University of Venda
Creating Future Leaders

UNIVERSITY OF VENDA

DOCTORAL THESIS

The Development and Application of Coupled Multiscale Models of Malaria Disease System

Author:
BOTHWELL MAREGERE
(17023777)

Supervisor:
Prof. Garira W.

Co-Supervisor:
Prof. Mathebula D.

A thesis submitted in fulfillment of the requirements
for the degree of Doctor of Philosophy (Applied Mathematics)

in the

Modelling Health and Environmental Linkages Research Group
Department of Mathematical and Computational Sciences
Faculty of Science, Engineering and Agriculture

September 2022

Declaration of Authorship

I, BOTHWELL MAREGERE (17023777), declare that this thesis titled, 'The Development and Application of Coupled Multiscale Models of Malaria Disease System' is my own work and it has never been submitted before for any degree or examination in any other university, where I have quoted from the work of others, the source is always given.

- This work was done wholly or mainly while in candidature for a research degree at this University.
- Where any part of this thesis has previously been submitted for a degree or any other qualification at this University or any other institution, this has been clearly stated.
- Where I have consulted the published work of others, this is always clearly attributed.
- Where I have quoted from the work of others, the source is always given. With the exception of such quotations, this thesis is entirely my own work.
- I have acknowledged all main sources of help.
- Where the thesis is based on work done by myself jointly with others, I have made clear exactly what was done by others and what I have contributed myself.

Signed: 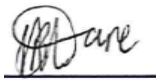

Date: 15/08/2022

Abstract

The purpose of this thesis is to develop coupled multi-scale dynamics of infectious disease systems. An infectious disease system consists of three subsystems interacting, which are the host, the pathogen, and the environment. Each level has two different interaction scales (micro-scale and macro-scale) and is organized into hierarchical levels of an organization, from the cellular level to the macro-ecosystem level, and is arranged into hierarchical levels of an organization. There are two main theories of infectious diseases: (i) the transmission mechanism theory, (ii) the replication-transmission relativity theory. A significant difference exists between these theories in that (i) the transmission mechanism theory considers transmission to be the primary cause of infectious disease spread at the macro-scale, while (ii) replication-transmission relativity theory is an extension of the first theory. It is important to consider the interaction between two scales when pathogen replication occurs within the host and transmission occurs between hosts (macro-scale). Our research primarily focuses on the replication-transmission relativity theory of pathogens. The main purpose of this study is to develop coupled multi-scale models of direct vector-borne diseases using malaria as a paradigm. We have developed a basic coupled multi-scale model with a combination of two other categories of multi-scale models, which are a nested multi-scale model in the human host and an embedded multi-scale model in the mosquito host. The developed multi-scale model consists of approaches of nonlinear differential equations that are employed to provide the mathematical results to the underlying issues of the multi-scale cycle of pathogen replication and transmission of malaria disease. Stability analyses of the models were evolved to substantiate that the infection-free equilibrium is locally and globally asymptotically stable whenever $R_0 < 1$, and the endemic equilibrium exists and is globally asymptotically stable whenever $R_0 > 1$. We applied the vaccination process as a governing measure on the multi-scale model of malaria with mosquito life cycle by comprising the three stages of vaccination, namely pre-erythrocyte stage vaccines, blood stage vaccines and transmission stage vaccines. The impact of vaccination on malaria disease has been proven. Through numerical simulation, it was found that when the comparative of vaccination efficacy is high, the community pathogen load (G_H and P_V) decreases and the reproductive number can be reduced by 89.09%, that is, the transmission of malaria can be reduced on the dynamics of individual level and population-level.We also evolved the multi-scale model with the human immune response on a within-human sub-model which is stimulated by the malaria parasite. We investigated the effect of immune cells on reducing malaria infection at both the between-host scale and within-host scale. We incorporate the environmental factor, such as temperature in the multi-scale model of the malaria disease system with a mosquito life cycle. We discovered that as the temperature enhances the mosquito population also increases which has the impact of increasing malaria infection at the individual level and at the community-scale. We also investigated the influence of the mosquito life cycle on the multi-scale model of the malaria disease system. The increase in eggs, larval and pupal stages of mosquitoes result in the increase of mosquito density and malaria transmission at the individual level and community-scale. Therefore, the suggestion is that immature and mature mosquitoes be controlled to lessen malaria transmission. The results indicated that the combination of malaria health

interventions with the highest efficacy has the influence of reducing malaria infection at the population-level. Models developed and analyzed in this study can play a significant role in preventing malaria outbreaks. Using the coupled multi-scale models that were developed in this study, we made conclusions about the malaria disease system based on the results obtained. It is possible to apply the multi-scale framework in this study to other vector-borne diseases as well.

Acknowledgements

I give thanks to the Almighty God, by His grace I receive the gift of life. I would like to express my deepest appreciation to my promoter, Prof. Garira W. and co-promoter Prof. Mathebula D, who continually and convincingly encouraged the spirit of adventure in relation to research and an excitement conveyed to teaching. Their guidance and persistence played a great role in this Thesis. Much appreciation also goes to fellow colleagues who were assisting tirelessly throughout the research. I wish there was a lot of space to write the names of my supporting cast, brothers and sisters: Edna Maregere, Editor Maregere, Amon Maregere, Munyaradzi Maregere and Nyasha Maregere. I would like to extend great thanks to Modelling Health and Environmental Linkages Research Group (MHELG) members who offered their time, support and commitment. Finally, I will conclude by extended my sincere gratitude to the work study and research for financial support.

Contents

List of Figures

List of Tables

Chapter 1

INTRODUCTION

1.1 Background of the infectious diseases

Infectious diseases remain the leading cause of morbidity and mortality worldwide, with HIV, malaria and tuberculosis being the leading cause of most deaths [2], particularly in low-income countries, particularly among children under 5 [3]. Infectious disease systems are described as illness triggered by organisms (such as bacteria, fungi, viruses, or parasites) that are transmitted either directly or indirectly from an infected person, animal or reservoir to a susceptible host [4]. Infectious disease systems are viewed as complex systems resulting from the interconnection of three subsystems (such as pathogen, host, and environmental) and these sub-systems are organised into hierarchical levels of organisation (that is from cell level to macro-ecosystem level), with multi-scales (i.e., micro-scale and macro-scale) [5, 6]. These diseases have endangered many people for centuries. Infections can be transmitted through direct or indirect contact with an infectious agent such as contaminated food, water, feces, bodily fluids or animal products, or through the air. There have been some improvements in infectious disease research, treatment, control and eradication, but they still face major public health challenges [7]. Mathematical models of the biological system have played an important role in improving our understanding of infectious disease systems at different organizational levels (e.g., cellular level, tissue level, organ level, micro-ecosystem level, host/organism level, community level, and macro-ecosystem level).

The field of mathematical models has long dealt with aspects of transmission mechanisms of infectious disease systems [8]. Daniel Bernoulli was the first to develop a mathematical modelling of infectious disease system in 1766, as models work on smallpox immunization [9]. Since that time until recently,

numerous single-scale mathematical model has been formulated to display and assess the transmission dynamics of various infectious diseases across different levels of organisation of an infectious disease system [10]. These traditional transmission mechanisms of mathematical models can be tracked back to Sir Ronald Ross 1916-1917 phenomenal models to investigation mosquito borne diseases [8]. In the early 1900s, Ross published a series of articles on mathematical models to explore the theory of transmission mechanisms of infectious disease systems. Most of George McDonald's models were developed by extending Rosss models by accounting for factors such as age-related differential susceptibility to malaria in human populations, acquired immunity, and host-parasite spatial and genetic heterogeneity[9]. Ronald Ross and George McDonald pioneered the theory of mosquito-borne disease transmission and the use of mathematics to model the transmission of infectious disease systems [9]. The Ross-McDonald models were an intentionally simplified set of models, concepts, and principles that could help illustrate certain related empirical phenomena related to pathogen transmission. The Ross-McDonald theory has contributed to improving the study of pathogen transmission and establishing strategies for the prevention of infectious diseases. Most mathematical models of infectious diseases in the transmission of pathogens are based on Ross-McDonald theory. In 1927, Kermack and McKendrick proposed the first Susceptible, Infected, and Recovered (SIR) model, refining and expanding the theory of pathogen transmission [9].

For over a century, almost all studies of infectious diseases have been based on the principle of Ross and McDonald, which has played an important role in developing the theory of pathogen transmission mechanisms. It is generally accepted that a better understanding of the theory of infectious disease transmission mechanisms can facilitate the development of new and improved prevention and control measures against the burdens and challenges of these infectious diseases across populations by using mathematical modeling methods [11]. The advantages of these transmission models are that they have improved our knowledge of the impact of different disease transmission mechanisms (e.g. fecal-oral transmission, sexual-oral transmission mechanisms, vector-borne transmission mechanisms, etc.) on the risk of infectious diseases on population health. These transmission models help us to compare and assess the effectiveness of different health interventions against these infectious diseases, either locally or globally.

1.2 Theories of infectious disease systems

Several theories have been developed to explain the infectious diseases, and the two main theories of infectious diseases are (i) the transmission mechanism theory and (ii) the replication-transmission-relativity theory [11]. The difference between these theories is that the first theory considers transmission as the main cause of infectious disease spread at macro-scale and the second theory considers replication transmission as the main cause of pathogen replication at lower/micro-scale. Scale and pathogen transmission at upper-scale/macro-scale. These theories of infectious disease systems are described as follows:

(1) ***The transmission mechanism theory***: The transmission mechanism theory is based on the assumption that transmission is the most important dynamic disease process at each hierarchical scale of organization (i.e. the cellular scale, the tissue scale, the organ scale, the micro-ecosystem scale, the host scale, the community scale, the macro-ecosystem scale) in the dynamics of infectious diseases and the transmission can be developed to study disease dynamics at a particular scale of organization. The majority of studies so far on mathematical modelling of infectious disease systems were confined to a single scale of organization (host-scale), thus creating distinct systems with their own questions. The development of these transmission models at any level are classifying at the population level (i.e., population of cells at the cellular scale, population of tissues at the tissue scale, population of organs at the organ scale, etc.) into compartments in which individuals behave in a homogeneous manner. However, we have seen number of mathematical models of infectious diseases developed based on the transmission mechanism theory. The mathematical models developed based on transmission mechanism theory demonstrated the infectious disease system on a single scale. Students working on infectious disease systems adopt transmission mechanism theory in their master's [12] and Ph.D [13] theses. This idea is based on three main transmission processes: (i) direct transmission mechanism, (ii) environmental transmission mechanism and (iii) vector transmitted transmission mechanism [11]. These transmission mechanisms can be summarized as follows:

(i) The directly transmitted mechanisms are infectious disease processes built on the transmission mechanism theory, in which transmission from one host to another occurs through host-to-host transmission. The mechanism of transmission can be sexually transmitted infection such as HIV/AIDS. The directly transmitted disease models are developed at the population level that has the following compartments Susceptible, Exposed, Infected, Recovering (SEIR) and variations of the paradigms (SI, SEI, SIR, etc.) at each hierarchical organizational level of an infectious disease system [11, 14, 15].

(ii) Environmentally transmitted mechanisms are the infectious disease systems where transmission of pathogens must pass through the environment to complete their disease life cycle [16, 17]. The models for environmentally transmitted disease systems have an additional compartment of environmental pathogen load and the following compartment built at the population level, i.e. H. Susceptible, Exposed, Infected, Recovered, and Environmental Pathogen Load (SEIRP) and variations of the paradigms (SIP, SEIP, SIRP, etc.) [11, 15].

(iii) Vector-borne transmitted mechanisms arising due to pathogens have a complex life cycle that requires the existence of two hosts (a vertebrate host and a vector host) for the pathogen to complete its life cycle. These infectious disease systems are either environmental or directly transmitted diseases [11, 18]. Vector-borne transmitted diseases have compartments for vertebrate hosts and vector hosts.

The transmission mechanism process has certain limitations such as: being incapable to offer system of level description of an infectious disease system that uses multiscale modeling approaches

that address both the microscale and the macroscale. Most models of the transmission mechanism also have limitations that are not sufficient to illustrate the phenomena of infectious disease dynamics that differ temporally and spatially at different scales [11]. These mathematical models of transmission mechanism theory have failed to recognize that the infectious disease system can be fully demonstrated by considering two bounding adjacent scales (i.e., the microscale and the macroscale), and they focus on a disease process on a single scale. The studies on infectious disease systems are mainly concerned with the theory of transmission mechanisms, that is of transmission at the population level, there is very little effort devoted to replicating pathogens.

(2) ***The replication-transmission relativity theory***: The need to consider the theory of relativity, which accounts for events (i.e. replication of pathogens) that lead to transmission and thus accounts for temporal and spatial variability. This theory is the extension of the first theory. The infectious disease systems that take into account pathogen replication and the theory of transmission mechanism are called the relativity theory of replication and transmission [11]. Replication-transfer relativity theory states that at each hierarchical level of organization of an infectious disease, there are interactions between the micro-scale and macro-scale sub-models. This infectious disease system research work addresses the replication-transmission relativity theory.

The replication-transmission relativity theory recognizes that there are two distinct processes at each hierarchical level of organization that influence each other through a positive feedback mechanism at the micro-scale (where pathogen replication often occurs) and at the macro-scale (where pathogens transmission occurs) when the dynamics of the infectious disease will spread and persist. These hierarchical levels organize and shape the dynamics of infectious diseases at each level as a multiscale loop that includes the influence between two scales (micro-scale and macro-scale) [11]. At each hierarchical level of an infectious disease system, the reciprocal influence between the micro-scale and macro-scale establishes a multi-scale cycle of pathogen replication and transmission [11]. The dynamics of infectious diseases are confronted with the circular causality of disease processes at each of the seven hierarchical levels of organization. These will unify the multi-scale cycle of replication and transmission. The two limiting scales (macroscale and microscale) interact with each other through the processes of (i) superinfection/infection (movement of pathogen from macroscale to micro-scale) and (ii) shedding/excretion (movement of pathogen from microscale to macroscale). The macro-scale is at the population level (between cell scale, between tissue scale, between organ scale, etc.) and the micro-scale is at the individual level (within cell scale, within tissue scale, etc.). Frequently, the scales at which pathogen repetition and transmission take place do not match [11]. The time scale on the microscale and the macroscale is different, that is, the microscale has a fast time scale while the macroscale has a slow time scale. At all levels we observe that there is pathogen replication and the process of transmission of pathogens linked by infection/superinfection and excretion/excretion processes. Studies have been concerned in transmission mechanism theory until multiscale modeling came about. The diagram in figure (1.1) shows the

reciprocal influence between the macroscale and the microscale.

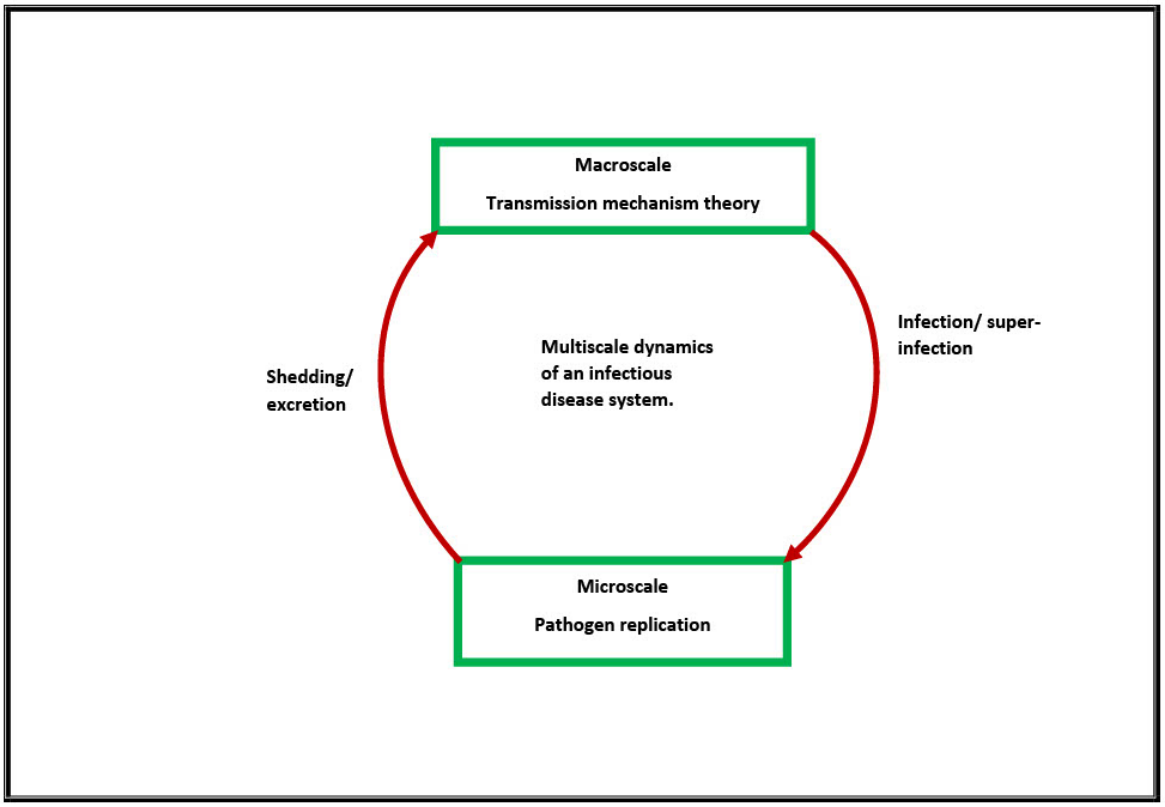

Figure 1.1: Conceptual diagram of replication-transmission multi-scale cycle.

1.3 The seven fundamental levels of organisation of infectious disease system

Infectious diseases are complex systems composed of multi-scale and multilevel dynamics. The seven main levels of organization of an infectious disease system at which disease can be resolved, and these levels are as follows: cellular level, tissue level, tissue level, organ level, micro-ecosystem level, host level, community level, and macro-ecosystem. Each level of organization of an infectious disease system is decomposed into two adjacent scales, the microscale and the macroscale, and these scales integrate in reciprocal ways. The interaction between two adjacent scales of an infectious disease system at different hierarchical levels of the biological organization of an infectious disease system, ranging from the cellular level to the macro-ecosystem level, is shown in the diagram in Figure 1.2. At each organizational level of an infectious disease system, there is an open scale boundary (enabling the bidirectional flow of information between scales) that demarcates each level into two adjacent scales (microscale and macroscale),

and the dynamics of infectious diseases at each hierarchical level creates a multiscale loop that entails the reciprocal (that is, in both directions) influence of the macro-scale and the micro-scale.At each organizational level, the macroscale influences the microscale through pathogen infection/superinfection, then follows the process of pathogen replication at the microscale. The micro-scale influences the macro-scale through shedding/excretion of pathogens and the process of pathogen transmission takes place at the macro-scale. These organizational levels of an infectious disease dynamics are briefly described as follows:

I. The cellular level: The micro-scale and macro-scale of this hierarchical level of organization are the within cellular scale and the between cellular scale, respectively. Infectious diseases, modelled at the cellular level of organization, are diseases in which the pathogen invades specific or target cells and damages the host cell. Integrating the intra-cell scale and the between cellular scale can account for different types of target cells in the multiscale dynamics of infectious disease systems, for example $CD4^+$ T cells and microphages for HIV, red blood cells and hepatocytes (liver cells) for malaria [3, 11].

II. The tissue level: The microscale and macroscale for this level are the within tissue and between tissue scales, respectively. Infectious disease systems, modelled at the tissue level of organization, are diseases in which the pathogen invades specific or target tissues and damages host tissues. The different types of tissues that can be considered in the multiscale cycle of the infectious disease dynamics encompass the granuloma for tuberculosis, or micro-abscesses triggered by certain bacterial infections [3, 11], epithelium, immune system, etc.

III. The organ level: This organizational level consists of two interacting scales, the within organ scale and the between organs scale as a micro-scale and macro-scale, respectively. Infectious disease modelled at the organ level are diseases in which the pathogen invades specific or targeted organs and damages the host organ. This level of organization is described in terms of a single pathogen strain and multiple organs/anatomical compartments. Some of the organs/anatomical compartments are as follows: lungs, brain, intestines, kidneys, heart, liver, etc. [3, 11].

IV. The micro ecosystem level: This level of organization is demonstrated by multiple organs/anatomical compartments and multiple pathogen strains/species replications. The various organs/anatomical compartments such as the lungs, intestines, kidneys, heart, liver etc. are taken into account as ecosystems. At this level of organization, the ecosystem process/interactions affect the infectious disease system, which includes the competing species/strain interactions and the mutual interplay between the multiple pathogen species/strains. This organizational level consists of two interacting scales, the within micro-ecosystem scale and the between micro-ecosystems scale as a micro-scale and macro-scale respectively [11].

V. The host/organism level: The micro-scale and macro-scale of this level are the within-host and inter-host scales, respectively. This level of organization is demonstrated in terms of single pathogen

species/strains as well as single host species and single community. The host-level disease system begins with infection/superinfection of the host by the pathogen. When infection of the host by the pathogen has successfully entered the host, replication of the pathogen at the intra-host level follows. The technique of pathogen replication is followed by pathogen shedding/excretion into the macroscale (between-host scale). The transmission process takes place at the macro scale. These illustrate the multiscale cycle of pathogen replication at the host level through infection/superinfection and excretion/excretion (i.e. the influence between macroscale and microscale) that connects the individual scale and the population scale within this level [11].

VI. The community level: Single pathogen species/strains, single host species, and multiple communities are used to demonstrate this level of organization. This organizational level has the within community scale and the between community scale as its micro scale and macro scale [11].

VII. The macro-ecosystem level: Single pathogen species/strains, single host species, and multiple communities are used to demonstrate this level of organization. This organizational level has the within community scale and the between community scale as its micro-scale and macro-scale, respectively [11].

The multiscale cycle can be differentiated into two types of reciprocal influence between the microscale and the macroscale: Type I reciprocal influence and Type II reciprocal influence [11]. These reciprocal influences are presented as follows:

(a) ***Type I reciprocal influence between macroscale and microscale within the levels of organisation.*** In this type, the microscale influences the macroscale through pathogen shedding/ excretion (movement of pathogen from microscale/lower scale/individual scale to macroscale/upper scale/population level). The macroscale influences the microscale by initial infection. This kind of reciprocal influence has a pathogen replication at micro-scale, the pathogen load on micro-scale increases by the pathogen replication [11].

(b) ***Type II reciprocal influence between macro-scale and micro-scale within each level of organisation.*** In this type, the micro-scale affects the macro-scale through shedding/excretion. The macro-scale affects the micro-scale through super-infection. This type of reciprocal influence between the micro-scale and macro-scale has no pathogen replication at the micro-scale, the pathogen load at the micro-scale increases due to the repeated infection [11].

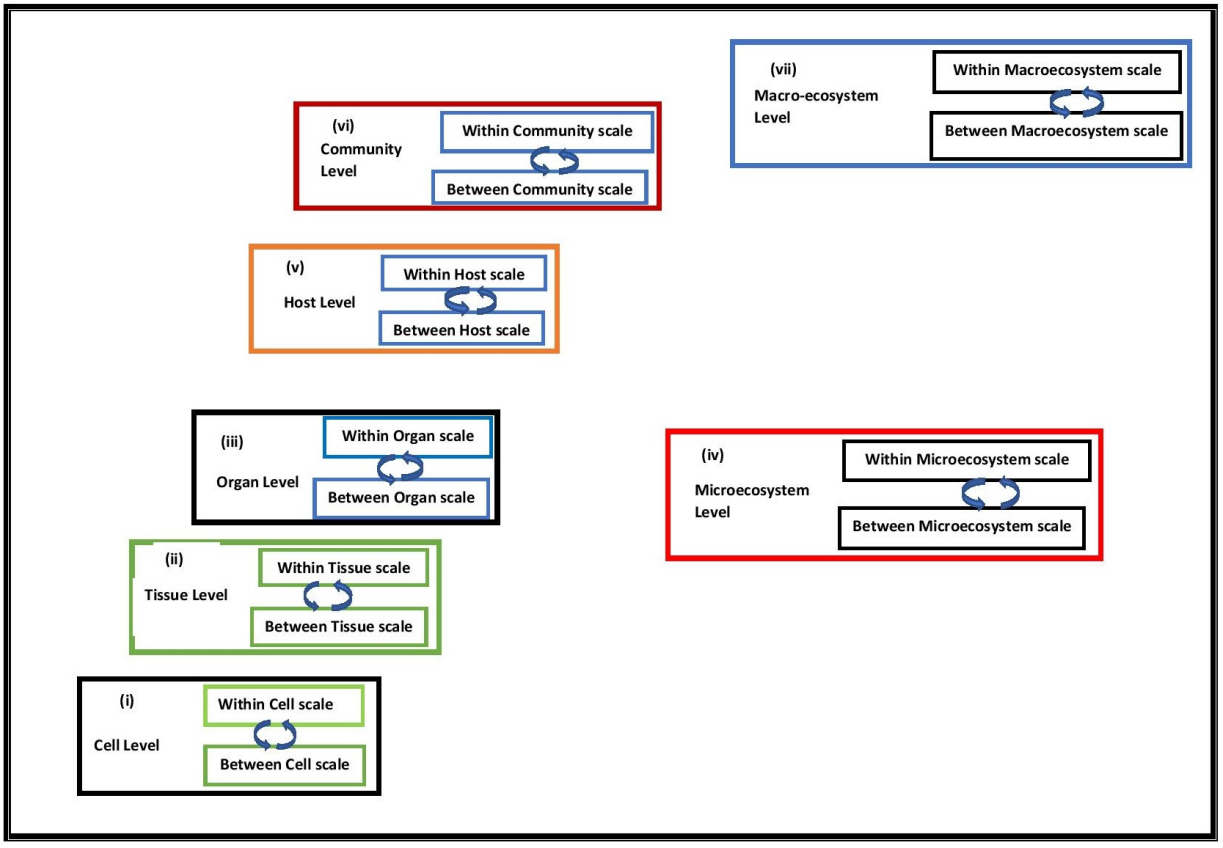

Figure 1.2: The seven hierarchical levels of organisation of infectious disease dynamics are illustrated in this conceptual diagram.

1.4 Problem statement

Multiscale modelling of the infectious disease dynamics has recently gained acceptance in the mathematical modelling community over the single-scale modelling which has mainly focused on the pathogen transmission mechanisms theory. Infectious diseases have been a serious threat on humans across the world, with the greatest impact in developing countries. The overall problem of the study is to re-engage the pathogen replication-transmission relativity theory, and since the theory was published [11], there have been few applications, although it is the overtake theory that provides a multi-scale modelling of infectious disease systems. The fundamental problem is the malaria disease system, which remains the leading cause of morbidity and mortality in the world. The malaria disease system has been modelled in the past, but there are still problems. We study the malaria disease system as an example to identify hierarchical levels of organization. There is no detailed work showing how the replication-transmission relativity theory can be applied to the malaria disease system and possible extension to other vector-borne diseases.

We change the whole Ross-Ronald setup that has been used to inform the modelling of malaria diseases over the last century, we reorganize the knowledge and illustrate that every aspect we can do, for example the issues of health interventions, environmental change system, and the human immune system can all be incorporated into multi-scale modelling. In addition to modeling the malaria disease system at a multiscale, we hope the idea can be generalized to other vector-borne diseases. Plasmodium parasites require both human hosts and mosquitoes to complete their life cycle in order to produce a realistic coupled multiscale model of malaria disease. There is a discussion of how health measures, environmental changes, and the immune system influence malaria disease development. The models we develop can serve as an important tool to address a variety of biomedical, biological, behavioral, environmental, and clinical problems related to malaria disease. The long-term contribution of biological and behavioral variability to the effectiveness-efficiency gap.

1.5 Aim and objectives

The main aim of this study is to develop coupled multiscale models of vector-borne disease system that consider the pathogen replication-transmission relativity theory using malaria as an example. The specific objectives of the study are as follows:

(i) To develop a basic coupled multi-scale model of malaria disease system with replication-transmission multi-scale cycle using *type I* reciprocal influence on humans and *type II* reciprocal influence on mosquitoes.

(ii) To extend the basic multi-scale model for malaria disease system by incorporating the human liver and blood stages and also to incorporating the vaccination process. Vaccines are also an important control measure that has been used successfully to prevent other infectious diseases. The vaccine prevents malaria in the stages of the life cycle of malaria and also prevents malaria infection on both within-host scale and between-host scale.

(iii) To investigate the impact of the human immune response on malaria disease system.

(iv) To incorporate the mosquito life cycle on multi-scale model of malaria disease system and considering the environmental changes aspects.

(v) To incorporate the malaria health intervention methods on multi-scale model of malaria disease dynamics with mosquito life cycle. We look at the three health interventions for malaria: egg-larval-pupa control, long-lasting insecticides treated bed nets (LLINs) and artemisinin-based combination therapy (ACT).

1.6 Preliminary of multiscale models of vector borne disease

Diseases transmitted by vectors such as mosquitoes, sand flies, black flies, ticks, tsetse flies, snails and others are vector-borne diseases caused by parasites, viruses and bacteria. Since vector-borne diseases have a complex life cycle, they require at least two hosts (i.e., vertebrate host and vector host). In addition to serving as parasite carriers, vectors also serve as organisms in which parasites mature and become infectious. There are two types of vector-borne diseases transmission mechanisms: (a) type I vector-borne disease systems, and (b) type II vector-borne disease systems [18]. We give brief summary of these types of vector-borne disease systems below.

a. ***Type I vector-borne disease systems:*** These are vector-borne diseases in which part of the pathogen life cycle is outside of the two hosts (vertebrate host and vector host) [19]. Infection of hosts with this type of vector-borne disease is caused by free-living infectious pathogens in the environment. These types of vector-borne diseases are also environmental disease systems. Examples of type I vector-borne disease systems are schistosomiasis in humans [20] and the guinea worm [21]. We have classified the type I vector-borne disease system or the environmental vector-borne disease system into three main groups, which are related to the level of organization of the infection where the pathogen at the micro-scale and the macro-scale influence each other. These groups are described as follows:

(i) ***Type I Environmentally transmitted vector-borne disease system***: These are vector-borne diseases in which pathogen replication is not observed at the microscale (type II reciprocal influence between the microscale and macroscale). The transmission process occurs at a macro scale. Pathogen load in an infected host increases as a result of superinfection or repeated infection. Examples of environmental type II diseases are schistosomiasis [20], guinea pig worm [21] and soil borne hookworm disease [11].

(ii) ***Type II Environmentally transmitted vector-borne disease system:*** These are environmentally transmitted vector borne disease systems which has pathogen replication at the micro-scale and transmission at the macro-scale. There use type I reciprocal influence between the micro-scale and the macro-scale. The examples of type II environmentally transmitted diseases are are air-borne viral infections e.g. influenza [22] and food-borne bacterial infections e.g. paratuberculosis species [23].

(iii) ***Type III Environmentally transmitted vector-borne disease systems:*** The pathogen reproduces at both the micro and macro scales in these type I vector-borne diseases. These vector-borne type I disease systems exhibit a combination of type I and type II mutual influences, showing the interaction between the micro and macro scales. The type III environmental diseases include cholera, salmonella enterica, and anthrax[11].

b. ***Type II vector-borne disease systems:*** Vector-borne diseases, of which the entire life cycle of the pathogen is strictly inside the hosts, are implicated in transmission of multiple-host infections[19].

The pathogen only survives in the interior environment of two hosts in this type of vector-borne disease system (i.e., the micro-scale). The majority of type II vector-borne diseases are spread by blood-feeding arthropods such mosquitos, ticks, and fleas. From Garira's work [18], we discovered that they are two groups of type II vector-borne disease systems which are summarized below.

i. This group of type II vector-borne disease systems that do not have a microscale pathogen replication cycle. Therefore, the reciprocal influence between the microscale and the macroscale of this group is a type II reciprocal influence. Example for this group is malaria in the vector host [24].

ii. This type II vector-borne disease system has pathogen-reproduce cycle at the microscale. Thus, micro-scale influences macro-scale through reciprocal influence of type I. Malaria is an example of a type II vector-borne disease system, where merozoites replicate at a micro-scale in the vertebrate host garira2019coupled.

This group of type II vector-borne disease systems that have a microscale pathogen replication cycle. Therefore, the reciprocal influence between the microscale and the macroscale is a Type I reciprocal influence. An example of this group of Type II vector-borne disease systems is malaria. In this case we have used malaria disease as a case study and we consider both the perspective of transmission mechanism theory and pathogen replication that make up the disease dynamics. We also regard the malaria disease system as the type II vector-borne disease systems. The basic problem in this study is the malaria disease system and it has caused damage in humans, and malaria has been modeled in the past, but they still have problems . We conduct a study of malaria disease systems at each hierarchical level of organization (the cellular level, the tissue level, the organ level, etc.). We're changing the entire setup used by Ronald Ross and George Mcdonald to model mosquito-borne diseases for the past century. We expand all Ross Mcdonald knowledge and explain that every aspect we can do, e.g. the issue of intervention, environmental change, etc., can all be included in the multiscale modeling where the merozoite life stage has the microscale replication cycle in the vertebrate host [24].

From the recent work of Garira [3, 7], the author presents five different main categories of multiscale models of infectious disease systems that integrate the two adjacent scales (i.e. the microscale and the macroscale) at the time of infection disease systems. These categories are: (I) Individual-Based Multiscale Models (IMSMs), (II) Nested Multiscale Models (NMSMs), (III) Embedded Multiscale Models (EMSMs), (IV) Hybrid Multiscale Models (HMSMs), and (V) Coupled Multiscale Models (CMSMs), where each category has more than one class. The categorization of these multiscale models of infectious disease systems that can be built at each of the seven levels of organization of infectious disease systems (i.e. cellular level, tissue level, organ level, microecosystem level, host level, the community level, and the macro-ecosystem level). These categories of multiscale models of infectious disease systems are summarized below.

I. ***Individuals-based multiscale models (IMSMs):***This category of multi-scale models of infectious disease systems that assume that the micro-scale sub-model illustrates the entire infection system both at the micro-scale and macro-scales. This category of multiscale models of infectious disease dynamics can be built at a particular level of organisation of an infectious disease system. There is no feedback from the macro-scale to the micro-scale and the macroscale is observed as emergent behaviour of the micro-scale entities. The microscale and the macro-scale are integrated through type I reciprocal influence. There are many examples of IMSMs which are as follows: graph-theoretic or network modeling, agent-based models (ABM), and cell automata (CA) [25–27].

II. ***Nested multiscale models (NMSMs):*** A category of multiscale models of infectious disease systems that are built on the assumption that there is a unidirectional flow of information, i.e. only from the microscale sub-model to the macroscale sub-model. This category of multiscale models of infectious disease dynamics is developed at a specific organizational level. The micro-scale sub-model and the macro-scale sub-model are integrated by Type I reciprocal influence. The micro-scale and macro-scale sub-models must be demonstrated by the same formalism or mathematical representation. Examples of NMSM can be found in [14, 28–30].

III. ***Embedded multiscale models (EMSMs):*** These are multiscale models of infectious disease systems that have a bi-directional flow of information between the micro-scale sub-model and the macro-scale sub-model. The micro-scale sub-model and the macro-scale sub-model are integrated by type II reciprocal influences. In both the micro-scale and macro-scale sub-models, the same mathematical representation must be used. Examples of EMSMs can be found in [11, 21, 31].

IV . ***Hybrid multiscale models (HMSMs):*** These are multiscale models of an infectious disease system that demonstrate the dynamics of infectious diseases at a specific organizational level. The micro-scale sub-model and the macro-scale sub-model are integrated by either Type I reciprocal influence or Type II reciprocal influence. The formalism or mathematical representation that demonstrates the micro-scale sub-model and the macro-scale sub-model must be different. The examples of HMSMs of such a paired formalism are deterministic/stochastic, mechanistic/phenomenological, ordinary differential equation (ODE)/partial differential equation (PDE), and ODE/ABM. The multiscale models in [32–34] are examples formulated on HMSMs.

V. ***Coupled multiscale models (CMSMs):*** These are multiscale models of infectious disease systems that include multiple levels of organization of infectious disease systems, multiple host infections, multiple strain infections, multiple group infections, multiple pathogen infections, multiple geographic environment infections, and multiple biological environment infections. This category of multiscale models of infectious disease dynamics integrates more than two scales and can be either Type I reciprocal influence or Type II reciprocal influence, or a combination of both types. The CMSMs differ from other categories of multiscale models (I, II, III, and IV), which focus on a specific combination of (i) a single host, (ii) a single pathogen, and (iii) a single organizational level of infectious disease systems. The other four categories of multiscale models (IMSMs, NMSMs,

EMSMs, and HMSMs) can be used as sub-models to demonstrate the dynamics of an infectious disease system across scales at each level of biological organization [3, 11]. The multi-scale models in [18, 20, 24, 35] are typical examples of CMSMs.

In this study, we develop a multiscale model of the malaria disease system, which is a vector-borne disease and a direct transmitted disease, and we illustrate the validity of the replication-transmission multi-scale cycle in the relationship between the micro-scale and the macro-scale sub-models become either demonstrated by Type I reciprocal influence or Type II reciprocal influence or a combination of both types. Characteristics of vector-borne disease systems are (i) multiple hosts (i.e., vertebrate host and vector host), (ii) effects of environmental change, and (iii) immune system. Therefore, in this study, we developed coupled multiscale models of the infectious disease system that feature a combination of embedded multiscale model with nested multiscale model that integrates two limiting neighboring scales at any hierarchical levels of organization to study the pathogen replication-transmission multiscale cycle at the microscale and the macro scale. We consider the embedded multiscale model in the vector-host since there is no pathogen replication cycle within the infected vector scale and the pathogen load increases due to repeated infection, i.e. superinfection. We apply the nested multiscale model in the vertebrate host because there is a pathogen replication cycle at the host level within the vertebrate, i.e. in merozoites. The within-host scale affects the between-host scale through pathogen shedding/shedding, while the between-host scale affects the within-host scale through initial infection, i.e. the pathogen load increases during the pathogen replication cycle.

The replication transmission multiscale cycle of vector-borne diseases is influenced by factors affecting vector numbers (e.g., warmer temperatures increase mosquito reproductive rates), contact between humans and vectors, imported pathogens (e.g., migration of non-immune humans). in areas where the disease is widespread), breeding grounds of the vectors [36]. The pathogen within the infected host scale is an infectious disease only if it can survive and multiply (i.e., pathogen replication with the infected host) at the infected host scale. Pathogens are very sensitive to environmental changes, i.e. temperature and precipitation [36].

1.7 Methodology

The study focuses on coupled multiscale models of infectious disease system based on ordinary differential equations that describe the dynamics of type II vector-borne transmitted disease system at any levels of organisation using the malaria disease system as a paradigm. We start by developing the malaria disease system to demonstrate the transmission mechanism theory that is at the macro-scale/ between-host scale. Then we followed by introducing the pathogen replication-transmission relativity theory to our model to form a multiscale circle, that is the interaction between the microscale and the macroscale sub-models. In other chapters, we consider the applications of the pathogen replication-transmission relativity theory.

Therefore, the single scale model make use of transmission mechanism theory, whereas other chapters with multiscale models use the replication transmission relativity theory.

In our mathematical analysis, we utilise numerous techniques to analyze all the models in this study, which are as follows: (i) Next generation operator, (ii) fixed point theory, (iii) Center Manifold theory, (iv) Descarte's sign change theory, (v) Routh-Hurwitz criteria, and (vi) Lyapunov function. We conduct sensitivity analysis to test the parameters which are sensitive to the models. We conducted sensitivity analysis using the Latin Hypercube Sampling (LHS) and Partial Rank Correlation Coefficients (PRCCs). The numerical simulation for the models were illustrated analytical solutions are obtained from these multiscale models using ODE solvers in Matlab and Python, that is ODE int function in the sci.integrate which solves systems of differential equations. These solvers are ode45 (Runge-Kutta Dormand-Prince method of order (4,5)) with default tolerance) [37].

1.7.1 Process of Multi-scale Modelling of Infectious Disease Systems

There are four main stages need to be followed in the development of multiscale models which are explained in [38]. These stages are summarized as follows:

Stage I: The first stage involves the identification of the infectious disease problem that need to be addressed by the multiscale modelling study of infectious disease system. In this stage, the modeller starts by state the aim and objectives of the multiscale modelling task of an infectious disease system. The modeller needs to discover the levels of organisation to be incorporated into a multiscale model and their associated scales. In this study of multiscale models of malaria disease system, the invasion of malaria parasite in human begins in the liver-cells, then follows the invasion of red-blood cells, which means the process of infection begins in at the cell-level. The study of multiscale models of malaria disease system can be at cell-level, tissue level, organ-level, host-level, and so on. Then there is need to decide which main categories of multiscale models which best fit your multiscale model. In case of our study of malaria disease system, the best category is coupled multiscale models (CMSMs) is the malaria parasite has a complex life cycle that needs two hosts to complete its life cycle and malaria can be studied at multiple levels of organisation. The reciprocal influence between the micro-scale sub-model and the macro-scale also helps to decide which appropriate categories will suit for your model. In case of our model, we develop coupled multiscale model of malaria disease system using the combination of (i) nested multiscale model in human-host where merozoites has a replication cycle at the microscale (that is in red-blood cells) and (ii) embedded multiscale model for vector-host where pathogen does not have a replication cycle at the micro-scale (that is for malaria, there is no replication cycle in the mosquito vector, pathogen progress from one stage to another). This multiscale model of malaria disease system which is linked through the exchange of single pathogen/strain [38].

Stage II : The second stage is to build a multiscale model of an infectious disease system using the information gathered in the first stage. The development of multiscale model of infectious disease system should involves the linkage of knowledge from four different multiscale modelling approaches. These four main modelling approaches are as follows: (i) empirical-based multiscale models (E-MSMs), (ii) mathematical-based multiscale models (M-MSMs), (iii) computational-based multiscale models (C-MSMs), and (iv) data-based multiscale models (D-MSMs). The process of development of multiscale models begins with the formulation of the E-MSMs of the infectious disease system, which is based on carrying out experiments, culture systems, clinical trials systems, observational systems, or surveillance systems which characterize an infectious disease system at multiple scales, that is where the data is being extracted. In the case of our multiscale model, we use secondary data from the published literature. The next process is to formulate the M-MSMs which involves the listing of the differential equations of all sub-models (i.e., within-host sub-model and between-host sub-model), explaining the meaning of each differential equation, variables and all the parameters utilised in the differential equations. All these differential equations, variables and parameters should be associated with each scale that integrates into multiscale model. It also involves down-scaling and up-scaling of variables and parameters when linking/integrating two scales (that is, micro-scale and macro-scale) into a complete multiscale model. The next process is the formulation of C-MSMs, which involves the developing of computational algorithms that interpret the M-MSMs and D-MSMs into numerical solutions and involves the use of software environments (i.e., use of Matlab, Python, Mathematica and e.t.c.). Then the last process is the formulation of D-MSMs that involves the transforming of multiscale data into knowledge about the dynamic of infectious disease system. These multiscale data can be applied to estimate probabilistic future trend of an infectious disease system derived from the previous behaviour characterized by the multiscale data [38].

State III: In this stage involves the evaluation of quality of the multiscale model of the infectious disease system. This stage involves the testing of the multiscale models of infectious disease systems by conducting multiscale model verification, multiscale model validation, and multiscale model sensitivity analysis and uncertainty analysis. The testing of quality multiscale model involves the examining whether it is mathematically and biologically well presented and the connection between the variables and between the scales are correctly presented. For testing the mathematically well posed, the modeller should use mathematical techniques to analyse the multiscale model of infectious disease system. These mathematical techniques are used to determine the feasible region of the equilibria of the multiscale scale, positivity of solutions, the basic reproductive number, the equilibrium points of the model, local and global stabilities of the equilibrium points, and numerical solutions. The conducting of sensitivity analysis assists in identifying the parameters which can be influenced by the disease control or elimination or eradication activities of infectious disease systems, which should be the critical points and need to be monitored and controlled during an

infectious disease system outbreak. There is also needed to state the limitations of the multiscale model which was developed [38].

Stage IV: In this last stage involves the use of multiscale models of infectious disease system in decision support. The process for multiscale models of infectious disease systems scientific agenda has four main items which are related to decision support which are described in [38], these are as follows: (a) use of multiscale models as a framework for understanding the influence of functionally organised complex systems of infectious disease dynamics, (b) utilize of multiscale models in predicting/forecasting of infectious disease dynamics, (c) use of multiscale models as strategic tools in analysing or understanding the underlining mechanisms of infectious disease dynamics, and (d) use of multiscale models in evaluation/analysis/formulation of policy for control or elimination or eradication of an infectious disease system.

When this iterative scheme on four main different stages in development of multiscale model are complete, then there should be a comparison between the results obtained and the real-world system in order to decide/conclude whether the outcome behaviour of the model and what is observed in the system matches. If the outcomes of the model obtained and the observation made from the system does not matches, then there is need to modify the model and begin again the iterative scheme for the development of multiscale model of infectious disease systems.

1.7.2 Multi-scale models and Vector-borne diseases

There are many mathematical models of malaria disease based on transmission mechanism theory, including [39–42] and work done on malaria disease systems within host scale [43–46]. From recent studies on the pathogen-replication-transmission relativity theory for *type I* vector-borne diseases (this takes into account environmentally-related infectious diseases), for example schistosomiasis [20] and Guinea worm disease [21] . Part of their pathogenic life cycle of these *type I* vector-borne diseases lies outside of the two hosts (vertebrate host and vector host). This type of environmentally transmitted infectious disease systems does not have a pathogen replication cycle at the micro-scale, rather there are only developmental stages of the pathogen that occur at this scale, while a process of pathogen transmission occurs at the macro-scale. Therefore, they integrate the micro-scale and macro-scale using the *Type II* reciprocal influence.

In the following, an overview of some of the existing coupled multiscale models that have been developed to describe the multiscale dynamics of *type II* vector-borne diseases is given. Agusto [35] developed a deterministically coupled multiscale model that combines the effects of microscale and macroscale dynamics on the *type II* transmitted disease system (i.e. the dynamics of malaria disease). They developed four sub-models (within-host scale, within-vector scale, between-host scale and between-vector scale) and these sub-models are linked using nested multi-scale models. Their coupled multi-scale model was built

at the host level. They use the transmission mechanism process in the macro-scale sub-models (between-host-scale and between-vector-scale) and use the replication process in the micro-scale sub-models (intra-host-scale and intra-vector-scale). In their model they use the *Type I* reciprocal influence between the macro-scale and the micro-scale, i.e. the macro-scale affects the micro-scale through initial infection, while the micro-scale affects the macro-scale through shedding/excretion of pathogens. We differentiate our multi-scale model with the model in [35], i.e. our model uses community pathogen load as a common metric for infectivity and disease transmission potential, while in [35] pathogens within the host are used as a measure of disease transmission, while the disease class between hosts (i.e., the infected class) is used as a measure of disease transmission .

Cai [34] adopted a hybrid multi-scale model approach for the dynamics of*type II* vectors that incorporates the vertebrate immune response to malaria transmission. They use age-structured partial differential equations for the between-host sub-model, they describe the asymptomatic and symptomatic infectious host population for malaria transmission. In their within-host sub-model, they use ordinary differential equations (ODEs) to demonstrate the replication of the malaria pathogen. When linking their sub-models, they use the mutual influence of *type I*, which demonstrates the interaction between the within-host scale and the inter-host scale. Your model was developed at the host level. Their model is difficult to simulate because one has to simulate their various components separately using special methods

Legros [47] worked on the evolution of resistance in a complex process influenced by transmission between-host dynamics and pathogen replication in intra-host dynamics. Their aim of the study was to investigate how these processes can be integrated at the micro-scale and macro-scale to influence the development of multi-pathogen infection (i.e. resistance in malaria parasites). They used a coupled multiscale model since the life cycle of the malaria parasite involves two hosts (i.e. the human host and the mosquito host). They also use nested multiscale models to link the within-host and the between-host scales (i.e. they apply *Type I* mutual influence between the microscale and the macroscale). They use a stochastic modeling framework to link transmission of malaria pathogens at the macro level and explicit pathogen replication at the micro level for two competing strains.

1.8 Outline of the thesis

Here is how the thesis is structured:

- Chapter 2 deals with the development of a single-scale model for the malaria disease system that only considers the theory of transmission mechanisms. We need to address the problem reflected in the epidemiological triad theory, which asserts that infectious diseases are the result of the interaction of three subsystems: host, pathogen, and environmental subsystems. The pathogen subsystem is not included in the SEIR models for directly transmitted diseases, and the direct transmission

mechanism shows the interaction of two subsystems: the host subsystem and the environmental subsystem. The extension of current models to multi-scale models is not realistic. For example, the time-since-infection models have pathogens at the microscale but no pathogen burden at the macroscale. Tracing the pathogen life cycle from the microscale to the macroscale becomes difficult when the two stages are linked. Integrating the two scales is particularly difficult because the scales have different units. In this chapter, we develop a directly transmitted mechanism of a vector-borne disease system with a community pathogen load (CPL) that can be extended to a multiscale model of the infectious disease system.

- From Chapter 3 to Chapter 7, we use the malaria disease system as an example to demonstrate the applicability of multiscale models of directly transmitted infectious disease systems with pathogen load at micro-scale and community pathogen load at macro-scale.
- Chapter 3 deals with the development of a basic coupled multiscale model of the malaria disease system by using the multiscale replication-transmission cycle with *type I* reciprocal influence on humans and with *type II* reciprocal influence on mosquitoes.
- In Chapter 4, extend the basic multi-scale model for malaria disease system by incorporating the human liver and blood stage and extend by incorporating the vaccination processes.
- Chapter 5 deals with investigation of the impact of the human immune response on multi-scale model of malaria disease dynamics.
- In Chapter 6, we investigate the mosquito life cycle on multi-scale model of malaria disease system and considering the impact of environmental changes.
- In Chapter 7, we investigate the impact of malaria health intervention methods on multi-scale model of malaria disease dynamics with mosquito life cycle.
- Chapter 8 provides conclusion and future research directions.

Chapter 2

A New Modelling Framework for Single Scale Models of Disease Dynamics Incorporating Direct Transmission

2.1 Introduction

One of the limitations of the transmission mechanism theory is that there is no common modeling framework to understand both directly transmitted infectious diseases and those that are environmentally transmitted. As a result, there is no measure of transmission or infectivity for either directly transmitted diseases or environmentally transmitted diseases. For direct communicable diseases, incidence and prevalence are the most common transmission metrics. However, for the dynamics of environmental disease, pathogen load is used as a measure of disease transmission. There is a need for a unified and standardized approach to modeling both direct and environmentally transmitted diseases. In an effort to address this limitation of transmission mechanism theory, we have proposed a new model science for directly transmitted diseases similar to an existing model science for environmentally transmitted infectious diseases. The method development for directly transmissible infectious disease models proposed in this study is based on the introduction of pathogen load as a new infectious disease variable, which is then used to define infection strength and transmission probability in models of disease dynamics. This transforms standard disease dynamics models based on Susceptible, Exposed, Infected, Recovered (SEIR) and variations of this paradigm (SI, SIS, SIR, etc.) for directly transmitted infectious diseases into disease dynamics models that are similar to the existing models for environmentally transmitted infectious diseases based

on Susceptible, Exposed, Infected, Recovered Pathogen Load (SEIRP) and variations of this paradigm (SIP, SISP, SIRP, etc.) where the community-wide pathogen load/pool in the environment is explicitly included in disease dynamics models.At the central to this modeling framework is the idea of using the total infection reservoir of the scale of analysis (TIR-SA) as the standard metric for disease transmission. This new metric of disease transmission is obtained by upscaling individual infectivity populations for directly transmitted infectious disease systems. The usefulness of such simple models is that they predict pathogens, the utility of which is threefold: [a.] as a measure to assess the effectiveness of treatment, [b.] as an indicator of a scale of community infectivity and likelihood of transmission, and [c.] as a proximal marker for the occurrence of infectious diseases and the possible spread of the disease.

2.1.1 Malaria Model Based on Direct Transmission Mechanism

[I.] Direct transmission of malaria in the human population: This sub-model is described by an SIS model. This sub-model is formulated based on monitoring the dynamics of two populations which are susceptible humans S_H, and infected humans I_H so that the total human population is given by $N_H = S_H + I_H$. We make the following assumptions for this sub-model.

[i.] There is no herd immunity in the human population as a result of prior exposure to the malaria infection or vaccination.

[ii.] The infected human population can recover naturally from malaria infection.

[iii.] The transmission parameter λ_V is a function of the number of infected mosquitoes so that $\lambda_V = \lambda_V(I_V)$.

[iv.] The dynamics of S_H and I_H are assumed to occur at slow time scale t compared to the within-human and within-mosquito submodels for malaria parasite population dynamics so that $S_H = S_H(t)$ and $I_H = I_H(t)$.

Based on these assumptions the malaria transmission dynamics using the human organism scale as the scale of observation and the community scale as scale of analysis becomes

$$\text{Direct transmission of malaria among humans} \begin{cases} 1.\ \dfrac{dS_H(t)}{dt} = \Lambda_H - \beta_V \lambda_V(I_V) S_H(t) - \mu_H S_H(t) + \gamma_H I_H, \\ 2.\ \dfrac{dI_H(t)}{dt} = \beta_V \lambda_V(I_V) S_H(t) - \Big[\mu_H + \delta_H + \gamma_H\Big] I_H(t). \end{cases} \tag{2.1.1.1}$$

The first equation in sub-model system (2.1.1.1) describes the dynamics of susceptible humans. The population of susceptible humans is assumed to increase at a constant rate Λ_H through birth. This population is depleted through infection of susceptible humans at a variable rate $\lambda_V(I_V)$ and natural death at a constant rate μ_H. The population of susceptible humans also increases through natural recovery of infected individuals at a rate γ_H. The second equation in sub-model system (2.1.1.1)

describes the dynamics of infected humans. This population increases through infection of susceptible humans and decreases through natural death at a rate μ_H, through disease induced death at a rate δ_H and through natural recovery at rate γ_H.

[II.] Direct transmission of malaria in the mosquito population in the Kermack-McKendrick Framework: This sub-model is described by an SI model and describes the transmission of malaria parasite from infected humans to susceptible mosquitoes. We make the following assumptions for this sub-model.

[i.] The infected mosquitoes do not recover naturally from malaria infection.

[ii.] The transmission parameter λ_H is a function of the number of infected humans so that $\lambda_H = \lambda_H(I_H)$.

[iii.] The dynamics of S_V and I_V are assumed to occur at slow time scale t compared to the within-human and within-mosquito submodels so that $S_V = S_V(t)$ and $I_V = I_V(t)$.

Based on these assumptions the malaria transmission dynamics using the mosquito organism scale as the scale of observation and the community scale as scale of analysis becomes

$$\text{Direct transmission of malaria among mosquitoes} \begin{cases} 1. \ \dfrac{dS_V(t)}{dt} = \Lambda_V - \beta_H \lambda_H(I_H) S_V(t) - \mu_V S_V(t), \\ 2. \ \dfrac{dI_V(t)}{dt} = \beta_H \lambda_H(I_H) S_V(t) - \Big[\mu_V + \delta_V\Big] I_V(t). \end{cases} \tag{2.1.1.2}$$

The first equation in sub-model system (2.1.1.2) describes the dynamics of susceptible mosquitoes. The first term on the right-hand side of this equation models the increase of susceptible mosquitoes through birth. The susceptible population of mosquitoes decreases through natural death at a constant rate μ_V, and through infection by humans at a variable rate $\lambda_H(I_H)$. The second equation in sub-model system (2.1.1.2) describes the dynamics of infected mosquitoes. The population of infected mosquitoes increases through infection of susceptible mosquitoes at a rate $\lambda_H(I_H)$. The same population decreases through natural death at a constant rate μ_V and also through infection induced death at a constant rate δ_V.

Putting together all the various derivations and assumptions the complete model for malaria transmission dynamics at the organism scale of observation (human organism and mosquito organism) and the community scale of analysis becomes

$$\text{Malaria model based on classical transmission mechanism theory} \begin{cases} 1.\ \dfrac{dS_H(t)}{dt} = \Lambda_H - \beta_V \lambda_V(I_V) S_H(t) - \mu_H S_H(t) + \gamma_H I_H, \\ 2.\ \dfrac{dI_H(t)}{dt} = \beta_V \lambda_V(I_V) S_H(t) - \Big[\mu_H + \delta_H + \gamma_H\Big] I_H(t), \\ 3.\ \dfrac{dS_V(t)}{dt} = \Lambda_V - \beta_H \lambda_H(I_H) S_V(t) - \mu_V S_V(t), \\ 4.\ \dfrac{dI_V(t)}{dt} = \beta_H \lambda_H(I_H) S_V(t) - \Big[\mu_V + \delta_V\Big] I_V(t). \end{cases} \tag{2.1.1.3}$$

We now re-cast this model of malaria into the proposed new modelling framework.

2.1.2 Malaria Model in the Proposed New Modelling Framework

If we assume that host (scale of observation) infectiousness is constant for a given host (scale of observation), for the entire duration of host infectiousness, but varies among hosts in a discrete way (e.g. by distinguishing several disease classes of hosts) so that average host infectiousness (determined by average pathogen load at the scale of observation) may be calculated, then we may get direct transmission models being of infectious disease system. In this case, details of pathogen-immune system interactions (which characterizes the replication and persistence of the pathogen within an infected host) at within-host scale are not modelled explicitly, instead, their interaction is rected in the choice of parameters used to characterize the between-host model which is represented mechanistically. Then we have a hybrid multiscale model of the mechanistic/phenomenological nature.

The first step in the integration of the two submodels is to make assumptions about the relationship between the dependent variables of the within-human and within-mosquito malaria parasite load dynamics which are N_h and N_v and the parameters of the human-to-mosquito and mosquito-to-human malaria parasite transmission at epidemiological scale which are $\lambda_V(I_V)$ and $\lambda_H(I_H)$. Details of the specific derivations and assumptions are as follows:

[a.] Further, we assume that the transmission parameter in the mosquito-to-human malaria transmission sub-model, λ_V is not just a function of the vector population alone $I_V(t)$, but of both the vector population $I_V(t)$ and sporozoite population N_v so that $\lambda_V = \lambda_V(N_v I_V(t))$. The net effect of this assumption is to up-scale individual mosquito infectiousness N_v to population level or community level infectiousness $N_v I_V(t)$. In addition, we interpret the quantity $N_v I_V(t)$ to be a new variable at epidemiological scale which we now denote by $P_V(t)$ so that $P_V(t) = N_v I_V(t)$, which is a product of the average individual infected mosquito's sporozoite load and the number of infected mosquitoes. Here, $P_V(t)$ is the total infectious reservoir of mosquitoes in the community which we refer to in this study as community sporozoite load. In terms of community sporozoite load,

the transmission parameter for mosquito-to-human malaria transmission sub-model becomes $\lambda_V = \lambda_V(P_V(t))$. We further assume a Holling type II functional form of the function $\lambda_V(P_V)$ so that the force of infection, denoted here by $\lambda_V(t)$, associated with infectivity of the community to humans becomes

$$\lambda_V(t) = \lambda_V[P_V(t)] = \frac{\beta_V P_V(t)}{P_0 + P_V(t)}, \tag{2.1.2.1}$$

where β_V is the exposure rate to a community with a population P_V of sporozoites per unit time, P_0 is the community sporozoite load that yields 50 percent chance of getting a human host infected with malaria after a bite by a mosquito in a particular community and

$$\lambda_V[P_V(t)] = \frac{\beta_V P_V(t)}{P_0 + P_V(t)}, \tag{2.1.2.2}$$

is probability that a random bite by a mosquito vector in a particular community with a community sporozoite load $P_V(t)$ will infect the individual with malaria in that community. However, $P_V(t)$, is a new variable at epidemiological scale which we have just introduced. In order to derive the differential equation governing $P_V(t)$, then the rate of change of community sporozoite load $P_V(t)$, in the entire community made of $I_V(t)$ unevenly distributed habitats/environments in the community becomes

$$\frac{dP_V(t)}{dt} = N_v \alpha_v I_V(t) - \alpha_V P_V(t), \tag{2.1.2.3}$$

where α_v is the shedding/excreting rate of the within-mosquito scale pathogen load to the community sporozoites load. α_V is the rate of sporozoite elimination in a particular geographical area/country/community so that the process of sporozoite elimination of community sporozoite load in a particular geographical area/country/community takes an average of $1/\alpha_V$ days. Since $P_V(t)$ is the total infectious reservoir of mosquitoes in a particular community defined here as community sporozoite load, then $1/\alpha_V$ days is the average time to eliminate the total infectious reservoir of mosquitoes and render all mosquitoes in a particular community non-infectious. Taking into account these derivations and assumptions the mosquito-to-human malaria transmission sub-model which is now coupled to the within-mosquito parasite population dynamics becomes

$$\begin{cases} 1.\ \dfrac{dS_H(t)}{dt} = \Lambda_H - \dfrac{\beta_V P_V(t)}{P_0 + P_V(t)} S_H(t) - \mu_H S_H(t) + \gamma_H I_H(t), \\ 2.\ \dfrac{dI_H(t)}{dt} = \dfrac{\beta_V P_V(t)}{P_0 + P_V(t)} S_H(t) - \Big[\mu_H + \gamma_H + \delta_H\Big] I_H(t), \\ 3.\ \dfrac{dP_V(t)}{dt} = N_v \alpha_v I_V(t) - \alpha_V P_V(t). \end{cases} \tag{2.1.2.4}$$

Community sporozoite load (CSL) $P_V(t)$, which is also a measure of the total infectious reservoir of mosquitoes in the community, is defined in this study as an aggregate population-level biomarker

of a community's sporozoite burden over a specific time period and is being proposed in this study as a useful metric for assessing the overall impact of malaria health interventions targeted at the mosquito vector or the uptake of malaria interventions targeted at the mosquito vector and quantifying their impact on transmission of malaria from mosquitoes to humans. In line with a similar metric for HIV/AIDS [48, 49], we therefore propose that this new public health measure of malaria transmission should be operationalized in the assessment of the path from control to elimination for malaria transmission in a particular community as (a) an indicator of a community's level of infectiousness and transmission probability of malaria to humans, (b) a measure of the effectiveness of malaria interventions targeted at the mosquito vector, and (c) a proximal maker of malaria incidence among mosquitoes and their potential to propagate malaria to humans.

[b.] Finally, we assume that the transmission parameter in the human-to-mosquito malaria transmission sub-model, λ_H is not just a function of the human population alone $I_H(t)$, but of both the human population $I_H(t)$ and gametocyte population N_h so that $\lambda_H = \lambda_H(N_h I_H(t))$. The net effect of this assumption is also to up-scale individual human infectiousness N_h to population level or community level infectiousness $N_h I_H(t)$. In addition, the quantity $N_h I_H(t)$ is also a new variable at epidemiological scale which we now denote by $G_H(t)$ so that $G_H(t) = N_h I_H(t)$, which is a product of the average individual infected human's gametocyte load and the number of infected humans. Here $G_H(t)$ is the total infectious reservoir of humans in the community which we refer to in this study as community gametocyte load. In terms of community gametocyte load, the transmission parameter for human-to-mosquito malaria transmission sub-model becomes $\lambda_H = \lambda_H(G_H(t))$. We further also assume a Holling type II functional form of the function $\lambda_H(G_H)$ so that the force of infection, denoted here by $\lambda_H(t)$, associated with infectivity of the community to mosquito becomes

$$\lambda_H(t) = \lambda_H(G_H(t)) = \frac{\beta_H G_H(t)}{G_0 + G_H(t)}, \tag{2.1.2.5}$$

where β_H is the exposure rate to a community with a population G_H of gametocytes per unit time, G_0 is the community gametocyte load that yields 50 percent chance of getting a mosquito vector infected with malaria after a bite of a human host by a mosquito in a particular community and

$$\lambda_H[G_H(t)] = \frac{\beta_H G_H(t)}{G_0 + G_H(t)}, \tag{2.1.2.6}$$

is the probability that a random bite of a human host by a mosquito vector in a particular community with a community gametocyte load $G_H(t)$ will infect the mosquito with malaria in that community. However, because $G_H(t)$, is also a new variable at epidemiological scale which we have just introduced. In order to derive the differential equation governing $G_H(t)$, since at any time t we have a total of $I_H(t)$ of these contaminated habitats/environments contaminated with an average of N_h gametocytes, then the rate of change of community gametocyte load, $G_H(t)$ in the entire community made of $I_H(t)$ homogeneous and unevenly distributed habitats/environments in the community

becomes

$$\frac{dG_H(t)}{dt} = N_h\alpha_h I_H(t) - \alpha_H G_H(t), \tag{2.1.2.7}$$

where α_h is the shedding/excreting rate of the within-human host scale pathogen load to the community gametocytes load. α_H is the rate of elimination of this total infectious reservoir of humans in the community so that the process of gametocyte elimination in a particular geographical area/-country/community takes an average of $\frac{1}{\alpha_H}$ days. Since $G_H(t)$ is the total infectious reservoir of humans in a particular community defined here as community gametocyte load, then $\frac{1}{\alpha_H}$ days is the average time to eliminate the total infectious reservoir of humans and render all humans in a particular community non-infectious to mosquitoes. Taking into account these derivations and assumptions the human-to-mosquito malaria transmission sub-model which is now coupled to the within-human parasite population dynamics becomes

$$\begin{cases} 1.\ \dfrac{dS_V(t)}{dt} = \Lambda_V - \dfrac{\beta_H G_H(t)}{G_0 + G_H(t)} S_V(t) - \mu_V S_V(t), \\ 2.\ \dfrac{dI_V(t)}{dt} = \dfrac{\beta_H G_H(t)}{G_0 + G_H(t)} S_V(t) - \Big[\mu_V + \delta_V\Big] I_V(t), \\ 3.\ \dfrac{dG_H(t)}{dt} = N_h\alpha_h I_H(t) - \alpha_H G_H(t). \end{cases} \tag{2.1.2.8}$$

The total infectious of the scale of analysis $G_H(t)$ when the human organism is the scale of observation, which is also a measure of the total infectious reservoir of humans in the community [24] (because the community scale is the scale of analysis), is defined in this study as an aggregate population-level biomarker of a community's gametocyte burden over a specific time period and is being proposed in this study as a useful public health measure of malaria transmission for assessing the overall impact of malaria health interventions targeted at the human host or the uptake of malaria interventions targeted at the human host and quantifying their impact on transmission of malaria from humans to mosquitoes. We therefore propose that this new measure should be operationalized in the assessment of the path from control to elimination for malaria transmission in a particular community as [a.] an indicator of a community's level of infectiousness and transmission probability of malaria to mosquitoes, [b.] a measure of the effectiveness of malaria interventions targeted at the human host, and [c.] a proximal maker of malaria incidence among humans and their potential to propagate malaria to mosquito vectors.

Based on all the derivations, mentioned assumptions, the diagram presented in Fig. (2.1) and description of variables in Table (2.1), the complete model for malaria transmission dynamics at the organism scale of observation (human organism and mosquito organism) and the community scale of analysis becomes

$$\text{Malaria model in the new framework} \begin{cases} 1.\ \dfrac{dS_H(t)}{dt} = \Lambda_H - \dfrac{\beta_V P_V(t)}{P_0 + P_V(t)} S_H(t) - \mu_H S_H(t) + \gamma_H I_H(t), \\ 2.\ \dfrac{dI_H(t)}{dt} = \dfrac{\beta_V P_V(t)}{P_0 + P_V(t)} S_H(t) - (\mu_H + \delta_H + \gamma_H) I_H(t), \\ 3.\ \dfrac{dP_V(t)}{dt} = N_v \alpha_v I_V(t) - \alpha_V P_V(t), \\ 4.\ \dfrac{dS_V(t)}{dt} = \Lambda_V - \dfrac{\beta_H G_H(t)}{G_0 + G_H(t)} S_V(t) - \mu_V S_V(t), \\ 5.\ \dfrac{dI_V(t)}{dt} = \dfrac{\beta_H G_H(t)}{G_0 + G_H(t)} S_V(t) - (\mu_V + \delta_V) I_V(t), \\ 6.\ \dfrac{dG_H(t)}{dt} = N_h \alpha_h I_H(t) - \alpha_H G_H(t), \end{cases} \tag{2.1.2.9}$$

No	Variable	Description
1	$S_H(t)$	Population of susceptible humans at time t
2	$I_H(t)$	Population of infected humans at time t
3	$G_H(t)$	Total infectious reservoir of humans (gametocyte load) of the scale of analysis at time t
4	$P_V(t)$	Total infectious reservoir of mosquito vectors (sporozoite load) of the scale of analysis at time t
5	$S_V(t)$	Population of susceptible mosquito vectors at time t
6	$I_V(t)$	Population of infected mosquito vectors at time t

Table 2.1: Table of variables and their description for the malaria model 2.1.2.9. For this malaria model, the scale of analysis is the community scale.

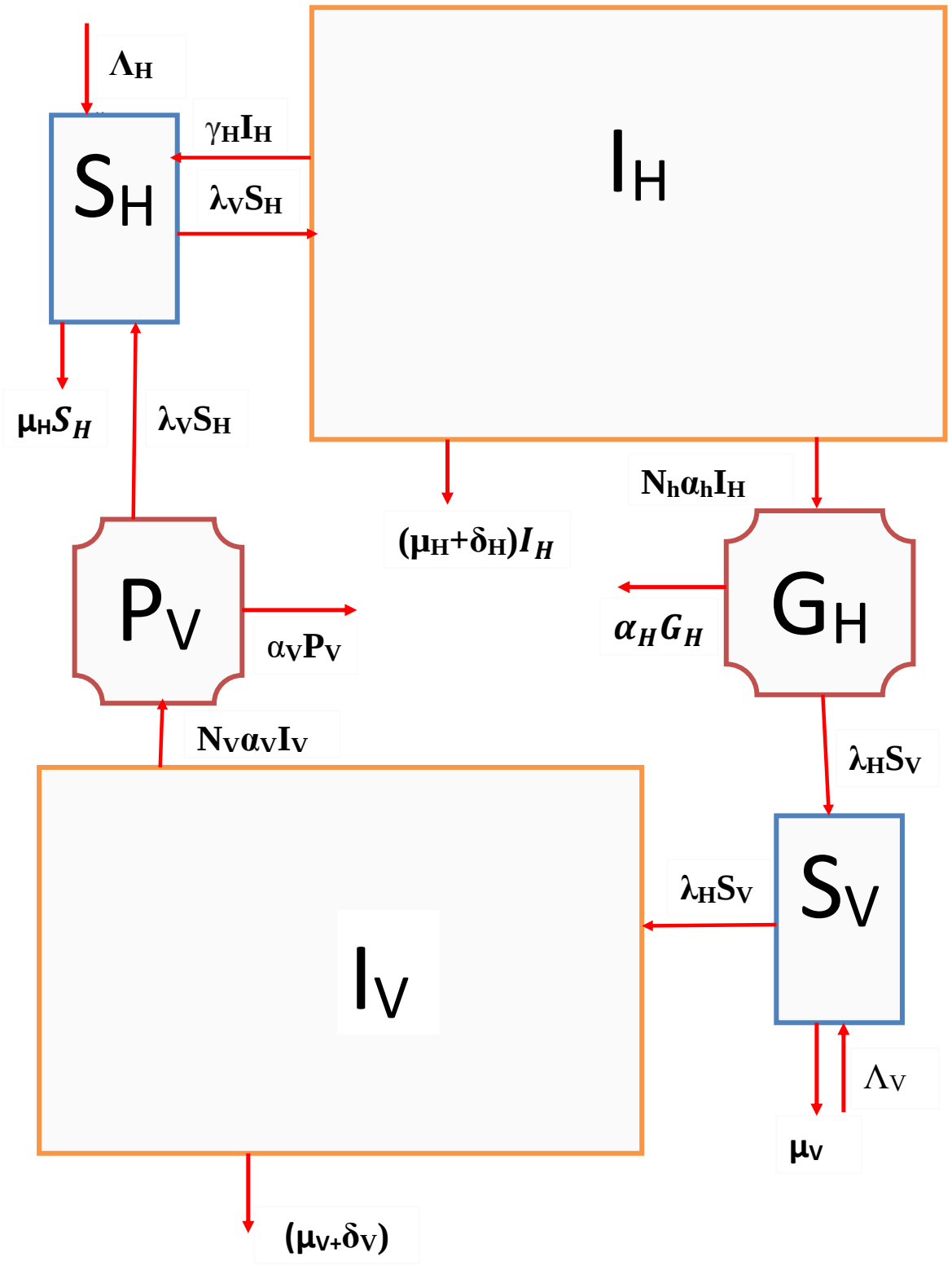

Figure 2.1: A conceptual diagram of the new model of malaria transmission dynamics based on the transmission mechanism theory using the organism scale (human organism and mosquito organism) as the scale of observation and the community scale as the scale of analsysis.

2.2 Analysis of the Model

We provide some qualitative analysis of the malaria model in this section. The aim is not to introduce new mathematical methods, but to show that the same simple methods for analyzing current models of disease dynamics are applicable to the proposed new modelling framework.

2.2.1 Positivity of solutions of the malaria model

Since the model given by (2.1.2.9) describes human, mosquito, and malaria parasite populations, all parameters in the model are non- negative and it can also be shown that the solutions of the model (2.1.2.9) are non-negative, given non-negative initial values ($S_H(0)$, $I_H(0)$, $G_H(0)$, $S_V(0)$, $I_V(0)$, $P_V(0)$), the solution/trajectories ($S_H(t)$, $I_H(t)$, $G_H(t)$, $S_V(t)$, $I_V(t)$, $P_V(t)$) of the model (2.1.2.9) will remain positive for all $t \geq 0$, so should be in consistence with the basic aspect of the biological reality. This is summarized in the following theorem.

Theorem 2.1. *Given that the initial conditions of the system of equations (2.1.2.9) remain non-negative (i.e.* $S_H(0), I_H(0) \geq 0, G_H(0) \geq 0, S_V(0) \geq 0, I_V(0) \geq 0, P_V(0) \geq 0$*), the resulting solutions* ($S_H(t)$, $I_H(t)$, $G_H(t)$, $S_V(t)$, $I_V(t)$, $P_V(t)$) *are all positive for all* $t \geq 0$.

Proof. From the system of equations (2.1.2.9), a differential inequality which demonstrates the dynamic of susceptible human population in time is given by

$$\frac{dS_H(t)}{dt} \geq -(\lambda_V(t) + \mu_H)S_H(t). \tag{2.2.1.1}$$

Hence, the expression of the differential inequality (2.2.1.1) can be solved by the separation of variables as follows

$$\frac{dS_H(t)}{S_H(t)} \geq -(\lambda_V(t) + \mu_H)dt. \tag{2.2.1.2}$$

We letting

$$\hat{t} = \sup\{t > 0 : S_H > 0, I_H > 0, G_H > 0, S_V > 0, I_V > 0, P_V > 0\} \in [0, t],$$

and integrating equation (2.2.1.2), we thus have

$$\ln(S_H(t)) \geq -(\mu_H t + \int_0^t \lambda_V(\hat{t})d\hat{t}) + \ln(S_H(0)). \tag{2.2.1.3}$$

Therefore, the solution of the differential inequality for the susceptible human population is given by

$$S_H(t) = S_H(0).\exp\left\{-(\mu_H t + \int_0^t \lambda_V(\hat{t})d\hat{t})\right\} > 0. \tag{2.2.1.4}$$

This implies that

$$\lim_{t\longrightarrow\infty} \inf(S_H(t)) \geq 0. \tag{2.2.1.5}$$

Based on the same principle, it can be shown that

$$\lim_{t\longrightarrow\infty} \inf(I_H(t)) \geq 0. \tag{2.2.1.6}$$

Using the last equation of the system of equations (2.1.2.9) that shows the evolution of the community gametocyte load, we can have the following differential inequality:

$$\frac{dG_H(t)}{dt} \geq -\alpha_H G_H(t). \tag{2.2.1.7}$$

Thus, by the separation of variables we obtain

$$G_H(t) \geq G_H(0).\exp\{-\alpha_H t\} > 0. \tag{2.2.1.8}$$

This implies that

$$\lim_{t\longrightarrow\infty} \inf(G_H(t)) \geq 0. \tag{2.2.1.9}$$

Using the same principle, it can be shown that

$$\begin{aligned} \lim_{t\longrightarrow\infty} \inf(S_V(t)) &\geq 0, \\ \lim_{t\longrightarrow\infty} \inf(I_V(t)) &\geq 0, \\ \lim_{t\longrightarrow\infty} \inf(P_V(t)) &\geq 0. \end{aligned} \tag{2.2.1.10}$$

The solution of the model, when starting with non-negative initial conditions in the system of equations (2.1.2.9), will remain non-negative for $t \geq 0$, and this completes the proof. □

2.2.2 Boundedness of solutions of the malaria model

In order to analyze the model (2.1.2.9), we split it into four parts, namely the human population, mosquito population, community gametocyte load and community sporozoite load. Consider the biologically feasible region consisting of

$$\Omega = \Omega_H \times \Omega_V \times \Omega_G \times \Omega_P \subset \mathbb{R}^2_+ \times \mathbb{R}^2_+ \times \mathbb{R}_+ \times \mathbb{R}_+ \tag{2.2.2.1}$$

where

$$\begin{cases} \Omega_H &= \left\{(S_H, I_H) \in \mathbb{R}^2_+ : 0 \leq N_H \leq \dfrac{\Lambda_H}{\mu_H}\right\}, \\ \Omega_V &= \left\{(S_V, I_V) \in \mathbb{R}^2_+ : 0 \leq N_V \leq \dfrac{\Lambda_V}{\mu_V}\right\}, \\ \Omega_G &= \left\{G_H \in \mathbb{R}_+ : 0 \leq G_H \leq \dfrac{N_h \alpha_h \Lambda_H}{\alpha_H \mu_H}\right\}, \\ \Omega_P &= \left\{P_V \in \mathbb{R}_+ : 0 \leq P_V \leq \dfrac{N_v \alpha_v \Lambda_V}{\alpha_V \mu_V}\right\}. \end{cases} \tag{2.2.2.2}$$

We follow the following steps to establish the positive invariance of Ω. Adding equations (1) and (2) and also adding equations (4) and (5) of model system (2.1.2.9) gives,

$$\begin{cases} 1.\ \dfrac{dN_H}{dt} &= \Lambda_H - \mu_H N_H - \delta_H I_H, \\ 2.\ \dfrac{dN_V}{dt} &= \Lambda_V - \mu_V N_V - \delta_V I_V, \\ 3.\ \dfrac{dP_V}{dt} &= N_v \alpha_v I_V - \alpha_V P_V, \\ 4.\ \dfrac{dG_H}{dt} &= N_h \alpha_h I_H - \alpha_H G_H. \end{cases} \Rightarrow \begin{cases} 1.\ \dfrac{dN_H}{dt} \leq \Lambda_H - \mu_H N_H, \\ 2.\ \dfrac{dN_V}{dt} \leq \Lambda_V - \mu_V N_V, \\ 3.\ \dfrac{dP_V}{dt} \leq N_v \alpha_v N_V - \alpha_V P_V, \\ 4.\ \dfrac{dG_H}{dt} \leq N_h \alpha_h N_H - \alpha_H G_H. \end{cases} \tag{2.2.2.3}$$

From which we obtain

$$\begin{cases} 1.\ N_H(t) \leq N_H(0) e^{-\mu_H t} + \dfrac{\Lambda_H}{\mu_H}\left[1 - e^{-\mu_H t}\right], \\ 2.\ N_V(t) \leq N_V(0) e^{-\mu_V t} + \dfrac{\Lambda_V}{\mu_V}\left[1 - e^{-\mu_V t}\right], \\ 3.\ P_V(t) \leq P_V(0) e^{-\alpha_V t} + \dfrac{N_v \alpha_v \Lambda_V}{\mu_V \alpha_V}\left[1 - e^{-\alpha_V t}\right], \\ 4.\ G_H(t) \leq G_H(0) e^{-\alpha_H t} + \dfrac{N_h \alpha_h \Lambda_H}{\mu_H \alpha_H}\left[1 - e^{-\alpha_H t}\right]. \end{cases} \tag{2.2.2.4}$$

where $N_H(0)$, $N_V(0)$, $P_V(0)$ and $G_H(0)$ represent the values of total human population, total mosquito

population, community sporozoite load (total infectious reservoir of mosquitoes) and community gametocyte load (total infectious reservoir of humans) evaluated at the initial values of the respective variables. Taking the limit as time gets large, we get the following expressions.

$$\begin{cases} 1. \ \lim\limits_{t\to\infty} \sup(N_H(t)) \leq \dfrac{\Lambda_H}{\mu_H}, \\ 2. \ \lim\limits_{t\to\infty} \sup(N_V(t)) \leq \dfrac{\Lambda_V}{\mu_V}, \\ 3. \ \lim\limits_{t\to\infty} \sup(P_V(t)) \leq \dfrac{N_v\alpha_v\Lambda_V}{\alpha_V\mu_V}, \\ 4. \ \lim\limits_{t\to\infty} \sup(G_H(t)) \leq \dfrac{N_h\alpha_h\Lambda_H}{\alpha_H\mu_H}. \end{cases} \tag{2.2.2.5}$$

Thus, the region Ω is positively invariant. Therefore, it is sufficient to consider the dynamics of the flow generated by (2.1.2.9) in Ω . In this region, the model is epidemiologically and mathematically well-posed. Thus, every solution of the mode (2.1.2.9) with initial conditions in Ω remains in Ω for all $t > 0$. Therefore, the Ω-limit sets of the model (2.1.2.9) are contained in Ω. We summarize this result in Theorem 2.2 below.

Theorem 2.2. *The region* $\Omega = \Omega_H \times \Omega_V \times \Omega_G \times \Omega_P \subset \mathbb{R}^2_+ \times \mathbb{R}^2_+ \times \mathbb{R}_+ \times \mathbb{R}_+$ *is positively invariant for the model system (2.1.2.9) with non-negative initial conditions in* $\mathbb{R}^6_+$.

2.2.3 Determination of the Basic Reproductive Number

An important question in malaria elimination is: how far has a particular scale of analysis gone in eliminating malaria and what more remains to be done? If a strategy for control interventions is that a particular scale of analysis has achieved $R_0 < 1$, then it is possible that maintaining current coverage levels of interventions would continue to reduce malaria transmission at a particular scale of analysis. However, if $R_0 > 1$, this gives way to an increase of malaria transmission at a particular scale of analysis. To obtain the reproductive number of the model system (2.1.2.9) we first obtain the disease-free equilibrium point by setting the left-hand side of this model equal to zero and also assume that $I_H = I_V = G_H = P_V = 0$ for the community scale as the scale of analysis. Thus we get

$$E^0 = (S^0_H, I^0_H, P^0_V, S^0_V, I^0_V, G^0_H) = \Big(\frac{\Lambda_H}{\mu_H}, 0, 0, \frac{\Lambda_V}{\mu_V}, 0, 0\Big), \tag{2.2.3.1}$$

where E^0 denotes the disease-free equilibrium of the model system (2.1.2.9). The local asymptotic stability of E^0 can be established using the basic reproductive number. In this study, we calculate the basic reproduction number of the model system (2.1.2.9) by using the next generation matrix approach [50].

In this case, the second and the third equations of the model system (2.1.2.9) form a subsystem that describes the generation and transition of infectious humans and the community pathogen load that are used to calculate $\mathcal{R}_0$. The Jacobian matrix associated with the linearized subsystem evaluated at the disease free equilibrium point, E^0, of the model system (2.1.2.9) is given by

$$J(E_0) = \begin{pmatrix} -(\mu_H + \delta_H + \gamma_H) & \frac{\beta_V \Lambda_H}{P_0 \mu_H} & 0 & 0 \\ 0 & -\alpha_V & N_v \alpha_v & 0 \\ 0 & 0 & -(\alpha_V + \delta_V) & \frac{\beta_H \Lambda_V}{G_0 \mu_V} \\ N_h \alpha_h & 0 & 0 & -\alpha_H \end{pmatrix} \tag{2.2.3.2}$$

Then, $J(E^0)$ is decomposed into two matrices F and V such that $J(E^0) = F - V$, where F is the transmission and non-negative matrix describing the generation of secondary infections, and V is the transition and non-singular matrix, describing the changes in individual states such as removal by death, recovery or excretion of gametocytes into the blood plasma by infected humans in the community. Following [51], we can give two different biological interpretations of the disease compartments and hence different next generation matrices from (2.1.2.2), to get two different $\mathcal{R}_0$ expressions for the compartmental single scale model (2.1.2.9) as follows.

[a.] *Assume that the community pathogen load is an extended state of host infectiousness*: This assumption holds since we upscaled individual host infectiousness $G_h(s)$ to population level infectiousness $G_H(t)$ and also the upscaling of within-mosquito host infectiousness $P_v(s)$ to population level infectiousness $P_V(t)$. In this case, the shedding of gametocytes (i.e. $N_h \alpha_h$) into the blood plasma and the shedding of sporozoites (i.e., $N_v \alpha_v$) into the mosquito salivary glands are placed in the V matrix rather than in the F matrix, so that matrices F and V become

$$F_I = \begin{pmatrix} 0 & \frac{\beta_V \Lambda_H}{P_0 \mu_H} & 0 & 0 \\ 0 & 0 & 0 & 0 \\ 0 & 0 & 0 & \frac{\beta_H \Lambda_V}{G_0 \mu_V} \\ 0 & 0 & 0 & 0 \end{pmatrix}, \quad V_I = \begin{pmatrix} (\mu_H + \delta_H + \gamma_H) & 0 & 0 & 0 \\ 0 & \alpha_V & N_v \alpha_v & 0 \\ 0 & 0 & (\alpha_V + \delta_V) & 0 \\ N_h \alpha_h & 0 & 0 & \alpha_H \end{pmatrix} \tag{2.2.3.3}$$

and

$$V_I^{-1} = \begin{pmatrix} \frac{1}{(\mu_H+\delta_H+\gamma_H)} & 0 & 0 & 0 \\ 0 & \frac{1}{\alpha_V} & -\frac{N_v\alpha_v}{\alpha_V(\mu_V+\delta_V)} & 0 \\ 0 & 0 & \frac{1}{(\alpha_V+\delta_V)} & 0 \\ -\frac{N_h\alpha_h}{\alpha_H(\mu_H+\delta_H+\gamma_H)} & 0 & 0 & \frac{1}{\alpha_H} \end{pmatrix} \tag{2.2.3.4}$$

Then the next generation matrix, $M_I = F_I V_I^{-1}$ is given by

$$M_I = \begin{pmatrix} 0 & \frac{\beta_V\Lambda_H}{\alpha_V P_0\mu_H} & \frac{-N_v\alpha_v}{(\alpha_V+\delta_V)}.\frac{\beta_V\Lambda_H}{\alpha_V P_0\mu_H} & 0 \\ 0 & 0 & 0 & 0 \\ \frac{-N_h\alpha_h}{(\mu_H+\delta_H+\gamma_H)}.\frac{\beta_H\Lambda_V}{\alpha_H G_0\mu_V} & 0 & 0 & \frac{\beta_H\Lambda_V}{\alpha_H G_0\mu_V} \\ 0 & 0 & 0 & 0 \end{pmatrix} \tag{2.2.3.5}$$

The basic reproductive number is the spectral radius (dominant eigenvalue) of the matrix $F_I V_I^{-1}$, that is, $\mathcal{R}_0^I = \rho(F_I V_I^{-1})$. Therefore, in this case, the basic reproduction number of the model system (2.1.2.9) becomes

$$R_0^I = \rho(F_I V_I^{-1}) = \sqrt[2]{\left[\frac{N_h\alpha_h}{(\mu_H+\delta_H+\gamma_H)}\frac{\Lambda_V\beta_H}{\mu_V\alpha_H G_0}\right]\left[\frac{N_v\alpha_v}{(\mu_V+\delta_V)}.\frac{\Lambda_H\beta_V}{\mu_H\alpha_V P_0}\right]} \tag{2.2.3.6}$$

[b.] *The community is assumed to act as a reservoir of the infective pathogen*: This assumption also holds since $N_h\alpha_h$ and $N_v\alpha_v$ are the rates that describes how much malaria pathogen load each infected individual (mosquito or human) contributes to the community pathogen load during their entire period of infectiousness. In this case, the shedding rate of malaria parasite (i.e. $N_h\alpha_h$ and $N_v\alpha_v$) are placed in the F matrix rather than in the V matrix, so that matrices F and V derived from

matrix (2.2.3.2) become

$$F_{II} = \begin{pmatrix} 0 & \frac{\beta_V \Lambda_H}{P_0} & 0 & 0 \\ 0 & 0 & N_v \alpha_v & 0 \\ 0 & 0 & 0 & \frac{\beta_H \Lambda_V}{G_0 \mu_V} \\ N_h \alpha_h & 0 & 0 & 0 \end{pmatrix},$$

$$V_{II} = \begin{pmatrix} (\mu_H + \delta_H + \gamma_H) & 0 & 0 & 0 \\ 0 & \alpha_V & 0 & 0 \\ 0 & 0 & (\alpha_V + \delta_V) & 0 \\ 0 & 0 & 0 & \alpha_H \end{pmatrix}, \tag{2.2.3.7}$$

and

$$V_{II}^{-1} = \begin{pmatrix} \frac{1}{(\mu_H + \delta_H + \gamma_H)} & 0 & 0 & 0 \\ 0 & \frac{1}{\alpha_V} & 0 & 0 \\ 0 & 0 & \frac{1}{(\alpha_V + \delta_V)} & 0 \\ 0 & 0 & 0 & \frac{1}{\alpha_H} \end{pmatrix} \tag{2.2.3.8}$$

Then the next generation matrix, $M_{II} = F_{II} V_{II}^{-1}$ is given by

$$M_{II} = \begin{pmatrix} 0 & \frac{\beta_V \Lambda_H}{\alpha_V P_0 \mu_H} & 0 & 0 \\ 0 & 0 & \frac{N_v \alpha_v}{(\mu_V + \delta_V)} & 0 \\ 0 & 0 & 0 & \frac{\beta_H \Lambda_V}{\alpha_H G_0 \mu_V} \\ \frac{N_h \alpha_h}{(\mu_H + \delta_H + \gamma_H)} & 0 & 0 & 0 \end{pmatrix} \tag{2.2.3.9}$$

The basic reproductive number is also the spectral radius (dominant eigenvalue) of the matrix $F_{II}V_{II}^{-1}$, that is, $\mathcal{R}_0^{II} = \rho(F_{II}V_{II}^{-1})$. In this case, the basic reproduction number of the model system (2.1.2.9) becomes

$$R_0^{II} = \rho(F_{II}V_{II}^{-1}) = \sqrt[4]{\left[\frac{N_h\alpha_h}{(\mu_H+\delta_H+\gamma_H)}\frac{\Lambda_V\beta_H}{\mu_V\alpha_H G_0}\right]\left[\frac{N_v\alpha_v}{(\mu_V+\delta_V)}.\frac{\Lambda_H\beta_V}{\mu_H\alpha_V P_0}\right]} \quad (2.2.3.10)$$

Therefore, the model system (2.1.2.9) is shown to have two reproductive numbers which are given by equation (2.2.3.6) and equation (2.2.3.10).

The two basic reproductive numbers $\mathcal{R}_0^I$ and $\mathcal{R}_0^{II}$ have each four main components which are: (i) the human-to-community partial reproductive number ($\mathcal{R}_{HC}$), and (ii) the community-to-mosquito partial reproductive number ($\mathcal{R}_{CV}$), (iii) the mosquito-to-community partial reproductive number ($\mathcal{R}_{VC}$), and (iv) the community-to-human partial reproductive number ($\mathcal{R}_{CH}$) so that

$$\begin{cases} 1.\ \mathcal{R}_0^I = \sqrt[2]{\left[\frac{N_h\alpha_h}{(\mu_H+\delta_H+\gamma_H)}\frac{\Lambda_V\beta_H}{\mu_V\alpha_H G_0}\right]\left[\frac{N_v\alpha_v}{(\mu_V+\delta_V)}.\frac{\Lambda_H\beta_V}{\mu_H\alpha_V P_0}\right]} = \sqrt[2]{\mathcal{R}_{HC}.\mathcal{R}_{CV}.\mathcal{R}_{VC}.\mathcal{R}_{CH}}, \\ 2.\ \mathcal{R}_0^{II} = \sqrt[4]{\left[\frac{N_h\alpha_h}{(\mu_H+\delta_H+\gamma_H)}\frac{\Lambda_V\beta_H}{\mu_V\alpha_H G_0}\right]\left[\frac{N_v\alpha_v}{(\mu_V+\delta_V)}.\frac{\Lambda_H\beta_V}{\mu_H\alpha_V P_0}\right]} = \sqrt[4]{\mathcal{R}_{HC}.\mathcal{R}_{CV}.\mathcal{R}_{VC}.\mathcal{R}_{CH}}. \end{cases} \quad (2.2.3.11)$$

Therefore, the basic reproductive number $\mathcal{R}_0^I$ or $\mathcal{R}_0^{II}$ in the human-to-human or mosquito-to-mosquito for human malaria transmission is made up of the following four partial reproductive numbers as follows.

[i.] *The human-to-community partial reproductive number ($\mathcal{R}_{HC}$)*: This partial reproductive number is given by

$$\mathcal{R}_{HC} = \frac{N_h\alpha_h}{(\mu_H+\delta_H+\gamma_H)}. \quad (2.2.3.12)$$

This is the average amount of infectious reservoir contributed to the community gametocyte load (CGL) by each infected human host during his or her entire period of of infectiousness. This quantity depends on the average number of gametocytes N_h, produced by each infected human, which is available for ingestion by a mosquito during her uptake of blood meals from an infected human during his or her entire period of infectiousness and is a composite parameter given by N_h In the expression for $\mathcal{R}_{HC}$, α_h is the rate at which gametocytes are shed/excreted into the blood plasma. Therefore, $N_h\alpha_h$ is the rate that describes how much each infected human host contributes to the community gametocyte load (the total infectious reservoir of humans in the community) during his/her entire period of infectiousness while $1/(\mu_H+\delta_H)$ is the average gametocyte carriage time by each infected human host.

[ii.] *The community-to-mosquito vector partial reproductive number ($\mathcal{R}_{CV}$)*: This partial reproductive number is given by

$$\mathcal{R}_{CV} = \frac{\Lambda_V \beta_H}{\mu_V \alpha_H G_0}. \tag{2.2.3.13}$$

It describes the average number of infected mosquitoes arising from each infectious dose of gametocytes ingested from the total infectious reservoir of humans in the community. This partial reproductive number depends on the effective supply rate of susceptible mosquitoes Λ_V, the average life span of each susceptible mosquito $1/\mu_V$, the rate of contact of the susceptible mosquitoes with the infectious reservoir of humans β_H, the average time it takes to eliminate the infectious reservoir of humans in the community $1/\alpha_H$ and the susceptibility coefficient, $1/G_0$ of mosquito vectors to infection by the CGL (the total human infectious reservoir in the community).

[iii.] *The mosquito-to-community partial reproductive number ($\mathcal{R}_{VC}$)*: This partial reproductive number is given by

$$\mathcal{R}_{VC} = \frac{N_v \alpha_v}{(\mu_V + \delta_V)}. \tag{2.2.3.14}$$

This is also the average amount of infectious reservoir contributed to the community sporozoite load (CSL) by each infected mosquito vector during her entire period of infectiousness. This quantity depends on the average number of sporozoites produced in each infected mosquito vector N_v, which is available for injection into a human host by a mosquito during uptake of blood meals from a human during her entire period of infectiousness and is a composite parameter which is also given by N_v. In the expression for $\mathcal{R}_{VC}$, α_v is the rate at which sporozoites are excreted/shed into the salivary glands of the mosquito. Therefore, $N_v \alpha_v$ is the rate that describes how much an infected mosquito contributes to the community sporozoite load (the total infectious reservoir of mosquitoes in the community) during her entire period of infectiousness while $1/(\mu_V + \delta_V)$ is the average sporozoite carriage time by each infected mosquito.

[iv.] *The community-to-human partial reproductive number ($\mathcal{R}_{CH}$)*: This reproductive number is given by

$$\mathcal{R}_{CH} = \frac{\Lambda_H \beta_V}{\mu_H \alpha_V P_0}. \tag{2.2.3.15}$$

It describes the average number of infected humans arising from each infectious dose of sporozoites injected from the total infectious reservoir of mosquitoes in the community. This partial reproductive number depends on the effective supply rate of susceptible mosquitoes Λ_H, the average life span of each susceptible humans $1/\mu_H$, the rate of contact of the susceptible humans with the infectious reservoir of mosquitoes β_V, the average time it takes to eliminate the infectious reservoir of mosquitoes in the community $1/\alpha_V$ and the susceptibility coefficient, $1/P_0$ of human hosts to infection by the CSL (the total mosquito infectious reservoir in the community).

Another informative way of interpreting $\mathcal{R}_0$ is to consider it as a product of two partial reproductive numbers which are the human-to-mosquito partial reproductive number $\mathcal{R}_{HV}$ and the mosquito-to-human partial reproductive number $\mathcal{R}_{VH}$ so that

$$\mathcal{R}_0 = \sqrt{\left[\frac{N_h\alpha_h}{(\mu_H+\delta_H+\gamma_H)}\frac{\Lambda_V\beta_H}{\mu_V\alpha_H G_0}\right]\left[\frac{N_v\alpha_v}{(\mu_V+\delta_V)}.\frac{\Lambda_H\beta_V}{\mu_H\alpha_V P_0}\right]} = \sqrt{R_{HV}.R_{VH}}. \tag{2.2.3.16}$$

In equation (2.2.3.16), the quantity $\mathcal{R}_{HV}$ is interpreted as follows. Consider a single newly infected human host entering a disease-free population of mosquitoes at equilibrium. This individual is still present and infectious and the expected number of mosquitoes infected by this human host is approximately

$$\mathcal{R}_{HV} = \frac{N_h\alpha_h}{(\mu_H+\delta_H+\gamma_H)}\frac{\Lambda_V\beta_H}{\mu_V\alpha_H G_0}. \tag{2.2.3.17}$$

Therefore, the human-to-mosquito transmission coefficient $\mathcal{R}_{HV}$ is composed of between-host disease parameters and within-human parameters. Similarly, in Eq. (2.2.3.16) the quantity $\mathcal{R}_{VH}$ is interpreted as follows. Consider a single newly infected mosquito vector entering a disease-free population of humans at equilibrium. This mosquito is still present and infectious and the expected number of humans infected by this mosquito is approximately

$$\mathcal{R}_{VH} = \frac{N_v\alpha_v}{(\mu_V+\delta_V)}.\frac{\Lambda_H\beta_V}{\mu_H\alpha_V P_0}. \tag{2.2.3.18}$$

From Eq. (2.2.3.18), we deduce that the mosquito-to-human transmission coefficient $\mathcal{R}_{VH}$ is also composed of between-host disease parameters and within-mosquito parameters.

2.2.4 Existence and uniqueness of the endemic equilibrium state

We let

$$E^* = (S_H^*, I_H^*, P_V^*, S_V^*, I_V^*, G_H^*), \tag{2.2.4.1}$$

denoting the endemic equilibrium points of the system of equations (2.1.2.9). We let the right-hand side of the system of equations (2.1.2.9) equal to zero to obtain

$$\begin{aligned}
\Lambda_H - \frac{\beta_V P_V^*}{P_0+P_V^*}S_H^* - \mu_H S_H^* + \gamma_H I_H^* &= 0,\\
\frac{\beta_V P_V^*}{P_0+P_V^*}S_H^* - (\mu_H+\gamma_H+\delta_H)I_H^* &= 0,\\
N_v\alpha_v I_V^* - \alpha_V P_V^* &= 0,\\
\Lambda_V - \frac{\beta_H G_H^*}{G_0+G_H} - (\mu_V+\delta_V)I_V^* &= 0,\\
N_h\alpha_h I_H^* - \alpha_H G_H^* &= 0.
\end{aligned} \tag{2.2.4.2}$$

From (2.2.4.2), the endemic equilibrium is given by

$$\begin{aligned}
S_H^*(P_V^*) &= \frac{\{\Lambda_H[a_2P_0+(a_1+a_2)P_V^*]+\gamma_H\beta_V\Lambda_HP_V^*\}(P_0+P_V^*)}{[a_2P_0+(a_1+a_2)P_V^*][\mu_HP_0+(\beta_V+\mu_H)P_V^*]},\\
I_H^*(P_V^*) &= \frac{\beta_V\Lambda_HP_V^*}{a_2P_0+(a_1+a_2)P_V^*},\\
G_H^*(P_V^*) &= \frac{N_h\alpha_h\beta_V\Lambda_HP_V^*}{\alpha_H[a_2P_0+(a_1+a_2)P_V^*]},\\
S_V^*(P_V^*) &= \frac{\Lambda_V\{G_0\alpha_H[a_2P_0+(a_1+a_2)P_V^*]+N_h\alpha_h\beta_V\Lambda_HP_V^*\}}{\mu_VG_0\alpha_H[a_2P_0+(a_1+a_2)P_V^*]+(\beta_H+\mu_V)N_h\alpha_h\beta_V\Lambda_HP_V^*},\\
I_V^*(P_V^*) &= \frac{N_h\alpha_h\beta_H\Lambda_V\beta_V\Lambda_HP_V^*}{(\mu_V+\delta_V)\{\mu_VG_0\alpha_H[a_2P_0+(a_1+a_2)P_V^*]+(\beta_H+\mu_V)N_h\alpha_h\beta_V\Lambda_HP_V^*\}},\\
P_V^* &= \frac{(\mu_V+\delta_V)\mu_HP_0(\mu_H+\delta_H+\gamma_H)\mu_V\alpha_HG_0}{\mu_VG_0\alpha_H(a_1+a_2)+(\beta_H+\mu_V)N_h\alpha_h\beta_V\Lambda_H}[R_0^2-1],
\end{aligned} \tag{2.2.4.3}$$

where

$$\begin{aligned}
a_1 &= \beta_V(\mu_H+\delta_H),\\
a_2 &= \mu_H(\mu_H+\gamma_H+\delta_H).
\end{aligned}$$

Therefore, we can conclude that there exists unique endemic equilibrium state for model (2.1.2.9) whenever $R_0 > 1$.

2.2.5 Numerical Study of the Malaria Model

In this subsection, we perform numerical simulations of the single-scale malaria model (2.1.2.9) using the parameter values given in Table (2.2). We illustrate the influence of parameters (α_v, α_H, α_V, β_H,β_V, δ_H, δ_V, G_0, γ_H, Λ_H, Λ_V, μ_V, N_h, N_v, P_0, α_h) on the model variables (I_H, G_H, I_V, P_V). The model developed in this work, was simulated using the initial value conditions given by $S_H(0) = 50000$, $I_H(0) = 7000$, $G_H(0) = 60000$, $S_V(0) = 150000$, $I_V(0) = 20000$, and $P_V(0) = 40000$.

Parameter	Description	Initial Value	Range	Units	Source
Λ_V	Recruitment rate of mosquitoes.	6000	5000–7000	Mosquitoes per day	[35]
β_V	Contact rate of susceptible humans with the infectious reservoir of mosquitoes.	0.52135	2.7×10^{-3}–0.64	day^{-1}	[35]
μ_V	Natural death rate of mosquitoes.	0.12	0.033-0.3	day^{-1}	[24]
δ_V	induced death rate of infected mosquitoes.	4.26×10^{-6}	$4.26\times10^{-6}-5.33\times10^{-6}$	day^{-1}	[24]
P_0	Half saturation constant associated with the infection of humans.	1×10^{8}	$1\times10^{6}-5\times10^{8}$	day^{-1}	[24]
N_v	Number of sporozoites available for excretion	3000	100-4000	Sporozoites per day	assumed
α_V	Rate of clearance of community sporozoite load.	0.3	0.09-0.99	day^{-1}	[24]
α_v	Shedding rate of sporozoites	0.25	0.016-1.0	day^{-1}	[24]
Λ_H	Recruitment rate of humans.	1000	100-1200	humans per day	[35]
β_H	Contact rate of susceptible mosquitoes with the infectious reservoir of humans.	0.356	0.072-0.64	day^{-1}	[35]
μ_H	Natural death rate of humans.	4.002×10^{-5}	$1\times10^{-5}--0.9$	day^{-1}	[24]
δ_H	induced death rate of infected humans.	0.0027	$1\times10^{-15}-0.0027$	day^{-1}	[24]
γ_H	Recovered rate from infection.	0.25	0.0014-0.7	day^{-1}	[24]
G_0	Half saturation constant associated with the infection of mosquitoes.	5×10^{8}	$1^{6}-5\times10^{9}$	day^{-1}	[24]
N_h	Number of gametocytes available for excretion	2000	10-2000	gametocytes per day	assumed
α_H	Rate of clearance of community gametocytes load.	0.913	$4.67\times10^{-5}-0.913$	day^{-1}	[24]
α_h	Shedding rate of gametocytes	0.4	0.01-0.9	day^{-1}	[24]

Table 2.2: Parameters values of model of malaria and their description.

Based on our numerical simulations, we determined the existence of malaria-endemic equilibrium, as figure (2.2) shows that each variable varies with time and reaches a constant value (i.e., at malaria-endemic equilibrium). Thus, Figure (2.2) displays the presence of malaria-endemic equilibrium for the model (2.1.2.9). Figure 2.3 and figure 2.4 are set of two graphs showing changes in four variables: I_H, I_V, G_H and P_V for different parameters: α_v, and α_h. Figure 2.3 shows the effect of rate at which sporozoites develop and become infectious to humans (α_v) on (i) population of infected humans I_H, (ii) community gametocytes load G_H, (iii) population of infected mosquitoes I_V and (iv) community sporozoites load P_V for different values of α_v: $\alpha_v = 0.25$, $\alpha_v = 0.45$, $\alpha_v = 0.85$. Figure 2.3 shows that as the rate at which sporozoites develop and become infectious to humans (α_v) increases, malaria disease transmission in the community also increases. Figure 2.4 shows the effect of rate at which gametocytes develop and become infectious to mosquitoes (α_h) on (i) population of infected humans I_H, (ii) community gametocytes load

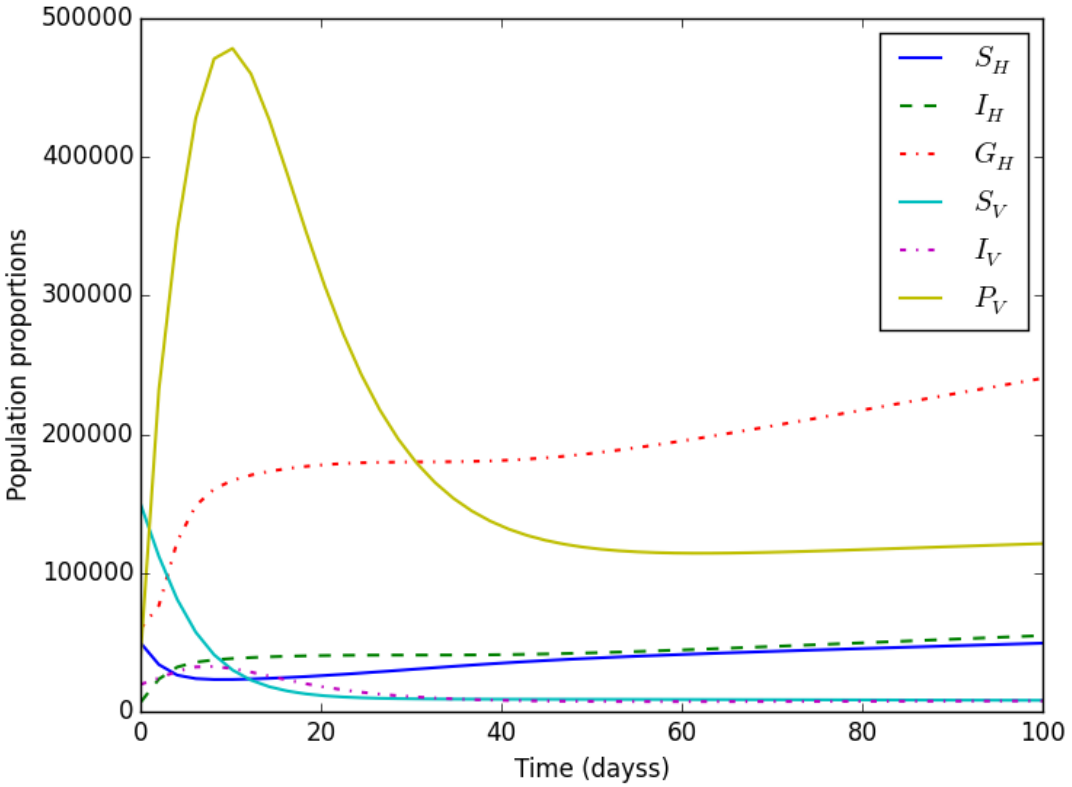

Figure 2.2: Variation of the Human and mosquito variables with time to verify the existence of malaria infection equilibrium.

G_H, (iii) population of infected mosquitoes I_V, and (iv) community sporozoites load P_V for different values of α_h: $\alpha_h = 0.4$, $\alpha_h = 0.6$, $\alpha_h = 0.8$. Similarly, Figure 2.4 shows that as the rate at which gametocytes develop and become infectious to mosquitoes (α_h) increases, malaria disease transmission in the community also increases. Overall Figure 2.3 and Figure 2.4 suggests that interventions that reduce the rate of development of gametocytes and sporozites to become infectious reduces malaria transmission for the specified scale of analysis, that is the community scale. Therefore, the use artemisinin-based combination therapy (ACT) which reduce the productions of gametocytes which will likely to reduce the malaria disease transmission.

Figure 2.5 and figure 2.6 are set of two graphs showing changes in four variables: I_H, I_V, G_H and P_V for different parameters: N_h, and N_v. Figure 2.5 shows the effect of the number of gametocytes available for excretion (N_h) on (i) population of infected humans I_H, (ii) community gametocytes load G_H, (iii) population of infected mosquitoes I_V, and (iv) community sporozoites load P_V for different values of the average number of gametocytes in the blood stream of an infected human (N_h): $N_h = 1800$, $N_h = 2000$, $N_h = 2200$. The numerical results in Figure 2.5 indicate that the variables (I_H, G_H, I_V, P_V) increase as the number of gametocytes available for excretion (N_h) increases, implying that as the number of gametocytes available for excretion (N_h) increases, malaria disease transmission in the community also increases.

Figure 2.6 shows the effect of number of sporozoites available for excretion (N_v) on (i) population of infected humans I_H, (ii) community gametocytes load G_H, (iii) population of infected mosquitoes I_V, and (iv) community sporozoites load P_V for different values of the average number of sporozoites in the salivary glands of each infected mosquito (N_v): $N_v = 2600$, $N_v = 2800$, $N_v = 3000$. The numerical results in Figure 2.6 also indicate that the variables (I_H, G_H, I_V, P_V) increase as the number of sporozoites available for excretion (N_v) increases, implying that as the number of sporozoites available for excretion (N_v) increases, malaria disease transmission in the community also increases.

Figure 2.7 and Figure 2.8 are set of two graphs showing changes in four variables: I_H, I_V, G_H and P_V for different parameters: β_H, and β_V. Figure 2.7 shows the effect of contact rate of susceptible humans with infectious mosquitoes (β_V) on (i) population of infected humans I_H, (ii) community gametocytes load G_H, (iii) population of infected mosquitoes I_V, and (iv) community sporozoites load P_V for different values of β_V: $\beta_V = 0.32135$, $\beta_V = 0.42135$, $\beta_V = 0.52135$. The results in Figure 2.7 shows that as the contact rate of susceptible humans with infectious reservoir of moquito vectors (β_V) increases, malaria transmission at community scale as the scale of analysis increases. Figure 2.8 shows effect of contact rate of susceptible mosquitoes with infectious humans (β_H) on (i) population of infected humans I_H, (ii) community gametocytes load G_H, (iii) population of infected mosquitoes I_V, and (iv) community sporozoites load P_V for different values of β_H: $\beta_H = 0.356$, $\beta_H = 0.456$, $\beta_H = 0.556$. Equally, the results in Figure 2.8 show that as the contact rate of susceptible mosquitoes with infectious reservoir of humans (β_H) increases, malaria transmission at community scale as the scale of analysis also increases. Overall, the results in Figure 2.7 and Fig. 2.8 suggest that the use of Long-lasting insecticidal nets (LLINs) have an beneficial impact of reducing malaria disease transmission in the community.

Figure 2.9 and Figure 2.10 are set of two graphs showing changes in four variables: I_H, I_V, G_H and P_V for different parameters: G_0, and P_0. Figure 2.9 effect of Half saturation constant associated with infection of mosquitoes (G_0) on (i) population of infected humans I_H, (ii) community gametocytes load G_H, (iii) population of infected mosquitoes I_V, and (iv) community sporozoites load P_V for different values of G_0: $G_0 = 3 \times 10^8$, $G_0 = 5 \times 10^8$, $G_0 = 7 \times 10^8$. We note from Figure (2.9) that as the half saturation constant associated with mosquito infection (G_0) increases, malaria disease transmission in the community decreases. Figure 2.10 shows effect of half saturation constant associated with infection of humans (P_0) on (i) population of infected humans I_H, (ii) community gametocytes load G_H, (iii) population of infected mosquitoes I_V, and (iv) community sporozoites load P_V for different values of P_0: $P_0 = 5 \times 10^7$, $P_0 = 1 \times 10^8$, $P_0 = 1.5 \times 10^7$. We also note from Figure (2.10) that as the half saturation constant associated human with infection (P_0) increases, malaria disease transmission in the community decreases.

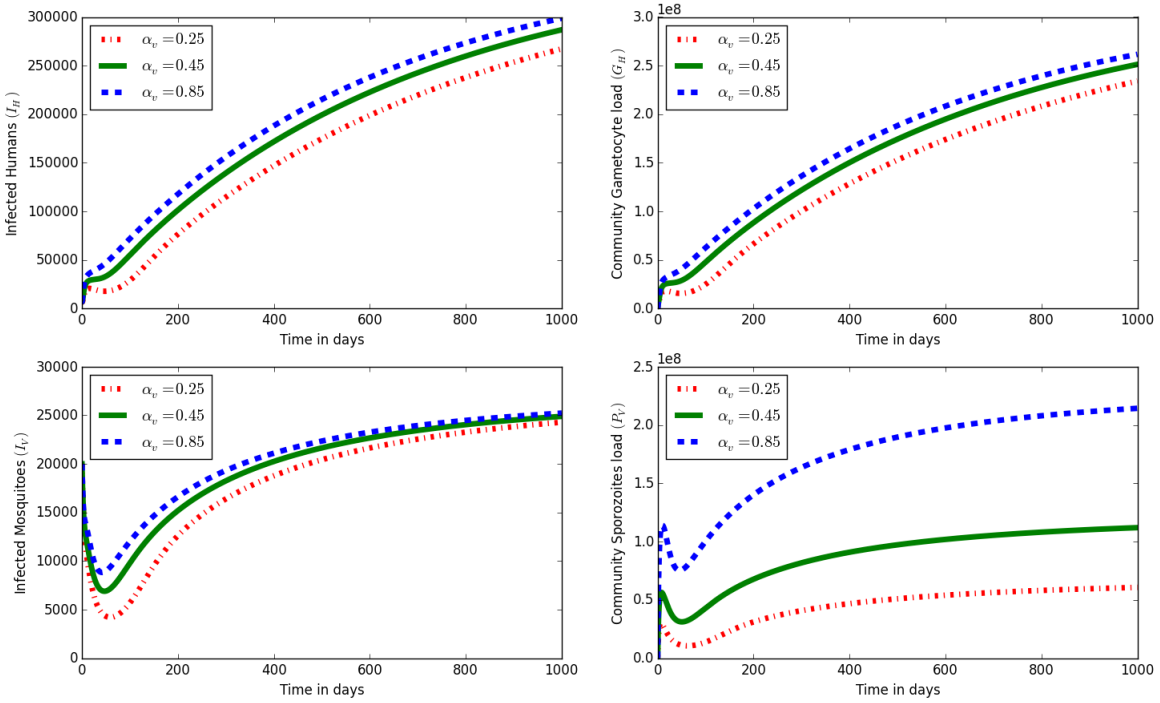

Figure 2.3: Graphs showing the effect of shedding rate of sporozoites (α_v) on (i) population of infected humans I_H (ii) community gametocytes load G_H (iii) population of infected mosquitoes I_V and (iv) community sporozoites load P_V for different values of α_v: $\alpha_v = 0.25$, $\alpha_v = 0.45$, $\alpha_v = 0.85$

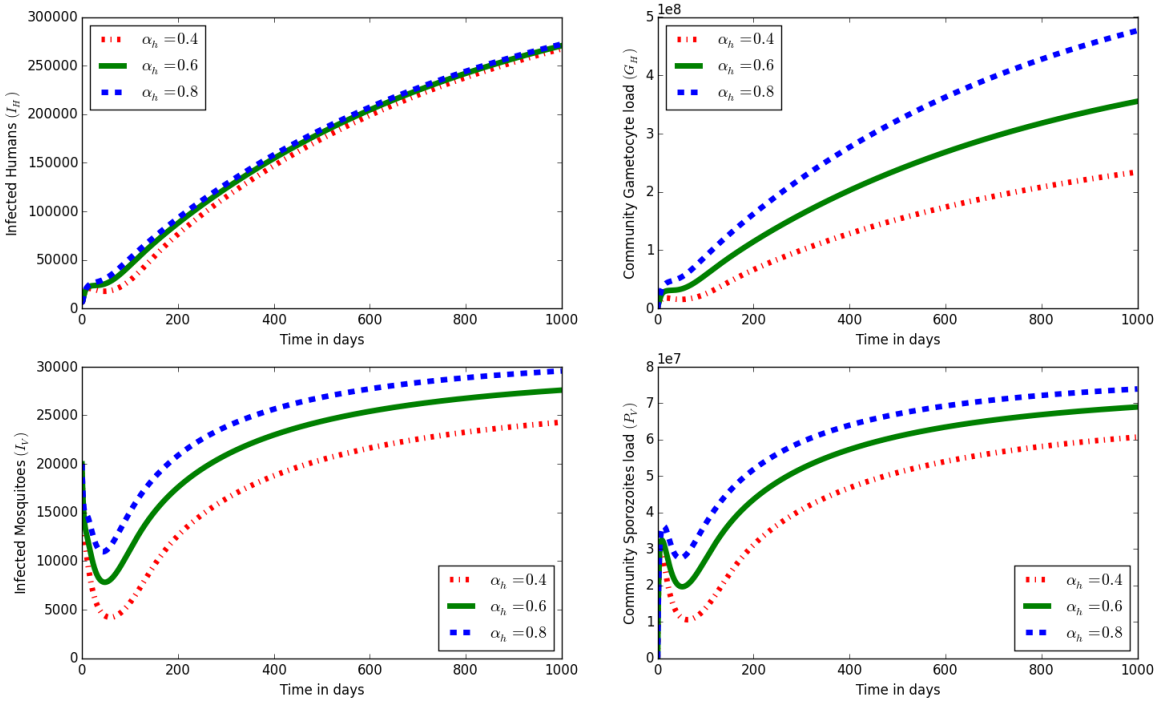

Figure 2.4: Graphs showing the effect of shedding rate of gametocytes (α_h) on (i) population of infected humans I_H (ii) community gametocytes load G_H (iii) population of infected mosquitoes I_V and (iv) community sporozoites load P_V for different values of α_h: $\alpha_h = 0.4$, $\alpha_h = 0.6$, $\alpha_h = 0.8$.

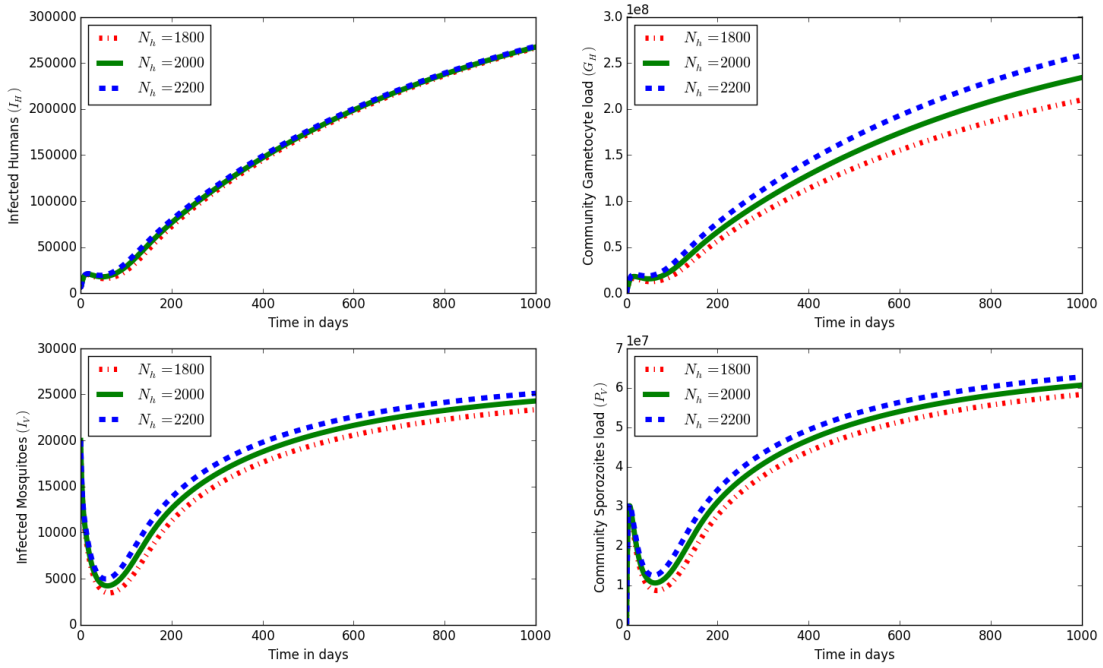

Figure 2.5: Graphs showing the effect of number of gametocytes available for excretion (N_h) on (i) population of infected humans I_H (ii) community gametocytes load G_H (iii) population of infected mosquitoes I_V and (iv) community sporozoites load P_V for different values of N_h: $N_h = 1800$, $N_h = 2000$, $N_h = 2200$.

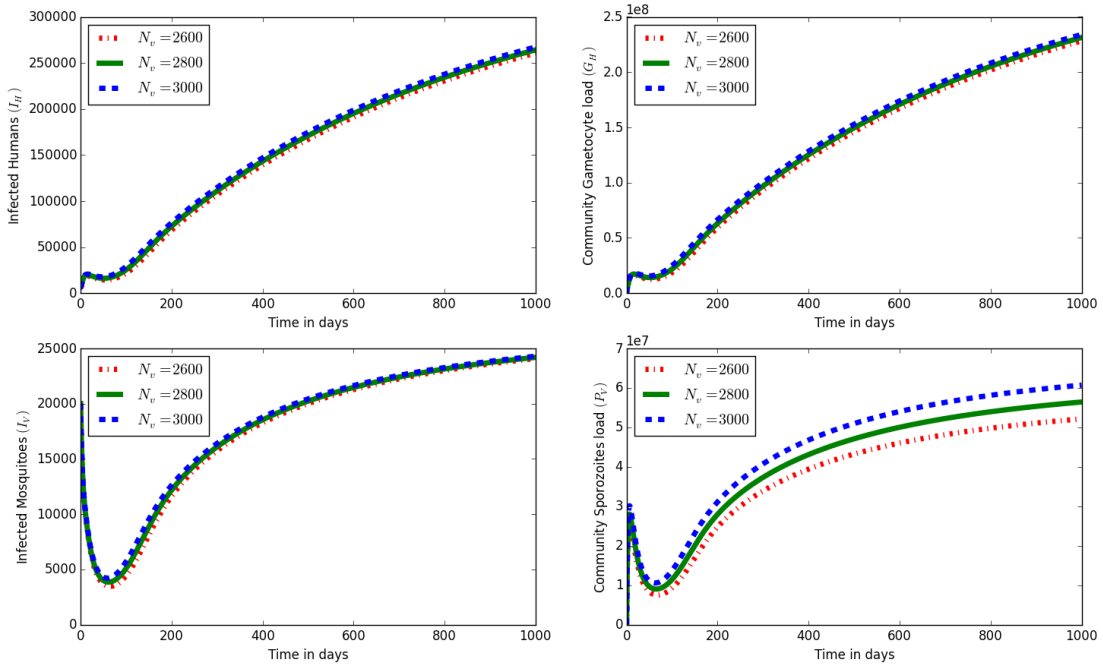

Figure 2.6: Graphs showing the effect of number of sporozoites available for excretion (N_v) on (i) population of infected humans I_H (ii) community gametocytes load G_H (iii) population of infected mosquitoes I_V and (iv) community sporozoites load P_V for different values of N_v: $N_v = 2600$, $N_v = 2800$, $N_v = 3000$.

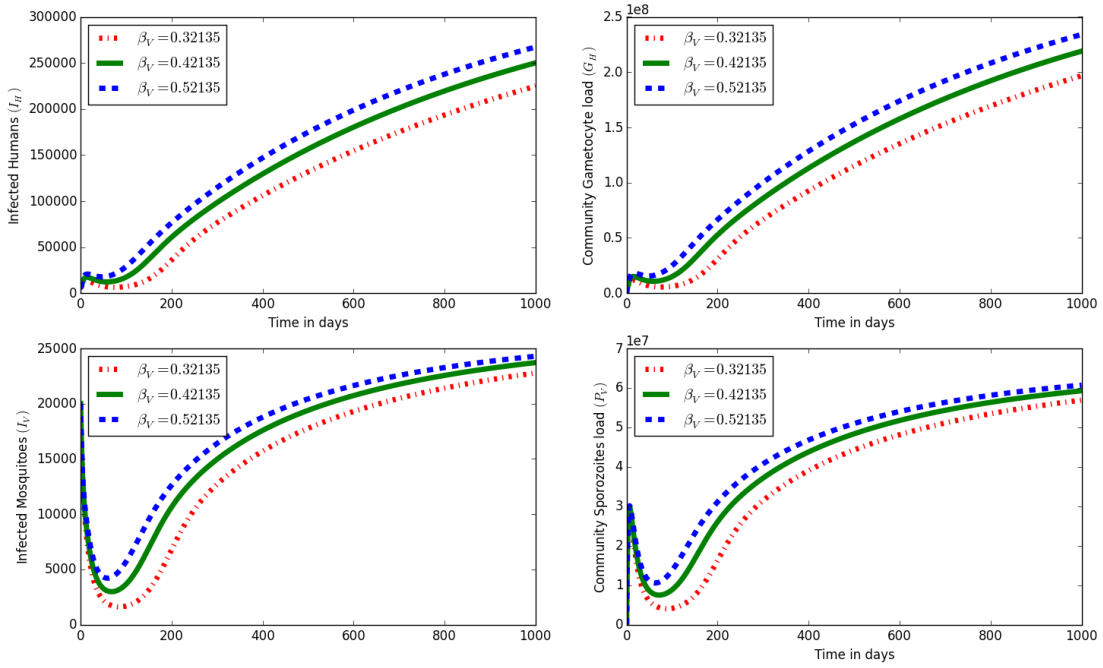

Figure 2.7: Graphs showing the effect of contact rate of susceptible humans with infectious mosquitoes (β_V) on (i) population of infected humans I_H (ii) community gametocytes load G_H (iii) population of infected mosquitoes I_V and (iv) community sporozoites load P_V for different values of β_V: $\beta_V = 0.32135$, $\beta_V = 0.42135$, $\beta_V = 0.52135$.

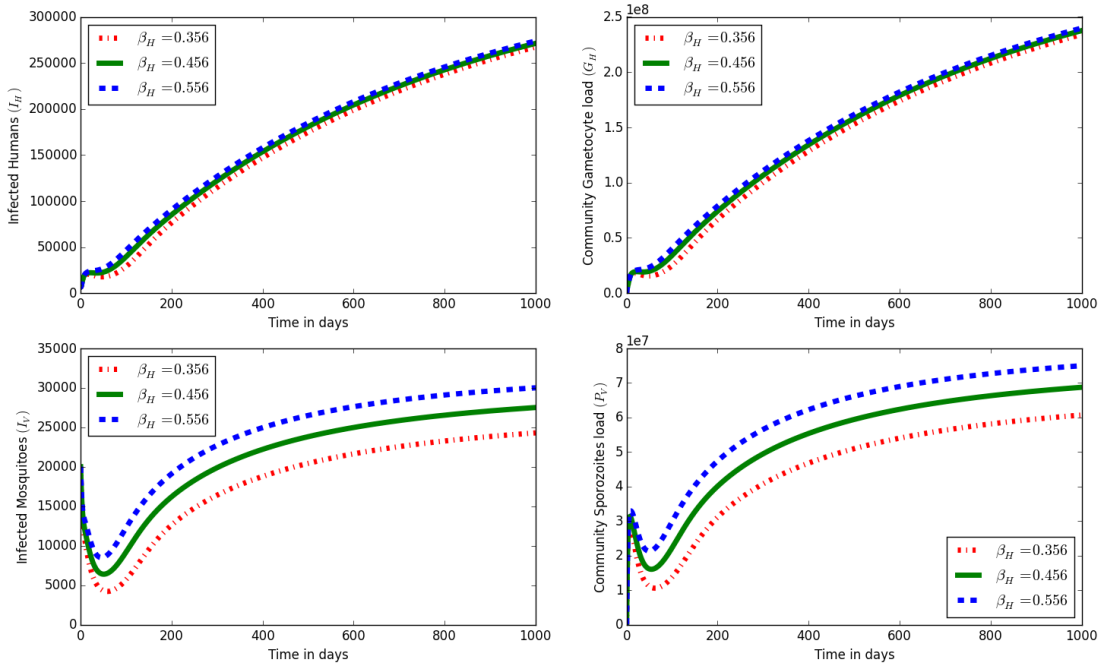

Figure 2.8: Graphs showing the effect of contact rate of susceptible mosquitoes with infectious humans (β_H) on (i) population of infected humans I_H (ii) community gametocytes load G_H (iii) population of infected mosquitoes I_V and (iv) community sporozoites load P_V for different values of β_H: $\beta_H = 0.356$, $\beta_H = 0.456$, $\beta_H = 0.556$.

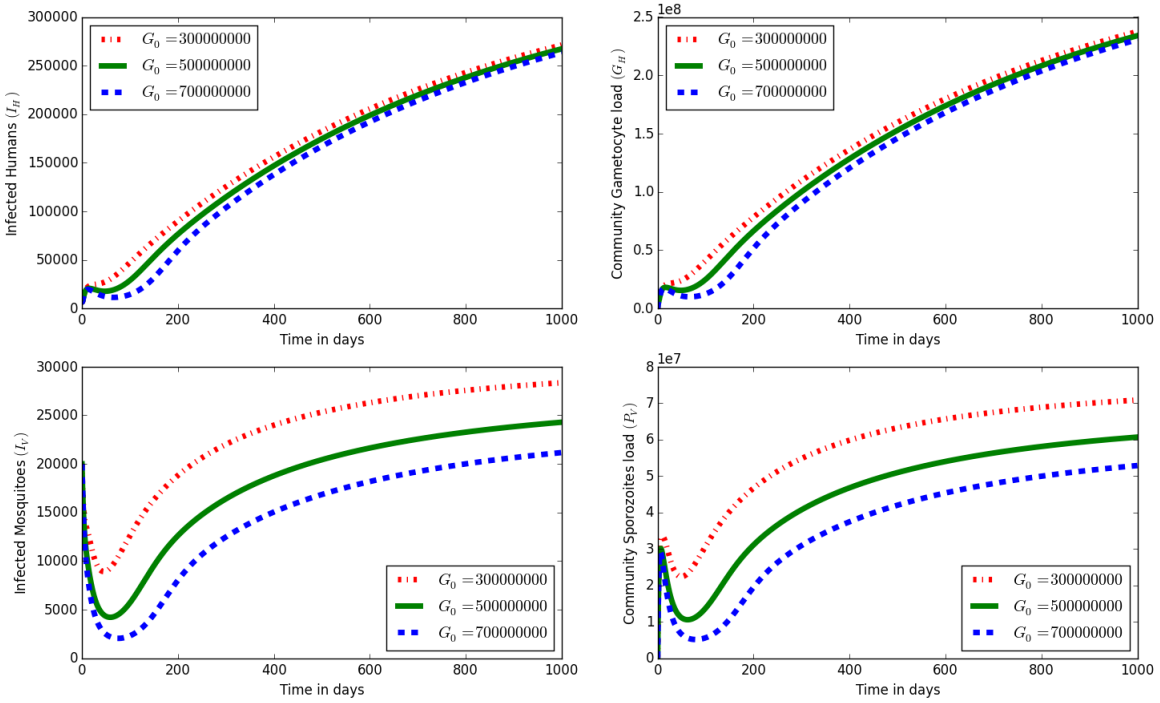

Figure 2.9: Graphs showing the effect of Half saturation constant associated with infection of mosquitoes (G_0) on (i) population of infected humans I_H (ii) community gametocytes load G_H (iii) population of infected mosquitoes I_V and (iv) community sporozoites load P_V for different values of G_0: $G_0 = 3\times10^8$, $G_0 = 5 \times 10^8$, $G_0 = 7 \times 10^8$.

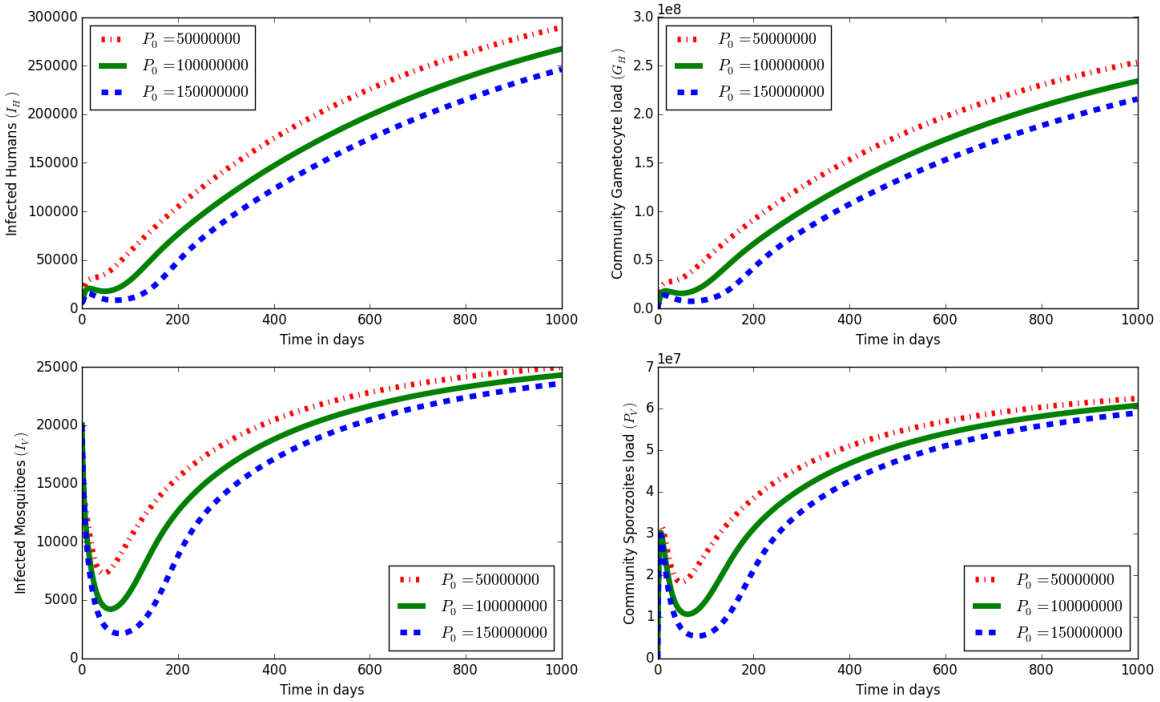

Figure 2.10: Graphs showing the effect of Half saturation constant associated with infection of humans (P_0) on (i) population of infected humans I_H (ii) community gametocytes load G_H (iii) population of infected mosquitoes I_V and (iv) community sporozoites load P_V for different values of P_0: $P_0 = 5\times10^7$, $P_0 = 1 \times 10^8$, $P_0 = 1.5 \times 10^7$.

By using pathogen load as a common metric of disease dynamics at all levels of organization of an infectious disease, this would ensure a common metric of control, elimination and eradication of disease in terms of pathogen load. Currently, single scale models of infectious disease systems at host level define disease burden in terms of incidence and prevalence. However, for some infectious diseases prevalence is not very informative, as the infectivity of individuals depends more on pathogen load than on whether one is infected or not. Incidence is difficult to measure directly. More importantly, the use of community pathogen load as a measure of disease burden also enables us to use a common metric for disease dynamics and burden across scales. Further, community pathogen also combines information from prevalence. Our revised manuscript explains this aspect in more detail [52].

2.3 The Modern Theory of Disease Dynamics

Although science has progressed over time by being able to summarize our existing knowledge of natural phenomena using certain scientific theories, it must be made clear that our description of natural phenomena using scientific theories is a dynamic process because these scientific theories often only adequately describe the phenomenon studied up to a certain time. As time progresses, new knowledge often emerges as we refine the domains of observation and the analysis to improve the accuracy of measurement. In this dynamic picture of science, the classical transmission mechanism theory of disease dynamics with its intellectual origins in the orginal work of Daniel Bernoulli [53], and later formulated and developed in its present form by Kermack and McKendrick [54–56] and others, remained unaltered for almost three centuries. However, because of the need to refine the domains of observation and scales of analysis of infectious disease dynamics, the transmission mechanism theory met its first obstacles around the turn of the nineteenth century. An increasing awareness of the complexity of infectious disease system, and of the challenges precipitated by the need to expand the scales of obervation and analsysis to much finer scales of observation and analysis than the scale of organization at which only transmission occurs required the development of new theory through novel extension of existing theory (the transmission mechanism theory) to advance the understanding of dynamics of infectious disease systems over the coming decades. The problem of directly transmitted diseases was recently successfully resolved by establishing a mathematical and computational description of infectious disease dynamics through a union of the microscale as a scale of observation where pathogen replication and macroscale where pathogen transmission often occurs resulted in a new theory of infectious disease dynamics called the replication-transmission mechanism theory which results in the description of phenomena involving simultaneously of both the pathogen transmission and pathogen replication. The main limitation of the transmission mechanism theory of disease dynamics is that it tends to disjoin the scales of description in order to simplify representation and understanding of infectious disease dynamics. This culminated in a radical scientific theory of infectious disease dynamics called the replication-transmission relativity theory of disease dynamics [11], in which old scientific knowledge of disease dynamics based on transmission mechanism theory was reordered into a new framework based on a revolutionary scientific theory called the replication-transmission mechanism

relativity theory. The replication-transmission relativity theory states that at any level of organization of an infectious disease system there is no privileged/absolute scale which would determine disease dynamics, only interactions between the microscale and macroscale [11]. It identifies an infectious disease system as a complex system which is organized into seven main hierarchical levels at which host-pathogen interactions can play out: (i) the cell level, (ii) the tissue level, (iii) the organ level, (iv) the microecosystem level, (v) the host/organism level, (vi) the community level, and (vii) the macroecosystem level. The replication-transmission relativity theory for multiscale dynamics of infectious disease ripped the entire fabric of classical transmission mechanism theory which has been in existence at least since Daniel Bernoulli developed a dynamic model of smallpox transmission and control in 1760 [53], which was later unified by Kermack and McKendrick in their seminal papers [54–56] into an idea now more widely known as mathematical epidemiology by 1933. The replication-transmission relativity theory for multiscale modelling of infectious disease dynamics [11] demolished the notion that transmission is the only main dynamic disease process. Therefore, the replication-transmission relativity theory is a radical paradigm shift from the scale specific transmission mechanism theory to modelling infectious disease systems.

Figure 2.11 is a conceptual representation of the replication-transmission relativity theory of disease dynamics. The theory makes the point that in multiscale dynamics of infectious diseases, there is an interacting multiscale cycle of four processes which are [a.] infection/super-infection by pathogen, [b.] pathogen replication, [c.] pathogen shedding/excretion, and [d.] pathogen transmission, which is repeated sequentially at each level of organization of an infectious disease system. These four processes are key to understanding infectious disease dynamics using the multiscale modelling methods. The linking of the scales in the development of multiscale as illustrated conceptually in Figure 2.11 involves linking or integration of microscale and macroscale. This involves up-scaling and down-scaling variables associated with some disease processes at these two scale as illustrated in Figure 2.11. This is because for an infectious disease system, the boundary between the microscale and macroscale for each hierarchical level of an infectious disease system indicate/represent shifts in disease processes. However, the greatest challenge in the development of multiscale models of infectious disease dynamics is in methodological difficulties on specific implementation approaches for downscaling and up-scaling in space and time and in converting dimensions across the microscale and macroscale when coupling the submodels of a multiscale model [3]. The lack of rigorous frameworks for down-scaling and up-scaling undermines progress in the development of multiscale models of infectious disease systems. Furthermore, down-scaling to microscale or up-scaling to macroscale involves developing conceptual models that adequately capture the dominant disease processes at these scales. In particular, we inevitably need to know more details when down-scaling while we also need to ignore some fine details when up-scaling. But another challenge is that when either down-scaling or up-scaling, we do not know in general how scale transition occurs. In particular when down-scaling, we do not know what microscale disease processes and parameters are essential in representing the macroscale processes and vice-versa when up-scaling.

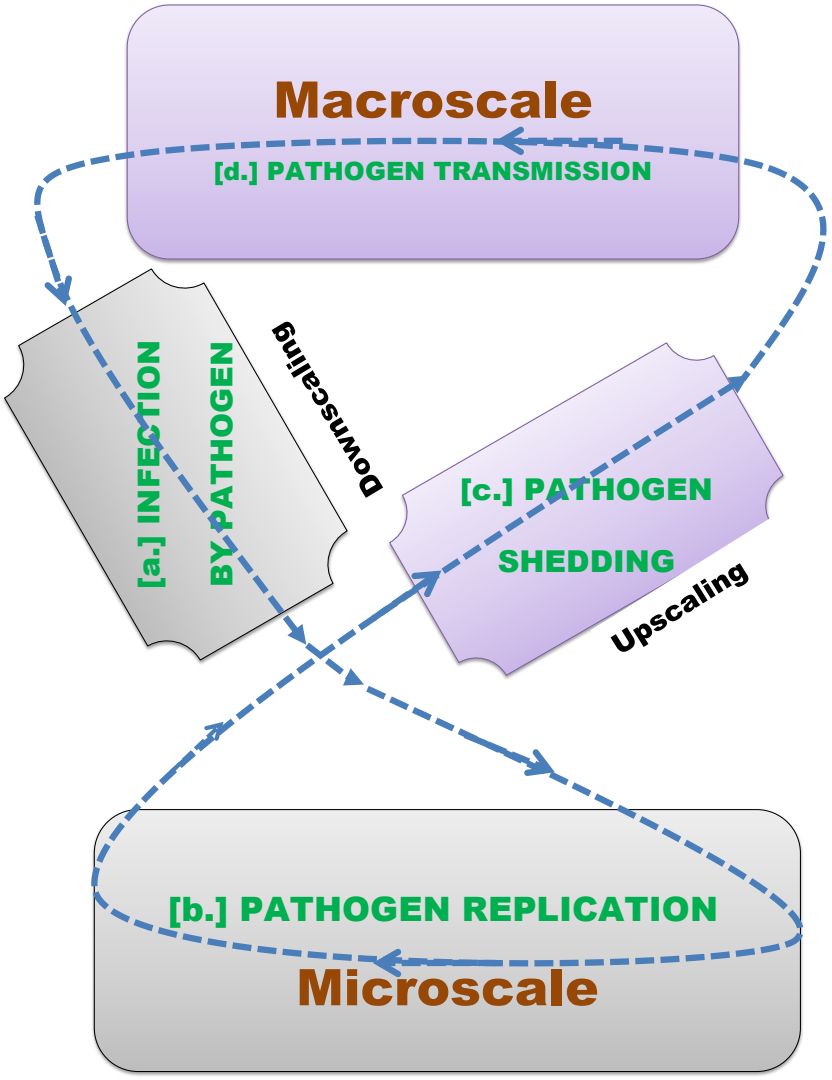

Figure 2.11: A conceptual representation of the replication-transmission relativity theory of disease dynamics.

This replication transmission mechanism theory is a radical paradigm shift from the scale specific transmission mechanism theory to modelling infectious disease systems. However, the passage from transmission mechanism theory of disease dynamics to the replication-transmission relativity theory of disease dynamics shares a feature that are common to all such transitions in which an old scientific theory gives way to a new one. In almost every situation where this transmission occurs there is usually a domain D_n of phenomena described by the new theory and a subdomain D_o wherein the old theory is reliable to a given accuracy. In the case of infectious disease dynamics, the domain D_n represents the level of multiscale observation described by the replication-transmission relativity theory while the subdomain D_0 represents the scale of observation described by the transmission mechanism theory. Further, in addition to numerical accuracy, the new theory often brings about radical conceptual changes. Therefore, unlike the transmission mechanism theory which bring down the complexity of an infectious disease system to manageable levels by discretizing or decomposing the infectious disease system into hierarchical scales

of organization, each of which can be analyzed independently using single scale modelling methods, the replication-transmission relativity theory enables us to bring down the complexity of an infectious disease system to manageable levels by discretizing or decomposing the infectious disease system into hierarchical levels of organization, each of which, can analyzed independently using multiscale modelling methods. This theory ripped the entire fabric of classical transmission mechanism theory which has been in existence at least since Daniel Bernoulli developed a dynamic model of smallpox transmission and control in 1760, which was later unified by Kermack and McKendrick in their seminal work, into an idea now more widely known as mathematical epidemiology. It demolished the notion that transmission is the only main dynamic process in infectious disease dynamics. It anticipates that the replication-transmission relativity theory will remain firmly established as the fundamental theory on which multiscale modelling of infectious disease dynamics is based on from the cell level to the macroecosystem level. Therefore, with a theory in place, we expect that multiscale modelling of infectious disease systems will evolve and expand in scope.

We anticipate that this landmark theory will uncannily transform mainstream thinking about modelling disease dynamics from a complex systems perspective. The basic principle behind the replication-transmission relativity theory is that it establishes that at every level of organization of an infectious disease system there is a replicative-transmission cascade in which a pathogen replicates at microscale while there is transmission at macroscale. This theory provides formal methodology, of describing the multiscale dynamics of infectious disease systems through the use of formal mathematics. It marks a breakthrough in a century long quest to build a working theory of the multiscale dynamics of infectious disease systems. This theory addresses data and observations with far-reaching implications for understanding key infectious disease processes and their fundamental consequences for human, plant and animal health. This theory guides model construction and experimentation, and to identify new organizing principles of infectious disease dynamics by establishing [a.] a common constructive framework multiscale models of infectious disease systems in which the scales are linked through exchange of organisms implicated in transmission of infectious disease system at all levels of organization of an infectious disease system (i.e., cell level, tissue level, organ level, microecosystem level, host level, community level, and macroecosystem level), and [b.] a theory to account for the reciprocal influence between pathogen replication and pathogen transmission, or persistence and dispersal in infectious disease dynamics at every level of organization of an infectious disease system. [c.] a common framework to link the scales of levels of biological organization of an infectious disease system. [c.] a framework to account for the reciprocal influence between the microscale and the macroscale at every level -dependency of information flow or other biological phenomena. Therefore, through out this thesis we are going to use the application of the replication-transmission relativity theory of infectious disease systems.

2.4 Discussion and conclusions

In this chapter we presented the transmission mechanism theory of disease dynamics and also explained its aims, assumptions and limitations. It is a scientific theory that has matured substantially over the past century and has established an enduring framework for the study of infectious disease dynamics using mathemtical and computational models. However, the transmission mechanism theory has limitations which undermine their usefulness. In an effort to address some of the limitations of the transmission mechanism theory we proposed a new modelling science for directly transmitted diseases similar to an existing modelling science for environmentally transmitted infectious diseases. The methods development for models of directly transmitted infectious diseases proposed in this study is based on introducing a new epidemiological variable called community pathogen load (CPL), which is then used to define the force of infection and transmission probability. This then converts standard epidemiological models based on susceptible, exposed, infected, recovered (SEIR) and variations of this paradigm (SI, SIS, SIR, etc.) for directly transmitted infectious diseases into epidemiological models similar to existing models for environmentally transmitted infectious diseases based on susceptible, exposed, infected, recovered, pathogen load (SEIRP) and variations of this paradigm (SIP, SISP, SIRP, etc.) in which community wide pathogen load/pool in the environment is explicitely incorporated into epidemiological models. At the centre of this modelling framework is the idea of using community pathogen load as the standard metric for assessing the effectiveness of TasP. We upscale individual microscale infectiousness to define macroscale infectiousness (community pathogen load) for directly transmitted infectious disease systems. Therefore, the incorporation of community pathogen load variable into the model (while useful as the metric to assess the effectiveness of TasP) is also done because of the need to represent transmission of an infectious disease systems more accurately at population level. The usefulness of such simple models is that they are predictive model for community pathogen load whose usefulness is three-fold: [a.] as a metric for assessing the effectiveness of Treatment as Prevention (TasP), [b.] as an indicator of a community's level of infectiousness and transmission probability, and [c.] as a proximal marker for infectious disease incidence and potential epidemic propagation. The concept of community pathogen load, which is an aggregate biomarker of a community's pathogen burden over a specific time period. We determined that when the community pathogen load is assumed to act as a reservoir for malaria parasites (i.e., $N_h\alpha_h$ and $N_v\alpha_v$) in human blood plasma and mosquito salivary glands is placed in F-matrix instead of V-matrix, then the reproductive number will be $R_0 = \sqrt[4]{R_{HV}R_{VH}}$.

Chapter 3

A Basic Multiscale Model of Malaria Disease Dynamics With Variable Super-infection of Mosquitoes

3.1 Introduction

Malaria disease is a type II vector-borne disease system that is initiated by protozoan parasites known as Plasmodium and it is transmitted to humans by a bite of an infected mosquito [57]. The malaria disease system in humans develops in two stages, the first is the exo-erythrocytic stage (i.e., the liver cells) and the second is the erythrocytic stage which occurs in the red blood cells. Malaria infection begins when an infected mosquito takes a blood meal from a susceptible human and thereby injects the malaria parasite (sporozoites) into the otherwise healthy human. This process is called mosquito to human transmission and the process occurs at the between-host scale (macro-scale). The processes which happen at the within-host scale (micro-scale) begin when the injected sporozoites migrate to liver-stage, by invading the liver cells, and they develop into schizonts which burst to produce merozoites and thus demonstrating the end of the exo-erythrocytic stage. The erythrocytic stage begins with the released merozoites entering the blood-stream and invading the red blood cells. The infected red blood cells burst releasing the merozoites which further invade the red blood cells to renew the cycle and maintain the infection or pathogen load, that is, the replication process that occurs at the micro-scale. The merozoites are the asexual form of the parasite, however, some of the released merozoites differentiate into the sexual form known as gametocytes. These gametocytes must be released into the community pathogen load such that the susceptible mosquitoes

take the blood meal from the community gametocytes load. When the mosquito is infected the parasite must progress from one stage to another within the infected mosquitoes [35]. The process of susceptible mosquitoes getting into contact with infected humans is called the human to mosquito transmission which occurs at the macro-scale.

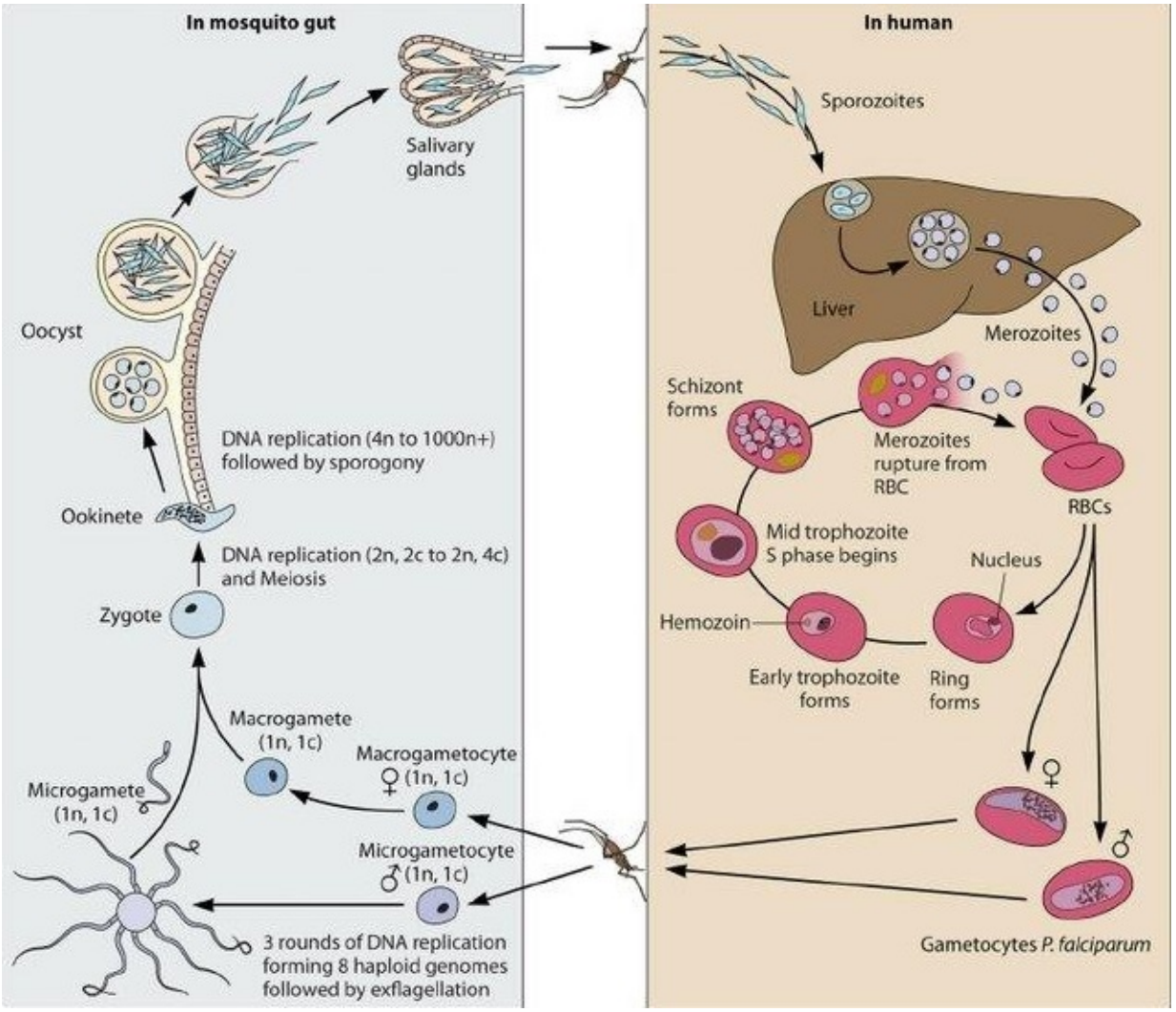

Figure 3.1: A diagram that demonstrates the life cycle of Malaria in Human and in Mosquito [1]

The malaria disease system has a complex life cycle, during sporogonic development, the malaria parasite has in close contact with the midgut, hemolymph, and salivary glands of vector-mosquito. The gametocytes which are consumed by the mosquito in blood meal cause the cycle of transmission to continue back to the mosquito. The gametocytes must cross the midgut of the mosquito, which performs as the first physical obstacle within the vector. The male and female gametocytes fuse within the mosquito forming diploid zygotes, which progress to ookinetes. The ookinetes migrate to the midgut of the mosquito, pass through the gut wall, and form the oocysts, which mature in the midgut's basal lamina. Upon the development, each oocyst bursts to discharge thousands of sporozoites, which then migrate to the salivary glands

of the female Anopheles mosquitoes to undergo further modifications that are necessary to continue the cycle of transmission back to humans [58]. The sporozoites must be released into the pool of pathogen load (i.e., the community sporozoites load).

Infectious disease systems are considered complex systems because of their multi-level and multi-scale nature [11]. As a result of multi-level and multi-scale as main features in infectious disease systems, has raised hopes for researchers in the mathematical modeling community has to lead them to multiscale modeling method for studying infectious diseases dynamics at any level of the organization. In this chapter, we present a coupled multi-scale model that has the combination of two other categories, which are the nested multiscale model and embedded multiscale model. The nested multi-scale model is at human-host and integrates the microscale sub-model and macro-scale sub-model at the host-level of an infectious disease system that has a pathogen replication-cycle at the microscale, that is, in merozoites. The pathogen load at the micro-scale increase through the pathogen replication cycle. The micro-scale sub-model influences the macro-scale sub-model through shedding/excretion, while the macro-scale sub-model influences the micro-scale sub-model through initial infection. The embedded multi-scale model is applied to mosquito-vector and integrates the micro-scale sub-model and the macro-scale sub-model at the host level, and there is no pathogen replication cycle at the micro-scale. The pathogen load at the micro-scale increase through repeated infection/ super-infection. The micro-scale sub-model influences the macro-scale sub-model through pathogen shedding/ excretion, whilst the macro-scale influences the micro-scale through repeated micro-scale through repeated infection/ super-infection.

The microscale sub-model and the macroscale sub-model can be integrated using the nested multiscale model at human-host and embedded multiscale model at mosquito-host, and the models can be developed at any level of organization of an infectious disease system, that is, at cell-level, tissue-level, organ-level, micro-ecosystem level, host-level, community-level, and micro-ecosystem level. At each level of organization, there is a transmission process at the macroscale sub-model and a replication cycle at the microscale sub-model. The two sub-models influence each other with type I or type II reciprocal influences. The objective of this study is to investigate how super-infection in mosquitoes has an influence on malaria disease dynamics for a pathogen with no replication cycle at the micro-scale and to investigate how initial infection in humans has an influence on malaria disease dynamics for a pathogen with a replication cycle at the micro-scale.

The research to date on malaria disease dynamics has tended to focus on the dynamics of malaria infection and investigating the influence of control measures that target at controlling, eliminating, and even eradicating this malaria disease system using a single-scale modeling approach, that is, within-host scale [43–45, 59, 60] and between-host scale [40–42]. From the literature, we observed the development of multiscale models of malaria infection in [34] using the time since infection, that is, the between-host

scale sub-model which modelled using partial differential equations (PDEs) and the within-host scale sub-model which are developed using ordinary differential equations (ODEs) and the sub-models are linked through a hybrid multiscale model approach. We also observed that all the research developed on infectious disease systems which use the coupled multiscale models as the main category, they linked the two multiscale using the combination of the same category in both human and vector. For example work by Garira [24] on a coupled multiscale model of malaria disease, the author linked the sub-models using the nested multiscale model on humans and linked sub-models using the nested multiscale model on vectors.

3.2 Derivation of the Basic Coupled Multiscale Model for Malaria Disease System

In this subsection, we develop a basic multiscale model of the malaria disease system which is at multiple hosts (that is, human-host and mosquito-host), with four sub-models which are within-host scale sub-models (within-human scale and within-mosquito scale), and between-host scale sub-models (between-human scale and between-mosquito scale). We obtain the nested multiscale model on human-host that links the between-human host sub-model which is related to the transmission dynamics of the malaria disease system and the within-human host sub-model which is related to the replication cycle of the malaria parasite within the infected humans. The between-human sub-model influences the within-human sub-model through initial infection whereas the within-human sub-model influences the between-human sub-model through shedding/ excretion of the pathogen. We also extract the embedded multiscale model on mosquito host that links the between -mosquito sub-model which is related to the transmission dynamics of malaria disease and within-mosquito sub-model which is associated with the replication cycle of the malaria parasite within the infected mosquitoes. The between-mosquito sub-model influences the within-mosquito sub-model through super-infection while the within-mosquito sub-model influences the between-mosquito sub-model through shedding/excretion of the pathogen. The human-host and mosquito-host are linked through the sharing of the pathogen (malaria parasite).

In this study, we adapted the work on a coupled multiscale model of malaria disease by Garira [24] with some minor modifications on the super-infection in mosquitoes. We make the following assumptions from the multiscale model system (3.2.0.1):

i. The transmission of infection of humans is only through direct contact with the sporozoites load (P_V), that is, from the infected mosquitoes whereas the transmission in mosquitoes is only through getting direct contact with the gametocytes load (G_H) from the infected humans.

ii. For embedded multiscale model, the dynamics of between-mosquito sub-model and the within-mosquito sub-model for malaria disease dynamics variables happen at the same time scale, that is, at a slow time scale, t, such that $S_V = S_V(t)$, $I_V = I_V(t)$, $P_V = P_V(t)$, $G_v = G_v(t)$, $G_m = G_m(t)$, $Z_v = Z_v(t)$, $O_v = O_v(t)$, and $P_v = P_v(t)$.

iii. For the nested multiscale model, we assume that the dynamics of between-human host sub-model and within-human host sub-model of malaria disease dynamics variables occur at different time scales. The between-human scale variables S_H, I_H and G_H occur at slow time scale, t, such that $S_H = S_H(t)$, $I_H = I_H(t)$, and $G_H = G_H(t)$, whilst the within-human scale variables R_h, R_m, M_h, and G_h occur at fast time scale , s, such that $R_h = R_h(s)$, $R_m = R_m(s)$, $M_h = M_h(s)$, and $G_h = G_h(s)$.

iv. Infected mosquitoes do not recover from malaria.

From the model diagram shown in figure (3.2), we have the following system of equations as our coupled multiscale model for malaria disease system transmission dynamics:

$$
\begin{aligned}
1.\quad & \frac{dS_H(t)}{dt} &&= \Lambda_H - \frac{\beta_V P_V(t)}{P_0 + P_V(t)} S_H(t) - \mu_H S_H(t) + \gamma_H I_H(t),\\
2.\quad & \frac{dI_H(t)}{dt} &&= \frac{\beta_V P_V(t)}{P_0 + P_V(t)} S_H(t) - [\mu_H + \gamma_H + \delta_H]\, I_H(t),\\
3.\quad & \frac{dR_h(s)}{ds} &&= \Lambda_h - \beta_h R_h(s) M_h(s) - \mu_b R_h(s),\\
4.\quad & \frac{dR_m(s)}{ds} &&= (1-\pi)\beta_h R_h(s) M_h(s) - \alpha_m R_m(s),\\
5.\quad & \frac{dM_h(s)}{ds} &&= N_m \alpha_m R_m(s) - \mu_m M_h(s),\\
6.\quad & \frac{dG_h(s)}{ds} &&= \pi \beta_h R_h(s) M_h(s) - [\alpha_h + \mu_h] G_h(s),\\
7.\quad & \frac{dG_H(t)}{dt} &&= N_h \alpha_h I_H(t) - \alpha_H G_H(t),\\
8.\quad & \frac{dS_V(t)}{dt} &&= \Lambda_V - \frac{\beta_H G_H(t)}{G_0 + G_H(t)} S_V(t) - \mu_V S_V(t),\\
9.\quad & \frac{dI_V(t)}{dt} &&= \frac{\beta_H G_H(t)}{G_0 + G_H(t)} S_V(t) - [\mu_V + \delta_V]\, I_V(t),\\
10.\quad & \frac{dG_v(t)}{dt} &&= \frac{\beta_H G_H(t)(S_V - 1)}{(G_0 + G_H)\phi_V (I_V + 1)} - [\alpha_g + \mu_g]\, G_v(t),\\
11.\quad & \frac{dG_m(t)}{dt} &&= N_g \alpha_g G_v(t) - [\alpha_s + \mu_s]\, G_m(t),\\
12.\quad & \frac{dZ_v(t)}{dt} &&= \frac{1}{2}\alpha_s G_m(t) - [\alpha_z + \mu_z]\, Z_v(t),\\
13.\quad & \frac{dO_v(t)}{dt} &&= \alpha_z Z_v(t) - [\alpha_k + \mu_k]\, O_v(s),\\
14.\quad & \frac{dP_v(t)}{dt} &&= N_k \alpha_k O_v(t) - [\alpha_v + \mu_v]\, P_v(t).\\
15.\quad & \frac{dP_V(t)}{dt} &&= P_v(t)\alpha_v\, (I_V(t) + 1) - \alpha_V P_V(t),
\end{aligned}
\tag{3.2.0.1}
$$

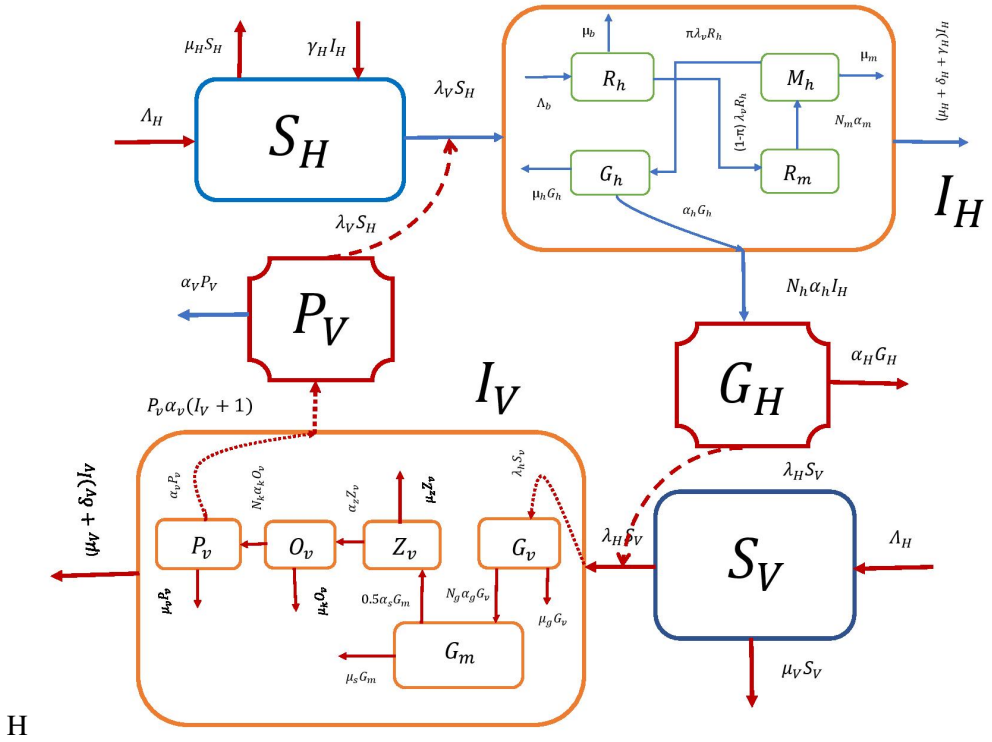

Figure 3.2: A conceptual diagram of the multiscale model of malaria disease dynamics

3.2.1 Analysis of the multi-scale model using fast-slow time-scale analysis

We observed from the embedded multi-scale model of system (3.2.0.1) that at mosquito-host level has same time scales which involved the between-mosquito host time scale (t) which associated with transmission at the population-level and the within-mosquito host time scale (t) associated with the growth of sporozoites population at the individual-level. We also note from the nested multi-scale model system (3.2.0.1) that at human host level, has different time scale which are the between-human host time scale (t) which associated with the transmission of malaria disease system and within-human host time scale (s) which associated with the replication of merozoites at an individual level. The analysis of the multi-scale model system (3.2.0.1) can be simplified by expressing the slow-time scale and fast time scale in terms of each other by using the form $t = \epsilon s$ such that the within-human-malaria disease dynamics can be written in the form of slow time scale.

3.2.1.1 Within-human malaria parasite population model

The within-host scale sub-model illustrate the time evolution of four population dynamics within an infected human host which are the population of uninfected red blood cells (Susceptible erythrocyte R_h), the population of infected red blood cells (merozoites infected erythrocytes R_m), the population of merozoites M_h, and the population of gametocyte infected erythrocytes G_h. The sub-model (3.2.1.1) has adopted the following assumptions from [24], which are:

i. There is no super-infection/repeated infection of humans.

ii. The immune response is not considered in the infected human.

iii. We only explicitly consider the blood-stage parasite population dynamics and consider the initial infection from the liver-stage of malaria parasite population dynamics which is captured through merozoites i.e., $M_h = M_h(0)$.

iv. The dynamics of the four populations of within an infected human occurs at a fast time scale, s, compared to between-host transmission dynamics, such that $R_h = R_h(s)$, $R_m = R_m(s)$, $M_h = M_h(s)$, and $G_h = G_h(s)$.

v. The within human gametocyte population G_h is a proxy for individual human infectiousness to mosquitoes.

When we consider all the assumptions, the sub-model describing the dynamics of the four within-human populations is proposed to be:

$$\begin{aligned}
1. \quad \frac{dR_h(s)}{ds} &= \Lambda_h - \beta_h R_h(s) M_h(s) - \mu_b R_h(s), \\
2. \quad \frac{dR_m(s)}{ds} &= (1-\pi)\beta_h R_h(s) M_h(s) - \alpha_m R_m(s), \\
3. \quad \frac{dM_h(s)}{ds} &= N_m \alpha_m R_m(s) - \mu_m M_h(s), \\
4. \quad \frac{dG_h(s)}{ds} &= \pi \beta_h R_h(s) M_h(s) - (\alpha_h + \mu_h) G_h(s).
\end{aligned} \tag{3.2.1.1}$$

The first equation in the system of equations (3.2.1.1), describes the dynamics of uninfected red blood cells (R_h). The population of uninfected red blood cells is assumed to increase through the supply of red blood cells from the bone marrow at a rate Λ_h and the population of uninfected red blood cells decrease through the infection of red blood cells. $\beta_h R_h(s) M_h(s)$ models the rate at which the merozoites get contact with the uninfected red blood cells, where β_h is the infection rate or contact rate. The susceptible erythrocytes are also reduced through natural decay at a constant rate μ_b. The second equation of sub-model (3.2.1.1) illustrates the dynamics of merozoites infected red blood cells (R_m). The dynamics of merozoites infected red blood cells increase through infection of susceptible red-blood cells with a propotion of $(1-\pi)$ and reduced through bursting of infected red blood cells to produce merozoites at a rate α_m. The third equation of sub-model (3.2.1.1) demonstrate the dynamics of population of merozoites. The dynamics of merozoites increase through the average number of merozoites releasedm in the human blood stream through bursting of infected red blood cells at a rate $N_m \alpha_m R_m(s)$. The population of merozoites reduced through natural decay at a rate μ_m. The last equation of sub-model (3.2.1.1) describe the dynamics of the population of gametocytes. The population of gametocytes increase through the population of gametocyte infected erythrocytes at a proportion π and the sub-model decrease through natural decay of gametocytes at a rate μ_h and through shedding/excretion of gametocytes at a rate α_h.

$$
\begin{aligned}
1. \quad \epsilon\frac{dR_h(t)}{dt} &= \Lambda_h - \beta_h R_h(t) M_h(t) - \mu_b R_h(t), \\
2. \quad \epsilon\frac{dR_m(t)}{dt} &= (1-\pi)\beta_h R_h(t) M_h(t) - \alpha_m R_m(t), \\
3. \quad \epsilon\frac{dM_h(t)}{dt} &= N_m \alpha_m R_m(t) - \mu_m M_h(t), \\
4. \quad \epsilon\frac{dG_h(t)}{dt} &= \pi\beta_h R_h(t) M_h(t) - (\alpha_h + \mu_h) G_h(t),
\end{aligned} \tag{3.2.1.2}
$$

where ϵ is a small constant number that is $0 < \epsilon \ll 1$ which highlights the fast time scale of the within-human host sub-model compared to the slow time scale of the between-host transmission sub-model [14, 24].

We use the next generation operator approach to obtain the basic reproductive number of the within-human host model (3.2.1.2). The model (3.2.1.2) can be written in the form

$$
\begin{aligned}
\frac{dX}{dt} &= f(X, Y, Z), \\
\frac{dY}{dt} &= g(X, Y, Z), \\
\frac{DZ}{dt} &= h(X, Y, Z),
\end{aligned}
$$

where

$$
\begin{aligned}
X &= (R_h), \\
Y &= (R_m, G_h), \\
Z &= (M_h).
\end{aligned} \tag{3.2.1.3}
$$

We define $\widetilde{g}(X^*, Z)$ by

$$
\begin{aligned}
g_1(X^*, Z) &= R_m = \frac{(1-\pi)\beta_h R_h M_h}{\alpha_m}, \\
g_2(X^*, Z) &= G_h = \frac{\pi\beta_h R_h M_h}{\alpha_h + \mu_h}.
\end{aligned} \tag{3.2.1.4}
$$

By substituting the values of R_m and G_h and letting $h_1 = \dfrac{dM_h}{dt}$ we obtain

$$
h_1 = \frac{dM_h}{dt} = N_m \alpha_m R_m - \mu_m M_h,
$$

therefore

$$\begin{aligned} h_1 &= \frac{(1-\pi)N_m\alpha_m\beta_h\Lambda_h M_h}{\alpha_m\mu_b} - \mu_m M_h, \\ A &= \frac{\partial h_1}{\partial M_h} = \frac{(1-\pi)N_m\alpha_m\beta_h\Lambda_h}{\alpha_m\mu_b} - \mu_m, \end{aligned} \tag{3.2.1.5}$$

where

$$\begin{aligned} A &= M - D, \\ M &= \frac{(1-\pi)N_m\alpha_m\beta_h\Lambda_h}{\alpha_m\mu_b}, \\ D &= \mu_m, \\ D^{-1} &= \frac{1}{\mu_m}, \\ MD^{-1} &= \frac{(1-\pi)N_m\alpha_m\beta_h\Lambda_h}{\alpha_m\mu_b\mu_m}. \end{aligned} \tag{3.2.1.6}$$

Therefore $\Re_0 = \rho(MD^{-1})$, the reproductive number is given by

$$\Re_0 = \frac{(1-\pi)N_m\beta_h\Lambda_h}{\mu_b\mu_m}. \tag{3.2.1.7}$$

The basic reproductive number number ($\Re_0$) of the within-human host submodel measures the total number of secondary infected red blood cells (IRBCs) produced by primary IRBCs in a host at the beginning of the infection.

Since $0 < \epsilon \ll 1$, we let $\epsilon = 0$ so that the within-human host sub-model becomes independent of time and which is given by:

$$\begin{aligned} \Lambda_h - \beta_h\widehat{R_h}\widehat{M_h} - \mu_b\widehat{R_h} &= 0, \\ (1-\pi)\beta_h\widehat{R_h}\widehat{M_h} - \alpha_m\widehat{R_m} &= 0, \\ N_m\alpha_m\widehat{R_m} - \mu_m\widehat{M_h} &= 0, \\ \pi\beta_h\widehat{R_h}\widehat{M_h} - \alpha_h\widehat{G_h} &= 0. \end{aligned} \tag{3.2.1.8}$$

The disease free equilibrium point of the within-human scale model, where there is no pathogen exists to infect the inside-host environment (human-host). The D.F.E is given by

$$\begin{aligned} E_0 &= \left(R_h^0, R_m^0, M_h^0, G_h^0\right), \\ &= \left(\frac{\Lambda_h}{\mu_b}, 0, 0, 0\right). \end{aligned} \tag{3.2.1.9}$$

The endemic equilibrium point of the within-human scale model, where the pathogen exists to infect the inside-host environment. The endemic equilibrium point is given by

$$E_1 = (\widehat{R_h}, \widehat{R_m}, \widehat{M_h}, \widehat{G_h}), \tag{3.2.1.10}$$

where

$$\begin{aligned} \widehat{R_h} &= \frac{\Lambda_h}{\mu_b \Re_0}, \\ \widehat{R_m} &= \frac{\mu_m \mu_b}{\beta_h N_m \alpha_m}(\Re_0 - 1), \\ \widehat{M_h} &= \frac{\mu_b}{\beta_h}(\Re_0 - 1), \\ \widehat{G_h} &= \frac{\pi \Lambda_h}{\Re_0(\alpha_h + \mu_h)}(\Re_0 - 1), \end{aligned} \tag{3.2.1.11}$$

where

$$\Re_0 = \frac{(1-\pi) N_m \beta_h \Lambda_h}{\mu_b \mu_m}. \tag{3.2.1.12}$$

The within-human host sub-model has a unique positive endemic equilibrium point when $\Re_0 > 1$ and no positive equilibrium point when $\Re_0 < 1$.

We note that from the multiscale model (3.2.0.1), the total number of gametocytes shed/excreted by each infected human in the environment (community gamocytes load) $N_h I_H$ is approximated by $\widehat{G}_h I_H$. Application of the notation $N_h = \widehat{G}_h$, which is the average number of the within-human host scale of the gamotocytes load (G_h) at the endemic equilibrium point is available for shedding/excretion into the community gametocyte load by each infected human. The multi-scale model (3.2.0.1) of the malaria disease system has been simplified to:

$$
\begin{aligned}
1.\quad \frac{dS_H(t)}{dt} &= \Lambda_H - \frac{\beta_V P_V(t)}{P_0 + P_V(t)} S_H(t) - \mu_H S_H(t) + \gamma_H I_H(t),\\
2.\quad \frac{dI_H(t)}{dt} &= \frac{\beta_V P_V(t)}{P_0 + P_V(t)} S_H(t) - [\mu_H + \gamma_H + \delta_H] I_H(t),\\
3.\quad \frac{dG_H(t)}{dt} &= N_h \alpha_h I_H(t) - \alpha_H G_H(t),\\
4.\quad \frac{dS_V(t)}{dt} &= \Lambda_V - \frac{\beta_H G_H(t)}{G_0 + G_H(t)} S_V(t) - \mu_V S_V(t),\\
5.\quad \frac{dI_V(t)}{dt} &= \frac{\beta_H G_H(t)}{G_0 + G_H(t)} S_V(t) - [\mu_V + \delta_V] I_V(t),\\
6.\quad \frac{dG_v(t)}{dt} &= \frac{\beta_H G_H(t)(S_V(t) - 1)}{(G_0 + G_H(t))\phi_V(I_V(t) + 1)} - [\alpha_g + \mu_g] G_v(t),\\
7.\quad \frac{dG_m(t)}{dt} &= N_g \alpha_g G_v(t) - [\alpha_s + \mu_s] G_m(t),\\
8.\quad \frac{dZ_v(t)}{dt} &= \frac{1}{2}\alpha_s G_m(t) - [\alpha_z + \mu_z] Z_v(t),\\
9.\quad \frac{dO_v(t)}{dt} &= \alpha_z Z_v(t) - [\alpha_k + \mu_k] O_v(t),\\
10.\quad \frac{dP_v(t)}{dt} &= N_k \alpha_k O_v(t) - [\alpha_v + \mu_v] P_v(t).\\
11.\quad \frac{dP_V(t)}{dt} &= P_v(t)\alpha_v (I_V(t) + 1) - \alpha_V P_V(t),
\end{aligned}
\tag{3.2.1.13}
$$

where

$$
\begin{aligned}
N_h &= \widehat{G_h} = \frac{\pi}{(1-\pi)}\left[\frac{(1-\pi)N_m\beta_h\Lambda_h - \mu_b\mu_m}{N_m\beta_h(\alpha_h + \mu_h)}\right] = \frac{\pi\Lambda_h}{(\alpha_h + \mu_h)\Re_0}\left[\Re_0 - 1\right],\\
\Re_0 &= \frac{(1-\pi)N_m\beta_h\Lambda_h}{\mu_b\mu_m}.
\end{aligned}
\tag{3.2.1.14}
$$

$\Re_0$ is the reproductive number of the within an infected human.

The first equation in system (3.2.1.13) describes the dynamics of uninfected humans (susceptible) S_H.The population is assumed to increase at a constant rate Λ_H through birth and immigrants and also increase through natural recovered of infected individual at a rate γ_H. This population is reduced through infection of susceptible humans at a rate to $\frac{\beta_V P_V}{P_0 + P_V}$, where β_V is the contact rate to a community sporozoite load $P_V(t)$ per unit time, P_0 is the community sporozoite load that yields 50% chance of getting a human host infected with malaria after a bite by a mosquito in a particular community. This equation also decreased by natural death at a constant rate μ_H.

The second equation in system (3.2.1.13) demonstrates the dynamics of infected individuals. The equation increases through infection of susceptible humans and also depleted through natural death rate μ_H,

recovery of the infected individual at rate γ_H and through disease induced death rate δ_H.

The third equation in system (3.2.1.13), demonstrates the dynamics of the community gametocyte load (G_H). The first term in the right-hand-side of this equation describes the total number of gametocytes load contributed by all infected individuals from within-host process to the community gametocytes load pool, where N_h is defined as the measure of the total volume of gametocytes produced within an infected host throughout the entire period of host infectiousness and α_h is the proportion of individuals who are infected. α_H is the rate of degradation of this class.

The fourth equation in system (3.2.1.13) describes the dynamics of uninfected mosquitoes (S_V). This equation increase through constant rate Λ_V. The equation depleted through infection of susceptible mosquitoes at a rate $\frac{\beta_H G_H}{G_0 + G_H}$, where β_H is the contact rate to a community gametocyte load G_H per unit time, G_0 is the community gametocyte load that yields 50% chance of getting a mosquito-vector infected with malaria after bite a human host in a particular community. This equation also decreased by natural death at a constant rate μ_V. The fifth equation in system (3.2.1.13) demonstrates the dynamics of infected mosquitoes. This equation increase through the infection of susceptible mosquitoes and also decreased through natural death rate μ_V and also disease induced death rate δ_V.

The sixth equation in system (3.2.1.13) demonstrates the dynamics of gametocytes infected erythrocytes within an infected mosquito after a mosquito gets a blood meal from an infected human. The first term on the right-hand-side of this equation is the new infection at an individual mosquito. This equation depleted through natural decay rate of gametocyte infected erythrocytes within an infected mosquito μ_g and also through α_g the rate at which gametocyte infected erythrocytes burst releasing sex cells called gametes. The seventh equation (3.2.1.13) describes the dynamics of the population of gametes within an infected mosquito. The first term of this equation is the rate of increase of gametes within an infected mosquito. The gametes decay at a rate μ_s and also depleted through male and female gametes fusing to form zygotes at a constant rate α_g. The eighth equation of system (3.2.1.13) demonstrates the dynamics of zygotes. The equation increase through gametes fuse to form zygotes at a rate $\frac{\alpha_s}{2}$ and depleted through natural decay μ_z and also through develop into oocysts at a rate α_s. The ninth equation of system (3.2.1.13) illustrates the dynamics of the population of oocysts in an infected mosquito. The first term in the right-hand-side of the ninth equation represent the rate of increase where the ookinetes transform into early oocysts. The second term is the rate of reduction of this population through either natural decay at a rate μ_k or burst and release sporozoites at a rate α_k. The tenth equation of system (3.2.1.13) describes the dynamics of sporozoites population in an infected mosquito. The first term of the RHS of the tenth equation is given by each oocysts bursts at a rate α_k releasing an average of N_k sporozoites upon bursting. Therefore, the rate of increase in sporozoites within an infected mosquito is given by $N_k \alpha_k O_v$. The tenth equation is reduced through either natural decay at a rate α_v or through the rate at which sporozoites mature and become infectious to humans and migrate to salivary glands of the infected mosquito.

The eleventh equation of system (3.2.1.13) describes the community sporozoites load P_V. The equation increase by the up-scaling of within-host scale excretion/shedding of pathogen which is given by $P_v\alpha_v(I_V+1)$ and reduced by α_V the rate of sporozoites eliminated from geographical area/ community area.

3.2.2 Positivity of Solutions

The system of equations (3.2.1.13) demonstrates the dynamics of human, mosquito and parasite populations and it is essential to show that these populations are positive for all ≥ 0. We have to prove the following theorem.

Theorem 3.1. *The solutions of the system of equations (3.2.1.13) satisfy the following initial conditions with strictly-positive components i.e. ($S_H > 0$, $I_H > 0$, $G_H > 0$, $S_V > 0$, $I_V > 0$, $P_V > 0$, $G_v > 0$, $G_m > 0$, $Z_v > 0$, $O_v > 0$, $P_v > 0$) for all $t > 0$.*

Proof. We prove that the solution of the model (3.2.1.13) of which the solution starts from a strictly positive point, all components are positive for $0 \leq t \leq t_0$

$$\frac{dS_H(t)}{dt} \geq -(\lambda_V(t)+\mu_H)S_H(t). \tag{3.2.2.1}$$

The equation can be solved by the separation of variables as follows:

$$\frac{dS_H(t)}{S_H(t)} \geq -(\lambda_V(t)+\mu_H)dt. \tag{3.2.2.2}$$

By letting

$$\begin{aligned}\hat{t} \;=\; & \sup\{t>0 : S_H>0, I_H>0, G_H>0, S_V>0, I_V>0, P_V>0, G_v>0, G_m>0, Z_v>0,\\ & O_v>0, P_v>0\} \in [0,t],\end{aligned}$$

and integrating equation (3.2.2.2) and we obtain

$$\begin{aligned}\ln(S_H(t)) &\geq -\left(\int_0^t \lambda_V(\hat{t})d\hat{t}+\mu_H t\right)+\ln(S_H(0)),\\ S_H(t) &\geq S_H(0).\exp\left\{-\left(\int_0^t \lambda_V(\hat{t})d\hat{t}+\mu_H t\right)\right\},\\ S_H(t) &\geq 0.\end{aligned} \tag{3.2.2.3}$$

It implies that

$$\lim_{t\to\infty}\inf(S_H(t)) \geq 0. \tag{3.2.2.4}$$

Using the similar method, it can be shown that

$$\begin{aligned}
\lim_{t\to\infty}\inf(I_H(t)) &\geq 0,\\
\lim_{t\to\infty}\inf(G_H(t)) &\geq 0,\\
\lim_{t\to\infty}\inf(S_V(t)) &\geq 0,\\
\lim_{t\to\infty}\inf(I_V(t)) &\geq 0,\\
\lim_{t\to\infty}\inf(P_V(t)) &\geq 0,\\
\lim_{t\to\infty}\inf(G_v(t)) &\geq 0\\
\lim_{t\to\infty}\inf(G_m(t)) &\geq 0,\\
\lim_{t\to\infty}\inf(Z_v(t)) &\geq 0,\\
\lim_{t\to\infty}\inf(O_v(t)) &\geq 0,\\
\lim_{t\to\infty}\inf(P_v(t)) &\geq 0.
\end{aligned} \tag{3.2.2.5}$$

Thus, when starting with non-negative initial value conditions in the model (3.2.1.13), the solutions of the model will remain non-negative for all $t \geq 0$, and this completes the proof. □

3.2.3 Feasible region of the equilibrium of the model

All the parameters and state variables for the model system (3.2.1.13) are assumed to be non-negative to be consistent with human and mosquito populations. Further, it can be verified that for model system (3.2.1.13), all solutions with non-negative initial conditions remain bounded and non-negative.
By letting $N_H = S_H + I_H$ and adding first and second equations in system (3.2.1.13)

$$\frac{dN_H}{dt} \leq \Lambda_H - \mu_H N_H. \tag{3.2.3.1}$$

It implies that

$$\lim_{t\longrightarrow\infty} Sup(N_H(t)) \leq \frac{\Lambda_H}{\mu_H}. \tag{3.2.3.2}$$

Using similar method by letting $N_V = S_V + I_V$ and adding fourth and fifth equations in system (3.2.1.13) gives

$$\frac{dN_V}{dt} \leq \Lambda_V - \mu_V N_V. \tag{3.2.3.3}$$

This implies that

$$\lim_{t\longrightarrow\infty} Sup(N_V(t)) \leq \frac{\Lambda_V}{\mu_V}. \tag{3.2.3.4}$$

Using equation (3.2.3.2) and (3.2.3.4) similar expressions can be derived for the remaining model variables. Therefore all feasible solutions of the model system (3.2.1.13) are positive and eventually enter the invariant attracting region

$$\Omega = (S_H, I_H, G_H, S_V, I_V, G_v, G_m, Z_v, O_v, P_v, P_V) \tag{3.2.3.5}$$

where

$$
\begin{aligned}
0 &\leq S_H + I_H \leq \frac{\Lambda_H}{\mu_H}, \\
0 &\leq S_V + I_V \leq \frac{\Lambda_V}{\mu_V}, \\
0 &\leq G_H \leq \frac{N_h\alpha_h}{\alpha_H}\frac{\Lambda_H}{\mu_H}, \\
0 &\leq G_v \leq \frac{1}{\alpha_g+\mu_g}\frac{1}{\phi_V}\frac{N_h\alpha_h\Lambda_H}{G_0\mu_H\alpha_H+N_h\alpha_h\Lambda_H}\frac{\beta_H(\Lambda_V-\mu_V)}{\Lambda_V+\mu_V}, \\
0 &\leq G_m \leq \frac{N_g\alpha_g}{\alpha_g+\mu_g}\frac{1}{\mu_s+\mu_s}\frac{1}{\phi_V}\frac{N_h\alpha_h\Lambda_H}{G_0\mu_H\alpha_H+N_h\alpha_h\Lambda_H}\frac{\beta_H(\Lambda_V-\mu_V)}{\Lambda_V+\mu_V}, \\
0 &\leq Z_v \leq \frac{1}{2}\frac{N_g\alpha_g}{\alpha_g+\mu_g}\frac{\alpha_s}{\mu_s+\mu_s}\frac{1}{\alpha_z+\mu_z}\frac{1}{\phi_V}\frac{N_h\alpha_h\Lambda_H}{G_0\mu_H\alpha_H+N_h\alpha_h\Lambda_H}\frac{\beta_H(\Lambda_V-\mu_V)}{\Lambda_V+\mu_V}, \\
0 &\leq O_v \leq \frac{1}{2}\frac{1}{2}\frac{N_g\alpha_g}{\alpha_g+\mu_g}\frac{\alpha_s}{\mu_s+\mu_s}\frac{\alpha_z}{\alpha_z+\mu_z}\frac{1}{\alpha_k+\mu_k}\frac{1}{\phi_V}\frac{N_h\alpha_h\Lambda_H}{G_0\mu_H\alpha_H+N_h\alpha_h\Lambda_H}\frac{\beta_H(\Lambda_V-\mu_V)}{\Lambda_V+\mu_V}, \\
0 &\leq P_v \leq \frac{1}{2}\frac{N_g\alpha_g}{\alpha_g+\mu_g}\frac{\alpha_s}{\mu_s+\mu_s}\frac{\alpha_z}{\alpha_z+\mu_z}\frac{N_k\alpha_k}{\alpha_k+\mu_k}\frac{1}{\alpha_v+\mu_v}\frac{1}{\phi_V}\frac{N_h\alpha_h\Lambda_H}{G_0\mu_H\alpha_H+N_h\alpha_h\Lambda_H}\frac{\beta_H(\Lambda_V-\mu_V)}{\Lambda_V+\mu_V}, \\
0 &\leq P_V \leq \frac{1}{2}\frac{N_g\alpha_g}{\alpha_g+\mu_g}\frac{\alpha_s}{\mu_s+\mu_s}\frac{\alpha_z}{\alpha_z+\mu_z}\frac{N_k\alpha_k}{\alpha_k+\mu_k}\frac{\alpha_v}{\alpha_v+\mu_v}\frac{1}{\phi_V}\frac{1}{\alpha_V}\frac{N_h\alpha_h\Lambda_H}{G_0\mu_H\alpha_H+N_h\alpha_h\Lambda_H}\frac{\beta_H(\Lambda_V-\mu_V)}{\mu_V},
\end{aligned}
\tag{3.2.3.6}
$$

for

$$\Lambda_V > \mu_V$$

Thus, the region Ω is positively invariant. It is sufficient to consider the dynamics of the flow generated by model system (3.2.1.13) in Ω. Thus, every solution of multiscale model (3.2.1.13) with initial condition in Ω remains in Ω for all $t > 0$.

3.2.4 Reproductive Number

We use the next generation operator approach to calculate the basic reproductive number and we use the [61]'s approach . Model system (3.2.1.13) can be written in the form

$$
\begin{aligned}
\frac{dX}{dt} &= f(X,Y,Z), \\
\frac{dY}{dt} &= g(X,Y,Z), \\
\frac{dZ}{dt} &= h(X,Y,Z),
\end{aligned}
\tag{3.2.4.1}
$$

where

$$
\begin{aligned}
X &= (S_H, S_V), \\
Y &= (I_H, I_V, G_v, G_m, Z_m, O_v, P_v), \\
Z &= (P_V, G_H).
\end{aligned}
\tag{3.2.4.2}
$$

Components of X denote the number of susceptibles, while combonents of Y represent the number of infected individuals that do not transmit the disease. Components of Z denotes the number of individuals capable of transmitting the disease. We define $\tilde{g}(X^*, Z)$ by

$$\begin{aligned}\tilde{g}(X^*, Z) &= (\tilde{g}_1(X^*, Z), \tilde{g}_2(X^*, Z), \tilde{g}_3(X^*, Z), \tilde{g}_4(X^*, Z), \tilde{g}_5(X^*, Z), \tilde{g}_6(X^*, Z), \\ &\quad \tilde{g}_7(X^*, Z)),\end{aligned} \tag{3.2.4.3}$$

with

$$\begin{aligned}
\tilde{g}_1(X^*, Z) &= \frac{1}{\mu_H + \gamma_H + \delta_H} \frac{\beta_V \Lambda_H}{\mu_H} \frac{P_V}{P_0 + P_V}, \\
\tilde{g}_2(X^*, Z) &= \frac{1}{\mu_V + \delta_V} \frac{\beta_H \Lambda_V}{\mu_V} \frac{G_H}{G_0 + G_H}, \\
\tilde{g}_3(X^*, Z) &= \frac{1}{\alpha_g + \alpha_g} \frac{1}{\phi_V} \frac{\beta_H(\Lambda_V - \mu_V)}{\mu_V} \frac{1}{I_V + 1} \frac{G_H}{G_0 + G_H}, \\
\tilde{g}_4(X^*, Z) &= \frac{N_g \alpha_g}{\alpha_g + \alpha_g} \frac{1}{\alpha_s + \mu_s} \frac{1}{\phi_V} \frac{\beta_H(\Lambda_V - \mu_V)}{\mu_V} \frac{1}{I_V + 1} \frac{G_H}{G_0 + G_H}, \\
\tilde{g}_5(X^*, Z) &= \frac{1}{2} \frac{N_g \alpha_g}{\alpha_g + \alpha_g} \frac{\alpha_s}{\alpha_s + \mu_s} \frac{1}{\alpha_z + \mu_z} \frac{1}{\phi_V} \frac{\beta_H(\Lambda_V - \mu_V)}{\mu_V} \frac{1}{I_V + 1} \frac{G_H}{G_0 + G_H}, \\
\tilde{g}_6(X^*, Z) &= \frac{1}{2} \frac{N_g \alpha_g}{\alpha_g + \alpha_g} \frac{\alpha_s}{\alpha_s + \mu_s} \frac{\alpha_z}{\alpha_z + \mu_z} \frac{1}{\alpha_k + \mu_k} \frac{1}{\phi_V} \frac{\beta_H(\Lambda_V - \mu_V)}{\mu_V} \frac{1}{I_V + 1} \frac{G_H}{G_0 + G_H}, \\
\tilde{g}_7(X^*, Z) &= \frac{1}{2} \frac{N_g \alpha_g}{\alpha_g + \alpha_g} \frac{\alpha_s}{\alpha_s + \mu_s} \frac{\alpha_z}{\alpha_z + \mu_z} \frac{N_k \alpha_k}{\alpha_k + \mu_k} \frac{1}{\alpha_v + \mu_v} \frac{1}{\phi_V} \frac{\beta_H(\Lambda_V - \mu_V)}{\mu_V} \frac{1}{I_V + 1} \frac{G_H}{G_0 + G_H}.
\end{aligned} \tag{3.2.4.4}$$

By substituting the values of I_H, I_V, G_v, G_m, Z_v, O_z and P_v and letting $h_1 = \frac{dP_V}{dt}$, $h_2 = \frac{dG_H}{dt}$ we obtain

$$\begin{aligned}
h_1 &= \frac{1}{2} \frac{N_g \alpha_g}{\alpha_g + \mu_g} \frac{N_k \alpha_k}{\alpha_k + \mu_k} \frac{\alpha_s}{\alpha_s + \mu_s} \frac{\alpha_z}{\alpha_z + \mu_z} \frac{\alpha_v}{\alpha_v + \mu_v} \frac{1}{\phi_V} \frac{\beta_H(\Lambda_V - \mu_V)}{\mu_V} \frac{G_H}{G_0 + G_{H|}} - \alpha_V P_V, \\
h_2 &= \frac{N_h \alpha_h}{\mu_H + \gamma_H + \delta_H} \frac{\beta_V \Lambda_H}{\mu_H} \frac{G_H}{G_0 + G_H} - \alpha_H G_H.
\end{aligned} \tag{3.2.4.5}$$

Let $A = D_z(X^*, \tilde{g}(X^*, 0), 0)$ and further assume that A can be written in the form $A = M - D$, where $M \geq 0$ and $D > 0$, a diagonal matrix.

$$A = \begin{pmatrix} \frac{\partial h_1}{\partial P_V} & \frac{\partial h_1}{\partial G_H} \\ \frac{\partial h_2}{\partial P_V} & \frac{\partial h_2}{\partial G_H} \end{pmatrix},$$

then A becomes

$$A = \begin{pmatrix} -\alpha_V & \frac{1}{2}\frac{N_g\alpha_g}{\alpha_g+\mu_g}\frac{N_k\alpha_k}{\alpha_k+\mu_k}\frac{\alpha_s}{\alpha_s+\mu_s}\frac{\alpha_z}{\alpha_z+\mu_z}\frac{\alpha_v}{\alpha_v+\mu_v}\frac{1}{\phi_V}\frac{1}{G_0}\frac{\beta_H(\Lambda_V-\mu_V)}{\mu_V} \\ \frac{1}{\mu_H+\gamma_H+\delta_H}\frac{N_h\alpha_h}{P_0}\frac{\beta_V\Lambda_H}{\mu_H} & -\alpha_H \end{pmatrix}. \tag{3.2.4.6}$$

We deduce matrices M and D to be

$$M = \begin{pmatrix} 0 & \frac{1}{2}\frac{N_g\alpha_g}{\alpha_g+\mu_g}\frac{N_k\alpha_k}{\alpha_k+\mu_k}\frac{\alpha_s}{\alpha_s+\mu_s}\frac{\alpha_z}{\alpha_z+\mu_z}\frac{\alpha_v}{\alpha_v+\mu_v}\frac{1}{\phi_V}\frac{1}{G_0}\frac{\beta_H(\Lambda_V-\mu_V)}{\mu_V} \\ \frac{1}{\mu_H+\gamma_H+\delta_H}\frac{N_h\alpha_h}{P_0}\frac{\beta_V\Lambda_H}{\mu_H} & 0 \end{pmatrix}, \tag{3.2.4.7}$$

and

$$D = \begin{pmatrix} \alpha_V & 0 \\ 0 & \alpha_H \end{pmatrix} \Longrightarrow D^{-1} = \begin{pmatrix} \frac{1}{\alpha_V} & 0 \\ 0 & \frac{1}{\alpha_H} \end{pmatrix}. \tag{3.2.4.8}$$

The basic reproductive number is a spectral radius (dominant eigenvalue) of the matrix MD^{-1}, that is $R_0 = \rho(MD^{-1})$. Therefore $R_0 =$

$$\sqrt{\left(\frac{1}{2}\frac{N_k\alpha_k}{\alpha_k+\mu_k}\frac{N_g\alpha_g}{\alpha_g+\mu_g}\frac{\alpha_s}{\alpha_s+\mu_s}\frac{\alpha_z}{\alpha_z+\mu_z}\frac{\alpha_v}{\alpha_v+\mu_v}\frac{1}{G_0}\frac{1}{\phi_V}\frac{1}{\alpha_H}\frac{\beta_H(\Lambda_V-\mu_V)}{\mu_V}\right)\left(\frac{N_h\alpha_h}{\alpha_V}\frac{1}{\mu_H+\gamma_H+\delta_H}\frac{1}{P_0}\frac{\beta_V\Lambda_H}{\mu_H}\right)}$$

where $\Lambda_V > \mu_V$.

3.2.5 Local Stability analysis of disease-free equilibrium point

We investigated the local stability of the disease-free-equilibrium.

Theorem 3.2. *The disease-free equilibrium point is locally asymptotically stable when* $R_0 < 1$.

Proof. We linearize the system of equations (3.2.1.13), obtain the Jacobian matrix J at the infection-free steady state E^*, and calculate the matrix $|J(E^*) - \lambda I|$ as follows, where λ is the eigenvalue and I is the identity matrix with the same dimension as $J(E^*)$. Where the disease-free equilibrium is given by

$$\begin{aligned} E^* &= (S_H^*, I_H^*, G_H^*, S_V^*, I_V^*, G_v^*, G_m^*, Z_v^*, O_v^*, P_v^*, P_V^*), \\ &= \left(\frac{\Lambda_H}{\mu_H}, 0, 0, \frac{\Lambda_V}{\mu_V}, 0, 0, 0, 0, 0, 0, 0\right). \end{aligned} \tag{3.2.5.1}$$

$$J(E^*) = \begin{bmatrix} -\mu_H & \gamma_H & 0 & 0 & 0 & 0 & 0 & 0 & 0 & 0 & -\frac{\beta_V \Lambda_H}{\mu_H P_0} \\ 0 & -k_1 & 0 & 0 & 0 & 0 & 0 & 0 & 0 & 0 & \frac{\beta_V \Lambda_H}{\mu_H P_0} \\ 0 & N_h\alpha_h & -\alpha_H & 0 & 0 & 0 & 0 & 0 & 0 & 0 & 0 \\ 0 & 0 & -\frac{\beta_H \Lambda_V}{\mu_V G_0} & -\mu_V & 0 & 0 & 0 & 0 & 0 & 0 & \\ 0 & 0 & \frac{\beta_H \Lambda_V}{\mu_V G_H} & 0 & -J_1 & 0 & & 0 & 0 & 0 & 0 \\ 0 & 0 & J_2 & 0 & 0 & -k_2 & 0 & 0 & 0 & 0 & 0 \\ 0 & 0 & 0 & 0 & 0 & N_g\alpha_g & -k_3 & 0 & 0 & 0 & 0 \\ 0 & 0 & 0 & 0 & 0 & 0 & \frac{1}{2}\alpha_s & -k_4 & 0 & 0 & 0 \\ 0 & 0 & 0 & 0 & 0 & 0 & 0 & \alpha_z & -k_5 & 0 & 0 \\ 0 & 0 & 0 & 0 & 0 & 0 & 0 & 0 & N_k\alpha_k & -k_6 & 0 \\ 0 & 0 & 0 & 0 & 0 & 0 & 0 & 0 & 0 & \alpha_v & -\alpha_V \end{bmatrix},$$

where $k_1 = (\mu_H + \gamma_H + \delta_H)$, $k_2 = (\alpha_g + \mu_g)$, $k_3 = \alpha_s + \mu_s$, $k_4 = \alpha_z + \mu_z$, $k_5 = (\alpha_k + \mu_k)$, $k_6 = (\alpha_v + \alpha_v)$, $J_1 = (\delta_V + \mu_V)$, and $J_2 = \dfrac{\beta_H(\Lambda_V - \mu_V)}{\mu_V \phi_V G_0}$.

$$\begin{aligned} |J(E^*) - \lambda I| &= 0, \\ (\mu_H + \lambda)(\mu_V + \lambda)(J_1 + \lambda)\{(k_1 + \lambda)(\alpha_H + \lambda)(k_2 + \lambda)(k_3 + \lambda)(k_4 + \lambda)(k_5 + \lambda)\times \\ (k_6 + \lambda)(\alpha_V + \lambda) - \frac{1}{2}N_h\alpha_h \frac{\beta_V \Lambda_H}{\mu_H P_0} \frac{\beta_H(\Lambda_V - \mu_V)}{\mu_V G_0 \phi_V} N_g\alpha_g\alpha_s\alpha_z N_k\alpha_k\alpha_v\Big\} &= 0. \end{aligned} \tag{3.2.5.2}$$

The disease-free steady state is locally asymptotically stable if and only if all the roots of the characteristic equation are negative or have negative real parts. $\lambda_1 = -\mu_H$, $\lambda_2 = -\mu_V$, $\lambda_3 = -(\delta_V + \mu_V)$ and

$$a_0\lambda^8 + a_1\lambda^7 + a_2\lambda^6 + a_3\lambda^5 + a_4\lambda^4 + a_5\lambda^3 + a_6\lambda^2 + a_7\lambda + a_8 = 0, \tag{3.2.5.3}$$

where

$$\begin{aligned} a_0 &= 1, \\ a_1 &= k_1 + k_2 + k_3 + k_4 + k_5 + k_6 + \alpha_H + \alpha_V, \\ a_2 &= k_1k_2 + k_1k_3 + k_1k_4 + k_1k_5 + k_1k_6 + k_1\alpha_H + k_1\alpha_V + k_2k_3 + k_2k_4 + k_2k_5 + k_2k_6 + k_2\alpha_H + k_2\alpha_V \\ &\quad + k_3k_4 + k_3k_5 + k_3k_6 + k_3\alpha_H + k_3\alpha_V + k_4k_5 + k_4k_6 + k_4\alpha_H + k_4\alpha_V + k_5k_6 + k_5\alpha_H + k_5\alpha_V + \\ &\quad k_6\alpha_H + k_6\alpha_V + \alpha_H\alpha_V, \end{aligned} \tag{3.2.5.4}$$

$$a_3 = k_1k_2k_3 + k_1k_2k_4 + k_1k_2k_5 + k_1k_2k_6 + k_1k_2\alpha_H + k_1k_2\alpha_V + k_1k_3k_4 + k_1k_3k_5 + k_1k_3k_6 + k_1k_3\alpha_H + k_1k_3\alpha_V + k_1k_4k_5 + k_1k_4k_6 + k_1k_4\alpha_H + k_1k_4\alpha_V + k_1k_5k_6 + k_1k_5\alpha_H + k_1k_5\alpha_V + k_1k_6\alpha_H + k_1k_6\alpha_V + k_1\alpha_H\alpha_V + k_2k_3k_4 + k_2k_3k_5 + k_2k_3k_6 + k_2k_3\alpha_H + k_2k_3\alpha_V + k_2k_4k_5 + k_2k_4k_6 + k_2k_4\alpha_H + k_2k_4\alpha_V + k_2k_5k_6 + k_2k_5\alpha_H + k_2k_5\alpha_V + k_2k_6\alpha_H + k_2k_6\alpha_V + k_2\alpha_H\alpha_V + k_3k_4k_5 + k_3k_4k_6 + k_3k_4\alpha_H + k_3k_4\alpha_V + k_3k_5k_6 + k_3k_5\alpha_H + k_3k_5\alpha_V + k_3k_6\alpha_H + k_3k_6\alpha_V + k_3\alpha_H\alpha_V + k_4k_5k_6 + k_4k_5\alpha_H + k_4k_5\alpha_V + k_4k_6\alpha_H + k_4k_6\alpha_V + k_4\alpha_H\alpha_V + k_5k_6\alpha_H + k_5k_6\alpha_V + k_5\alpha_H\alpha_V + k_6\alpha_H\alpha_V, \quad (3.2.5.5)$$

$$a_4 = k_1k_2k_3k_4 + k_1k_2k_3k_5 + k_1k_2k_3k_6 + k_1k_2k_3\alpha_H + k_1k_2k_3\alpha_V + k_1k_2k_4k_5 + k_1k_2k_4k_6 + k_1k_2k_4\alpha_H + k_1k_2k_4\alpha_V + k_1k_2k_5k_6 + k_1k_2k_5\alpha_H + k_1k_2k_5\alpha_V + k_1k_2k_6\alpha_H + k_1k_2k_6\alpha_V + k_1k_2\alpha_H\alpha_V + k_1k_3k_4k_5 + k_1k_3k_4k_6 + k_1k_3k_4\alpha_H + k_1k_3k_4\alpha_V + k_1k_3k_5k_6 + k_1k_3k_5\alpha_H + k_1k_3k_5\alpha_V + k_1k_3k_6\alpha_H + k_1k_3k_6\alpha_V + k_1k_3\alpha_H\alpha_V + k_1k_4k_5k_6 + k_1k_4k_5\alpha_H + k_1k_4k_5\alpha_V + k_1k_4k_6\alpha_H + k_1k_4k_6\alpha_V + k_1k_4\alpha_H\alpha_V + k_1k_5k_6\alpha_H + k_1k_5k_6\alpha_V + k_1k_5\alpha_H\alpha_V + k_1k_6\alpha_H\alpha_V + k_2k_3k_4k_5 + k_2k_3k_4k_6 + k_2k_3k_4\alpha_H + k_2k_3k_4\alpha_V + k_2k_3k_5k_6 + k_2k_3k_5\alpha_H + k_2k_3k_5\alpha_V + k_2k_3k_6\alpha_H + k_2k_3k_6\alpha_V + k_2k_3\alpha_H\alpha_V + k_2k_4k_5k_6 + k_2k_4k_5\alpha_H + k_2k_4k_5\alpha_V + k_2k_4k_6\alpha_H + k_2k_4k_6\alpha_V + k_2k_4\alpha_H\alpha_V + k_2k_5k_6\alpha_H + k_2k_5k_6\alpha_V + k_2k_6\alpha_H\alpha_V + k_3k_4k_5k_6 + k_3k_4k_5\alpha_H + k_3k_4k_5\alpha_V + k_3k_4k_6\alpha_H + k_3k_4k_6\alpha_V + k_3k_4\alpha_H\alpha_V + k_3k_5k_6\alpha_H + k_3k_5k_6\alpha_V + k_3k_5\alpha_H\alpha_V + k_3k_6\alpha_H\alpha_V + k_4k_5k_6\alpha_H + k_4k_5k_6\alpha_V + k_4k_5\alpha_H\alpha_V + k_4k_6\alpha_H\alpha_V + k_5k_6\alpha_H\alpha_V, \quad (3.2.5.6)$$

$$a_5 = k_1k_2k_3k_4k_5 + k_1k_2k_3k_4k_6 + k_1k_2k_3k_4\alpha_H + k_1k_2k_3k_4\alpha_V + k_1k_2k_3k_5k_6 + k_1k_2k_3k_5\alpha_H + k_1k_2k_3k_5\alpha_V + k_1k_2k_3k_6\alpha_H + k_1k_2k_3k_6\alpha_V + k_1k_2k_3\alpha_H\alpha_V + k_1k_2k_4k_5k_6 + k_1k_2k_4k_5\alpha_H + k_1k_2k_4k_5\alpha_V + k_1k_2k_4k_6\alpha_H + k_1k_2k_4k_6\alpha_V + k_1k_2k_4\alpha_H\alpha_V + k_1k_2k_5k_6\alpha_H + k_1k_2k_5k_6\alpha_V + k_1k_2k_5\alpha_H\alpha_V + k_1k_2k_6\alpha_H\alpha_V + k_1k_3k_4k_5k_6 + k_1k_3k_4k_5\alpha_H + k_1k_3k_4k_5\alpha_V + k_1k_3k_4k_6\alpha_H + k_1k_3k_4k_6\alpha_V + k_1k_3k_4\alpha_H\alpha_V + k_1k_3k_5k_6\alpha_H + k_1k_3k_5k_6\alpha_V + k_1k_3k_5\alpha_H\alpha_V + k_1k_3k_6\alpha_H\alpha_V + k_1k_4k_5k_6\alpha_H + k_1k_4k_5k_6\alpha_V + k_1k_4k_5\alpha_H\alpha_V + k_1k_4k_6\alpha_H\alpha_V + k_1k_5k_6\alpha_H\alpha_V + k_2k_3k_4K_5k_6 + k_2k_3k_4K_5\alpha_H + k_2k_3k_4K_5\alpha_V + k_2k_3k_4K_6\alpha_H + k_2k_3k_4K_6\alpha_V + k_2k_3k_4\alpha_H\alpha_V + k_2k_3k_5k_6\alpha_H + k_2k_3k_5k_6\alpha_V + k_2k_3k_5\alpha_H\alpha_V + k_2k_3k_6\alpha_H\alpha_V + k_2k_4k_5k_6\alpha_H + k_2k_4k_5k_6\alpha_V + k_2k_4k_5\alpha_H\alpha_V + k_2k_4k_6\alpha_H\alpha_V + k_2k_5k_6\alpha_H\alpha_V + k_3k_4k_5k_6\alpha_H + k_3k_4k_5k_6\alpha_V + k_3k_4k_5\alpha_H\alpha_V + k_3k_4k_6\alpha_H\alpha_V + k_3k_5k_6\alpha_H\alpha_V + k_4k_5k_6\alpha_H\alpha_V, \quad (3.2.5.7)$$

$$a_6 = k_1k_2k_3k_4k_5k_6 + k_1k_2k_3k_4k_5\alpha_H + k_1k_2k_3k_4k_5\alpha_V + k_1k_2k_3k_4k_6\alpha_H + k_1k_2k_3k_4k_6\alpha_V + k_1k_2k_3k_4\alpha_H\alpha_V + k_1k_2k_3k_5k_6\alpha_H + k_1k_2k_3k_5k_6\alpha_V + k_1k_2k_3k_5\alpha_H\alpha_V + k_1k_2k_3k_6\alpha_H\alpha_V + k_1k_2k_4k_5k_6\alpha_H + k_1k_2k_4k_5k_6\alpha_V + k_1k_2k_4k_5\alpha_H\alpha_V + k_1k_2k_4k_6\alpha_H\alpha_V + k_1k_2k_5k_6\alpha_H\alpha_V + k_1k_3k_4k_5k_6\alpha_H + k_1k_3k_4k_5k_6\alpha_V + k_1k_3k_4k_5\alpha_H\alpha_V + k_1k_3k_4k_6\alpha_H\alpha_V + k_1k_3k_5k_6\alpha_H\alpha_V + k_1k_4k_5k_6\alpha_H\alpha_V + k_2k_3k_4k_5k_6\alpha_H + k_2k_3k_4k_5k_6\alpha_V + k_2k_3k_4k_5\alpha_H\alpha_V + k_2k_3k_4k_6\alpha_H\alpha_V + k_2k_3k_5k_6\alpha_H\alpha_V + k_2k_4k_5k_6\alpha_H\alpha_V + k_3k_4k_5k_6\alpha_H\alpha_V, \quad (3.2.5.8)$$

$$a_7 = k_1k_2k_3k_4k_5k_6\alpha_H + k_1k_2k_3k_4k_5k_6\alpha_V + k_1k_2k_3k_4k_6\alpha_H\alpha_V + k_1k_2k_3k_4k_5\alpha_H\alpha_V + k_1k_2k_3k_5k_6\alpha_H\alpha_V + k_1k_2k_4k_5k_6\alpha_H\alpha_V + k_1k_3k_4k_5k_6\alpha_H\alpha_V + k_2k_3k_4k_5k_6\alpha_H\alpha_V, \quad (3.2.5.9)$$

$$a_8 = k_1k_2k_3k_4k_5k_6\alpha_H\alpha_V\left[1 - R_0^2\right]. \quad (3.2.5.10)$$

It is clear that $a_0 > 0$, $a_1 > 0$, $a_2 > 0$, $a_3 > 0$, $a_4 > 0$, $a_5 > 0$, $a_6 > 0$ and $a_7 > 0$ and $a_8 > 0$ whenever $R_0 < 1$. To confirm that all the roots of the systems of equations (3.2.5.2) have negative real parts, we shall use Descarte's law of signs to determine the possible number of positive roots of equation (3.2.5.3) as shown in table (3.1).

use Descartes' Rule of signs change, we observe that on characteristic equation (3.2.5.3) there is no sign changes in the sequence of coefficients and so there is zero real positive roots.

Table 3.1: Possible number of positive roots of the characteristic equation (3.2.5.3)

	a_0	a_1	a_2	a_3	a_4	a_5	a_6	a_7	a_8	**The number of positive roots**
$R_0 < 1$	+	+	+	+	+	+	+	+	+	0
$R_0 > 1$	+	+	+	+	+	+	+	+	-	1

When $R_0 < 1$ we notice that $a_8 > 0$ and there is no change of sign and conclude that the equation (3.2.5.3) has zero positive roots. When $R_0 > 1$, we observe that $a_8 < 0$, and there is only one change of sign and conclude that the characteristic equation (3.2.5.3) has atleast one positive root. The roots of the characteristic equation (3.2.5.2) are all negative or have negative real parts. Therefore, all the eigenvalues of the Jacobian matrix $J(E^*)$ are negative or have negative real parts when $R_0 < 1$. This proves that E^* is locally stable when$R_0 \leq 1$. □

3.2.6 Determination of endemic equilibrium

The equilibrium point of the model are obtained by setting the right-hand-side of the systems of equations (3.2.1.13) to zero.

$$
\begin{aligned}
\tilde{S}_H &= \frac{\Lambda_H(\delta_H+\gamma_H+\mu_H)(P_0+\tilde{P}_V)}{a_1(P_0+P_V)+a_2\tilde{P}_V},\\
\tilde{I}_H &= \frac{\beta_V\Lambda_H\tilde{P}_V}{a_1(P_0+P_V)+a_2\tilde{P}_V},\\
\tilde{S}_V &= \frac{\Lambda_V\left[N_h\alpha_h\beta_V\Lambda_H\tilde{P}_V+\alpha_H G_0[a_1(P_0+\tilde{P}_V)+a_2\tilde{P}_V]\right]}{N_h\alpha_h\beta_V\Lambda_H\tilde{P}_V(\beta_H+\mu_V)+\mu_V\alpha_H G_0[a_1(P_0+\tilde{P}_V)+a_2\tilde{P}_V]},\\
\tilde{I}_V &= \frac{N_h\alpha_h\beta_V\Lambda_H\beta_H\Lambda_V\tilde{P}_V}{(\mu_V+\delta_V)\left[N_h\alpha_h\beta_V\Lambda_H\tilde{P}_V(\beta_H+\mu_V)+\alpha_H G_0\mu_V[a_1(P_0+\tilde{P}_V)+a_2\tilde{P}_V]\right]},\\
\tilde{G}_H &= \frac{N_h\alpha_h\beta_V\Lambda_H\tilde{P}_V}{\alpha_H[a_1(P_0+\tilde{P}_V)+a_2\tilde{P}_V]},\\
\tilde{G}_v &= \frac{N_h\alpha_h\beta_V\Lambda_H\beta_H\tilde{P}_V\left[a_1\alpha_H G_0P_0(\Lambda_V-\mu_V)+b_1\tilde{P}_V\right]}{[b_2\tilde{P}_V+\alpha_H a_1G_0P_0]\phi(\tilde{I}_V+1)(\alpha_g+\mu_g)(b_3\tilde{P}_V+a_1\mu_V\alpha_H G_0P_0)},\\
\tilde{G}_m &= \frac{N_g\alpha_g N_h\alpha_h\beta_V\Lambda_H\beta_H\tilde{P}_V\left[a_1\alpha_H G_0P_0(\Lambda_V-\mu_V)+b_1\tilde{P}_V\right]}{(\alpha_s+\mu_s)[b_2\tilde{P}_V+\alpha_H a_1G_0P_0]\phi(\tilde{I}_V+1)(\alpha_g+\mu_g)(b_3\tilde{P}_V+a_1\mu_V\alpha_H G_0P_0)},\\
\tilde{Z}_v &= \frac{0.5N_g\alpha_g\alpha_s N_h\alpha_h\beta_V\Lambda_H\beta_H\tilde{P}_V\left[b_1\tilde{P}_V+a_1\alpha_H G_0P_0(\Lambda_V-\mu_V)\right]}{(\alpha_s+\mu_s)(\alpha_z+\mu_z)[b_2\tilde{P}_V+\alpha_H a_1G_0P_0]\phi(\tilde{I}_V+1)(\alpha_g+\mu_g)(b_3\tilde{P}_V+a_1\mu_V\alpha_H G_0P_0)},\\
\tilde{O}_v &= \frac{0.5N_g\alpha_g\alpha_s\alpha_z N_h\alpha_h\beta_V\Lambda_H\beta_H\tilde{P}_V\left[b_1\tilde{P}_V+a_1\alpha_H G_0P_0(\Lambda_V-\mu_V)\right]}{(\alpha_s+\mu_s)(\alpha_z+\mu_z)(\alpha_k+\mu_k)[b_2\tilde{P}_V+\alpha_H a_1G_0P_0]\phi(\tilde{I}_V+1)(\alpha_g+\mu_g)(b_3\tilde{P}_V+a_1\mu_V\alpha_H G_0P_0)},\\
\tilde{P}_v &= \frac{c_1\tilde{P}_V\left[b_1\tilde{P}_V+a_1\alpha_H G_0P_0(\Lambda_V-\mu_V)\right]}{c_2(I_V+1)(b_2\tilde{P}_V+a_1\alpha_H G_0P_0)(b_3\tilde{P}_V+a_1\mu_V\alpha_H G_0P_0)},\\
\tilde{P}_V &= \frac{c_1\alpha_v\tilde{P}_V\left[b_1\tilde{P}_V+a_1\alpha_H G_0P_0(\Lambda_V-\mu_V)\right]}{c_2\alpha_V(b_2\tilde{P}_V+a_1\alpha_H G_0P_0)(b_3\tilde{P}_V+a_1\mu_V\alpha_H G_0P_0)}\\
\tilde{P}_V &= \frac{-D_2+\sqrt{D_2^2-4D_1D_3}}{2(D_1)},
\end{aligned}
\tag{3.2.6.1}
$$

where

$$\begin{aligned} a_1 &= \mu_H(\delta_H + \gamma_H + \mu_H), \\ a_2 &= \beta_V(\delta_H + \mu_H), \\ b_1 &= \alpha_H G_0(a_1 + a_2)(\Lambda_V - \mu_V) + N_h\alpha_h\beta_V\Lambda_H[\Lambda_V - (\beta_H + \mu_V)], \\ b_2 &= N_h\alpha_h\beta_V\Lambda_H + \alpha_H G_0(a_1 + a_2), \\ b_3 &= N_h\alpha_h\beta_V\Lambda_H(\beta_H + \mu_V) + \mu_V\alpha_H G_0(a_1 + a_2), \end{aligned} \tag{3.2.6.2}$$

$$\begin{aligned} c_1 &= 0.5N_k\alpha_k N_g\alpha_g\alpha_s\alpha_z N_h\alpha_h\beta_H\beta_V\Lambda_H, \\ c_2 &= \phi(\alpha_v + \mu_v)(\alpha_s + \mu_s)(\alpha_z + \mu_z)(\alpha_k + \mu_k)(\alpha_g + \mu_g), \\ D_1 &= b_2b_3c_2\alpha_V, \\ D_2 &= a_1c_2\alpha_H\alpha_V G_0P_0(\mu_V b_2 + b_3) - b_1c_1\alpha_v, \\ D_3 &= -a_1^2\alpha_H^2 G_0^2P_0^2c_2\alpha_V\mu_V\left[R_0^2 - 1\right]. \end{aligned}$$

1. $\tilde{P}_V = 0$, if $R_0 = 1$, $D_1 > 0$, and $D_3 = 0$, therefore $\tilde{P}_V$ will be at the disease free equilibrium point.

2. $\tilde{P}_V < 0$, when $R_0 < 1$, $D_1 > 0$, $D_3 > 0$.Therefore, $\tilde{P}_V$ is not a positive equilibrium point because of Descartes rule of signs, there is no sign of change from the coefficients.

3. $\tilde{P}_V > 0$, when $R_0 > 1$, $D_1 > 0$, $D_3 < 0$, the co-efficient D_2 could be positive or negative, therefore $\tilde{P}_V$ is a positive equilibrium point, according to Descartes rule of signs.

Therefore, we conclude that there exist a positive endemic equilibrium points when $R_0 > 1$.

3.2.6.1 Local Stability analysis of endemic equilibrium point

The endemic equilibrium is given by

$$E^{**} = \left(\tilde{S}_H, \tilde{I}_H, \tilde{G}_H, \tilde{S}_V, \tilde{I}_V, \tilde{G}_v, \tilde{G}_m, \tilde{Z}_v, \tilde{O}_v, \tilde{P}_v, \tilde{P}_V\right).$$

The infected steady state exists if and only if $R_0 > 1$. The following results shows the chronic infection is established when $R_0 > 1$.

Theorem 3.3. *The endemic equilibrium point E^{**} of systems of equations 3.2.1.13 is locally asymptotically stable when $R_0 > 1$.*

Proof. We obtain the Jacobian matrix at the endemic equilibrium (E^{**}) and calculate the Jacobian matrix $J(E^{**})$ is given by

$$J(E^{**}) = \begin{bmatrix} -j_0 & \gamma_H & 0 & 0 & 0 & 0 & 0 & 0 & 0 & 0 & -\frac{\beta_V P_0 \tilde{S}_H}{(P_0+\tilde{P}_V)^2} \\ \frac{\beta_V \tilde{P}_V}{P_0+\tilde{P}_V} & -j_1 & 0 & 0 & 0 & 0 & 0 & 0 & 0 & 0 & \frac{\beta_V P_0 \tilde{S}_H}{(P_0+\tilde{P}_V)^2} \\ 0 & N_h\alpha_h & -\alpha_H & 0 & 0 & 0 & 0 & 0 & 0 & 0 & 0 \\ 0 & 0 & -j_2 & -j_3 & 0 & 0 & 0 & 0 & 0 & 0 & 0 \\ 0 & 0 & j_2 & j_4 & -j_7 & 0 & 0 & 0 & 0 & 0 & 0 \\ 0 & 0 & j_6 & j_5 & -j_{14} & -j_8 & 0 & 0 & 0 & 0 & 0 \\ 0 & 0 & 0 & 0 & 0 & N_g\alpha_g & -j_9 & 0 & 0 & 0 & 0 \\ 0 & 0 & 0 & 0 & 0 & 0 & \frac{1}{2}\alpha_s & -j_{10} & 0 & 0 & 0 \\ 0 & 0 & 0 & 0 & 0 & 0 & 0 & \alpha_z & -j_{11} & 0 & 0 \\ 0 & 0 & 0 & 0 & 0 & 0 & 0 & 0 & N_k\alpha_k & -j_{12} & 0 \\ 0 & 0 & 0 & 0 & \alpha_v\tilde{P}_v & 0 & 0 & 0 & 0 & j_{13} & -\alpha_V \end{bmatrix},$$

where

$$j_0 = \mu_H + \frac{\beta_V \tilde{P}_V}{P_0+\tilde{P}_V}, \quad j_1 = (\delta_H + \gamma_H + \mu_H), \quad j_2 = \frac{\beta_H G_0 \tilde{S}_V}{(G_0+\tilde{G}_H)^2},$$
$$j_3 = \frac{\beta_H \tilde{G}_H}{G_0+\tilde{G}_H} + \mu_V, \quad j_4 = \frac{\beta_H \tilde{G}_H}{G_0+\tilde{G}_H}, \quad j_5 = \frac{\beta_H \tilde{G}_H}{(G_0+\tilde{G}_H)\phi_V(\tilde{I}_V+1)},$$
$$j_6 = \frac{\beta_H G_0(\tilde{S}_V-1)}{(G_0+\tilde{G}_H)^2\phi_V(\tilde{I}_V+1)}, \quad j_7 = (\delta_V + \mu_V), \quad j_8 = (\alpha_g + \mu_g),$$
$$j_9 = (\alpha_s + \mu_s), \quad j_{10} = (\alpha_z + \mu_z), \quad j_{11} = (\alpha_k + \mu_k),$$
$$j_{12} = (\alpha_v + \mu_v), \quad j_{13} = \alpha_v(\tilde{I}_V+1), \quad \text{and } j_{14} = \frac{\beta_H \tilde{G}_H(\tilde{S}_V-1)}{(G_0+\tilde{G}_H)\phi_V(\tilde{I}_V+1)^2}$$

Where $\tilde{S}_H$, $\tilde{G}_H$, $\tilde{S}_V$, $\tilde{I}_V$, $\tilde{P}_V$ and $\tilde{P}_v$ are given in equations (3.2.6.1). The characteristic equation of the Jacobian matrix evaluated at the endemic equilibrium point (E^{**}) is given by

$$|J(E^{**}) - \lambda I| = 0. \tag{3.2.6.3}$$

To find the eigenvalues of the characteristic equation (3.2.6.3), we use numerical solutions. Parameter values are given in the tables (3.2) and (3.3). The eigenvalues are given by

$$\lambda_1 = -96.606, \quad \lambda_2 = -58.08, \quad \lambda_3 = -1.424,$$
$$\lambda_4 = -0.4760, \quad \lambda_5 = -0.0002720, \quad \lambda_6 = -0.00009130,$$
$$\lambda_7 = -0.028467, \quad \lambda_8 = -0.02510, \quad \lambda_9 = -0.2100,$$
$$\lambda_{10} = -0.120004 \quad \textbf{and } \lambda_{11} = -0.9000$$

All the eigenvalues of the Jacobian matrix are negative. This proves that E^{**} is locally asymptotically stable. □

3.3 Results

3.3.1 Numerical Simulation

We compute the model system (3.2.0.1) to outline the influence of variation on parameter values. The behaviour of model system (3.2.0.1) was analysed using numerical simulations using a python program version 2.7. The numerical simulation of the model system was used to predict malaria disease system for long term trends for human population and mosquito population. The numerical simulations were performed utilising a set of within-host scale (human and mosquito) and between-host(human and mosquito) parameters defined in Table 3.3 and Table 3.2 for within-mosquito and between-host respectively. The reason why some parameter values are assumed or estimated is that the multiscale modeling of malaria infectious disease, which includes the within-human host scale and within-mosquito scale, are limited or the parameter values found in existing literature are not suitable for this model. The dynamics of some epidemiological class of the model are simulated with time and also the effects of sensitivity parameters to demonstrate the behaviour of the model. The dynamics of some epidemiological class of the model are simulated with time as well as the influences of sensitivity parameters to demonstrate the behaviour of the model in the following, we display the outcomes of simulations for model system (3.2.0.1) in graphical form. We use the coupled multiscale models of infectious disease system and in this case we use embedded multiscale models and nested multiscale models as sub-models. Embedded multiscale models developed at host level is that the within-host scale and the between-host scale influences each other in a reciprocal way i.e. bi-directional flow of information. Nested multiscale model developed at host level is demonstrated by the within-host scale influence the between-host scale through shedding/excretion of pathogens and the between-host scale influence within-host scale through initial infection i.e. there is unidirectional flow of information. In this work, we use numerical simulations to illustrate and verify this structure of coupled multiscale model (3.2.0.1) and indicate the measures for control, elimination and eradication of malaria disease system. We investigate the influence of the within-host scale parameters on between-host scale variables for malaria disease system and to investigate the influence of between-host scale parameters on within-host scale variables.

Table 3.2: Between-human and between-mosquito parameter values and their description.

Parameter	Description	Initial Value	Units	Source
Λ_H	Rate of recruitment of susceptible humans	400	Humans per day	[35, 62]
Λ_V	Rate of recruitment of susceptible mosquitoes	0.525	Mosquitoes per day	Assumed
β_V	Infection rate of susceptible humans	0.32135	day^{-1}	[24, 62]
μ_H	Natural death rate of humans	0.00004002	day^{-1}	[24, 43]
γ_H	Natural recovery rate of humans	0.0092	day^{-1}	[35]
P_0	Saturation constant rate of community sporozoite load	1 000 000	day^{-1}	[24]
δ_H	Disease induced death rate	0.000345	day^{-1}	[35, 62]
G_0	Saturation constant rate of community gametocyte load	5 000 000	day^{-1}	[24]
β_H	infection rate of susceptible mosquitoes	0.356	day^{-1}	[24, 35, 62]
μ_V	Natural death rate of mosquitoes	0.12	day^{-1}	[24, 43]
δ_V	Induced death rate of infected mosquitoes	0.00000426	day^{-1}	[24]
α_H	Rate of clearance of community gametocyte load	0.0000913	day^{-1}	[24]
ϕ	Down scaling	0.0001	day^{-1}	Assumed
α_V	Rate of clearance of community sporozoite load	0.3	day^{-1}	[24]

Table 3.3: Within-mosquito parameter values and their description.

Parameter	Description	Initial Value	Units	Source
α_z	Rate at which zygotes develop into oocysts	0.4240	day^{-1}	[24]
α_h	Rate at which gametocytes develop and become infectious	0.4	day^{-1}	[24, 47]
α_g	Rate at which gametocyte infected erythrocytes burst	96	day^{-1}	[24, 43]
μ_z	Natural death rate of oocysts	1	day^{-1}	[24, 43]
μ_g	Decay rate of gametocytes	0.0625	day^{-1}	[24, 43]
α_s	Fertilization of gametes	0.2	day^{-1}	Assumed
N_m	Number of merozoites produced per bursting erythrocytes	16	day^{-1}	[24, 63, 64]
μ_s	Natural death rate of gametes	58	day^{-1}	[24]
N_g	Number of gametes produced per gametocyte infected erythrocyte	2	day^{-1}	[24]
N_k	Number of sporozoites produced per bursting oocyst	3 000	day^{-1}	[24]
α_v	Rate at which sporozoites become infectious to humans	0.025	day^{-1}	[24]
α_k	Bursting rate of oocysts to produce sporozoites	0.2	day^{-1}	[24]
μ_k	Natural death rate of oocysts	0.01	day^{-1}	[24]
μ_h	Natural death rate of gametocyte infected erythrocytes within infected humans	0.0625	day^{-1}	[24]
μ_v	Natural death rate of sporozoites	0.0001	day^{-1}	[24]
Λ_h	Rate of supply of uninfected red blood cells(erythrocytes)	200	Cells per day	[24]
β_h	the rate of infection of erythrocytes by free merozoites	0.3	day^{-1}	[24]
μ_b	Natural decay of erythrocytes	0.0083	day^{-1}	[24]
π	Proportion of gametocytes infected erythrocytes	0.4	day^{-1}	[24]
μ_m	Natural decay of rate of free merozoites	0.001	day^{-1}	[24]
α_m	Rate at which erythrocytes burst to produce merozoites	0.5	day^{-1}	[24]

3.3.1.1 Sensitivity Analysis

Using the parameter values in Table (3.2) and (3.3), we compute sensitivity analysis to assess the relative change in R_0, $\tilde{P}_V$ and $\tilde{G}_H^*$ when between-host parameters of the model varies. Sensitivity index help us to detect the change in the reproductive number (R_0), the community sporozoites load $(\tilde{P}_V)$ and the community gametocytes load $(\tilde{G}_H)$ when parameter changes. The normalised forward sensitivity index of variable to parameter is defined as the relation of the relative change in the variable to the relative change in the parameter. The sensitivity analysis of R_0, $\tilde{P}_V$ and $\tilde{G}_H$ against parameters from the model based on the method developed by [21] is presented. The purpose of study is to investigate the model output sensitivity with changes in model parameters or recognise parameters with crucial reservations on the model output. We compute R_0, $\tilde{P}_V$ and $\tilde{G}_H$ using differentiable function of the parameter i. The normalised forward sensitivity index of R_0, $\tilde{P}_V$ and $\tilde{G}_H$ at i is defined as $\Upsilon_i^{R_0} = \dfrac{\partial R_0}{\partial i} \times \dfrac{i}{R_0}$, $\Upsilon_i^{\tilde{P}_V} = \dfrac{\partial \tilde{P}_V}{\partial i} \times \dfrac{i}{\tilde{P}_V}$ and $\Upsilon_i^{\tilde{G}_H} = \dfrac{\partial \tilde{G}_H}{\partial i} \times \dfrac{i}{\tilde{G}_H}$.

The results of sensitivity indices of R_0, $\tilde{P}_V$ and $\tilde{G}_H$ to the different model parameters are shown in the Table:(3.4). The sensitivity index value sign indicates whether the parameter have effects on increases the reproduction number, R_0, community sporozoite load, $\tilde{P}_V$ and community gametocyte load $\tilde{G}_H$ or reduces R_0, $\tilde{P}_V$ and $\tilde{G}_H$. We notice from the values that there are four between-host scale parameters (μ_V, ϕ, α_V and Λ_V) which are sensitive to endemic equilibrium point $\tilde{P}_V$. The within-host scale parameters which are sensitive to $\tilde{P}_V$ are α_s, μ_z, α_s, μ_s, N_g and N_k. We note that the endemic equilibrium point $\tilde{G}_H$ is sensitive to between-host scale parameters, which are Λ_H, Λ_V, β_V, γ_H, P_0, μ_V, α_H, ϕ and α_V, and within-host scale parameters which are μ_z, α_s, μ_s, N_g, N_k, Λ_h and π. We also discover the parameters (Λ_H, Λ_V, β_V, β_H, α_z, α_s, N_g, N_k, Λ_h and π) which have effect in increasing the reproductive number (R_0), whilst the parameters which have effects in reducing R_0 are (γ_H, P_0, G_0, μ_V, α_H, ϕ, α_v, μ_z and μ_s).

Table 3.4: Sensitivity indices of reproduction number R_0 to parameter for the model system, evaluated at the parameter values

Number	**Parameter**	P_V	G_H	R_0
1	Λ_H	-0.250899266417443	0.796246060144495	0.500000000000000
2	Λ_V	5.66302415329643	4.59891134480741	0.648148148148148
3	β_V	-0.250879052719156	0.608937009344156	0.500000000000000
4	μ_H	0.251928072243536	-0.630918594174446	-0.502086506562063
5	γ_H	0.240791963300044	-0.584453490304655	-0.479896509274522
6	P_0	0.250878990140534	-0.608357128208763	-0.500000000000000
7	δ_H	0.00905828359302024	-0.189810985009550	-0.0180169841634152
8	G_0	0.250899266417444	0.203753939855506	-0.500000000000000
9	β_H	-3.43063855634498	-2.78600305236642	0.500000000000000
10	μ_V	-1.73416974300393	-1.40830988691442	-0.648148148148148
11	δ_V	0	0	0
12	α_H	0.250899266417444	-0.796246060144495	-0.500000000000000
13	ϕ	-1.00002616577141	-0.812115850890962	-0.500000000000000
14	α_V	-1.00002616577141	-0.812115850890961	-0.500000000000000
15	α_z	0.451360409938765	0.366547352381680	0.351123595505618
16	α_h	-0.0339053062726275	0.107600818938445	0.0675675675675675
17	α_g	-0.250254520800838	-0.203230345420720	0.000325309043591481
18	μ_z	-0.702265565850710	-0.570306075063878	-0.351123595505618
19	μ_g	-0.000650635111106969	-0.000528377261477529	-0.000325309043591412
20	α_s	0.747743563350139	0.607238511334258	0.499311294765840
21	N_m	-3.61538857890509e-9	1.14736848056915e-8	7.20486106779192e-9
22	μ_s	-0.998648719262085	-0.810997234016456	-0.499311294765840
23	N_g	0.749121009859466	0.608357128208764	0.500000000000000
24	N_k	0.749121009859466	0.608357128208764	0.500000000000000
25	α_v	-0.246920987920824	-0.200523201363907	0.00199203187250988
26	α_k	-0.203284862303783	-0.165086539306438	0.0238095238095239
27	μ_k	-0.0476202936081624	-0.0386721833757601	-0.0238095238095238
28	μ_h	0.0339053062726275	-0.107600818938445	-0.0675675675675676
29	μ_v	-0.00398416799112116	-0.00323552131829068	-0.00199203187250996
30	Λ_h	-0.250899270032832	0.796246071618180	0.500000007204861
31	β_h	-3.61538876643451e-9	1.14736844261895e-8	7.20486112664761e-9
32	μ_b	3.61538878693143e-	-1.14736847125536e-8	-7.20486121493116e-9
33	π	-0.250899264007185	0.796246052495371	0.499999995196759
34	μ_m	3.61538878693143e-9	-1.14736847125536e-8	-7.20486121493116e-9
35	α_m	0	0	0

Using the tornado plot sensitivity analysis will allow us to establish which factors influence the model outcomes when we decrease or increase certain parameter values. We need to discover which parameters should we target to decrease the R_0, P_V and G_H.

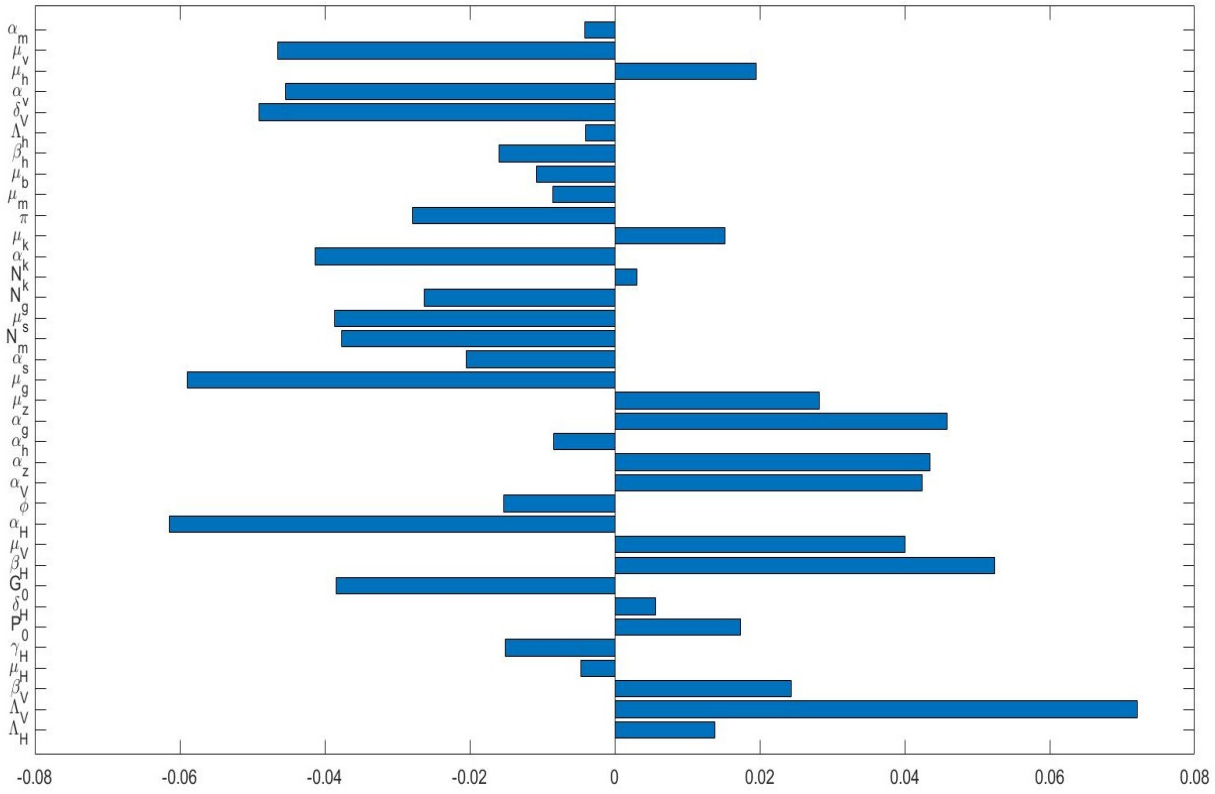

Figure 3.3: Tornado plot showing Partial Rank Correlation Coefficients of the reproduction number (R_0)

Figure (3.3), showing the sensitivity analysis of reproductive number (R_0) using the tornado plot. If the parameter values are positive, partial rank correlation coefficients (PRCCs) increase the value of R_0 if their parameter values are increased. The parameter values which have negative PRCCs have impact of reducing the value of R_0 when we increase the parameter values. The parameters Λ_H, Λ_V, β_V, β_H, α_z and α_g have the effect in raising the value of R_0 when these parameter values are increased. The parameters α_H, G_0, ϕ, μ_g and μ_v have the effect in reducing the value of R_0 when these parameter values are increased. The parameter values may have either positive or negative PRCCs, it is important to discover whether there is an increasing or decreasing trend when the parameter values are varied.

Figure (3.4), tornado plot showing Partial Rank Correlation Coefficients of the endemic equilibrium point ($\tilde{P}_V$). The parameters Λ_H, Λ_V, β_H, β_V, α_z, α_h, α_g, α_s, N_g and α_v have an impact in increasing the value of $\tilde{P}_V$ when these parameters values are increased. The parameters α_V, G_0, π, P_0, μ_g, and μ_k have the impact on decreasing the value of community sporozoites load ($\tilde{P}_V$) when these parameter values are increased. In figure (3.5) illustrate tornado plot which show the PRCCs of the endemic equilibrium equilibrium point ($\tilde{G}_H$). The parameters (β_h, α_v, π, N_k, N_m, α_s, α_h, α_z, Λ_H, Λ_V and β_V) that have impact in increasing the value of $\tilde{G}_H$ when the parameter value is increased, whilst parameters (P_0, ϕ, α_V, μ_v, μ_z and μ_k) have the impact on reducing the value of the endemic equilibrium point $\tilde{G}_H$.

In general, we find that evaluating the sensitivity of the malaria disease transmission, which are: the basic reproductive number R_0, the endemic equilibrium value of community sporozoites load $\tilde{P}_H$ and the endemic equilibrium value of the community load $\tilde{G}_H$ to the multiscale model parameters was useful to guide the data collection for model parameterization and to recognize parameters that are important in the control and elimination of the malaria disease system [65].

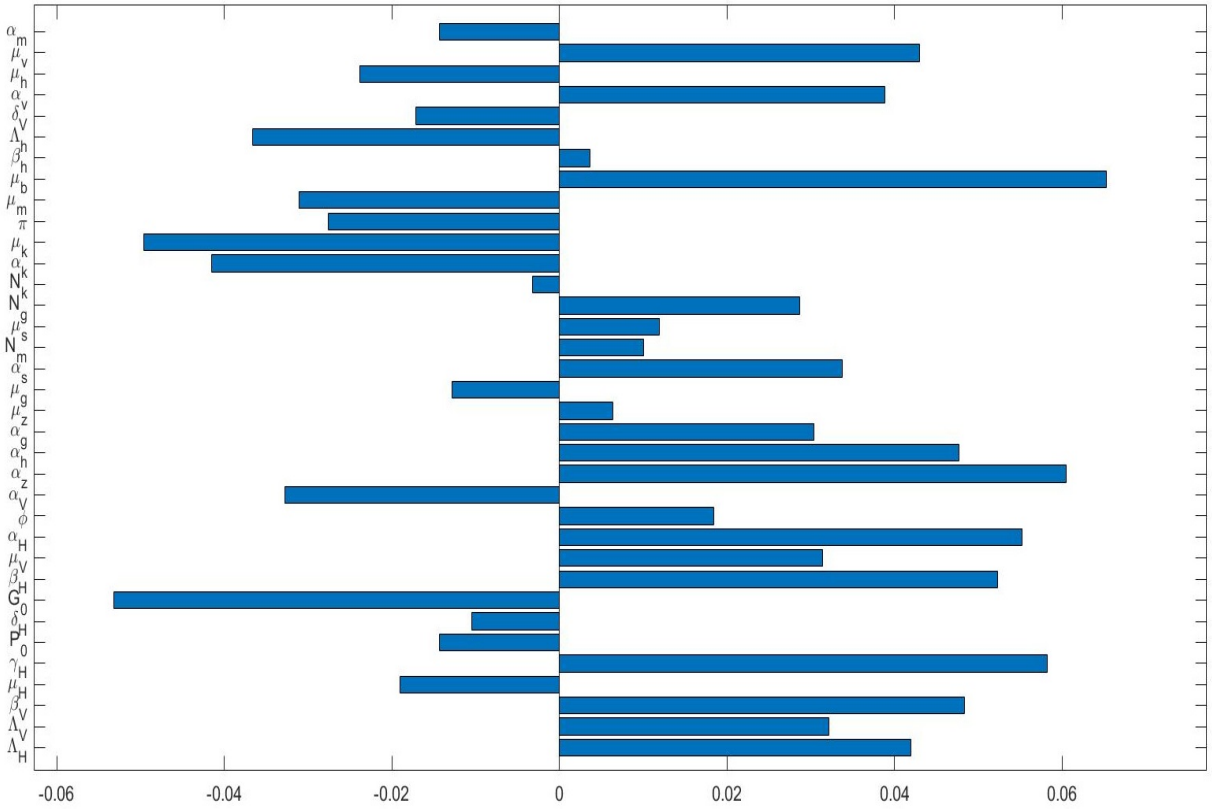

Figure 3.4: Tornado plot showing Partial Rank Correlation Coefficients of the community sporozoites load (P_V)

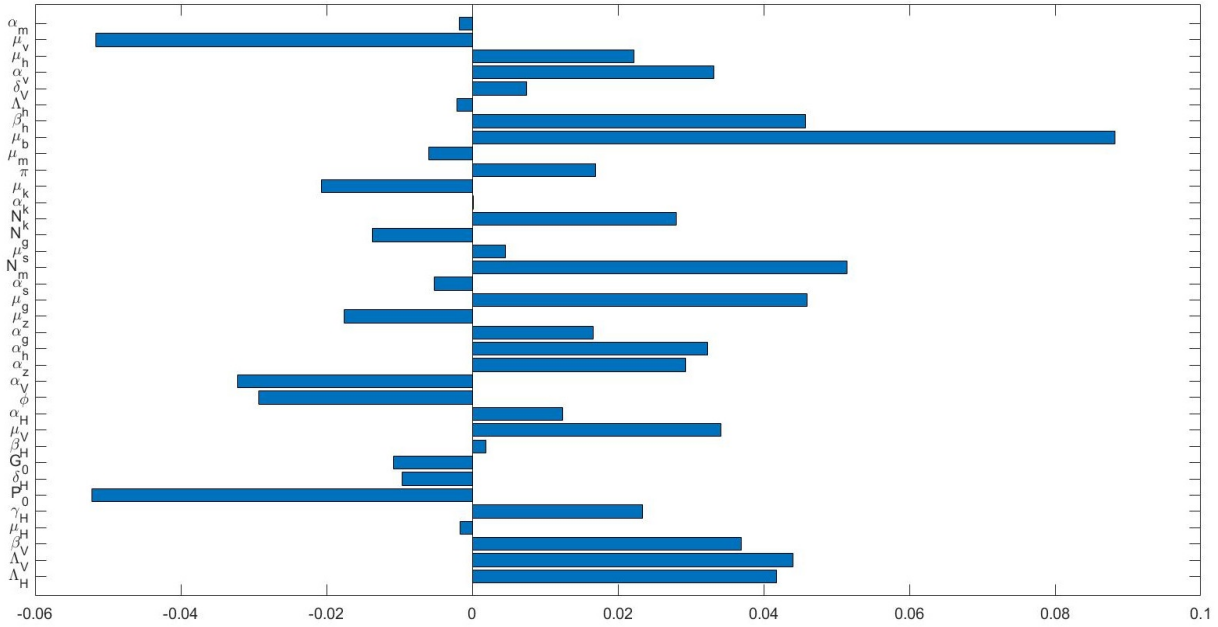

Figure 3.5: Tornado plot showing Partial Rank Correlation Coefficients of the community gametocytes load (G_H)

3.3.2 The impact of initial infection on the within-human scale of malaria infection dynamics

In figure (3.6), we illustrate through numerical solutions of the coupled multiscale model (3.2.0.1) the impact of between-host (human and mosquito) scale malaria disease dynamics on within-human scale variables for malaria incfection dynamics. We are varying the initial value condition that is initial infection $M_h(0)$, the susceptible erythrocytes within human scale acquire infection by have interacting with the merozoites for different values and we evaluate its influence on the dynamics of within-host scale variables ((a) population of infected erythrocyte R_h, (b) population of merozoites M_h and (c) population of gametocytes G_h). The results presented that as the initial condition of merozoites increase, there is a visible slightly changes in the dynamics of within-host scale variables ((a) population of infected erythrocyte R_h, (b) population of merozoites M_h and (c) population of gametocytes G_h) within the first day. When the host is infected, then the replication process follows in the within-host scale to sustains the disease dynamics at within-host scale.

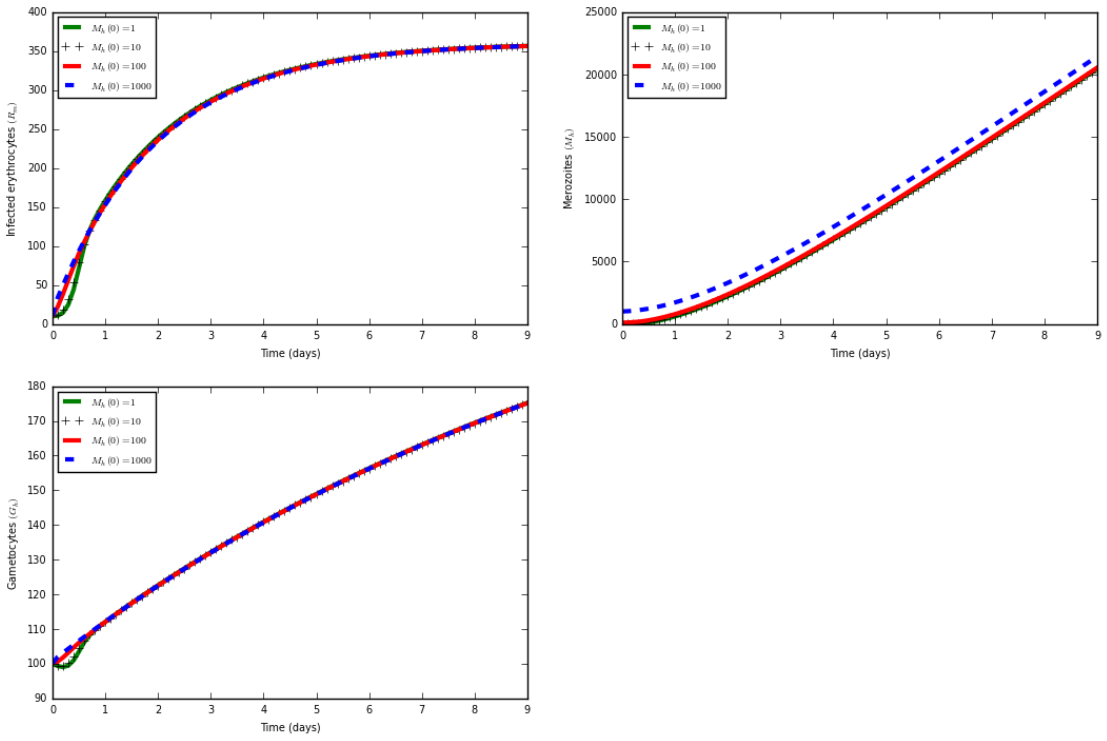

Figure 3.6: Numerical simulation of multiscale model (3.2.0.1) showing the evolution with time of (a) population of infected erythrocyte within-infected humans B_h^*, (b) the population of merozoites M_h and (c) the population of gametocytes within infected human G_h for different values of initial value condition of the within human scale $M_h(0)$: $M_h(0) = 1$, $M_h(0) = 10$, $M_h(0) = 100$ and $M_h(0) = 1000$.

3.3.3 To investigate the influence of between-human parameters on the within-mosquito scale of malaria disease dynamics

In this sub-section, we illustrate through numerical simulations of multi-scale model (3.2.0.1) the influence of between-human dynamics on within-mosquito scale variables for malaria disease dynamics ((a). population of gametocytes within-infected mosquito G_v, (b). population of gametes G_m, (c). population of zygotes Z_v and (d). the population of sporozoites P_v). We vary the between-human parameters (β_H, G_0 and γ_H) and investigate their influence on the dynamics of the within-mosquito scale variables.

Figure (3.7)shows graphs of numerical results of the system of equations (3.2.0.1) showing the evolution in time of (a) population of gametocytes within-infected mosquito G_v, (b) population of gametes G_m, (c) population of zygotes Z_v and (d) population of sporozoites P_v for different values of infection rate of susceptible mosquitoes with infectious reservoir of humans β_H: $\beta_H = 0.356$, $\beta_H = 0.656$ and $\beta_H = 0.956$. The results in figure (3.7) indicate that an increase in the infection rate of susceptible mosquitoes

with infectious reservoir of humans has important public health effects at the within-mosquito scale for malaria disease dynamics and we observe an increase in the population of gametocytes G_v, the population of gametes G_m, the population of zygotes Z_v and the population of sporozoites P_v. Hence, any prevention measures (i.e., use of LLNs, mosquito repelent and protective efficacy of humans from mosquitoes) are important in both at the between-human scales for malaria dynamics and the within-infected mosquito will prevent the malaria parasite to complete its life-cycle which have an impact in reducing the malaria infection at individual mosquitoes.

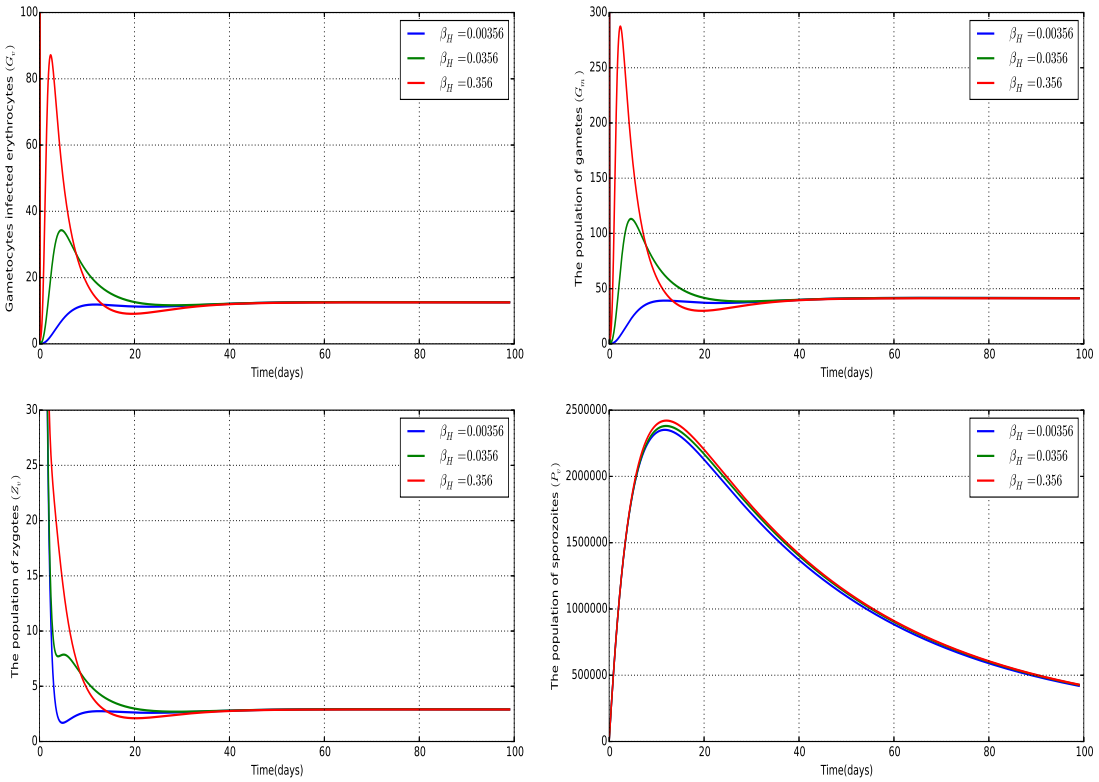

Figure 3.7: Simulation of model (3.2.0.1) showing the evolution with time of (a) population of gametocytes within-infected mosquitoes G_v, (b) the population of gametes G_m, (c) the population of zygotes Z_v and (d) the population of sporozoites P_v for different values of infection rate of susceptible mosquitoes with infectious reservoir of humans β_H: $\beta_H = 0.356$, $\beta_H = 0.656$ and $\beta_H = 0.956$.

Figure (3.8) demonstrates the dynamics in within-mosquito variables, that is, (a) the population of gametocytes G_v, (b) the population of gametes G_m, (c) the population of zygotes Z_v and (d) the population of sporozoites P_v for the variation of between-human scale, that is the half saturation constant of between-human scale, that is, the half saturation constant associated with infection of mosquitoes G_0: $G_0 = 100000000$, $G_0 = 500000000$ and 900000000. The numerical solutions in fig. (3.8) depicts that as the half saturation constant associated with infection of mosquitoes increases, we observe reduction on

malaria disease dynamics at within-mosquito scale (a) the population of gametocytes G_v, (b) the population of gametes G_m, (c) the population of zygotes Z_v and (d) the population of sporozoites P_v. Therefore, the reduction of susceptibility to malaria infection in the gametocytes community, that is, the use of transmission blocking vaccine have an impact in reducing the malaria disease in both between-human scale and at the within-mosquito scale.

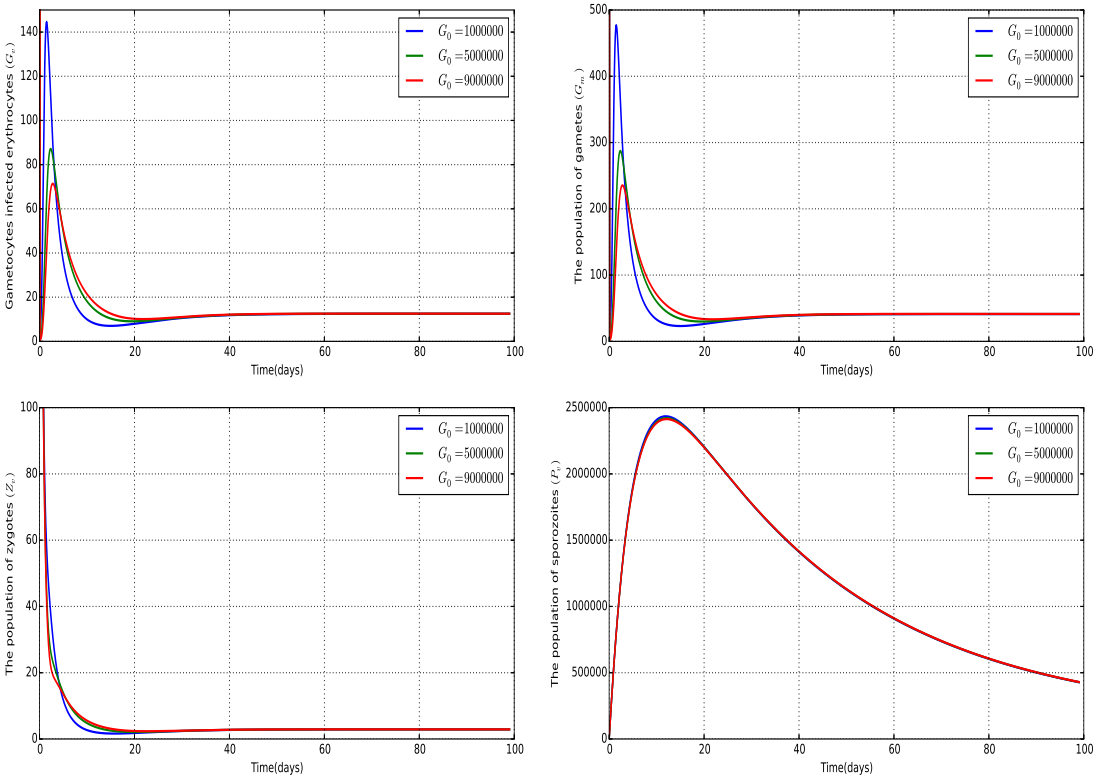

Figure 3.8: Graphs of numerical solution of multi-scale model (3.2.0.1) showing the evolution in time of (a) population of gametocytes within-infected mosquito G_v, (b) population of gametes G_m, (c) the population of zygotes Z_v and (d) the population of sporozoites P_v for different values of half saturation constant rate of community gametocyte load G_0: $G_0 = 100000000$, $G_0 = 500000000$ and $G_0 = 900000000$

Figure (3.9) illustrates the dynamics in the within-mosquito malaria disease dynamics (a) the population of gametocytes G_v, (b) the population of gametes G_m, (c) the population of zygotes Z_v, and (d) the population of sporozoites P_v for different values of human recovery rate from malaria infection γ_H: $\gamma_H = 0.0092$, $\gamma_H = 0.092$, and $\gamma_H = 0.92$. The numerical solution in figure (3.9) indicate that as the huma recovery rate from malaria infection increases, we notice a reduction in malaria infection within-infected mosquito, that is, there is reduction in population of gametocytes and population of gametes and we also notice that there is no change in the population of zygotes and population of sporozoites.

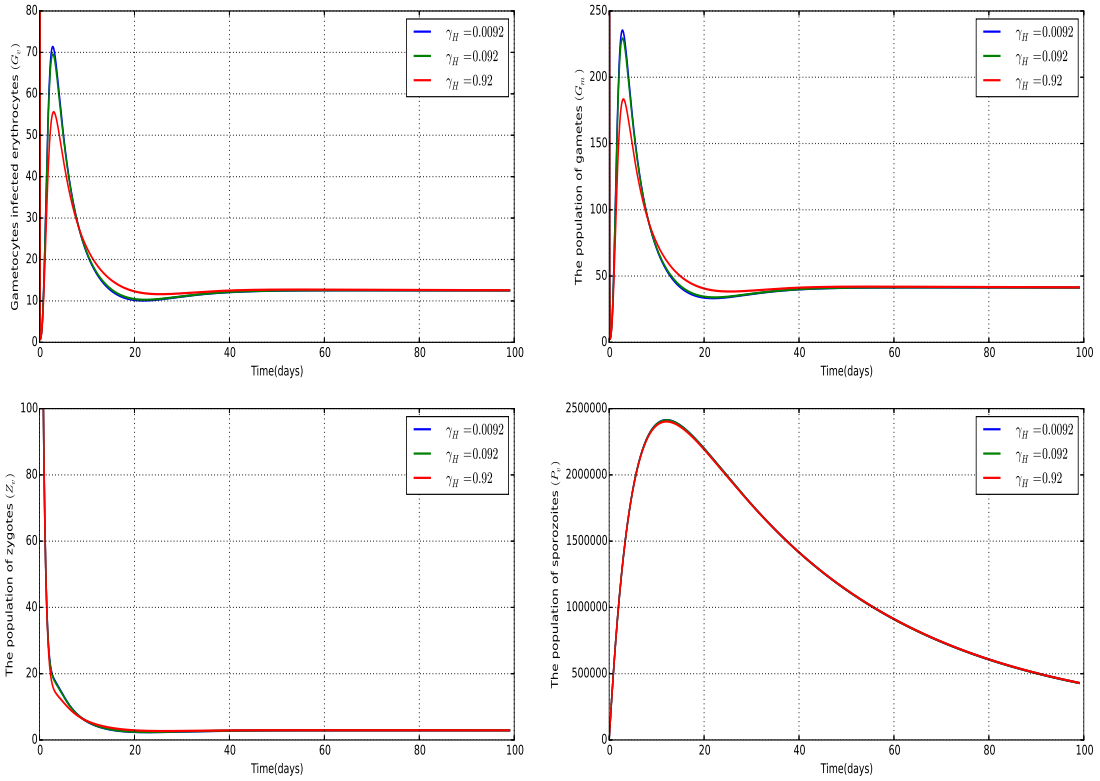

Figure 3.9: Simulation of multi-scale model (3.2.0.1) showing the changes in (a) the population of gametocytes within-infected mosquito G_v, (b) the population of gametes G_m, (c) the population of zygotes Z_v and (d) the population of sporozoites P_v for different values of recovery rate of infected humans γ_H: $\gamma_H = 0.0092$, $\gamma_H = 0.092$ and $\gamma_H = 0.92$

3.3.4 Assessment of the influence of between-mosquito parameters on within-mosquito variables.

In this sub-section, we demonstrate through numerical simulations of the multiscale model (3.2.0.1) the impact of between-mosquito scale parameters on the within-mosquito scale variable for malaria disease dynamics. We describe the variation of the between-mosquito scale parameters (β_V, Λ_V, P_0 and μ_V) and analyse their influence on the within-mosquito scale variables. Figure (3.10) presents graphs of numerical results of the system of equations (3.2.0.1) presenting the dynamics of (a) the population of gametocytes G_v, (b) the population of gametes G_m, (c) the population of zygotes Z_v and (d) the population of sporozoites P_v for different values of the contact rate of susceptible humans with the infectious reservoir of mosquitoes (β_V) with values $\beta_V = 0.0052135$, $\beta_V = 0.052135$ and $\beta_V = 0.52135$. The increase in β_V has an impact in increasing the within-mosquito scale variables (G_v, G_m, Z_v and P_v). The results indicate that an increase in the contact rate of susceptible humans with the infectious reservoir of mosquitoes

result in the increase of malaria infection on within-mosquito scale, that is, we notice an increase in the population of gametocytes, population of gametes, population of zygotes and population of sporozoites. Therefore, any prevention measures that prevent the contacts of susceptible humans and infected mosuitoes has an impact in reducing the transmitting malaria infection in the population level and as well as at the within-mosquito scale.

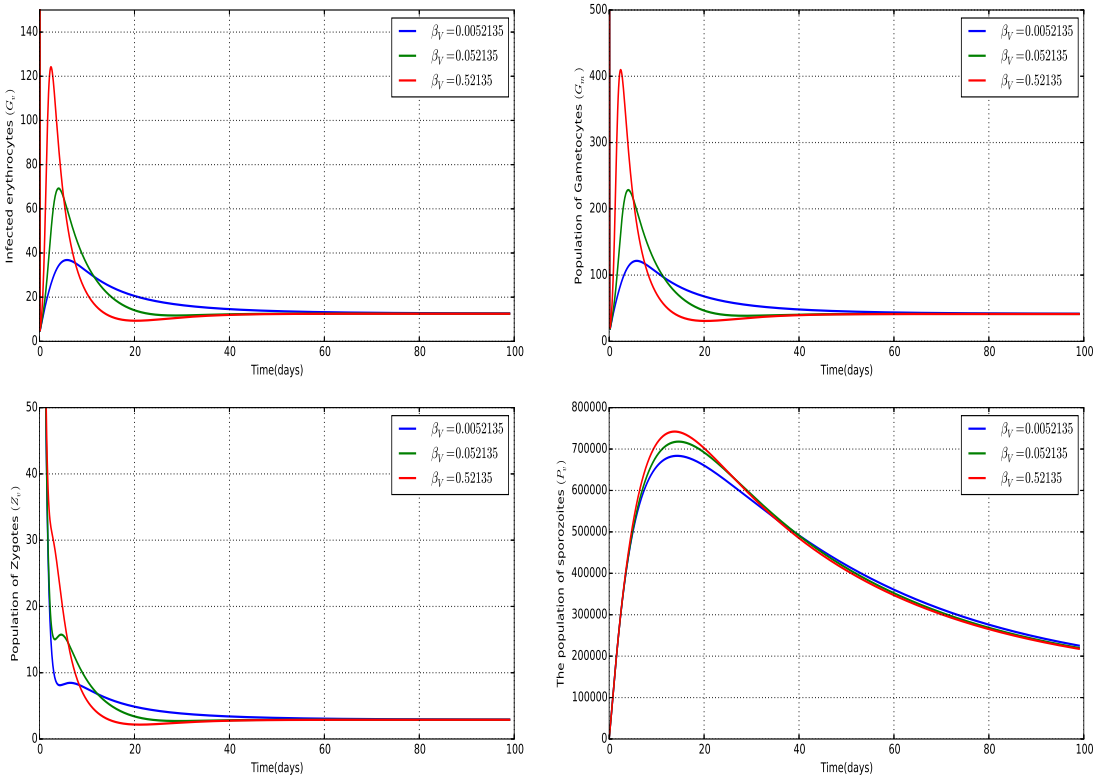

Figure 3.10: Graphs of numerical results of the model (3.2.0.1) presenting the changes in (a) the population of gametocytes within-infected mosquito G_v, (b) the population of gametes G_m, (c) the population of zygotes Z_v and (d) the population of sporozoites P_v for different values of the contact rate of susceptible humans with the infectious reservoir of mosquitoes β_V: $\beta_V = 0.0052135$, $\beta_V = 0.052135$ and $\beta_V = 0.52135$

In figure (3.11) presents the the dynamics in (a) the population of gametocytes G_v, (b) the population of gametes G_m, (c) the population of zygotes Z_v and (d) the population of sporozoites P_v for different values of recruitment rate of susceptible mosquitoes (Λ_V): $\Lambda_V = 20$, $\Lambda_V = 200$ and $\Lambda_V = 2000$. The results indicate that as the recruitment rate of mosquitoes increases, the transmission of malaria infection at within-mosquito scale also increases. Hence, these results will help us to come up with control measures on the immature mosquitoes which will result in reducing the malaria infection at a community-level and also at within-mosquito level.

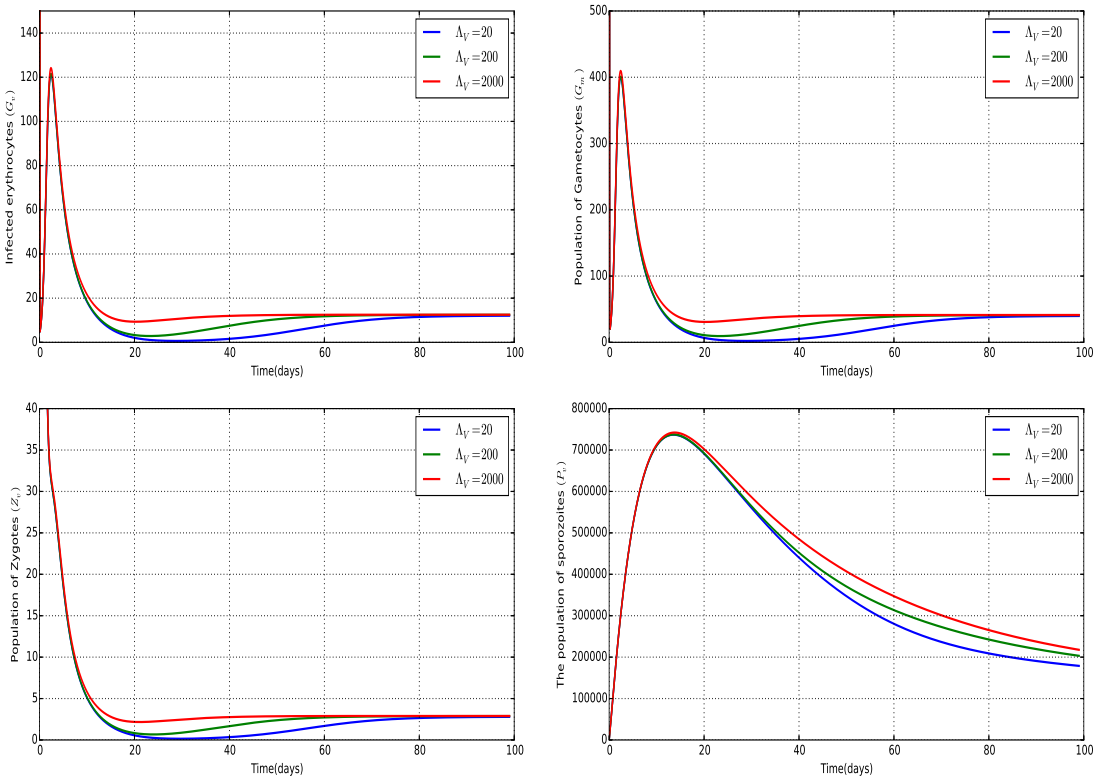

Figure 3.11: Graphs of numerical simulations of model (3.2.0.1) showing the evolution with time 0f (a) the population of gametocytes G_v, (b) the population of gametes G_m, (c) the population of zygotes Z_v and (d) the population of sporozoites P_v for different values of the recruitment rate of mosquitoes Λ_V: $\Lambda_V = 20$, $\Lambda_V = 200$ and $\Lambda_V = 2000$

Figure (3.12) illustrates the evolution with time of within-mosquito scale dynamics ((a) the population of gametocytes G_v, (b) the population of gametes G_m, (c) the population of zygotesZ_v and (d) the population of sporozoites P_v) for different values of saturation constant rate of community sporozoites load P_0: $P_0 = 50000$, $P_0 = 500000000$ and $P_0 = 500000000$. The numerical solutions indicate that an increase in the half saturation constant rate of community sporozoites load has an impact in the reducing the transmission of malaria infection on within-mosquito scale variable, that is, on the population of gametocytes, the population of gametes, the population of zygotes and the population of sporozoites.

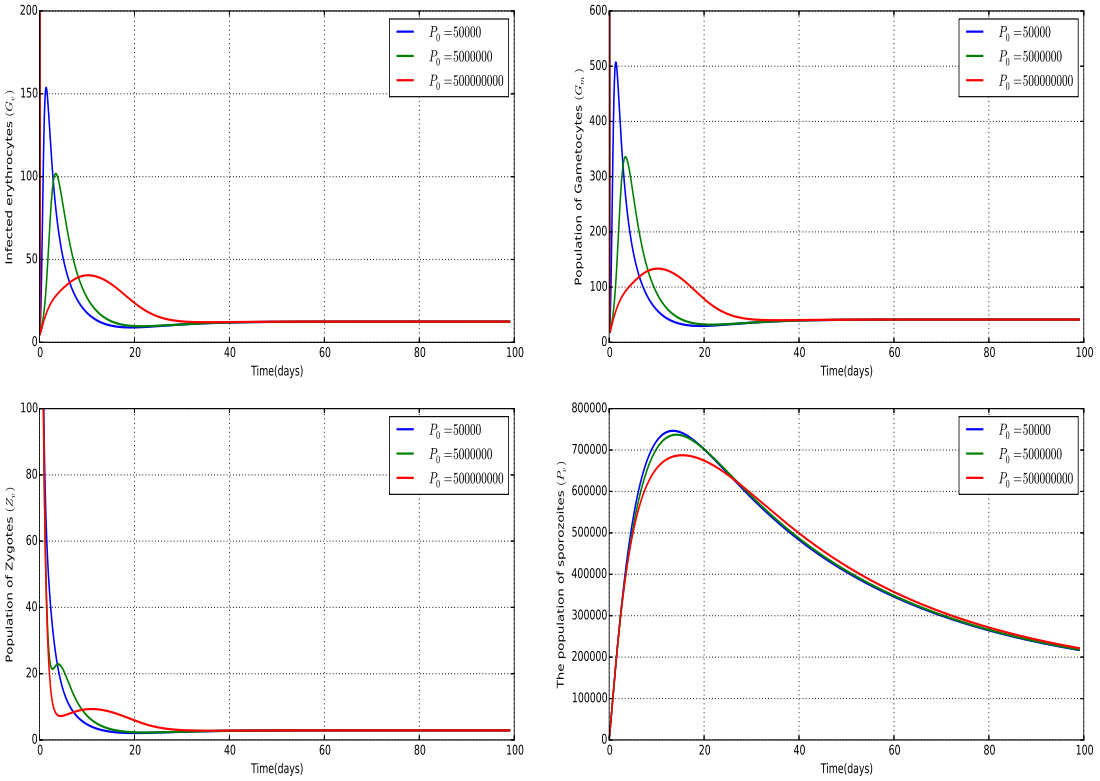

Figure 3.12: Graphs of numerical simulations of model (3.2.0.1) showing the evolution with time 0f (a) the population of gametocytes G_v, the population of gametes G_m, (c) the population of zygotes Z_v and (d) the population of sporozoites P_v for different values of saturation constant rate of community sporozoites load P_0: $P_0 = 50000$, $P_0 = 5000000$ and $P_0 = 500000000$.

Figure (3.13) pictures the numerical simulations of multi-scale model (3.2.0.1) showing the changes in the dynamics of within-mosquito scale variables ((a) the population of gametocytes G_v, (b) the population of gametes G_m, (c) the population of zygotes Z_v and (d) the population of sporozoites P_v) for different values of the proportion of new infected mosquitoes in the total infected mosquito population ϕ_V: $\phi_V = 0.0001$, $\phi_V = 0.0002$ and $\phi_V = 0.0003$. The numerical results shows that an increase in the proportion of infected mosquitoes in the total infected mosquito population results in the reduction of transmission of malaria infection of within-mosquito variables ((a) the population of gametocytes G_v, (b) the population of gametes G_m, (c) the population of zygotes Z_v and (d) the population of sporozoites P_v).

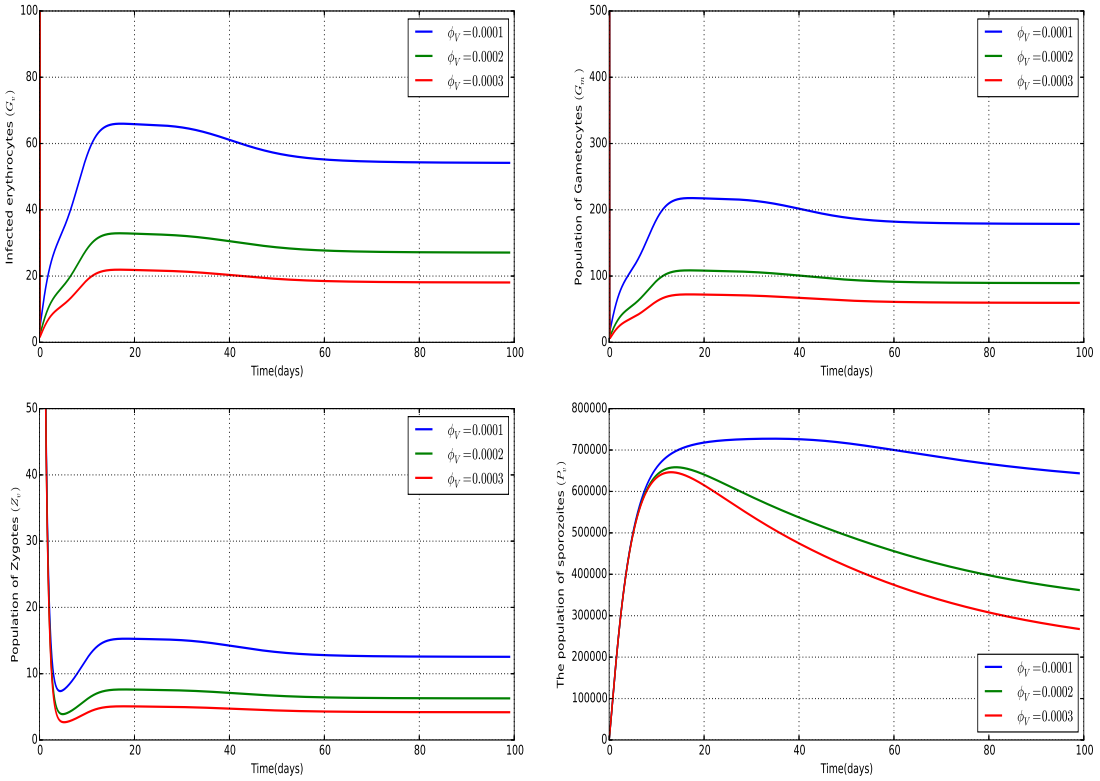

Figure 3.13: Graphs of numerical simulation of multi-scale model (3.2.0.1) showing the dynamics of (a) the population of gametocytes G_v, (b) the population of gametes G_m, (c) the population of zygotes Z_v and (d) the population of sporozoites P_v for different values of the proportion of new infected mosquitoes in the total infected mosquito population ϕ_V: $\phi_V = 0.0001$, $\phi_V = 0.0002$ and $\phi_V = 0.0003$

3.3.5 Analysing the influence of within-human parameters on between-host variables.

In this sub-section, we analyse numerically the influence of the within-human scale parameters (α_h, π and μ_h) on the between-host scale malaria disease transmission dynamics that is (a) the population of infected humans I_H, (b) the population of community gametocytes load G_H, (c) the population of infected mosquitoes I_V and (d) the population of community sporozoites load P_V using the multi-scale model (3.2.0.1) for malaria disease system. Figure (3.14) presents the graphs of numerical results of system of equations (3.2.0.1) indicating changes in dynamics of (a) population of infected humans I_H, (b) the population of community gametocytes load, (c) the population of infected mosquitoes I_V and (d) the population of community sporozoites load P_V for different values of the shedding/excretion rate of gametocytes from within-human scale into between-host scale α_h: $\alpha_h = 0.002$, $\alpha_h = 0.02$ and $\alpha_h = 0.2$. The numerical results display that an increase of excretion rate of gametocytes from within-human scale into the population level by each infected human individual has significant in public health influence at population level since

there is an observable increase in the between-host scale malaria malaria transmission on the population of infected humans I_H and the population of community gametocytes load G_H and there is slightly increase in the population of infected mosquitoes I_V and the population of community sporozoites load P_V.

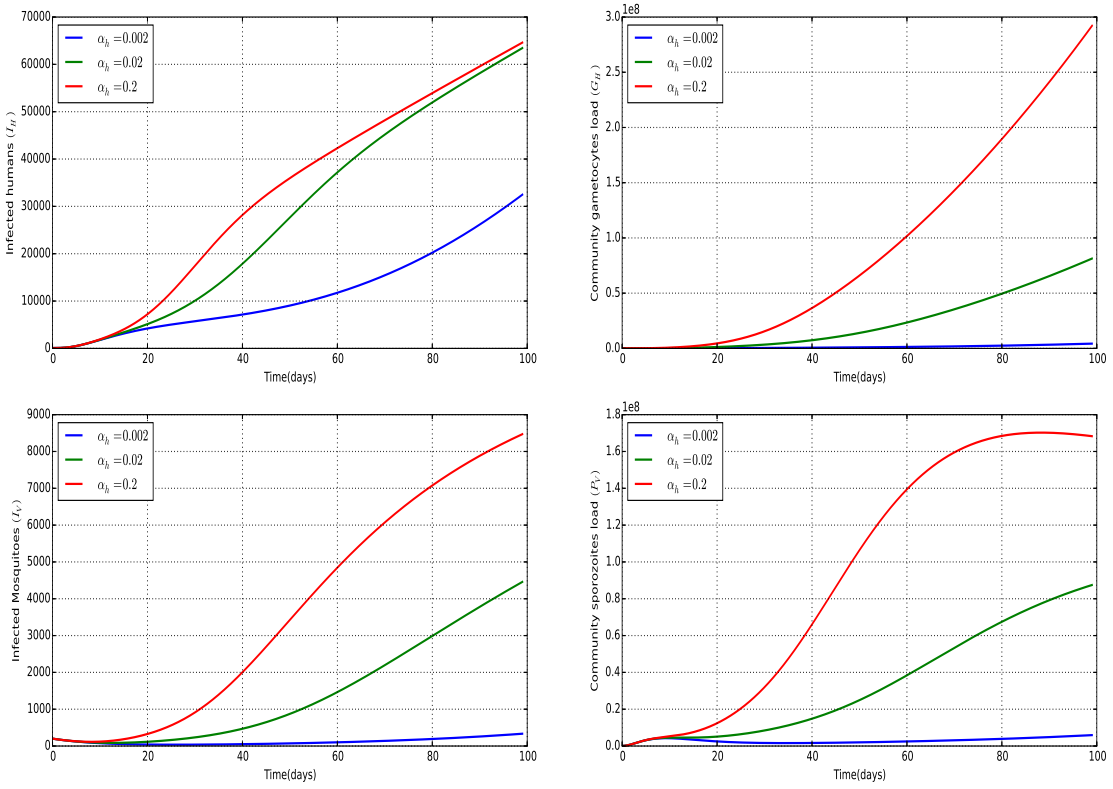

Figure 3.14: Graphs of numerical results of the multiscale model (3.2.0.1) picturing the evolution in time of dynamics of (a) population of infected humans I_H, (b) the population of community gametocytes load, (c) the population of infected mosquitoes I_V and (d) the population of community sporozoites load P_V for different values of the shedding/excretion rate of gametocytes from within-human scale to between-host scale α_h: $\alpha_h = 0.002$, $\alpha_h = 0.02$ and $\alpha_h = 0.2$.

In figure (3.14), we demonstrate the numerical results of multiscale model (3.2.0.1) showing changes in the between-host scale malaria infection dynamics ((a) the population of infected humans I_H, (b) the population community gametocytes load G_H, (c) the population of infected mosquitoes I_V and (d) the population of community sporozoites load P_V) for different values of the proportion of gametocytes infected erythrocytes within infected human π: $\pi = 0.2$, $\pi = 0.4$ and $\pi = 0.6$. The numerical results indicate that an increase of the proportion of gametocytes infected erythrocytes within infected humans has an impact in decreasing malaria disease transmission at between-human scale that is at population of infected humans and the population of community sporozotes load and at between-mosquito scale (the

population of infected mosquitoes and the population of community sporozoites load), we notice a light reduction in malaria transmission for 100 days.

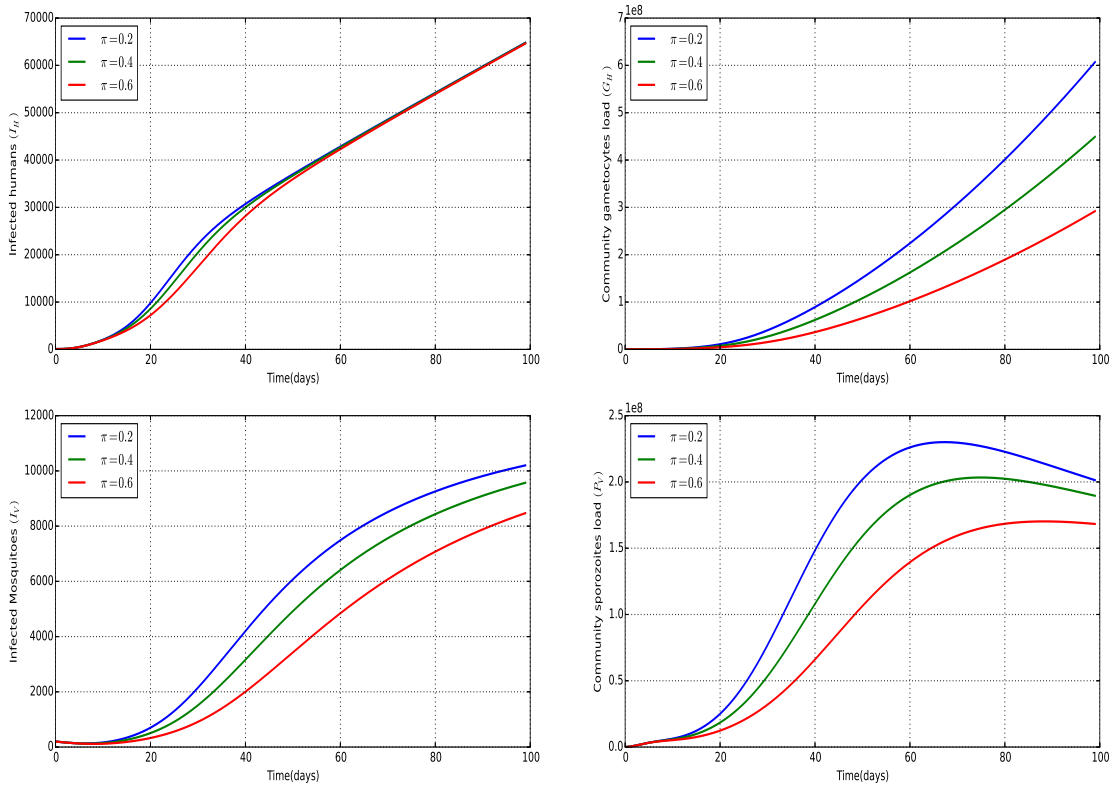

Figure 3.15: Graphs of numerical results of the multiscale model (3.2.0.1) picturing the evolution in time of dynamics of (a) population of infected humans I_H, (b) the population of community gametocytes load, (c) the population of infected mosquitoes I_V and (d) the population of community sporozoites load P_V for different values of the proportion of gametocytes infected erythrocytes π: $\pi = 0.2$, $\pi = 0.4$ and $\pi = 0.6$

In figure (3.16), we illustrate the simulations of multi-scale model (3.2.0.1) showing the evolution in time of between-host scale dynamics ((a) the population of infected humans I_H, (b) the population of community gametocytes load G_H, (c) the population of infected mosquitoes I_V and (d) the population of community sporozoites load P_V) for variation of the natural decay rate of gametocyte infected erythrocytes within infected humans μ_h: $\mu_h = 0.0325$, $\mu_h = 0.0625$ and $\mu_h = 0.0925$. The numerical results shows that an increase in the natural decay rate of gametocyte infected erythrocytes within infected humans,has an impact of reducing malaria disease transmission at the between-human scale, that is, we notice a reduction of the population of infected humans and the population of community gametocyte load and we notice that there is no difference in the population of infected mosquitoes and the population

of community sporozoites load. Therefore, the use of ACTs which kills the gametocytes within the infected humans is important in reducing the malaria disease transmission at within-human scale and also at population-level.

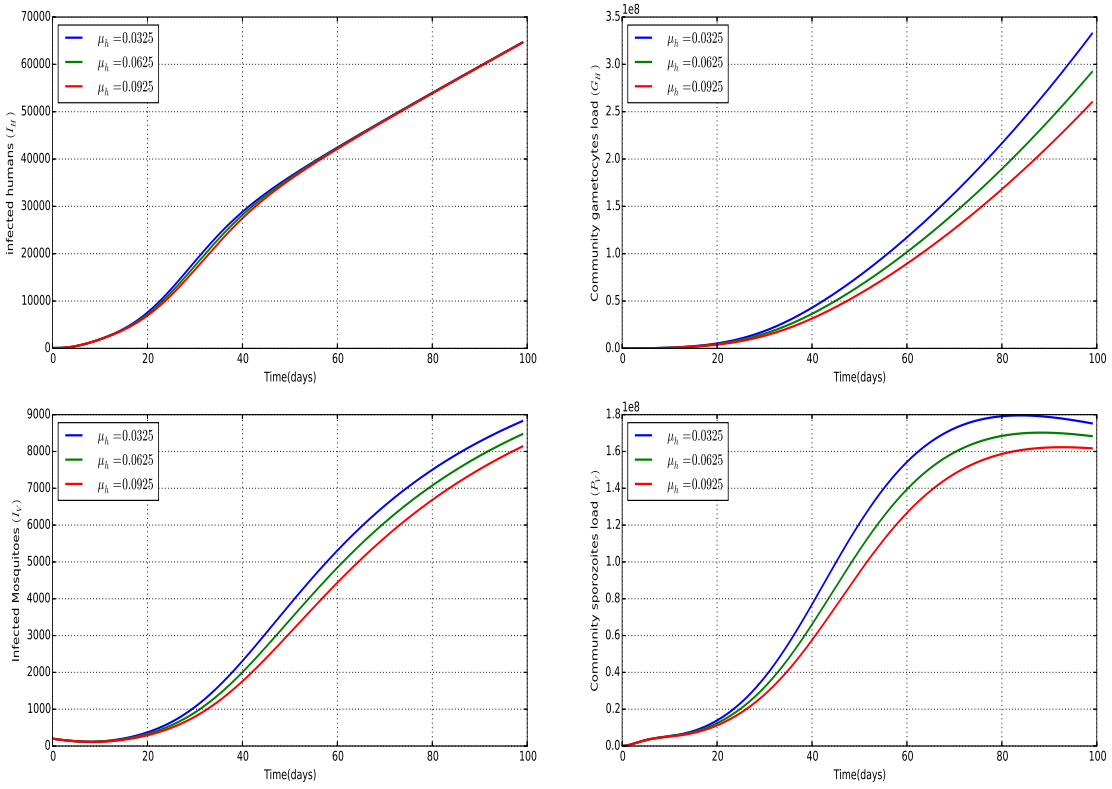

Figure 3.16: Graphs of numerical results of the multiscale model (3.2.0.1) picturing the evolution in time of dynamics of (a) population of infected humans I_H, (b) the population of community gametocytes load, (c) the population of infected mosquitoes I_V and (d) the population of community sporozoites load P_V for different values of the natural decay rate of gametocyte infected erythrocytes within infected humans μ_h: $\mu_h = 0.0325$, $\mu_h = 0.0625$ and $\mu_h = 0.0925$

3.3.6 The influence of within-mosquito scale parameters on the between-host scale malaria transmission dynamics

In this sub-section, we illustrate through numerical results of coupled multi-scale model (3.2.0.1) the influence of within-mosquito scale dynamics on between-host scale variables for malaria disease transmission dynamics. We vary within-mosquito scale parameters (α_s, α_z, N_k, α_k, N_g, α_v, μ_k, μ_s and μ_z) for different values and analyse the influence on the dynamics of the between-host scale for malaria disease system (the population of infected humans I_H, the community gametocytes load G_H, the population of infected mosquitoes I_V and the community sporozoites load P_V).

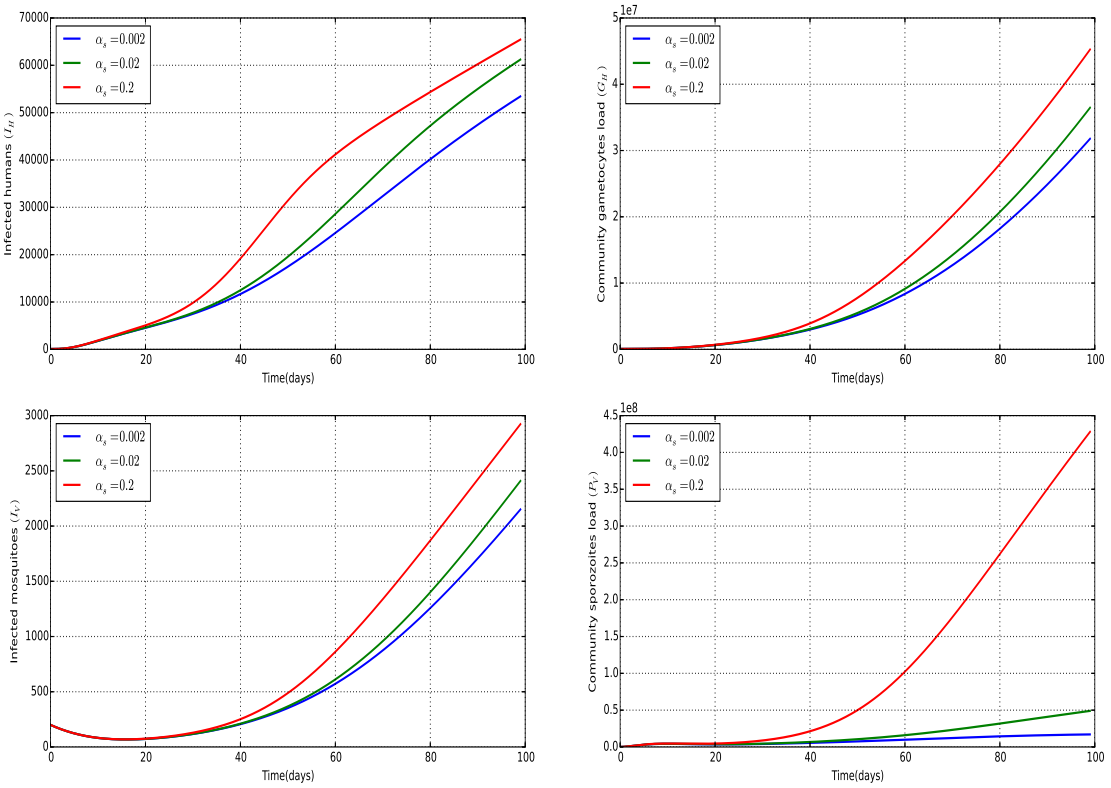

Figure 3.17: Graphs presenting changes in (a) the population of infected humans I_H, the community gametocytes load G_H, the population of infected mosquitoes I_V and the communit sporozoites load P_V for distinct values of fertilization of gametes within infected mosquitoes α_s: $\alpha_s = 0.002$, $\alpha_s = 0.02$ and $\alpha_s = 0.2$.

Figure (3.17) displays graphs of numerical solutions of the system of eqution (3.2.0.1) showing the dynamics of (a) the population of infected humans I_H, (b) the community gametocytes load G_H, (c) the population of infected mosquitoes I_V and (d) the community sporozoites load P_V for variation of fertilization of gametes within infected mosquito α_s: $\alpha_s = 0.002$, $\alpha_s = 0.02$ and $\alpha_s = 0.2$. The results demonstrate that an increase in the fertilization of gametes also has an influence of increasing malaria disease transmission at the between-human scale (the population of infected humans and the community gametocytes load) and the malaria transmission at the between-mosquito scale, we observe no different on malaria transmission at the population of infected mosquitoes and there is slightly increase in the community sporozoites load for the first 100 days.

Figure (3.18) displays graphs of numerical results of the system of equations (3.2.0.1) presenting the dynamics of (a) the population of infected humans I_H, (b) the community gametocytes load G_H, (c) the population of infected mosquitoes I_V and the community sporozoites load P_V for different values of the

development rate of zygotes into oocysts within infected mosquito α_z: $\alpha_z = 0.024$, $\alpha_z = 0.424$ and $\alpha_z = 0.824$. The results in Fig.(3.18) indicate that reducing the development rate of zygotes into oocysts have an effects of reducing the malaria transmission at the between-host scale. This implies that any interventions that are focused on the development rate of zygoges into oocysts within infected vector is likely to have impact in reducing malaria transmission.

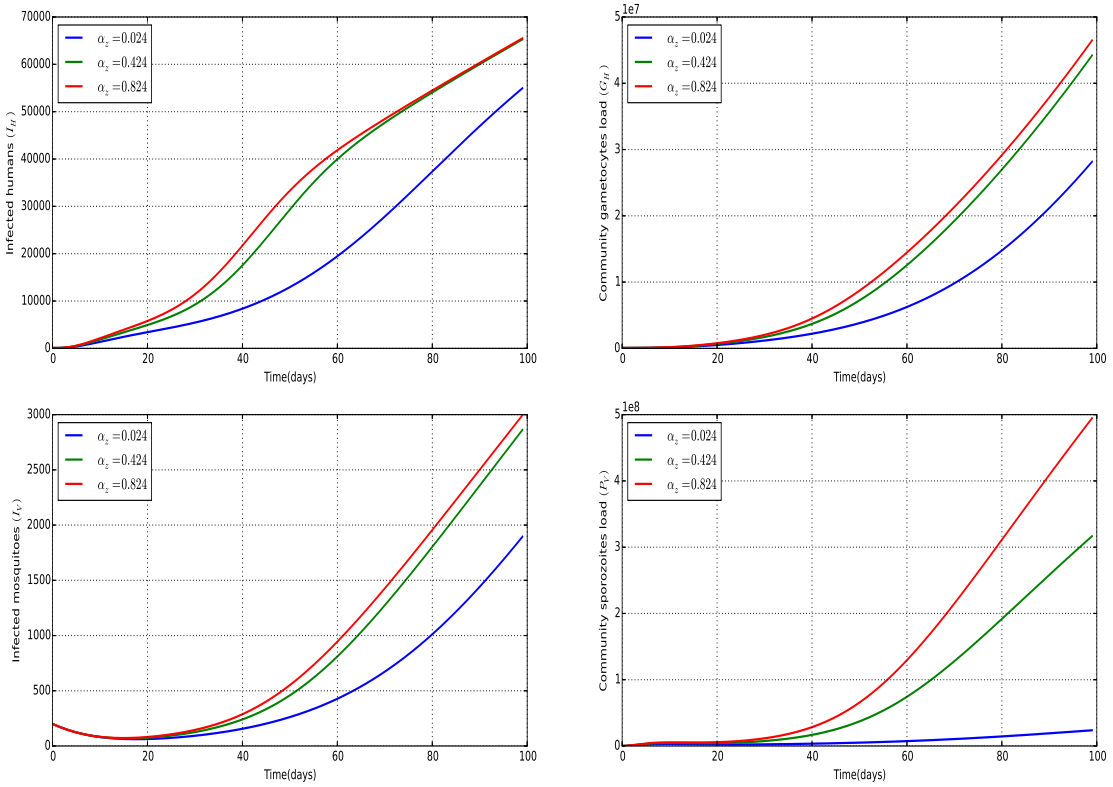

Figure 3.18: Graphs presenting changes in (a) the population of infected humans I_H, the community gametocytes load G_H, the population of infected mosquitoes I_V and the community sporozoites load P_V for distinct values of the development rate of zygotes into oocysts within infected mosquitoes α_z: $\alpha_z = 0.024$, $\alpha_z = 0.424$ and $\alpha_z = 0.824$.

Figure (3.19) presents changes in (a) the population of infected humans I_H, the community gametocytes load G_H, the population of infected mosquitoes I_V and the community sporozoites load P_V for distinct values of the number of sporozoites produced per bursting oocyst within infected mosquitoes N_k: $N_k = 1000$, $N_k = 2000$ and $N_k = 3000$. The results indicate that as the number of sporozoites produced per bursting oocyst within infected mosquito has impact of increasing the malaria transmission at a population-level that is at between-host scale. Hence, any intervention that targets the number of sporozoites produced per bursting oocyst has an impact of reducing mosquito-to human malaria transmission.

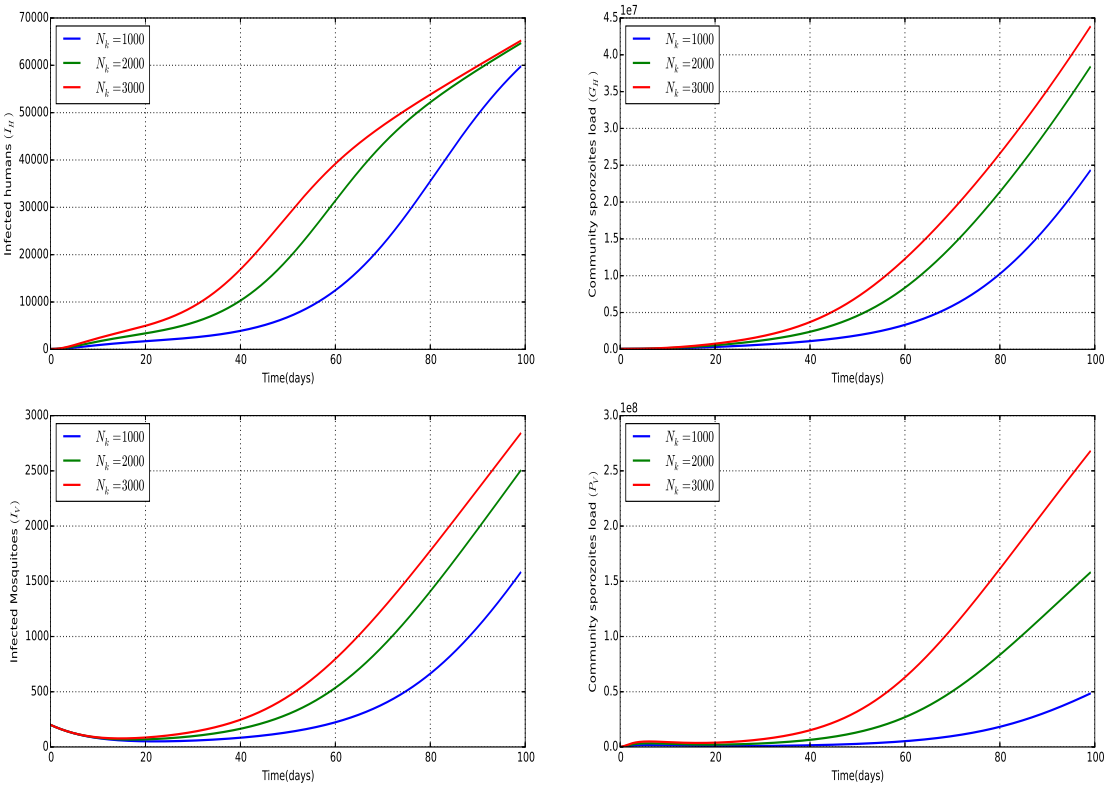

Figure 3.19: Graphs presenting changes in (a) the population of infected humans I_H, the community gametocytes load G_H, the population of infected mosquitoes I_V and the community sporozoites load P_V for distinct values of the number of sporozoites produced per bursting oocyst within infected mosquitoes N_k: $N_k = 1000$, $N_k = 2000$ and $N_k = 3000$.

Figure (3.20) presents changes in (a) the population of infected humans I_H, the community gametocytes load G_H, the population of infected mosquitoes I_V and the community sporozoites load P_V for distinct values of the bursting rate of oocysts to produce sporozoites within infected mosquitoes α_k: $\alpha_k = 0.2$, $\alpha_k = 0.7$ and $\alpha_k = 1.2$. The results show that as the bursting rate of oocysts to produce sporozoites within infected mosquitoes increases, there is also observable increase on between-host scale malaria transmission,that is, the population of infected humans I_H, the community gametocytes load G_H, the population of infected mosquitoes I_V and the community sporozoites load P_V. Therefore, the results suggest that intervention measures which targets at the bursting rate of oocysts to release sporozoites within infected mosquitoes are important for the community in reducing transmission of malaria infection at population level.

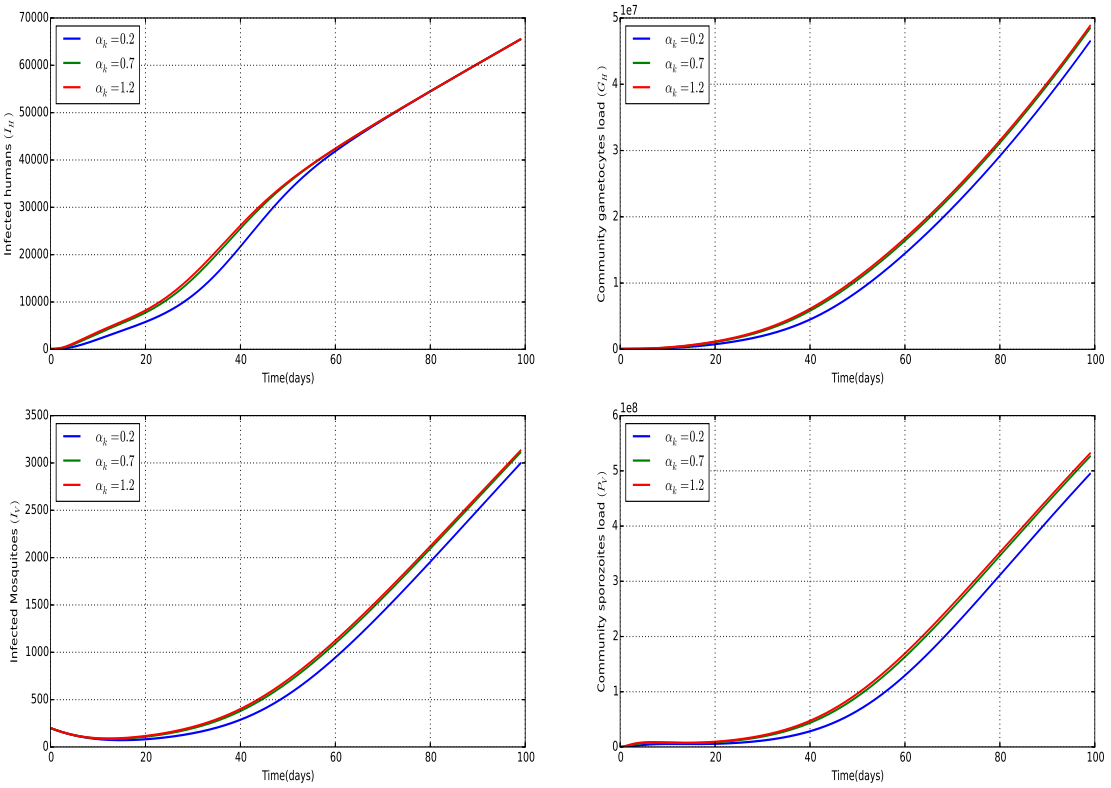

Figure 3.20: Graphs presenting changes in (a) the population of infected humans I_H, the community gametocytes load G_H, the population of infected mosquitoes I_V and the community sporozoites load P_V for distinct values of the bursting rate of oocysts to produce sporozoites within infected mosquitoes α_k: $\alpha_k = 0.2$, $\alpha_k = 0.7$ and $\alpha_k = 1.2$.

Figure (3.21) pictures the changes in (a) the population of infected humans I_H, (b) the community gametocytes load G_H, (c) the population of infected mosquitoes I_V and the community sporozoites load for different values of the number of gametes released per gametocyte infected erythrocyte within infected mosquitoes N_g: $N_g = 4$, $N_g = 12$ and $N_g = 22$. The results show that an increase in the number of gametes released per gametocyte infected erythrocyte within infected mosquitoes has impact in increasing the malaria transmission at community-level, that is, the population of infected humans I_H, the community gametocytes load G_H, the population of infected mosquitoes I_V and the community sporozoites load P_V.

Figure (3.22) depicts variation in (a) the population of infected humans I_H, (b) the community gametocytes load G_H, (c) the population of infected mosquitoes I_V and the community sporozoites load for different values of the rate at which sporozoites becomes infectious to humans α_v: $\alpha_v = 0.025$, $\alpha_v = 0.25$ and $\alpha_v = 0.5$. The results indicate that as the rate at which sporozoites becomes infectious to humans

increase, there is a corresponding increase in the malaria transmission at the community-level, that is, at the population of infected humans I_H, the community gametocytes load G_H, the population of infected mosquitoes I_V and the community sporozoites load P_V.

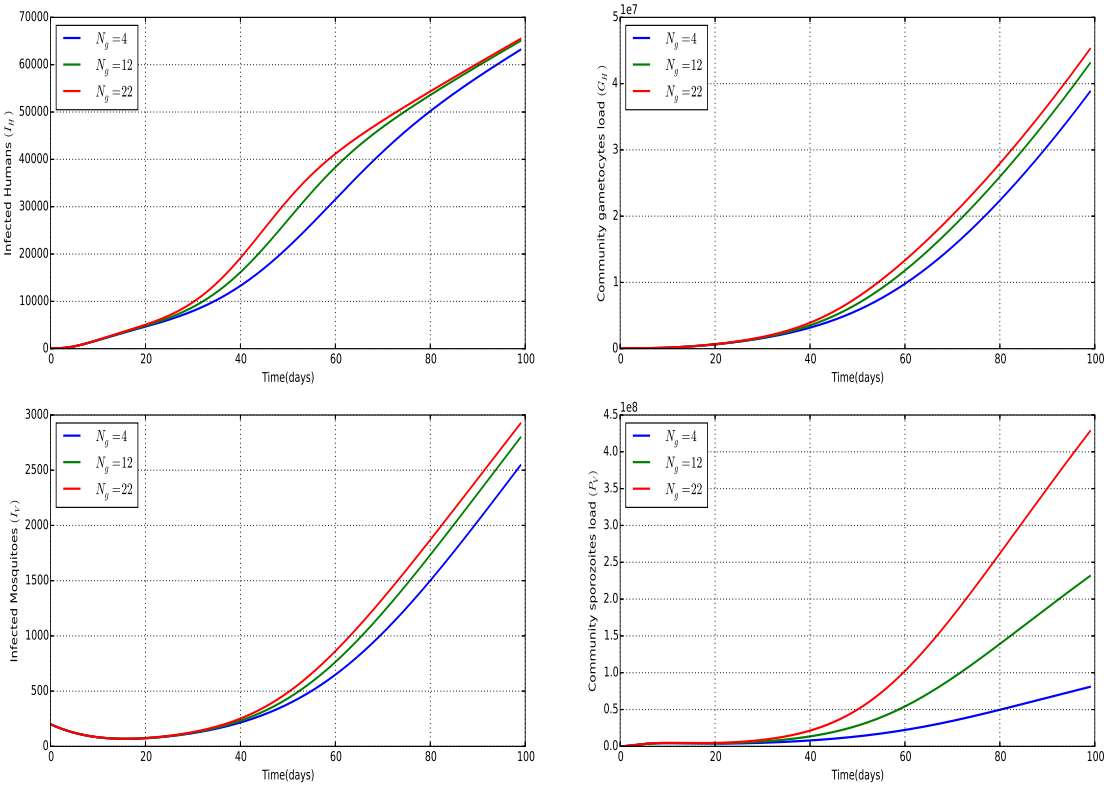

Figure 3.21: Graphs presenting changes in (a) the population of infected humans I_H, the community gametocytes load G_H, the population of infected mosquitoes I_V and the community sporozoites load P_V for distinct values of the number of gametes produced per gametocyte infected erythrocyte within infected mosquitoes N_g: $N_g = 4$, $N_g = 12$ and $N_g = 22$.

Figure (3.23) depicts the evolution in time of (a) the population of infected humans I_H, (b) the community gametocytes load G_H, (c) the population of infected mosquitoes I_V and the community sporozoites load for different values of the natural decay rate of oocysts within infected mosquitoes μ_k: $\mu_k = 0.01$, $\mu_k = 0.1$ and $\mu_k = 1$. The results depict that an increase in the natural decay rate of oocysts within infected mosquitoes has an impact in reducing the malaria transmission at community-level, that is, the population of infected humans I_H, the community gametocytes load, the population of infected mosquitoes I_V, the community sporozoites load P_V. However, any interventions that kills the oocysts within infected mosquitoes has an impact in reducing the malaria transmission at community-level, that is , the population of infected humans, the community gametocytes load, the population of infected mosquitoes and the community sporozoites load.

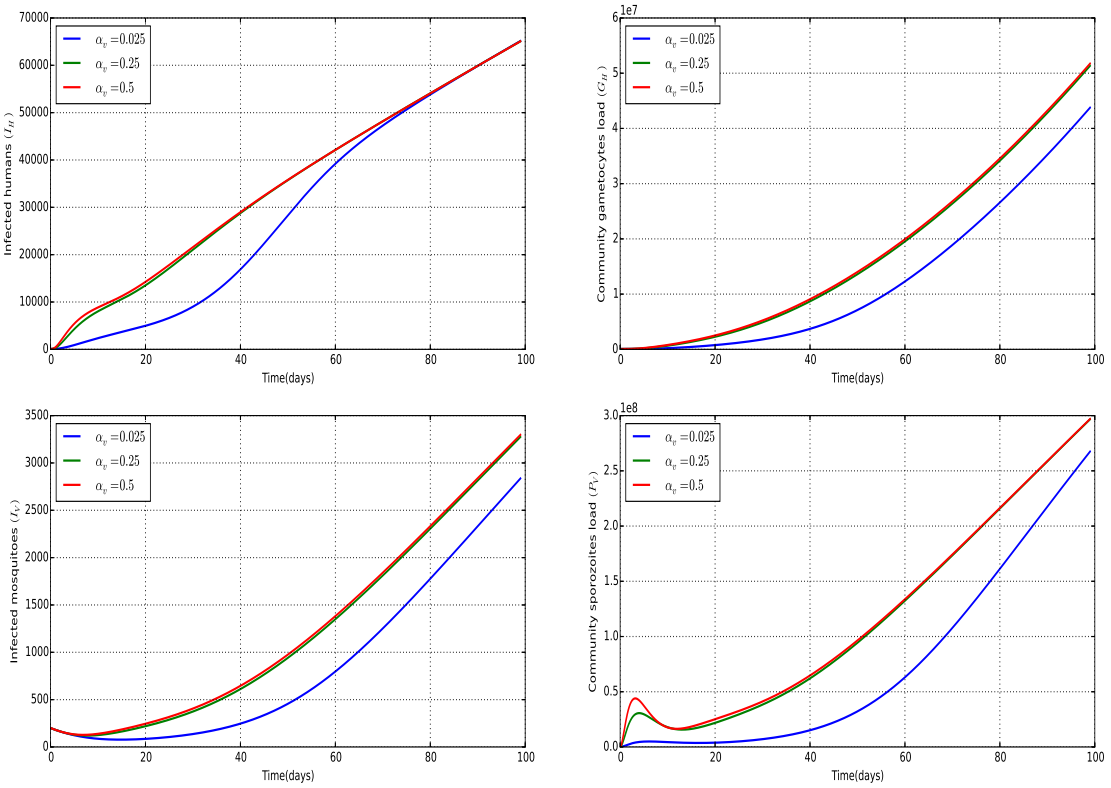

Figure 3.22: Graphs presenting changes in (a) the population of infected humans I_H, the community gametocytes load G_H, the population of infected mosquitoes I_V and the community sporozoites load P_V for different values of the rate at which sporozoites become infectious to humans α_v: $\alpha_v = 0.025$, $\alpha_v = 0.25$ and $\alpha_v = 0.5$.

Figure (3.24) depicts the changes in (a) the population of infected humans I_H, (b) the community gametocytes load G_H, (c) the population of infected mosquitoes I_V and the community sporozoites load for different values of natural decay rate of gametes within infected mosquitoes μ_s: $\mu_s = 38$, $\mu_s = 58$ and $\mu_s = 78$. From the results, it can be seen that as the natual decay rate of gametes within infected mosquitoes increases, there is a corresponding increase in the malaria transmission on community-level, that is, the population of infected humans, the community gametocytes, the infected mosquitoes and the community sporozoites load.

Figure (3.25) demonstrates the dynamics of (a) the population of infected humans I_H, (b) the community gametocytes load G_H, (c) the population of infected mosquitoes I_V and the community sporozoites load for different values of natural decay rate of zygotes within infected mosquitoes μ_z: $\mu_z = 0.01$, $\mu_z = 0.1$ and $\mu_z = 1.0$. The results depict that an increase in natural decay rate of zygotes has an effect in reducing

the malaria transmission at community-level, that is, the population of infected humans, the community gametocytes, the population of infected mosquitoes and the community sporozoites load.

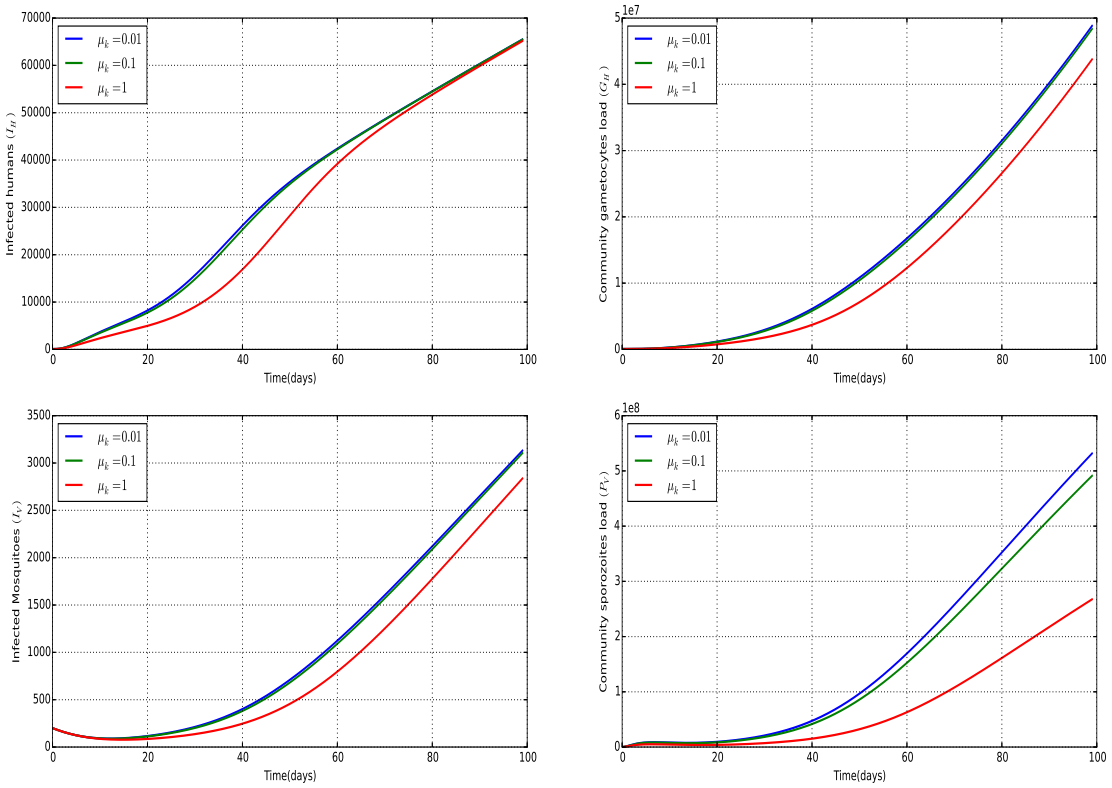

Figure 3.23: Graphs presenting changes in (a) the population of infected humans I_H, the community gametocytes load G_H, the population of infected mosquitoes I_V and the community sporozoites load P_V for distinct values of the natural decay rate of oocysts within infected mosquitoes μ_k: $\mu_k = 0.01$, $\mu_k = 0.1$ and $\mu_k = 1$.

We note from the results in figure (3.14)- figure (3.25) that between-host variables ((a) population of infected humans I_H, (b) community gametocyte load G_H, (c) population of infected mosquitoes I_V and (d) community sporozoite load P_V) are importantly sensitive to the variation of the within-host (human and mosquito) scales parameters (α_h, π and μ_h) and (α_s, α_z, N_k, α_v, μ_k, μ_s and μ_z) respectively. From the results in fig. (3.7)-fig.(3.13), we also note the within-mosquito variables ((a)population of G_v, (b) population of gametes G_m, (c) population of zygotes Z_v and population of sporozoites p_v) are crucially sensitive to the variation of the between-host (human and mosquito) scales parameters (β_H, G_0 and γ_H) and (β_V, Λ_V, P_0 and μ_V) respectively. We conclude from the observation obtain from the numerical results in fig. (3.6)-fig.(3.25) that:

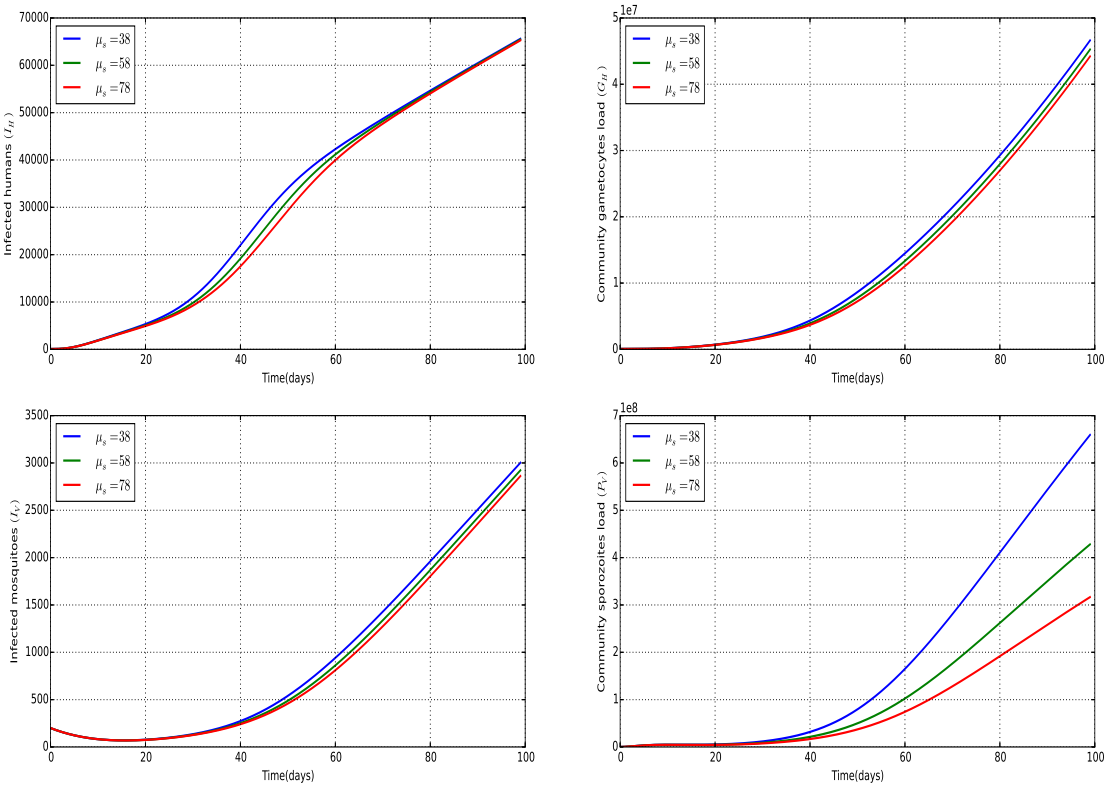

Figure 3.24: Graphs presenting changes in (a) the population of infected humans I_H, the community gametocytes load G_H, the population of infected mosquitoes I_V and the community sporozoites load P_V for distinct values of the natural decay rate of gametes within infected mosquitoes μ_s: $\mu_s = 38$, $\mu_s = 58$ and $\mu_s = 78$.

(1) Within-host (human and mosquito) scales influence the dynamics of malaria disease system at between host scale throughout the whole process of infection through shedding/excretion of malaria pathogen.

(2) The between host scale influence the within-human scale through initial infection of pathogen and then the within-human scale pathogen load increase through replication-cycle. The process of the pathogen replication cycle contributed much compared to the initial infection.

(3) The between-host scale influences the within-mosquito scale through super-infection, the within-mosquito pathogen load increase through repeated infection.

(4) We also notice that the nested multiscale model has a unidirectional flow of information from microscale to macroscale, that is, micro-scale influences macro-scale through shedding or excretion of pathogens whereas macro-scale influences micro-scale through initial infection.

(5) We also notice that the embedded multiscale model has a bidirectional flow of information, that is, the within-mosquito scale influences the between-host scale through shedding/excretion of pathogen whilst the between-host scale influences the within-mosquito scale through repeated infection/ super-infection.

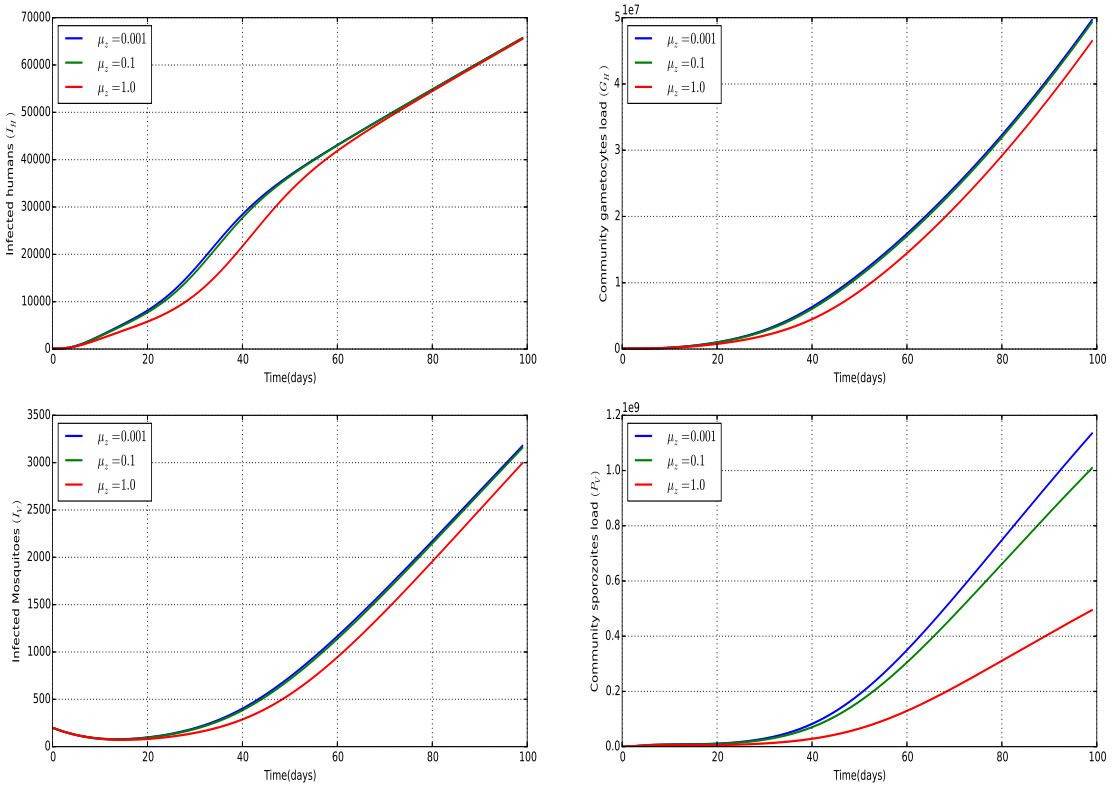

Figure 3.25: Graphs presenting changes in (a) the population of infected humans I_H, the community gametocytes load G_H, the population of infected mosquitoes I_V and the community sporozoites load P_V for distinct values of the natural decay rate of zygotes within infected mosquitoes μ_z: $\mu_z = 0.01$, $\mu_z = 0.1$ and $\mu_z = 1.0$.

3.4 Summary

The objective of the study is to investigate how super-infection/re-infection in mosquitoes has an impact on dynamics of type II-vector borne disease transmission with no pathogen replication cycle at the microscale and to investigate how initial infection in humans has an influence on multiscale model dynamics of an infectious disease with the pathogen replication cycle at the microscale. The coupled multiscale model of type II vector-borne disease has a combination of a nested multiscale model and an embedded multiscale model for integrating the microscale and the macroscale sub-models. The coupled multiscale

model in this study was derived from work by Garira in [11] and we modify the model by including the influence of super-infection on mosquitoes. The coupled multiscale model of type II vector-borne disease transmission presents the replication-transmission multiscale cycle in both mosquito and human populations. The embedded multiscale model was used on mosquitoes to examine the influence of super-infection on the multiscale model of the malaria disease system. There is no pathogen replication cycle at the within-mosquito scale and pathogen load increase through super-infection/re-infection. While the nested multiscale model on the human population was used to investigate the influence of initial infection with pathogen replication cycle at within-human sub-model. From the results, we discovered that the embedded multiscale model has the bidirectional flow of information, that is, the within-host scale influences the between-host scale throughout the infection through shedding/excretion whereas between host scale influences the within-host scale throughout the infection through super-infection. On the other hand, the results indicate that the nested multiscale model has a unidirectional flow of information, that is, the within-host scale influences the between-host scale throughout the infection through pathogen shedding/excretion, whilst the between-host scale influences the within-host scale through initial infection and the pathogen load within infected host increased through pathogen replication. The sensitivity used to discover the parameters that are sensitive to the decrease or increase of the basic reproductive number R_0, community sporozoites load P_V, and community gametocyte load G_H, which help to suggest appropriate health intervention measures.

Chapter 4

A Multiscale Model of Malaria Disease Dynamics to Access Vaccine Components

4.1 Introduction

In the previous chapter, we develop a coupled multiscale model for the malaria disease system with a combination of a nested multiscale model and an embedded multiscale model. We used an embedded multiscale model in mosquitoes to investigate the influence of super-infection/re-infection on malaria disease dynamics whilst in humans, we used a nested multiscale to investigate the impact of initial infection on malaria disease dynamics. In this chapter, we demonstrate a coupled multiscale model of malaria disease dynamics with the combination of two embedded multiscale models, that is, an embedded multiscale model on humans and an embedded multiscale model on mosquitoes. We perform the processes that happen in the infectious disease system from the work by Garira in [11], which are (i) infection/ super-infection, (ii) pathogen replication cycle, (iii) pathogen shedding/excretion, and (iv) pathogen transmission. The microscale and the macroscale influence each other in a reciprocal way and these processes can occur at any hierarchical level of organization for infectious disease systems. In humans, the macroscale influences the microscale through super-infection/re-infection of pathogens whereas the microscale influences the macroscale through shedding/excretion of the pathogens. There is pathogen replication in microscale that is in merozoites and there is a transmission cycle at the macroscale. In mosquitoes, we adapt the processes in the previous chapter. At every hierarchical level of organization for infectious disease dynamics which involves pathogen replication-transmission multiscale cycle.

Malaria is an infectious disease system caused by the Plasmodium parasite which has a complex life cycle such that they require at least multiple-host which are (i) human-host and (ii) vector host, for the malaria parasite to have fully completed its life cycle process. In addition to acting as a carrier, the mosquito provides an environment where the Pasmodium parasite can develop to an infectious state before it is transmitted to vertebrate hosts. The Plasmodium life cycle can be divided into three main phases: (1) the vector phase, which happens in the midgut and salivary glands of female Anopheles mosquitoes, (2) The liver stage, which occurs in the hepatocytes of the secondary host, in this case, its humans, and (3) the erythrocytic stage, which occurs in the red blood cells of the secondary host, [35]. Taking into consideration the burden of malaria infection, there is a need for a malaria vaccine that would reduce the gap left by other medical and public health interventions [66]. A Malaria vaccine would be an important tool in controlling malaria because the current struggle against disease is on a variety of these interventions, that include the distribution of LLNs, the promotion of indoor spraying, and the development of new medicines and insecticides [66]. However, the malaria vaccine is designed to act at these three stages during the life cycle of the Plasmodium parasite. There are three main classes of vaccine which are (i) pre-erythrocytic vaccine (PEV), (ii) blood-stage vaccine (BSV), and (iii) transmission-blocking vaccine (TBV) which inhibits the malaria infections in the pre-erythrocytic stage, erythrocytic stage, and in mosquitoes on preventing from transmitting the infection to the next person, respectively [45, 67]. These sub-units are desribed as follows:

(i) The pre-erythrocytic vaccine aims to inhibit the early phase of malaria infection, the phase at which the plasmodium parasite enters or matures in an infected human's liver cells [45, 67].

(ii) The blood-stage vaccine targets the malaria parasite at its most destructive phase, the rapid reduction of the organism in human red red-blood cells. This vaccine do not aim to block all infection, but it ia expected to minimize the number of malaria parasites in the blood system, and this will reduce the severity of the disease [45, 67].

(iii) The transmission-blocking vaccine seeks to disrupt the life cycle of plasmodium parasite by stimulating antibodies that inhibit the malaria parasite from maturing in the mosquito after feeding blood meal from a vaccinated person. This transmission-blocking vaccine would not inhibit a human from getting malaria, nor would diminish the symptoms of the disease. The TBV, which the processes are carried into mosquito after taking a blood meal and their disruption with in-vector parasite development [43, 45, 67].

The vaccine has provided a cost-effective and efficacious means of inhibiting malaria disease and reducing the mortality rate, boosting the immune system in the fight against parasites [67].

The recent studies of malaria vaccines are on single scale models which are either immunological (within-host scale) [45] or epidemiological (between-host scale) by [67]. There were none of the studies that attempted to evaluate the possible impacts of malaria vaccines in controlling malaria parasites on both

scales (within-host scale and between-host scale). There has been relatively little literature published on coupled multiscale models for malaria disease systems. Garira [24] developed a new coupled multiscale model for malaria infection which can enlighten policy and guide malaria control and elimination. They demonstrated their model using nested multiscale models for linking within-host scale sub-model and between-host scale sub-model. In their model, they incorporate the two malaria public health interventions (i.e., artemisinin-based combination therapy (ACT) and long-lasting insecticides treated nets) which they used comparative effectiveness of malaria health interventions. Agusto [35] developed a coupled multiscale model of malaria disease system with immune response, where they also demonstrated their model using the nested multiscale model for linking the within-host scale sub-model and the between-host scale sub-model. None of these investigations has tried to examine the possible influence of malaria vaccines in controlling clinical Plasmodium falciparum parasites in all the parasite stages.

In this study, we formulate a more detailed coupled multiscale model for the malaria disease system considering the contact of malaria parasites with liver cells, red blood cells, human population level, and mosquito population level. The objective of this study is to investigate the influence of vaccine on the multiscale model of the malaria disease system. However, we consider the intra-organ level and extra-organ level. On the intra-organ level, we are investigating the interaction of malaria parasites and the liver cells whereas, at the extra-organ level, we are investigating malaria parasites outside the liver stage.

4.2 The Mathematical Model

We formulate a coupled multiscale model that traces the malaria parasite's life cycle of malaria disease systems. The malaria parasite's life cycle should involve two distinct environments which are: biological human host environment and biological mosquito vector environment. In this work we presented a full coupled multiscale model based on monitoring the dynamics of eighteen populations at time t, which are susceptible humans $S_H(t)$ and infected humans $I_H(t)$; community gametocytes load $G_H(t)$- in human biological environment; susceptible mosquito $S_V(t)$ and infected mosquito $I_V(t)$; community sporozoites load $P_V(t)$- in mosquito biological environment; sporozoites population $P_h(t)$, uninfected liver cells $L_h(t)$, infected liver cells $L_h^*(t)$, uninfected red blood cells $B_h(t)$, infected red blood cells $B_h^*(t)$, population of merozoites $M_h(t)$ and population of gametocytes $G_h(t)$ within-human biological environment; population of gametocytes within infected mosquito $G_v(t)$, population of gametes $G_m(t)$, population of zygotes $Z_v(t)$, population of oocysts $O_v(t)$ and population of sporozoites $P_v(t)$ -in mosquito biological environment.

This coupled multiscale model express the transmission of malaria parasite from mosquito to human using SIP sub-model with variables which are susceptible humans $S_H(t)$, infected humans $I_H(t)$ and community sporozoites load P_V, where by the transmission of malaria parasite at between-human scale from

community infectious reservoir of mosquitoes to humans occurs at a rate $\lambda_V(t) = \frac{\beta_V P_V(t) S_H(t)}{P_0 + P_V(t)}$, where β_V is the contact rate to the community with a population $P_V(t)$ sporozoites per unit time [20]. The community sporozoite load that yields 50% probability of human host get infected with malaria after mosquito bites in a certain community, which is denoted by P_0. Similarly, the model illustrate the transmission of malaria pathogen from human to mosquito using SIP sub-model with variables which are susceptible mosquitoes $S_V(t)$, infected mosquitoes $I_V(t)$ and community gametocytes load $G_H(t)$ and the transmission of malaria pathogen at between-mosquito scale from community infectious reservoir of humans to mosquitoes happen at rate $\lambda_H(t) = \frac{\beta_H G_H(t)}{G_0 + G_H(t)}$. Where β_H is the rate of contact to the community with a population $G_H(t)$ gametocytes per unit time and which is considered as a method of evaluate the human biting rate. Where G_0 models the community gametocyte load that yields 50% likelihood of mosquito getting infected with malaria after mosquito biting an infected human in a certain community.

The S_H and S_V increases at a constant recruitment rate Λ_H and Λ_V respectively. The susceptible humans are decreasing due to the transmission of malaria parasite at between-human scale from community infectious reservoir of mosquito $P_V(t)$ to human hosts occurs at a rate $\beta_V \lambda_V(P_V) S_H(t)$. The susceptible mosquitoes are decreasing due to transmission of malaria pathogen at between-mosquito scale from community infectious reservoir of humans G_H to mosquitoes occurs at a rate $\beta_H \lambda_H(t)(G_H(t)) S_V(t)$. From between-host scale variables, the susceptible host populations ($S_H(t)$ and $S_V(t)$) are reduced through natural death at rates μ_H and μ_V respectively. $S_H(t)$ also increase through natural recovery of infected population at a rate γ_H. Infected human populations $(I_H(t))$ and Infected mosquito populations $(I_V(t))$ increase through $\beta_V \lambda_V(t)(P_V(t)) S_H(t)$ and $\beta_H \lambda_H(t)(G_H(t)) S_V(t)$ respectively and they reduced through natural death at rates (μ_H and μ_V) and also reduced by mortality due to infection at rates δ_H and δ_V. $I_H(t)$ is also reduced due to natural recovery from infection at a rate γ_H. In community sporozoites load $(P_V(t))$, the first term on the right hand side of the equation (18) of model (4.2.0.1) is modeled by $(I_V(t) + 1)\alpha_v P_v(t)$, where every infected mosquito sheds/excretes the within-mosquito scale pathogens (sporozoites) at a rate $\alpha_v P_v(t)$ and for a total of $I_v(t) = I_V(t) + 1$ infected mosquitoes which the model involves the upscaling (for linking of within-mosquito scale to the between-mosquito scale) [18, 20]. P_V diminished by the elimination of the total community sporozoite load at a rate α_V. From community gametocytes load $(G_H(t))$, the first term of the right hand side of the equation (10) of model (4.2.0.1) is showed by $(I_H(t) + 1)\alpha_h G_h(t)$, where every infected human excretes the within-human scale pathogen (gametocytes) at a rate $\alpha_h G_h(t)$ and for a total of $I_h(t) = I_H(t) + 1$ infected mosquitoes is the upscaling of within-human scale to the between-human scale. $G_H(t)$ decreases due to elimination of the total community gametocytes load.

We show features for the derivation of a coupled multiscale model for directly transmitted vector-borne disease (i.e. malaria disease systems) in which the Plasmodium falciparum does not have a replication cycle at both within-human scale and within-mosquito scale as a way of complete its life-cycle. The pathogen load at both within-human scale and within-mosquito scale grows only through super-infection.

The coupled multiscale model of malaria disease systems is demonstrated in Figure (4.1). The infection process at human usually starts with an infected mosquito sucking blood meal and injecting sporozoites in the human blood system. The sporozoites in mosquito will be injected into human system and constitutes the sporozoites population in the first life-stage at within-human scale denoted by $P_h(t)$ and may increase through super-infection at a rate $\lambda_v(t)S_h(t) = \frac{\beta_V P_V(t)(S_H(t)-1)}{(P_0+P_V(t))\phi_H(I_H(t)+1)}$, where ϕ_H is the proportion of new infection or decay naturally at rate μ_p. This process of super-infection involves the down-scaling whereby we integrate the between-host scale parameter and variables to the within-human sub-model. The first intermediate life stage of within-human sub-model which is the uninfected liver cells which is given by $L_h(t)$, increase through the rate of supply of unifected liver cells Λ_l. Uninfected liver cells decrease due to infection of liver cells by sporozoites which is given by $\beta_l P_h(t)L_h(t)$ where β_l is the contact rate of sporozoites with uninfected liver cells. The first intermediate life-stage of within-human scale die naturally at a rate μ_l. The infected liver cells is the second intermediate life stage of within-human scale and which is denoted by $L_h^*(t)$. The second intermediate life stage increase through infection of uninfected liver cells $\beta_l P_h(t)L_h(t)$, or decay naturally at rate μ_l or bursting of liver cells at rate α_l. The uninfected red blood cells is the third intermediate life stage of within-human scale which is given by $B_h(t)$, which increase through the rate of supply of uninfected red blood cells Λ_h, and decrease by infection of uninfected cells by merozoites which is given by $\beta_h M_h(t)B_h(t)$ where β_h is the contact rate of merozoites and unifected red blood cells, or decay naturally at rate μ_b. Infected red blood cells is the fourth intermediate life stage of within-human scale which is denoted by $B_h^*(t)$, increase throughthe rate of proportion of infection of liver cells $(1-\pi)\beta_h M_h(t)B_h(t)$ and or decay natually at rate μ_b or bursting of infected-red blood cells to produce merozoites α_m. The merozoites population is the last stage of the intermediate life stage of within-human scale which is given by $M_h(t)$, the merozoites in the human blood system increase due to bursting of infected liver cells which is given by $N_l\alpha_l L_h^*(t)$ and through the rate of increase of merozotes in the human blood system through bursting of infected red blood cells which is given by $N_m\alpha_m B_h^*(t)$ The population of merozoites assumed to decay naturally at rate μ_m. The population of gametocytes is the last life stage of within-human scale which is given by $G_h(t)$. This last life stage increase through the proportion of the total population of merozoites infected liver cells $\pi\beta_h M_h(t)B_h(t)$, or decrease through the rate of natural decay of gametocytes infected erythrocytes (μ_h) or by (α_h) which is the rate of shed/ excretion of infectious gametocytes from within-infected human blood system to the community gametocytes load.

The infection process of malaria disease system at within-mosquito scale is initiated with the mosquito draw blood meal from an infected human. The gametocytes which are consumed up by the mosquito in blood meal and must cross through the midgut of mosquito, which performance are the first physical obstacle inside the mosquito [58]. The gametocytes population is the initial life-phase at within-mosquito scale which is indicated by $G_v(t)$ in the flow diagram in Figure (4.1) and gametocytes population may increase through super-infection at rate $\lambda_h(t)S_v(t) = \frac{\beta_H G_H(t)(S_V(t)-1)}{(G_0+G_H(t))\phi_V(I_V(t)+1)}$, where ϕ_V is the proportion of new infection or decay naturally at rate μ_g or proceed to the initial intermediate life stage

that is gametes population at rate α_g. We can say α_g is the rate at which gametocytes within-infected mosquitoes burst releasing sex cells called gametes (either male or female gametes). The population of gametes $G_m(t)$ increase by $N_g\alpha_g G_v(t)$, where we assume that for every bursting gametocytes within an infected mosquito, it releases an average of N_g gametes upon bursting. The gametes population decreases through natural decay at rate μ_s or at rate α_s where gametes also get depleted through male and female gametes fusing to form zygotes which is the second intermediate life-phase. The population of zygotes $Z_v(t)$ increase through the developmental processes which is udergone by gametes to mature and pair-up and fuse to form zygotes at rate $\frac{\alpha_s}{2}G_m(t)$. The zygote population either decay naturally at rate μ_z or proceed to further developmental changes into ookinetes and migrates to the midgut of the mosquito by pass through the gull wall and then form the oocysts at rate α_z. The oocysts population $(O_v(t))$ is the last intermediate life-stage on within-mosquito scale where increase through developmental changes in ookinetes to become oocysts at $\alpha_z Z_v(t)$ and decrease through natural decay at rate μ_k or through bursting of oocysts to release sporozoites at α_k. The population of sporozoites $(P_v(t))$ increase by $N_k\alpha_k O_v(t)$, where we assume that each oocyst bursts at a rate of α_k producing an average of N_k sporozoites upon bursting. The population of sporozoites decrease through natural decay at rate μ_v or at rate α_v which is the excretion/shedding rate of mature sporozoites into the salivary glands of within-infected mosquito to the community sporozoites load.

From the diagram shown in Figure (4.1), we have the following system of equations as a coupled multi-scale model for malaria disease system transmission dynamics which is given by model (4.2.0.1).

$$
\begin{aligned}
1.\quad \frac{dS_H(t)}{dt} &= \Lambda_H - \frac{\beta_V P_V(t)}{P_0 + P_V(t)} S_H(t) - \mu_H S_H(t) + \gamma_H I_H(t),\\
2.\quad \frac{dI_H(t)}{dt} &= \frac{\beta_V P_V(t)}{P_0 + P_V(t)} S_H(t) - [\mu_H + \gamma_H + \delta_H]\, I_H(t),\\
3.\quad \frac{dP_h(t)}{dt} &= \frac{\beta_V P_V(t)(S_H(t)-1)}{(P_0 + P_V(t))\phi_H(I_H(t)+1)} - \mu_p P_h(t),\\
4.\quad \frac{dL_h(t)}{dt} &= \Lambda_l - \beta_l P_h(t) L_h(t) - \mu_l L_h(t),\\
5.\quad \frac{dL_h^*(t)}{dt} &= \beta_l P_h(t) L_h(t) - \alpha_l L_h^*(t),\\
6.\quad \frac{dB_h(t)}{dt} &= \Lambda_h - \beta_h M_h(t) B_h(t) - \mu_b B_h(t),\\
7.\quad \frac{dB_h^*(t)}{dt} &= (1-\pi)\beta_h M_h(t) B_h(t) - \alpha_m B_h^*(t),\\
8.\quad \frac{dM_h(t)}{dt} &= N_l \alpha_l L_h^*(t) + N_m \alpha_m B_h^*(t) - \mu_m M_h(t) - \beta_h M_h(t) B_h(t),\\
9.\quad \frac{dG_h(t)}{dt} &= \pi \beta_h M_h(t) B_h(t) - (\alpha_h + \mu_h) G_h(t).\\
10.\quad \frac{dG_H(t)}{dt} &= G_h(t)\alpha_h(I_H(t)+1) - \alpha_H G_H(t),\\
11.\quad \frac{dS_V(t)}{dt} &= \Lambda_V - \frac{\beta_H G_H(t)}{G_0 + G_H(t)} S_V(t) - \mu_V S_V(t),\\
12.\quad \frac{dI_V(t)}{dt} &= \frac{\beta_H G_H(t)}{G_0 + G_H(t)} S_V(t) - [\mu_V + \delta_V]\, I_V(t),\\
13.\quad \frac{dG_v(t)}{dt} &= \frac{\beta_H G_H(t)(S_V(t)-1)}{(G_0 + G_H(t))\phi_V(I_V(t)+1)} - [\alpha_g + \mu_g]\, G_v(t),\\
14.\quad \frac{dG_m(t)}{dt} &= N_g \alpha_g G_v(t) - [\alpha_s + \mu_s]\, G_m(t),\\
15.\quad \frac{dZ_v(t)}{dt} &= \frac{1}{2}\alpha_s G_m(t) - [\alpha_z + \mu_z]\, Z_v(t),\\
16.\quad \frac{dO_v(t)}{dt} &= \alpha_z Z_v(t) - [\alpha_k + \mu_k]\, O_v(t),\\
17.\quad \frac{dP_v(t)}{dt} &= N_k \alpha_k O_v(t) - [\alpha_v + \mu_v]\, P_v(t).\\
18.\quad \frac{dP_V(t)}{dt} &= P_v(t)\alpha_v\,(I_V(t)+1) - \alpha_V P_V(t).
\end{aligned}
\tag{4.2.0.1}
$$

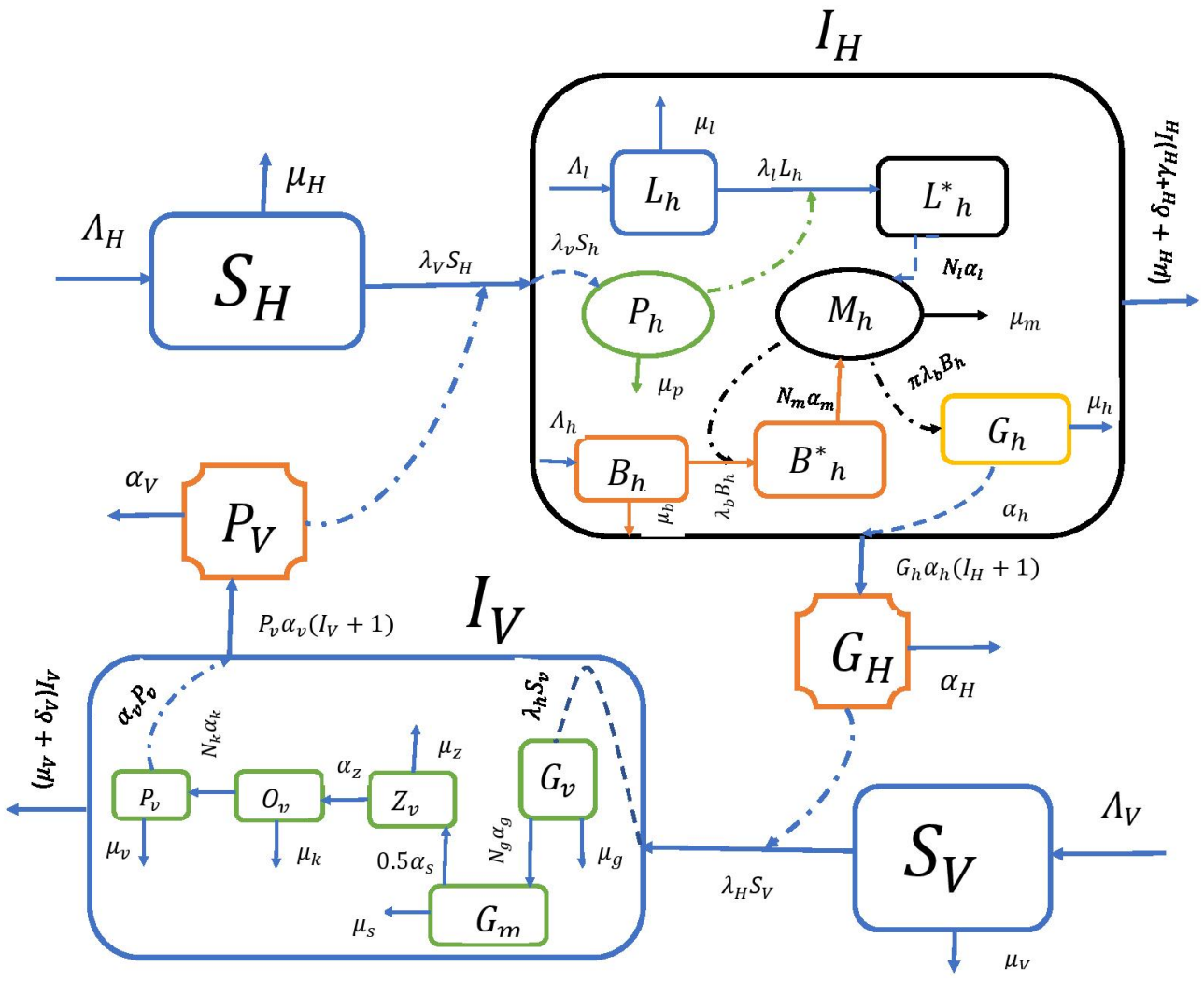

Figure 4.1: A conceptual diagram of a coupled multiscale model (4.2.0.1) of malaria disease dynamics.

4.2.1 Reproductive Number

Using the next generation operator approach to calculate the basic reproductive number and we use the [61]'s approach. The model system (4.2.0.1) can be written in the form

$$\begin{aligned} \frac{dX}{dt} &= f(X, Y, Z), \\ \frac{dY}{dt} &= g(X, Y, Z), \\ \frac{dZ}{dt} &= h(X, Y, Z), \end{aligned} \tag{4.2.1.1}$$

where

$$\begin{aligned} X &= (S_H(t), L_h(t), B_h(t), S_V(t)), \\ Y &= (I_H(t), P_h(t), L_h^*(t), B_h^*(t), G_h(t), I_V(t), G_v(t), G_m(t), Z_v(t), O_v(t), P_v(t)), \\ Z &= (M_h(t), G_H(t), P_V(t)). \end{aligned} \tag{4.2.1.2}$$

We define $\widetilde{g}(X^*, Z)$ by The disease free equilibrium is given by

$$\begin{aligned} E_0 &= (S_H^0, I_H^0, P_h^0, L_h^0, L_h^{*0}, B_h^0, B_h^{*0}, M_h^0, G_h^0, G_H^0, S_V^0, I_V^0, G_v^0, G_m^0, Z_v^0, O_v^0, P_v^0, P_V^0), \\ &= \left(\frac{\Lambda_H}{\mu_H}, 0, 0, \frac{\Lambda_l}{\mu_l}, 0, \frac{\Lambda_h}{\mu_b}, 0, 0, 0, 0, \frac{\Lambda_V}{\mu_V}, 0, 0, 0, 0, 0, 0, 0\right). \end{aligned} \tag{4.2.1.3}$$

By letting $h_1 = \dfrac{dM_h}{dt}$, $h_2 = \dfrac{dG_H}{dt}$ and $h_3 = \dfrac{dP_V}{dt}$ we obtain

$$\begin{aligned} h_1 &= \frac{N_l\alpha_l}{\alpha_l+\mu_l}\frac{\beta_l\Lambda_l\beta_V(\Lambda_H-\mu_H)(\mu_H+\gamma_H+\delta_H)P_V}{\mu_p\mu_l\phi_H[\beta_V\Lambda_H P_V+\mu_H(\mu_H+\gamma_H+\delta_H)(P_0+P_V)]} \\ &\quad + \frac{N_m\alpha_m}{\alpha_m+\mu_b}\frac{(1-\pi)\beta_h\Lambda_h M_h}{\mu_b} - \frac{(\mu_m\mu_b+\beta_h\Lambda_h)M_h}{\mu_b} \\ h_2 &= \frac{\alpha_h}{\alpha_h+\mu_h}\frac{\pi\beta_h\Lambda_h[\beta_V\Lambda_H P_V+\mu_H(\mu_H+\gamma_H+\delta_H)(P_0+P_V)]M_h}{\mu_b\mu_H(\mu_H+\gamma_H+\delta_H)(P_0+P_V)} - \alpha_H G_H, \\ h_3 &= \frac{1}{2}\frac{N_g\alpha_g}{\alpha_g+\mu_g}\frac{\alpha_s}{\alpha_s+\mu_s}\frac{\alpha_z}{\alpha_z+\mu_z}\frac{N_k\alpha_k}{\alpha_k+\mu_k}\frac{\alpha_v}{\alpha_v+\mu_v}\frac{\beta_H(\Lambda_V-\mu_V)G_H}{\mu_V\phi_V(G_0+G_H)} - \alpha_V P_V, \end{aligned} \tag{4.2.1.4}$$

$A = M - D$, where $M > 0$ and $D > 0$, a diagonal matrix.

$$\begin{aligned} A &= \begin{pmatrix} \dfrac{\partial h_1}{\partial M_h} & \dfrac{\partial h_1}{\partial G_H} & \dfrac{\partial h_1}{\partial P_V} \\ \dfrac{\partial h_2}{\partial M_h} & \dfrac{\partial h_2}{\partial G_H} & \dfrac{\partial h_2}{\partial P_V} \\ \dfrac{\partial h_3}{\partial M_h} & \dfrac{\partial h_3}{\partial G_H} & \dfrac{\partial h_3}{\partial P_V} \end{pmatrix}, \\ &= \begin{pmatrix} \dfrac{N_m\alpha_m}{\alpha_m+\mu_b}\dfrac{(1-\pi)\beta_h\Lambda_h}{\mu_b} - \dfrac{\mu_m\mu_b+\beta_h\Lambda_h}{\mu_b} & 0 & \dfrac{N_l\alpha_l}{\alpha_l+\mu_l}\dfrac{\beta_l\Lambda_l\beta_V(\Lambda_H-\mu_H)}{\mu_p\mu_l\mu_H\phi_H P_0} \\ \dfrac{\alpha_h}{\alpha_h+\mu_h}\dfrac{\pi\beta_h\Lambda_h}{\mu_b} & -\alpha_H & 0 \\ 0 & a_1 & -\alpha_V \end{pmatrix}, \end{aligned} \tag{4.2.1.5}$$

$$M = \begin{pmatrix} \frac{N_m\alpha_m}{\alpha_m+\mu_b}\frac{(1-\pi)\beta_h\Lambda_h}{\mu_b} & - & \frac{\mu_m\mu_b+\beta_h\Lambda_h}{\mu_b} & 0 & \frac{N_l\alpha_l}{\alpha_l+\mu_l}\frac{\beta_l\Lambda_l\beta_V(\Lambda_H-\mu_H)}{\mu_p\mu_l\mu_H\phi_H P_0} \\ \frac{\alpha_h}{\alpha_h+\mu_h}\frac{\pi\beta_h\Lambda_h}{\mu_b} & & & 0 & 0 \\ 0 & & & a_1 & 0 \end{pmatrix} \quad (4.2.1.6)$$

$$D = \begin{pmatrix} \frac{\mu_m\mu_b+\beta_h\Lambda_h}{\mu_b} & 0 & 0 \\ 0 & \alpha_H & 0 \\ 0 & 0 & \alpha_V \end{pmatrix}, \quad (4.2.1.7)$$

$$D^{-1} = \begin{pmatrix} \frac{\mu_b}{\mu_m\mu_b+\beta_h\Lambda_h} & 0 & 0 \\ 0 & \frac{1}{\alpha_H} & 0 \\ 0 & 0 & \frac{1}{\alpha_V} \end{pmatrix}, \quad (4.2.1.8)$$

where $a_1 = \frac{1}{2}\frac{N_g\alpha_g}{\alpha_g+\mu_g}\frac{\alpha_s}{\alpha_s+\mu_s}\frac{\alpha_z}{\alpha_z+\mu_z}\frac{N_k\alpha_k}{\alpha_k+\mu_k}\frac{\alpha_v}{\alpha_v+\mu_v}\frac{\beta_H(\Lambda_V-\mu_V)}{\mu_V\phi_V G_0}$.

$$MD^{-1} = \begin{pmatrix} \frac{N_m\alpha_m}{\alpha_m+\mu_b}\frac{(1-\pi)\beta_h\Lambda_h}{\mu_m\mu_b+\beta_h\Lambda_h} & 0 & \frac{N_l\alpha_l}{\alpha_l+\mu_l}\frac{\beta_l\Lambda_l\beta_V(\Lambda_H-\mu_H)}{\mu_p\mu_l\mu_H\alpha_V\phi_H P_0} \\ \frac{\alpha_h}{\alpha_h+\mu_h}\frac{\pi\beta_h\Lambda_h}{\mu_m\mu_b+\beta_h\Lambda_h} & 0 & 0 \\ 0 & Q_V & 0 \end{pmatrix}, \quad (4.2.1.9)$$

where

$$\begin{aligned} Q_V &= \frac{1}{2}\frac{N_g\alpha_g}{\alpha_g+\mu_g}\frac{\alpha_s}{\alpha_s+\mu_s}\frac{\alpha_z}{\alpha_z+\mu_z}\frac{N_k\alpha_k}{\alpha_k+\mu_k}\frac{\alpha_v}{\alpha_v+\mu_v}\frac{\beta_H(\Lambda_V-\mu_V)}{\mu_V\alpha_H\phi_V G_0} \\ Q_H &= \frac{\alpha_h}{\alpha_h+\mu_h}\frac{\pi\beta_h\Lambda_h}{\mu_m\mu_b+\beta_h\Lambda_h}\frac{N_l\alpha_l}{\alpha_l+\mu_l}\frac{\beta_l\Lambda_l\beta_V(\Lambda_H-\mu_H)}{\mu_p\mu_l\mu_H\alpha_V\phi_H P_0} \end{aligned} \quad (4.2.1.10)$$

$R_0 = \rho(MD^{-1})$, which is given by

$$\lambda^3 + b_2\lambda^2 + b_1\lambda + b_0 = 0, \tag{4.2.1.11}$$

where

$$\begin{aligned} b_2 &= -\frac{N_m\alpha_m}{\alpha_m + \mu_b}\frac{(1-\pi)\beta_h\Lambda_h}{\mu_m\mu_b + \beta_h\Lambda_h} \\ b_1 &= 0, \\ b_0 &= -Q_V Q_H, \end{aligned} \tag{4.2.1.12}$$

where

$$\begin{aligned} \Lambda_H &> \mu_H, \\ \Lambda_V &> \mu_V. \end{aligned} \tag{4.2.1.13}$$

The solution is given by the cubic formulae

$$\begin{aligned} \lambda_1 &= -\frac{1}{3}b_2 + (H+O), \\ \lambda_2 &= -\frac{1}{3}b_2 - \frac{1}{2}(H+O) - \frac{1}{2}\sqrt{3(O-H)}, \\ \lambda_3 &= -\frac{1}{3}b_2 - \frac{1}{2}(H+O) + \frac{1}{2}\sqrt{3(O-H)}, \end{aligned} \tag{4.2.1.14}$$

where

$$\begin{aligned} H &= \sqrt[3]{R+\sqrt{D}}, \\ O &= \sqrt[3]{R-\sqrt{D}}, \\ D &= Q^3 + R^2, \\ Q &= \frac{3b_1 - b_2^2}{9}, \\ R &= \frac{9b_1b_2 - 27b_0 - 2b_2^3}{54}. \end{aligned} \tag{4.2.1.15}$$

Since $b_0 < 0$, $b_1 = 0$ and $b_2 < 0$, therefore

$$\begin{aligned} Q &= -\frac{b_2^2}{9} < 0, \\ R &= \frac{-27b_0 - 2b_2^3}{54} > 0, \\ D &= \left(-\frac{b_2^2}{3^2}\right)^3 + \left(-\frac{3^3 b_0 + 2b_2^3}{2 \times 3^3}\right)^2, \\ &= \frac{-4b_2^6 + 3^6 b_0^2 + 2 \times 3^3 b_0 b_2^3 + 4b_2^6}{2^2 \times 3^6}, \\ &= \frac{3^3(3^3 b_0 + 2b_2^3)}{2^2 \times 3^3 \times 3^3}, \\ D &= \frac{b_0(27b_0 + 2b_2^3)}{108} > 0. \end{aligned} \tag{4.2.1.16}$$

(4.2.1.17)

Since $R > 0$ and $D > 0$, therefore

$$\begin{aligned} H &= \sqrt[3]{R + \sqrt{D}} > 0, \\ O &= \sqrt[3]{R - \sqrt{D}} > 0, \\ H &> O, \\ O - H &< 0. \end{aligned} \tag{4.2.1.18}$$

There are three possible values which may represent the value of reproductive number, these are mathematically correct but not all of them gives us real positive solutions, some are complex numbers. We take the real positive numbers only. Therefore $\lambda_1 > 0$, and λ_2 and λ_3 are the imaginary roots of polynomial equaton (4.2.1.11). Therefore we conclude that our reproductive number is given by

$$\begin{aligned} R_0 &= \lambda_1 = -\frac{1}{3}b_2 + (H + O), \\ &= -\frac{1}{3}b_2 + \left[\sqrt[3]{R + \sqrt{D}} + \sqrt[3]{R - \sqrt{D}}\right], \\ &= -\frac{1}{3}b_2 + \left[\sqrt[3]{\frac{-27b_0 - 2b_2^3}{54} + \sqrt{\frac{b_0(27b_0 + 2b_2^3)}{108}}} + \sqrt[3]{\frac{-27b_0 - 2b_2^3}{54} - \sqrt{\frac{b_0(27b_0 + 2b_2^3)}{108}}}\right], \\ &= \frac{1}{3}\frac{N_m\alpha_m}{\alpha_m + \mu_b}\frac{(1-\pi)\beta_h\Lambda_h}{\mu_m\mu_b + \beta_h\Lambda_h} \end{aligned} \tag{4.2.1.19}$$

$$+\sqrt[3]{\frac{27Q_VQ_H + 2\left(\frac{N_m\alpha_m}{\alpha_m+\mu_b}\frac{(1-\pi)\beta_h\Lambda_h}{\mu_m\mu_b+\beta_h\Lambda_h}\right)^3}{54} + \sqrt{\frac{Q_VQ_H\left(27Q_VQ_H + 2\left(\frac{N_m\alpha_m}{\alpha_m+\mu_b}\frac{(1-\pi)\beta_h\Lambda_h}{\mu_m\mu_b+\beta_h\Lambda_h}\right)^3\right)}{108}}}$$

$$+\sqrt[3]{\frac{27Q_VQ_H + 2\left(\frac{N_m\alpha_m}{\alpha_m+\mu_b}\frac{(1-\pi)\beta_h\Lambda_h}{\mu_m\mu_b+\beta_h\Lambda_h}\right)^3}{54} - \sqrt{\frac{Q_VQ_H\left(27Q_VQ_H + 2\left(\frac{N_m\alpha_m}{\alpha_m+\mu_b}\frac{(1-\pi)\beta_h\Lambda_h}{\mu_m\mu_b+\beta_h\Lambda_h}\right)^3\right)}{108}}}$$

4.2.2 Positivity of solutions

The multiscale model (4.2.0.1) describes the dynamics of human, mosquito and parasite populations and it is essential to show that these populations are positive for all $t \geq 0$. We have to prove the following theorem.

Theorem 4.1. *The solutions of the multiscale model (4.2.0.1) satisfy the following initial conditions which strictly positive components i.e. ($SH > 0$, $I_H > 0$, $P_h > 0$, $L_h > 0$, $L_h^* > 0$, $B_h > 0$, $B_h^8 > 0$, $M_h > 0$, $G_h > 0$, $G_H > 0$, $S_V > 0$, $I_V > 0$, $G_v > 0$, $G_m > 0$, $Z_v > 0$, $O_v > 0$, $P_v > 0$,$P_V > 0$) for all $t > 0$.*

Proof. We prove that the solution of the multiscale model (4.2.0.1) of which the solution starts from a strictly positive point, all components are positive for $0 \leq t \leq t_0$.

$$\frac{dS_H(t)}{dt} =\geq -(\lambda_V(t) + \mu_H)S_H(t), \tag{4.2.2.1}$$

The equation can be solved by the separable variable as follows.

$$\frac{dS_H(t)}{S_H(t)} \geq -(\lambda_V(t) + \mu_H)dt. \tag{4.2.2.2}$$

By leting

$$\begin{aligned}\hat{t} \quad = \quad & \sup\{t > 0 : S_H > 0, I_H > 0, P_h > 0, L_h > 0, L_h^* > 0, B_h > 0, B_h^* > 0, M_h > 0, G_h > 0, \\ & G_H > 0, S_V > 0, I_V > 0, G_v > 0, G_m > 0, Z_v > 0, O_V.0, P - [v].0, P - [V].0\} \in [0, t],\end{aligned}$$

and integrating equation (4.2.2.2), and we obtain

$$\begin{aligned}\ln(S_H(t)) \quad \geq \quad & -\left(\int_0^t \lambda_V(\hat{t})d\hat{t} + \mu_H t\right) + \ln(S_H(0)), \\ S_H(t) \quad \geq \quad & S_H(0)\exp\left\{-\left(\int_0^t \lambda_V(\hat{t})d\hat{t} + \mu_H t\right)\right\}.\end{aligned}$$

It implies that

$$\lim_{t\to\infty} \inf(S_H(t)) \geq 0.$$

Using similar method, we obtain

$$\begin{aligned}I_H(t) \quad \geq \quad & I_H(0)\exp\{-(\mu_H + \gamma_H + \delta_H)t\}, \\ \lim_{t\to} \inf(I_H) \quad \geq \quad & 0.\end{aligned}$$

Using similar principle on the sporozoites population (P_h) within-human dynamics, we obtain

$$\begin{aligned}P_h(t) \quad \geq \quad & P_h(0)\exp\{-\mu_p t\}, \\ \lim_{t\to\infty} \inf(P_h(t)) \quad \geq \quad & 0.\end{aligned} \tag{4.2.2.3}$$

Using Similar method, it can be shown that

$$\begin{aligned}
\lim_{t\to\infty}(L_h(t)) &\geq 0,\\
\lim_{t\to\infty}(L_{h^*}(t)) &\geq 0,\\
\lim_{t\to\infty}(B_h(t)) &\geq 0,\\
\lim_{t\to\infty}(B_h^*(t)) &\geq 0,\\
\lim_{t\to\infty}(M_h(t)) &\geq 0,\\
\lim_{t\to\infty}(G_h(t)) &\geq 0,\\
\lim_{t\to\infty}(G_H(t)) &\geq 0,\\
\lim_{t\to\infty}(S_V(t)) &\geq 0,\\
\lim_{t\to\infty}(I_V(t)) &\geq 0,\\
\lim_{t\to\infty}(G_v(t)) &\geq 0,\\
\lim_{t\to\infty}(G_m(t)) &\geq 0,\\
\lim_{t\to\infty}(Z_v(t)) &\geq 0,\\
\lim_{t\to\infty}(O_v(t)) &\geq 0,\\
\lim_{t\to\infty}(P_v(t)) &\geq 0,\\
\lim_{t\to\infty}(P_V(t)) &\geq 0,
\end{aligned} \tag{4.2.2.4}$$

Thus, when starting with no-negative initial value conditions in the multiscale model (4.2.0.1), the solutions of the model will remain non-negative for all $t \geq 0$, and this completes the proof. □

4.2.3 Invariant Region

Let N_H represent the total human population and by letting $N_H = S_H + I_H$ and adding first and second equations in system (4.2.0.1)

$$\begin{aligned}
\frac{dN_H}{dt} &= \frac{dS_H}{dt} + \frac{dI_H}{dt},\\
&= \Lambda_H - \mu_H N_H - \delta_H I_H,\\
&\leq \Lambda_H - \mu_H N_H.
\end{aligned} \tag{4.2.3.1}$$

It implies that

$$\lim_{t\to\infty} Sup(N_H(t)) \leq \frac{\Lambda_H}{\mu_H}. \tag{4.2.3.2}$$

Applying the similar method letting $N_V = S_V + I_V$, where N_V is the total mosquitoes population, and by adding fourth and fifth equations in system (4.2.0.1), we obtain

$$\frac{dN_V}{dt} \leq \Lambda_V - \mu_V N_V. \tag{4.2.3.3}$$

It implies that

$$\lim_{t\longrightarrow\infty} Sup(N_V(t)) \leq \frac{\Lambda_V}{\mu_V}. \tag{4.2.3.4}$$

Let N_h represent the total liver cells population, where $N_h = L_h + L_h^*$. By adding equations thirteen and fourteen we obtain

$$\frac{dN_h}{dt} \leq \Lambda_l - \mu_l N_h. \tag{4.2.3.5}$$

It implies that

$$\lim_{t\to\infty} Sup(N_h(t)) \leq \frac{\Lambda_l}{\mu_l}. \tag{4.2.3.6}$$

Let the total red blood cells population be N_r, such that $N_r = B_h + B_h^*$. From adding the equations fifteen and sixteen of the system (4.2.0.1), we obtain

$$\frac{dN_r}{dt} \leq \Lambda_h - \mu_b N_r. \tag{4.2.3.7}$$

This implies that

$$\lim_{t\to\infty} Sup(N_r(t)) \leq \frac{\Lambda_h}{\mu_b}. \tag{4.2.3.8}$$

Therefore all feasible solutions of the model system (4.2.0.1) are positive and eventually enter the invariant attracting region

$$\begin{aligned}\Omega \quad = \quad & ((S_H, I_H, P_h, L_h, L_h^*, B_h, B_h^*, M_h, G_h, G_H, S_V, I_V, G_v, G_m, Z_v, O_v, P_v, P_V) : \\ & 0 \leq S_H + I_H \leq \Omega_1, 0 \leq S_V + I_V \leq \Omega_2, 0 \leq L_h + L_h^* \leq \Omega_3, 0 \leq B_h + B_h^* \leq \Omega_4, \\ & 0 \leq M_h \leq \Omega_5, 0 \leq G_h \leq \Omega_6, 0 \leq G_H \leq \Omega_7, 0 \leq G_v \leq \Omega_8, 0 \leq G_m \leq \Omega_9, \\ & 0 \leq Z_v \leq \Omega_{10}, 0 \leq O_v \leq \Omega_{11}, 0 \leq P_v \leq \Omega_{12}, 0 \leq P_V \leq \Omega_{13}),\end{aligned} \tag{4.2.3.9}$$

where

$$
\begin{aligned}
\Omega_1 &= \frac{\Lambda_H}{\mu_H}, \\
\Omega_2 &= \frac{\Lambda_V}{\mu_V}, \\
\Omega_3 &= \frac{\Lambda_l}{\mu_l}, \\
\Omega_4 &= \frac{\Lambda_h}{\mu_b}, \\
\Omega_5 &= \frac{N_l\alpha_l\mu_b\Lambda_l + N_m\alpha_m\mu_l\Lambda_h}{\mu_l(\mu_m\mu_b + \beta_h\Lambda_h)}, \\
\Omega_6 &= \frac{1}{\alpha_h+\mu_h}\frac{\pi\beta_h\Lambda_h\left[N_l\alpha_l\mu_b\Lambda_l + N_m\alpha_m\mu_l\Lambda_h\right]}{\mu_l\mu_b(\mu_m\mu_r + \beta_h\Lambda_h)}, \\
\Omega_7 &= \frac{\alpha_h}{\alpha_h+\mu_h}\frac{\pi\beta_h\Lambda_h d_1}{\alpha_H\mu_H\mu_L\mu_r(\mu_m\mu_r + \beta_h\Lambda_h)}, \\
\Omega_8 &= \frac{1}{\alpha_g+\mu_g}\frac{\pi\alpha_h\beta_h\Lambda_h\beta_H(\Lambda_V-\mu_V)d_1}{\phi_V(\Lambda_V+\mu_V)d_2}, \\
\Omega_9 &= \frac{N_g\alpha_g}{\alpha_g+\mu_g}\frac{1}{\alpha_s+\mu_s}\frac{\pi\alpha_h\beta_h\Lambda_h\beta_H(\Lambda_V-\mu_V)d_1}{\phi_V(\Lambda_V+\mu_V)d_2}, \\
\Omega_{10} &= \frac{1}{2}\frac{N_g\alpha_g}{\alpha_g+\mu_g}\frac{\alpha_s}{\alpha_s+\mu_s}\frac{1}{\alpha_z+\mu_z}\frac{\pi\alpha_h\beta_h\Lambda_h\beta_H(\Lambda_V-\mu_V)d_1}{\phi_V(\Lambda_V+\mu_V)d_2}, \\
\Omega_{11} &= \frac{1}{2}\frac{N_g\alpha_g}{\alpha_g+\mu_g}\frac{\alpha_s}{\alpha_s+\mu_s}\frac{\alpha_z}{\alpha_z+\mu_z}\frac{1}{\alpha_k+\mu_k}\frac{\pi\alpha_h\beta_h\Lambda_h\beta_H(\Lambda_V-\mu_V)d_1}{\phi_V(\Lambda_V+\mu_V)d_2}, \\
\Omega_{12} &= \frac{1}{2}\frac{N_k\alpha_k}{\alpha_k+\mu_k}\frac{N_g\alpha_g}{\alpha_g+\mu_g}\frac{\alpha_s}{\alpha_s+\mu_s}\frac{\alpha_z}{\alpha_z+\mu_z}\frac{1}{\alpha_v+\mu_v}\frac{\pi\alpha_h\beta_h\Lambda_h\beta_H(\Lambda_V-\mu_V)d_1}{\phi_V(\Lambda_V+\mu_V)d_2}, \\
\Omega_{13} &= \frac{1}{2}\frac{N_k\alpha_k}{\alpha_k+\mu_k}\frac{N_g\alpha_g}{\alpha_g+\mu_g}\frac{\alpha_s}{\alpha_s+\mu_s}\frac{\alpha_z}{\alpha_z+\mu_z}\frac{\alpha_v}{(\alpha_v+\mu_v)}\frac{\pi\alpha_h\beta_h\Lambda_h\beta_H(\Lambda_V-\mu_V)d_1}{\alpha_V\mu_V\phi_V d_2},
\end{aligned}
\tag{4.2.3.10}
$$

where

$$
\begin{aligned}
d_1 &= (\Lambda_H+\mu_H)\left[N_l\alpha_l\mu_b\Lambda_l + N_m\alpha_m\mu_l\Lambda_h\right], \\
d_2 &= G_0\mu_H\alpha_H\mu_l\mu_b(\alpha_h+\mu_h)(\mu_m\mu_b+\beta_h\Lambda_h) + \alpha_h\pi\beta_h\Lambda_h d_1.
\end{aligned}
\tag{4.2.3.11}
$$

Any solution of the model (4.2.0.1) which commences in Ω at any time $t \geq 0$ will always remain confined in the region. Whenever $\Lambda_H > \mu_H$ and $\Lambda_V > \mu_V$, Ω is positively invariant and attracting and it is sufficient to consider solutions of the system of equations (4.2.0.1) in Ω. So the model (4.2.0.1) is hence well presented mathematically and biologically.

4.3 Numerical Simulation

In this section, we carry out a numerical simulations of a coupled multiscale model of malaria disease system, in order to illustrate some of the analytical results obtained in this work. We compute the model system to outline the effect of different parameter values. The behaviour of model system (4.2.0.1) was

investigated using Python program version (2.7) in the windows operation system (Windows 10). The parameter values used for model simulation are presented and described in Tables (4.1), (4.2), (4.3) and (4.4). Some of the parameter values utilised in this research work were taken from published literature and some were estimated from experimental studies. The reason why some parameter values are assumed or estimated is that the multiscale modeling of malaria infectious disease, which includes the within-human host scale and within-mosquito scale, are limited or the parameter values found in existing literature are not suitable for this model. The model developed in this work, was simulated using the initial value conditions given by $S_H(0) = 10000$, $I_H(0) = 70$, $P_h(0) = 1000$, $L_h(0) = 100$, $L_h^*(0) = 10$, $B_h(0) = 10$, $B_h^*(0) = 10$, $M_h(0) = 10$, $G_h(0) = 100$, $G_H(0) = 60000$, $S_V(0) = 100000$, $I_V(0) = 200$, $G_v(0) = 100$, $G_m(0) = 100$, $Z_v(0) = 10$, $O_v(0) = 10$, $P_v(0) = 10$ and $P_V(0) = 40000$.

Table 4.1: Between-mosquito scale parameter values and their description.

Parameter	Description	Initial Value	Range	Units	Source
Λ_V	Rate of recruitment of susceptible mosquitoes.	2000	1000-3000	Mosquitoes per day	[35]
β_V	Contact rate of susceptible humans with the infectious reservoir of mosquitoes.	0.32135	2.7×10^{-3}-0.64	day^{-1}	[35]
μ_V	Natural death rate of mosquitoes.	0.12	0.033-0.3	day^{-1}	[24]
δ_V	induced death rate of infected mosquitoes.	0.00000426	$4.26 \times 10^{-6} - 5.33 \times 10^{-6}$	day^{-1}	[24]
P_0	Half saturation constant associated with the infection of humans.	1×10^8	$1^7 - 5 \times 10^8$	day^{-1}	[24]
ϕ_V	Proportion of new infected mosquitoes in the total infected mosquito population.	0.0001	0.0001-0.01	day^{-1}	Assumed
α_V	Rate of clearance of community sporozoite load.	0.3	0.09-0.99	day^{-1}	[24]

Table 4.2: Between-human scale parameter values and their description.

Parameter	Description	Initial Value	Range	Units	Source
Λ_H	Rate of recruitment of Susceptible humans.	600	10-800	Humans per day	[35]
β_H	Infection rate of susceptible mosquitoes.	0.356	0.072-0.64	day^{-1}	[35]
μ_H	Natural death rate of humans.	0.00004	0.00001-0.00008	day^{-1}	[24]
δ_H	Disease induced death rate of humans.	0.003454	$1 \times 10^{-15} - 4.1 \times 10^{-4}$	day^{-1}	[35]
γ_H	Natural recovery rate of humans.	0.0092	0.0014-0.017	day^{-1}	[35]
G_0	Half saturation constant associated with the infection of mosquitoes.	5×10^8	$1\times10^8 - 1\times10^9$	day^{-1}	[24]
ϕ_H	Proportion of new infected humans in the total infected human population.	0.0001	0.0001-0.01	day^{-1}	Assumed
α_H	Rate of clearance of community gametocyte load.	0.0000913	0.0000467-0.000274	day^{-1}	[24]

Table 4.3: Within-mosquito scale parameter values and their description.

Parameter	Description	Initial Value	Range	Units	Source
α_g	Rate at which gametocyte infected erythrocytes burst within ifected mosquito.	96	90-100	day^{-1}	[24]
μ_g	Decay rate of gametocytes within infected mosquito.	0.0625	0.0326-0.0725	day^{-1}	[24]
N_g	Number of gametes produced per gametocyte infected erythrocyte within infected mosquito.	2	1-3	day^{-1}	[24]
α_z	Rate at which zygote develop into oocysts.	0.4240	0.01-0.5	day^{-1}	[24]
μ_z	Natural death rate of zygote.	1	1-4	day^{-1}	[24]
α_s	Fertilisation of gametes.	0.2	0.01-0.2	day^{-1}	Assumed
μ_s	Natural death rate of gametes.	58	40-129	day^{-1}	[24]
α_k	Bursting rate of oocysts to produce sporozoites.	0.2	0-1	day^{-1}	[24]
N_k	Number of sporozoites produced per bursting oocysts.	3 000	1000-10000	day^{-1}	[24]
μ_k	Natural death rate of oocysts.	0.01	0.071-0.143	day^{-1}	[24]
α_v	Rate at which sporozoites become infectious to humans.	0.025	0.0167-1	day^{-1}	[24]
μ_v	Natural death rate of sporozoites.	0.0001	0.0001-0.01	day^{-1}	[24]

Table 4.4: Within-human scale parameter values and their description.

Parameter	Description	Initial Value	Range	Units	Source
Λ_l	Rate of supply of uninfected liver cells.	3000		Cells per day	[60]
μ_p	Decay rate of sporozoites.	1.2×10^{-11}		day^{-1}	[45]
β_l	Rate of infection of hepatocytes by sporozoites.	1×10^{-6}		day^{-1}	[45]
μ_l	Natural decay rate of liver cells.	0.029		day^{-1}	[45]
α_l	Rate at which infected liver cell bursts.	0.02		day^{-1}	[45]
N_l	Number of merozoites produced per bursting pre-erythrocytes.	10 000		day^{-1}	[45]
Λ_h	Rate of suppy of uninfected red blood cells.	200	100-300	cells per day	[24]
β_h	Rate of infection of red blood cells (erythrocytes).	0.1	2×10^{-9}-0.2	day^{-1}	[24]
α_h	Rate at which gametocytes develop and become infectious within infected human.	0.4	0.01-0.9	day^{-1}	[24, 47]
μ_h	Natural death rate of gametocyte infected erythrocytes within infected human.	0.0625	0.0600-0.0625	day^{-1}	[24]
μ_b	Natural decay rate of red blood cells.	0.0083	0.006-0.1	day^{-1}	[24]
μ_m	Natural decay rate of free merozoites	0.001	0.001-0.5	day^{-1}	
π	Proportion of gametocytes infected erythrocytes.	0.1	0.1-0.5	day^{-1}	[24]
N_m	Number of merozoites produced per bursting erythrocytes.	16	10-30	day^{-1}	[24]
α_m	Rate at which erythrocytes burst to produce merozoites.	0.5	0.1-1.0	day^{-1}	[24]

4.3.1 Global sensitivity analysis

Employing the tornado plot sensitivity analysis will allow us to establish which parameters influences the model outcomes when we decrease or increase certain parameter values. We need to determine which parameters should we target to reduce the reproductive number (R_0).

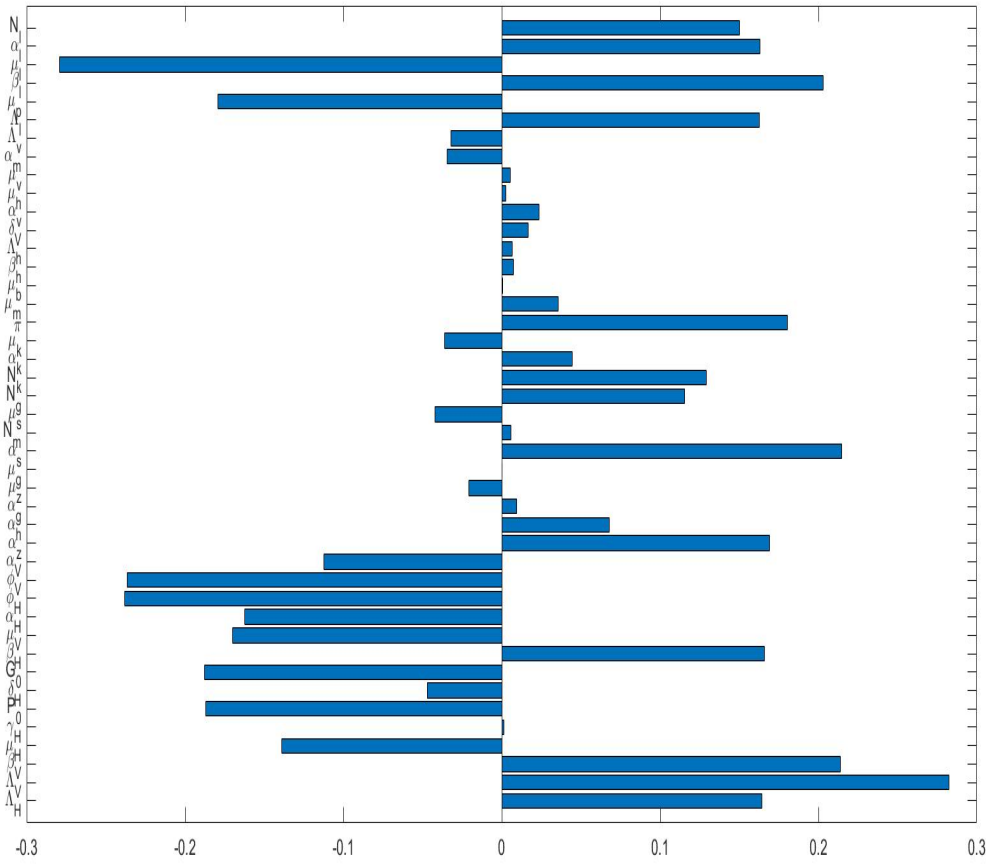

Figure 4.2: Tornado plot showing Partial Rank Correlation Coefficients of the reproductive number (R_0)

In Figure (4.2), showing the global sensitivity analysis of reproductive number (R_0) using the tornado plot. If the parameter values are positive, partial rank correlation coefficients (PRCCs) has a potential to increase the value of R_0 if the parameter values are increased. The parameter values which have negative PRCCs have influence of reducing the value of R_0 when we increase the parameter values. The parameters Λ_V, β_V, α_s, β_l, π, Λ_H, β_H, α_z, N_l, α_l and Λ_l have the highest impact in raising the value of R_0 when these parameters are increased. The parameters μ_l, ϕ_H, ϕ_V, P_0, G_0, α_H, μ_V and μ_p have the highest impact in reducing the value of R_0 when these parameter values are increased. The parameter values may have either positive or negative PRCCs, it is crucial to discover whether there is an increasing or decreasing trend when the parameter values are varied.

4.3.2 The influence of between-human scale parameters on within-human scale variables for malaria infection

This subsection demonstrates through numerical analysis results of coupled multiscale model (4.2.0.1) the evidence for the influence of between-human scale parameters on within-human scale variables for malaria infection dynamics. We evaluate the different values of between-human scale parameters (ϕ_H, α_H, β_H and G_0) and assess their influence on the dynamics of the within-human scale variables ((a) population of infected liver-cells L_h^*, (b) population of infected red-blood cells B_h^*, (c) population of merozoites M_h and (d) population of gametocytes G_h).

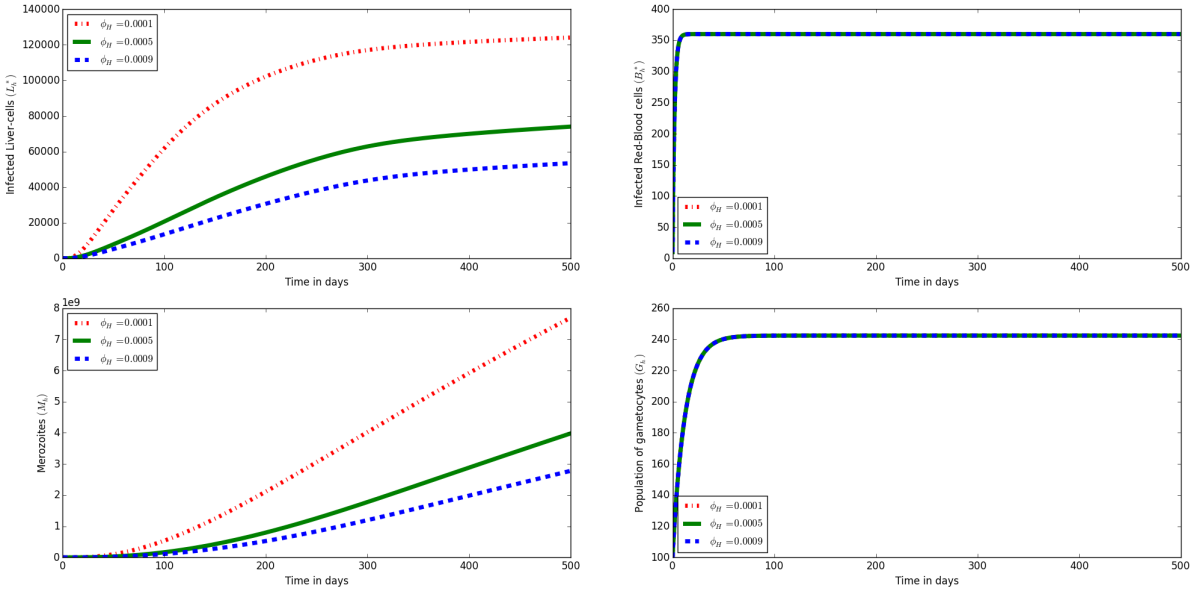

Figure 4.3: Simulation of model (4.2.0.1) showing the evolution in time of (a) population of infected liver cells L_h^*, (b) population of infected red blood cells B_h^*, (c) population of merozoites M_h and (d) population of gametocytes G_h for different values of the proportion of new incfected humans ϕ_H: $\phi_H = 0.0001$, $\phi_H = 0.0005$ and $\phi_H = 0.0009$.

Figure (4.3) demonstrates graphs of numerical results of the coupled multiscale model system (4.2.0.1) presenting the dynamics on (a) population of infected liver-cells L_h^*, (b) population of infected red-blood cells B_h^*, (c) population of merozoites M_h and (d) population of gametocytes G_h for different values of the proportion of new infected humans ϕ_H: $\phi_H = 0.0001$, $\phi_H = 0.0005$ and $\phi_H = 0.0009$. The results show that as the proportion of nwe infected humans increase, there is a observable decrease in the population of infected liver-cells and population of merozoites and there is no change in population of infected red blood cells and population of gametocytes. Therefore, ϕ_H has an impact in the reduction of malaria infection in liver cells and also in the production of merozoites.

In Figure (4.4), illustrates graphs of numerical solutions of the coupled multiscale model (4.2.0.1) showing the changes on (a) population of infected liver cells L_h^*, (b) population of infected red blood cells B_h^*, (c)

population of merozoites M_h and (d) population of gametocytes G_h for different values of clearance rate of community gametocytes load α_H: $\alpha_H = 0.0000913$, $\alpha_H = 0.000913$ and $\alpha_H = 0.00913$. The results in Figure (4.4) indicate that as the clearance rate of community gametocytes load α_H increase, there is observable decrease in the population of infected liver cells L_h^* and population of merozoites M_h no changes in the population of infected red blood cells B_h^* and the population of infected gametocytes G_h^*. This also give evidence of the influence of the between-human scale parameters on the malaria infection dynamics at the within-human scale.

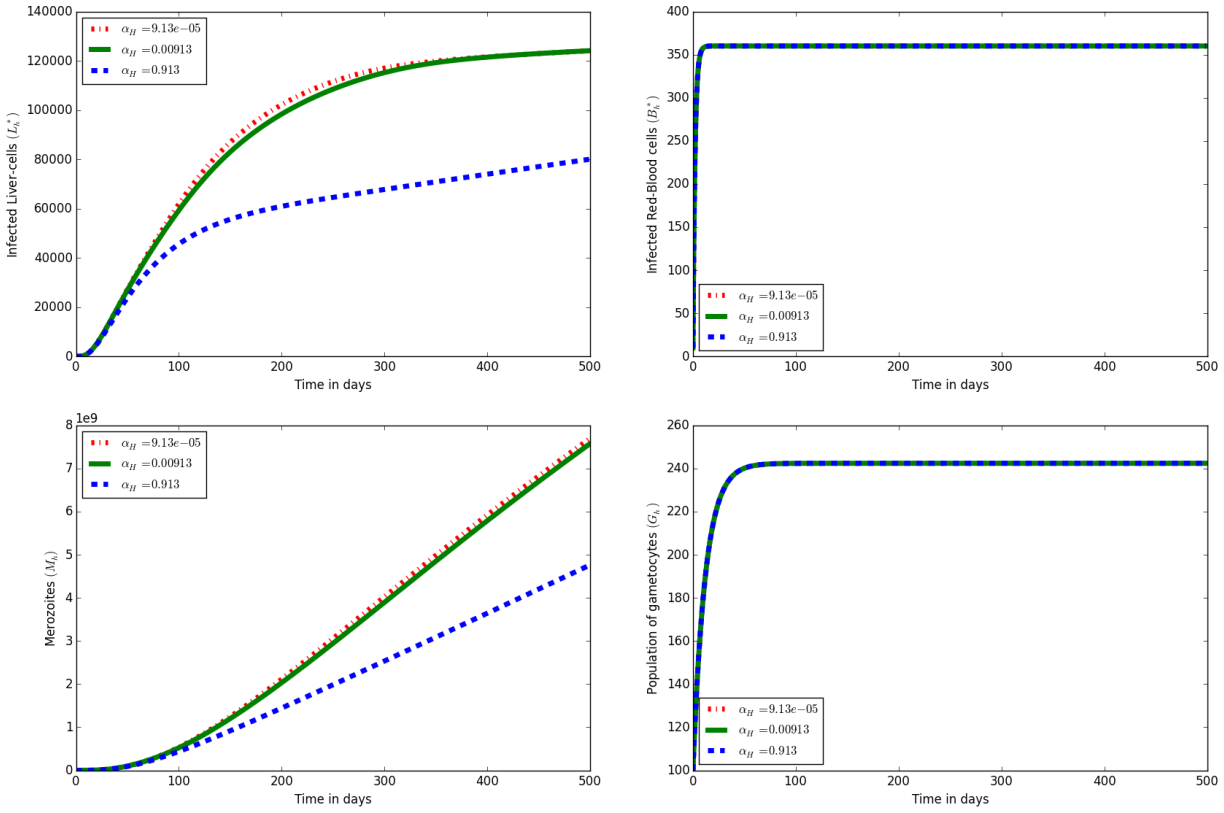

Figure 4.4: Simulation of model (4.2.0.1) showing the evolution with time of (a) population of infected liver cells L_h^*, (b) population of infected red blood cells B_h^*, (c) population of merozoites M_h and (d) population of gametocytes G_h for different values of clearance rate of community gametocytes load α_H: $\alpha_H = 0.0000913$, $\alpha_H = 0.000913$ and $\alpha_H = 0.00913$.

Figure (4.5) demonstrates the changes in (a) population of infected liver cells L_h^*, (b) population of infected red blood cells B_h^*, (c) population of merozoites M_h and (d) population of gametocytes G_h for different values of the infection rate of susceptible mosquitoes β_H: $\beta_H = 0.00356$, $\beta_H = 0.0356$ and $\beta_H = 0.356$. The results from figure (4.5) show that as the increase in the infection rate of susceptible mosquitoes β_H, there is also observable increase in the within human scale malaria infection (population of infected liver cells L_h^* and population of merozoites M_h) and there is no influence on population of infected red blood cells and population of gametocytes.

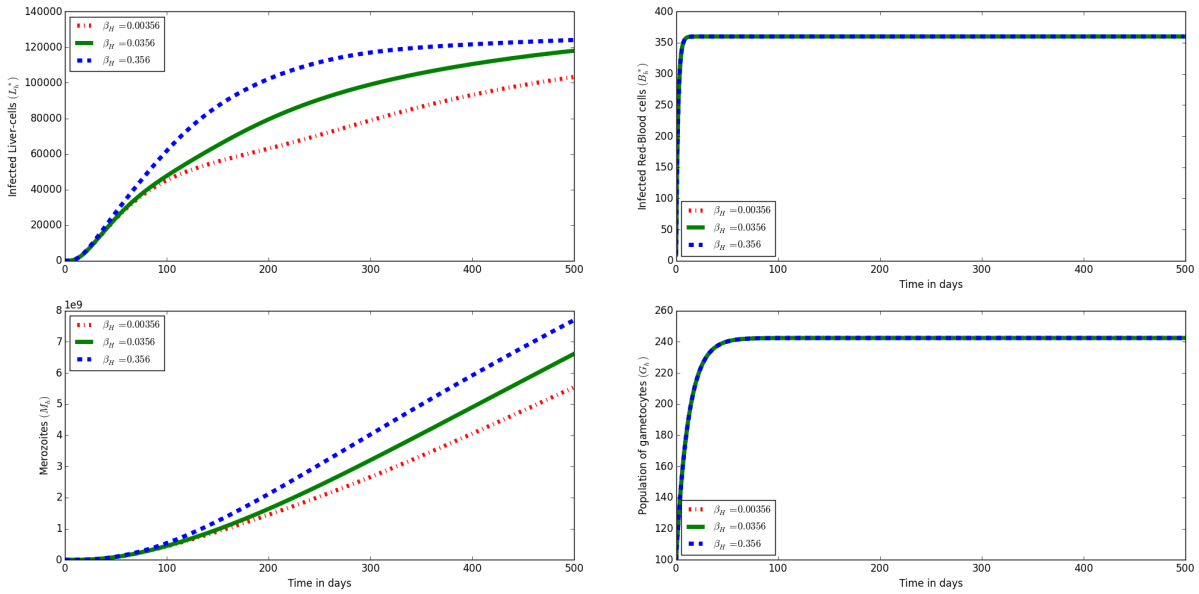

Figure 4.5: Simulation of model (4.2.0.1) showing the evolution with time of (a) population of infected liver cells L_h^*, (b) population of infected red blood cells B_h^*, (c) population of merozoites M_h and (d) population of gametocytes G_h for different values of the infection rate of susceptible mosquitoes β_H: $\beta_H = 0.00356$, $\beta_H = 0.0356$ and $\beta_H = 0.356$.

Figure (4.6) presents graphs of numerical simulation of the coupled multiscale model (4.2.0.1) depicts the dynamics of (a) population of infected liver cells L_h^*, (b) population of infected red blood cells B_h^*, (c) population of merozoites M_h and (d) population of gametocytes G_h for different values of half saturation constant associated with the infection of mosquitoes (G_0): $G_0 = 100000000$, $G_0 = 500000000$ and $G_0 = 900000000$. The results indicate that as the half saturation constant associated with the infection of mosquitoes G_0 increase, there is a noticeable decrease in in the within human malaeia infection that is population of infected liver cells L_h^* and population of merozoites M_h and there is no difference in the within host malaria infection dynamics on population of infected red blood cellsn B_h^* and population of gametocytes G_h. Therefore, the between-human scale parameter will assist in administration of vaccine which will have effect on the within-human disease dynamics. This again give evidence that the between-human disease parameterhave influence on within-human disease processes.

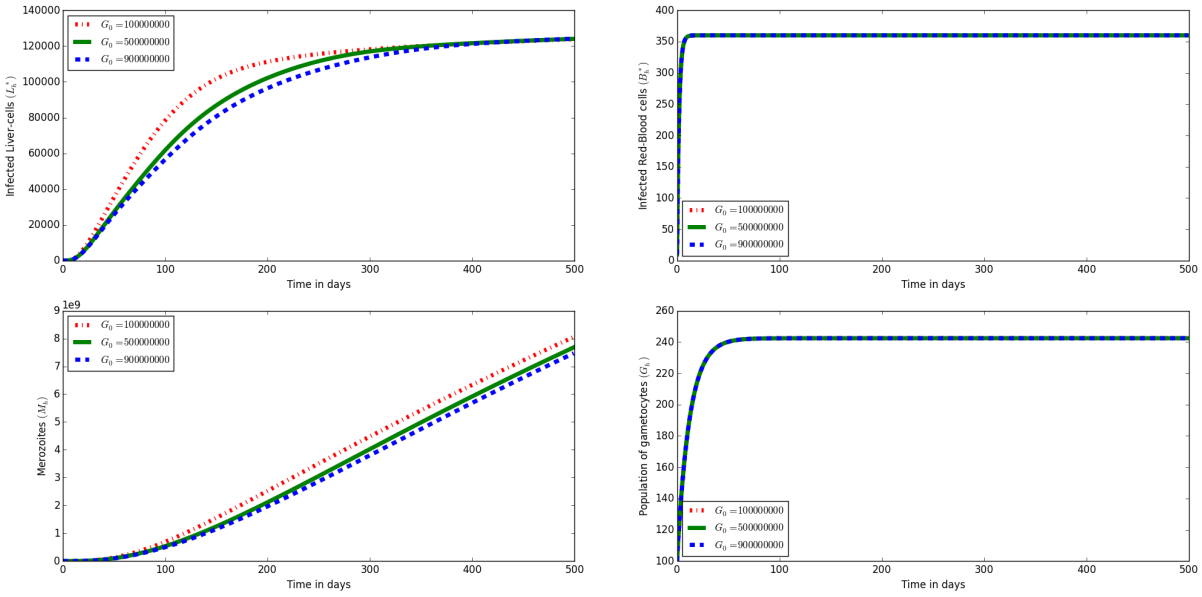

Figure 4.6: Simulation of model (4.2.0.1) showing the evolution with time of (a) the population of infected liver cells L_h^*, (b) the population of infected red blood cells B_h^*, (c) the population of merozoites M_h and (d) the population of gametocytes G_h for different values of half saturation constant associated with the infection of mosquitoes G_0: $G_0 = 100000000$, $G_0 = 500000000$ and $G_0 = 900000000$.

4.3.3 The influence of between-human scale parameters on within-mosquito scale variables for malaria infection

In this sub-section, we examine numerically the effect of the between-human sub-model parameters (β_H and G_0) on within-mosquito scale malaria infection variables ((a) population of gametocytes within infected mosquitoes G_v, (b) population of gametes G_m, (c) population of zygotes Z_v and (d) population of sporozoites P_v). Figure (4.7) demonstrates graphs of numerical solutions of multiscale model (4.2.0.1) showing the changes in (a) population of gametocytes within infected mosquitoes G_v, (b) population of gametes G_m, (c) population of zygotes Z_v and (d) population of sporozoites P_v for different values of half saturation constant associated with the infection of mosquitoes G_0: $G_0 = 5000000$, $G_0 = 50000000$ and $G_0 = 500000000$. The solutions in fig.(4.7) depict as the half saturation constant associated with the infection rate of mosquitoes G_0increase, thre is visible decrease im malaria infction on within-mosquito dynamics (G_v, G_m, Z_v and P_v). However, this between-human scale parameter is targeted for administering of vaccine which has an impact on reducing malaria infection in both between-host scale and within-mosquito scale.

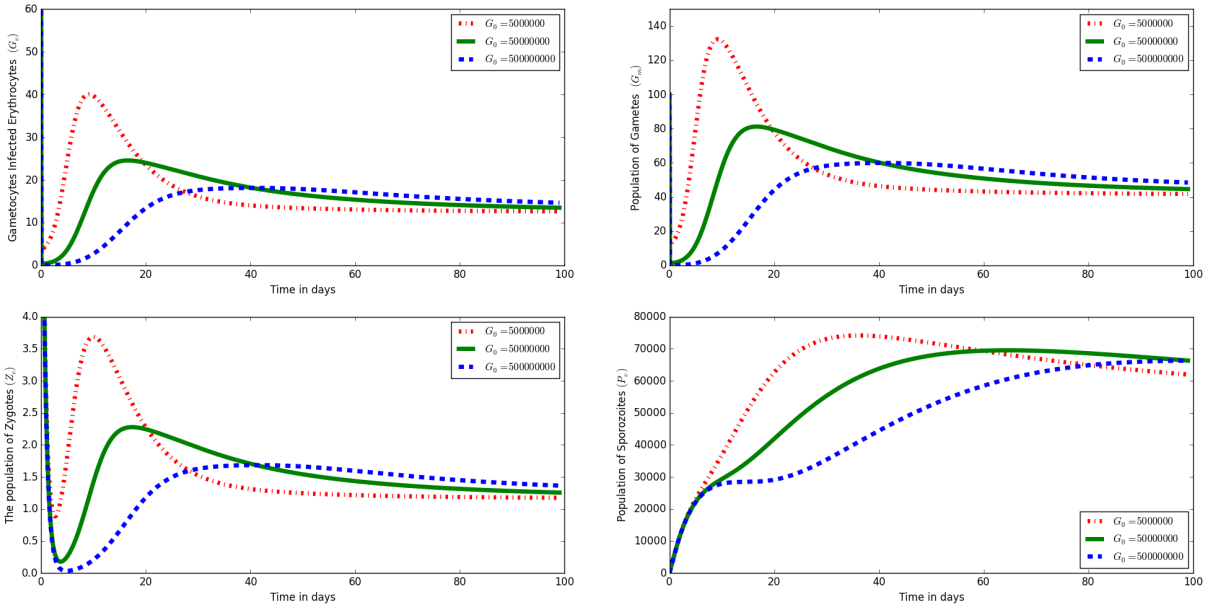

Figure 4.7: Graphs showing the changes in (a) population of gametocytes within infected mosquitoes G_v, (b) population of gametes G_m, (c) population of zygotes Z_v and (d) population of sporozoites P_v for different values of half saturation constant associated with the infection of mosquitoes G_0: $G_0 = 5000000$, $G_0 = 50000000$ and $G_0 = 500000000$.

Figure (4.8) examines graphs of numerical solutions of the multiscale model (4.2.0.1) presenting the changes in (a) population of gametocytes within infected mosquitoes G_v, (b) population of gametes G_m, (c) population of zygotes Z_v and (d) population of sporozoites P_v for different values of the clearance rate of community gametocyte load (α_H): $\alpha_H = 0.0000913$, $\alpha_H = 0.00913$ and $\alpha_H = 0.913$. The results in fig.(4.8) indicate that as the clearance rate of community sporozoites load α_H increase, there is observble slightly decrease in malaioa infection on all within-mosquito scale variables ((a) population of gametocytes within infected mosquitoes G_v, (b) population of gametes G_m, (c) population of zygotes Z_v and (d) population of sporozoites P_v).

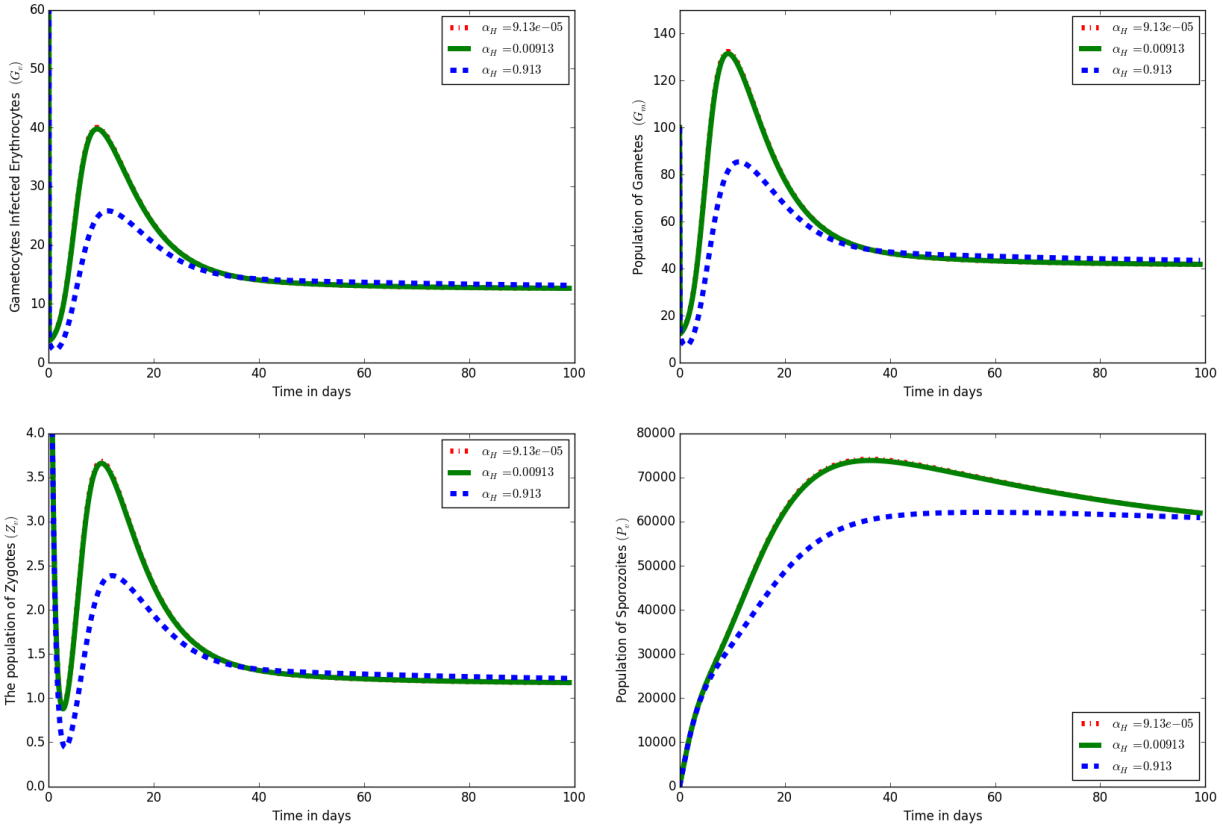

Figure 4.8: Graphs showing the changes in (a) population of gametocytes within infected mosquitoes G_v, (b) population of gametes G_m, (c) population of zygotes Z_v and (d) population of sporozoites P_v for different values of the clearance rate of community gametocyte load (α_H): $\alpha_H = 0.0000913$, $\alpha_H = 0.00913$ and $\alpha_H = 0.913$.

Figure(4.9) illustrates the dynamics in (a) population of gametocytes within infected mosquitoes G_v, (b) population of gametes G_m, (c) population of zygotes Z_v and (d) population of sporozoites P_v for different values of the contact rate of susceptible mosquitoes with the infectious reservoir of humans β_H: $\beta_H = 0.00356$, $\beta_H = 0.0356$ and $\beta_H = 0.356$. The results in fig.(4.9) demontrate that an increase in the contact rate of susceptible mosquitoes with the infectious reservoir of humans β_H results in an increase of malaria infection in within-mosquito variables ((a) population of gametocytes within infected mosquitoes G_v, (b) population of gametes G_m, (c) population of zygotes Z_v and (d) population of sporozoites P_v).

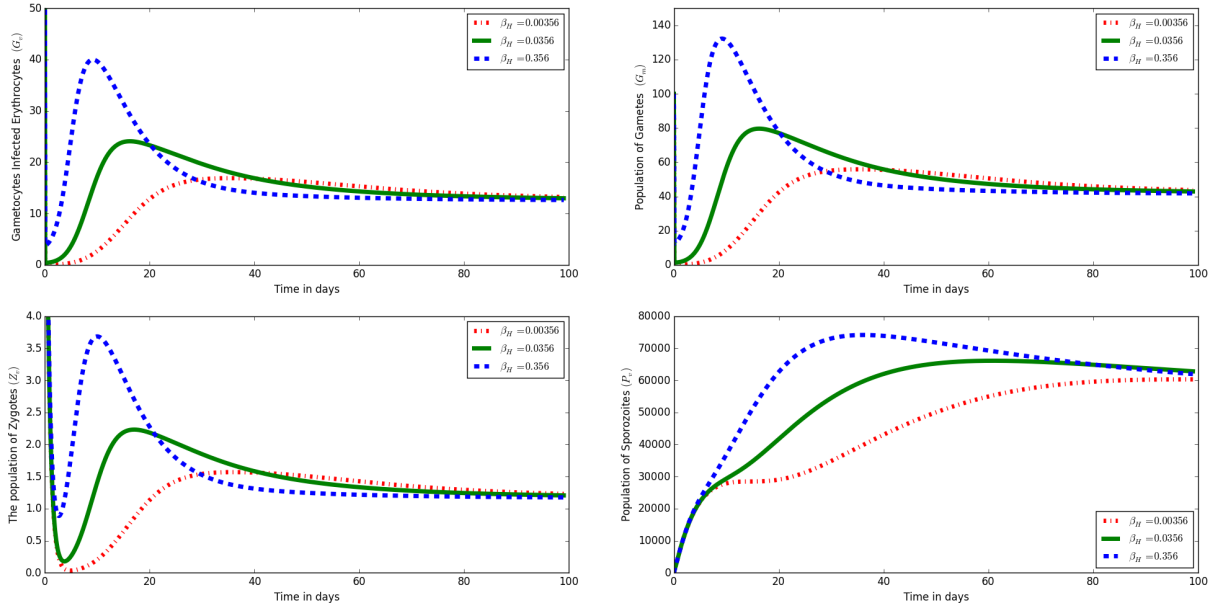

Figure 4.9: Graphs showing the changes in (a) population of gametocytes within infected mosquitoes G_v, (b) population of gametes G_m, (c) population of zygotes Z_v and (d) population of sporozoites P_v for different values of the contact rate of susceptible mosquitoes with the infectious reservoir of humans β_H: $\beta_H = 0.00356$, $\beta_H = 0.0356$ and $\beta_H = 0.356$.

4.3.4 The influence of between-mosquito scale parameters on within-human scale variables for malaria infection

In this sub-section, we examine numerically the impact of between-mosquito sub-model parameters (ϕ_V, α_V, β_V, δ_V, Λ_V, μ_V and P_0) on the within-human sub-model for malaria pathogen interacting with the liver-cells and red-blood cells within a single infected human.Fig. (4.10)- fig.(4.16) present the influence in the different values of between mosquito parameters (ϕ_V, α_V, β_V, δ_V, Λ_V, μ_V and P_0) on the malaria infection dynamics of the within-scale variables ((a) the population of infected liver-cells L_h^*, (b) population of infected red blood cells B_h^*, (c) population of merozoites M_h and (d) population of gametocytes G_h).

Figure (4.10) demonstrates graphs of numerical simulations of the multiscale model (4.2.0.1) presenting the changes in (a) the population of infected liver-cells L_h^*, (b) population of infected red blood cells B_h^*, (c) population of merozoites M_h and (d) population of gametocytes G_h for different values of proportion of new infected mosquitoes in the total infected mosquito population ϕ_V: $\phi_V = 0.0001$, $\phi_V = 0.001$ and $\phi_V = 0.01$. The simulation in figure (4.10) show that as the proportion of new infected mosquitoes in the total infected mosquito population ϕ_V increase, there is observable slightly reduction in the population of infected liver-cells L_h^* and population of merozoites M_h and there is no difference in the infected red-blood cells B_h^* and the population of gametocytes G_h. These results indicate that the variation of

the proportion of new infected mosquitoes for different values influence the within-huiman scale disease dynamics on infection of liver cells and the production of merozoites. However, if there is an intervention that increase the between-mosquito parameter ϕ_V will have an impact in reducing the malaria infection on within-human scale.

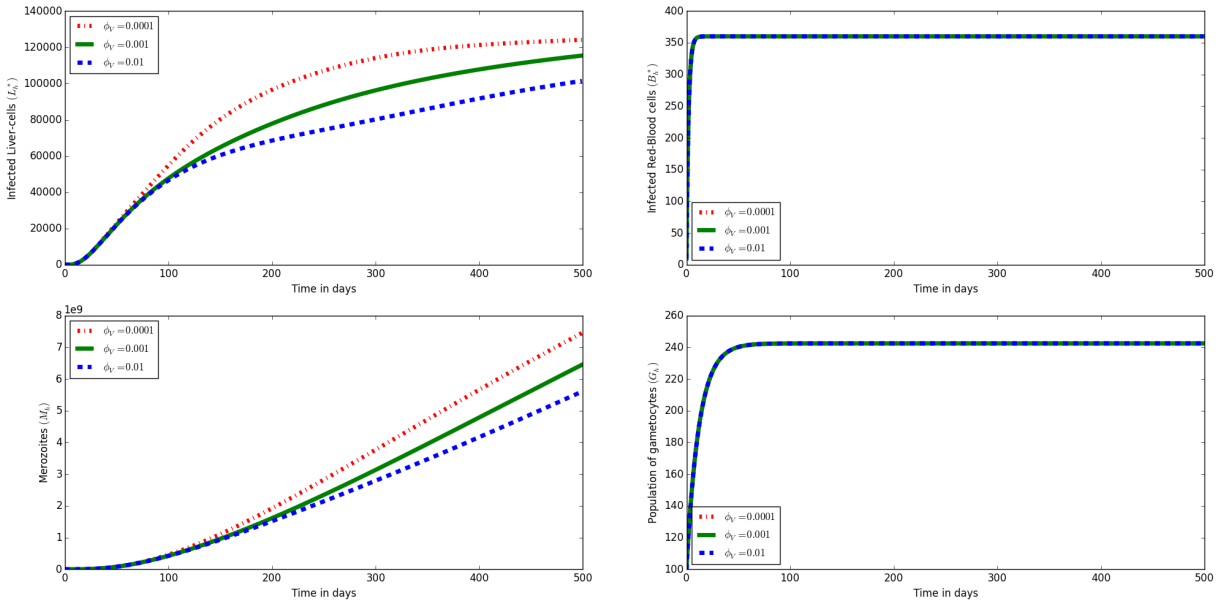

Figure 4.10: Simulations of multiscale model (4.2.0.1) depicting the evolution in time of (a) population of infected liver cells L_h^*, (b) population of infected red blood cells B_h^*, (c)population of merozoites M_h and (d) population of gametocytes G_h for varying the values of proportion of new infected mosquitoes in the total infected population ϕ_V: $\phi_V = 0.0001$, $\phi_V = 0.001$ and $\phi_V = 0.01$.

Figure (4.11) depicts graphs of numerical simulations of the multiscale model (4.2.0.1) presenting the varation of (a) population of infected liver-cells L_h^*, (b) population of infected red blood cells B_h^*, (c) population of merozoites M_h and population of gametocytes G_h for different values of clearance rate of community sporozoites α_V: $\alpha_V = 0.1$, $\alpha_V = 0.3$ and $\alpha_V = 0.5$. The solutions in figure (4.11) indicate that as the clearance rate of community sporozoites load α_V increase, there is a visible reduction in the population of infected liver-cells L_h^* and population of merozoites M_h and we also notice that there is no difference on the disease dynamics of population of infected red blood cells B_h^* and population of gametocytes G_h. Therefore, this indicate that between-mosquito scale parameter has impact on within-human scale malaria infection dynamics.

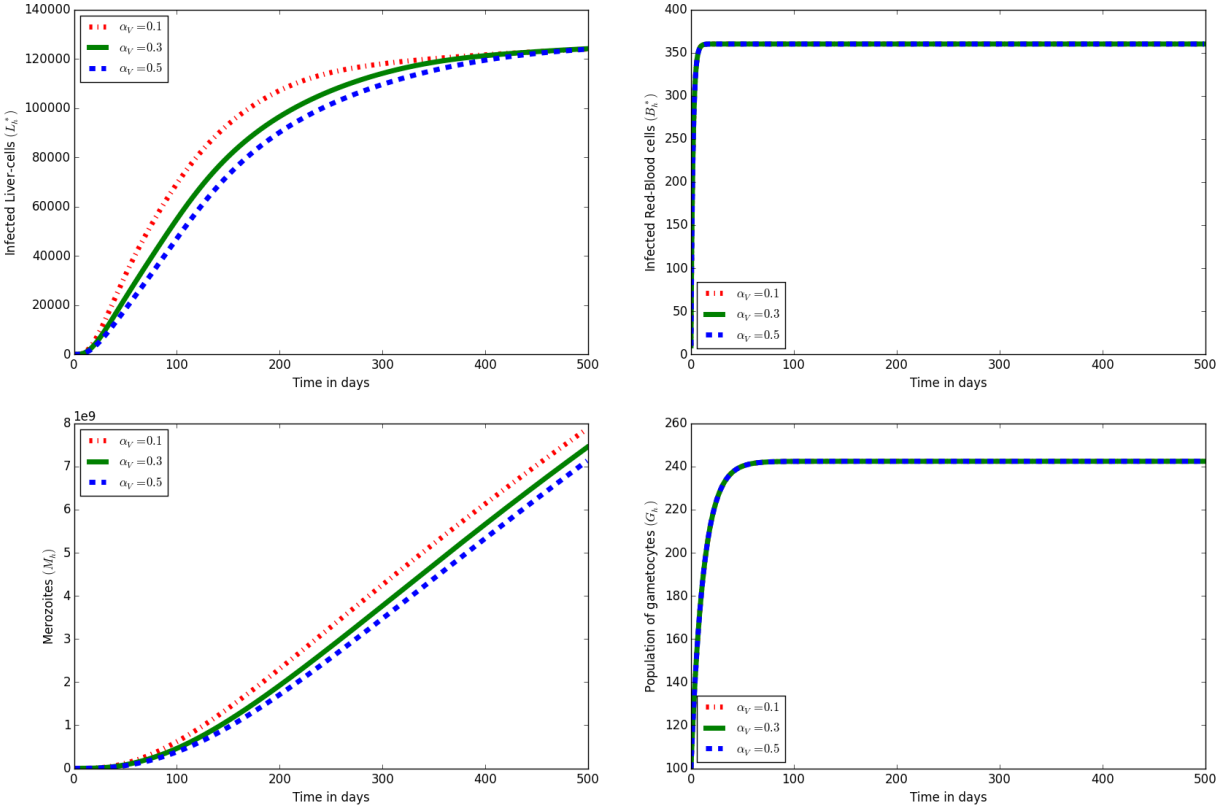

Figure 4.11: Simulations of multiscale model (4.2.0.1) depicting the evolution in time of (a) population of infected liver cells L_h^*, (b) population of infected red blood cells B_h^*, (c)population of merozoites M_h and (d) population of gametocytes G_h for varying the values of clearance rate of community sporozoites load α_V: $\alpha_V = 0.1$, $\alpha_V = 0.3$ and $\alpha_V = 0.5$.

Figure (4.12) depicts the simulations of the multiscale model (4.2.0.1) presenting the variation of (a) population of infected liver cells L_h^*, (b) population of infected red blood cells B_h^*, (c) population of merozoites M_h and (d) population of gametocytes G_h for different values of contact rate of susceptible humans with the infectious reservoir of mosquitoes β_V: $\beta_V = 0.0032135$, $\beta_V = 0.032135$ and $\beta_V = 0.32135$. The solutions in figure (4.12) present that as the contact rate of susceptible humans with infectious reservoir of mosquitoes β_V increase, we observe an increase in the population of infected liver cells L_h^* and population of merozoites M_h and we also observe that there is no difference in the population of infected red blood cells B_h^* and population of gametocytes G_h. Therefore, this results gives evidence that the between mosquito parameter has influence on the invasion of liver-cells and the production of merozoites.

Figure (4.13) presents the numerical solutions of the multiscale model (4.2.0.1) illustrating the variations of (a) population of infected liver cells L_h^*, population of infected red blood cells B_h^*, (c) population of merozoites M_h and (d) population of gametocytes G_h for different values of induced death rate of infectected mosquitoes δ_V: $\delta_V = 0.00000426$, $\delta_V = 0.000426$ and $\delta_V = 0.0426$. The results in figure (4.13) demonstrate that as the induced death rate of infected mosquitoes increase, there is observable

reduction in the malaria infection on the population of liver-cells L_h^* and the population of merozoites M_h and there is no difference in the population of infected red-blood cells B_h^* and population of gametocytes G_h. Therefore, any intervention that increase the death rate of mosquitoes has an impact in reducing the malaria infection within-infected humans.

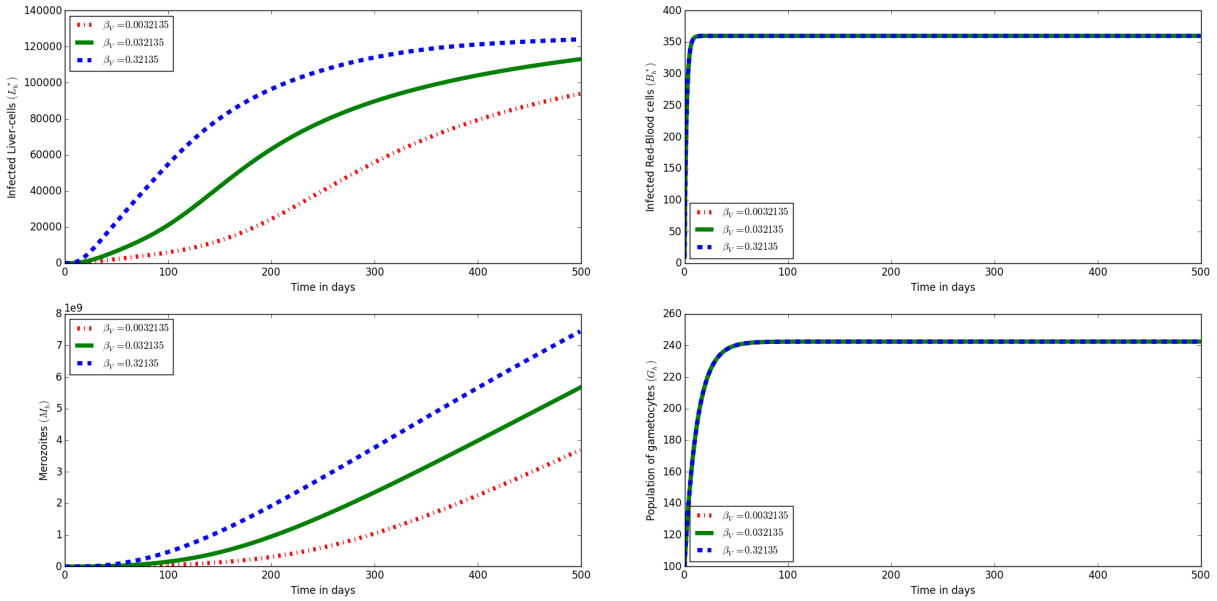

Figure 4.12: Simulations of multiscale model (4.2.0.1) depicting the evolution in time of (a) population of infected liver cells L_h^*, (b) population of infected red blood cells B_h^*, (c)population of merozoites M_h and (d) population of gametocytes G_h for varying the values of contact rate of susceptible humans with the infectious reservoir of mosquitoes β_V: $\beta_V = 0.0032135$, $\beta_V = 0.032135$ and $\beta_V = 0.32135$.

Figure (4.14) depicts the dynamics the dynamics in the (a) population of infected liver-cells L_h^*, (b) population of infected red blood cells B_h^*, (c) population of merozoites M_h and (d) population of gametocytes G_h for different values of supply rate of mosquitoes Λ_V: $\Lambda_V = 1000$, $\Lambda_V = 2000$ and $\Lambda_V = 3000$. The results in fig.(4.14) show that as the supply rate of mosquitoes increase, there is observable increase in the population of infected liver cells L_h^* and population of merozoites M_h and there is no changes in the dynamics of the population of infected red blood cells B_h^* and population of gametocytes G_h. Therefore, any intervention that inhibits the breeding of mosquitoes has an influence in reducing malaria infecion at within human scale.

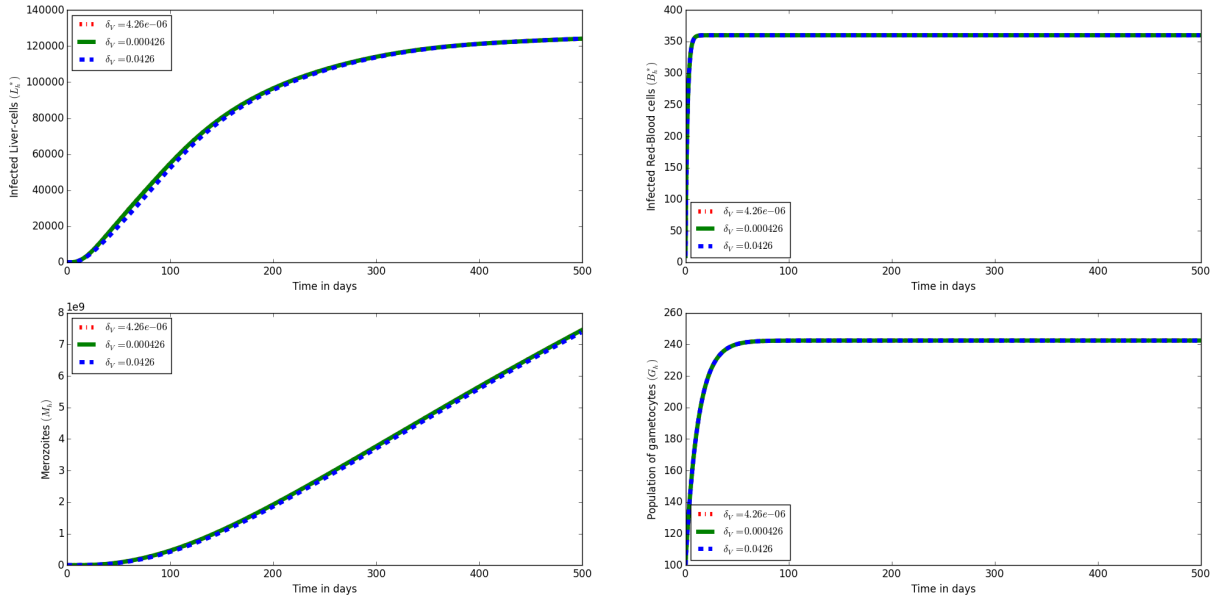

Figure 4.13: Simulations of multiscale model (4.2.0.1) depicting the evolution in time of (a) population of infected liver cells L_h^*, (b) population of infected red blood cells B_h^*, (c)population of merozoites M_h and (d) population of gametocytes G_h for varying the values of induced death rate of mosquitoes δ_V: $\delta_V = 0.00000426$, $\delta_V = 0.000426$ and $\delta_V = 0.0426$.

Figure (4.15) demonstrates the changes in (a) population of infected liver cells L_h^*, (b) population of infected red blood cells B_h^*, (c) population of merozoites M_h and (d) population of gametocytes G_h for different values of natural decay rate of mosquitoes μ_V: $\mu_V = 0.0012$, $\mu_V = 0.012$ and $\mu_V = 0.12$. The results in fig.(4.15) show that as the natural death rate of mosquitoes increase, there is visible reduction of within-human scale malaria infection on population of infected liver cells L_h^* and population of merozoites M_h and there is no difference in the population of infected red blood cells B_h^* and population of gametocytes G_h. However, this indicate that the variation of natural decay rate of mosquitoes for different values influence the within-human malaria disease dynamics only on invasion of liver cells and production of merozoites.

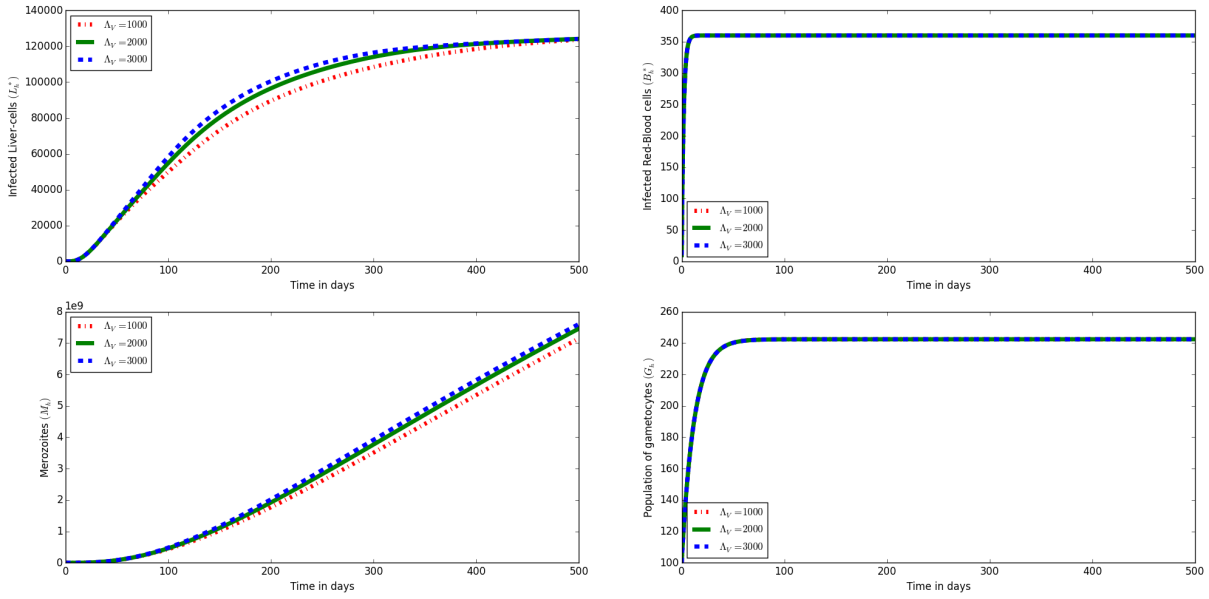

Figure 4.14: Simulations of multiscale model (4.2.0.1) depicting the evolution in time of (a) population of infected liver cells L_h^*, (b) population of infected red blood cells B_h^*, (c)population of merozoites M_h and (d) population of gametocytes G_h for varying the values of recruitment rate of mosquitoes Λ_V: $\Lambda_V = 1000$, $\Lambda_V = 2000$ and $\Lambda_V = 3000$.

Figure (4.16) presents graphs of numerical simulutions of multiscale model (4.2.0.1) presenting the variation of (a) population of infected liver cells L_h^*, (b) population of infected red blood cells B_h^*, (c) population of merozoites M_h and (d) population of gametocytes G_h for different values of half saturation constant associated with the infection of humans P_0: $P_0 = 50000000$, $P_0 = 100000000$ and $P_0 = 150000000$. The numerical solutions in fig(4.16) depicts that as the half saturation constant associated with the infection of humans P_0 increase, there is visible reduction in malaria infection on population of infected liver cells L_h^* and population of merozoites M_h and we observe that there is no difference in the malaria disease dynamics on population of infectect red blood cells B_h^* and population of gametocytes G_h. The administration of vaccine is effective on this between-host parameter which has an impact of reducing the malaria infection on within human scale variables.

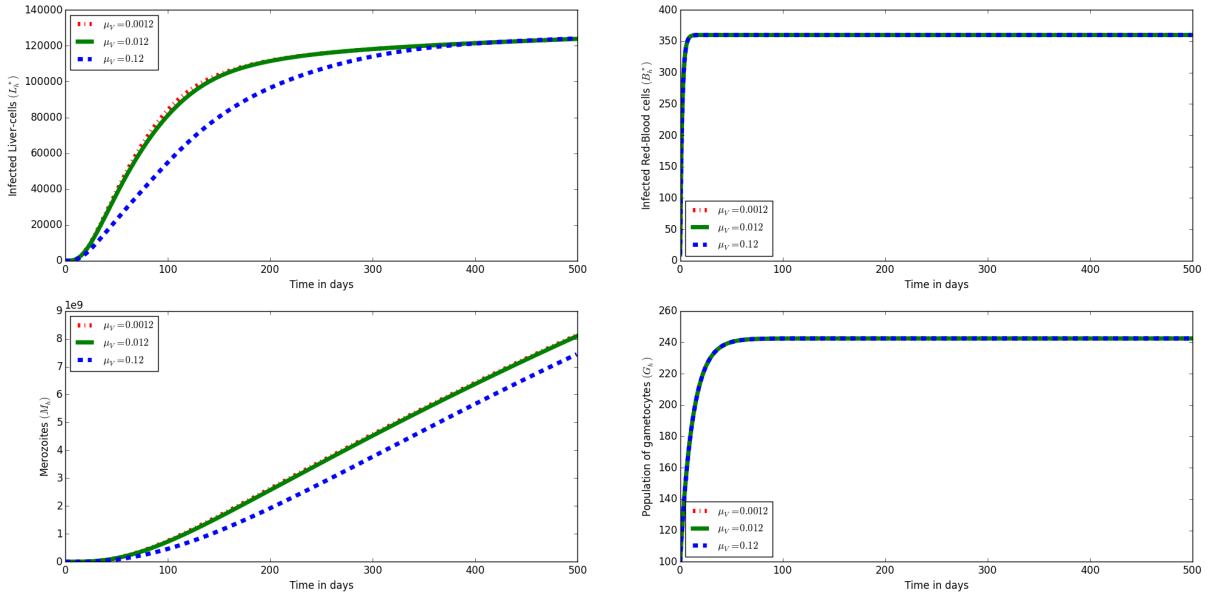

Figure 4.15: Simulations of multiscale model (4.2.0.1) depicting the evolution in time of (a) population of infected liver cells L_h^*, (b) population of infected red blood cells B_h^*, (c)population of merozoites M_h and (d) population of gametocytes G_h for varying the values of natural decay rate of mosquitoes μ_V: $\mu_V = 0.0012$, $\mu_V = 0.012$ and $\mu_V = 0.12$

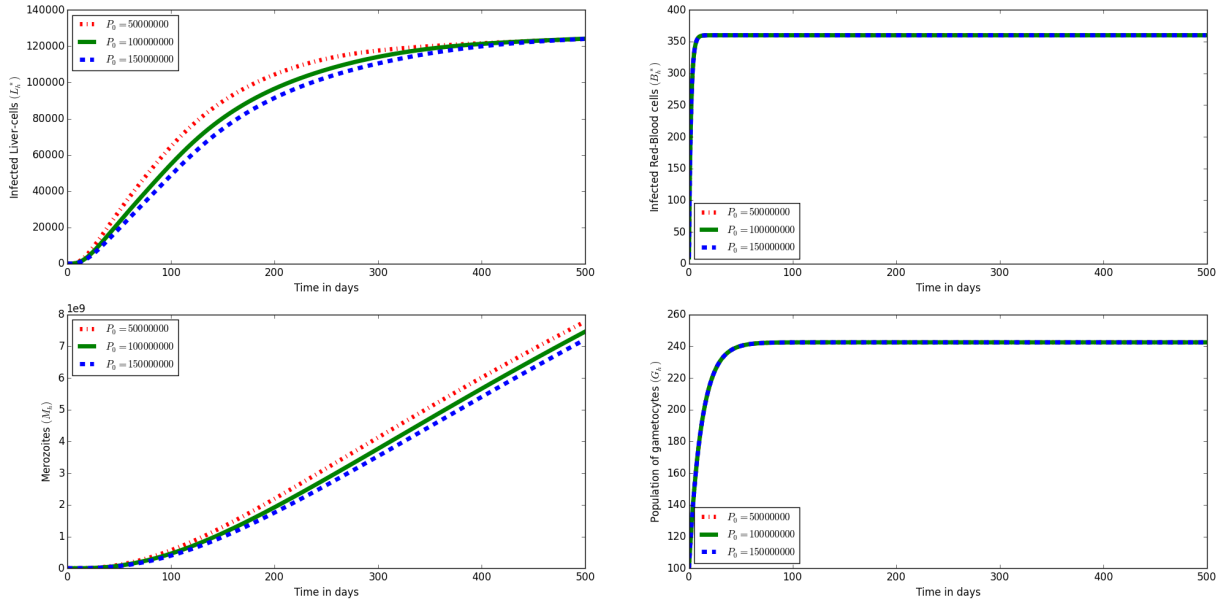

Figure 4.16: Simulations of multiscale model (4.2.0.1) depicting the evolution in time of (a) population of infected liver cells L_h^*, (b) population of infected red blood cells B_h^*, (c)population of merozoites M_h and (d) population of gametocytes G_h for varying the values of half saturation constant associated with the infection of humans P_0: $P_0 = 50000000$, $P_0 = 100000000$ and $P_0 = 150000000$.

4.3.5 Assessment of the influence of between-mosquito scale parameters on within-mosquito scale variables for malaria infection

In this sub-section, we investigate the numerically the influence of between-mosquito sub-model parameters (ϕ_V, α_V, and β_V) on within-mosquito sub-model for malaria dynamic of ((a) population of gametocytes for within infected mosquitoes G_v, (b) population of gametes G_m, (c) population of zygotes Z_v and (c) population of sporozoites P_v).

Figure (4.17) demonstrates graphs of numerical results of the multiscale model (4.2.0.1) showing the dynamics of (a) population of gametocytes within infected mosquitoes G_v, (b) population of gametes G_m, (c) population of zygotes Z_v and (d) population of sporozoites P_v for different values of proportion of new infected mosquitoes in the total infected mosquito population ϕ_V: $\phi_V = 0.0001$, $\phi_V = 0.0003$ and $\phi_V = 0.0005$. From our numerical simulation in fig. (4.17), we note that as the proportion of new infected mosquitoes in the total infected mosquito population ϕ_V increase, there is visible decrease in within-mosquito scale variables ((a) population of gametocytes within infected mosquitoes G_v, (b) population of gametes G_m, (c) population of zygotes Z_v and (d) population of sporozoites P_v). Therefore, there is evidence that between-mosquito dynamics have an impact on within-mosquito scale malaria infection.

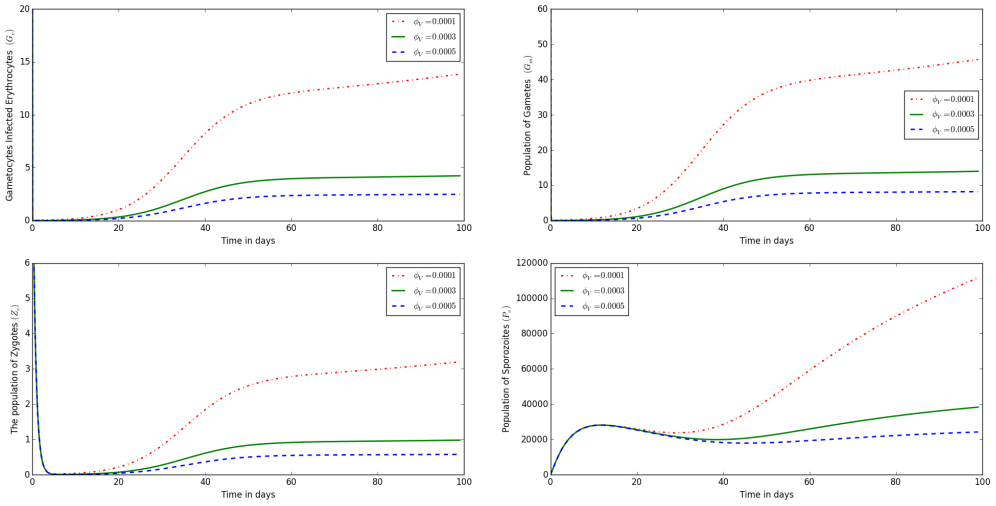

Figure 4.17: Graphs showing changes in (a) population of gametocytes within infected mosquitoes G_v, (b) population of gametes G_m, (c) population of zygotes Z_v and (d) population of sporozoites P_v for different values of proportion of new infected mosquitoes in the total infected mosquito population ϕ_V: $\phi_V = 0.0001$, $\phi_V = 0.0003$ and $\phi_V = 0.0005$.

Figure(4.18) demonstrates graphs of numerical simulations of multiscale model (4.2.0.1) showing the changes in (a) population of gametocytes within infected mosquitoes G_v, (b) population of gametes G_m, (c) population of zygotes Z_v and (d) population of sporozoites P_v for different values of clearance rate of community sporozoite load α_V: $\alpha_V = 0.1$, $\alpha_V = 0.3$ and $\alpha_V = 0.5$. From the numerical solutions in fig.

(4.18) present that as the clearance rate of community sporozoite load α_V increase, there is visible slightly decrease in tha malaria infection on within-mosquito dynamics of (a) population of gametocytes within infected mosquitoes G_v, (b) population of gametes G_m, (c) population of zygotes Z_v and (d) population of sporozoites P_v. Therefore, any interventions that clearace the community sporozoity load has an impact of reducing malaria infection in both between-mosquito scale and within-mosquito scale.

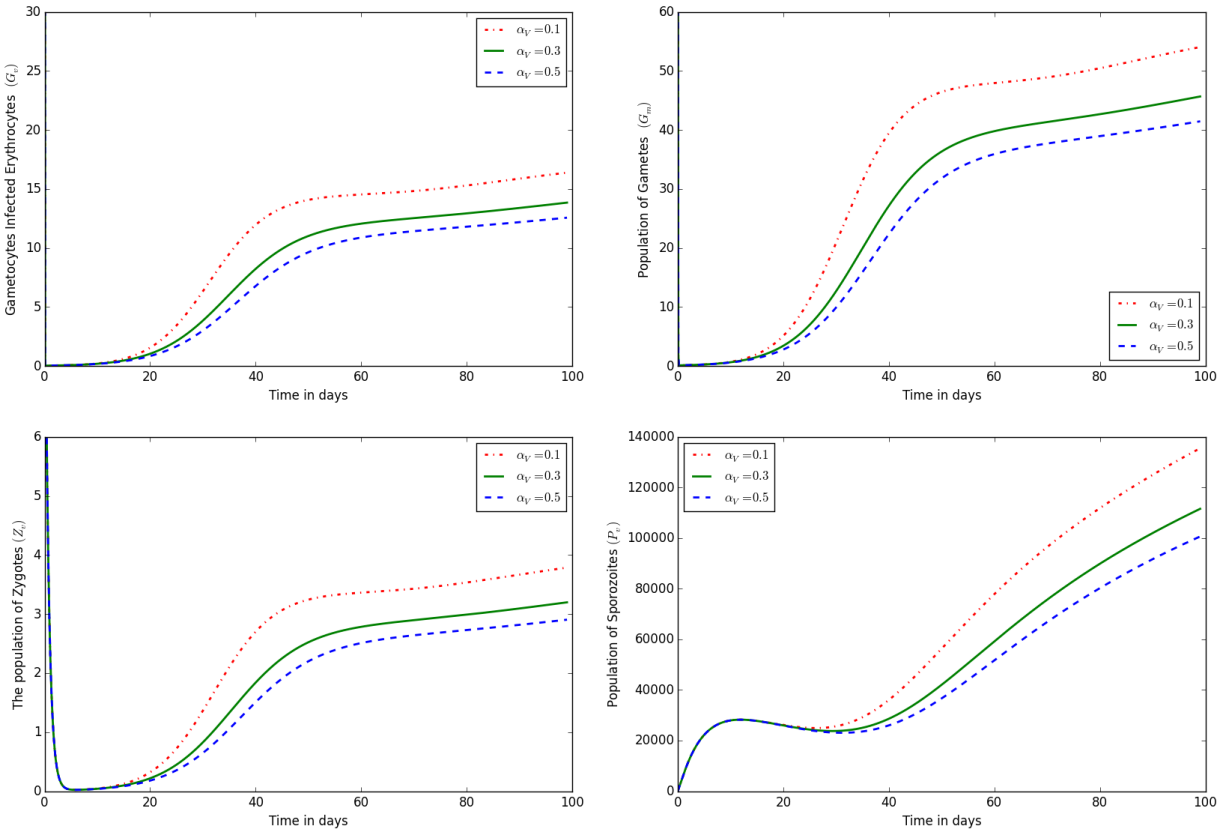

Figure 4.18: Graphs showing changes in (a) population of gametocytes within infected mosquitoes G_v, (b) population of gametes G_m, (c) population of zygotes Z_v and (d) population of sporozoites P_v for different values of clearance rate of community sporozoite load α_V: $\alpha_V = 0.1$, $\alpha_V = 0.3$ and $\alpha_V = 0.5$.

Figure (4.19) illustrates graphs of numerical simulations of the multiscale model (4.2.0.1) showing changes in (a) population of gametocytes within infected mosquitoes G_v, (b) population of gametes G_m, (c) population of zygotes Z_v and (d) population of sporozoites P_v for different values of contact rate of susceptible humans with the infectious reservoir of mosquitoes $\beta_V = 0.0052135$, $\beta_V = 0.052135$ and $\beta_V = 0.52135$. From the numerical simulations in fig.(4.19) display that as the contact rate of susceptible humans with the infectious reservoir of mosquitoes increase, we discover that there is an increase of malaria infection on within-mosquito scale that is on the dynamics of (a) population of gametocytes within infected mosquitoes G_v, (b) population of gametes G_m, (c) population of zygotes Z_v and (d) population of sporozoites P_v. Therefore, any interventions that prevent the contact of human hosts with the mosquitoes have an impact in reducing malaria infection on within-mosquito scale.

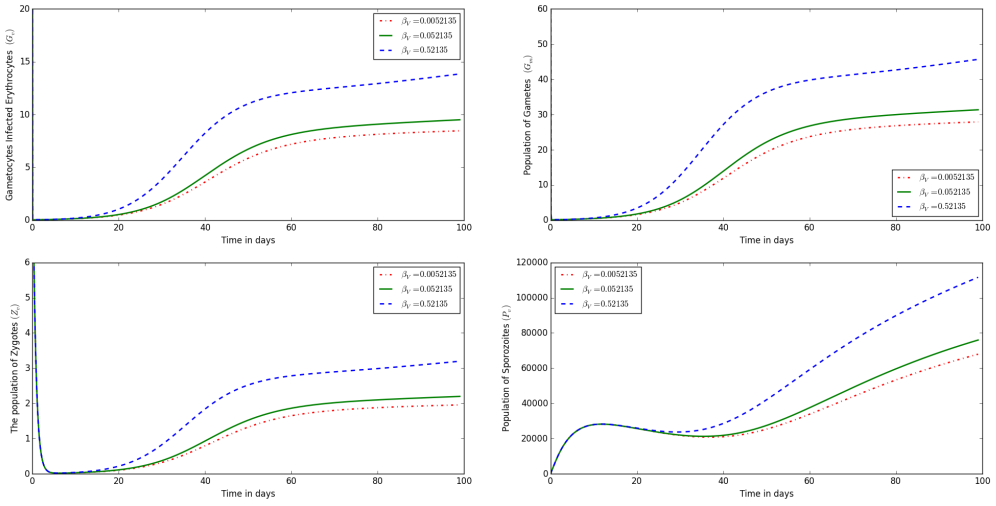

Figure 4.19: Graphs showing changes in (a) population of gametocytes within infected mosquitoes G_v, (b) population of gametes G_m, (c) population of zygotes Z_v and (d) population of sporozoites P_v for different values of contact rate of susceptible humans with the infectious reservoir of mosquitoes $\beta_V = 0.0052135$, $\beta_V = 0.052135$ and $\beta_V = 0.52135$.

4.3.6 The influence of within-human scale parameters on between-hosts scale variables for malaria infection

In this sub-section, we illutrate the numerical results of multiscale model (4.2.0.1) present the changes in (a) population of infected humans I_H, (b) community gametocyte load G_H, (c) population of infected mosquyitoes I_V and (d) community sporozoite load P_V over time in days for different values of four within-human scale selected parameters (π, α_h, and μ_h). We demonstrate the influence of these four within human scale malaria infection dynamics parameters (π, α_h, and μ_h) on between host scale variables ((a) population of infected humans I_H, (b) community gametocyte load G_H, (c) population of infected mosquyitoes I_V and (d) community sporozoite load P_V).

Figure (4.20) presents variations in (a) population of infected humans I_H, (b) community gametocyte load G_H, (c) population of infected mosquyitoes I_V and (d) community sporozoite load P_V over time in days for different values of proportion of gametocytes infected erythrocytes π: $\pi = 0.1$, $\pi = 0.3$ and $\pi = 0.5$. The numerical results indicate that as the proportion of gametocytes infected erythrocytes π within infected humans increase, there is also a visible increase in the population of infected humans I_H , community gametocyte load G_H, population of infected mosquitoes I_V and community sporozoite load P_V.

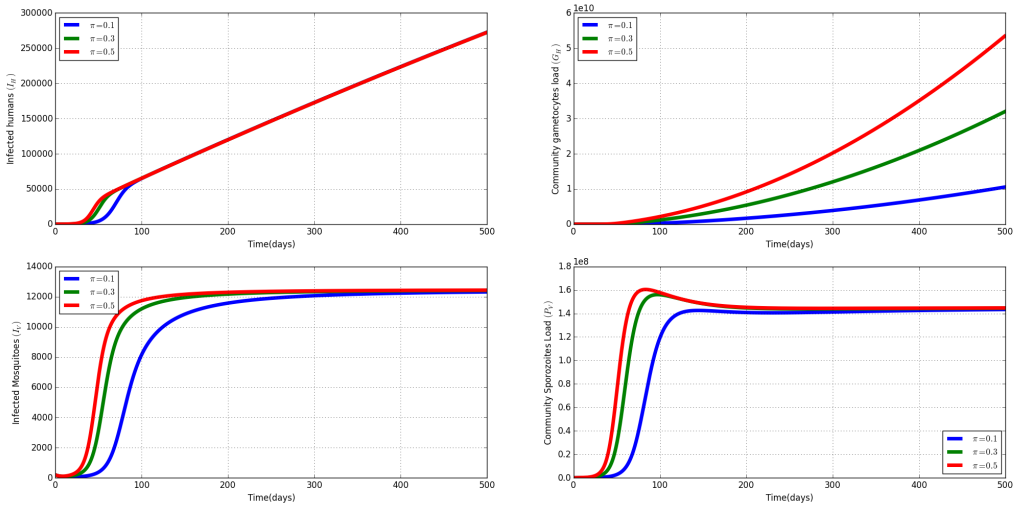

Figure 4.20: Numerical solutions presenting changes in (a) population of infected humans I_H, (b) community gametocyte load G_H, (c) population of infected mosquyitoes I_V and (d) community sporozoite load P_V over time in days for different values of proportion of gametocytes infected erythrocytesπ: $\pi = 0.1$, $\pi = 0.3$ and $\pi = 0.5$.

Figure (4.21) presents dynamics of (a) population of infected humans I_H, (b) community gametocyte load G_H, (c) population of infected mosquyitoes I_V and (d) community sporozoite load P_V over time in days for different values of rate at which gametocytes develop and become infectious within infected human α_h: $\alpha_h = 0.002$, $\alpha_h = 0.02$ and $\alpha_h = 0.2$. The numerical simulation results present that as the rate at which gametocytes develop and become infectious within infected human increase, visible increase in population of infected humans, community gametocyte load, infected mosquitoes and community sporozoite load. The results suggest that intervention measures that aimed at reducing the shedding/excretion rate at which gametocytes develop and become infectious within infected human which has an impact in reducing the transmission of malaria at population-level.

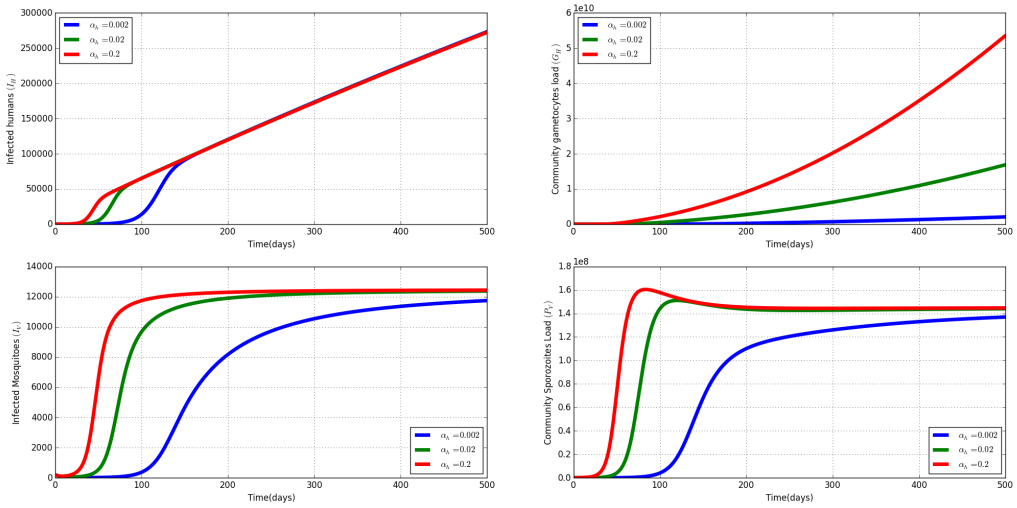

Figure 4.21: Numerical solutions presenting changes in (a) population of infected humans I_H, (b) community gametocyte load G_H, (c) population of infected mosquyitoes I_V and (d) community sporozoite load P_V over time in days for different values of rate at which gametocytes develop and become infectious within infected human α_h: $\alpha_h = 0.002$, $\alpha_h = 0.02$ and $\alpha_h = 0.2$.

Figure (4.22) shows the evolution of (a) population of infected humans I_H, (b) community gametocyte load G_H, (c) population of infected mosquitoes I_V and (d) community sporozoite load P_V over time in days for different values of natural decay rate of gametocytes within infected human $\mu_h = 0.00625$, $\mu_h = 0.0625$ and $\mu_h = 0.625$. The numerical simulation results in fig. (4.22) show that as natural decay rate of gametocytes within infected human increase, there is visible reduction on between-host malaria dynamics of population of infected humans I_H, community gametocyte load G_H, population of infected mosquitoes I_V and community sporozoites load P_V. The results suggest that intervention measures targeted at giving treatments that kills gametocyte within infected humans have an impact on reducing the transmission of malaria disease at population-level.

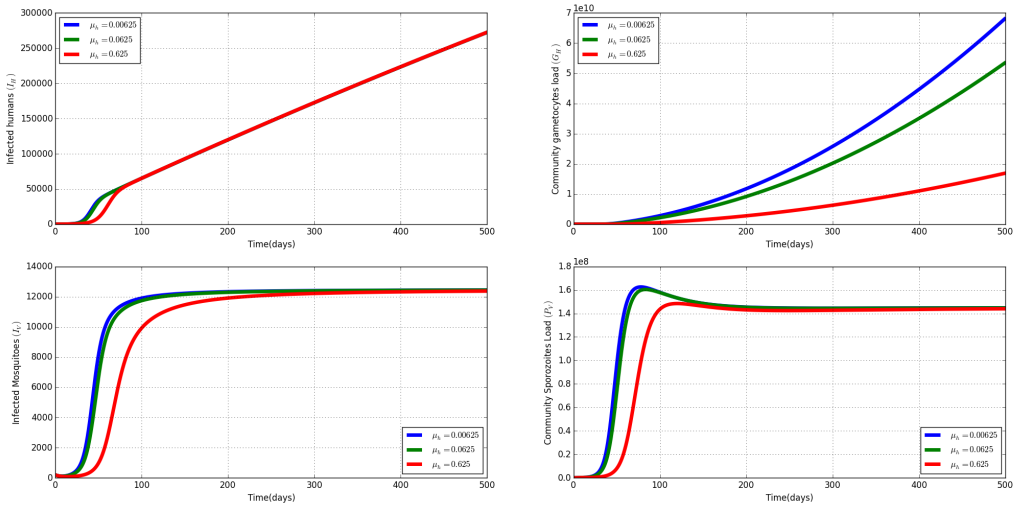

Figure 4.22: Numerical solutions presenting changes in (a) population of infected humans I_H, (b) community gametocyte load G_H, (c) population of infected mosquyitoes I_V and (d) community sporozoite load P_V over time in days for different values of natural decay rate of gametocytes within infected human $\mu_h = 0.00625$, $\mu_h = 0.0625$ and $\mu_h = 0.625$.

4.3.7 The influence of within-mosquito scale parameters on between-hosts scale variables for malaria infection

In this sub-section, we illutrate the numerical results of multiscale model (4.2.0.1) present the changes in (a) population of infected humans I_H, (b) community gametocyte load G_H, (c) population of infected mosquyitoes I_V and (d) community sporozoite load P_V over time in days for different values of within-mosquito scale selected parameters (N_k, α_k, α_s, α_v, α_z, N_g, μ_k, μ_s, μ_v and μ_z). We demonstrate the influence of these within-mosquito scale malaria infection dynamics parameters (N_k, α_k, α_s, α_v, α_z, N_g, μ_k, μ_s, μ_v and μ_z) on between host scale variables ((a) population of infected humans I_H, (b) community gametocyte load G_H, (c) population of infected mosquyitoes I_V and (d) community sporozoite load P_V).

Figure (4.23) present the changes in (a) population of infected humans I_H, (b) community gametocyte load G_H, (c) population of infected mosquyitoes I_V and (d) community sporozoite load P_V over time in days for different values of number of sporozoites produced per bursting oocysts within infected mosquitoes N_k: $N_k = 1000$, $N_k = 2000$ and $N_k = 3000$. The numerical simulation results in fig. (4.23) present that as the number of sporozoites produced per bursting oocysts within-infected mosquitoes increase, there is visible increase on malaria transmission of dynamics of population of infected humans, community gametocyte load, population of infected mosquitoes and community sporozoites load. The results recommend the intervention measures that targeted to reduce the number of sporozoites produced per bursting oocysts within-infected mosquitoes which is good in reducing the malaria transmission at population-level.

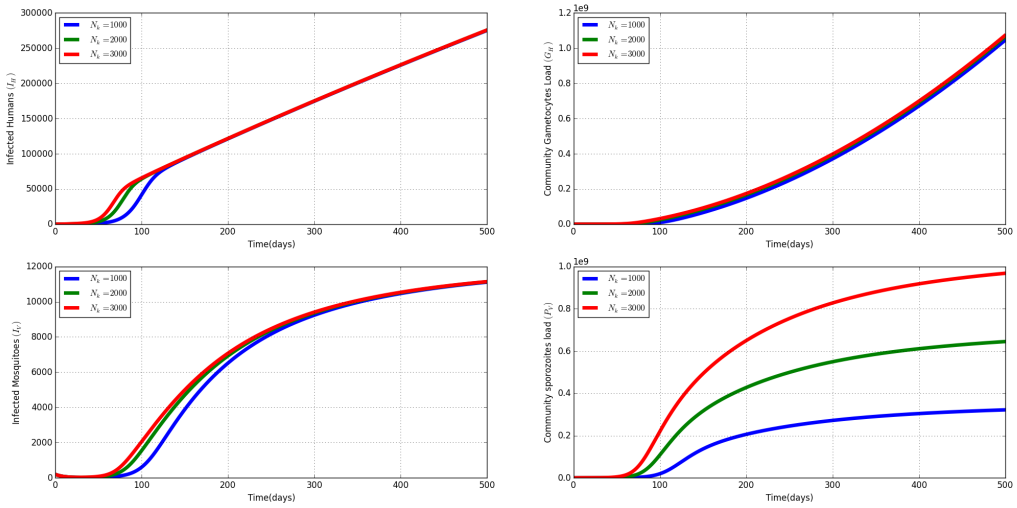

Figure 4.23: Numerical solutions of model (4.2.0.1) presenting changes in (a) population of infected humans I_H, (b) community gametocyte load G_H, (c) population of infected mosquyitoes I_V and (d) community sporozoite load P_V over time in days for different values of number of sporozoites produced per bursting oocysts within infected mosquitoes N_k: $N_k = 1000$, $N_k = 2000$ and $N_k = 3000$.

Figure (4.24) demonstrate the dynamics of (a) population of infected humans I_H, (b) community gametocyte load G_H, (c) population of infected mosquyitoes I_V and (d) community sporozoite load P_V over time in days for different values of bursting rate of oocysts to produce sporozoites within infected mosquitoes α_k: $\alpha_k = 0.2$, $\alpha_k = 0.6$ and $\alpha_k = 1$. The numerical simulation results in fig.(4.24 show that as the bursting rate of oocysts to produce sporozoites within infected mosquitoes increase, there is noticable slight increase on transmission of malaria dynamics of population of infected humans, community gametocyte load, population of infected mosquitoes and community sporozoite load. The numerical simulation results imply that intervention measures that targeted to reduce the bursting rate of oocysts to produce sporozoites within infected mosquitoes have impact in reducing the malaria transmission at population level.

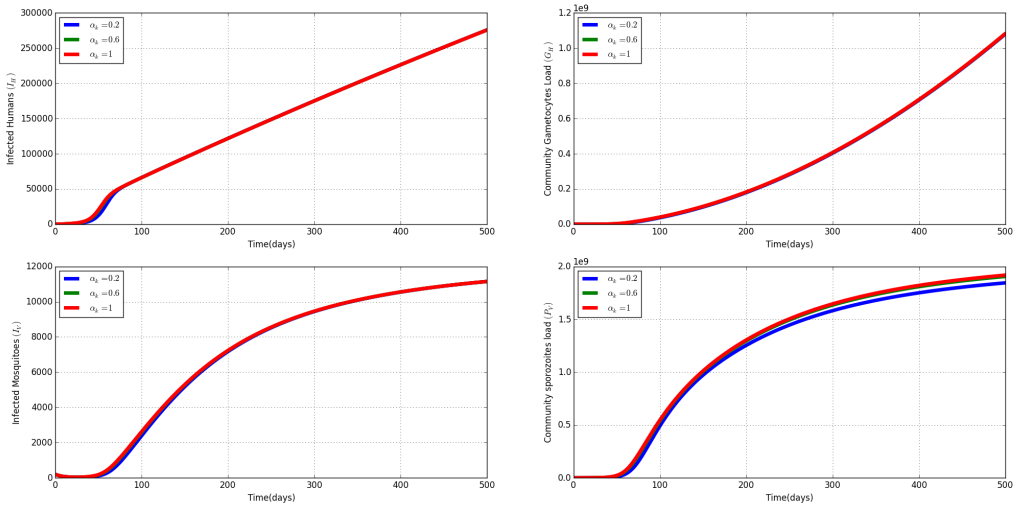

Figure 4.24: Numerical solutions of multiscale model (4.2.0.1) presenting changes in (a) population of infected humans I_H, (b) community gametocyte load G_H, (c) population of infected mosquyitoes I_V and (d) community sporozoite load P_V over time in days for different values of α_k: $\alpha_k = 2$, $\alpha_k = 06$ and $\alpha_k = 0.1$

Figure (4.25) presents the numerical solutions of multiscale model (4.2.0.1) presenting changes in (a) population of infected humans I_H, (b) community gametocyte load G_H, (c) population of infected mosquyitoes I_V and (d) community sporozoite load P_V over time in days for different values of fertilisation of gametes within infected mosquitoes α_s: $\alpha_s = 0.2$, $\alpha_s = 0.5$ and $\alpha_s = 0.8$. The numerical simulation results in fig.(4.25 show that as the fertilisation of gametes within infected mosquitoes increase, there is noticable increase on transmission of malaria dynamics of population of infected humans, community gametocyte load, population of infected mosquitoes. The numerical simulation results imply that intervention measures that targeted to reduce the fertilisation of gametes within infected mosquitoes have impact in reducing the malaria transmission at population level.

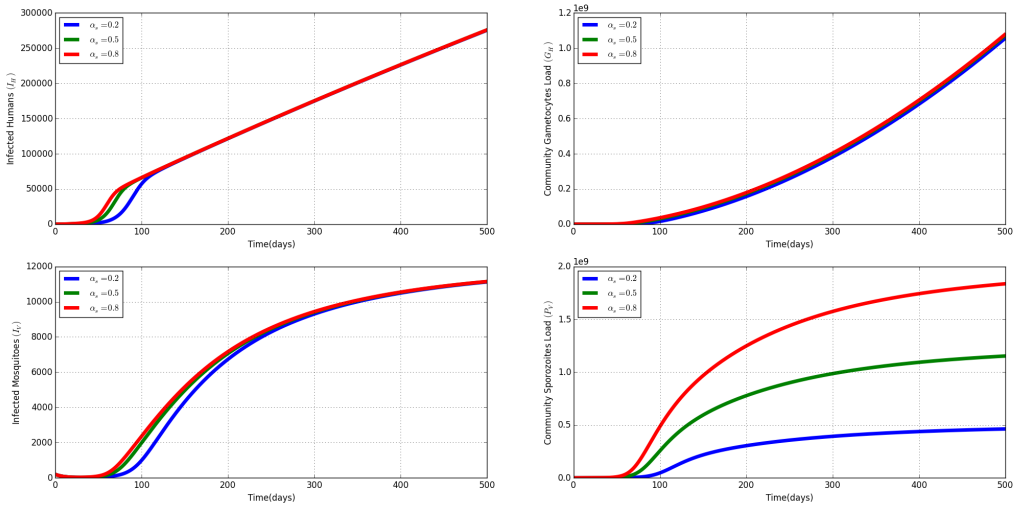

Figure 4.25: Numerical solutions of multiscale model (4.2.0.1) presenting changes in (a) population of infected humans I_H, (b) community gametocyte load G_H, (c) population of infected mosquyitoes I_V and (d) community sporozoite load P_V over time in days for different values of fertilisation of gametes within infected mosquitoes α_s: $\alpha_s = 0.2$, $\alpha_s = 0.5$ and $\alpha_s = 0.8$.

Figure (4.26) presents the numerical solutions of multiscale model (4.2.0.1) presenting changes in (a) population of infected humans I_H, (b) community gametocyte load G_H, (c) population of infected mosquyitoes I_V and (d) community sporozoite load P_V over time in days for different values of shedding/excretion rate of sporozoites become infectious to humans within infected mosqiotoes α_v: $\alpha_v = 0.0025$, $\alpha_v = 0.025$ and $\alpha_v = 0.25$. The numerical simulation results in fig.(4.26) show that as the shedding/excretion rate of sporozoites becomes infectious to human within infected mosquitoes increase, there is noticable increase on transmission of malaria dynamics of population of infected humans, community gametocyte load, population of infected mosquitoes and community sporozoite load. The numerical simulation results imply that intervention measures that targeted to reduce the shedding/excretion rate of sporozoites becomes infectious to human within infected mosquitoes have impact in reducing the malaria transmission at population level.

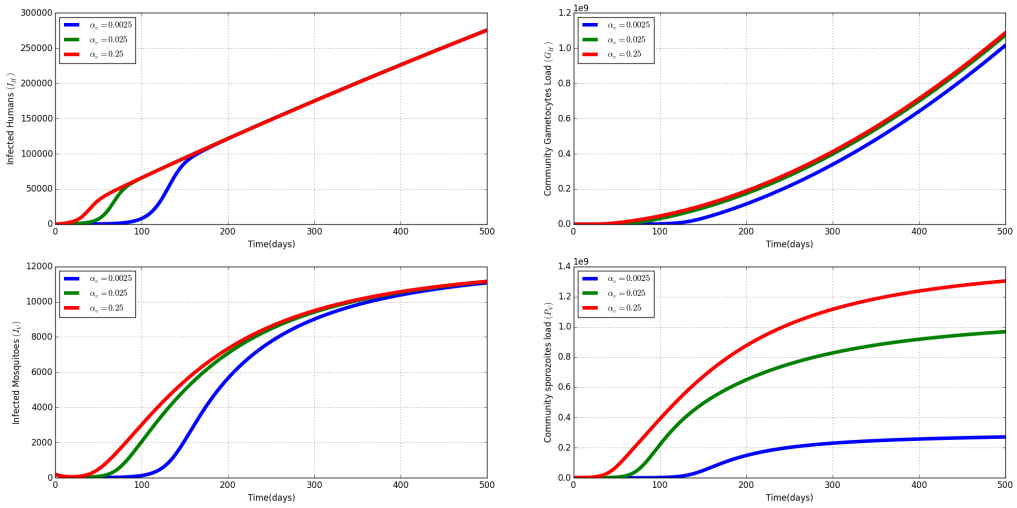

Figure 4.26: Numerical solutions of multiscale model (4.2.0.1) presenting changes in (a) population of infected humans I_H, (b) community gametocyte load G_H, (c) population of infected mosquyitoes I_V and (d) community sporozoite load P_V over time in days for different values of shedding/excretion rate of sporozoites become infectious to humans within infected mosqiotoes α_v: $\alpha_v = 0.0025$, $\alpha_v = 0.025$ and $\alpha_v = 0.25$.

Figure (4.27) presents the numerical solutions of multiscale model (4.2.0.1) presenting changes in (a) population of infected humans I_H, (b) community gametocyte load G_H, (c) population of infected mosquyitoes I_V and (d) community sporozoite load P_V over time in days for different values of progression rate at which zygote develop into oocysts within infected mosquitoes α_z: $\alpha_z = 0.024$, $\alpha_z = 0.424$ and $\alpha_z = 0.824$. The numerical simulation results in fig.(4.27) show that as the progression rate at which zygote develop into oocysts within infected mosquitoes increase, there is noticable increase on transmission of malaria dynamics of population of infected humans, community gametocyte load, population of mosquitoes, and community sporozoite load. The numerical simulation results imply that intervention measures that targeted to reduce the progression rate at which zygote develop into oocysts within infected mosquitoes have impact in reducing the malaria transmission at population level.

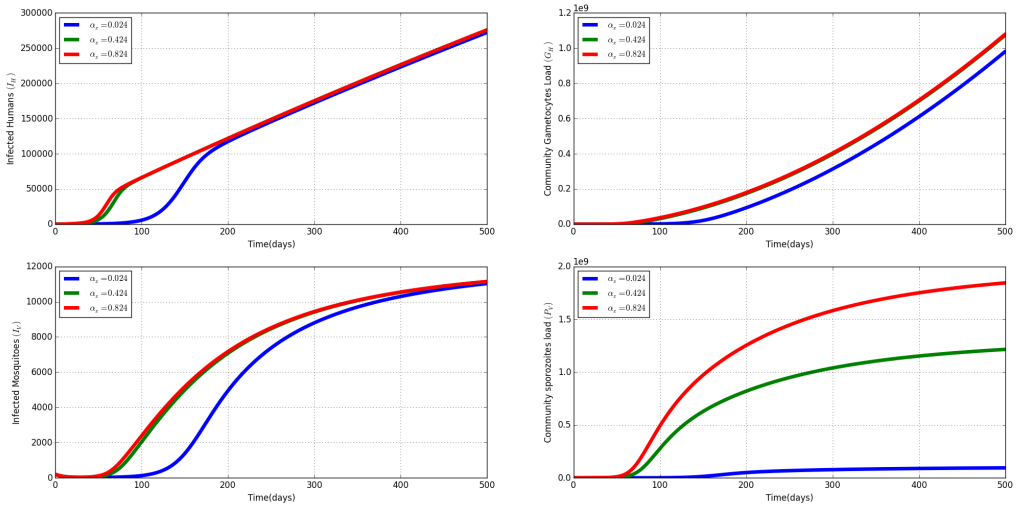

Figure 4.27: Numerical solutions of multiscale model (4.2.0.1) presenting changes in (a) population of infected humans I_H, (b) community gametocyte load G_H, (c) population of infected mosquyitoes I_V and (d) community sporozoite load P_V over time in days for different values of progression rate at which zygote develop into oocysts α_z: $\alpha_z = 0.024$, $\alpha_z = 0.424$ and $\alpha_z = 0.824$.

Figure (4.28) present the changes in (a) population of infected humans I_H, (b) community gametocyte load G_H, (c) population of infected mosquyitoes I_V and (d) community sporozoite load P_V over time in days for different values of gametes produced per gametocyte infectes erythrocyte within infected mosquitoes N_g: $N_g = 2$, $N_g = 6$ and $N_g = 10$. The numerical simulation results in fig. (4.28) present that as the gametes produced per gametocyte infectes erythrocyte within infected mosquitoes increase, there is visible increase on malaria transmission of dynamics of population of infected humans, community gametocyte load, population of infected mosquitoes, and community sporozoites load. The results recommend the intervention measures that targeted to reduce the gametes produced per gametocyte infectes erythrocyte within infected mosquitoes which is good in reducing the malaria transmission at population-level.

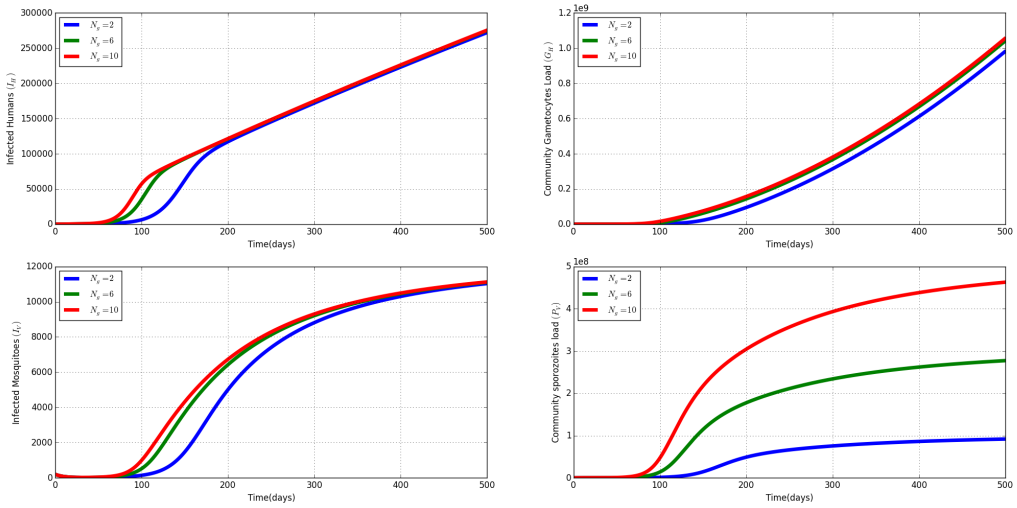

Figure 4.28: Numerical solutions of multiscale model (4.2.0.1) presenting changes in (a) population of infected humans I_H, (b) community gametocyte load G_H, (c) population of infected mosquyitoes I_V and (d) community sporozoite load P_V over time in days for different values of number of gametes produced per gametocyte infectes erythrocyte within infected mosquitoes N_g: $N_g = 2$, $N_g = 6$ and $N_g = 10$.

Figure (4.29) presents the numerical solutions of multiscale model (4.2.0.1) presenting changes in (a) population of infected humans I_H, (b) community gametocyte load G_H, (c) population of infected mosquyitoes I_V and (d) community sporozoite load P_V over time in days for different values of natural decay rate of oocysts within-infected mosquitoes μ_k: $\mu_k = 0.01$, $\mu_k = 0.1$ and $\mu_k = 1$. The numerical simulation results in fig.(4.29) show that as the natural decay rate of oocysts within-infected mosquitoes increase, there is noticable decrease on transmission of malaria dynamics of population of infected humans, community gametocyte load and community sporozoite load and we also notice that there is no difference on the transmission of malaria dynamics on population of infected mosquitoes. The numerical simulation results imply that intervention measures that aimed at killing of oocysts within-infected mosquitoes have impact in reducing the malaria transmission at population level.

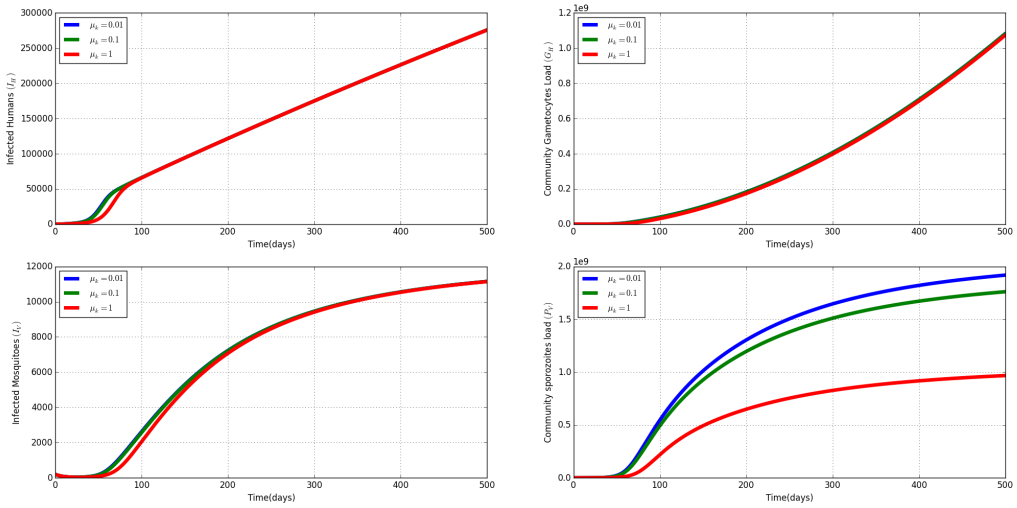

Figure 4.29: Numerical solutions of multiscale model (4.2.0.1) presenting changes in (a) population of infected humans I_H, (b) community gametocyte load G_H, (c) population of infected mosquyitoes I_V and (d) community sporozoite load P_V over time in days for different values of natural decay rate of oocysts within-infected mosquitoes μ_k: $\mu_k = 0.01$, $\mu_k = 0.1$ and $\mu_k = 1$.

Figure (4.30) presents the numerical solutions of multiscale model (4.2.0.1) presenting changes in (a) population of infected humans I_H, (b) community gametocyte load G_H, (c) population of infected mosquyitoes I_V and (d) community sporozoite load P_V over time in days for different values of natural decay rate of gametes within-infected mosquitoes μ_s: $\mu_s = 28$, $\mu_s = 58$ and $\mu_s = 88$. The numerical simulation results in fig.(4.30) show that as the natural decay rate of gametes within-infected mosquitoes increase, there is noticable decrease on transmission of malaria dynamics of population of infected humans, community gametocyte load, population of infected mosquitoes and community sporozoite load. The numerical simulation results imply that intervention measures that targeted for killing gametes within-infected mosquitoes have impact in reducing the malaria transmission at population level.

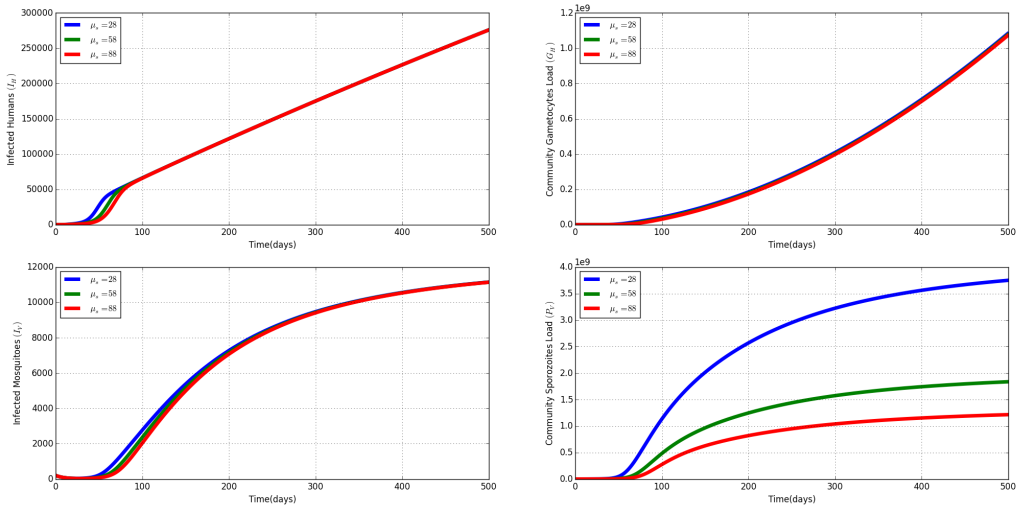

Figure 4.30: Numerical solutions of multiscale model (4.2.0.1) presenting changes in (a) population of infected humans I_H, (b) community gametocyte load G_H, (c) population of infected mosquyitoes I_V and (d) community sporozoite load P_V over time in days for different values of natural decay rate of gametes within-infected mosquitoes μ_s: $\mu_s = 28$, $\mu_s = 58$ and $\mu_s = 88$.

Figure (4.31) presents the numerical solutions of multiscale model (4.2.0.1) presenting changes in (a) population of infected humans I_H, (b) community gametocyte load G_H, (c) population of infected mosquyitoes I_V and (d) community sporozoite load P_V over time in days for different values of natural death rate of sporozoites within-infected mosquitoes μ_v: $\mu_v = 0.01$, $\mu_v = 0.1$ and $\mu_v = 1$. The numerical simulation results in fig.(4.31) show that as the natural death rate of sporozoites within-infected mosquitoes increase, there is noticable decrease on transmission of malaria dynamics of population of infected humans, community gametocyte load, population of infected mosquitoes and community sporozoite load. The numerical simulation results imply that intervention measures that aimed at killing sporozoites within infected mosquitoes have impact in reducing the malaria transmission at population level.

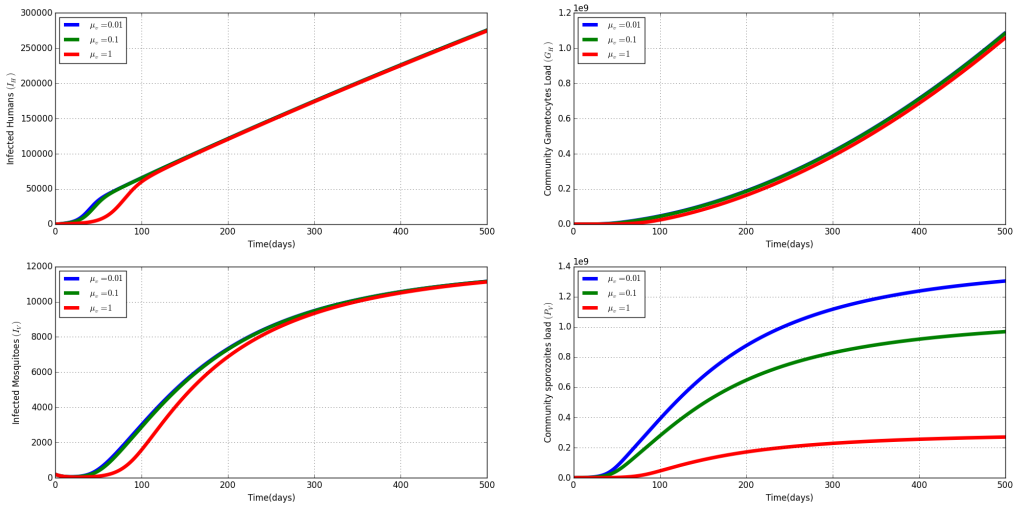

Figure 4.31: Numerical solutions of multiscale model (4.2.0.1) presenting changes in (a) population of infected humans I_H, (b) community gametocyte load G_H, (c) population of infected mosquyitoes I_V and (d) community sporozoite load P_V over time in days for different values of natural death rate of sporozoites within-infected mosquitoes μ_v: $\mu_v = 0.01$, $\mu_v = 0.1$ and $\mu_v = 1$.

Figure (4.32) presents the numerical solutions of multiscale model (4.2.0.1) presenting changes in (a) population of infected humans I_H, (b) community gametocyte load G_H, (c) population of infected mosquyitoes I_V and (d) community sporozoite load P_V over time in days for different values of natural death rate of zygote within-infected mosquitoes μ_z: $\mu_z = 0.01$, $\mu_z = 0.1$ and $\mu_z = 1$. The numerical simulation results in fig.(4.32) show that as the natural death rate of zygote within-infected mosquitoes increase, there is noticable decrease on transmission of malaria dynamics of the community sporozoite load and we also notice that there is slightly decrease on the transmission of malaria dynamics on population of infected humans, community gametocyte load and population of infected mosquitoes. The numerical simulation results suggest that intervention measures that aimed at killing zygotes within infected mosquitoes have impact in reducing the malaria transmission at population level.

In summary, the numerical results in fig.(4.3)-fig.(4.32) present that:

(1) The between-host scale influences the within-host scale through super-infection or repeated infection.

(2) When the infection of the within-host scale has successfully been established then the process of pathogen replication will take over.

(3) Within-host scale continuously influences the dynamics of disease at the between-host scale through shedding /excretion of pathogen throughout the infection.

(4) We notice that the model has a bidirectional flow of information.

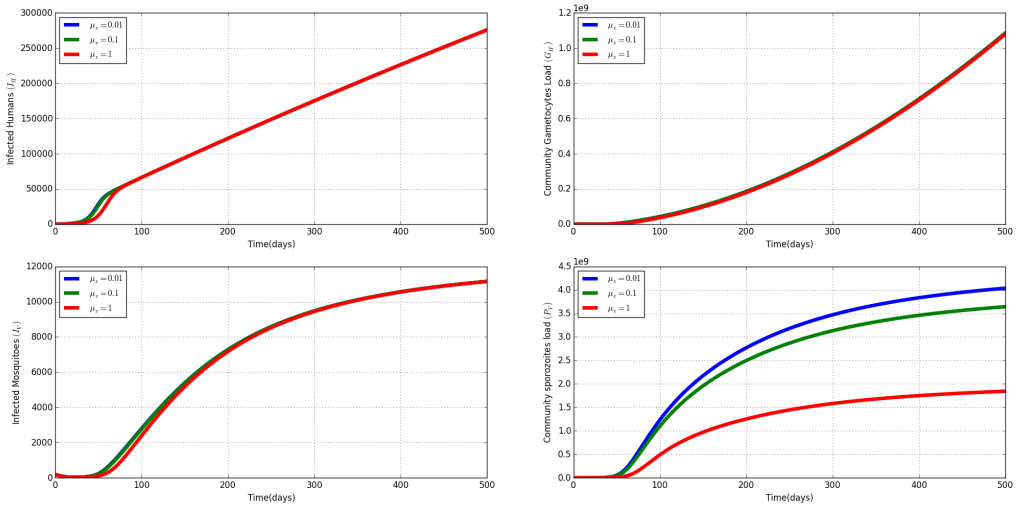

Figure 4.32: Numerical solutions of multiscale model (4.2.0.1) presenting changes in (a) population of infected humans I_H, (b) community gametocyte load G_H, (c) population of infected mosquyitoes I_V and (d) community sporozoite load P_V over time in days for different values of natural death rate of zygote within-infected mosquitoes μ_z: $\mu_z = 0.0025$, $\mu_z = 0.0625$ and $\mu_z = 0.1225$.

4.4 Model extension

We extend the malaria model with liver stage by including the vaccination processes which are: pre-erythrocytic vaccine (PEV), blood stage vaccine (BSV) and transmission blocking vacine (TBV). The parameter $(1-\nu)$ can be taken as an aspect by which pre-erythrocytic vaccine (PEV) reduces invasion of hepatocytes by the malaria sporozoites, where $0 < \nu < 1$ is the efficacy of the pre-erythrocytic vaccine. $\nu = 1$ shows that the vaccine is fully efficient (i.e. all the malaria sporozoites are cleared before or during their development in the liver) whereas $\nu = 0$ shows that the vaccine is totally ineffective. The eliminating of infected hepatocytes deminishes the burst size of the infected hepatocytes. This is denoted by the term $(1-b)$, where $0 < b < 1$ is the probability with which the vaccine inhibits merozoite emergence from infected liver cells. The BSV is expected to reduce the number of parasites in the blood and in so doing deminish the severity of disease. The effects of BSV on the transmission of red blood cells is modelled by $(1-\varepsilon)$, where $0 < \varepsilon < 1$ is represent the efficacy of the BSV. The effect of BSV is modelled by parater $(1+\theta_1)$, where θ_1 is the rate at which recovered rate of infected humans are increased, where $0 < \theta_1 < 1$. $1-\theta_2$ is the rate at which the disease related death rate in infected human population is reduced due to the effects of vaccine on blood stages of the parasite, where $0 < \theta_2 < 1$. BSV diminishes the density of merozoites that are discharged per bursting blood schizont, which is given by $(1-a)$, where $0 < a < 1$ accounts for the vaccine-induced decline of merozoites discharged per bursting infected red blood cells. The TBV seek to interrupt the life cycle of the parasite by inducing antibodies that preventthe parasite

from maturing in the mosquito after it takes a blood meal from a vaccinated person. These will prevent the transmission of malaria from spreading to new hosts. This effect is denoted by a parameter χ where $0 < \chi < 1$. The summary of the action of malaria vaccination is given in Table (4.5).

Table 4.5: Summary of the action of vaccination on malaria transmission dynamics

No.	**Health intervention**	**Mechanism of intervention action**	**Modelling effect of intervention**
1.	Pre-erythrocytic vaccine	Rate at which malaria sporozoites invade the hepatocytes parameter β_l is reduced. The rate at which vaccine-induced deminishes of merozoites released per bursting size of an infected hepatocytes N_l.	$\beta_l \longrightarrow \beta_l(1-\nu)$ $N_l \longrightarrow N_l(1-b)$
2.	Blood-stage vaccine	Rate at which merozoites invade the red blood cells parameter β_h is reduced. Rate at which recovered rate of infected humans γ_H are increased. The rate at which the disease related death rate in infected humans δ_H is reduced. The rate of vaccine -induced reduce of merozoites released per bursting size of infected red blood cells N_m.	$\beta_h \longrightarrow \beta_h(1-\varepsilon)$ $\gamma_H \longrightarrow \gamma_H(1+\theta_1)$ $\delta_H \longrightarrow \delta_H(1-\theta_2)$ $N_m \longrightarrow N_m(1-a)$
3.	Transmission blocking vaccine	Reduce susceptibility to malaria infection in the sporozoites community and gametocytes community by reducing the susceptibility coefficient $\frac{1}{P_0}$ and $\frac{1}{G_0}$ respectively and therefore increase P_0 and G_0 respectively.	$P_0 \longrightarrow P_0(1+\chi_1)$, $G_0 \longrightarrow G_0(1+\chi_2)$

The extended model is given by

$$
\begin{aligned}
1.\quad \frac{dS_H(t)}{dt} &= \Lambda_H - \frac{\beta_V P_V(t)}{P_0(1+\chi_1)+P_V(t)} S_H(t) - \mu_H S_H(t) + (1+\theta_1)\gamma_H I_H(t),\\
2.\quad \frac{dI_H(t)}{dt} &= \frac{\beta_V P_V(t)}{P_0(1+\chi_1)+P_V(t)} S_H(t) - [\mu_H + \gamma_H(1+\theta_1) + \delta_H(1-\theta_2)] I_H(t),\\
3.\quad \frac{dP_h(t)}{dt} &= \frac{\beta_V P_V(t)(S_H(t)-1)}{(P_0(1+\chi_1)+P_V(t))\phi_H(I_H(t)+1)} - \mu_p P_h(t),\\
4.\quad \frac{dL_h(t)}{dt} &= \Lambda_l - (1-\nu)\beta_l P_h(t) L_h(t) - \mu_l L_h(t),\\
5.\quad \frac{dL_h^*(t)}{dt} &= (1-\nu)\beta_l P_h(t) L_h(t) - (\mu_l + \alpha_l) L_h^*(t),\\
6.\quad \frac{dB_h(t)}{dt} &= \Lambda_h - (1-\varepsilon)\beta_h M_h(t) B_h(t) - \mu_b B_h(t),\\
7.\quad \frac{dB_h^*(t)}{dt} &= (1-\varepsilon)(1-\pi)\beta_h M_h(t) B_h(t) - (\mu_b + \alpha_m) B_h^*(t),\\
8.\quad \frac{dM_h(t)}{dt} &= (1-b) N_l \alpha_l L_h^* + (1-a) N_m \alpha_m B_h^*(t) - \mu_m M_h(t) - \beta_h M_h B_h, \qquad (4.4.0.1)\\
9.\quad \frac{dG_h(t)}{dt} &= (1-\varepsilon)\pi\beta_h M_h(t) B_h - (\alpha_h + \mu_h) G_h(t),\\
10.\quad \frac{dG_H(t)}{dt} &= G_h(t)\alpha_h(I_H(t)+1) - \alpha_H G_H(t),\\
11.\quad \frac{dS_V(t)}{dt} &= \Lambda_V - \frac{\beta_H G_H(t)}{G_0(1+\chi_2)+G_H(t)} S_V(t) - \mu_V S_V(t),\\
12.\quad \frac{dI_V(t)}{dt} &= \frac{\beta_H G_H(t)}{G_0(1+\chi_2)+G_H(t)} S_V(t) - (\mu_V + \delta_V) I_V(t),\\
13.\quad \frac{dG_v(t)}{dt} &= \frac{\beta_H G_H(t)(S_V(t)-1)}{(G_0(1+\chi_2)+G_H(t))\phi_V(I_V(t)+1)} - (\alpha_g + \mu_g) G_v(t),\\
14.\quad \frac{dG_m(t)}{dt} &= N_g \alpha_g G_v(t) - (\alpha_s + \mu_s) G_m(t),\\
15.\quad \frac{dZ_v(t)}{dt} &= \frac{1}{2}\alpha_s G_m(t) - (\alpha_z + \mu_z) Z_v(t),\\
16.\quad \frac{dO_v(t)}{dt} &= \alpha_z Z_v - (\alpha_k + \mu_k) O_v(t),\\
17.\quad \frac{dP_v(t)}{dt} &= N_k \alpha_k O_v(t) - (\alpha_v + \mu_v) P_v(t),\\
18.\quad \frac{dP_V(t)}{dt} &= P_v(t)\alpha_v(I_V(t)+1) - \alpha_V P_V(t).
\end{aligned}
$$

The effective reproduction number is given by

$$
\begin{aligned}
R_{0E} &= \frac{1}{3}Q_{he} + \sqrt[3]{\frac{27Q_{VE}Q_{HE}+2Q_{he}^3}{54} + \sqrt{\frac{Q_{VE}Q_{HE}\left(27Q_{VE}Q_{HE}+2Q_{he}^3\right)}{108}}}\\
&\quad + \sqrt[3]{\frac{27Q_{VE}Q_{HE}+2Q_{he}^3}{54} - \sqrt{\frac{Q_{VE}Q_{HE}\left(27Q_{VE}Q_{HE}+2Q_{he}^3\right)}{108}}}, \qquad (4.4.0.2)
\end{aligned}
$$

where

$$\begin{aligned} Q_{he} &= \frac{(1-a)N_m\alpha_m}{\alpha_m+\mu_b}\frac{(1-\varepsilon)(1-\pi)\beta_h\Lambda_h}{\mu_b\mu_m+\beta_h\Lambda_h}, \\ Q_{HE} &= \frac{(1-b)N_l\alpha_l}{\mu_p\mu_l}\frac{(1-\nu)\beta_l\Lambda_l}{\alpha_l+\mu_l}\frac{\alpha_h}{\alpha_h+\mu_h}\frac{(1-\varepsilon)\pi\beta_h\Lambda_h}{\mu_b\mu_m+\beta_h\Lambda_h}\frac{\beta_V(\Lambda_H-\mu_H)}{\alpha_V\mu_H\phi_H P_0(1+\chi_1)}, \\ Q_{VE} &= \frac{1}{2}\frac{N_g\alpha_g}{\alpha_g+\mu_g}\frac{\alpha_s}{\alpha_s+\mu_s}\frac{\alpha_z}{\alpha_z+\mu_z}\frac{N_k\alpha_k}{\alpha_k+\mu_k}\frac{\alpha_v}{\alpha_v+\mu_v}\frac{\beta_H(\Lambda_V-\mu_V)}{\mu_V\phi_V\alpha_H G_0(1+\chi_2)}. \end{aligned} \tag{4.4.0.3}$$

The percentage reduction of the public health measure is given by

$$\%\text{age reduction of}R_0 = \frac{R_0 - R_{0V}}{R_0} \times 100\%, \tag{4.4.0.4}$$

where R_{0V} is the reproductive number where the vaccine efficacy is applied. In Table (4.6), we illustrate the influence of vaccination processes on reproductive number (R_0). As the rate of efficacy for malaria vaccine increase, we observe that the percentage reduction of R_0 also increase. We also observe that an increase in the vaccine combination have an influence in the increase of the percentage reduction of R_0. We compute the comparative effectiveness as follows: (i) low efficacy which is given by $\nu = \varepsilon = \chi_1 = \chi_2 = 30\%$, (ii) medium efficacy is given by $\nu = \varepsilon = \chi_1 = \chi_2 = 60\%$ and (iii) high efficacy is given by $\nu = \varepsilon = \chi_1 = \chi_2 = 90\%$.

From the Table (4.6), we evaluate the comparative effectiveness of the three phases in malaria vaccination (PEV, BSV and TBV) using the basic reproductive number as the guide of intervention effectiveness using efficacy data. The Table (4.6) presenting the outcomes of the assessment of the comparative effectiveness of three phases in the malaria vaccination and their related mechanisms using the percentage reduction in the basic reproductive number as the guide on the effectiveness of malaria vaccine. From Table (4.6), we conclude the following outcomes:

(a) Considering the use malaria vaccination as the only malaria health intervention. We note that this intervention has three phases of malaria vaccines which are:

(i) efficacy of the PEV,

(ii) efficacy of the BSV, and

(iii) the efficacy of the TBV.

The outcomes presents that the efficacy of PEV have highest comparative effectiveness, while the efficacy of BSV has a lowest comparative effectiveness comparing with other phases of vaccines components as a complex malaria health intervention.

(b) Comparing the effectiveness of two stages of malaria vaccination components. The combination of PEV and BSV has the highest comparative effectiveness while the combination of PEV and TBV has the lowest comparative effectiveness.

(c) The combination of three phases of malaria vaccination with comparative effectiveness efficacy of (i) 90% (at high efficacy) can reduce malaria in a particular region/community by an approximation of 89.04% of basic reproductive number when used in combination, (ii) 60% (at medium efficacy) can reduce malaria infection in a particular community by approximate of 62.24% of the basic reproductive number when used in combination and (iii) 30% (at low efficacy) can reduce malaria infection in a particular community by approximate of 32.44% of the basic reproductive number when used in combination

Table 4.6: Indicating the results of analysis of comparative effectiveness of vaccination on malaria transmission dynamics employing the percentage reduction of basic reproduction number (R_0) as a guide of malaria intervention effectiveness when each of these phases of malaria vaccination are assumed to have: (a) low-efficacy of 30%, (b) medium-efficacy of 60% and (c) high-efficacy of 90%.

Number	Parameter	Calculated R_{0V}-Low	Ranking	Calculated R_{0V}-Medium	Ranking	Calculated R_{0V}-High	Ranking
1	R_0	0	1	0	1	0	1
2	$R_{0\varepsilon}$	11.21	2	26.33	4	53.59	4
3	$R_{0\chi_1}$	11.24	3	21.66	2	30.96	2
4	$R_{0\chi_2}$	11.24	3	21.66	2	30.96	2
5	$R_{0\nu}$	14.27	5	34.57	5	65.79	5
6	$R_{0\varepsilon\chi_1}$	21.19	6	42.28	6	67.96	6
7	$R_{0\varepsilon\chi_2}$	21.19	6	42.28	6	67.96	6
8	$R_{0\varepsilon\nu}$	23.89	8	51.8	10	84.13	10
9	$R_{0\chi_1\nu}$	23.9	9	48.74	8	76.38	8
10	$R_{0\chi_2\nu}$	23.9	9	48.74	8	76.38	8
11	$R_{0\varepsilon\chi_1\nu}$	32.44	11	62.24	11	89.04	11
12	$R_{0\varepsilon\chi_2\nu}$	32.44	11	62.24	11	89.04	11

The impact of vaccine-induced reduction of merozoites released per bursting size of infected red blood cells is controlled by differentiating R_{0E} with respect to a. We obtain

$$\begin{aligned}\frac{\partial R_{0E}}{\partial a} = & -\frac{1}{3}\frac{(1-\varepsilon)(1-\pi)N_m\alpha_m\beta_h\Lambda_h}{(\alpha_m+\mu_b)(\beta_h\Lambda_h+\mu_b\mu_m)}\left\{1+\left(\frac{27Q_{VE}Q_{HE}+2Q_{he}^3}{54}+\right.\right.\\ & \left.\sqrt{\frac{Q_{VE}Q_{HE}(27Q_{VE}Q_{HE}+2Q_{he}^3)}{108}}\right)^{-\frac{2}{3}}\left[\frac{1}{9}Q_{he}^2+\frac{1}{36}\left(\frac{Q_{VE}Q_{HE}(27Q_{VE}Q_{HE}+2Q_{he}^3)}{108}\right)^{-\frac{1}{2}}\right.\\ & \left.\times Q_{VE}Q_{HE}Q_{he}^2\right]+\left(\frac{27Q_{VE}Q_{HE}+2Q_{he}^3}{54}-\sqrt{\frac{Q_{VE}Q_{HE}(27Q_{VE}Q_{HE}+2Q_{he}^3)}{108}}\right)^{-\frac{2}{3}}\times\\ & \left.\left[\frac{1}{9}Q_{he}^2-\frac{1}{36}Q_{VE}Q_{HE}Q_{he}^2\left(\frac{Q_{VE}Q_{HE}(27Q_{VE}Q_{HE}+2Q_{he}^3)}{108}\right)^{-\frac{1}{2}}\right]\right\}<0. \qquad (4.4.0.5)\end{aligned}$$

From the derivation, we observe that the vaccine reproductive number R_{0E} decreases with the increasing value of a.

The impact of the vaccine-induced reduction of merozoites released per bursting size of an infected hepatocytes is controlled by differentiating R_{0E} with respect to b. We obtain

$$\begin{aligned}\frac{\partial R_{0E}}{\partial b} &= -\frac{1}{3}Q_{VE}\frac{N_l\alpha_l}{\mu_l\mu_p}\frac{(1-\nu)\beta_l\Lambda_l}{\alpha_l+\mu_l}\frac{\alpha_h}{\alpha_h+\mu_h}\frac{(1-\varepsilon)\pi\beta_h\Lambda_h}{\mu_b\mu_m+\beta_h\Lambda_h}\frac{\beta_V(\Lambda_H-\mu_H)}{\alpha_V\mu_H\phi_H P_0(1+\chi_1)}\left\{\left(\frac{27Q_{VE}Q_{HE}+2Q_{he}^3}{54}\right.\right.\\ &\left.+\sqrt{\frac{Q_{VE}Q_{HE}(27Q_{VE}Q_{HE}+2Q_{he}^3)}{108}}\right)^{-\frac{2}{3}}\left[\frac{1}{2}+\frac{1}{2}\left(\frac{Q_{VE}Q_{HE}(27Q_{VE}Q_{HE}+2Q_{he}^3)}{108}\right)^{-\frac{1}{2}}\times\right.\\ &\left.\left(\frac{27Q_{VE}Q_{HE}+2Q_{he}^3}{108}+\frac{1}{4}Q_{VE}Q_{HE}\right)\right]+\left(\frac{27Q_{VE}Q_{HE}+2Q_{he}^3}{54}-\right.\\ &\left.\sqrt{\frac{Q_{VE}Q_{HE}(27Q_{VE}Q_{HE}+2Q_{he}^3)}{108}}\right)^{-\frac{2}{3}}\left[\frac{1}{2}-\frac{1}{2}\left(\frac{Q_{VE}Q_{HE}(27Q_{VE}Q_{HE}+2Q_{he}^3)}{108}\right)^{-\frac{1}{2}}\times\right.\\ &\left.\left.\left(\frac{27Q_{VE}Q_{HE}+2Q_{he}^3}{108}+\frac{1}{4}Q_{VE}Q_{HE}\right)\right]\right\}<0. \qquad (4.4.0.6)\end{aligned}$$

We observe from diffentiation that the vaccine reproductive number R_{0E} decreases with the increasing value of b.

We differentiate R_{0E} with respect to vaccine efficacy ν. This gives

$$\begin{aligned}\frac{\partial R_{0E}}{\partial \nu} &= -\frac{1}{3}Q_{VE}\frac{(1-b)N_l\alpha_l}{\mu_p\mu_l}\frac{\beta_l\Lambda_l}{\alpha_l+\mu_l}\frac{\alpha_h}{\alpha_h+\mu_h}\frac{(1-\varepsilon)\pi\beta_h\Lambda_h}{\mu_b\mu_m+\beta_h\Lambda_h}\frac{\beta_V(\Lambda_H-\mu_H)}{\alpha_V\mu_H\phi_H P_0(1+\chi_1)}\left\{\left(\frac{27Q_{VE}Q_{HE}+2Q_{he}^3}{54}\right.\right.\\ &\left.+\sqrt{\frac{Q_{VE}Q_{HE}(27Q_{VE}Q_{HE}+2Q_{he}^3)}{108}}\right)^{-\frac{2}{3}}\left[\frac{1}{2}+\frac{1}{2}\left(\frac{Q_{VE}Q_{HE}(27Q_{VE}Q_{HE}+2Q_{he}^3)}{108}\right)^{-\frac{1}{2}}\times\right.\\ &\left.\left(\frac{Q_{VE}Q_{HE}+2Q_{he}^3}{108}\right)\right]+\left(\frac{27Q_{VE}Q_{HE}+2Q_{he}^3}{54}-\sqrt{\frac{Q_{VE}Q_{HE}(27Q_{VE}Q_{HE}+2Q_{he}^3)}{108}}\right)^{-\frac{2}{3}}\left[\frac{1}{2}\right.\\ &\left.\left.-\frac{1}{2}\frac{54Q_{VE}Q_{HE}+2Q_{he}^3}{108}\left(\frac{Q_{VE}Q_{HE}(27Q_{VE}Q_{HE}+2Q_{he}^3)}{108}\right)^{-\frac{1}{2}}\right]\right\}<0. \qquad (4.4.0.7)\end{aligned}$$

We observe that R_{0E} is a decreasing function of the pre-erythrocytic vaccine ν. The concentration of infected hepatocytes decreases with increasing values of ν.

By differentiating R_{0E} with respect to vaccines efficacy χ_1, χ_2 and ε respectively, yields

$$\begin{aligned} \frac{\partial R_{0E}}{\partial \chi_1} &< 0 \\ \frac{\partial R_{0E}}{\partial \chi_2} &< 0 \\ \frac{\partial R_{0E}}{\partial \varepsilon} &< 0. \end{aligned} \tag{4.4.0.8}$$

We observe that R_{0E} decreases with increasing with χ_1, χ_2 and ε. From our differentiation, we observe that PEV, BST and TBV have impact in the reduction in the basic reproductive number.

In Figure (4.33) and (4.34) we show the evidence for the impact of the variation of combination of malaria vaccines (PEV, BSV and TBV) on community gametocytes load G_H. We observe that the highly efficacious combination of malaria vaccines has a potential to reduce the number of gametocytes in the blood stream, thereby minimizing the community gametocytes load (G_H).

In figure (4.35) we demonstrate the influence of variation in combination of malaria vaccines (PEV, bsv and TBV) on community sporozoites load P_V. We observe that an increase in the combination of malaria vaccines will results in reduction of the community sporozoites load. In Figure (4.36) and (4.37) we present the evidence of influence of the variation of malaria vaccines on population of merozoites (M_h). We notice that the increase of efficacy in combination of malaria vaccines would reduce the merozoites in the blood stream thereby minimizing parasite transmission to mosquitoes and subsequently to other human beings. We observe from Figure (4.38) that the variation in the rate at which vaccine-induced deminishes merozoites released per bursting size of an infected hepatocytes and also the rate of vaccine-induced reduces of merozoites released per bursting size of infected red blood cells have influence on the merozoites population.

In Figure (4.39) to (4.42) we demonstrate the influence of varying the efficacy of pre-erythrocytic vaccine on infected liver cells. A highly efficacy of PEV has a potential to significantly reduce the number of malaria sporozoites in the liver-stage, which results in minimizing the parasite transmission to mosquitoes and subsequently to other human beings.

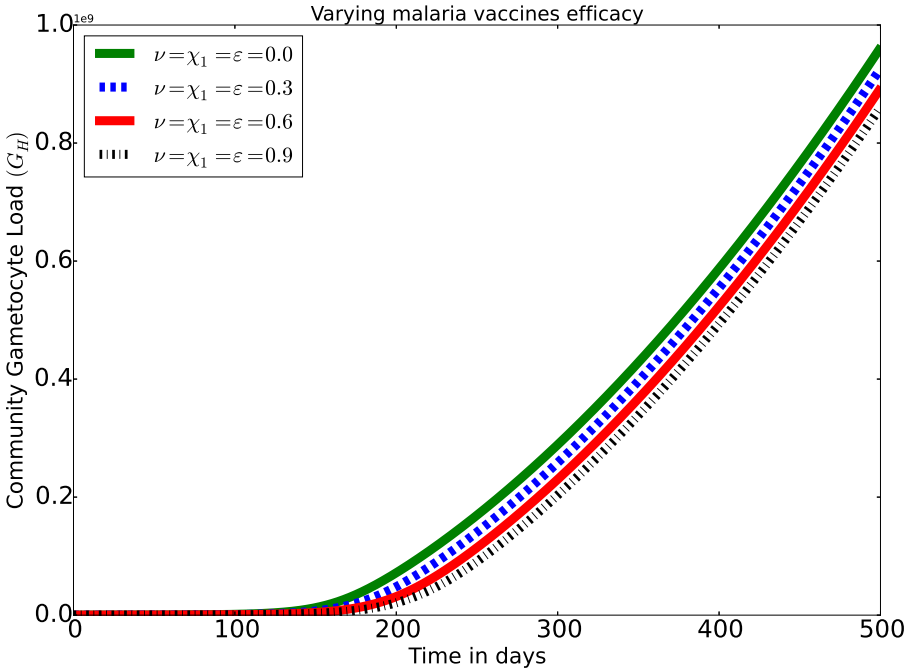

Figure 4.33: The graph showing changes in Community Gametocytes Load (G_H^*) for varying all the efficacy i.e pre-erythrocytic vaccine ν, blood stage vaccine ε, and transmission blocking vaccine χ_1.

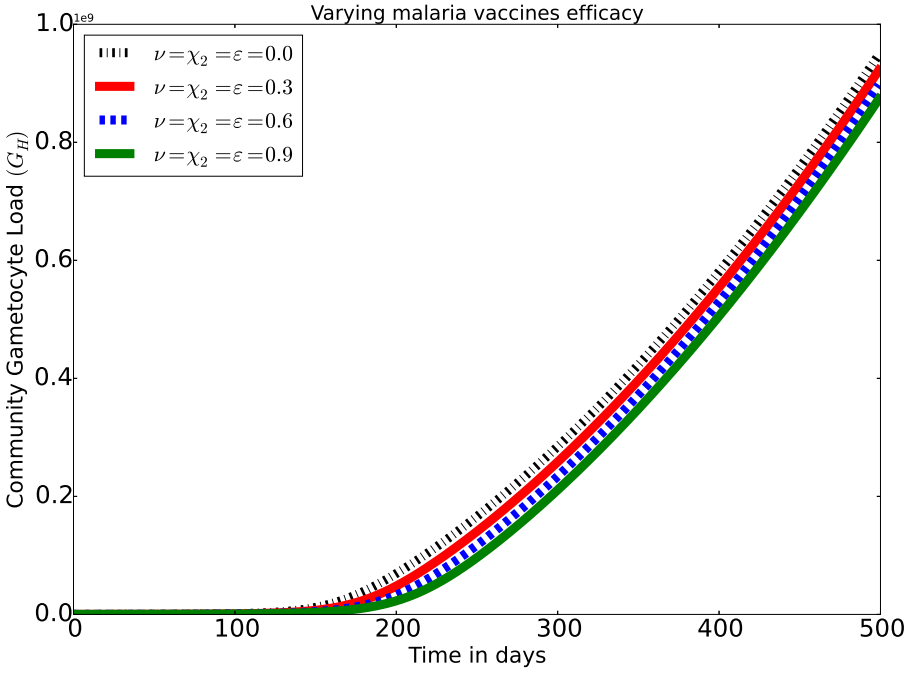

Figure 4.34: The graph showing changes in Community Gametocytes Load (G_H^*) for varying all the efficacy i.e pre-erythrocytic vaccine ν, blood stage vaccine ε, and transmission blocking vaccine χ_2.

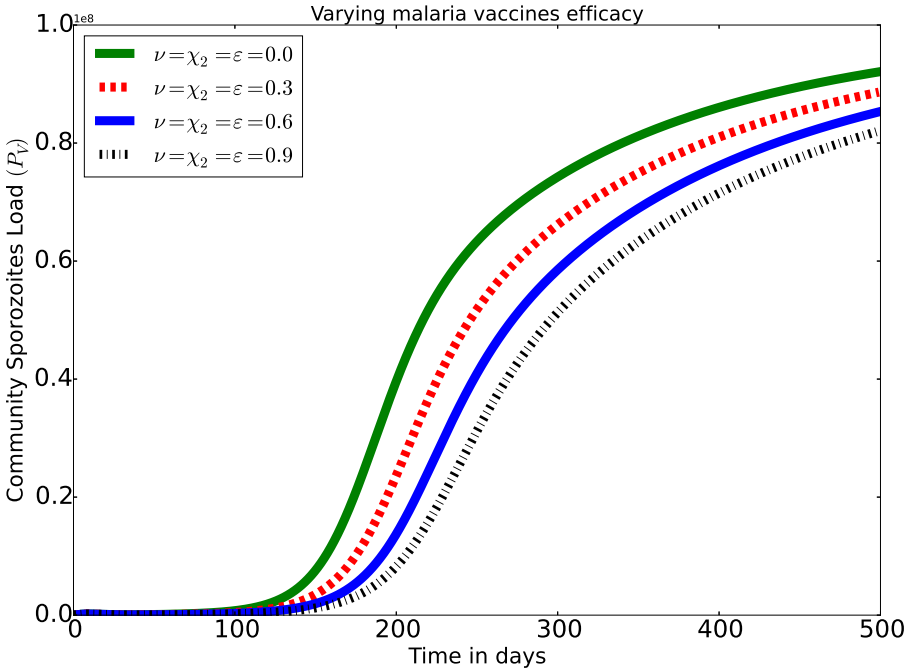

Figure 4.35: The graph showing changes in Community Sporozoites Load (P_V^*) for varying all the efficacy i.e pre-erythrocytic vaccine ν, blood stage vaccine ε, and transmission blocking vaccine χ_2.

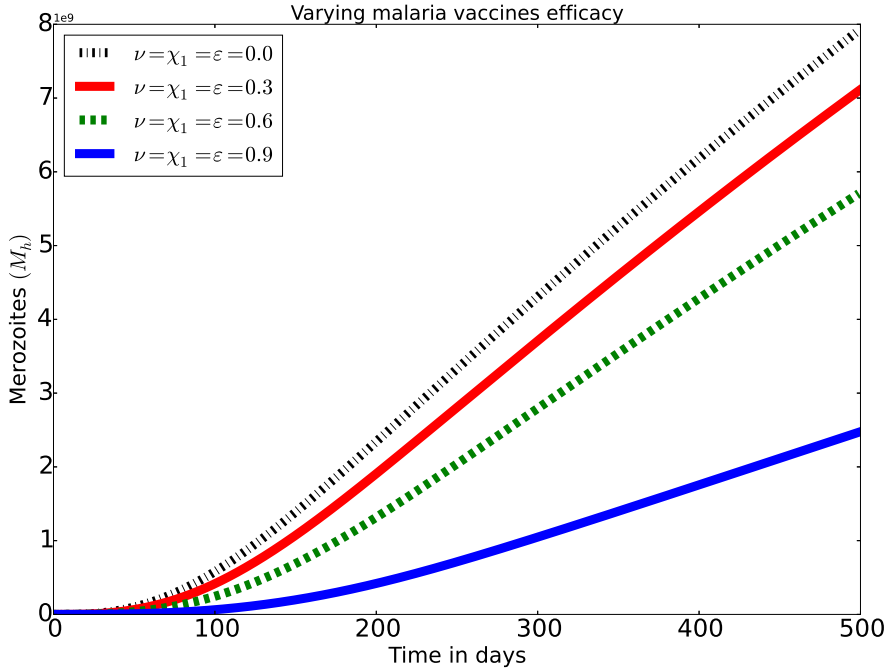

Figure 4.36: The graph showing the profile of merozoites population (M_h) in the presence of malaria vaccines. The efficacy of malaria vaccines are varied from 0 to 1.

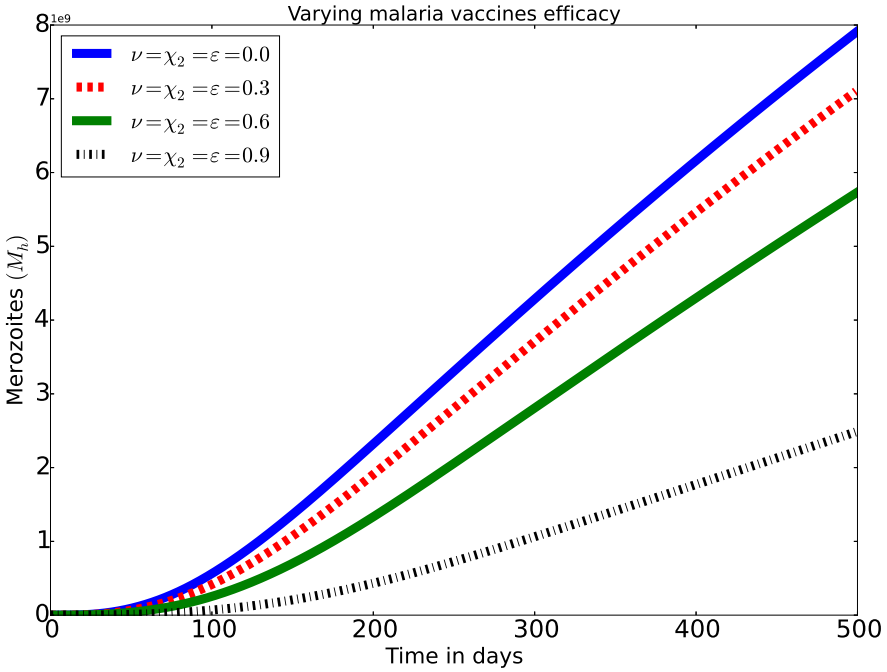

Figure 4.37: The graph showing the profile of merozoites population (M_h) in the presence of malaria vaccines. The efficacy of malaria vaccines are varied from 0 to 1.

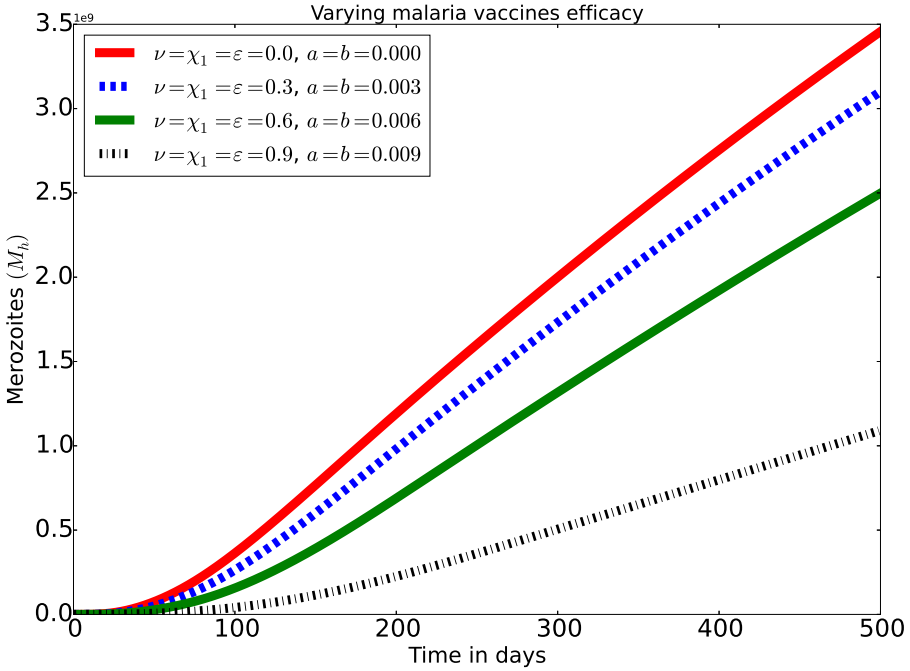

Figure 4.38: The graph showing the profile of merozoites population (M_h) in the presence of malaria vaccines. The efficacy of malaria vaccines are varied from 0 to 1.

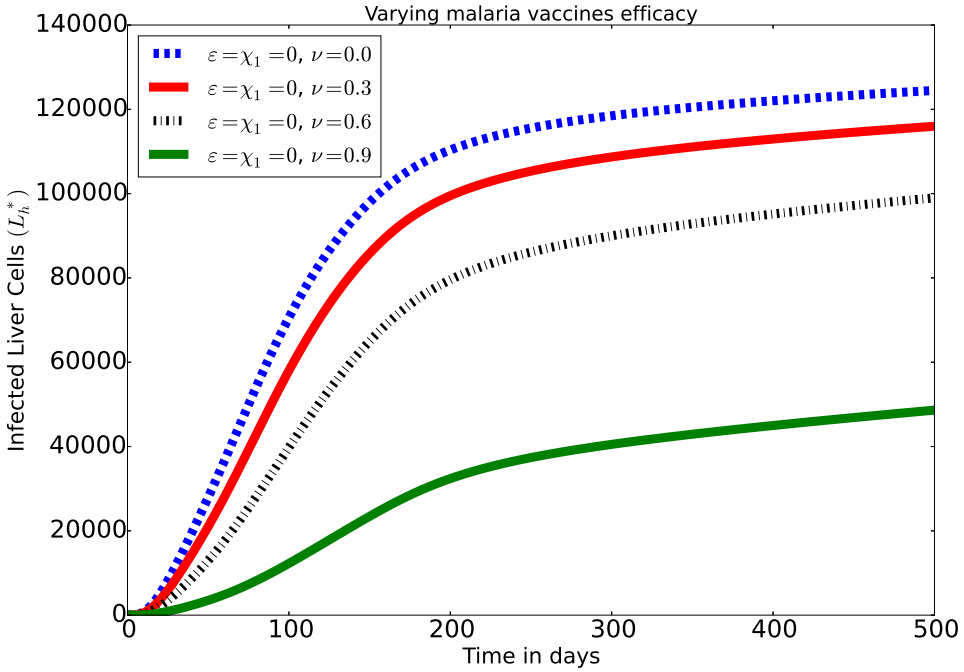

Figure 4.39: The graph showing changes in infected liver cells $(L_h^*)$for $\varepsilon = \chi_1 = 0$ with the varying efficacy of pre-erythrocytic vaccine ν.

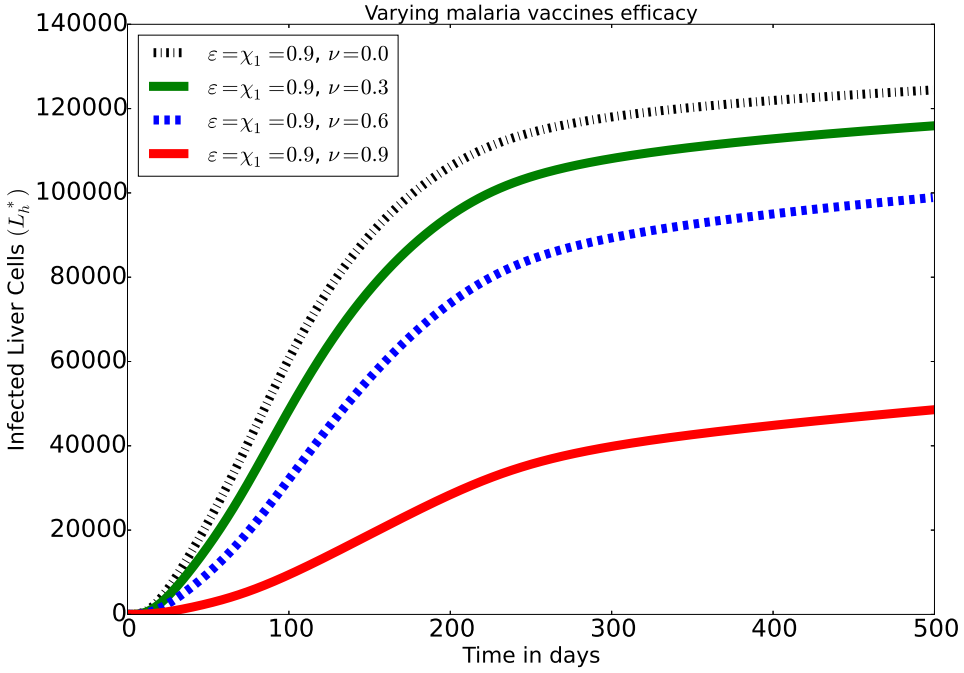

Figure 4.40: The graph showing changes in infected liver cells $(L_h^*)$for $\varepsilon = \chi_1 = 0.9$ with the varying efficacy of pre-erythrocytic vaccine ν.

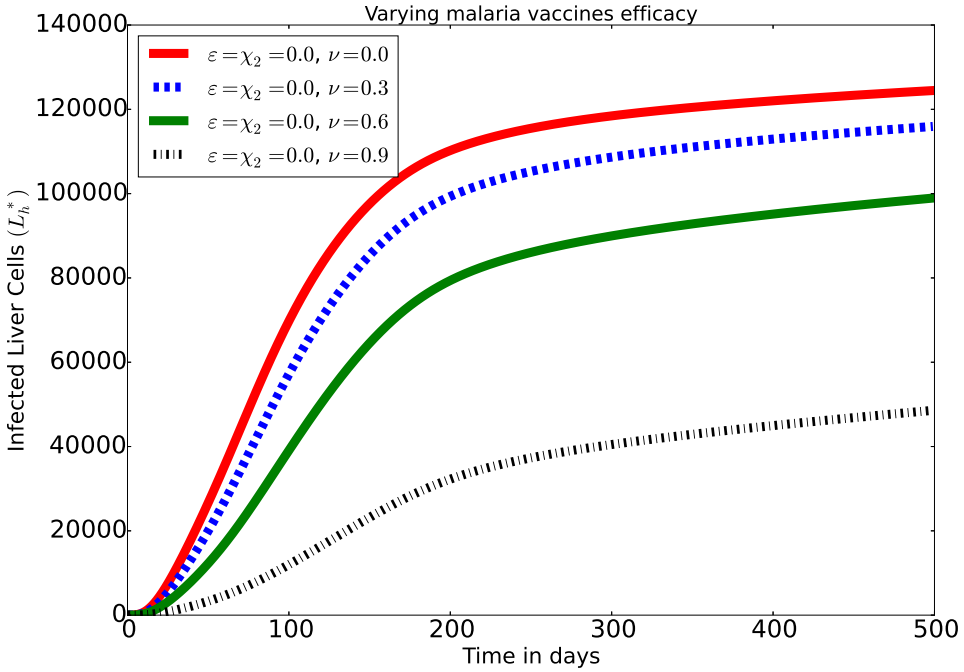

Figure 4.41: The graph showing changes in infected liver cells $(L_h^*)$for $\varepsilon = \chi_2 = 0$ with the varying efficacy of pre-erythrocytic vaccine ν.

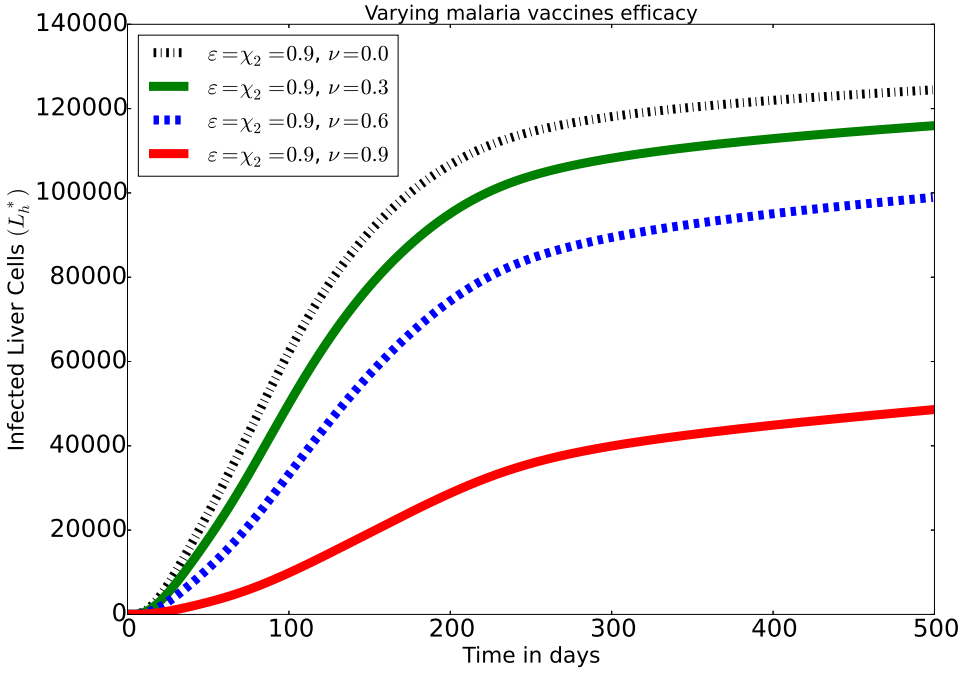

Figure 4.42: The graph showing changes in infected liver cells $(L_h^*)$for $\varepsilon = \chi_2 = 0.9$ with the varying efficacy of pre-erythrocytic vaccine ν.

4.5 Summary

In this chapter, we developed a coupled multiscale model of type II vector-borne disease dynamics which represents transmission in both mosquito and human populations. The objective of this chapter is to investigate the influence of the human liver stage on the multiscale model for the malaria disease system. We also investigate how the super-infection on humans has an influence on the multiscale model of malaria disease dynamics and in which there is a pathogen replication cycle at the microscale. This coupled multiscale model of type II vector-borne disease dynamics has developed on a combination of two multiscale models that integrate the microscale and the macroscale. The results of an embedded multiscale model from numerical simulation demonstrate that the transmission of the malaria disease system at the between-host scale influences the disease dynamics at the within-host scale throughout the infection. Sensitivity analysis of the model parameters was also executed using the reproductive number and the community sporozoites load as the metric for infectiousness and disease transmission. From the simulation, we observe that the activation of malaria vaccines has a considerable effect on reducing the transmission of malaria infectious disease. The extended coupled multiscale model of the malaria disease system results incorporates the vaccination processes at different stages of the pathogen life cycle which are: pre-erythrocytic vaccine (PEV), blood-stage vaccine (BSV), and transmission-blocking stage (TBS). The comparative effectiveness of the combination of malaria vaccines results in major reductions in the transmission of malaria disease, that is, reproductive number and community pathogen loads. The results suggest that the highest percentages of the combination of malaria vaccines have the potential to boost the immune system, which results in the reduction of the population of infected liver cells, the population of infected red blood cells, and merozoites. The presented multiscale model of the malaria disease system provides helpful insight on the need to improve the efficacy of current malaria vaccines in the development and the need to try vaccine combinations in controlling the transmission of malaria infection at the individual level and the population level.

Chapter 5

A Multiscale Model of Malaria Disease Dynamics With Immune Response

5.1 Introduction

This chapter extends our previous work by adding the human immune response to the multiscale models of the malaria disease system discussed in the previous chapter. Malaria is a type II-vector-borne disease that is caused by the Plasmodium parasite transmitted from one person to another by the bite of infected Anopheles mosquito [35]. The Plasmodium parasite needs two hosts to successful complete its life cycle, which is vector-host i.e. female anopheles mosquito and human-host [68]. Malaria in humans develops in two stages, which are: the first stage is the exo-erythrocyte which involves the liver-cells and the second stage is the erythrocyte that involves the red-blood cells. Malaria disease cause significant public health burden in endemic areas [68]. In 2018, an estimated of 405,000 death due to malaria disease infection were recorded worldwide from an estimated of 228 million cases worldwide [69]. When malaria parasites evolve in the host, they can stimulate the activation of the immune cells in the human host which release the immune response to fight against the infection. The immune response can either prevent the re-invasion/replication of merozoites or increase the death rate of infected red blood cells. The immune response is stimulated by plasmodium surface antigens discharged during schizont rupture.

An understudied aspect of infectious disease systems is that their transmission is the result of complex dynamic relationships that occur on different spatial and temporal scales [7]. Therefore, the dynamics of infectious diseases may require an interaction between different temporal and spatial scales related to

the levels of biological organization (i.e. cellular, tissue, organ, organism/host, community and ecosystems) [7]. Recent studies demonstrate that there are 3 types of infectious disease transmission mechanisms which are: (i) directly transmission mechanism, (ii) environmental transmission mechanism and (iii) vector-borne transmission mechanism [11]. This study focus on malaria disease dynamics which is a directly transmitted and vector-borne transmission mechanisms, with the goal to increasing understanding of how the pathogen can be shared between two hosts (human and mosquito) [18]. Malaria disease system is also a directly transmitted and the transmission models are at cellular-level. This study is being developed at the cellular level, therefore the multiscale model developed at the cellular level of an infectious disease system describes the infection of the whole body/organism that uses the cell as the multiscale unit of analysis [3]. At the cellular level, the organization of an infectious disease system provides another pathogenic habitat or environment in which the pathogen can survive, grow, shed/excrete, reproduce and be transmitted on different scales of an infectious disease system [3]. Mathematical models of vector-borne pathogen transmission have been useful in understanding and identifying major epidemiological and immunological features, to assess the transmission intensity and growth of pathogen, and also to guide disease control programs.

Multiscale models of infectious disease system can demonstrates the replication-transmission relativity theory, which illustrates how the disease being transmitted among humans, animals, and vectors and how the pathogen can replicate within the infected host. This helps to identify new approaches to prevention and control that guide in design the public health policy. Multiscale models of infectious disease testing and analysis guide in policy making and improved in scientific understanding. The development in the design of appropriate control measures for the prevalence of malaria disease have led to an interest in understanding the interaction of malaria parasites and the human immune system. A complete multi-scale model of an infectious disease system can be conceptualized as a complex system model that contains many interactive sub-systems that are related to the four main levels of organization of an infectious disease system. These sub-systems are as follows: (a) the host/organism sub-system (human, animal, vector, plant), (b) the pathogen sub-system (viruses, prions, helminths, protozoa, bacteria, fungi), (c) the health interventions sub-system (medical and public health interventions), and (d) the environmental sub-system (inside-host or biological environment and outside-host environment with all its different domains, including physical, geographical, social, economic, etc). Each of these four organizational levels of an infectious disease system can be decomposed into two different scales, which are: the micro-scale and the macro-scale.

A considerable amount of literature has been published to date on mathematical modelling of malaria disease transmission with immune response [45, 59, 70]. These studies has managed to focus on single scale models which is under transmission mechanism theory. However, there has been relatively few mathematical modelling on malaria disease dynamics developed to investigate the dynamics of immune response on two different scales that is within-host scale and between-host scale which are under

replication-transmission relativity theory [34, 35]. These models they did not consider the role played by human-host liver stage on within-host dynamics. The different between our multiscale model and theirs is that, our multiscale model uses pathogen load as a metric for infectiousness and disease transmission potential across two scales, whilst in [34, 35], they apply within-host scale pathogen load as the metric for pathogen transmission whereas between-host scale disease uses infected class as the metrioc for disease transmission. Bridging the gap between two interacting scales (i.e. within-host scale and between-host scale) that is in replication-transmission relativity theory and empirical studies is at the current heart of the rising field of study in linking the within-host scale and between-host scale [34].

In this chapter, we develop a theoretical framework that describes the interaction of human-host immune response system and the malaria parasite at cell-level. The objective of this study is to investigate the impact of immune response on the multiscale model for malaria disease system. Therefore, in this study we develop the coupled multiscale modelling for malaria disease system approaches that are needed to demonstrate how immune responses at individual level/ within-human host scale can influence the population-level/between-host scale dynamics. We extend the previous chapter of coupled multiscale model for malaria disease dynamics which includes the human liver stage and incorporate the human immune response.

5.2 Within-human host model

The development of malaria Plasmodium is a complex system which comprising of multiple phases that can be decompose into sexual (sporogonic) and asexual phases. These phases take place in the Anopheles mosquitoes and in humans respectively. We establish a within-human sub-model of malaria infection to understand the immune system reactions that are stimulated by the malaria parasite and the development of the infection in the host at cell-level and host-level. Plasmodium falcipalum malaria is a main trigger of mortality in the tropics, where the transmission is through the bite of infected mosquito which releases sporozoites into the bloodstream and migrate quickly into the human liver cells. While in the liver stage the sporozoites infect the hepatocytes, reproducing asexually and asymptotically for an estimated period of 6 to 15 days [70]. The infected liver cells differentiate to produce thousands of merozoites which after bursting of their host cells, escapes into blood and infect red-blood cells (RBCs), which is the beginning of erythrocytic stage of the Plasmodium Falcipalum life-cycle. The infected red-blood cells raptures releasing merozoites daughter parasites which will repeat invade fresh erythrocytes to renew the cycle. This repeating cycle maintains the infection and generates symptoms. This cycle repeated many times, and some merozoites immediately generate into sexual form of the parasites called gametocytes, which are the communicable forms of the malaria parasite from a human to a mosquito-vector. The successive erythrocytic cycle will lead to an increase in parasitaemia until the immune response activates.

The within-human host sub-model that include the immune response in malaria disease dynamics is derived from [24, 59] models of erythrocyte cycle, using the systems of differential equations. We develop a within-human host sub-model with immune response that presents the dynamics of sporozoites in the infected liver $P_h(s)$, susceptible uninfected health liver cells $L_h(s)$, infected liver cells $L_h^*(s)$, population of uninfected health red blood cells $B_h(s)$, population of infected red blood cells $B_h^*(s)$, population of free merozoites $M_h(s)$, the population of gametocytes $G_h(s)$, concentration of immune cells $D(s)$ and concentration of antibodies $A(s)$. The assumptions of within-host scale sub-model with immune response are as follows:

(1) The sporozoites are injected into the human body at a one-off time through the bite of an infected mosquito.

(2) Assume that the sporozoites supply rate $\Lambda_h = 0$.

(3) Infected red blood cells die at a constant rate and are also killed by the presence of immune effectors. They produce merozoites by bursting.

(4) The production rate of merozoites is reduced by immune cells. These free pathogens suffer a natural death, are eliminated from circulating by immune cells, and are also reduced through infecting red blood cells.

(5) Immune cells are produced at a constant rate and their production is stimulated by the presence of infected liver cells, infected red blood cells, and merozoites. They are also reduced by natural decay at a constant rate.

(6) Antibodies that inhibit the invasion of red blood cells proliferate in the presence of merozoites. Antibodies decay at a constant rate.

The within-human host model of malaria disease with immune response is given in system of equations (5.2.0.1).

$$
\begin{aligned}
1.\quad \frac{dP_h(s)}{ds} &= -\mu_p P_h(s) - \theta_p D_h(s) P_h(s),\\
2.\quad \frac{dL_h(s)}{ds} &= \Lambda_l - \frac{\beta_l P_h(s) L_h(s)}{1+\alpha_a D_h(s)} - \mu_l L_h(s),\\
3.\quad \frac{dL_h^*(s)}{ds} &= \frac{\beta_l P_h(s) L_h(s)}{1+\alpha_a D_h(s)} - \alpha_l L_h^*(s) - \theta_l D_h(s) L_h^*(s),\\
4.\quad \frac{dB_h(s)}{ds} &= \Lambda_b - \frac{\beta_h M_h(s) B_h(s)}{1+\alpha_0 A_h(s)} - \mu_b B_h(s),\\
5.\quad \frac{dB_h^*(s)}{ds} &= \frac{(1-\pi)\beta_h M_h(s) B_h(s)}{1+\alpha_0 A_h(s)} - \alpha_m B_h^*(s) - \theta_b D_h(s) B_h^*(s),\\
6.\quad \frac{dM_h(s)}{ds} &= \frac{N_l \alpha_l L_h^*(s)}{1+\alpha_2 D_h(s)} + \frac{N_m \alpha_m B_h^*(s)}{1+\alpha_1 D_h(s)} - \mu_m M_h(s) - \theta_m D_h(s) M_h(s) - \frac{\beta_h M_h(s) B_h(s)}{1+\alpha_0 A_h(s)},\\
7.\quad \frac{dG_h(s)}{ds} &= \frac{\pi \beta_h M_h(s) B_h(s)}{1+\alpha_0 A_h(s)} - (\alpha_h + \mu_h) G_h(s) - \theta_g D_h(s) G_h(s),\\
8.\quad \frac{dD_h(s)}{ds} &= \Lambda_d + \left(\frac{\rho_l L_h^*}{f_0 + L_h^*(s)} + \frac{\rho_b B_h^*(s)}{f_1 + B_h^*(s)} + \frac{\rho_m M_h(s)}{f_2 + M_h(s)} \right) D_h(s) - \mu_d D_h(s),\\
9.\quad \frac{dA_h(s)}{ds} &= \frac{\eta M_h(s) D_h(s)}{f_2 + M_h(s)} - \mu_a A_h(s).
\end{aligned}
\tag{5.2.0.1}
$$

The first equation in model (5.2.0.1) is the dynamics of sporozoites parasites $P_h(s)$, demonstrates the injection of sporozoites into the human skin by infected Anopheles mosquito. The sporozoites are reduced by the natural decay at a rate μ_p and also eliminated by immune cells θ_p. The second equation in the model (5.2.0.1) is the dynamics of uninfected liver cells $L_h(s)$. The population of uninfected liver-cells are recruited at a constant rate Λ_l, liver cells become infected by sporozoites at a constant rate β_l and the rate of infection is reduced by $\frac{1}{1+\alpha_a D_h(s)}$, where α_a is the efficiency of immune cells $(D_h(s))$ to inhibit invasion of Hepatocytic liver cells (HLCs) by sporozoites. The uninfected liver-cells are reduced by natural death at a constant rate μ_l. The third equation is the dynamics of infected liver cells $L_h^*(s)$, The infected liver cells increase through the infected of liver cells. The infected liver cells reduced through bursting of infected liver-cells at a constant rate α_m to release the meteorites into the blood stream and by also apoptosis at a constant rate θ_l.

The fourth equation in the sub-model (5.2.0.1) demonstrate the dynamics of uninfected red blood cells $B_h(s)$. The red blood cells are supplied by bone marrow at a constant rate Λ_b. The number of uninfected red are reduced by merozoites at an infection rate β_h and the rate of infection is reduced by $\frac{1}{1+\alpha_0 A_h(s)}$, which represents the role played by antibodies in controlling parasitemia, where α_0 is the efficacy of antibodies in reducing erythrocytic invasion. Uninfected red blood cells also reduced through natural death at a constant rate μ_b. The fifth equation of the sub-model (5.2.0.1), describe the dynamics of merozoites infected erythrocytes or infected red blood cells. The merozoites that infects the red-blood cells has one or two condition (i) it may either become a trophozoite and replicate the cycle in the production of merozoites, or (ii) it may change into a trophozoite and then it goes through gametocytogenesis, which is the

process of gametocytes are formed within-host erythocyte [24]. B_h^* increase through a proportion $(1-\pi)$ of the total population of merozoite infected erythrocytes. The infected red blood cells reduced by immune cells estimated by infection of red blood cells at a constant rate θ_b, and through bursting to produce merozoites at a rate α_m.

The sixth equation in the sub-model (5.2.0.1) models the rate of change of merozoites $M_h(s)$. Merozoites are supplied at an average rate N_l and N_m upon the bursting of infected liver cells α_l and infected red-blood cells α_m, respectively. An average of N_l merozoites are released per bursting each infected liver-cells and an average of N_m merozoites are released per bursting each red blood cells. The production rate of merozoites by infected cells are inhibited by immune cells with a factor $\dfrac{1}{1+\alpha_2 D_h(s)}$ and $\dfrac{1}{1+\alpha_1 D_h(s)}$, where α_2 and α_1 are the efficacy of immune cells inhibiting the production of merozoites. The infected liver-cells rupture and merozoites are released into uninfected red blood cells. Merozoites are reduced through natural decay at a constant rate μ_m and are also eliminated by immune cells at a constant rate θ_m. The seventh equation of sub-model (5.2.0.1) models the rate of change of gametocytes $G_h(s)$. The equation describes the dynamics of remaining proportion, π, of the total population of merozoite infected red-blood cells. The population of gametocytes decrease through which gametocyte within erythrocytes mature and become infectious to mosquitoes at a constant rate α_h, through natural decay at a rate μ_h and also eliminated by immune cells at a rate θ_g.

The eighth equation in sub-model (5.2.0.1) models the rate of change of immune cells $D_h(s)$. The immune cells are supplied at rate Λ_d, which is the combined of immune cells (e.g.macrophages, natural killer-cells, $CD4^+$ T-cells). This stimulation term

$$\left(\frac{\rho_l L_h^*(s)}{f_0+L_h^*(s)}+\frac{\rho_b B_h^*(s)}{f_1+B_h^*(s)}+\frac{\rho_m M_h(s)}{f_2+M_h(s)}\right)D_h(s)$$

for immune cells in the presence of infected liver-cells $L_h^*(s)$, infected red-blood cells $B_h^*(s)$ and merozoites $M_h(s)$, wherebρ_l, ρ_b and ρ_m represents the immunogenecity of infected liver-cells, infected red-blood cells and merozoites respectively. The parameter f_0 is the density of of infected liver-cells at which immune cells grow in the absense of sporozoites, f_1 is the density of infected red blood-cells at which immune cells grow in the absence of merozotes and f_2 is the density of merozoites at which immune cells grow in the absence of red blood-cells. Immune cells reduced through natural death, at a rate μ_d. The last equation in sub-model (5.2.0.1) describes the rate of change of antibodies. The antibodies is stimulated at term $\dfrac{\eta D_h(s) M_h(s)}{f_2+M_h(s)}$, where η is the maximum rate of increase of antibodies. The antibodies are reduced through natural death at a constant rate μ_a.

5.2.1 Positivity of Solutions

The system of equations (5.2.0.1) demonstrates the dynamics of within-human sub-model and the parasite populations and it is essential to show these compartments are positive for all time $s \geq 0$. We have to prove the following theorem.

Theorem 5.1. *The solution of the system of equations (5.2.0.1) satisfy the following initial conditions with strictly positive components i.e. ($P_h > 0$, $L_h > 0$, $L_h^* > 0$, $B_h > 0$, $B_h^* > 0$, $M_h > 0$, $G_h > 0$, $D_h > 0$, $A_h > 0$) for all $s > 0$.*

Proof. We present the following proof. This follow from system of equations in (5.2.0.1) of the solution starts from a strictly positive point, all component positive for $o \leq s \leq s_0$

$$\frac{dP_h(s)}{ds} \geq -(\mu_p + \theta_p D_h(s))P_h(s), \tag{5.2.1.1}$$

The equation (5.2.1.1) can be solve using separable variables as follows

$$\frac{dP_h(s)}{P_h(s)} \geq -(\mu_p + \theta_p D_h(s))ds. \tag{5.2.1.2}$$

By letting

$$\begin{aligned} \hat{s} \quad = \quad & \sup\{s > 0 : P_h > 0, L_h > 0, L_h^* > 0, B_h > 0, B_h^* > 0, M_h > 0, G_h > 0, D_h > 0, \\ & A_h > 0\} \in [0, s], \end{aligned} \tag{5.2.1.3}$$

and integrating equation (5.2.1.2) and we obtain

$$\begin{aligned} \ln(P_h(s)) \quad &\geq \quad -\left(\mu_p s + \theta_p \int_0^s D_h(\hat{s})d\hat{s}\right) + \ln(P_h(0)) \\ P_h(s) \quad &\geq \quad P_h(0)\exp\left\{-\left(\mu_p s + \theta_p \int_0^s D_h(\hat{s})d\hat{s}\right)\right\}. \end{aligned}$$

It implies that

$$\lim_{s\to\infty} \inf(P_h(s)) \geq 0. \tag{5.2.1.4}$$

Using similar method, we obtain

$$\begin{aligned} L_h(s) \quad &\geq \quad L_h(0)\exp\left\{-\left(\int_0^s \frac{\beta_l P_h(\hat{s})}{1 + \alpha_a D_h(\hat{s})} + \mu_l s\right)\right\} \\ \lim_{s\to\infty} \inf(L_h(s)) \quad &\geq \quad 0, \\ L_h^*(s) \quad &\geq \quad L_h^*(0)\exp\left\{-\left(\alpha_l s + \theta_l \int_0^s D_h(\hat{s})d\hat{s}\right)\right\} \\ \lim_{s\to\infty} \inf(L_h^*(s)) \quad &\geq \quad 0. \end{aligned}$$

Using the same principle, it can be shown that

$$\begin{aligned}
B_h(s) &\geq B_h(0)\exp\left\{-\left(\int_0^s \frac{\beta_h M_h(\hat{s})}{1+\alpha_0 A_h(\hat{s})}d\hat{s}+\mu_b s\right)\right\},\\
\lim_{s\to\infty}\inf(B_h(s)) &\geq 0.\\
B_h^*(s) &\geq B_h^*(0)\exp\left\{-\left(\alpha_m s+\theta_b\int_0^s D_h(\hat{s})d\hat{s}\right)\right\},\\
\lim_{s\to\infty}\inf(B_h^*(s)) &\geq 0,\\
M_h(s) &\geq M_h(0)\exp\left\{-\left(\mu_m s+\theta_m\int_0^s D_h(\hat{s})d\hat{s}+\int_0^s \frac{\beta_h B_h(\hat{s})}{1+\alpha_0 A_h(\hat{s})}d\hat{s}\right)\right\},\\
\lim_{s\to\infty}\inf(M_h(s)) &\geq 0.\\
G_h(s) &\geq G_h(0)\exp\left\{-\left((\alpha_h+\mu_h)+\theta_g\int_0^s D_h(\hat{s})d\hat{s}\right)\right\},\\
\lim_{s\to\infty}\inf(G_h(s)) &\geq 0,\\
D_h(s) &\geq D_h(0)\exp\{-\mu_d s\},\\
\lim_{s\to\infty}\inf(D_h(s)) &\geq 0,\\
A_h(s) &\geq A_h(0)\exp\{-\mu_a s\},\\
\lim_{s\to\infty}\inf(A_h(s)) &\geq 0.
\end{aligned}$$

Thus, when starting with non-negative initial value conditions in the model system (5.2.0.1), this indicates that the solution $(P_h(s), L_h(s), L_h^*(s), B_h(s), B_h^*(s), M_h(s), G_h(s), D_h(s), A_h(s))$ is always no-negative for every $s \geq 0$. □

The within-host model (5.2.0.1) has a disease free equilibrium, obtained by setting the right-hand sides of the equations in the model to zero. The equilibrium is given as

$$\begin{aligned}
E_0 &= (P_h^0, L_h^0, L_h^{*0}, B_h^0, B_h^{*0}, M_h^0, G_h^0, D_h^0, A_h^0),\\
&= \left(0, \frac{\Lambda_l}{\mu_l}, 0, \frac{\Lambda_b}{\mu_b}, 0, 0, 0, \frac{\Lambda_d}{\mu_d}, 0\right).
\end{aligned} \tag{5.2.1.5}$$

The linear stability of E_0 can be established utilising the next generation operator approach to calculate the basic reproductive number and we use the [71]'s approach. The model system (5.2.0.1) can be written in the form

$$\begin{aligned}
\frac{dX}{dt} &= f(X,Y,Z),\\
\frac{dY}{dt} &= g(X,Y,Z),\\
\frac{dZ}{dt} &= h(X,Y,Z),
\end{aligned} \tag{5.2.1.6}$$

where

$$\begin{aligned} X &= (L_h, B_h, D_h), \\ Y &= (P_h, L_h^*, B_h^*, G_h, A_h), \\ Z &= (M_h). \end{aligned} \tag{5.2.1.7}$$

We define $\widetilde{g}(X^*, Z)$ by

$$\begin{aligned} g_1(X^*, Z) &= P_h = 0 \\ g_2(X^*, Z) &= L_h^* = \frac{\beta_l L_h P_h}{(1+\alpha_a)(\alpha_l + \theta_l D_h)} = 0, \\ g_3(X^*, Z) &= B_h^* = \frac{(1-\pi)\beta_h B_h \mu_a M_h (f_2 + M_h)}{[f_2\mu_a + (\mu_a + \alpha_0\eta D_h)M_h](\alpha_m + \theta_b D_h)}, \\ g_4(X^*, Z) &= G_h = \frac{\pi\beta_h B_h \mu_a M_h (f_2 + M_h)}{[f_2\mu_a + (\mu_a + \alpha_0\eta D_h)M_h](\mu_h + \alpha_h + \theta_g D_h)}, \\ g_5(X^*, Z) &= A_h = \frac{\eta D_h M_h}{\mu_a}, \end{aligned}$$

By substituting the values of P_h, L_h^*, B_h^*, G_h and A_h and letting $h_1 = \dfrac{dM_h}{dts}$ we obtain

$$\begin{aligned} h_1 = {} & \frac{N_l \alpha_l \beta_l L_h P_h}{(1+\alpha_a D_h)(1+\alpha_2)(\alpha_l + \theta_l D_h)} + \frac{(1-\pi)N_m \alpha_m \beta_h B_h \mu_a}{(1+\alpha_1)(\alpha_m + \theta_b D_h)} \frac{M_h(f_2 + M_h)}{[f_2\mu_a + (\mu_a + \alpha_0\eta D_h)M_h]} \\ & - (\mu_m + \theta_m D + \beta_h B_h)\, M_h, \end{aligned} \tag{5.2.1.8}$$

$$\frac{\partial h_1}{\partial M_h} = \frac{(1-\pi)N_m \alpha_m \beta_h B_h}{(1+\alpha_1 D_h)(\alpha_m + \theta_b D_h)} - (\mu_m + \theta_m D_h + \beta_h B_h).$$

We compute $A = M - D$, where $M > 0$ and $D > 0$, a diagonal matrix.

$$\begin{aligned} A &= \frac{(1-\pi)N_m \alpha_m \beta_h B_h}{(1+\alpha_1 D_h)(\alpha_m + \theta_b D_h)} - (\mu_m + \theta_m D_h + \beta_h B_h), \\ M &= \frac{(1-\pi)N_m \alpha_m \beta_h B_h}{(1+\alpha_1 D_h)(\alpha_m + \theta_b D_h)}, \\ D &= (\mu_m + \theta_m D_h + \beta_h B_h), \\ D^{-1} &= \frac{1}{(\mu_m + \theta_m D_h + \beta_h B_h)}. \\ MD^{-1} &= \frac{(1-\pi)N_m \alpha_m \beta_h B_h}{(1+\alpha_1 D_h)(\alpha_m + \theta_b D_h)(\mu_m + \theta_m D_h + \beta_h B_h)}. \end{aligned} \tag{5.2.1.9}$$

Therefore the reproduction number is given by $\Re_0 = \rho(MD^{-1})$. Therefore

$$\Re_0 = \frac{(1-\pi)N_m \alpha_m \beta_h \frac{\Lambda_b}{\mu_b}}{(1+\alpha_1 \frac{\Lambda_d}{\mu_d})(\alpha_m + \theta_b \frac{\Lambda_d}{\mu_d})(\mu_m + \theta_m \frac{\Lambda_d}{\mu_d} + \beta_h \frac{\Lambda_b}{\mu_b})} \tag{5.2.1.10}$$

The threshold quantity $\Re_0$ (i.e. the basic reproduction number) measures the total number of secondary infected red blood cells (IRBCs) produced by primary IRBC in a host at the beginning of the infection. This local stability result indicates that, if the initial sub-population of the model is within the attraction of E_0, the pathogen can be eliminated from the bloodstream if $\Re_0 < 1$. To ensure that this clearance is independent of the initial concentrations of red blood cells (RBCs), IRBC and merozoites, the global asymptotic stability must be established for the disease free equilibrium E_0.

Lemma 5.2. *The disease free equilibrium E_0 is locally asymptotically stable if $\Re_0 < 1$ and unstable if $\Re_0 > 1$.*

Proof. Now, we consider the local stability analysis of the disease free equilibrium in system of equations (5.2.0.1). We first, linearize the system of equations (5.2.0.1) at infection-free equilibrium point (E_0), we yield the following Jacobian matrix:

$$J(E_0) = \begin{pmatrix} -x_1 & -x_3 & 0 & 0 & 0 & 0 & 0 & k_2 & 0 \\ -x_2 & -x_4 & 0 & 0 & 0 & 0 & 0 & k_20 & \\ x_2 & x_3 & -y_1 & 0 & 0 & 0 & 0 & -\beta_l k_2 & 0 \\ 0 & 0 & 0 & -\mu_b & 0 & -m_1 & 0 & 0 & 0 \\ 0 & 0 & 0 & 0 & -z_2 & (1-\pi)m_1 & 0 & 0 & 0 \\ 0 & 0 & y_2 & 0 & z_3 & -m_2 & 0 & 0 & 0 \\ 0 & 0 & 0 & 0 & 0 & \pi m_1 & -k_1 & 0 & 0 \\ 0 & 0 & y_3 & 0 & z_4 & m_3 & 0 & -\mu_d & 0 \\ 0 & 0 & 0 & 0 & 0 & m_4 & 0 & 0 & -\mu_a \end{pmatrix}, \tag{5.2.1.11}$$

where $x_1 = \dfrac{\beta_l \frac{\Lambda_l}{\mu_l}}{1+\alpha_a \frac{\Lambda_d}{\mu_d}} + \mu_p$, $x_2 = \dfrac{\beta_l \frac{\Lambda_l}{\mu_l}}{1+\alpha_a \frac{\Lambda_d}{\mu_d}}$, $x_3 = \dfrac{\beta_l \frac{\Lambda_h}{\mu_p}}{1+\alpha_a \frac{\Lambda_d}{\mu_d}}$, $x_4 = \dfrac{\beta_l \frac{\Lambda_h}{\mu_p}}{1+\alpha_a \frac{\Lambda_d}{\mu_d}} + \mu_l$, $y_1 = \left(\alpha_l + \theta_l \dfrac{\Lambda_d}{\mu_d}\right)$, $y_2 = \dfrac{N_l \alpha_l}{1+\alpha_2 \frac{\Lambda_d}{\mu_d}}$, $y_3 = \dfrac{\rho_l}{f_0}\dfrac{\Lambda_d}{\mu_d}$, $z_2 = \left(\alpha_m + \theta_b \dfrac{\Lambda_d}{\mu_d}\right)$, $z_3 = \dfrac{N_m \alpha_m}{1+\alpha_1 \frac{\Lambda_d}{\mu_d}}$, $z_4 = \dfrac{\rho_b}{f_1}\dfrac{\Lambda_d}{\mu_d}$, $m_1 = \beta_h \dfrac{\Lambda_b}{\mu_b}$, $m_2 = \left(\mu_m + \theta_m \dfrac{\Lambda_d}{\mu_d} + \beta_h \dfrac{\Lambda_b}{\mu_b}\right)$, $m_3 = \dfrac{\rho_m}{f_2}\dfrac{\Lambda_d}{\mu_d}$, $m_4 = \dfrac{\eta}{f_2}\dfrac{\Lambda_d}{\mu_d}$, $k_1 = \left(\mu_h + \alpha_h + \theta_g \dfrac{\Lambda_d}{\mu_d}\right)$ and $k_2 = \dfrac{\alpha_a \frac{\Lambda_h}{\mu_p}\frac{\Lambda_l}{\mu_l}}{(1+\alpha_a \frac{\Lambda_d}{\mu_d})^2}$.

The characteristic equation is given by $|J(E_0) - \lambda I| = 0$. We observe that the eigenvalues $\lambda_1 = -y_1$, $\lambda_2 = -\mu_b$, $\lambda_3 = -k_1$, $\lambda_4 = -\mu_d$, $\lambda_5 = -\mu_a$ are negative and the other remaining eigenvalues are decided by the following characteristic equation

$$a_4\lambda^4 + a_3\lambda^3 + a_2\lambda^2 + a_1\lambda + a_0 = 0, \tag{5.2.1.12}$$

where

$$\begin{aligned} a_4 &= 1, \\ a_3 &= (x_1 + x_4) + (z_2 + m_2) > 0, \\ a_2 &= [(x_1x_4 - x_2x_3) + (x_1 + x_4)(z_2 + m_2) + (m_2z_2 - (1-\pi)m_1z_3)(x_1x_4 - x_3x_2)], \\ a_1 &= [(x_1x_4 - x_2x_3) + (x_1 + x_4)(m_2z_2 - (1-\pi)m_1z_3)], \\ a_0 &= [(m_2z_2 - (1-\pi)m_1z_3)(x_1x_4 - x_2x_3)]. \end{aligned} \tag{5.2.1.13}$$

Therefore

$$\begin{aligned} x_1x_4 - x_2x_3 &= \frac{\beta_l}{1 + \alpha_a \frac{\Lambda_d}{\mu_d}}(\Lambda_l + \Lambda_h) + \mu_l\mu_p > 0, \\ m_2z_2 - (1-\pi)m_1z_3 &= (\alpha_m + \theta_b\frac{\Lambda_d}{\mu_d})(\mu_m + \theta_m\frac{\Lambda_d}{\mu_d} + \beta_h\frac{\Lambda_b}{\mu_b})(1 - \Re_0). \end{aligned} \tag{5.2.1.14}$$

Clearly, if $\Re_0 < 1$, we have $a_4 > 0$, $a_3 > 0$, $a_2 > 0$, $a_1 > 0$ and $a_0 > 0$. To confirm that all the roots of the systems of equations (5.2.0.1) have negative real parts, we shall use Descartes' Rule of signs change, we observe that on characteristic equation (5.2.1.13) there is no sign changes in the sequence of coefficients and so there is zero real positive roots [72, 73].

$$\begin{aligned} f(\lambda) &= a_4\lambda^4 + a_3\lambda^3 + a_2\lambda^2 + a_1\lambda + a_0 \\ f(-\lambda) &= a_4\lambda^4 - a_3\lambda^3 + a_2\lambda^2 - a_1\lambda + a_0 \end{aligned} \tag{5.2.1.15}$$

When we find $f(\lambda)$ we observe that there is no sign changes and when we find $f(-\lambda)$ we observe that there are four sign changes. Therefore, we have zero positive eigenvalalues and four real negative eigenvalues. Then all the eigenvalues of the Jacobian matrix $J(E_0)$ are negative or have negative real real parts when $\Re_0 < 1$. Which shows that the local stability of E_0 is stable when $\Re_0 < 1$ and unstable when $\Re_0 > 1$. □

The within-human host sub-model is in terms of fast time scale s. We can write the model (5.2.0.1) using the slow time scale t by assuming a relation between the fast and slow time-scales to be of the form $t = \epsilon s$ [14, 24], such that the within-human host sub-model can be written in terms of the slow time-scale as

follows:

$$
\begin{aligned}
1.\quad \epsilon\frac{dP_h(t)}{dt} &= -\mu_p P_h(t) - \theta_p D_h(t) P_h(t),\\
2.\quad \epsilon\frac{dL_h(t)}{dt} &= \Lambda_l - \frac{\beta_l P_h(t) L_h(t)}{1+\alpha_a D_h(t)} - \mu_l L_h(t),\\
3.\quad \epsilon\frac{dL_h^*(t)}{dt} &= \frac{\beta_l P_h(t) L_h(t)}{1+\alpha_a D_h(t)} - \alpha_l L_h^*(t) - \theta_l D_h(t) L_h^*(t),\\
4.\quad \epsilon\frac{dB_h(t)}{dt} &= \Lambda_b - \frac{\beta_h M_h(t) B_h(t)}{1+\alpha_0 A_h(t)} - \mu_b B_h(t),\\
5.\quad \epsilon\frac{dB_h^*(t)}{dt} &= \frac{(1-\pi)\beta_h M_h(t) B_h(t)}{1+\alpha_0 A_h(t)} - \alpha_m B_h^*(t) - \theta_b D_h(t) B_h^*(t),\\
6.\quad \epsilon\frac{dM_h(t)}{dt} &= \frac{N_l \alpha_l L_h^*(t)}{1+\alpha_2 D_h(t)} + \frac{N_m \alpha_m B_h^*(t)}{1+\alpha_1 D_h(t)} - \mu_m M_h(t) - \theta_m D_h(t) M_h(t) - \frac{\beta_h M_h(t) B_h(t)}{1+\alpha_0 A_h(t)},\\
7.\quad \epsilon\frac{dG_h(t)}{dt} &= \frac{\pi\beta_h M_h(t) B_h(t)}{1+\alpha_0 A_h(t)} - (\alpha_h + \mu_h) G_h(t) - \theta_g D_h(t) G_h(t),\\
8.\quad \epsilon\frac{dD_h(t)}{dt} &= \Lambda_d + \left(\frac{\rho_l L_h^*(t)}{f_0 + L_h^*(t)} + \frac{\rho_b B_h^*(t)}{f_1 + B_h^*(t)} + \frac{\rho_m M_h(t)}{f_2 + M_h(t)}\right) D_h(t) - \mu_d D_h(t),\\
9.\quad \epsilon\frac{dA_h(t)}{dt} &= \frac{\eta M_h(t) D_h(t)}{f_2 + M_h(t)} - \mu_a A_h(t),
\end{aligned}
\tag{5.2.1.16}
$$

where ϵ is a small constant number that is $0 < \epsilon << 1$ which highlights the fast time scale of the within-human host sub-model compared to the slow time scale of the between-host transmission sub-model [14, 24]. We obtain the endemic equilibrium of model (5.2.1.16) by setting the right-hand side of the equations to zero and we obtain

$$
E_1 = \left(\widehat{P_h}, \widehat{L_h}, \widehat{L_h^*}, \widehat{B_h}, \widehat{B_h^*}, \widehat{M_h}, \widehat{G_h}, \widehat{G_h}, \widehat{D_h}, \widehat{A_h}\right). \tag{5.2.1.17}
$$

The endemic equilibrium is given by

$$
\begin{aligned}
\widehat{P_h}(t) &= P_h(0)e^{-(\mu_p+\theta_p D_h)t},\\
\widehat{L_h}(t) &= \frac{\Lambda_l}{\mu_l+\frac{\beta_l\widehat{P_h}}{1+\alpha_a\widehat{D_h}}}+\left[L_h(0)-\frac{\Lambda_l}{\mu_l+\frac{\beta_l\widehat{P_h}}{1+\alpha_a\widehat{D_h}}}\right]e^{-(\mu_l+\frac{\beta_l\widehat{P_h}}{1+\alpha_a\widehat{D_h}})t},\\
\widehat{L_h^*}(t) &= \frac{\beta_l\widehat{P_h}\widehat{L_h}}{(\alpha_l+\theta_l\widehat{D_h})(1+\alpha_a\widehat{D_h})}+\left[L_h^*(0)-\frac{\beta_l\widehat{P_h}\widehat{L_h}}{(\alpha_l+\theta_l\widehat{D_h})(1+\alpha_a\widehat{D_h})}\right]e^{-(\alpha_l+\theta_p\widehat{D_h})t},\\
\widehat{B_h}(t) &= \frac{\Lambda_b(1+\alpha_0\widehat{A_h})}{\beta_h\widehat{M_h}+\mu_p(1+\alpha_0\widehat{A_h})}+\left[B_h(0)-\frac{\Lambda_b(1+\alpha_0\widehat{A_h})}{\beta_h\widehat{M_h}+\mu_p(1+\alpha_0\widehat{A_h})}\right]e^{-(\frac{\beta_h\widehat{M_h}+\mu_b(1+\alpha_0\widehat{A_h})}{1+\alpha_0\widehat{A_h}})t},\\
\widehat{B_h^*}(t) &= \frac{(1-\pi)\beta_h\widehat{M_h}\widehat{B_h}}{(1-\alpha_0\widehat{A_h})(\alpha_m+\theta_b\widehat{D_h})}+\left[\widehat{B_h^*}(0)-\frac{(1-\pi)\beta_h\widehat{M_h}\widehat{B_h}}{(1-\alpha_0\widehat{A_h})(\alpha_m+\theta_b\widehat{D_h})}\right]e^{-(\alpha_m+\theta_b\widehat{D_h})t}\\
\widehat{M_h}(t) &= \frac{\frac{N_l\alpha_l\widehat{L_h^*}}{1+\alpha_2\widehat{D_h}}+\frac{N_m\alpha_m\widehat{B_h^*}}{1+\alpha_1\widehat{D_h}}}{\mu_m+\theta_m\widehat{D_h}+\frac{\beta_h\widehat{B_h}}{1+\alpha_0\widehat{A_h}}}+\left[\widehat{M_h}(0)-\frac{\frac{N_l\alpha_l\widehat{L_h^*}}{1+\alpha_2\widehat{D_h}}+\frac{N_m\alpha_m\widehat{B_h^*}}{1+\alpha_1\widehat{D_h}}}{\mu_m+\theta_m\widehat{D_h}+\frac{\beta_h\widehat{B_h}}{1+\alpha_0\widehat{A_h}}}\right]e^{-(\mu_h+\theta_m\widehat{D_h}+\frac{\beta_h\widehat{B_h}}{1+\alpha_0\widehat{A_h}})t},\\
\widehat{G_h}(t) &= \frac{\pi\beta_h\widehat{M_h}\widehat{B_h}}{(1+\alpha_0\widehat{A_h})(\alpha_h+\mu_h+\theta_g)}+\left[G_h(0)-\frac{\pi\beta_h\widehat{M_h}\widehat{B_h}}{(1+\alpha_0\widehat{A_h})(\alpha_h+\mu_h+\theta_g)}\right]e^{-(\alpha_h+\mu_h+\theta_g\widehat{D_h})t}\\
\widehat{D_h}(t) &= \frac{\Lambda_d}{\mu_d-\left(\frac{\rho_l\widehat{L_h^*}}{df_0+\widehat{L_h^*}}+\frac{\rho_b\widehat{B_h^*}}{f_1+\widehat{B_h^*}}+\frac{\rho_m\widehat{M_h}}{f_2+\widehat{M_h}}\right)}+[D_h(0)-\\
&\quad\left.\frac{\Lambda_d}{\mu_d-\left(\frac{\rho_l\widehat{L_h^*}}{df_0+\widehat{L_h^*}}+\frac{\rho_b\widehat{B_h^*}}{f_1+\widehat{B_h^*}}+\frac{\rho_m\widehat{M_h}}{f_2+\widehat{M_h}}\right)}\right]e^{-\left(\mu_d-\left(\frac{\rho_l\widehat{L_h^*}}{df_0+\widehat{L_h^*}}+\frac{\rho_b\widehat{B_h^*}}{f_1+\widehat{B_h^*}}+\frac{\rho_m\widehat{M_h}}{f_2+\widehat{M_h}}\right)\right)t},\\
\widehat{A_h}(t) &= \frac{\eta\widehat{M_h}\widehat{D_h}}{\mu_a(f_2+\widehat{M_h})}+\left[A_h(0)-\frac{\eta\widehat{M_h}\widehat{D_h}}{\mu_a(f_2+\widehat{M_h})}\right]e^{-\mu_a t}.
\end{aligned}
\tag{5.2.1.18}
$$

When $t=0$ we obtain $\widehat{P_h}=P_h(0)$, $\widehat{L_h}=L_h(0)$, $\widehat{L_h^*}=L_h^*(0)$, $\widehat{B_h}=B_h(0)$, $\widehat{B_h^*}=B_h^*(0)$, $\widehat{M_h}=M_h(0)$, $\widehat{G_h}=G_h(0)$, $\widehat{D_h}=D_h(0)$ and $\widehat{A_h}=A_h(0)$.

From the first equation of the system of equations (5.2.1.18), it implies that when s get larger, $P_h(s)$converges to zero. That is

$$P_h(s)\to 0 \textbf{ as } s\to\infty.$$

As $t \to \infty$, eventually, endemic equilibrium converges to the following::

$$\begin{aligned}
\widehat{P_h}(t) &\to 0, \\
\widehat{L_h}(t) &\to \frac{\Lambda_l}{\mu_l + \frac{\beta_l \widehat{P_h}}{1+\alpha_a \widehat{D_h}}}, \\
\widehat{L_h^*}(t) &\to \frac{\beta_l \widehat{P_h} \widehat{L_h}}{(\alpha_l + \theta_l \widehat{D_h})(1+\alpha_a \widehat{D_h})}, \\
\widehat{B_h}(t) &\to \frac{\Lambda_b (1+\alpha_0 \widehat{A_h})}{\beta_h \widehat{M_h} + \mu_p (1+\alpha_0 \widehat{A_h})}, \\
\widehat{B_h^*}(t) &\to \frac{(1-\pi)\beta_h \widehat{M_h} \widehat{B_h}}{(1-\alpha_0 \widehat{A_h})(\alpha_m + \theta_b \widehat{D_h})}, \\
\widehat{M_h}(t) &\to \frac{\frac{N_l \alpha_l \widehat{L_h^*}}{1+\alpha_2 \widehat{D_h}} + \frac{N_m \alpha_m \widehat{B_h^*}}{1+\alpha_1 \widehat{D_h}}}{\mu_m + \theta_m \widehat{D_h} + \frac{\beta_h \widehat{B_h}}{1+\alpha_0 \widehat{A_h}}}, \\
\widehat{G_h}(t) &\to \frac{\pi \beta_h \widehat{M_h} \widehat{B_h}}{(1+\alpha_0 \widehat{A_h})(\alpha_h + \mu_h + \theta_g)}, \\
\widehat{D_h}(t) &\to \frac{\Lambda_d}{\mu_d - \left(\frac{\rho_l \widehat{L_h^*}}{df_0 + \widehat{L_h^*}} + \frac{\rho_b \widehat{B_h^*}}{f_1 + \widehat{B_h^*}} + \frac{\rho_m \widehat{M_h}}{f_2 + \widehat{M_h}} \right)}, \\
\widehat{A_h}(t) &\to \frac{\eta \widehat{M_h} \widehat{D_h}}{\mu_a (f_2 + \widehat{M_h})}.
\end{aligned} \tag{5.2.1.19}$$

There is a weakness in this model. It is difficult to solve the endemic equilibrium point to an explicit solution with only parameters.

5.3 Within-mosquito host model

We adapt the within-mosquito malaria model in chapter 3. Mosquitoes are the main host for malaria parasites, where the sexual phase of the parasite's life cycle occurs in a process called morphologically different phases of life, called sporogony. This leads to the development of parasitic infections called sporozoites. The within-mosquito malaria parasite dynamics is modelled by the following time evolution of five different parasite stages in the infected mosquito which are the population of gametocyte infected erythrocytes, $G_v(s)$, the population of gametes, $G_m(s)$, the population of zygotes, $Z_v(s)$, the population of oocysts, $O_v(s)$, and the population of sporozoites, $P_v(s)$. We use the same assumptions in [24]'s work. In the within-mosquito sub-model, we assume that there is no immune response. The within-mosquito

malaria parasite dynamics is given by the system of equations in (5.3.0.1).

$$\begin{aligned}
1. \quad \frac{dG_v(s)}{ds} &= \Lambda_v - (\alpha_g + \mu_g)G_v(s), \\
2. \quad \frac{dG_{m(s)}}{ds} &= N_g\alpha_g G_v(s) - (\alpha_s + \mu_s)G_m(s), \\
3. \quad \frac{dZ_v(s)}{ds} &= \frac{1}{2}\alpha_s G_m(s) - (\alpha_z + \mu_z)Z_v(s), \\
4. \quad \frac{dO_v(s)}{ds} &= \alpha_z Z_v(s) - (\alpha_k + \mu_k)O_v(s), \\
5. \quad \frac{dP_v(s)}{ds} &= N_k\alpha_k O_v(s) - (\alpha_v + \mu_v)P_v(s),
\end{aligned} \tag{5.3.0.1}$$

The first equation in system of equations (5.3.0.1) demonstrates the population of gametocytes $G_v(s)$ within an infected mosquito after a mosquito suck blood from an infected human host. The first term, Λ_v models the super-infection of infected mosquitoes. The population of gametocytes infected erythrocytes is reduced either by the bursting of gametocytes infected erythrocytes releasing sex cells called gametes at a constant rate α_g, or through natural decay at rate μ_g. The second equation of model system (5.3.0.1) demonstrates the dynamics of the population of gametes $G_m(s)$. The first term of the population of gametes models the rate of increase of gametes within an infected mosquito, which is given by $N_g\alpha_g G_v(s)$, where N_g is the number of gametes released per each bursting gametocyte infected erythrocyte within an infected mosquito. The population of gametes also get depleted through combination of male and female gametes to form zygotes at a constant rate α_s.

The third equation in system of equations (5.3.0.1) demonstrates the dynamics of zygotes $Z_v(s)$. The population of zygotes within an infected mosquito increase at rate $\frac{\alpha_s G_m(s)}{2}$, which models the grouping of male and female gametes and combining them to form zygotes. We assume that the population of zygotes are reduced either through natural decay at rate μ_z , or through developmental changes into oocysts at constant rate α_z. The fourth equation of system of equations (5.3.0.1) describes the dynamics of oocysts $O_v(s)$. The first term of $O_v(s)$ demonstrates the rate of increase of oocysts within an infected mosquito, which is given by $\alpha_z Z_v(s)$.The population of oocysts is reduced either through natural decay at constant rate μ_k or through the bursting of oocysts to release sporozoites at rate α_k. The last equation of system (5.3.0.1) describe the dynamics of population sporozoites, $P_v(s)$. The rate of increase of sporozoites within infected mosquito is given by $N_k\alpha_k O_v(s)$, where N_k is the number of sporozoites per each bursting oocyst. The population of sporozoites reduced either through natural decay at constant rate μ_v or through the excretion/shedding of mature sporozoites into salivary glands of an infected mosquito at constant rate α_v.

The within-mosquito malaria transmission sub-model is in terms of fast time-scale s, while the between-host malaria transmission sub-model are in terms of a slow scale t. We simplify the model by writing the systems of equations (5.3.0.1) using the slow time scale t by assuming a relation between the fast and

slow time-scales to be of the form $t = \epsilon s$, such that we can write the within-mosquito malaria transmission sub-model in slow time-scale as follows:

$$\begin{aligned}
1. \quad \epsilon\frac{dG_v(t)}{dt} &= \Lambda_v - (\alpha_g + \mu_g)G_v(t), \\
2. \quad \epsilon\frac{dG_{m(t)}}{dt} &= N_g\alpha_g G_v(t) - (\alpha_s + \mu_s)G_m(t), \\
3. \quad \epsilon\frac{dZ_v(t)}{dt} &= \frac{1}{2}\alpha_s G_m(t) - (\alpha_z + \mu_z)Z_v(t), \\
4. \quad \epsilon\frac{dO_v(t)}{dt} &= \alpha_z Z_v(t) - (\alpha_k + \mu_k)O_v(t), \\
5. \quad \epsilon\frac{dP_v(t)}{dt} &= N_k\alpha_k O_v(t) - (\alpha_v + \mu_v)P_v(t),
\end{aligned} \tag{5.3.0.2}$$

The ϵ is a small constant term, that is $0 < \epsilon << 1$, highlighting the fast time-scale of the within-mosquito sub-model of relationship with the time -scale of between-host malaria transmission sub-model.

The endemic equilibrium of within-mosquito host model is given by

$$\begin{aligned}
\widetilde{G_v} &= \frac{\Lambda_v}{\alpha_g + \mu_g} + \left[G_v(0) - \frac{\Lambda_v}{\alpha_g + \mu_g}\right] e^{-(\alpha_g + \mu_g)t}, \\
\widetilde{G_m} &= \frac{N_g\alpha_g}{\alpha_s + \mu_s}\widetilde{G_v} + \left[G_m(0) - \frac{N_g\alpha_g}{\alpha_s + \mu_s}\widetilde{G_v}\right] e^{-(\alpha_s + \mu_s)t} \\
\widetilde{Z_v} &= \frac{1}{2}\frac{\alpha_s}{\alpha_z + \mu_z}\widetilde{G_m} + \left[Z_v(0) - \frac{1}{2}\frac{\alpha_s}{\alpha_z + \mu_z}\widetilde{G_m}\right] e^{-(\alpha_z + \mu_z)t}, \\
\widetilde{O_v} &= \frac{\alpha_z}{\alpha_k + \mu_k}\widetilde{Z_v} + \left[O_v(0) - \frac{\alpha_z}{\alpha_k + \mu_k}\widetilde{Z_v}\right] e^{-(\alpha_k + \mu_k)t}, \\
\widetilde{P_v} &= \frac{N_k\alpha_k}{\alpha_v + \mu_v}\widetilde{O_v} + \left[P_v(0) - \frac{N_k\alpha_k}{\alpha_v + \mu_v}\widetilde{O_v}\right] e^{-(\alpha_v + \mu_v)t}.
\end{aligned} \tag{5.3.0.3}$$

When $t = 0$, we obtain

$$\begin{aligned}
\widetilde{G_v} &= G_v(0), \\
\widetilde{G_m} &= G_m(0), \\
\widetilde{Z_v} &= Z_v(0), \\
\widetilde{O_v} &= O_v(0), \\
\widetilde{P_v} &= P_v(0).
\end{aligned} \tag{5.3.0.4}$$

When $t \to \infty$, the endemic equilibrium state converges, which is given by

$$\begin{aligned}
\widetilde{G_v} &\to \frac{\Lambda_v}{\alpha_g+\mu_g}, \\
\widetilde{G_m} &\to \frac{N_g\alpha_g}{\alpha_g+\mu_g}\frac{\Lambda_v}{\alpha_s+\mu_s}, \\
\widetilde{Z_v} &\to \frac{1}{2}\frac{N_g\alpha_g}{\alpha_g+\mu_g}\frac{\alpha_s}{\alpha_s+\mu_s}\frac{\Lambda_v}{\alpha_z+\mu_z}, \\
\widetilde{O_v} &\to \frac{1}{2}\frac{N_g\alpha_g}{\alpha_g+\mu_g}\frac{\alpha_s}{\alpha_s+\mu_s}\frac{\alpha_z}{\alpha_z+\mu_z}\frac{\Lambda_v}{\alpha_k+\mu_k}, \\
\widetilde{P_v} &\to \frac{1}{2}\frac{N_g\alpha_g}{\alpha_g+\mu_g}\frac{\alpha_s}{\alpha_s+\mu_s}\frac{\alpha_z}{\alpha_z+\mu_z}\frac{N_k\alpha_k}{\alpha_k+\mu_k}\frac{\Lambda_v}{\alpha_v+\mu_v}.
\end{aligned} \tag{5.3.0.5}$$

5.4 Coupled Multiscale model

The between-hosts (human and mosquitoes) describe the transmission and spread of malaria dynamics at population level. We use susceptible-infected-susceptible (SIS) model on between-human host sub-model. This sub-model is formulated based on two dynamical population, which are susceptible humans (S_H) and infected humans infected human populations I_H. We assume that the infected human classes are associated to the within-human host dynamics of particular individual. The total human population is given by $N_H(t)$ at time t, and now $N_H(t) = S_H(t) + I_H(t)$. We adapt the assumptions of this sub-model from [24] which are as follows:

i. The infected human population can recover naturally from malaria infection or through immune response.

ii. The transmission to human parameter $\widehat{\beta_V}$ is the function of the number of infected mosquito population that is $\widehat{\beta_V} = \widehat{\beta_V}(I_V)$.

iii. The between-human host dynamics are assumed to occur at slow time scale t as compared to within-host (human and mosquito) sub-models for malaria disease dynamics, that is $S_H = S_H(t)$ and $I_H = I_H(t)$.

The assumptions above direct us to the following sub-model of between-human host of malaria disease system.

$$\begin{aligned}
\frac{dS_H(t)}{dt} &= \Lambda_H - \widehat{\beta_V}(I_V)S_H(t) - \mu_H S_H(t) + \hat{\widehat{\gamma_H}} I_H(t), \\
\frac{dI_H(t)}{dt} &= \widehat{\beta_V}(I_V)S_H(t) - (\mu_H + \widehat{\delta_H} + \widehat{\gamma_H})I_H(t).
\end{aligned} \tag{5.4.0.1}$$

The first equation of sub-model (5.4.0.1) models the dynamics of susceptible human population. We assume the population of susceptible humans increase either through recruitment at a constant rate Λ_H that is through birth or through recovery of human infected population at a constant rate $\widehat{\gamma_H}$. The population

reduced either through the malaria infection of susceptible humans at a variable $\widehat{\beta_V}(I_V)$ or through natural death at a constant rate μ_H. The second equation of sub-model (5.4.0.1) models the dynamics of malaria infected human population. This population increases through malaria infection of susceptible humans and decreases through natural death at a constant rate μ_H, through disease induced death at rate $\widehat{\delta_H}$ and recovery of infected population at rate $\widehat{\gamma_H}$.

In a similar way, $N_V(t)$ denotes the total mosquito population size at time t. We use susceptible-infected (SI) model for between-mosquito host sub-model, since the mosquitoes do not recover from their infection. The population of mosquitoes is divided into susceptible mosquitoes (S_V) and malaria infected mosquitoes (I_V). Now $N_V(t) = S_V(t) + I_V(t)$. For between-mosquito host sub-model, we adapt the assumptions in [24], which are given as following:

i. Infected mosquitoes do not recover naturally from their malaria infection.

ii. The malaria transmission parameter $\widehat{\beta_H}$ is the function of the number of malaria infected humans, which is given by $\widehat{\beta_H} = \widehat{\beta_H}(I_H)$.

iii. The dynamics of between-mosquito host sub-model is assumed to occur at slow time scale t, when we compare with the within-host (human and mosquito) sub-models variables of malaria disease dynamics, which is given by $S_V = S_V(t)$ and $I_V(t)$.

From the assumption, the between-mosquito host sub-model is given by:

$$\begin{aligned} \frac{dS_V(t)}{dt} &= \Lambda_V - \widehat{\beta_H}(I_H)S_V(t) - \mu_V S_V(t), \\ \frac{dI_V(t)}{dt} &= \widehat{\beta_H}(I_H)S_V(t) - (\mu_V + \widehat{\delta_V})I_V(t). \end{aligned} \tag{5.4.0.2}$$

The first equation of sub-model (5.4.0.2) models the dynamics of population of susceptible mosquitoes. The susceptible mosquitoes increase through the supply rate Λ_V that is through birth. This population decreases either through natural decay at a constant rate μ_V or through malaria infection by humans at rate $\widehat{\beta_H}(I_H)$. The second equation of system (5.4.0.2) models the dynamics of population of infected mosquitoes. The population of infected mosquitoes increases though the infection of susceptible mosquitoes and decrease either through natural death at a constant rate μ_V or through malaria infection induced death at a constant rate $\widehat{\delta_V}$.

We integrate the following four sub-models (5.2.1.16), (5.3.0.2), (5.4.0.1) and (5.4.0.2) into a single coupled multiscale model. We adapt the method used in [14, 24] to integrate all the four sub-models. Now we have to illustrate how to couple the sub-models into a single multiscale model. These sub-model involves the coupling of between-host (human and mosquito) scale to within- host (human and mosquito) scale through the process of super-infection or infection. The within-host sub-models and between-host sub-models are linked through the nested multiscale model, where within-host scale influence between-host

scale through pathogen shedding/excretion whilst between-host scale influences within-host scale sub-model through initial infection. Whereas human and mosquitoes are linked through sharing of pathogen.

We understand that, G_h, M_h and P_v integrates the within-host scale to between-host scale which illustrates the pathogen shedding/excretion. The between-host scale parameters $\widehat{\beta_H}(I_H)$, $\widehat{\beta_V}(I_V)$, $\widehat{\delta_H}$, $\widehat{\delta_V}$ and $\widehat{\gamma_H}$ are functions of within-host scale. Considering the ecosystems concepts, We integrate the disease induced death rate to malaria parasite/ immune cells dynamics in the infected human host. $\widehat{\delta_H} = \widehat{\delta_H}(M_h(t), D(t))$, where $M_h(t)$ is the malaria merozoites and $D(t)$ is the density of immune cells within symptomatically infected humans. The recovery rate can be written as $\widehat{\gamma_H} = \widehat{\gamma_H}(M_h, D(t))$, which integrate the dynamics of infected-host by immune-cells, Using similar way, the infection induced death of mosquito is given by $\widehat{\delta_V} = \widehat{\delta_V}(P_v(t))$, where P_v is the population of sporozites within an infected mosquitoes.

We consider that the transmission of parasite in the vector-host to vertebrate host malaria transmission dynamics is described by $\widehat{\beta_V}$, which is a function of product of infected vector host (I_V) and the population of sporozoites (P_v), which is given by $\widehat{\beta_V} = \widehat{\beta_V}\,(P_v(s)I_V(t))$. Therefore, $P_v(s)I_V(t)$ to be the variable at between-host scale which is denoted by $P_V(t)$, that is $P_V(t) = P_v(s)I_V(t)$, which is the products of the average number of sporozoites within an infected mosquito and the number of infected mosquitoes. $P_V(t)$ is the total infectious reservoir of mosquitoes in the community which we refer to the community sporozoites load. This gives $\widehat{\beta_V} = \widehat{\beta_V}(P_V(t))$. The force of infection can be given by

$$\beta_V \lambda_V(P_V(t)) = \widehat{\beta_V}(P_V(t)) = \frac{\beta_V P_V(t)}{P_0 + P_V(t)},$$

where β_V is the contact rate to a community with population $P_V(t)$, of sporozoites per unit time, which can be considered as the measure of vertebrate-host biting rate. P_0 which is the community sporozoites load that yields 50% chance of getting human host get infected with malaria disease system after a successful bite by a mosquito in a certain community.

The rate at which sporozoites becomes infectious to human within an infected mosquitoes α_v, integrates the within-mosquito scale to between-host scale. The population of sporozoites $P_v(s)$ and the shedding/excretion rate of sporozoites within an infected mosquito α_v in the community sporozoites load link the within-mosquito scale variable and parameter to the between-human host scale in a uni-directional way. The community sporozoites load is modelled by

$$\frac{dP_V(t)}{dt} = P_v(s)\alpha_v I_V(t) - \alpha_V P_V(t). \tag{5.4.0.3}$$

The equation (5.4.0.3) demonstrate the dynamics of the community sporozoites load. The first term to

$P_V(t)$ describes the total number of sporozoites load contributed by all infected individuals from within-mosquito processes to the community sporozoites load pool, where $N_h = \widetilde{P_v}(s)$ is defined as the measure of total volume of sporozoites produced within an infected mosquito throughout the entire period of mosquito infectiousness and α_v is the proportion of individual mosquitoes who are infected. α_V is the rate of degradation of the community sporozoites load.

Similarly, we also consider the transmission of parasite in the vertebrate-host to vector-host malaria transmission dynamics is described by $\widehat{\beta_H}$, which is the function of product of infected human host (I_H) and the population of gametocytes (G_h), which is given by $\widehat{\beta_H} = \widehat{\beta_H}(G_h(s)I_H(t))$. This product $G_h(s)I_H(t)$ is a variable at between- host scale which is denoted by $G_H(t)$, therefore $G_H(t) = G_h(s)I_H(t)$, which is the product of the average number of gametocytes within an infected humans and the average of infected humans. Where $G_H(t)$ is the community gametocytes load that is responsible for transmission of pathogen at between-host scale from community of infectious reservoir of humans to mosquitoes. Therefore $\widehat{\beta_H} = \widehat{\beta_H}(G_H(t))$. The force of infection can be given by

$$\beta_H \lambda_H(G_H(t)) = \widehat{\beta_H}(G_H(t)) = \frac{\beta_H G_H}{G_0 + G_H(t)},$$

where β_H is the contact rate to the community with population $G_H(t)$ and G_0 is half saturation constant associated with infection of mosquitoes.

α_h is the rate at which the gametocytes population become infectious to mosquitoes which are shed/excreted into specific anatomical compartments of an infected human host [18].The population of gametocytes $G_h(s)$ and the shedding/excretion rate of gametocytes within an infected human α_h in the community gametocytes load link the within-human host scale variable and parameter to the between-mosquitoes scale in a unidirectional way. The community gametocytes load is given by

$$\frac{dG_H(t)}{dt} = G_h(s)\alpha_h I_H(t) - \alpha_H G_H(t). \tag{5.4.0.4}$$

The community gametocytes load is increased through shedding/ excreting the gametocytes at a rate $G_h(s)\alpha_h$ into specific anatomical compartment of human host. $\frac{1}{\alpha_H}$ is the average time to eliminate the total community gametocyte load.

The coupled multiscale model of malaria disease system can be reduced to

$$
\begin{aligned}
1.\quad \frac{dS_V(t)}{dt} &= \Lambda_V - \widehat{\beta_H}(G_H(t))S_V(t) - \mu_V S_V(t),\\
2.\quad \frac{dI_V(t)}{dt} &= \widehat{\beta_H}(G_H(t))S_V(t) - \left[\mu_V + \widehat{\delta_V}(P_v(s))\right] I_V(t),\\
3.\quad \frac{dP_V(t)}{dt} &= P_v(s)\alpha_v I_V(t) - \alpha_V P_V(t).\\
4.\quad \frac{dS_H(t)}{dt} &= \Lambda_H - \widehat{\beta_V}(P_V(t))S_H(t) - \mu_H S_H(t) + \widehat{\gamma_H}(M_h(s), D(s))I_H(t),\\
5.\quad \frac{dI_H(t)}{dt} &= \widehat{\beta_V}(P_V(t))S_H(t) - \left[\mu_H + \widehat{\gamma_H}(M_h(s), D(s)) + \widehat{\delta_H}(M_h(s), D(s))\right] I_H(t),\\
6.\quad \frac{dG_H(t)}{dt} &= G_h(s)\alpha_h I_H(t) - \alpha_H G_H(t),
\end{aligned}
\tag{5.4.0.5}
$$

We let

$$
\begin{aligned}
\gamma_H &= \widehat{\gamma_H}(M_h(s), D(s)) \text{ a constant parameter},\\
\delta_H &= \widehat{\delta_H}(M_h(s), D(s)) \text{ a constant parameter},\\
\delta_V &= \widehat{\delta_V}(P_v(s)) \text{ a constant parameter},\\
N_v &= \widetilde{P_v},\\
N_h &= \widehat{G_h},\\
\frac{\beta_H G_H(t)}{G_0 + G_H(t)} &= \widehat{\beta_H}(G_H(t)),\\
\frac{\beta_V P_V(t)}{P_0 + P_V(t)} &= \widehat{\beta_V}(P_V(t)),
\end{aligned}
\tag{5.4.0.6}
$$

the full multiscale model of malaria disease dynamics is simplified in dimension

$$
\begin{aligned}
1.\quad \frac{dS_V(t)}{dt} &= \Lambda_V - \frac{\beta_H G_H(t)}{G_0 + G_H(t)} S_V(t) - \mu_V S_V(t),\\
2.\quad \frac{dI_V(t)}{dt} &= \frac{\beta_H G_H(t)}{G_0 + G_H(t)} S_V(t) - [\mu_V + \delta_V] I_V(t),\\
3.\quad \frac{dP_V(t)}{dt} &= N_v \alpha_v I_V(t) - \alpha_V P_V(t).\\
4.\quad \frac{dS_H(t)}{dt} &= \Lambda_H - \frac{\beta_V P_V(t)}{P_0 + P_V(t)} S_H(t) - \mu_H S_H(t) + \gamma_H I_H(t),\\
5.\quad \frac{dI_H(t)}{dt} &= \frac{\beta_V P_V(t)}{P_0 + P_V(t)} S_H(t) - [\mu_H + \gamma_H + \delta_H] I_H(t),\\
6.\quad \frac{dG_H(t)}{dt} &= N_h \alpha_h I_H(t) - \alpha_H G_H(t),
\end{aligned}
\tag{5.4.0.7}
$$

5.4.1 Disease-free equilibrium states

The disease free equilibrium points of multiscale model (5.4.0.7 is given by

$$E^{00} = (S_V^{00}, I_V^{00}, P_V^{00}, S_H^{00}, I_H^{00}, G_H^{00}) = \left(\frac{\Lambda_V}{\mu_V}, 0, 0, \frac{\Lambda_H}{\mu_H}, 0, 0\right). \tag{5.4.1.1}$$

5.4.2 Reproductive Number

Using the next generation operator approach to calculate the basic reproductive number and we use the [71]'s approach. The model system (5.4.0.5) can be written in the form

$$\begin{aligned} \frac{dX}{dt} &= f(X, Y, Z), \\ \frac{dY}{dt} &= g(X, Y, Z), \\ \frac{dZ}{dt} &= h(X, Y, Z), \end{aligned} \tag{5.4.2.1}$$

where

$$\begin{aligned} X &= (S_V, S_H), \\ Y &= (I_V, I_H), \\ Z &= (P_V, G_H). \end{aligned} \tag{5.4.2.2}$$

We define $\widetilde{g}(X^*, Z)$ by

$$\begin{aligned} g_1(X^*, Z) &= I_V = \frac{\beta_H S_V G_H}{(\mu_V + \delta_V)(G_0 + G_H)}, \\ g_2(X^*, Z) &= I_H = \frac{\beta_V S_H P_V}{(\mu_H + \gamma_H + \delta_H)(P_0 + P_V)}. \end{aligned} \tag{5.4.2.3}$$

By substituting the value of I_V and I_H and letting $h_1 = \frac{dP_V}{dt}$, $h_2 = \frac{dG_H}{dt}$ we obtain

$$\begin{aligned} h_1 &= \frac{1}{2}\frac{N_v \alpha_v \beta_H S_V G_H}{(\mu_V + \delta_V)(G_0 + G_H)} - \alpha_V P_V, , \\ h_2 &= \frac{N_h \alpha_h \beta_V S_H P_V}{(\mu_H + \gamma_H + \delta_H)(P_0 + P_V)} - \mu_H G_H, , \end{aligned} \tag{5.4.2.4}$$

We compute $A = M - D$, where $M > 0$ and $D > 0$, a diagonal matrix.

$$A = \begin{pmatrix} \frac{\partial h_1}{\partial P_V} & \frac{\partial h_1}{\partial G_H} \\ \frac{\partial h_2}{\partial P_V} & \frac{\partial h_2}{\partial G_H} \end{pmatrix}, \tag{5.4.2.5}$$

therefore $A =$

$$\begin{pmatrix} -\alpha_V & \frac{N_v\alpha_v\beta_H\Lambda_V}{\mu_V G_0(\mu_V+\delta_V)} \\ \frac{N_h\alpha_h\beta_V\Lambda_V}{\mu_H P_0(\mu_H+\gamma_H+\delta_H)} & -\alpha_H \end{pmatrix}, \tag{5.4.2.6}$$

where

$$\begin{aligned} N_v &= \frac{1}{2}\frac{N_g\alpha_g}{\alpha_g+\mu_g}\frac{\alpha_s}{\alpha_s+\mu_s}\frac{\alpha_z}{\alpha_z+\mu_z}\frac{N_k\alpha_k}{\alpha_k+\mu_k}\frac{\Lambda_v}{\alpha_v+\mu_v}, \\ N_h &= \widehat{G_h}, \end{aligned} \tag{5.4.2.7}$$

$$M = \begin{pmatrix} 0 & \frac{N_v\alpha_v\beta_H\Lambda_V}{\mu_V G_0(\mu_V+\delta_V)} \\ \frac{N_h\alpha_h\beta_V\Lambda_V}{\mu_H P_0(\mu_H+\gamma_H+\delta_H)} & 0 \end{pmatrix}, \tag{5.4.2.8}$$

$$D = \begin{pmatrix} \alpha_V & 0 \\ 0 & \alpha_H \end{pmatrix}, \tag{5.4.2.9}$$

$$D^{-1} = \begin{pmatrix} \frac{1}{\alpha_V} & 0 \\ 0 & \frac{1}{\alpha_H} \end{pmatrix} \tag{5.4.2.10}$$

and $MD^{-1} =$

$$\begin{pmatrix} 0 & \frac{N_v\alpha_v\beta_H\Lambda_V}{\mu_V G_0\alpha_H(\mu_V+\delta_V)} \\ \frac{N_h\alpha_h\beta_V\Lambda_V}{\mu_H P_0\alpha_V(\mu_H+\gamma_H+\delta_H)} & 0 \end{pmatrix}. \tag{5.4.2.11}$$

$R_0 = (MD^{-1})$, which is given by

$$\lambda^2 - \frac{N_v\alpha_v\beta_H\Lambda_V}{\mu_V G_0\alpha_H(\mu_V+\delta_V)}\frac{N_h\alpha_h\beta_V\Lambda_H}{\mu_H P_0\alpha_V(\mu_H+\gamma_H+\delta_H)} = 0, \tag{5.4.2.12}$$

where

$$\begin{aligned} N_h &= \widehat{G_h}, \\ N_v &= \widetilde{P_v} = \frac{1}{2}\frac{N_g\alpha_g}{\alpha_g+\mu_g}\frac{\alpha_s}{\alpha_s+\mu_s}\frac{\alpha_z}{\alpha_z+\mu_z}\frac{N_k\alpha_k}{\alpha_k+\mu_k}\frac{\Lambda_v}{\alpha_v+\mu_v}. \end{aligned} \tag{5.4.2.13}$$

Therefore

$$R_0 = \sqrt{\frac{N_v\alpha_v\beta_H\Lambda_V}{\mu_V G_0\alpha_H(\mu_V+\delta_V)}\frac{N_h\alpha_h\beta_V\Lambda_H}{\mu_H P_0\alpha_V(\mu_H+\gamma_H+\delta_H)}}. \tag{5.4.2.14}$$

5.4.3 The local stability analysis of disease free equilibrium state

To determine the local stability analysis of disease free-equilibrium state of the multiscale model (5.4.0.7), we linearize equations of system of equations (5.4.0.7), to obtain the Jacobian matrix and then solve it at

the disease free equilibrium point E^{00}, to obtain

$$J(E^{00}) = \begin{pmatrix} -\mu_V & 0 & 0 & 0 & 0 & -\frac{\beta_H \Lambda_V}{G_0 \mu_V} \\ 0 & -(\mu_V + \delta_V) & 0 & 0 & 0 & \frac{\beta_H \Lambda_V}{G_0 \mu_V} \\ 0 & N_v \alpha_v & -\alpha_V & 0 & 0 & 0 \\ 0 & 0 & -\frac{\beta_V \Lambda_H}{P_0 \mu_H} & -\mu_H & \gamma_H & 0 \\ 0 & 0 & \frac{\beta_V \Lambda_H}{P_0 \mu_H} & 0 & -(\mu_H + \gamma_H + \delta_H) & 0 \\ 0 & 0 & 0 & 0 & N_h \alpha_h & -\alpha_H \end{pmatrix}. \quad (5.4.3.1)$$

The eigenvalues of $J(E^{00})$ are calculated using $det(J(E^{00}) - \lambda I) = 0$. The characteristic equation of the eigenvalues is given by

$$(\lambda + \mu_V)(\lambda + \mu_H)(a_4\lambda^4 + a_3\lambda^3 + a_2\lambda^2 + a_1\lambda + a_0) = 0, \quad (5.4.3.2)$$

where

$$\begin{aligned} a_4 &= 1, \\ a_3 &= \alpha_V + \alpha_H + (\mu_V + \delta_V) + (\mu_H + \gamma_H + \delta_H), \\ a_2 &= \alpha_V\alpha_H + (\alpha_V + \alpha_H)(\mu_V + \delta_V) + (\mu_H + \gamma_H + \delta_H)[\alpha_V + \alpha_H + (\mu_V + \delta_V)], \\ a_1 &= \alpha_V\alpha_H(\mu_V + \delta_V) + (\mu_H + \gamma_H + \delta_H)[\alpha_V\alpha_H + (\alpha_V + \alpha_H)(\mu_V + \delta_V)], \\ a_0 &= \alpha_V\alpha_H(\mu_V + \delta_V)(\mu_H + \gamma_H + \delta_H)\left[1 - R_0^2\right]. \end{aligned} \quad (5.4.3.3)$$

From (5.4.3.2) it is clear that two eigenvalues are equal to $\lambda_1 = -\mu_V$ and $\lambda_2 = -\mu_H$. Now, the other remaining eigenvalues are obtained from the polynomial

$$a_4\lambda^4 + a_3\lambda^3 + a_2\lambda^2 + a_1\lambda + a_0 = 0, \quad (5.4.3.4)$$

It is clear that a_4, a_3, a_2 and a_1 are positive and it's also clear that $a_0 > 0$ whenever $R_0 < 1$ and $a_0 < 0$ when $R_0 > 1$. Since all the coefficient in the polynomial are positive when $R_0 > 1$, therefore to confirm that all the roots of the systems of equations (5.4.3.4) have negative real parts, we shall use Descartes' Rule of signs change, we observe that on characteristic equation (5.4.3.4) there is no sign changes in the sequence of coefficients and so there is zero real positive roots [72, 73]. Therefore we have four real negative eigenvalues. Then all the eigenvalues of the Jacobian matrix $J(E^{00})$ are negative or have negative real parts when $R_0 < 1$. Which shows that the local stability of E^{00} is stable when $R_0 < 1$ and unstable when $R_0 > 1$.

5.4.4 The global stability analysis of disease free equilibrium state

In this subsection, we perform the proof that the DFE is globally asymptotically stable, we state the theorem below.

Theorem 5.3. *The disease free equilibrium state* (E^{00}) *is globally asymptotically stable in the positively invariant region when* $R_0 \leq 1$.

Proof. We define V: $\{(S_V, I_V, P_V, S_H, I_H, G_H) \in \Omega: S_V > 0, S_H > 0\} \to \mathbb{R}$ by

$$V = S_V - S_V^{00}\ln(S_V) + I_V + aP_V + S_H - S_H^{00}\ln(S_H) + I_H + bG_H. \tag{5.4.4.1}$$

We differentiate V with respect to time and is given as follows:

$$\begin{aligned}
\frac{dV}{dt} &= \frac{dS_V}{dt} - \frac{S_V^{00}}{S_V}\frac{dS_V}{dt} + \frac{dI_V}{dt} + a\frac{dP_V}{dt} + \frac{dS_H}{dt} - \frac{S_H^{00}}{S_H}\frac{dS_H}{dt} + \frac{dI_H}{dt} + b\frac{dG_H}{dt},\\
&= \frac{1}{S_V}\left(S_V - S_V^{00}\right)\frac{dS_V}{dt} + \frac{dI_V}{dt} + a\frac{dP_V}{dt} + \frac{1}{S_H}\left(S_H - S_H^{00}\right)\frac{dS_H}{dt} + \frac{dI_H}{dt} + b\frac{dG_H}{dt},\\
&= \frac{1}{S_V}\left(S_V - S_V^{00}\right)\left[\Lambda_V - \frac{\beta_H G_H S_V}{G_0 + G_H} - \mu_V S_V\right] + \frac{\beta_H G_H S_V}{G_0 + G_H} - (\mu_V + \delta_V)I_V +\\
&\quad a(N_v\alpha_v I_V - \alpha_V P_V) + \frac{1}{S_H}\left(S_H - S_H^{00}\right)\left[\Lambda_H - \frac{\beta_V P_V S_H}{P_0 + P_V} - \mu_H S_H + \gamma_H I_H\right]\\
&\quad + \frac{\beta_V P_V S_H}{P_0 + P_V} - (\mu_H + \gamma_H + \delta_H)I_H + b(N_h\alpha_h I_H - \alpha_H G_H),\\
&= -\frac{\mu_V}{S_V}\left(S_V - S_V^{00}\right)\left[S_V - \frac{\Lambda_V}{\mu_V}\right] - \frac{\beta_V G_H}{G_0 + G_H}(S_V - S_V^{00}) + \frac{\beta_H G_H S_V}{G_0 + G_H}\\
&\quad -(\mu_V + \delta_V)I_V + aN_v\alpha_v I_V - a\alpha_V P_V - \frac{\mu_H}{S_H}\left(S_H - S_H^{00}\right)\left[S_H - \frac{\Lambda_H}{\mu_H}\right]\\
&\quad - \frac{\beta_V P_V}{P_0 + P_V}(S_V - S_V^{00}) + \frac{\beta_V P_V S_H}{P_0 + P_V} + \gamma_H\frac{I_H}{S_H}(S_H - S_H^{00}) + \frac{\beta_V P_V S_H}{P_0 + P_V}\\
&\quad -(\mu_H + \gamma_H + \delta_H)I_H + bN_h\alpha_h I_H - b\alpha_H G_H,\\
&= -\frac{\mu_V}{S_V}\left(S_V - S_V^{00}\right)^2 + I_V\left[N_v\alpha_v a - (\mu_V + \delta_V)\right] + G_H\left[\frac{\beta_H S_V^{00}}{G_0 + G_H} - \alpha_H b\right]\\
&\quad -\frac{\mu_H}{S_H}\left(S_H - S_H^{00}\right)^2 + I_H\left[N_h\alpha_h b - (\mu_H + \gamma_H + \delta_H)\right] + P_V\left[\frac{\beta_V S^{00}}{P_0 + P_V} - a\alpha_V\right]\\
&\quad + \gamma_H\frac{I_H}{S_H}\left(S_H - S_H^{00}\right).
\end{aligned} \tag{5.4.4.2}$$

We now choose the a such that $\dfrac{\beta_V S_H^{00}}{P_0 + P_V} - a\alpha_V = 0$, since $P_V = 0$ at DFE, we then make a the subject of formula and obtain $a = \dfrac{\beta_V S_H^{00}}{P_0\alpha_V}$.

We also choose b such that $\dfrac{\beta_H S_V^{00}}{G_0 + G_H} - b\alpha_H = 0$, since $G_H = 0$ at DFE and make b the subject of formula and we obtain $b = \dfrac{\beta_H S_V^{00}}{G_0\alpha_H}$.

We substitute the value of a and b into equation (5.4.4.2), we obtain.

$$\begin{aligned}
\frac{dV}{dt} &= -\frac{\mu_V}{S_V}(S_V - S_V^{00})^2 + I_V\left[N_v\alpha_v\frac{\beta_V S_H^{00}}{P_0\alpha_V} - (\mu_V+\delta_V)\right] - \frac{\mu_H}{S_H}(S_H - S_H^{00})^2 \\
&\quad + I_H\left[N_h\alpha_h\frac{\beta_H S_V^{00}}{G_0\alpha_H} - (\mu_H+\gamma_H+\delta_H)\right] + \gamma_H\frac{I_H}{S_H}(S_H - S_H^{00}), \\
&= -\frac{\mu_V}{S_V}(S_V - S_V^{00})^2 + I_V\left[N_v\alpha_v\frac{\beta_V\Lambda_H}{P_0\alpha_V\mu_H(\mu_V+\delta_V)} - 1\right](\mu_V+\delta_V) \\
&\quad -\frac{\mu_H}{S_H}(S_H - S_H^{00})^2 + I_H\left[N_h\alpha_h\frac{\beta_H\Lambda_V}{G_0\alpha_H\mu_V(\mu_H+\gamma_H+\delta_H)} - 1\right](\mu_H+\gamma_H+\delta_H) \\
&\quad +\gamma_H\frac{I_H}{S_H}(S_H - S_H^{00}), \\
&= -\frac{\mu_V}{S_V}(S_V - S_V^{00})^2 + I_V\left[R_{VH} - 1\right](\mu_V+\delta_V) - \frac{\mu_H}{S_H}(S_H - S_H^{00})^2 \\
&\quad + I_H\left[R_{HV} - 1\right](\mu_H+\gamma_H+\delta_H) + \gamma_H\frac{I_H}{S_H}(S_H - S_H^{00}), \qquad (5.4.4.3) \\
&\leq 0,
\end{aligned}$$

where $R_{VH} = \dfrac{N_v\alpha_v\beta_V\Lambda_H}{P_0\alpha_V\mu_H(\mu_V+\delta_V)}$, $R_{HV} = \dfrac{N_h\alpha_h\beta_H\Lambda_V}{G_0\alpha_H\mu_V(\mu_H+\gamma_H+\delta_H)}$, and $R_0 = \sqrt{R_{VH}R_{HV}}$. $\dfrac{dV}{dt} = 0$ when $S_V = S_V^{00}$ and $S_H = S_H^{00}$ and all other compartments are zero at this point. This means that the DFE is the only equilibrium point that exists at that particular singleton and according to LaSalle's invariant principle and the properties of the constructed Lyapunov function, the DFE is globally asymptotically stable when $R_0 \leq 1$ that is $R_{VH} \leq 1$ and $R_{HV} \leq 1$. □

5.4.5 The Existence of the Endemic Equilibrium State

The endemic equilibrium is denoted by

$$\overline{E} = (\overline{S_V}, \overline{I_V}, \overline{P_V}, \overline{S_H}, \overline{I_H}, \overline{G_H}), \qquad (5.4.5.1)$$

where

$$\begin{aligned}
\overline{S_V}(\overline{G_H}) &= \frac{\Lambda_V(G_0+\overline{G_H})}{\beta_H\overline{G_H} + \mu_V(G_0+\overline{G_H})}, \\
\overline{I_V}(\overline{G_H}) &= \frac{\beta_H\Lambda_V\overline{G_H}}{(\mu_V+\delta_V)[\beta_H\overline{G_H} + \mu_V(G_0+\overline{G_H})]}, \\
\overline{P_V}(\overline{G_H}) &= \frac{N_v\alpha_v\beta_H\Lambda_V\overline{G_H}}{\alpha_V(\mu_V+\delta_V)[\beta_H\overline{G_H} + \mu_V(G_0+\overline{G_H})]}, \qquad (5.4.5.2) \\
\overline{S_H}(\overline{G_H}) &= \frac{\Lambda_H[b_1 + (b_2 + N_v\alpha_v\gamma_H\beta_H\Lambda_V\beta_V)\overline{G_H}](b_3 + b_4\overline{G_H})}{(b_1+b_2\overline{G_H})[\mu_H b_3 + (\mu_H b_4 + \beta_V N_v\alpha_v\beta_H\Lambda_V)\overline{G_H}]}, \\
\overline{I_H}(\overline{G_H}) &= \frac{N_v\alpha_v\beta_H\Lambda_V\beta_V\Lambda_H\overline{G_H}}{b_1 + b_2\overline{G_H}},
\end{aligned}$$

where

$$\begin{aligned} a_1 &= \mu_H P_0(\mu_H + \gamma_H + \delta_H), \\ a_2 &= \mu_H(\mu_H + \gamma_H + \delta_H) + \beta_V(\mu_H + \delta_H), \\ b_1 &= a_1\alpha_V\mu_V G_0(\mu_V + \delta_V), \\ b_2 &= a_1\alpha_V(\mu_V + \delta_V)(\beta_H + \mu_V) + a_2 N_v\alpha_v\beta_H\Lambda_V, \\ b_3 &= \mu_V G_0 P_0\alpha_V(\mu_V + \delta_V), \\ b_4 &= P_0\alpha_V(\mu_V + \delta_V)(\beta_H + \mu_V) + N_v\alpha_v\beta_H\Lambda_V, \\ N_h &= \widehat{G_h}, \\ N_v &= \widetilde{P_v} = \frac{1}{2}\frac{N_g\alpha_g}{\alpha_g + \mu_g}\frac{\alpha_s}{\alpha_s + \mu_s}\frac{\alpha_z}{\alpha_z + \mu_z}\frac{N_k\alpha_k}{\alpha_k + \mu_k}\frac{\Lambda_v}{\alpha_v + \mu_v}. \end{aligned} \tag{5.4.5.3}$$

By substituting the expressions in (5.4.5.2) in the equation for G_H which is given by

$$\frac{dG_H}{dt} = N_h\alpha_h I_H - \alpha_H G_H.$$

We obtain disease free equilibrium state given by

$$E^{00} = \left(S_V^{00}, I_V^{00}, P_V^{00}, S_H^{00}, I_H^{00}, G_H^{00}\right) = \left(\frac{\Lambda_V}{\mu_V}, 0, 0, \frac{\Lambda_H}{\mu_H}, 0, 0\right), \tag{5.4.5.4}$$

when $\overline{G_H} = 0$.
The endemic equilibrium is given by

$$\overline{E} = (\overline{S_V}, \overline{I_V}, \overline{P_V}, \overline{S_H}, \overline{I_H}, \overline{G_H})$$

when

$$\overline{G_H} = \frac{\mu_H P_0\alpha_H\mu_V G_0\mu_V(\mu_V + \delta_V)(\mu_H + \gamma_H + \delta_H)[R_0^2 - 1]}{\alpha_H b_2}, \tag{5.4.5.5}$$

where b_2 is define above in expression (5.4.5.3). From the expression of $\overline{G_H}$, we conclude that there exists one unique endemic equilibrium for the model system (5.4.0.5) whenever $R_0 > 1$.

5.4.6 Local stability analysis of endemic equilibrium state

We establish a local stability of endemic equilibrium state using the center manifold theory [74]. We use center manifold theorem to determine the stability of malaria disease at an endemic equilibrium state. The bifurcation analysis is carried out at the disease-free equilibrium state by utilising the center manifold theory as described in Castillo-Chavez and Song [74]. To using the center manifold theory, we then introducing the following simplification and change of variables. We rewrite the model (5.4.0.5) using the state variables of the malaria disease model and the center manifold approach on the system. We let $x_1 = S_V(t)$, $x_2 = I_V(t)$, $x_3 = P_V(t)$, $x_4 = S_H(t)$, $x_5 = I_H(t)$, $x_6 = G_H(t)$, $\beta^* = \beta_H$ and $\beta_V = k\beta_H$.

Using vector notation, we denote $X = (x_1, x_2, x_3, x_4, x_5, x_6)^T$, the system of equations (5.4.0.5) can written in the form $F = (f_1, f_2, f_3, f_4, f_5, f_6)^T$. By writing the system of equations (5.2.0.1) in vector form as:

$$\begin{aligned}
\frac{dx_1}{dt} &= f_1 = \Lambda_V - \frac{\beta^* x_6}{G_0 + x_6} x_1 - \mu_V x_1, \\
\frac{dx_2}{dt} &= f_2 = \frac{\beta^* x_6}{G_0 + x_6} x_1 - (\mu_V + \delta_V) x_2, \\
\frac{dx_3}{dt} &= f_3 = N_v \alpha_v x_2 - \alpha_V x_3, \\
\frac{dx_4}{dt} &= f_4 = \Lambda_H - \frac{k\beta^* x_3}{P_0 + x_3} x_4 - \mu_H x_4 + \gamma_H x_5, \\
\frac{dx_5}{dt} &= f_5 = \frac{k\beta^* x_3}{P_0 + x_3} x_4 - (\mu_H + \gamma_H + \delta_H) x_5, \\
\frac{dx_6}{dt} &= f_6 = N_h \alpha_h x_5 - \alpha_H x_6.
\end{aligned} \tag{5.4.6.1}$$

We consider $R_0 = 1$ and solving β^* as a bifurcation parameter, we obtain

$$\beta^* = \sqrt{\frac{\mu_V G_0 \alpha_H (\mu_V + \delta_V)}{N_v \alpha_v \Lambda_V} \frac{\mu_H \alpha_V P_0 (\mu_H + \gamma_H + \delta_H)}{N_h \alpha_h k \Lambda_H}}. \tag{5.4.6.2}$$

The Jacobian matrix at disease-free equilibrium is given by

$$J(E_0, \beta^*) = \begin{pmatrix}
-\mu_V & 0 & 0 & 0 & 0 & -\frac{\beta^* \Lambda_V}{\mu_V G_0} \\
0 & -(\mu_V + \delta_V) & 0 & 0 & 0 & \frac{\beta^* \Lambda_V}{\mu_V G_0} \\
0 & N_v \alpha_v & -\alpha_V & 0 & 0 & 0 \\
0 & 0 & -\frac{k\beta^* \Lambda_H}{\mu_H P_0} & -\mu_H & \gamma_H & 0 \\
0 & 0 & \frac{k\beta^* \Lambda_H}{\mu_H P_0} & 0 & -(\mu_H + \gamma_H + \delta_H) & 0 \\
0 & 0 & 0 & 0 & N_h \alpha_h & -\alpha_H
\end{pmatrix}. \tag{5.4.6.3}$$

The eigenvalues of the Jacobian matrix are given by $\lambda_1 = -\mu_V$, $\lambda_2 = -\mu_H$ and

$$a_4 \lambda^4 + a_3 \lambda^3 + a_2 \lambda^2 + a_1 \lambda + a_0 = 0, \tag{5.4.6.4}$$

where

$$\begin{aligned} a_4 &= 1, \\ a_3 &= (\mu_V + \delta_V) + \alpha_V + \alpha_H + (\mu_H + \gamma_H + \delta_H), \\ a_2 &= \alpha_V(\mu_V + \delta_V) + \alpha_H[(\mu_V + \delta_V + \alpha_V)] + (\mu_H + \gamma_H + \delta_H)[(\mu_V + \delta_V) + \alpha_V + \alpha_H], \\ a_1 &= \alpha_H\alpha_V(\mu_V + \delta_V) + (\mu_H + \gamma_H + \delta_H)[\alpha_V(\mu_V + \delta_V) + \\ &\quad \alpha_H[(\mu_V + \delta_V) + \alpha_V]], \\ a_0 &= \alpha_H\alpha_V(\mu_V + \delta_V)(\mu_H + \gamma_H + \delta_H)[1 - R_0^2]. \end{aligned} \tag{5.4.6.5}$$

We notice that $a_4 > 0$, $a_3 > 0$, $a_2 > 0$ and $a_1 > 0$. $a_0 > 0$ when $R_0 < 1$, $a_0 < 0$ when $R_0 > 1$ and when $R_0 = 1$ $a_0 = 0$.

When $R_0 = 1$ we can clearly notice that the Jacobian of the linearized system has a simple zero eigenvalue and all other eigenvalues are negative or have negative real parts. Therefore, the center manifold theory is the appropriate to use in analysing the dynamics of the system of equations (5.4.0.5). When $R_0 = 1$, It is clear that the Jacobian matrix has a right eigenvector that is associated to the zero eigenvalue, given by

$$\mathcal{W} = (w_1 \quad w_2 \quad w_3 \quad w_4 \quad w_5 \quad w_6)^T.$$

We obtain

$$\begin{aligned} w_1 &= -\frac{\beta^*\Lambda_V}{\mu_V^2 G_0} w_6, \\ w_2 &= \frac{\beta^*\Lambda_V}{\mu_V G_0(\mu_V + \delta_V)} w_6, \\ w_3 &= \frac{N_v\alpha_v\beta^*\Lambda_V}{\alpha_V\mu_V G_0(\mu_V + \delta_V)} w_6, \\ w_4 &= -\frac{k\beta^*\Lambda_H(\mu_H + \delta_H)}{\mu_H^2 P_0(\mu_H + \gamma_H + \delta_H)} \frac{N_v\alpha_v\beta^*\Lambda_V}{\alpha_V\mu_V G_0(\mu_V + \delta_V)} w_6, \\ w_5 &= \frac{k\beta^*\Lambda_H}{\mu_H P_0(\mu_H + \gamma_H + \delta_H)} \frac{N_v\alpha_v\beta^*\Lambda_V}{\alpha_V\mu_V G_0(\mu_V + \delta_V)} w_6, \end{aligned} \tag{5.4.6.6}$$

(5.4.6.7)

and we let $w_6 = w_6 > 0$.

Similarly, we denote

$$\mathcal{V} = \begin{pmatrix} v_1 \\ v_2 \\ v_3 \\ v_4 \\ v_5 \\ v_6 \end{pmatrix}^T,$$

as the left eigenvector associated to the zero eigenvalue. We obtain

$$\begin{aligned} v_1 &= v_4 = 0, \\ v_2 &= \frac{N_v\alpha_v k\beta^*\Lambda_H}{\alpha_V\mu_H P_0(\mu_V+\delta_V)}\frac{N_h\alpha_h}{(\mu_H+\gamma_H+\delta_H)}v_6, \\ v_3 &= \frac{N_h\alpha_h k\beta^*\Lambda_H}{\alpha_V\mu_H P_0(\mu_H+\gamma_H+\delta_H)}v_6, \\ v_5 &= \frac{N_h\alpha_h}{\mu_H+\gamma_H+\delta_H}v_6, \end{aligned} \tag{5.4.6.8}$$

and we let $v_6 = v_6 > 0$.

Using the condition $\mathcal{W}\cdot\mathcal{V} = 1$ to obtain the values of v_6 and w_6. Therefore, we obtain

$$v_6 = \frac{\alpha_V(\mu_V+\delta_V)(\mu_H+\gamma_H+\delta_H)}{w_6[(\mu_H+\gamma_H+\delta_H)\{\alpha_H\alpha_V+(\mu_V+\delta_V)(\alpha_H+\alpha_V)\}+\alpha_H\alpha_V(\mu_V+\delta_V)]}.$$

We set $w_6 = 1$. Thus

$$v_6 = \frac{\alpha_V(\mu_V+\delta_V)(\mu_H+\gamma_H+\delta_H)}{[(\mu_H+\gamma_H+\delta_H)\{\alpha_H\alpha_V+(\mu_V+\delta_V)(\alpha_H+\alpha_V)\}+\alpha_H\alpha_V(\mu_V+\delta_V)]}. \tag{5.4.6.9}$$

We shall demonstrate the conditions on parameter values a bifurcation to occur in the system, based on the use of center Manifold theory, from the work in [74]. We compute the bifurcation coefficients a and b, for the transformed system (5.4.6.1), and are defined as follows:

$$\begin{aligned} a &= \sum_{i,j,k=1}^{6} v_k w_i w_j \frac{\partial^k(E_0,\beta^*)}{\partial x_i\partial x_j}, \\ b &= \sum_{i,k=1}^{6} v_k w_i \frac{\partial^2 f_k(E_0,\beta^*)}{\partial x_i\partial\beta^*} \end{aligned} \tag{5.4.6.10}$$

Now,

$$\begin{aligned} a &= \sum_{i,j,k=1}^{6} v_2 w_1 w_6 \frac{\partial^2 f_2}{\partial x_1\partial x_6} + \sum_{i,j,k=1}^{6} v_5 w_3 w_4 \frac{\partial^2 f_5}{\partial x_3\partial x_4} + \sum_{i,j,k=1}^{6} v_2 w_6^2 \frac{\partial^2 f_2}{\partial x_6^2} + \sum_{i,j,k=1}^{6} v_5 w_3^2 \frac{\partial^2 f_5}{\partial x_3^2}, \\ &= -\frac{N_v\alpha_v k\beta^*\Lambda_V}{\alpha_V\mu_H P_0(\mu_V+\delta_V)}\frac{N_h\alpha_h\beta^{*2}\Lambda_V v_6 w_6^2}{\mu_V^2 G_0^2(\mu_V+\gamma_H+\delta_H)}\left[1+\frac{N_v\alpha_v k\beta^*\Lambda_V(\mu_H+\delta_H)}{\alpha_V P_0(\mu_V+\delta_V)}\right] \\ &\quad -2\frac{N_h\alpha_h\beta^*\Lambda_H}{\mu_H+\gamma_H+\delta_H}\frac{N_v\alpha_v k\beta^*\Lambda_V}{\mu_H\alpha_V\mu_V G_0^2 P_0(\mu_V+\delta_V)}v_6 w_6^2\left[1+\frac{N_v\alpha_v\beta^*\Lambda_V}{\alpha_V\mu_V P_0(\mu_V+\delta_V)}\right]. \end{aligned} \tag{5.4.6.11}$$

$$\begin{aligned} b &= \sum_{i,k=1}^{6} v_2 w_6 \frac{\partial^2 f_2}{\partial x_6\partial\beta^*} + \sum_{i,k=1}^{6} v_5 w_3 \frac{\partial^2 f_5}{\partial x_3\partial\beta^*}, \\ &= 2\frac{N_v\alpha_v k\beta^*\Lambda_H}{\alpha_V\mu_V P_0(\mu_V+\delta_V)}\frac{N_h\alpha_h\Lambda_V}{\mu_V G_0(\mu_H+\gamma_H+\delta_H)}v_6 w_6. \end{aligned} \tag{5.4.6.12}$$

We notice that the bifurcation coefficients $a < 0$ and $b > 0$, then it follows that the model will undergo trans-critical bifurcation at $R_0 = 1$. We can conclude that the locally stability of the presents of malaria disease equilibrium state of system (5.2.0.1) is stable when $R_0 > 1$ but close to 1.

5.4.7 Global stability analysis of endemic equilibrium state

Theorem 5.4. *The endemic equilibrium state is globally asymptotically stable when* $R_0 > 1$.

Proof. We prove the global stability analysis of endemic equilibrium state by using the definition of lyapunov function [75].

$$\begin{aligned} V &= \int_{S_V^*}^{S_V} \left(1 - \frac{S_V^*}{x}\right) dx + \int_{I_V^*}^{I_V} \left(1 - \frac{I_V^*}{x}\right) dx + a \int_{P_V^*}^{P_V} \left(1 - \frac{P_V^*}{x}\right) dx + \int_{S_H^*}^{S_H} \left(1 - \frac{S_H^*}{x}\right) dx \\ &+ \int_{I_H^*}^{I_H} \left(1 - \frac{I_H^*}{x}\right) dx + a \int_{G_H^*}^{G_H} \left(1 - \frac{G_H^*}{x}\right) dx. \end{aligned} \tag{5.4.7.1}$$

The derivative of V is given by:

$$\begin{aligned} \frac{dV}{dt} &= \left(1 - \frac{\overline{S_V}}{S_V}\right) \frac{dS_V}{dt} + \left(1 - \frac{\overline{I_V}}{I_V}\right) \frac{dI_V}{dt} + a \left(1 - \frac{\overline{P_V}}{P_V}\right) \frac{dP_V}{dt} + \left(1 - \frac{\overline{S_H}}{S_H}\right) \frac{dS_H}{dt} \\ &\left(1 - \frac{\overline{I_H}}{I_H}\right) \frac{dI_H}{dt} + b \left(1 - \frac{\overline{G_H}}{G_H}\right) \frac{dG_H}{dt}. \end{aligned} \tag{5.4.7.2}$$

At the endemic equilibrium, we consider the following:

$$\begin{aligned} \Lambda_V &= \frac{\beta_H \overline{G_H S_V}}{G_0 + \overline{G_H}} + \mu_V \overline{S_V}, \\ (\mu_V + \delta_V) &= \frac{\beta_H \overline{G_H S_V}}{(G_0 + \overline{G_H})\overline{I_V}}, \\ \alpha_V &= \frac{N_v \alpha_v \overline{I_V}}{\overline{P_V}}, \\ \Lambda_H &= \frac{\beta_V \overline{P_V S_H}}{P_0 + \overline{P_V}} + \mu_H \overline{S_H} - \gamma_H \overline{I_H}, \\ (\mu_H + \gamma_H + \delta_H) &= \frac{\beta_V \overline{P_V S_H}}{P_0 + \overline{P_V}}, \\ \alpha_H &= \frac{N_h \alpha_h \overline{I_H}}{\overline{G_H}}. \end{aligned} \tag{5.4.7.3}$$

Using (5.4.7.2) and (5.4.7.3), we obtain

$$\begin{aligned}\frac{dV}{dt} &= \left(1-\frac{\overline{S_V}}{S_V}\right)\left[\frac{\beta_H\overline{G_HS_V}}{G_0+\overline{G_H}}+\mu_V\overline{S_V}-\frac{\beta_HG_HS_V}{G_0+G_H}-\mu_VS_V\right]\\&+\left(1-\frac{\overline{I_V}}{I_V}\right)\left[\frac{\beta_HG_HS_V}{G_0+G_H}-\frac{\beta_H\overline{G_HS_V}}{G_0+\overline{G_H}}\frac{I_V}{\overline{I_V}}\right]+a\left(1-\frac{\overline{P_V}}{P_V}\right)\left[N_v\alpha_vI_V-N_v\alpha_v\overline{I_V}\frac{P_V}{\overline{P_V}}\right]\\&+\left(1-\frac{\overline{S_H}}{S_H}\right)\left[\frac{\beta_V\overline{P_VS_H}}{P_0+\overline{P_V}}+\mu_H\overline{S_H}-\gamma_H\overline{I_H}-\frac{\beta_VP_VS_H}{P_0+P_V}-\mu_HS_H+\gamma_HI_H\right] \qquad (5.4.7.4)\\&+\left(1-\frac{\overline{I_H}}{I_H}\right)\left[\frac{\beta_VP_VS_H}{P_0+P_V}-\frac{\beta_V\overline{P_VS_H}}{P_0+\overline{P_V}}\frac{I_H}{\overline{I_H}}\right]+b\left(1-\frac{\overline{G_H}}{G_H}\right)\left[N_h\alpha_hI_H-N_h\alpha_h\overline{I_H}\frac{G_H}{\overline{G_H}}\right],\end{aligned}$$

$$\begin{aligned}\frac{dV}{dt} &= -\frac{\mu_V}{S_V}(S_V-\overline{S_V})^2-\frac{\mu_H}{S_H}(S_H-\overline{S_H})^2+2\frac{\beta_H\overline{G_HS_V}}{G_0+\overline{G_H}}-\frac{\beta_H\overline{G_HS_V}}{G_0+\overline{G_H}}\frac{\overline{S_V}}{S_V}+\frac{\beta_HG_HS_V}{G_0+G_H}\frac{\overline{S_V}}{S_V}\\&-\frac{\beta_HG_HS_V}{G_0+G_H}\frac{\overline{I_V}}{I_V}+I_V\left[aN_v\alpha_v-\frac{\beta_H\overline{G_HS_V}}{(G_0+\overline{G_H})\overline{I_V}}\right]-aN_v\alpha_vI_H\frac{\overline{P_V}}{P_V}-aN_v\alpha_v\overline{I_V}\frac{P_V}{\overline{P_V}}\\&+aN_v\alpha_v\overline{I_V}+2\frac{\beta_V\overline{P_VS_H}}{P_0+\overline{P_V}}+\frac{\beta_VP_VS_H}{P_0+P_V}\frac{\overline{S_H}}{S_H}-\frac{\beta_V\overline{P_VS_H}}{P_0+\overline{P_V}}\frac{\overline{S_H}}{S_H}-\frac{\beta_VP_VS_H}{P_0+P_V}\frac{\overline{I_H}}{I_H}\\&+I_H\left[bN_h\alpha_h-\frac{\beta_V\overline{P_VS_H}}{(P_0+\overline{P_V})\overline{I_H}}\right]+\gamma_HI_H-\gamma_H\overline{I_H}+\gamma_H\overline{I_H}\frac{\overline{S_H}}{S_H}-\gamma_HI_H\frac{\overline{S_H}}{S_H}-bN_h\alpha_hI_H\frac{\overline{G_H}}{G_H}\\&-bN_h\alpha_h\overline{I_H}\frac{\overline{G_H}}{G_H}+bN_h\alpha_h\overline{I_H}. \qquad (5.4.7.5)\end{aligned}$$

We let

$$aN_v\alpha_v-\frac{\beta_H\overline{G_HS_V}}{(G_0+\overline{G_H})\overline{I_V}}=0,$$

then we solve for a and we obtain

$$a=\frac{\beta_H\overline{G_HS_V}}{N_v\alpha_v(G_0+\overline{G_H})\overline{I_V}}. \qquad (5.4.7.6)$$

We also let

$$bN_h\alpha_h-\frac{\beta_V\overline{P_VS_H}}{(P_0+\overline{P_V})\overline{I_H}}=0,$$

then we solve for b and obtain

$$b=\frac{\beta_V\overline{P_VS_H}}{N_h\alpha_h(P_0+\overline{P_V})\overline{I_H}}. \qquad (5.4.7.7)$$

We substitute (5.4.7.6) and (5.4.7.7) into (5.4.7.2), and we obtain

$$\begin{aligned}
\left(1-\frac{\overline{S_V}}{S_V}\right)\frac{dS_V}{dt} &= \left(1-\frac{\overline{S_V}}{S_V}\right)\left[\Lambda_V-\frac{\beta_H G_H S_V}{G_0+G_H}-\mu_V S_V\right] \\
&= \left(1-\frac{\overline{S_V}}{S_V}\right)\left[\frac{\beta_H \overline{G_H S_V}}{G_0+\overline{G_H}}+\mu_V\overline{S_V}-\frac{\beta_H G_H S_V}{G_0+G_H}-\mu_V S_V\right] \\
&= \left(1-\frac{\overline{S_V}}{S_V}\right)\left[\mu_V\overline{S_V}-\mu_V S_V\right]+\left(1-\frac{\overline{S_V}}{S_V}\right)\left[\frac{\beta_H \overline{G_H S_V}}{G_0+\overline{G_H}}-\frac{\beta_H G_H S_V}{G_0+G_H}\right] \\
&= -\mu_V S_V\left(1-\frac{\overline{S_V}}{S_V}\right)^2+\overline{\lambda_H S_V}\left(1-\frac{\overline{S_V}}{S_V}\right)\left[1-\frac{\lambda_H S_V}{\overline{\lambda_H S_V}}\right] \\
&\leq \overline{\lambda_H S_V}\left(1-\frac{\overline{S_V}}{S_V}\right)\left[1-\frac{\lambda_H S_V}{\overline{\lambda_H S_V}}\right] \\
&\leq \overline{\lambda_H S_V}\left[1-\frac{\lambda_H S_V}{\overline{\lambda_H S_V}}-\frac{\overline{S_V}}{S_V}+\frac{\lambda_H}{\overline{\lambda_H}}\right],
\end{aligned} \tag{5.4.7.8}$$

$$\begin{aligned}
\left(1-\frac{\overline{I_V}}{I_V}\right)\frac{dI_V}{dt} &= \left(1-\frac{\overline{I_V}}{I_V}\right)\left[\frac{\beta_H G_H S_V}{G_0+G_H}-(\mu_V+\delta_V)I_V\right] \\
&= \left(1-\frac{\overline{I_V}}{I_V}\right)\left[\frac{\beta_H G_H S_V}{G_0+G_H}-\frac{\beta_H \overline{G_H S_V}}{G_0+\overline{G_H}}\frac{I_V}{\overline{I_V}}\right] \\
&= \overline{\lambda_H S_V}\left(1-\frac{\overline{I_V}}{I_V}\right)\left(\frac{\lambda_H S_V}{\overline{\lambda_H S_V}}-\frac{I_V}{\overline{I_V}}\right) \\
&= \overline{\lambda_H S_V}\left[\frac{\lambda_H S_V}{\overline{\lambda_H S_V}}-\frac{I_V}{\overline{I_V}}-\frac{\lambda_H S_V \overline{I_V}}{\overline{\lambda_H S_V} I_V}+1\right],
\end{aligned} \tag{5.4.7.9}$$

$$\begin{aligned}
\frac{\beta_H \overline{G_H S_V}}{N_v\alpha_v(G_0+\overline{G_H})\overline{I_V}}\left(1-\frac{\overline{I_V}}{I_V}\right)\frac{P_V}{dt} &= \frac{\beta_H \overline{G_H S_V}}{N_v\alpha_v(G_0+\overline{G_H})\overline{I_V}}\left(1-\frac{\overline{I_V}}{I_V}\right)\left[N_v\alpha_v I_V-\alpha_V P_V\right] \\
&= \frac{\beta_H \overline{G_H S_V}}{N_v\alpha_v(G_0+\overline{G_H})\overline{I_V}}\left(1-\frac{\overline{I_V}}{I_V}\right)\left[N_v\alpha_v I_V-N_v\alpha_v\overline{I_V}\frac{P_V}{\overline{P_V}}\right] \\
&= \overline{\lambda_H S_V}\left(1-\frac{\overline{P_V}}{P_V}\right)\left(\frac{I_V}{\overline{I_V}}-\frac{I_V}{\overline{P_V}}\right) \\
&= \overline{\lambda_H S_V}\left[\frac{I_V}{\overline{I_V}}-\frac{P_V}{\overline{P_V}}-\frac{\overline{P_V} I_V}{P_V\overline{I_V}}+1\right],
\end{aligned} \tag{5.4.7.10}$$

$$\begin{aligned}
\left(1-\frac{\overline{S_H}}{S_H}\right)\frac{dS_H}{dt} &= \left(1-\frac{\overline{S_H}}{S_H}\right)\left[\Lambda_H-\frac{\beta_V P_V S_H}{P_0+P_V}-\mu_H S_H+\gamma_H I_H\right] \\
&= \left(1-\frac{\overline{S_H}}{S_H}\right)\left[\frac{\beta_V \overline{P_V S_H}}{P_0+\overline{P_V}}+\mu_H\overline{S_H}-\gamma_H\overline{I_H}-\frac{\beta_V P_V S_H}{P_0+P_V}-\mu_H S_H+\gamma_H I_H\right] \\
&= \left(1-\frac{\overline{S_H}}{S_H}\right)\left(\frac{\beta_V \overline{P_V S_H}}{P_0+\overline{P_V}}-\frac{\beta_V P_V S_H}{P_0+P_V}\right)+\left(1-\frac{\overline{S_H}}{S_H}\right)\left[\mu_H\overline{S_H}-\mu_H S_H\right] \\
&\quad +\left(1-\frac{\overline{S_H}}{S_H}\right)\left[\gamma_H I_H-\gamma_H\overline{I_H}\right] \qquad (5.4.7.11) \\
&= \overline{\lambda_V S_H}\left(1-\frac{\overline{S_H}}{S_H}\right)\left(1-\frac{\lambda_V S_H}{\overline{\lambda_V S_H}}\right)-\mu_H S_H\left(1-\frac{\overline{S_H}}{S_H}\right)^2+ \\
&\quad \gamma_H\overline{I_H}\left(1-\frac{\overline{S_H}}{S_H}\right)\left(\frac{I_H}{\overline{I_H}}-1\right) \\
&\leq \overline{\lambda_V S_H}\left(1-\frac{\overline{S_H}}{S_H}\right)\left(1-\frac{\lambda_V S_H}{\overline{\lambda_V S_H}}\right)+\gamma_H\overline{I_H}\left(1-\frac{\overline{S_H}}{S_H}\right)\left(\frac{I_H}{\overline{I_H}}-1\right) \\
&\leq \overline{\lambda_V S_H}\left[1-\frac{\lambda_V S_H}{\overline{\lambda_V S_H}}-\frac{\overline{S_H}}{S_H}+\frac{\Lambda_V}{\overline{\lambda_V}}\right]+\gamma_H\overline{I_H}\left[\frac{I_H}{\overline{I_H}}-1-\frac{\overline{S_H}I_H}{S_H\overline{I_H}}+\frac{\overline{S_H}}{S_H}\right],
\end{aligned}$$

$$\begin{aligned}
\left(1-\frac{\overline{I_H}}{I_H}\right)\frac{dI_H}{dt} &= \left(1-\frac{\overline{I_H}}{I_H}\right)\left[\frac{\beta_V P_V S_H}{P_0+P_V}-(\mu_H+\gamma_H+\delta_H)I_H\right] \\
&= \left(1-\frac{\overline{I_H}}{I_H}\right)\left[\frac{\beta_V P_V S_H}{P_0+P_V}-\frac{\beta_V\overline{P_V S_H}}{P_0+\overline{P_V}}\frac{I_H}{\overline{I_H}}\right] \qquad (5.4.7.12) \\
&= \overline{\lambda_V S_H}\left(1-\frac{\overline{I_H}}{I_H}\right)\left(\frac{\lambda_V S_V}{\overline{\lambda_V S_H}}-\frac{I_H}{\overline{I_H}}\right) \\
&= \left[\frac{\lambda_V S_V}{\overline{\lambda_V S_H}}-\frac{I_H}{\overline{I_H}}-\frac{\lambda_V S_V\overline{I_H}}{\overline{\lambda_V S_H}I_H}+1\right],
\end{aligned}$$

and

$$\begin{aligned}
b\left(1-\frac{\overline{G_H}}{G_H}\right)\frac{dG_H}{dt} &= \frac{\beta_V\overline{P_V S_H}}{N_h\alpha_h(P_0+\overline{P_V})\overline{I_H}}\left(1-\frac{\overline{G_H}}{G_H}\right)\left[N_h\alpha_h I_H-\alpha_H G_H\right] \\
&= \frac{\overline{\lambda_V S_H}}{N_h\alpha_h\overline{I_H}}\left(1-\frac{\overline{G_H}}{G_H}\right)\left[N_h\alpha_h I_H-N_h\alpha_h\overline{I_H}\frac{G_H}{\overline{G_H}}\right] \qquad (5.4.7.13) \\
&= \overline{\lambda_V S_H}\left(1-\frac{\overline{G_H}}{G_H}\right)\left[\frac{I_H}{\overline{I_H}}-\frac{G_H}{\overline{G_H}}\right] \\
&= \overline{\lambda_V S_H}\left[\frac{I_H}{\overline{I_H}}-\frac{G_H}{\overline{G_H}}-\frac{\overline{G_H}I_H}{G_H\overline{I_H}}+1\right].
\end{aligned}$$

$$\begin{aligned}
\frac{dV}{dt} &\leq \overline{\lambda_H S_V}\left[1-\frac{\lambda_H S_V}{\overline{\lambda_H S_V}}-\frac{\overline{S_V}}{S_V}+\frac{\lambda_H}{\overline{\lambda_H}}\right]+\overline{\lambda_H S_V}\left[\frac{\lambda_H S_V}{\overline{\lambda_H S_V}}-\frac{I_V}{\overline{I_V}}-\frac{\lambda_H S_V \overline{I_V}}{\overline{\lambda_H S_V} I_V}+1\right]+\\
&\quad \overline{\lambda_H S_V}\left[\frac{I_V}{\overline{I_V}}-\frac{P_V}{\overline{P_V}}-\frac{\overline{P_V} I_V}{P_V \overline{I_V}}+1\right]+\overline{\lambda_V S_H}\left[1-\frac{\lambda_V S_H}{\overline{\lambda_V S_H}}-\frac{\overline{S_H}}{S_H}+\frac{\Lambda_V}{\overline{\lambda_V}}\right]+\\
&\quad \gamma_H \overline{I_H}\left[\frac{I_H}{\overline{I_H}}-1-\frac{\overline{S_H} I_H}{S_H \overline{I_H}}+\frac{\overline{S_H}}{S_H}\right]+\left[\frac{\lambda_V S_V}{\overline{\lambda_V S_H}}-\frac{I_H}{\overline{I_H}}-\frac{\lambda_V S_V \overline{I_H}}{\overline{\lambda_V S_H} I_H}+1\right]+\\
&\quad \overline{\lambda_V S_H}\left[\frac{I_H}{\overline{I_H}}-\frac{G_H}{\overline{G_H}}-\frac{\overline{G_H} I_H}{G_H \overline{I_H}}+1\right]. \qquad (5.4.7.14)\\
&\leq \overline{\lambda_H S_V}\left[2-\frac{\overline{S_V}}{S_V}+\frac{\lambda_H}{\overline{\lambda_H}}-\frac{I_V}{\overline{I_V}}-\frac{\lambda_H S_V \overline{I_V}}{\overline{\lambda_H S_V} I_V}\right]+\overline{\lambda_H S_V}\left[\frac{I_V}{\overline{I_V}}-\frac{P_V}{\overline{P_V}}-\frac{\overline{P_V} I_V}{P_V \overline{I_V}}+1\right]\\
&\quad \overline{\lambda_V S_H}\left[2-\frac{\overline{S_H}}{S_H}+\frac{\lambda_V}{\overline{\lambda_V}}-\frac{I_H}{\overline{I_H}}-\frac{\lambda_V S_H \overline{I_H}}{\overline{\lambda_V S_H} I_H}\right]+\overline{\lambda_V S_H}\left[\frac{I_H}{\overline{I_H}}-\frac{G_H}{\overline{G_H}}-\frac{\overline{G_H} I_H}{G_H \overline{I_H}}+1\right]\\
&\quad \gamma_H \overline{I_H}\left[\frac{I_H}{\overline{I_H}}-1-\frac{\overline{S_H} I_H}{S_H \overline{I_H}}+\frac{\overline{S_H}}{S_H}\right].
\end{aligned}$$

Let $g(x) = 1 - x + \ln(x)$, and as we know that $x > 0$, therefore $g(x) \leq 0$. And when $x = 1$, then $g(x) = 0$.

$$\begin{aligned}
\frac{dV}{dt} &\leq \overline{\lambda_H S_V}\left[g\left(\frac{\overline{S_V}}{S_V}\right)+\ln\left(\frac{\overline{S_V}}{S_V}\right)-\frac{I_V}{\overline{I_V}}+g\left(\frac{\lambda_H S_V \overline{I_V}}{\overline{\lambda_H S_V} I_V}\right)+\ln\left(\frac{\lambda_H}{\overline{\lambda_H}}\right)-\ln\left(\frac{\overline{S_V}}{S_V}\right)-\ln\left(\frac{I_V}{\overline{I_V}}\right)+\frac{\lambda_H}{\overline{\lambda_H}}\right]\\
&\quad +\overline{\lambda_H S_V}\left[\frac{I_V}{\overline{I_V}}-\frac{P_V}{\overline{P_V}}+g\left(\frac{\overline{P_V} I_V}{P_V \overline{I_V}}\right)+\ln\left(\frac{\overline{P_V} I_V}{P_V \overline{I_V}}\right)\right]+\overline{\lambda_V S_H}\left[g\left(\frac{\overline{S_H}}{S_H}\right)+\ln\left(\frac{\overline{S_H}}{S_H}\right)-\frac{I_H}{\overline{I_H}}+\right.\\
&\quad \left. g\left(\frac{\lambda_V S_H \overline{I_H}}{\overline{\lambda_V S_H} I_H}\right)+\ln\left(\frac{\lambda_V}{\overline{\lambda_V}}\right)-\ln\left(\frac{\overline{S_H}}{S_H}\right)-\ln\left(\frac{I_H}{\overline{I_H}}\right)+\frac{\lambda_V}{\overline{\lambda_V}}\right]+\overline{\lambda_V S_H}\left[\frac{I_H}{\overline{I_H}}-\frac{G_H}{\overline{G_H}}+g\left(\frac{\overline{G_H} I_H}{G_H \overline{I_H}}\right)\right.\\
&\quad \left.+\ln\left(\frac{\overline{G_H} I_H}{G_H \overline{I_H}}\right)\right]+\gamma_H \overline{I_H}\left[\frac{I_H}{\overline{I_H}}+g\left(\frac{\overline{S_H} I_H}{S_H \overline{I_H}}\right)+\ln\left(\frac{\overline{S_H} I_H}{S_H \overline{I_H}}\right)+\frac{\overline{S_H}}{S_H}-2\right], \qquad (5.4.7.15)\\
&\leq \overline{\lambda_H S_V}\left[g\left(\frac{\lambda_H S_V \overline{I_V}}{\overline{\lambda_H S_V} I_V}\right)+g\left(\frac{\overline{S_V}}{S_V}\right)-\frac{I_V}{\overline{I_V}}-\ln\left(\frac{I_V}{\overline{I_V}}\right)-\ln\left(\frac{G_H}{\overline{G_H}}\right)-\frac{G_H}{\overline{G_H}}+\frac{G_H}{\overline{G_H}}+g\left(\frac{G_0+G_H}{G_0+\overline{G_H}}\right)\right.\\
&\quad \left.-\frac{G_0+G_H}{G_0+\overline{G_H}}-\frac{G_H(G_0+\overline{G_H})}{\overline{G_H}(G_0+G_H)}+1\right]+\overline{\lambda_H S_V}\left[g\left(\frac{I_V \overline{P_V}}{\overline{I_H} P_V}\right)+\frac{I_V}{\overline{I_V}}-\frac{P_V}{\overline{P_V}}+\ln\left(\frac{I_V}{\overline{I_V}}\right)-\ln\left(\frac{P_V}{\overline{P_V}}\right)\right]\\
&\quad +\overline{\lambda_V S_H}\left[g\left(\frac{\lambda_V S_H \overline{I_H}}{\overline{\lambda_V S_H} I_H}\right)+g\left(\frac{\overline{S_H}}{S_H}\right)-\frac{I_H}{\overline{I_H}}-\ln\left(\frac{I_H}{\overline{I_H}}\right)+\ln\left(\frac{P_V}{\overline{P_V}}\right)-\frac{P_V}{\overline{P_V}}\frac{P_V}{\overline{P_V}}+g\left(\frac{P_0+P_V}{P_0+\overline{P_V}}\right)\right.\\
&\quad \left.-\frac{P_0+P_V}{P_0+\overline{P_V}}-\frac{P_V(P_0+\overline{P_V})}{\overline{P_V}(P_0+P_V)}+1\right]+\overline{\lambda_V S_H}\left[g\left(\frac{I_H \overline{G_H}}{\overline{I_H} G_H}\right)+\frac{I_H}{\overline{I_H}}-\frac{G_H}{\overline{G_H}}+\ln\left(\frac{I_H}{\overline{I_H}}-\ln\left(\frac{G_H}{\overline{G_H}}\right)\right)\right]\\
&\quad +\gamma_H \overline{I_H}\left[\frac{I_H}{\overline{I_H}}+g\left(\frac{\overline{S_H} I_H}{S_H \overline{I_H}}\right)+\ln\left(\frac{\overline{S_H}}{S_H}\right)+\ln\left(\frac{I_H}{\overline{I_H}}\right)+\frac{\overline{S_H}}{S_H}-2\right]
\end{aligned}$$

$$\begin{aligned}\frac{dV}{dt} \leq\ & \overline{\lambda_H S_V}\left[g\left(\frac{\lambda_H S_V \overline{I_V}}{\overline{\lambda_H S_V} I_V}\right)+g\left(\frac{\overline{S_V}}{S_V}\right)-\frac{I_V}{\overline{I_V}}-\ln\left(\frac{I_V}{\overline{I_V}}\right)+\ln\left(\frac{P_V}{\overline{P_V}}\right)+\frac{P_V}{\overline{P_V}}\right]\\ &+\overline{\lambda_H S_V}\left[g\left(\frac{G_0+G_H}{G_0+\overline{G_H}}\right)-\frac{G_0+G_H}{G_0+\overline{G_H}}-\frac{G_H(G_0+\overline{G_H})}{\overline{G_H}(G_0+G_H)}-\frac{P_V}{\overline{P_V}}+1\right]+\\ &\overline{\lambda_H S_V}\left[g\left(\frac{I_V\overline{P_V}}{\overline{I_V}P_V}\right)+\frac{I_V}{\overline{I_V}}-\frac{P_V}{\overline{P_V}}+\ln\left(\frac{I_V}{\overline{I_V}}\right)-\ln\left(\frac{P_V}{\overline{P_V}}\right)\right]+\overline{\lambda_V S_H}\left[g\left(\frac{\lambda_V S_H \overline{I_H}}{\overline{\lambda_V S_H} I_H}\right)\right.\\ &\left.+g\left(\frac{\overline{S_H}}{S_H}\right)-\frac{I_H}{\overline{I_H}}-\ln\left(\frac{I_H}{\overline{I_H}}\right)+\ln\left(\frac{G_H}{\overline{G_H}}\right)+\frac{I_H}{\overline{I_H}}\right]+\overline{\lambda_V S_H}\left[g\left(\frac{P_0+P_V}{P_0+\overline{P_V}}\right)-\frac{P_0+P_V}{P_0+\overline{P_V}}\right.\\ &\left.+\frac{P_V(P_0+\overline{P_V})}{\overline{P_V}(P_0+P_V)}-\frac{G_H}{\overline{G_H}}+1\right]+\overline{\lambda_V S_H}\left[g\left(\frac{I_H\overline{G_H}}{\overline{I_H}G_H}\right)+\frac{I_H}{\overline{I_H}}-\frac{G_H}{\overline{G_H}}+\ln\left(\frac{I_H}{\overline{I_H}}\right)-\ln\left(\frac{G_H}{\overline{G_H}}\right)\right]\\ &+\gamma_H\overline{I_H}\left[\frac{I_H}{\overline{I_H}}+g\left(\frac{\overline{S_H}I_H}{S_H\overline{I_H}}\right)+\ln\left(\frac{\overline{S_H}}{S_H}\right)+\ln\left(\frac{I_H}{\overline{I_H}}\right)+\frac{S_H}{\overline{S_H}}-2\right].\end{aligned}$$

Consequently, we gain

$$\begin{aligned}\frac{dV}{dt} \leq\ & \overline{\lambda_H S_V}\left[\frac{P_V}{\overline{P_V}}-\frac{I_V}{\overline{I_V}}-\ln\left(\frac{I_V}{\overline{I_V}}\right)+\ln\left(\frac{P_V}{\overline{P_V}}\right)\right]+\overline{\lambda_H S_V}\left[\frac{I_V}{\overline{I_V}}-\frac{P_V}{\overline{P_V}}+\ln\left(\frac{I_V}{\overline{I_V}}\right)-\ln\left(\frac{P_V}{\overline{P_V}}\right)\right]\\ &+\overline{\lambda_V S_H}\left[\frac{G_H}{\overline{G_H}}-\frac{I_H}{\overline{I_H}}+\ln\left(\frac{G_H}{\overline{G_H}}\right)-\ln\left(\frac{I_H}{\overline{I_H}}\right)\right]+\overline{\lambda_V S_H}\left[\frac{I_H}{\overline{I_H}}-\frac{G_H}{\overline{G_H}}+\ln\left(\frac{I_H}{\overline{I_H}}\right)-\ln\left(\frac{G_H}{\overline{G_H}}\right)\right].\end{aligned} \tag{5.4.7.16}$$

Hence, $\frac{dV}{dt} \leq 0$ for all $(S_V, I_V, P_V, S_H, I_H, G_H) > 0$ and $\frac{dV}{dt} = 0$ only when $S_V = \overline{S_V}$, $I_H = \overline{I_V}$, $P_V = \overline{P_V}$, $S_H = \overline{S_H}$, $I_V = \overline{I_H}$ and $G_H = \overline{G_H}$. It is clear that the largest invariant subset, where $\frac{dV}{dt} = 0$, is $\overline{E}$. Applying the LaSalle's invariance principle [76] we conclude that the endemic equilibrium state $(\overline{E})$ is globally asymptotically stable when $R_0 > 1$. □

5.5 Numerical Simulation

In this section, we perform the numerical simulation for the coupled multiscale model (5.2.0.1) using Matlab version 2019 and python 2.7 with built-in function of Odeint, which implements the version of Runge-kutta scheme. The parameter values that we use for numerical simulations are estimates from published studies. These parameter values we use are in Tables (5.1)-(5.5). We use the following initial conditions $S_V(0) = 100000$, $I_V(0) = 200$, $P_V = 40000$, $S_H(0) = 10000$, $I_H(0) = 70$, $P_h(0) = 45$, $L_h(0) = 400$, $L_h^*(0) = 50$, $B_h(0) = 500$, $B_h^*(0) = 5$, $M_h(0) = 50$, $G_h(0) = 15$, $D(0) = 30$, $A(0) = 10$ and $G_H(0) = 1000$. However, this coupled multiscale model forecasts on the outcome of immune system have when contacts with the pathogen and determine its influence on the host-level. Our key focus is on the parameters associated with immune response and determine how they have influence on between-host scale malaria infection dynamics of (a) population of infected humans (I_H), (b) community gametocyte load (G_H), (c) population of infected mosquitoes (I_V) and (d) community sporozoite load (P_V).

Table 5.1: Between-mosquito scale parameter values and their description.

Parameter	Description	Initial Value	Range	Units	Source
Λ_V	Rate of recruitment of susceptible mosquitoes.	6000	5000-7000	Mosquitoes per day	[24]
β_V	Contact rate of susceptible humans with the infectious reservoir of mosquitoes.	0.52135	2.7×10^{-3}-0.64	day^{-1}	[35]
μ_V	Natural death rate of mosquitoes.	0.12	0.033-0.3	day^{-1}	[24]
δ_V	induced death rate of infected mosquitoes.	0.00000426	$4.26 \times 10^{-6} - 5.33 \times 10^{-6}$	day^{-1}	[24]
P_0	Half saturation constant associated with the infection of humans.	1×10^7	$1\times10^6-5\times10^8$	day^{-1}	Assumed.
α_V	Rate of clearance of community sporozoite load.	0.3	0.09-0.99	day^{-1}	[24]

Table 5.2: Between-human scale parameter values and their description.

Parameter	Description	Initial Value	Range	Units	Source
Λ_H	Rate of recruitment of Susceptible humans.	1000	1000-2000	Human per day	[24]
β_H	Infection rate of susceptible mosquitoes.	0.556	0.072-0.64	day^{-1}	[35]
μ_H	Natural death rate of humans.	0.004	0.00001-0.008	day^{-1}	Assumed
δ_H	Disease induced death rate of humans.	0.03454	$1 \times 10^{-15} - 4.1 \times 10^{-2}$	day^{-1}	[35]
γ_H	Natural recovery rate of humans.	0.025	0.0014-0.037	day^{-1}	Assumed
G_0	Half saturation constant associated with the infection of mosquitoes.	5×10^7	$1\times10^6-1\times10^9$	day^{-1}	Assumed.
α_H	Rate of clearance of community gametocyte load.	0.0000913	0.0000467-0.000274	day^{-1}	[24]

Table 5.3: Within-mosquito scale parameter values and their description.

Parameter	**Description**	**Initial Value**	**Range**	**Units**	**Source**
Λ_v	The rate of supply of gametocytes within infected mosquitoes.	3000	100-3000	Gametocytes per day	Assumed
α_g	Rate at which gametocyte infected erythrocytes burst within ifected mosquito.	96	90-100	day^{-1}	[24]
μ_g	Decay rate of gametocytes within infected mosquito.	0.0625	0.0326-0.0725	day^{-1}	[24]
N_g	Number of gametes produced per gametocyte infected erythrocyte within infected mosquito.	2	1-3	Gametes per day	[24]
α_z	Rate at which zygote develop into oocysts.	0.4240	0.01-0.5	day^{-1}	[24]
μ_z	Natural death rate of zygote.	1	1-4	day^{-1}	[24]
α_s	Fertilisation of gametes.	0.2	0.01-0.2	day^{-1}	[24]
μ_s	Natural death rate of gametes.	58	40-129	day^{-1}	[24]
α_k	Bursting rate of oocysts to produce sporozoites.	0.2	0-1	day^{-1}	[24]
N_k	Number of sporozoites produced per bursting oocysts.	3 000	1000-10000	Sporozoites per day	[24]
μ_k	Natural death rate of oocysts.	0.01	0.071-0.143	day^{-1}	[24]
α_v	Rate at which sporozoites become infectious to humans.	0.025	0.0167-1	day^{-1}	[24]
μ_v	Natural death rate of sporozoites.	0.0001	0.0001-0.01	day^{-1}	[24]

Table 5.4: Within-human scale parameter values and their description.

Parameter	Description	Initial Value	Range	Units	Source
Λ_h	The rate of injection of sporozoites into pre-erythrocytes due to mosquito bites	30	18-35	Sporozoites per day	[45]
θ_l	Destruction rate of sporozoites	0.03	0.001- 0.9	day^{-1}	Assumed.
Λ_l	Rate of supply of uninfected liver cells.	3000	1000- 10000	Cells per day	[60]
μ_p	Decay rate of sporozoites.	1.2×10^{-3}	$10^{-12} - 10^{-1}$	day^{-1}	Assumed
β_l	Rate of infection of hepatocytes by sporozoites.	1×10^{-1}	10^{-6}- 0.1	day^{-1}	[45]
μ_l	Natural decay rate of liver cells.	0.029	0.001- 0.1	day^{-1}	[45]
α_l	Rate at which infected liver cell bursts.	0.02	0.01- 0.1	day^{-1}	[45]
N_l	Number of merozoites produced per bursting pre-erythrocytes.	1 000	1000-10000	Merozoites per day	[45]
Λ_b	Rate of suppy of uninfected red blood cells.	200	100-300	Cells per day	[24]
β_h	Rate of infection of red blood cells (erythrocytes).	0.3	2×10^{-9}-0.4	day^{-1}	Assumed
θ_b	The destruction rate of merozoites into infected red-blood cells	0.03	$(10^{-8} - 0.06)$ cells	day^{-1}	[35].
α_h	Rate at which gametocytes develop and become infectious within infected human.	0.4	0.01-0.9	day^{-1}	[24]
μ_h	Natural death rate of gametocyte infected erythrocytes within infected human.	0.0625	0.0600-0.0625	day^{-1}	[24]
μ_b	Natural decay rate of red blood cells.	0.0083	0.006-0.1	day^{-1}	[24]
μ_m	Natural decay rate of free merozoites	0.001	0.001-0.5	day^{-1}	[24]
π	Proportion of gametocytes infected erythrocytes.	0.4	0.1-0.5	day^{-1}	[24]
N_m	Number of merozoites produced per bursting erythrocytes.	16	10-30	Merozoites per day	[77]
α_m	Rate at which erythrocytes burst to produce merozoites.	0.5	0.1-1.0	day^{-1}	[24].

Table 5.5: Within-human scale parameter values and their description.

Parameter	Description	Initial Value	Range	Units	Source
θ_m	Destruction rate of merozoites by immune cells	0.06	$(10^{-8} - 0.12)$ cells	day^{-1}	[35].
θ_g	Destruction rate of gametocytes by immune cells.	0.03	$(10^{-8} - 0.06)$ cells	day^{-1}	[35].
Λ_d	Supply rate of immune cells	30	1-300	day^{-1}	[70].
ρ_l	Immunogenecity of infected hepatocytes.	0.001	0.001- 0.1		Assumed
ρ_b	Immuno-sensitivity of infected red-blood-cells.	0.06	$(2 \times 10^{-8} - 0.12)$ cells	day^{-1}	[35].
ρ_m	Immuno-sensitivity of merozoites cells	0.6	$(3\times10^{-8}-1.2)$ cells	day^{-1}	[35].
μ_d	decay rate of immune cells	$\frac{1}{20}$	$\left(\frac{1}{25} - \frac{3}{50}\right)$	day^{-1}	[35].
η	The maximum rate of increase of antibodies.	0.6	0.01- 0.9	day^{-1}	[70].
μ_a	Decay rate of antibodies	0.4	0.01- 0.9	day^{-1}	[70].
α_a	Inhibition rate of immune cells response in infected liver-cells	0.5	0.001- 0.7	day^{-1}	Assumed.
α_0	Efficiency of antibodies in infected red-blood cells	0.6	0.01-0.8	day^{-1}	[59]
α_1	Rate of parasite production by infected red-blood cells is inhibited	0.85	0.1-0.9	day^{-1}	[59]
α_2	The rate of parasite production by infected liver cells is inhibited.	0.55	0.05- 0.9	day^{-1}	Assumed.
f_0	Stimulation constant for immune cells due to infected liver-cells.	1700	1000- 2000	Cells per day	Assumed.
f_1	Stimulation constant for immune cells due to infected red-blood cells.	2000	1000- 3000	Cells per day	[59]
f_2	Stimulation constant for immune cells due to merozoites	1500	500- 2000	Merozoites per day	[77]

5.5.1 The influence of within-human host parameters on between host dynamics

In this section, we explore the influence of within-human host scale parameters on between-host (humans and mosquitoes) scale malaria infection dynamics of (a) population of infected humans (I_H), (b) community gametocyte load (G_H), (c) population of infected mosquitoes (I_V) and (d) community sporozoite load (P_V). Applying the categorization of multiscale models of infectious disease system presented in [3, 7], the coupled multiscale model in (5.4.0.7) is classified as a nested multiscale model of malaria disease dynamics. Hence, the flow of information in uni-directionally linked in that the within-host scale sub-model influences the between-host scale sub-model without any reciprocal feedback. We demonstrate the effects

of key within-human host scale parameters that associated with immune response on between-host scale variables (I_H, G_H, I_V and P_V).

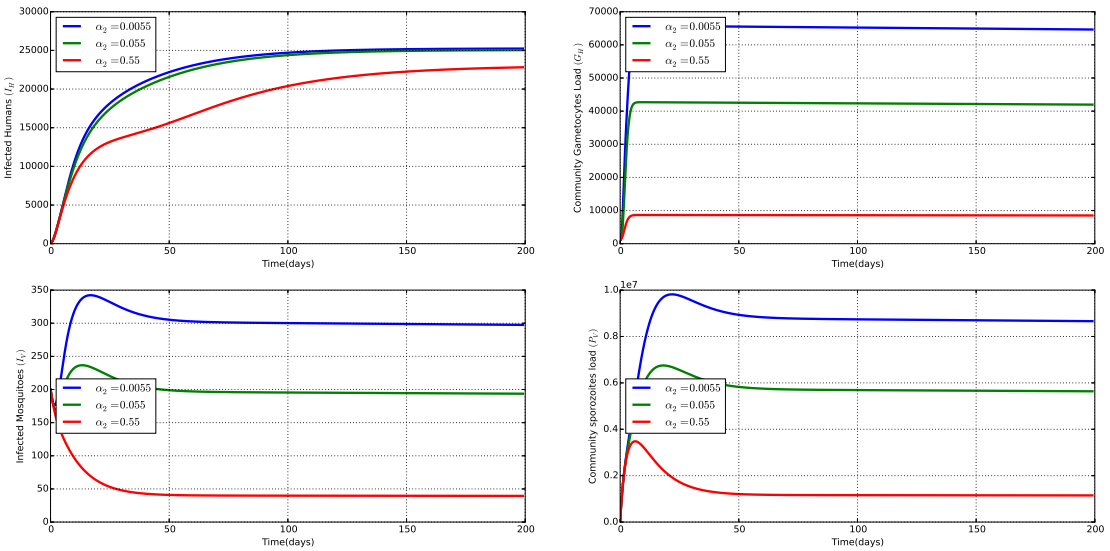

Figure 5.1: Graphs illustrating changes in Infected Humans (I_H), Community gametocytes load (G_H), Infected mosquitoes (I_V) and Community sporozoites load (P_V) for the variation in values of the efficacy of immune cells inhibiting the production of merozoites α_2: $\alpha_2 = 0.0055$, $\alpha_2 = 0.055$ and $\alpha_2 = 0.55$.

In figure (5.1), displays variation of population of infected humans (I_H), community gametocytes load (G_H), population of infected mosquitoes (I_V) and community sporozoites load (P_V) for different values of the efficacy of immune cells inhibiting the production of merozoites (α_2): $\alpha_2 = 0.0055$, $\alpha_2 = 0.055$ and $\alpha_2 = 0.55$. The simulations display that these four between- host scale variables (I_H, G_H, I_V and P_V) are influenced by the within-host scale parameter α_2. The simulation indicates that as the efficacy of immune cells inhibiting the production of merozoites increases, (I_H, G_H, I_V and P_V) also decreases. Hence, health interventions that inhibits merozoites within-human host scale will likely to minimize the transmission of malaria disease dynamics at between-host scale.

Figure (5.2) indicates the time evolution of between-host scale malaria infection dynamics of ((a) population of infected humans I_H, (b) community gametocyte load G_H, (c) population of infected mosquitoes I_V and (d) community sporozoites load P_V) for different values of the supply of immune cells Λ_d: $\Lambda_d = 30$, $\Lambda_d = 60$ and $\Lambda_d = 90$. The simulations indicates that the four between-host scale malaria infection dynamics of ((a) population of infected humans I_H, (b) community gametocyte load G_H, (c) population of infected mosquitoes I_V and (d) community sporozoite load P_V) are influenced by the within-human host scale parameter Λ_d. Hence, we observe that as the supply rate of immune cells increases, the transmission of malaria disease dynamics at between-host scale malaria infection dynamics of (I_H, G_H, I_V and

P_V) also decreases. Therefore, health interventions that promotes the supply of immune cells have the potential to reduce the transmission of malaria disease dynamics at between-host scale.

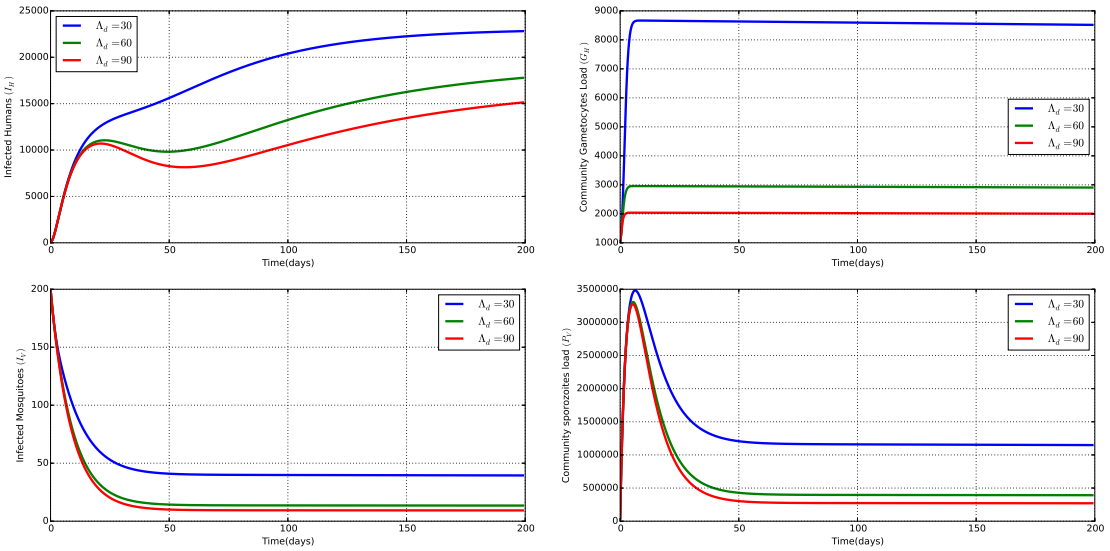

Figure 5.2: Graphs illustrating changes in Infected Humans (I_H), Community gametocytes load (G_H), Infected mosquitoes (I_V) and Community sporozoites load (P_V) for the different values of the supply of immune cells Λ_d: $\Lambda_d = 30$, $\Lambda_d = 60$ and $\Lambda_d = 90$.

Figure (5.3) illustrates the changes in between-host scale for malaria ifction dynamics of ((a) population of infected humans I_H, (b) community gametocyte load G_H, (c) population of infected mosquitoes I_V and (d) community sporozoites load P_V) for different values of the destruction rate of merozoites into red blood cells (θ_b): $\theta_b = 0.003$, $\theta_b = 0.03$ and $\theta_b = 0.3$). The graphs also indicate that the rate of destruction of infected red-blood cells increases, we notice a slightly decrease on between-host scale variables (I_H, G_H, I_V and P_V). The solutions imply that control measures aimed at giving health interventions that kills the infected red-blood cells within-the infected human red-blood cells, which also be good for the community in that they reduce the transmission of malaria disease at between-host scale.

Figure (5.4) displays the numerical solutions of the multiscale model (5.4.0.7) showing the dynamics of (a) population of infected humans I_H, (b) community gametocyte load G_H, (c) population of infected mosquitoes I_V and (d) community sporozoite load P_V for different values of the killing rate of the gametocytes by human immune cellsθ_g: $\theta_g = 0.003$, $\theta_g = 0.03$ and $\theta_g = 0.3$. The numerical results in figure (5.4) indicate that the between-host malaria dynamics of (a) population of infected humans I_H, (b) community gametocyte load G_H, (c) population of mosquitoes I_V and community sporozoites load P_V decrease in respond to the increase of killing rate of gametocytes by immune cells within-infected human.The results desplay that the killing of gametocytes by immune cells on the last life stage of pathogen

life cycle within-infected human has an impact in reducing the transmission of malaria at community level. Hence, any intervention methods that is intendd to kill the gametocytes within infected humans has significant effect on reducing the transmission of malaria infection at community level.

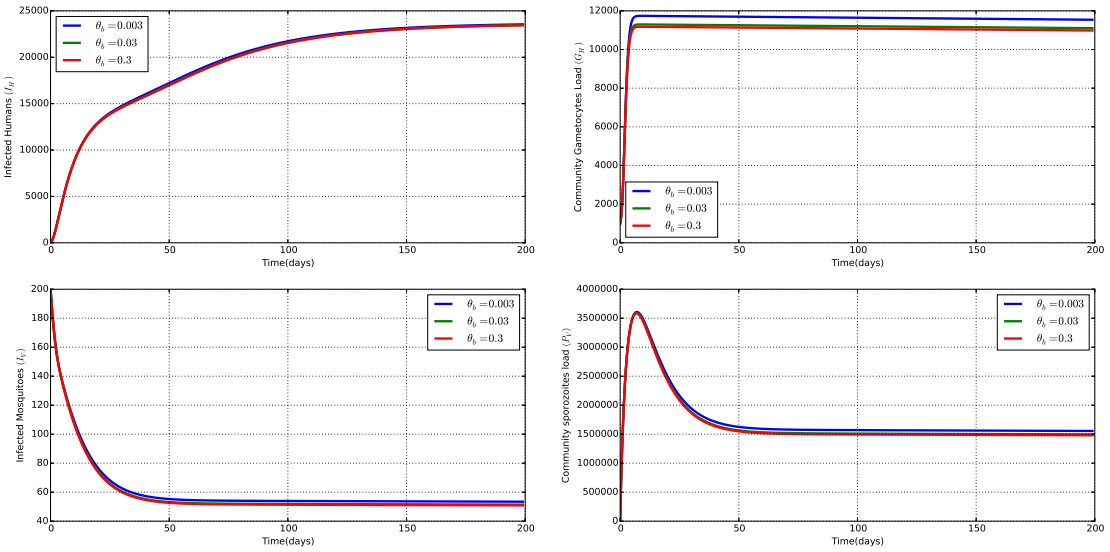

Figure 5.3: Graphs illustrating changes in Infected Humans (I_H), Community gametocytes load (G_H), Infected mosquitoes (I_V) and Community sporozoites load (P_V) for the variation in values of the destruction rate of merozoites into red-blood cells by immune cells θ_b: $\theta_b = 0.003$, $\theta_b = 0.03$ and $\theta_b = 0.3$.

Figure (5.5) displays the numerical solution of the multiscale model (5.4.0.7) showing variation of (a) population of infected humans I_H, (b) community gametocyte load G_H, (c) population of infected mosquitoes I_V and (d) community sporozoite load P_V for different values of the killing rate of sporozoites in liver-cells by human immune cells (θ_l): $\theta_l = 0.01$, $\theta_l = 0.03$ and $\theta_l = 0.06$. From the numerical results in figure (5.5) presents that as the killing rate of sporozoites in the liver cells by human immune cells increase, there is observable reasonable decrease in the transmission of malaria infection on the dynamics of (a) population of infected humans I_V, (b) community gametocytes load G_H, (c) population of infected mosquitoes and (d) community sporozoites load P_V. However, any intervention that kills the sporozoites within-the human liver cells has significant effect in reducing malaria transmission at community level and at also population level.

Figure (5.6) displays the numerical results of multiscale model (5.4.0.7) displaying the variation of (a) population of infected humans I_H, (b) community gametocyte load G_H, (c) population of infected mosquitoes I_V and (d) community sporozoites load P_V for diffent values of killing rate of merozoites by immune cells within-infected human θ_m: $\theta_m = 0.006$, $\theta_m = 0.06$ and $\theta_m = 0.6$. The numerical results in figure (5.6)

present that the between-host scale malaria dynamics of (a) population of infected humans I_H, (b) community gametocyte load G_H, (c) population of infected mosquitoes I_V and (d) community sporozoites load P_V decrease in response to the increase of killing rate of merozoites by human immune cells. This implies that immune response has a significant influence on transmission of malaria infection on population level.

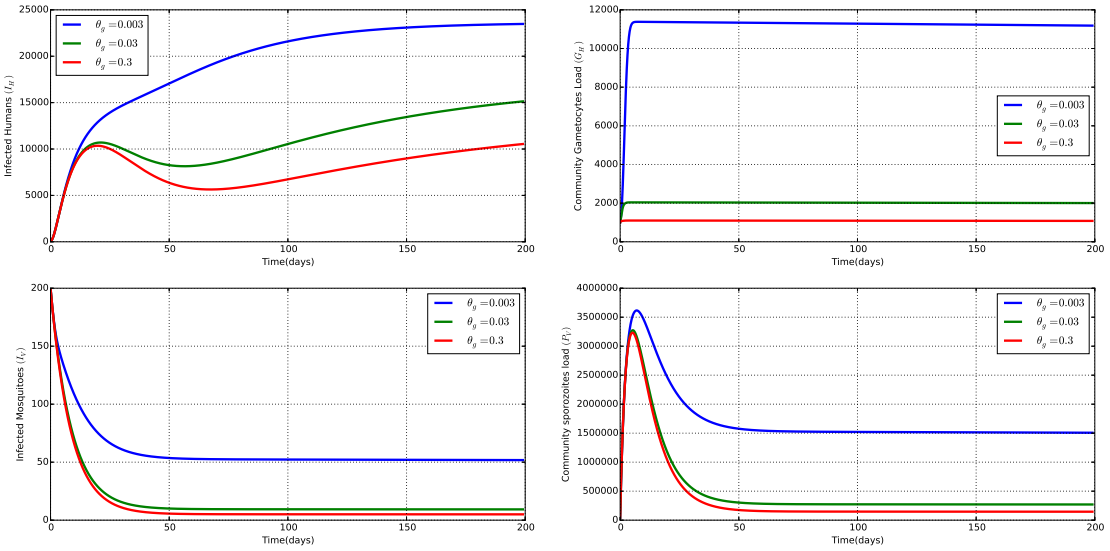

Figure 5.4: Graphs illustrating changes in Infected Humans (I_H), Community gametocytes load (G_H), Infected mosquitoes (I_V) and Community sporozoites load (P_V) for the variation in values of the destruction rate of gametocytes by immune cells θ_g: $\theta_g = 1e-08$, $\theta_g = 0.0003$ and $\theta_g = 0.03$.

Figure (5.7) pictures the numerical results of multiscale model (5.4.0.7) displaying the variation of (a) population of infected humans I_H, (b) community gametocyte load G_H, (c) population of infected mosquitoes I_V and (d) community sporozoites load P_V for different values of the efficacy of antibodies in reducing erythrocytic invasion α_0: $\alpha_0 = 0.01$, $\alpha_0 = 0.6$ and $\alpha_0 = 0.8$. The numerical simulations in figure (5.7) display that the between-host scale malaria dynamics of (a) population of infected humans I_H, (b) community gametocyte load G_H, (c) population of infected mosquitoes I_V and (d) community sporozoites load P_V decrease slightly in response to the increase in the values of the efficacy of antibodies in reducing erythrocytic invasion α_0 at within-infected human. From these analysis we observe that the immune response have significant influence in reducing the transmission of malaria disease dynamics at population level.

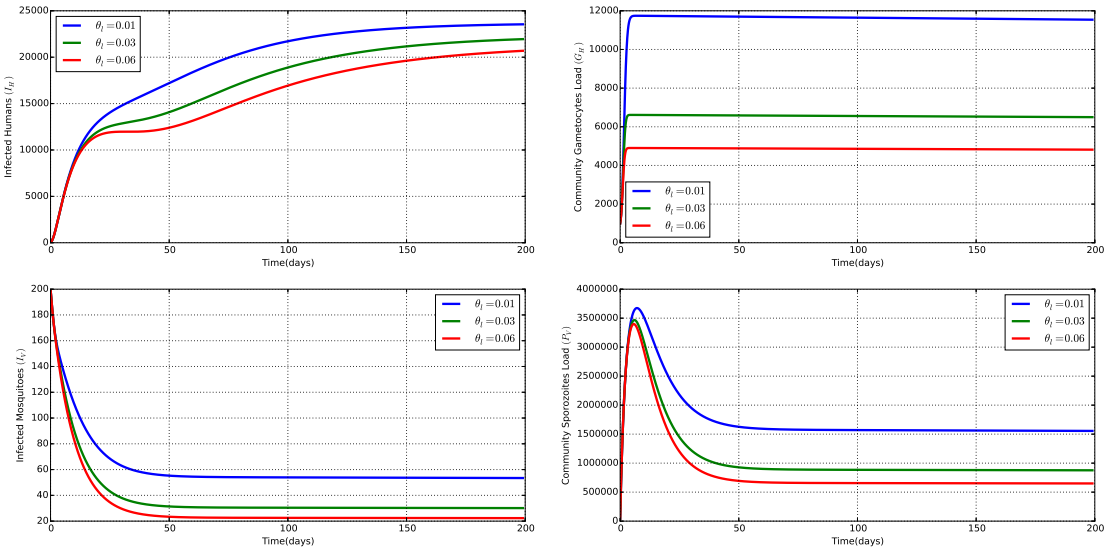

Figure 5.5: Graphs illustrating changes in Infected Humans (I_H), Community gametocytes load (G_H), Infected mosquitoes (I_V) and Community sporozoites load (P_V) for the different values of the destruction rate of sporozoites in liver-cells by immune cells θ_l: $\theta_l = 0.01$, $\theta_l = 0.03$ and $\theta_l = 0.06$.

In summary, the numerical results demonstrated in this chapter on the within-human scale parameters for immune cells are helpfull when considering the vaccination intervention as a way of preventive measures against malaria infection. The preventive health intervention by vaccination of an infectious disease system will help to boost the effectiveness of the immune system on fight against the disease infection which will likely reduce the transmission of the infection to others. This confirms that during malaria transmission dynamics within-host scale has a significant influence on the between-host scale for malaria infection dynamics.

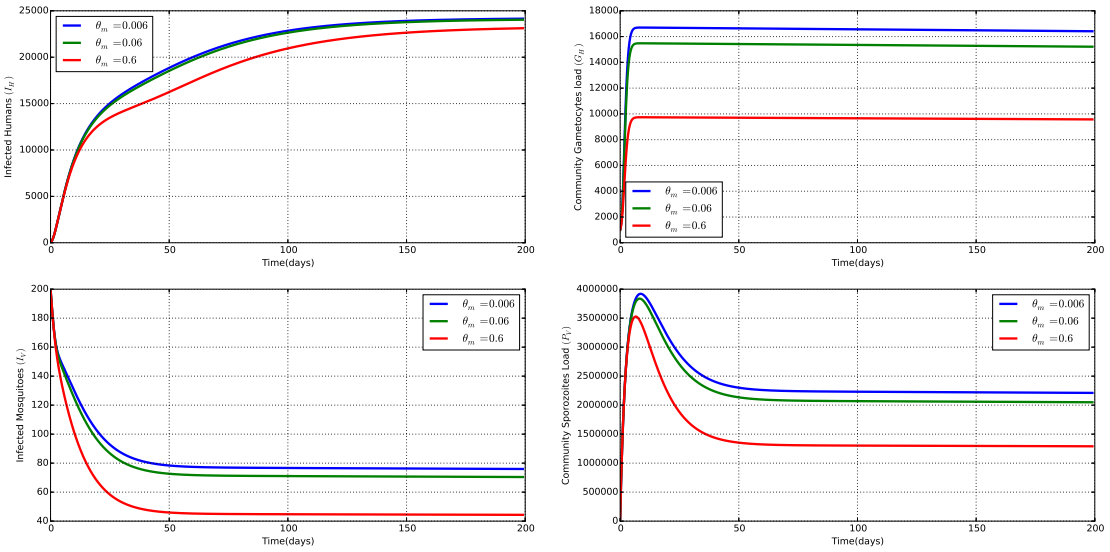

Figure 5.6: Graphs illustrating changes in Infected Humans (I_H), Community gametocytes load (G_H), Infected mosquitoes (I_V) and Community sporozoites load (P_V) for the different values of the destruction rate of merozoites by immune cells θ_m: $\theta_m = 0.006$, $\theta_m = 0.06$ and $\theta_m = 0.6$.

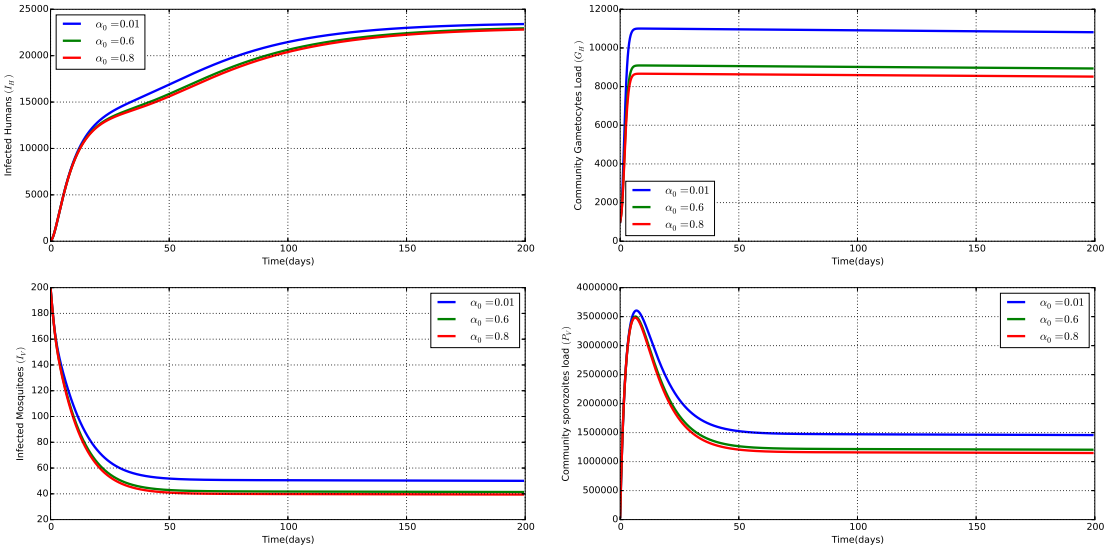

Figure 5.7: Graphs illustrating changes in Infected Humans (I_H), Community gametocytes load (G_H), Infected mosquitoes (I_V) and Community sporozoites load (P_V) for the variation in values of the efficacy of antibodies in reducing erythrocyte invasion α_0: $\alpha_0 = 0.01$, $\alpha_0 = 0.6$ and $\alpha_0 = 0.8$.

5.6 Summary

In this study, we displayed a multiscale model of malaria disease dynamic which is *type II* vector-borne disease, in which pathogen replication cycle is at the within-human host scale and no pathogen replication at the within-mosquito scale. A coupled multiscale model for malaria disease system dynamics was developed utilising the modelling framework. The coupled multiscale model was used to examine the influence of immune response on malaria disease systems at population level. The community pathogen load (community gametocyte load or community sporozoite load) were used to assess the human community-level infectious or mosquito community-level infectious. This community pathogen load were obtained by up-scaling of within-host (human and mosquito) scale infectious to between-host (human and mosquito) scale infectiousness.Our results suggest that malaria disease in the inside-host (human) and at the population level can be controlled by reducing the number of sporozoites in the liver cells and merozoites in the red blood cells. Sporozoites invade the liver cells to release merozoites and the meroroides invade the red blood cells, the replication process in the infected red blood cells continuously produce more merozoites, making the disease more difficult to control. Most available antimalarial drugs work only by slowing down the replication process of merozoites, but the liver will continue to depositing merozoites in the red blood cells. Drugs that directly kill sporozoites, as well as those that delay the development of merozoites, should also be available for treatment to be more effective. We demonstrated the role played by the human immune response in fight against malaria parasite which has an influence at population-level. This study assist in identify the vaccines that boost the human immune response in fight against malaria parasite stages which have an impact on reduction of malaria disease at population-level. The numerical results recommend that the coupled multiscale model of malaria disease system with human immune response can be used to guide the effectiveness control of malaria disease system in the community. We expected that the numerical solutions shown in this work will enlighten in making decisions about malaria disease control, elimination and eradication. This multiscale model for malaria disease in general help in developing strategies for their control, advising disease management, recognising the targets for new drugs and vaccines, and in turn assessing the effect of these medical interventions.

Chapter 6

A Multiscale Model of Malaria Disease Dynamics that incorporate the Effects of Temperature Changes

6.1 Introduction

The malaria disease system is the major public health challenge in most parts of the world. Mosquitoes are vectors that cause malaria transmission and are the main targets of public health interventions. Malaria disease is a *type II* vector-borne disease, where vector-borne diseases are infectious disease systems that caused by infectious agents (viruses, bacteria, protozoa, and helminths), have a complex life cycle, that requiring two hosts (e.g., vertebrate host and host vector). Malaria disease system is transmitted through the blood meal of infectious female mosquitoes called Anopheles. Global warming can significantly have effect on the spread and severity of malaria disease worldwide, especially in mosquito-borne diseases are extremely sensitive to climate change [78]. Even though representing only one source of possible increases in death rates and the rate of disease in a population, changes in the severity and global distribution of vector-borne diseases are believed to represent a significant biological influence of this change.

In this work, we consider the replication-transmission multiscale cycle of the *type II* vector-borne disease system in which there is no pathogen replication cycle on the within-vector host scale and where there is

pathogen replication cycle on the within-human host scale. The multi-scale model of malaria disease system presented in this work is a coupled multi-scale model that has combination of nested multi-scale models on humans and embedded multi-scale models on mosquitoes. Multiscale model of infectious diseases system are complex systems caused by the interaction of three sub-systems that are (i) the host sub-system (i.e human-host subsystem and mosquito-host subsystem), (ii) the pathogenic subsystem and (ii) the environmental subsystem [38]. In general an infectious disease system has seven main levels of organisation which are: the cell level, the tissue level, the organ level, the micro-ecosystem level, the host level, the community level, and the macro-ecosystem level, with each level reduced into two adjacent scales, that is, the cell level as the lowest organisational level that is decomposed into two adjacent scales which are within-cell scale and between-cell scale and the macro-ecosystem level as the highest level of organisation and that is decomposed into the within-macro-ecosystem scale and the between- macro-ecosystem scale. The pathogen subsystem consists of two main levels of organisation, where each level is being the same as a scale, namely, single pathogen species/strain level/scale and the multiple pathogen species/strains level/scale. The environmental subsystem consists of a main level of organisation which is the environmental level that can be decomposed into two limiting scales which are (a) the micro-environmental scale which is the inside-host environmental scale (i.e. the biological environment), and (b) the macro-environmental scale which is the outside-host environmental scale (geographical environment) [7]. This work consists of two hosts subsystems (mosquitoes and humans), single pathogen species/strain level/scale and utilises the inside-host environment as the environmental subsystem.

The main objective of this chapter is to investigate the influence of climate changes effect on the multi-scale model for malaria disease system. This study examines the influence of environmental changes on the mosquito life cycle and the growth of the malaria parasite at the individual level, and the transmission of malaria at the population level. Environmental change system is a type of functionally organised complex system that consists of two main levels/scales [38] which are:

(i) The micro-environmental change level/scale which takes place at the inside-host environment, which includes the use of drugs, immune response, etc.

(ii) Macro-environmental change level/scale that occurs at the outside-host environmental scale and the factors influences the infectious disease system are (a) caused by a naturally induced mechanism or (b) caused by human-induced mechanisms [7, 38]. These can influence the presence and growth of populations, survival and reproductive capacity of vectors and pathogens on a macro-environmental scale [38]. Examples of macro-environmental scales are as follows: temperature, rainfall, humidity, population growth, extreme weather events, natural disasters, climate change, agriculture, etc. This work is on macro-environmental change level/scale where we evaluate the impact of temperature changes on malaria disease systems.

A considerable amount of literature has been published on mathematical modelling on the effect of weather and climate changes on malaria transmission, focusing primarily on temperature and precipitation and how anthropogenic climate changes could influence the (potential) burden of the illness and these models are on transmission mechanism theory [39, 78–80]. Climate changes are expected to influence malaria disease system because the vector and parasite have a life cycle that is highly dependent on temperature and rainfall. Anthropogenic climate change can alter the (potential) distribution of malaria diseases, which has been central to many mechanistic (or process-based) models of malaria transmission.

In other studies on replication-transmission multiscale cycle of infectious disease system, the mosquito life cycle is generally ignored because eggs, larvae, and pupae are not directly involved in the transmission cycle [24, 35]. The mosquito life cycle is a useful simplification of the system, but the results of these models unfortunately cannot predict the intensity of malaria in most endemic areas. There are some mathematical models on transmission mechanism theory that focus on mosquito populations and/or the impact of environmental managers, such as temperature and precipitation. From these mathematical models, those that include temperature predict a spike in vector abundance at higher temperatures than those observed in combination with malaria transmission in the field. The influences of temperature on the mosquito life cycle and malaria parasite development have been recognized for many years but are rarely used in multiscale models to predict parasite growth and malaria transmission. The multiscale model for evaluating the influences of temperature change on malaria disease consists of several related systems: the climate system, the malaria system (which is divided between the human host sub-system and mosquito-host sub-system), and the impact system [81].

In this study, we develop a multiscale model of the malaria disease system that begins with the complex nonlinear temperature relationships that exist throughout the mosquito life cycle, as well as the growth of parasites and transmission of the malaria disease between two hosts (human and mosquito). The multiscale model of malaria disease dynamics with two hosts, which are human host and mosquito host, where mosquitoes are formulated in a similar fashion but rely on two compartments: one for the aqueous phases of mosquitoes (eggs, larvae and pupae) and one for the terrestrial (adult) mosquito stages, which consists of parasite growth on within-mosquito host scale and the malaria transmission on between-mosquito host scale. Temperature is included in all stages of development, spawning and mortality. Temperature affects the potential for malaria transmission in the mosquito population at population-level and the growth of the parasite at individual-level.

6.2 Mathematical Model

The aim of this study is to use the concept of two potential impacts of temperature change that does have influence in malaria growth and transmission, using ordinary non-linear differential equations. We are developing a multiple model of human dynamics (within-human host and between-human host scales)

and mosquito dynamics (or within-mosquito host and between-mosquito host scales) for malaria disease systems. We consider the conditions of the parasite to depend on the temperature and not the life cycle of the mosquito. This study incorporates the juvenile stage of the mosquito into malaria growth and transmission dynamics which is highly dependent on the surrounding environmental conditions.

In developing a framework for understanding the influence of temperature on malaria dynamics, a deterministic transmission model is developed. We present a multiscale model based on monitoring the dynamics of between-mosquito host model at slow-time scale (t), where the mosquito is divided into immature mosquito i.e. the juvenile mosquito $(L_M(t))$ and adult mosquito population of which are susceptible mosquitoes $(S_V(t))$, infected mosquitoes $(I_V(t))$ and community sporozoites load $(P_V(t))$, within-mosquito host dynamics at slow-time scale (t), which are population of erythrocyte gametocytes within-infected mosquito $(G_v(t))$, population of gametes $(G_m(t))$, population of zygotes $(Z_v(t))$, population of oocysts $(O_v(t))$ and population of sporozoites $(P_v(t))$. The dynamics of between-host scale are modelled at slow-time scale t, which are: susceptible humans $(S_H(t))$, infected humans $(I_H(t))$ and community gametocytes load $(G_{H(t)})$ and within-human host dynamics are modelled at fast-time scale (s), which are uninfected red-blood cells $(R_h(s))$, infected red-blood cells $(R_m(s))$, population of merozoites $(M_h(s))$ and population of gametocytes $(G_h(s))$. The total mosquito population is given by $N_V(t) = S_V(t) + I_V(t)$ and the total human populations is given by $N_H(t) = S_H(t) + I_H(t)$. The rate of infection of a susceptible humans is dependent on the mosquito's biting rate $a(T)$ and the proportion of bites by infected mosquitoes on susceptible humans that produce infection b_H. Blood meal taken by an infectious female anopheles mosquito on a susceptible human will cause sporozoites to be injected into the human bloodstream and will be carried to the liver stage.

The female Anopheles mosquitoes rest for a few days after taking blood meal from the human host. The mosquito digests blood and develops eggs, the process of which depends on temperature. The dynamics of juvenile mosquitoes $(L_M(t))$ increase through the logistic growth rate for immature mosquitoes and is represented by $\Lambda_L(T)\left(1 - \frac{L_M(t)}{K}\right) N_V(t)$ where k is the carrying capacity and $\Lambda_L(T)$ is the deposition rate for susceptible and infected mosquitoes [79]. The dynamics of juvenile mosquito is decrease through the temperature dependent natural decay at a rate $\mu_L(T)\left(1 - \frac{L_M(t)}{K}\right) L_M(t)$, through temperature dependent maturation at a rate $\alpha_L(T)$ and death rate due to other things (δ_L). The single compartment $L_M(t)$ represents the three aquatic stages of mosquitoes, i.e., egg, larva, and pupa.

The susceptible mosquitoes $S_V(t)$ increase through the development of juvenile mosquitoes to adult mosquitoes at rate $\alpha_L(T)$. The susceptible mosquitoes decrease either through temperature dependent natural decay at a rate $\mu_V(T)$ or through malaria infection by humans at rate $\frac{\beta_H(T)G_H(t)}{G_0 + G_H(t)}$, where $\beta_H(T)$ is temperature dependent contact rate of susceptible mosquitoes with infected humans and G_0 is the half saturation constant associated with the infection of mosquitoes. The third equation of model (6.2.1.12)

demonstrates the dynamics of infected mosquitoes $(I_H(t))$. The infected mosquitoes increase through the infection of susceptible mosquitoes and decrease either through natural decay at a rate $\mu_V(T)$ or through malaria induced death rate δ_V.

The fourth equation in the model (6.2.1.12) describes the dynamics of erythrocytic gametocytes within-infected mosquitoes $(G_v(t))$. $G_v(t)$ is the first life stage of the pathogen at within-mosquito scale. The first -life stage increase through super-infection at a rate $\lambda_h(T)S_v = \dfrac{\beta_H(T)G_H(t)(S_V(t)-1)}{(G_0+G_H(t))\phi_V(I_V(t)+1)}$, which is the down-scaling of pathogen from between-host scale to within-mosqito scale. $G_v(t)$decrease either through natural decay at a rate μ_g or through proceed to the first intermediate life stage at rate α_g. α_g is the rate at which gametocytes within-infected mosquito burst releasing sex cells called gametes (either male or female). The fifth equation in model (6.2.1.12) models the dynamics of population of gametes $(G_m(t))$. $G_m(t)$ is the first intermediate life stage at within-mosquito scale. The first intermmediate life stage increase by $N_g\alpha_g G_v(t)$, where we assume that for every bursting gametocytes within an infected mosquito, it releases han average of N_g gametes upon bursting. The gametes population decrease either through natural decay at rate μ_s or at rate α_s, where gametes get depleted through male and female gametes fusing to form zygotes which is the second intermediate life stage.

The second intermediate life-stage for within-infected mosquito is represented by the population of zygotes $(Z_v(t))$. $Z_v(t)$ increase through the developmental processes done by gametes to mature and pair-up and fuse to form zygotes at a rate $\dfrac{\alpha_s}{2}G_m(t)$. The population of zygotes decrease either through natural decay at a rate μ_z or through the progression of zygote into oocysts at a rate α_z. The last intermediate life stage at within-infected mosquito scale is given by O_v, which is the population of oocysts. The population of oocysts increase through the progression from zygotes into ookinetes to become oocusts at $\alpha_z Z_v(t)$. The last intermediate life stage decrease either through natural decay at a rate μ_k or through the progression to sporozoites population at a rate α_k, which is the bursting of oocysts to release sporozoites.

The last life-stage on within-mosquito scale is given by P_v, which is the population of sporozoites. $P_v(t)$ increase by $N_k\alpha_k O_v(t)$, where each oocyst bursts at a rate of α_k to producing an average of N_k sporozoites upon bursting. The last life stage of within-infected mosquito scale decrease either through natural decay or through the excretion/shedding of mature sporozoites the the community sporozoity load at α_v.

The ninth equation in system (6.2.1.12) describes the dynamics of community sporozoites load (P_V). The community sporozoites load increase through up-scaling of individual excretion/shedding of pathogen which is modelled by $P_v(t)\alpha_v(I_V(t)+1)$. The influence of within-mosquito scale on between-mosquito scale through pathogen shedding/excretion can be modelled by up-scaling individual host excretion/shedding of the pathogen from within-mosquito scale at a rate $\alpha_v P_v(t)$ to between-mosquito scale [11, 24].

The tenth equation of system (6.2.1.12) describe the rate of change in time, of the susceptible human population $(S_H(t))$. The $S_H(t)$ increase through supply rate/ birth at a constant rate Λ_H and the number of infected individual humans who recovered from malaria infection and join the susceptible human class at a rate γ_H. Susceptible humans decreases due to natural death at a rate μ_H and through infection susceptible humans at a rate $\lambda_V(T) = \dfrac{\beta_V(T)P_V}{P_0 + P_V}$, with temperature dependent parameter $\beta_V(T)$ being the contact rate of susceptible humans with the infectious reservoir of mosquitoes and P_0 is the half saturation constants associated with the infection of humans. The eleventh equation in system (6.2.1.12) describes the changes in time of the population of infected humans $(I_H(t))$. Infected humans increase through the infection of susceptible humans and proceed to infected class at a constant rate $\lambda_V(t)$. The population of infected human class reduces due to natural death at a rate μ_H, or through disease induced death at a rate δ_H or through the recovered of infected humans to join the $S_H(t)$ at a rate γ_H.

The last equation of system (6.2.1.12) describes the dynamics of community gametocytes load $(G_H(t))$. Community gametocytes load increase through shedding/excretion of the pathogen from within-infected human to between-host scale modelled by $N_h\alpha_h I_H(t)$. α_h is the excretion/shedding rate of last-life stage of within-infected human into the layer of the skin and N_h is the average number of within-infected human gametocytes pathogen load excreted into the layer of each infected individuals [18, 24]. $N_h\alpha_h$ used to links the within-human scale to between-host scale. The community gametocytes load decreases through decay at a constant rate α_H.

We adapt the method used in [24] to demonstrate the dynamics of within-host scales and also the linking method applied to couple the within-host scale and between host scale.

$$
\begin{aligned}
1.\quad \frac{dL_M(t)}{dt} &= [\Lambda_L(T)N_V(t) - \mu_L(T)L_M(t)]\left(1 - \frac{L_M(t)}{K}\right) - (\alpha_L(T) + \delta_L)L_M(t),\\
2.\quad \frac{dS_V(t)}{dt} &= \Lambda_V(T) - \frac{\beta_H(T)G_H(t)S_V(t)}{G_0 + G_H(t)} - \mu_V(T)S_V(t),\\
3.\quad \frac{dI_V(t)}{dt} &= \frac{\beta_H(T)G_H(t)S_V(t)}{G_0 + G_H(t)} - (\mu_V(T) + \delta_V)I_V(t),\\
4.\quad \frac{dG_v(t)}{dt} &= \frac{\beta_H(T)G_H(t)(S_V(t) - 1)}{(G_0 + G_H(t))\phi_V(I_V(t) + 1)} - [\alpha_g + \mu_g]\, G_v(t),\\
5.\quad \frac{dG_m(t)}{dt} &= N_g\alpha_g G_v(t) - [\alpha_s + \mu_s]\, G_m(t),\\
6.\quad \frac{dZ_v(t)}{dt} &= \frac{1}{2}\alpha_s G_m(t) - [\alpha_z + \mu_z]\, Z_v(t),\\
7.\quad \frac{dO_v(t)}{dt} &= \alpha_z Z_v(t) - [\alpha_k + \mu_k]\, O_v(t),\\
8.\quad \frac{dP_v(t)}{dt} &= N_k\alpha_k O_v(t) - [\alpha_v + \mu_v]\, P_v(t),\\
9.\quad \frac{dP_V(t)}{dt} &= P_v(t)\alpha_v(I_V(t) + 1) - \alpha_V P_V(t),\\
10.\quad \frac{dS_H(t)}{dt} &= \Lambda_H - \frac{\beta_V(T)P_V(t)S_H(t)}{P_0 + P_V(t)} - \mu_H S_H(t) + \gamma_H I_H(t),\\
11.\quad \frac{dI_H(t)}{dt} &= \frac{\beta_V(T)P_V(t)S_H(t)}{P_0 + P_V(t)} - (\mu_H + \gamma_H + \delta_H)I_H(t),\\
12.\quad \frac{dR_h(s)}{ds} &= \Lambda_h - \beta_h R_h(s)M_h(s) - \mu_b R_h(s),\\
13.\quad \frac{dR_m(s)}{ds} &= (1 - \pi)\beta_h R_h(s)M_h(s) - \alpha_m R_m(s),\\
14.\quad \frac{dM_h(s)}{ds} &= N_m\alpha_m R_m(s) - \mu_m M_h(s),\\
15.\quad \frac{dG_h(s)}{ds} &= \pi\beta_h R_h(s)M_h(s) - (\alpha_h + \mu_h)G_h(s),\\
16.\quad \frac{dG_H(t)}{dt} &= G_h(s)\alpha_h I_H(t) - \alpha_H G_H(t),
\end{aligned}
\tag{6.2.0.1}
$$

where

$$\Lambda_V(T) = \frac{\alpha_L(T)L_M(t)}{2}.$$

6.2.1 Analysis of the multi-scale model using fast-slow time-scale analysis

We observe from the embedded multi-scale model of system (6.2.0.1) that at mosquito-host level has same time scales which involved the between-mosquito host time scale (t) which associated with transmission at the population-level and the within-mosquito host time scale (t) associated with the growth of sporozoites population at the individual-level. We also note from the nested multi-scale model system (6.2.0.1) that at human host level, has different time scale which are the between-human host time scale (t) which associated with the transmission of malaria disease system and within-human host time scale (s) which

associated with the replication of merozoites at an individual level. The analysis of the multi-scale model system (6.2.0.1) and can be simplified by expressing the slow-time scale and fast time scale in terms of each other by using the form $t = \epsilon s$ such that the within-human-malaria disease dynamics can be written in the from of slow time scale as follows:

6.2.1.1 Within-human malaria parasite population model

The within-host scale model is given by following ordinary differential equations

$$\begin{aligned}
1. \quad \epsilon\frac{dR_h(t)}{dt} &= \Lambda_h - \beta_h R_h(t) M_h(t) - \mu_b R_h(t), \\
2. \quad \epsilon\frac{dR_m(t)}{dt} &= (1-\pi)\beta_h R_h(t) M_h(t) - \alpha_m R_m(t), \\
3. \quad \epsilon\frac{dM_h(t)}{dt} &= N_m \alpha_m R_m(t) - \mu_m M_h(t), \\
4. \quad \epsilon\frac{dG_h(t)}{dt} &= \pi\beta_h R_h(t) M_h(t) - (\alpha_h + \mu_h) G_h(t),
\end{aligned} \tag{6.2.1.1}$$

where ϵ is a small constant number that is $0 < \epsilon \ll 1$ which highlights the fast time scale of the within-human host sub-model compared to the slow time scale of the between-host transmission sub-model [14, 24].

We use the next generation operator approach to obtain the basic reproductive number of the within-human host model (6.2.1.1). The model (6.2.1.1) can be written in the form

$$\begin{aligned}
\frac{dX}{dt} &= f(X, Y, Z), \\
\frac{dY}{dt} &= g(X, Y, Z), \\
\frac{DZ}{dt} &= h(X, Y, Z),
\end{aligned}$$

where

$$\begin{aligned}
X &= (R_h), \\
Y &= (R_m, G_h), \\
Z &= (M_h).
\end{aligned} \tag{6.2.1.2}$$

We define $\widetilde{g}(X^*, Z)$ by

$$\begin{aligned}
g_1(X^*, Z) &= R_m = \frac{(1-\pi)\beta_h R_h M_h}{\alpha_m}, \\
g_2(X^*, Z) &= G_h = \frac{\pi\beta_h R_h M_h}{\alpha_h + \mu_h}.
\end{aligned} \tag{6.2.1.3}$$

By substituting the values of R_m and G_h and letting $h_1 = \frac{dM_h}{dt}$ we obtain

$$h_1 = \frac{dM_h}{dt} = N_m \alpha_m R_m - \mu_m M_h,$$

therefore

$$\begin{aligned} h_1 &= \frac{(1-\pi) N_m \alpha_m \beta_h \Lambda_h M_h}{\alpha_m \mu_b} - \mu_m M_h, \\ A &= \frac{\partial h_1}{\partial M_h} = \frac{(1-\pi) N_m \alpha_m \beta_h \Lambda_h}{\alpha_m \mu_b} - \mu_m, \end{aligned} \tag{6.2.1.4}$$

where

$$\begin{aligned} A &= M - D, \\ M &= \frac{(1-\pi) N_m \alpha_m \beta_h \Lambda_h}{\alpha_m \mu_b}, \\ D &= \mu_m, \\ D^{-1} &= \frac{1}{\mu_m}, \\ MD^{-1} &= \frac{(1-\pi) N_m \alpha_m \beta_h \Lambda_h}{\alpha_m \mu_b \mu_m}. \end{aligned} \tag{6.2.1.5}$$

Therefore $\Re_0 = \rho(MD^{-1})$, the reproductive number is given by

$$\Re_0 = \frac{(1-\pi) N_m \beta_h \Lambda_h}{\mu_b \mu_m}. \tag{6.2.1.6}$$

The basic reproductive number number ($\Re_0$) of the within-human host submodel measures the total number of secondary infected red blood cells (IRBCs) produced by primary IRBCs in a host at the beginning of the infection.

Since $0 < \epsilon \ll$, we let $\epsilon = 0$ so that the within-human host sub-model becomes independent of time and which is given by:

$$\begin{aligned} \Lambda_h - \beta_h \overline{R_h M_h} - \mu_b \overline{R_h} &= 0, \\ (1-\pi)\beta_h \overline{R_h M_h} - \alpha_m \overline{R_m} &= 0, \\ N_m \alpha_m \overline{R_m} - \mu_m \overline{M_h} &= 0, \\ \pi \beta_h \overline{R_h M_h} - \alpha_h \overline{G_h} &= 0. \end{aligned} \tag{6.2.1.7}$$

The disease free equilibrium point of the within-human scale model, where there is no pathogen exists to infect the inside-host environment (human-host). The D.F.E is given by

$$\begin{aligned} E_0 &= \left(R_h^0, R_m^0, M_h^0, G_h^0\right), \\ &= \left(\frac{\Lambda_h}{\mu_b}, 0, 0, 0\right). \end{aligned} \tag{6.2.1.8}$$

The endemic equilibrium point of the within-human scale model, where the pathogen exists to infect the inside-host environment. The endemic equilibrium point is given by

$$E_1 = (\overline{R_h}, \overline{R_m}, \overline{M_h}, \overline{G_h}), \tag{6.2.1.9}$$

where

$$\begin{aligned} \overline{R_h} &= \frac{\Lambda_h}{\mu_b \Re_0}, \\ \overline{R_m} &= \frac{\mu_m \mu_b}{\beta_h N_m \alpha_m}(\Re_0 - 1), \\ \overline{M_h} &= \frac{\mu_b}{\beta_h}(\Re_0 - 1), \\ \overline{G_h} &= \frac{\pi \Lambda_h}{\Re_0(\alpha_h + \mu_h)}(\Re_0 - 1), \end{aligned} \tag{6.2.1.10}$$

where

$$\Re_0 = \frac{(1-\pi) N_m \beta_h \Lambda_h}{\mu_b \mu_m}. \tag{6.2.1.11}$$

The within-human host sub-model has a unique positive endemic equilibrium point when $\Re_0 > 1$ and no positive equilibrium point when $\Re_0 < 1$.

We note that from the multiscale model (6.2.0.1), the total number of gametocytes shed/excreted by each infected human in the environment (community gamocytes load) $N_h I_H$ is now approximated by $\overline{G}_h I_H$. Application of the notation $N_h = \overline{G}_h$, which is the average number of the within-human host scale of the gamotocytes load (G_h) at the endemic equilibrium point is available for shedding/excretion into the community gametocyte load by each infected human. The multi-scale model (6.2.0.1) of the malaria disease system has been simplified to:

$$
\begin{aligned}
1.\quad \frac{dL_M(t)}{dt} &= [\Lambda_L(T)N_V(t) - \mu_L(T)L_M(t)]\left(1 - \frac{L_M(t)}{K}\right) - (\alpha_L(T) + \delta_L)L_M(t),\\
2.\quad \frac{dS_V(t)}{dt} &= \Lambda_V(T) - \frac{\beta_H(T)G_H(t)}{G_0 + G_H(t)}S_V(t) - \mu_V(T)S_V(t),\\
3.\quad \frac{dI_V(t)}{dt} &= \frac{\beta_H(T)G_H(t)}{G_0 + G_H(t)}S_V(t) - [\mu_V(T) + \delta_V]\, I_V(t),\\
4.\quad \frac{dG_v(t)}{dt} &= \frac{\beta_H(T)G_H(t)(S_V(t) - 1)}{(G_0 + G_H(t))\phi_V(I_V(t) + 1)} - [\alpha_g + \mu_g]\, G_v(t),\\
5.\quad \frac{dG_m(t)}{dt} &= N_g\alpha_g G_v(t) - [\alpha_s + \mu_s]\, G_m(t),\\
6.\quad \frac{dZ_v(t)}{dt} &= \frac{1}{2}\alpha_s G_m(t) - [\alpha_z + \mu_z]\, Z_v(t),\\
7.\quad \frac{dO_v(t)}{dt} &= \alpha_z Z_v(t) - [\alpha_k + \mu_k]\, O_v(t),\\
8.\quad \frac{dP_v(t)}{dt} &= N_k\alpha_k O_v(t) - [\alpha_v + \mu_v]\, P_v(t).\\
9.\quad \frac{dP_V(t)}{dt} &= P_v(t)\alpha_v\,(I_V(t) + 1) - \alpha_V P_V(t),\\
10.\quad \frac{dS_H(t)}{dt} &= \Lambda_H - \frac{\beta_V(T)P_V(t)}{P_0 + P_V(t)}S_H(t) - \mu_H S_H(t) + \gamma_H I_H(t),\\
11.\quad \frac{dI_H(t)}{dt} &= \frac{\beta_V(T)P_V(t)}{P_0 + P_V(t)}S_H(t) - [\mu_H + \gamma_H + \delta_H]\, I_H(t),\\
12.\quad \frac{dG_H(t)}{dt} &= N_h\alpha_h I_H(t) - \alpha_H G_H(t),
\end{aligned}
\tag{6.2.1.12}
$$

where

$$
\begin{aligned}
\Lambda_V(T) &= \frac{\alpha_L(T)L_M(t)}{2},\\
N_h &= G_h^* = \frac{\pi}{(1-\pi)}\left[\frac{(1-\pi)N_m\beta_h\Lambda_h - \mu_b\mu_m}{N_m\beta_h(\alpha_h + \mu_h)}\right] = \frac{\pi\Lambda_h}{(\alpha_h + \mu_h)\Re_0}\left[\Re_0 - 1\right],\\
\Re_0 &= \frac{(1-\pi)N_m\beta_h\Lambda_h}{\mu_b\mu_m}.
\end{aligned}
\tag{6.2.1.13}
$$

N_h is the average number of the within-human host scale for malaria causing gametocytes load (at the within-human host endemic equilibrium) shed/excrete into the between-host scale by each infected humans. $\Re_0$ is the reproductive number of the within an infected human.

6.2.2 Feasible region of the coupled multiscale model

We now consider that all parameters and state variables for multiscale model (6.2.1.12) are assumed to be positive to be consistent with human (within-human and between-human scales) and mosquito juvenile and adult (within-mosquito and between-mosquito scales).

We consider $N_H(t)$ denote the total number of humans, whereby $N_H(t) = S_H(t) + I_H(t)$. Therefore

$$\begin{aligned}\frac{dN_H(t)}{dt} &= \Lambda_H - \mu_H(S_H(t) + I_H) - \delta_H I_H, \\ &= \Lambda_H - \mu_H N_H - \delta_H I_H, \\ &\leq \Lambda_H - \mu_H N_H.\end{aligned} \tag{6.2.2.1}$$

This implies that

$$\lim_{t\longrightarrow\infty} \sup(N_H(t)) \leq \frac{\Lambda_H}{\mu_H}. \tag{6.2.2.2}$$

It also implies that

$$L_M \leq \frac{K[\Lambda_L(T)\alpha_L(T) - 2\mu_V(T)(\mu_L(T) + \alpha_L(T) + \delta_L)]}{\Lambda_L(T)\alpha_L(T) - 2\mu_L(T)\mu_V(T)}. \tag{6.2.2.3}$$

We let $N_V(t)$ denote the total number of mosquitoes, such that $N_V(t) = S_V(t) + I_V(t)$. Therefore

$$\begin{aligned}\frac{dN_V(t)}{dt} &= \Lambda_V(T) - \mu_V(T)(S_V(t) + I_V(t)) - \delta_V I_V(t) \\ &= \frac{\alpha_L(T)L_M(t)}{2} - \mu_V(T)N_V - \delta_V I_V(t) \\ &\leq \frac{\alpha_L(T)L_M(t)}{2} - \mu_V(T)N_V.\end{aligned} \tag{6.2.2.4}$$

It implies that

$$\begin{aligned}\lim_{t\longrightarrow\infty} \sup(N_V(t)) &\leq \frac{\alpha_L(T)L_M(t)}{2\mu_V(T)}, \\ N_V(t) &\leq \frac{\alpha_L(T)}{2\mu_V(T)} \frac{K[\Lambda_L(T)\alpha_L(T) - 2\mu_V(T)(\mu_L(T) + \alpha_L(T) + \delta_L)]}{\Lambda_L(T)\alpha_L(T) - 2\mu_L(T)\mu_V(T)}.\end{aligned} \tag{6.2.2.5}$$

6.2.3 The disease free equilibrium state for coupled multiscale model

At disease-free eduilibrium (DFE) there is no infection. Thus, no pathogen exists to infect the mosquito-hosts and also the human-hosts.

$$E_{00} = (L_M^{00}, S_V^{00}, I_V^{00}, G_v^{00}, G_m^{00}, Z_v^{00}, O_v^{00}, P_v^{00}, P_V^{00}, S_H^{00}, I_H^{00}, G_H^{00}), \tag{6.2.3.1}$$

where

$$\begin{aligned}L_M^{00} &= \frac{K[\Lambda_L(T)\alpha_L(T) - 2\mu_V(T)(\mu_L(T) + \alpha_L(T) + \delta_L)]}{\Lambda_L(T)\alpha_L(T) - 2\mu_L(T)\mu_V(T)}, \\ S_V^{00} &= \frac{\Lambda_V(T)}{\mu_V(T)} = \frac{\alpha_L(T)}{2\mu_V(T)} \frac{K[\Lambda_L(T)\alpha_L(T) - 2\mu_V(T)(\mu_L(T) + \alpha_L(T) + \delta_L)]}{\Lambda_L(T)\alpha_L(T) - 2\mu_L(T)\mu_V(T)}, \\ S_H^{00} &= \frac{\Lambda_H}{\mu_H}, \\ I_V^{00} &= G_v^{00} = G_m^{00} = Z_v^{00} = O_v^{00} = P_v^{00} = P_V^{00} = I_H^{00} = G_H^{00} = 0.\end{aligned} \tag{6.2.3.2}$$

6.2.4 The reproductive number of coupled multiscale model

We use next-generation operator approach to compute the basic reproductive number and we use the [61]'s approach. The systems of equations (6.2.1.12) can be written in the form

$$\begin{aligned} \frac{dX}{dt} &= f(X,Y,Z), \\ \frac{dY}{dt} &= g(X,Y,Z), \\ \frac{dZ}{dt} &= h(X,Y,Z), \end{aligned} \tag{6.2.4.1}$$

where

$$\begin{aligned} X &= (L_M, S_V, S_H) \\ Y &= (I_V, G_v, G_m, Z_v, O_v, P_v, I_H), \\ Z &= (P_V, G_H). \end{aligned} \tag{6.2.4.2}$$

We denote $\widetilde{g}(X^*, Z)$ by

$$\begin{aligned} \widetilde{g}_1(X^*,Z) &= I_V = \frac{\beta_H(T) S_V G_H}{(\mu_V(T)+\delta_V)(G_0+G_H)}, \\ \widetilde{g}_2(X^*,Z) &= G_v = \frac{1}{\alpha_g+\mu_g}\frac{\beta_H(T) G_H(S_V-1)}{(G_0+G_H)\phi_V(I_V+1)}, \\ \widetilde{g}_3(X^*,Z) &= G_m = \frac{N_g\alpha_g}{\alpha_g+\mu_g}\frac{1}{\alpha_s+\mu_s}\frac{\beta_H(T) G_H(S_V-1)}{(G_0+G_H)\phi_V(I_V+1)}, \\ \widetilde{g}_4(X^*,Z) &= Z_v = \frac{1}{2}\frac{N_g\alpha_g}{\alpha_g+\mu_g}\frac{\alpha_s}{\alpha_s+\mu_s}\frac{1}{\alpha_z+\mu_z}\frac{\beta_H(T) G_H(S_V-1)}{(G_0+G_H)\phi_V(I_V+1)}, \\ \widetilde{g}_5(X^*,Z) &= O_v = \frac{1}{2}\frac{N_g\alpha_g}{\alpha_g+\mu_g}\frac{\alpha_s}{\alpha_s+\mu_s}\frac{\alpha_z}{\alpha_z+\mu_z}\frac{1}{\alpha_k+\mu_k}\frac{\beta_H(T) G_H(S_V-1)}{(G_0+G_H)\phi_V(I_V+1)}, \\ \widetilde{g}_6(X^*,Z) &= P_v = \frac{1}{2}\frac{N_g\alpha_g}{\alpha_g+\mu_g}\frac{\alpha_s}{\alpha_s+\mu_s}\frac{\alpha_z}{\alpha_z+\mu_z}\frac{N_k\alpha_k}{\alpha_k+\mu_k}\frac{1}{\alpha_v+\mu_v}\frac{\beta_H(T) G_H(S_V-1)}{(G_0+G_H)\phi_V(I_V+1)}, \\ &= P_v = \frac{N_v\beta_H(T) G_H(S_V-1)}{(G_0+G_H)\phi_V(I_V+1)}, \\ \widetilde{g}_7(X^*,Z) &= I_H = \frac{1}{\mu_H+\gamma_H+\delta_H}\frac{\beta_V(T) S_H P_V}{P_0+P_V}, \end{aligned} \tag{6.2.4.3}$$

where

$$N_v = \frac{1}{2}\frac{N_g\alpha_g}{\alpha_g+\mu_g}\frac{\alpha_s}{\alpha_s+\mu_s}\frac{\alpha_z}{\alpha_z+\mu_z}\frac{N_k\alpha_k}{\alpha_k+\mu_k}\frac{1}{\alpha_v+\mu_v}. \tag{6.2.4.4}$$

Let $h_1 = \frac{dP_V}{dt}$ and $h_2 = \frac{dG_H}{dt}$ and we obtain

$$\begin{aligned} h_1 &= \frac{N_v\alpha_v\beta_H(T)G_H(S_V-1)}{(G_0+G_H)\phi_V} - \alpha_V P_V, \\ h_2 &= \frac{N_h\alpha_h\beta_V S_H P_V}{(\mu_H+\gamma_H+\delta_H)(P_0+P_V)} - \alpha_H G_H. \end{aligned} \tag{6.2.4.5}$$

We assume that $A = M - D$, where $M \geq 0$ and $D \geq 0$, a diagonal matrix.

$$A = \begin{pmatrix} \frac{\partial h_1}{\partial P_V} & \frac{\partial h_1}{\partial G_H} \\ \frac{\partial h_2}{\partial P_V} & \frac{\partial h_2}{\partial G_H} \end{pmatrix},$$

then

$$A = \begin{pmatrix} -\alpha_V & \frac{N_v\alpha_v\beta_H(T)(S_V^{00}-1)}{G_0\phi_V} \\ \frac{N_h\alpha_h\beta_V(T)\Lambda_H}{(\mu_H+\gamma_H+\delta_H)\mu_H P_0} & -\alpha_H \end{pmatrix}, \tag{6.2.4.6}$$

$$M = \begin{pmatrix} 0 & \frac{N_v\alpha_v\beta_H(T)(S_V^{00}-1)}{G_0\phi_V} \\ \frac{N_h\alpha_h\beta_V(T)\Lambda_H}{(\mu_H+\gamma_H+\delta_H)P_0\mu_H} & 0 \end{pmatrix}, \tag{6.2.4.7}$$

$$D = \begin{pmatrix} \alpha_V & 0 \\ 0 & \alpha_H \end{pmatrix} \quad D^{-1} = \begin{pmatrix} \frac{1}{\alpha_V} & 0 \\ 0 & \frac{1}{\alpha_H} \end{pmatrix},$$

$$MD^{-1} = \begin{pmatrix} 0 & \frac{N_v\alpha_v\beta_H(T)(S_V^{00}-1)}{\alpha_H G_0\phi_V} \\ \frac{N_h\alpha_h\beta_V(T)\Lambda_H}{(\mu_H+\gamma_H+\delta_H)P_0\mu_H\alpha_V} & 0 \end{pmatrix}. \tag{6.2.4.8}$$

$R_0 = \rho(MD^{-1})$

$$\begin{aligned} R_0 &= \sqrt{\frac{N_h\alpha_h}{\mu_H+\gamma_H+\delta_H}\frac{\beta_H(T)(S_V^{00}-1)}{G_0\alpha_H}.\frac{N_v\alpha_v\beta_V(T)\Lambda_H}{\phi_V P_0\mu_H\alpha_V}}, \\ &= \sqrt{R_{HV}R_{VH}}, \\ R_{HV} &= \frac{N_h\alpha_h}{\mu_H+\gamma_H+\delta_H}\frac{\beta_H(T)(S_V^{00}-1)}{G_0\alpha_H}, \\ R_{VH} &= \frac{N_v\alpha_v\beta_V(T)\Lambda_H}{\phi_V P_0\mu_H\alpha_V}, \end{aligned} \tag{6.2.4.9}$$

where

$$\begin{aligned} N_h &= \overline{G_h} = \frac{\pi\Lambda_h}{\Re_0(\alpha_h+\mu_h)}(\Re_0-1), \\ N_v &= \frac{1}{2}\frac{N_g\alpha_g}{\alpha_g+\mu_g}\frac{\alpha_s}{\alpha_s+\mu_s}\frac{\alpha_z}{\alpha_z+\mu_z}\frac{N_k\alpha_k}{\alpha_k+\mu_k}\frac{1}{\alpha_v+\mu_v}, \\ S_V^{00} &= \frac{\alpha_L(T)}{2\mu_V(T)}\frac{K[\Lambda_L(T)\alpha_L(T)-2\mu_V(T)(\mu_L(T)+\alpha_L(T)+\delta_L)]}{\Lambda_L(T)\alpha_L(T)-2\mu_L(T)\mu_V(T)}. \end{aligned} \tag{6.2.4.10}$$

R_{HV} is the human-host to vector (mosquito) reproductive number. R_{VH} is the vector to human reproductive number. $\Re_0$ is the reproductive number for within-human host model. Our R_0 consist of parameters which are from within-host and between-host scales.

6.2.5 Local Stability Analysis of the Disease-free Equilibrium (D.F.E)

We determine the local stability analysis of the D.F.E point of the multiscale model (6.2.1.12), the D.F.E. is asymptotically stable when $R_0 < 1$ and unstable when $R_0 > 1$. We linearize the multiscale model (6.2.1.12), to obtain the Jacobian matrix and then compute at the D.F.E (E_{00}), to obtain by $J(E_{00}) =$

$$\begin{bmatrix}
-c_1 & 0 & 0 & 0 & 0 & 0 & 0 & 0 & 0 & 0 & 0 & 0 \\
\frac{\alpha_L(T)}{2} & -\mu_V(T) & 0 & 0 & 0 & 0 & 0 & 0 & 0 & 0 & 0 & -c_3 \\
0 & 0 & -c_2 & 0 & 0 & 0 & 0 & 0 & 0 & 0 & 0 & c_3 \\
0 & 0 & 0 & -a_1 & 0 & 0 & 0 & 0 & 0 & 0 & 0 & c_4 \\
0 & 0 & 0 & N_g\alpha_g & -a_2 & 0 & 0 & 0 & 0 & 0 & 0 & 0 \\
0 & 0 & 0 & 0 & \frac{1}{2}\alpha_s & -a_3 & 0 & 0 & 0 & 0 & 0 & 0 \\
0 & 0 & 0 & 0 & 0 & \alpha_z & -a_4 & 0 & 0 & 0 & 0 & 0 \\
0 & 0 & 0 & 0 & 0 & 0 & N_k\alpha_k & -a_5 & 0 & 0 & 0 & 0 \\
0 & 0 & 0 & 0 & 0 & 0 & 0 & \alpha_v & -\alpha_V & 0 & 0 & 0 \\
0 & 0 & 0 & 0 & 0 & 0 & 0 & 0 & -\frac{\beta_V(T)S_H^{00}}{P_0} & -\mu_H & \gamma_H & 0 \\
0 & 0 & 0 & 0 & 0 & 0 & 0 & 0 & \frac{\beta_V(T)S_H^{00}}{P_0} & 0 & -a_6 & 0 \\
0 & 0 & 0 & 0 & 0 & 0 & 0 & 0 & 0 & 0 & N_h\alpha_h & -\alpha_H
\end{bmatrix},$$

where $a_1 = (\alpha_g+\mu_g)$, $a_2 = (\alpha_s+\mu_s)$, $a_3 = (\alpha_z+\mu_z)$, $a_4 = (\alpha_k+\mu_k)$, $a_5 = (\alpha_v+\mu_v)$, $a_6 = (\mu_H+\gamma_H+\delta_H)$, $c_1 = \frac{\Lambda_L(T)\alpha_L(T)}{2\mu_V(T)}$, $c_2 = (\mu_V(T)+\delta_V)$, $c_3 = \frac{\beta_H(T)S_V^{00}}{G_0}$ and $c_4 = \frac{\beta_H(T)(S_V^{00}-1)}{G_0\phi_V}$.

We obtain the eigenvalues of $J(E_{00})$ by computing the $det(J(E_{00})-\lambda I)=0$. The characteristic equation of the eigenvalues is given by

$$(\lambda+c_1)(\lambda+\mu_V(T))(\lambda+c_2)(\lambda+\mu_H)[b_8\lambda^8+b_7\lambda^7+b_6\lambda^6+b_5\lambda^5+b_4\lambda^4+b_3\lambda^3+b_2\lambda^2b_1\lambda_1+b_0]=0. \tag{6.2.5.1}$$

We obtain $\lambda_1=-c_1$, $\lambda_2=-\mu_V(T)$, $\lambda_3=-c_2$, $\lambda_4=-\mu_H$ and $\lambda_5...\lambda_{12}$ is given by the equation

$$b_8\lambda^8+b_7\lambda^7+b_6\lambda^6+b_5\lambda^5+b_4\lambda^4+b_3\lambda^3+b_2\lambda^2b_1\lambda_1+b_0=0. \tag{6.2.5.2}$$

$$\begin{aligned}
b_8 &= 1>0,\\
b_7 &= a_1+a_2+a_3+a_4+a_5+a_6+\alpha_V+\alpha_H>0,\\
b_6 &= a_1a_2+a_1a_3+a_1a_4+a_1a_5+a_1a_6+a_1\alpha_V+a_1\alpha_H+a_2a_3+a_2a_4+a_2a_5+a_2a_6+a_2\alpha_V\\
&\quad +a_2\alpha_H+a_3a_4+a_3a_5+a_3a_6+a_3\alpha_V+a_3\alpha_H+a_4a_5+a_4a_6+a_4\alpha_V+a_4\alpha_H+a_5a_6+a_5\alpha_V\\
&\quad +a_5\alpha_H+a_6\alpha_V+a_6\alpha_H+\alpha_V\alpha_H>0,\\
b_5 &= a_1a_2a_3+a_1a_2a_4+a_1a_2a_5+a_1a_2a_6+a_1a_2\alpha_V+a_1a_2\alpha_H+a_1a_3a_4+a_1a_3a_5+a_1a_3a_6+\\
&\quad a_1a_3\alpha_V+a_1a_3\alpha_H+a_1a_4a_5+a_1a_4a_6+a_1a_4\alpha_V+a_1a_4\alpha_H+a_1a_5a_6+a_1a_5\alpha_V+a_1a_5\alpha_H+\\
&\quad a_1a_6\alpha_V+a_1a_6\alpha_H+a_1\alpha_V\alpha_H+a_2a_3a_4+a_2a_3a_5+a_2a_3a_6+a_2a_3\alpha_V+a_2a_3\alpha_H+a_2a_4a_5+\\
&\quad a_2a_4a_6+a_2a_4\alpha_V+a_2a_4\alpha_H+a_2a_5a_6+a_2a_5\alpha_V+a_2a_5\alpha_H+a_2a_6\alpha_V+a_2a_6\alpha_H+a_2\alpha_V\alpha_H\\
&\quad +a_3a_4a_5+a_3a_4a_6+a_3a_4\alpha_V+a_3a_4\alpha_H+a_3a_5a_6+a_3a_5\alpha_V+a_3a_5\alpha_H+a_3a_6\alpha_V+a_3a_6\alpha_H\\
&\quad +a_3\alpha_V\alpha_H+a_4a_5a_6+a_4a_5\alpha_V+a_4a_5\alpha_H+a_4a_6\alpha_V+a_4a_6\alpha_H+a_4\alpha_V\alpha_H+a_5a_6\alpha_V+a_5a_6\alpha_H\\
&\quad +a_5\alpha_V\alpha_H+a_6\alpha_V\alpha_H>0,\\
b_4 &= a_1a_2a_3a_4+a_1a_2a_3a_5+a_1a_2a_3a_6+a_1a_2a_3\alpha_V+a_1a_2a_3\alpha_H+a_1a_2a_4a_5+a_1a_2a_4a_6+a_1a_2a_4\alpha_V\\
&\quad +a_1a_2a_4\alpha_H+a_1a_2a_5a_6+a_1a_2a_5\alpha_V+a_1a_2a_5\alpha_H+a_1a_2a_6\alpha_V+a_1a_2a_6\alpha_H+a_1a_2\alpha_V\alpha_H+\\
&\quad a_1a_3a_4a_5+a_1a_3a_4a_6+a_1a_3a_4\alpha_V+a_1a_3a_4\alpha_H+a_1a_3a_5a_6+a_1a_3a_5\alpha_V+a_1a_3a_5\alpha_H+a_1a_3a_6\alpha_V\\
&\quad +a_1a_3a_6\alpha_H+a_1a_3\alpha_V\alpha_H+a_1a_4a_5a_6+a_1a_4a_5\alpha_V+a_1a_4a_5\alpha_H+a_1a_4a_6\alpha_V+a_1a_4a_6\alpha_H+\\
&\quad a_1a_4\alpha_V\alpha_H+a_1a_5a_6\alpha_V+a_1a_5a_6\alpha_H+a_1a_5\alpha_V\alpha_H+a_1a_6\alpha_V\alpha_H+a_2a_3a_4a_5+a_2a_3a_4a_6+\\
&\quad a_2a_3a_4\alpha_V+a_2a_3a_4\alpha_H+a_2a_3a_5a_6+a_2a_3a_5\alpha_V+a_2a_3a_5\alpha_H+a_2a_3a_6\alpha_V+a_2a_3a_6\alpha_H+\\
&\quad a_2a_3\alpha_V\alpha_H+a_2a_4a_5a_6+a_2a_4a_5\alpha_V+a_2a_4a_5\alpha_H+a_2a_4a_6\alpha_V+a_2a_4a_6\alpha_H+a_2a_4\alpha_V\alpha_H+\\
&\quad a_2a_5a_6\alpha_V+a_2a_5a_6\alpha_H+a_2a_5\alpha_V\alpha_H+a_2a_6\alpha_V\alpha_H+a_3a_4a_5a_6+a_3a_4a_5\alpha_V+a_3a_4a_5\alpha_H+\\
&\quad a_3a_4a_6\alpha_V+a_3a_4a_6\alpha_H+a_3a_4\alpha_V\alpha_H+a_3a_5a_6\alpha_V+a_3a_5a_6\alpha_H+a_3a_5\alpha_V\alpha_H+a_3a_6\alpha_V\alpha_H+\\
&\quad a_4a_5a_6\alpha_V+a_4a_5a_6\alpha_H+a_4a_5\alpha_V\alpha_H+a_4a_6\alpha_V\alpha_H+a_5a_6\alpha_V\alpha_H>0,
\end{aligned} \tag{6.2.5.3}$$

$$
\begin{aligned}
b_3 &= a_1a_2a_3a_4a_5 + a_1a_2a_3a_4a_6 + a_1a_2a_3a_4\alpha_V + a_1a_2a_3a_4\alpha_H + a_1a_2a_3a_5a_6 + a_1a_2a_3a_5\alpha_V + \\
&\quad a_1a_2a_3a_5\alpha_H + a_1a_2a_3a_6\alpha_V + a_1a_2a_3a_6\alpha_H + a_1a_2a_3\alpha_V\alpha_H + a_1a_2a_4a_5a_6 + a_1a_2a_4a_5\alpha_V + \\
&\quad a_1a_2a_4a_5\alpha_H + a_1a_2a_4a_6\alpha_V + a_1a_2a_4a_6\alpha_H + a_1a_2a_4\alpha_V\alpha_H + a_1a_2a_5a_6\alpha_V + a_1a_2a_5a_6\alpha_H + \\
&\quad a_1a_2a_5\alpha_V\alpha_H + a_1a_2a_6\alpha_V\alpha_H + a_1a_3a_4a_5a_6 + a_1a_3a_4a_5\alpha_V + a_1a_3a_4a_5\alpha_H + a_1a_3a_4a_6\alpha_V + \\
&\quad a_1a_3a_4a_6\alpha_H + a_1a_3a_4\alpha_V\alpha_H + a_1a_3a_5a_6\alpha_V + a_1a_3a_5a_6\alpha_H + a_1a_3a_5\alpha_V\alpha_H + a_1a_3a_6\alpha_V\alpha_H + \\
&\quad a_1a_4a_5a_6\alpha_V + a_1a_4a_5a_6\alpha_H + a_1a_4a_5\alpha_V\alpha_H + a_1a_4a_6\alpha_V\alpha_H + a_1a_4a_5\alpha_V\alpha_H + a_2a_3a_4a_5a_6 + \\
&\quad a_2a_3a_4a_5\alpha_V + a_2a_3a_4a_5\alpha_H + a_2a_3a_4a_6\alpha_V + a_2a_3a_4a_6\alpha_H + a_2a_3a_4\alpha_V\alpha_H + a_2a_3a_5a_6\alpha_V + \\
&\quad a_2a_3a_5a_6\alpha_H + a_2a_3a_5\alpha_V\alpha_H + a_2a_3a_6\alpha_V\alpha_H + a_2a_4a_5a_6\alpha_V + a_2a_4a_5a_6\alpha_H + a_2a_4a_5\alpha_V\alpha_H + \\
&\quad a_2a_4a_6\alpha_V\alpha_H + a_2a_5a_6\alpha_V\alpha_H + a_3a_4a_5a_6\alpha_V + a_3a_4a_5a_6\alpha_H + a_3a_4a_5\alpha_V\alpha_H + a_3a_4a_6\alpha_V\alpha_H + \\
&\quad a_3a_5a_6\alpha_V\alpha_H + a_4a_5a_6\alpha_V\alpha_H > 0,
\end{aligned}
$$

$$
\begin{aligned}
b_2 &= a_1a_2a_3a_4a_5a_6 + a_1a_2a_3a_4a_5\alpha_V + a_1a_2a_3a_4a_5\alpha_H + a_1a_2a_3a_4a_6\alpha_V + a_1a_2a_3a_4a_6\alpha_H + \\
&\quad a_1a_2a_3a_4\alpha_V\alpha_H + a_1a_2a_3a_5a_6\alpha_V + a_1a_2a_3a_5a_6\alpha_H + a_1a_2a_3a_5\alpha_V\alpha_H + a_1a_2a_3a_6\alpha_V\alpha_H + \\
&\quad a_1a_2a_4a_5a_6\alpha_V + a_1a_2a_4a_5a_6\alpha_H + a_1a_2a_4a_5\alpha_V\alpha_H + a_1a_2a_4a_6\alpha_V\alpha_H + a_1a_2a_5a_6\alpha_V\alpha_H + \\
&\quad a_1a_3a_4a_5a_6\alpha_V + a_1a_3a_4a_5a_6\alpha_H + a_1a_3a_4a_5\alpha_V\alpha_H + a_1a_3a_4a_6\alpha_V\alpha_H + a_1a_3a_5a_6\alpha_V\alpha_H + \\
&\quad a_1a_4a_5a_6\alpha_V\alpha_H + a_2a_3a_4a_5a_6\alpha_V + a_2a_3a_4a_5a_6\alpha_H + a_2a_3a_4a_5\alpha_V\alpha_H + a_2a_3a_4a_6\alpha_V\alpha_H + \\
&\quad a_2a_3a_5a_6\alpha_V\alpha_H + a_2a_4a_5a_6\alpha_V\alpha_H + a_3a_4a_5a_6\alpha_V\alpha_H > 0, \qquad (6.2.5.4)
\end{aligned}
$$

$$
\begin{aligned}
b_1 &= a_1a_2a_3a_4a_5a_6\alpha_V + a_1a_2a_3a_4a_5a_6\alpha_H + a_1a_2a_3a_4a_5\alpha_V\alpha_H + a_1a_2a_3a_4a_6\alpha_V\alpha_H + \\
&\quad a_1a_2a_3a_5a_6\alpha_V\alpha_H + a_1a_2a_4a_5a_6\alpha_V\alpha_H + a_1a_3a_4a_5a_6\alpha_V\alpha_H + a_2a_3a_4a_5a_6\alpha_V\alpha_H > 0,
\end{aligned}
$$

$$
\begin{aligned}
b_0 &= a_1a_2a_3a_4a_5a_6\alpha_V\alpha_H\left(1 - \frac{c_4}{\alpha_V}\frac{N_g\alpha_g}{a_1}\frac{\alpha_s}{2a_2}\frac{\alpha_z}{a_3}\frac{N_k\alpha_k}{a_4}\frac{\alpha_v}{a_5}\frac{\beta_V(T)S_H^{00}}{P_0\alpha_V}\frac{N_h\alpha_h}{a_6}\right), \\
&= a_1a_2a_3a_4a_5a_6\alpha_V\alpha_H\left(1 - R_0^2\right).
\end{aligned}
$$

Table 6.1: Possible number of positive roots of equation (6.2.5.2)

	b_7	b_6	b_5	b_4	b_3	b_2	b_1	b_0	**The number of positive roots**
$R_0 < 1$	+	+	+	+	+	+	+	+	0
$R_0 > 1$	+	+	+	+	+	+	+	-	1

Using Descarte's law of signs to determine the possible number of positive roots of equation (6.2.5.2) as shown in table (6.1). It is clear that $b_7 > 0$, $b_6 > 0$, $b_5 > 0$, $b_4 > 0$, $b_3 > 0$, $b_2 > 0$ and $b_1 > 0$. When $R_0 < 1$ we notice that $b_0 > 0$ and there is no change of sign and conclude that the equation (6.2.5.2) has zero positive roots. When $R_0 > 1$, we observe that $b_0 < 0$, and there is only one change of sign and conclude that the characteristic equation (6.2.5.2) has atleast one positive root. The roots of equation

(6.2.5.2) are all negative or have negative real parts. We shown that there is no change of sign when $R_0 < 1$, and confirms that the disease free equilibrium is locally asymptotically stable and unstable when $R_0 > 1$.

6.2.6 Global Stability of Disease-Free Equilibrium (D.F.E)

We determine the global stability of D.F.E by following Castillo-Chavez's approach [71]. We rewrite the model system (6.2.1.12) in the form

$$\begin{aligned} \frac{dX}{dt} &= F(X,Z), \\ \frac{dZ}{dt} &= G(X,Z), \\ G(X,0) &= 0, \end{aligned} \tag{6.2.6.1}$$

where $X = (L_M, S_V, S_H) \in \mathbb{R}^3_+$- comprises of the uninfected components and
$Z = (I_V, G_v, G_m, Z_v, O_v, P_v, P_V, I_H, G_H) \in \mathbb{R}^9_+$ comprises of the infected and infectious components.

We let

$$E_{00} = (X^*, 0) = (L_M^{00}, S_V^{00}, 0, 0, 0, 0, 0, 0, 0, S_H^{00}, 0, 0)$$

to denote the disease free equilibrium of the multiscale model. The conditions of H_1 and H_2 must holds, for E_{00} to be globally asymptotically stable:

H_1**:** For $\dfrac{dX}{dt} = F(X,0)$, X^* is globally asymptotically stable,

H_2**:** $G(X,Z) = AZ - \widehat{G}(X,Z)$, $\widehat{G}(X,Z) \geq 0$ for $(X,Z) \in \mathbb{R}^{12}_+$,

where $A = D_Z G(X,0)$, is an M matrix (the off diagonal elements 0f A are non-negative) and $\mathbb{R}^{12}_+$ is the region where the model is meaningful biologically.

Theorem 6.1. *The fixed point E_{00} is a globally asymptotically stable equilibrium point of the model (6.2.1.12) provided $R_0 < 1$ and assumptions H_1 and H_2 hold.*

Proof. Using the multiscale model (6.2.1.12), we determine if the conditions H_1 and H_2 hold. We observe that

$$F(X,0) = \begin{bmatrix} [\Lambda_L(T)N_V - \mu_L(T)L_M]\left(1 - \dfrac{L_M}{K}\right) - (\alpha_L(T) + \delta_L)L_M \\ \dfrac{\alpha_L(T)}{2}\dfrac{K[\Lambda_L(T)\alpha_L(T) - 2\mu_V(T)(\mu_L(T) + \alpha_L(T) + \delta_L)]}{\Lambda_L(T)\alpha_L(T) - 2\mu_L(T)\mu_V(T)} - \mu_V(T)S_V \\ \Lambda_H - \mu_H S_H \end{bmatrix},$$

and the matrix A is given by

$$\begin{bmatrix} -b_1 & 0 & 0 & 0 & 0 & 0 & 0 & 0 & \frac{\beta_H(T)S_V^{00}}{G_0} \\ 0 & -b_2 & 0 & 0 & 0 & 0 & 0 & 0 & \frac{\beta_H(T)(S_V^{00}-1)}{G_0\phi_V} \\ 0 & N_g\alpha_g & -b_3 & 0 & 0 & 0 & 0 & 0 & 0 \\ 0 & 0 & \frac{1}{2}\alpha_s & -b_4 & 0 & 0 & 0 & 0 & 0 \\ 0 & 0 & 0 & \alpha_z & -b_5 & 0 & 0 & 0 & 0 \\ 0 & 0 & 0 & 0 & N_k\alpha_k & -b_6 & 0 & 0 & 0 \\ 0 & 0 & 0 & 0 & 0 & \alpha_v & -\alpha_V & 0 & 0 \\ 0 & 0 & 0 & 0 & 0 & 0 & \frac{\beta_V(T)S_H^*}{P_0} & -b_7 & 0 \\ 0 & 0 & 0 & 0 & 0 & 0 & 0 & N_h\alpha_h & -\alpha_H \end{bmatrix}$$

where $b_1 = (\mu_V(T) + \delta_V)$, $b_2 = (\alpha_g + \mu_g)$, $b_3 = (\alpha_s + \mu_s)$, $b_4 = (\alpha_z + \mu_z)$, $b_5 = (\alpha_k + \mu_k)$, $b_6 = (\alpha_v + \mu_v)$ and $b_7 = (\mu_H + \gamma_H + \delta_H)$.

The matrices of AZ and $G(X, Z)$ are given by

$$AZ = \begin{bmatrix} -(\mu_V(T) + \delta_V)I_V + \frac{\beta_H(T)G_HS_V^{00}}{G_0} \\ -(\alpha_g + \mu_g)G_v + \frac{\beta_H(T)G_H(S_V^{00}-1)}{\phi_V G_0} \\ N_g\alpha_g G_v - (\alpha_s + \mu_s)G_m \\ \frac{1}{2}\alpha_s - (\alpha_z + \mu_z)Z_v \\ \alpha_z Z_v - (\alpha_k + \mu_k)O_v \\ N_k\alpha_k O_v - (\alpha_v + \mu_v)P_v \\ \alpha_v P_v - \alpha_V P_V \\ \frac{\beta_V(T)P_V S_H^{00}}{P_0} - (\mu_H + \gamma_H + \delta_H)I_H \\ N_h\alpha_h I_H - \alpha_H G_H \end{bmatrix} \quad \text{and } G(X, Z) = \begin{bmatrix} \frac{\beta_H(T)G_HS_V}{G_0+G_H} - (\mu_V(T) + \delta_V)I_V \\ \frac{\beta_H G_H(S_V-1)}{(G_0+G_H)\phi_V(I_V+1)} - (\alpha_g + \mu_g)G_v \\ N_g\alpha_g G_v - (\alpha_s + \mu_s)G_m \\ \frac{1}{2}\alpha_s G_m - (\alpha_z + \mu_z)Z_v \\ \alpha_z Z_v - (\alpha_k + \mu_k)O_v \\ N_k\alpha_k O_v - (\alpha_v + \mu_v)P_v \\ P_v\alpha_v(I_V+1) - \alpha_V P_V \\ \frac{\beta_V(T)P_V S_H}{P_0+P_V} - (\mu_H + \gamma_H + \delta_H)I_H \\ N_h\alpha_h I_H - \alpha_H G_H \end{bmatrix}$$

Therefore, $\widehat{G}(X,Z) = AZ - G(X,Z)$,

$$\widehat{G}(X,Z) = \begin{bmatrix} \left(\frac{s_V^{00}}{G_0} - \frac{S_V}{G_0+G_H}\right)\beta_H(T)G_H \\ \left(\frac{(S_V^{00}-1)}{G_0} - \frac{(S_V-1)}{(G_0+G_H)(I_V+1)}\right)\frac{\beta_H(T)G_H}{\phi_V} \\ 0 \\ 0 \\ 0 \\ 0 \\ 0 \\ \left(\frac{S_H^{00}}{P_0} - \frac{S_H}{P_0+P_V}\right) \\ 0 \end{bmatrix},$$

where $\widehat{G}(X,Z) \geq 0$ for all $X, Z \in \mathbb{R}_+^{12}$, if $\left(\frac{s_V^{00}}{G_0} \geq \frac{S_V}{G_0+G_H}\right)$, $\left(\frac{(S_V^{00}-1)}{G_0} \geq \frac{(S_V-1)}{(G_0+G_H)(I_V+1)}\right)$ and $\left(\frac{S_H^{00}}{P_0} \geq \frac{S_H}{P_0+P_V}\right)$. Therefore, it is clear that A is an M-matrix because of the off diagonal elements of A are non-negative, , so the condition is satisfied. Hence, the disease-free equilibrium point is globally asymptotically stable. □

6.3 Endemic equilibrium point for coupled multiscale model

We define

$$\begin{aligned} V^{**} &= \lambda_V(T) = \frac{\beta_V(T)P_V^{**}}{P_0+P_V^{**}}, \\ H^{**} &= \lambda_H(T) = \frac{\beta_H(T)G_H^{**}}{G_0+G_H^{**}}. \end{aligned} \tag{6.3.0.1}$$

We obtain the equilibrium points by equating the right hand side of system of equations (6.2.1.12) to zero and solve the simultaneous equations.

$$\begin{aligned}
[\Lambda_L(T)N_V^{**}(t) - \mu_L(T)L_M^{**}]\left(1 - \frac{L_M^{**}}{K}\right) - (\alpha_L(T) + \delta_L)L_M^{**} &= 0,\\
\Lambda_V(T) - H^{**}S_V^{**} - \mu_V(T)S_V^{**} &= 0,\\
H^{**}S_V^{**} - (\mu_V(T) + \delta_V)I_V^{**} &= 0,\\
\frac{H^{**}(S_V^{**} - 1)}{\phi_V(I_V^{**} + 1)} - [\alpha_g + \mu_g]\, G_v^{**} &= 0,\\
N_g\alpha_g G_v^{**} - [\alpha_s + \mu_s]\, G_m^{**} &= 0,\\
\psi_v - [\alpha_z + \mu_z]\, Z_v^{**} &= 0,\\
\alpha_z Z_v^{**} - [\alpha_k + \mu_k]\, O_v^{**} &= 0,\\
N_k\alpha_k O_v^{**} - [\alpha_v + \mu_v]\, P_v^{**} &= 0,\\
P_v^{**}\alpha_v(I_V^{**} + 1) - \alpha_V P_V^{**} &= 0,\\
\Lambda_H - V^{**}S_H^{**} - \mu_H S_H^{**} + \gamma_H I_H^{**} &= 0,\\
V^{**}S_H^{**} - (\mu_H + \gamma_H + \delta_H)I_H^{**} &= 0,\\
N_h\alpha_h I_H^{**} - \alpha_H G_H^{**} &= 0,
\end{aligned} \tag{6.3.0.2}$$

where

$$\begin{aligned}
N_h &= \overline{G_h} = \frac{\pi\Lambda_h}{\Re_0(\alpha_h + \mu_h)}(\Re_0 - 1),\\
\Re_0 &= \frac{(1-\pi)N_m\beta_h\Lambda_h}{\mu_b\mu_m},\\
\Lambda_V(T) &= \frac{\alpha_L L_M^{**}}{2}.\\
\psi_v &= \frac{\alpha_s G^{**}}{2}.
\end{aligned} \tag{6.3.0.3}$$

The disease free equilibrium point can be simplified when $H^{**} = 0$ and $V^{**} = 0$ to obtain

$$E_{00} = (L_M^{00}, S_V^{00}, I_V^{00}, G_v^{00}, G_m^{00}, Z_v^{00}, O_v^{00}, P_v^{00}, P_V^{00}, S_H^{00}, I_H^{00}, G_H^{00}), \tag{6.3.0.4}$$

where

$$\begin{aligned}
L_M^{00} &= \frac{K[\Lambda_L(T)\alpha_L(T) - 2\mu_V(T)(\mu_L(T) + \alpha_L(T) + \delta_L)]}{\Lambda_L(T)\alpha_L(T) - 2\mu_L(T)\mu_V(T)},\\
S_V^{00} &= \frac{\Lambda_V(T)}{\mu_V(T)} = \frac{\alpha_L(T)}{2\mu_V(T)}\frac{K[\Lambda_L(T)\alpha_L(T) - 2\mu_V(T)(\mu_L(T) + \alpha_L(T) + \delta_L)]}{\Lambda_L(T)\alpha_L(T) - 2\mu_L(T)\mu_V(T)},\\
S_H^{00} &= \frac{\Lambda_H}{\mu_H},\\
I_V^{00} &= G_v^{00} = G_m^{00} = Z_v^{00} = O_v^{00} = P_v^{00} = P_V^{00} = I_H^{00} = G_H^{00} = 0.
\end{aligned} \tag{6.3.0.5}$$

The endemic equilibrium point can be simplified in terms of H^{**} and V^{**} to obtain

$$E_2 = (L_M^{**}, S_V^{**}, I_V^{**}, G_v^{**}, G_m^{**}, Z_v^{**}, O_v^{**}, P_v^{**}, S_H^{**}, I_H^{**}, G_H^{**}), \tag{6.3.0.6}$$

where

$$\begin{aligned}
L_M^{**} &= \frac{b \pm \sqrt{b^2 - 4K\Lambda_L(T)N_V^{**}\mu_L(T)}}{2\mu_L(T)} \\
S_V^{**} &= \frac{\alpha_L(T)L_M^{**}}{2(H^{**} + \mu_V(T))}, \\
I_V^{**} &= \frac{H^{**}}{\mu_V(T) + \delta_V} \frac{\alpha_L(T)L_M^{**}}{2(H^{**} + \mu_V(T))}, \\
G_v^{**} &= \frac{1}{\alpha_g + \mu_g} \frac{H^{**}}{\phi_V(I_V^{**} + 1)} \left[\frac{\alpha_L(T)L_M^{**}}{2(H^{**} + \mu_V(T))} - 1\right] \\
G_m^{**} &= \frac{N_g\alpha_g}{\alpha_g + \mu_g} \frac{1}{\alpha_s + \mu_s} \frac{H^{**}}{\phi_V(I_V^{**} + 1)} \left[\frac{\alpha_L(T)L_M^{**}}{2(H^{**} + \mu_V(T))} - 1\right], \\
Z_v^{**} &= \frac{\psi_v}{\alpha_z + \mu_z}, \\
O_v &= \frac{\alpha_z}{\alpha_z + \mu_z} \frac{\psi_v}{\alpha_k + \mu_k}, \\
P_v^{**} &= \frac{\alpha_z}{\alpha_z + \mu_z} \frac{N_k\alpha_k}{\alpha_k + \mu_k} \frac{\psi_v}{\alpha_v + \mu_v}, \\
P_V^{**} &= \frac{N_v\alpha_v H^{**}}{\alpha_V\phi_V} \left[\frac{\alpha_L(T)L_M^{**}}{2(H^{**} + \mu_V(T))} - 1\right], \\
S_H^{**} &= \frac{\Lambda_H(\mu_H + \gamma_H + \delta_H)}{\mu_H(\mu_H + \gamma_H + \delta_H) + V^{**}(\mu_H + \delta_H)}, \\
I_H^{**} &= \frac{\Lambda_H V^{**}}{\mu_H(\mu_H + \gamma_H + \delta_H) + V^{**}(\mu_H + \delta_H)}, \\
G_H^{**} &= \frac{N_h\alpha_h}{\alpha_H} \frac{\Lambda_H V^{**}}{[\mu_H(\mu_H + \gamma_H + \delta_H) + V^{**}(\mu_H + \delta_H)]},
\end{aligned} \tag{6.3.0.7}$$

where

$$\begin{aligned}
N_h &= \overline{G_h} = \frac{\pi\Lambda_h}{\Re_0(\alpha_h + \mu_h)}(\Re_0 - 1), \\
\Lambda_V(T) &= \frac{\alpha_L(T)L_M}{2}, \\
\psi_v &= \frac{\alpha_s G^{**}}{2}, \\
N_v &= \frac{1}{2} \frac{N_g\alpha_g}{\alpha_g + \mu_g} \frac{\alpha_s}{\alpha_s + \mu_s} \frac{\alpha_z}{\alpha_z + \mu_z} \frac{N_k\alpha_k}{\alpha_k + \mu_k} \frac{1}{\alpha_v + \mu_v}, \qquad (6.3.0.8) \\
b &= [\Lambda_L(T)N_V^{**} + K(\mu_L(T) + \alpha_L(T) + \delta_L)], \\
N_V^{**} &= \frac{\alpha_L(T)}{2\mu_V(T)} \frac{K[\Lambda_L(T)\alpha_L(T) - 2\mu_V(T)(\mu_L(T) + \alpha_L(T) + \delta_L)]}{\Lambda_L(T)\alpha_L(T) - 2\mu_L(T)\mu_V(T)}. \qquad (6.3.0.9)
\end{aligned}$$

The positivity of the endemic equilibrium of the systems of equations (6.2.1.12) can be obtained by evaluating the fixed points of H^{**} and V^{**} in equations (6.3.0.1) and substituting the results into systems of

equations (6.3.0.7) [82, 83]. The expressions of H^{**} and V^{**} are given by

$$H^{**} = \frac{\beta_H(T)N_h\alpha_h\Lambda_H V^{**}}{G_0\alpha_H[\mu_H(\mu_H+\gamma_H+\delta_H)+V^{**}(\mu_H+\delta_H)]+N_h\alpha_h\Lambda_H V^{**}}, \tag{6.3.0.10}$$

$$V^{**} = \frac{N_v\alpha_v\beta_V(T)H^{**}[\alpha_L(T)L_M^{**}-2(H^{**}+\mu_V(T))]}{2P_0\phi_V\alpha_V(H^{**}+\mu_V(T))+N_v\alpha_v H^{**}[\alpha_L(T)L_M^{**}-2(H^{**}+\mu_V(T))]}, \tag{6.3.0.11}$$

We define

$$\begin{pmatrix} H^{**} \\ V^{**} \end{pmatrix} = f(H,V) = \begin{pmatrix} f_1(V) \\ f_2(H) \end{pmatrix}.$$

When $H^{**}=0$ and $V^{**}=0$ is a fixed point of $f_1(V)$ and $f_2(H)$ which match up with the disease free equilibrium point. We develop conditions which illustrate that f has a unique nonzero fixed point corresponding to the positive endemic equilibrium point whose coordinates are equations (6.2.1.12) [84].

$$f_1(V) = \frac{\beta_H(T)N_h\alpha_h\Lambda_H V}{G_0\alpha_H[\mu_H(\mu_H+\gamma_H+\delta_H)+V(\mu_H+\delta_H)]+N_h\alpha_h\Lambda_H V}, \tag{6.3.0.12}$$

Since $f_1(0)=0$ and $\lim_{V\to\infty} f_1(V) = \dfrac{\beta_H(T)N_h\alpha_h}{G_0\alpha_H(\mu_H+\delta_H)+N_h\alpha_h\Lambda_H} < \infty$, then $0 \le f_1(V) < \infty$. This signify that $f_1(V)$ is bounded. Therefore

$$\frac{\partial f_1}{\partial V} = \frac{G_0\alpha_H\beta_H(T)N_h\alpha_h\Lambda_H\mu_H(\mu_H+\gamma_H+\delta_H)}{[G_0\alpha_H[\mu_H(\mu_H+\gamma_H+\delta_H)+V(\mu_H+\delta_H)]+N_h\alpha_h\Lambda_H V]^2} > 0, \tag{6.3.0.13}$$

$$\frac{\partial^2 f_1}{\partial V^2} = \frac{-2G_0\alpha_H\beta_H(T)N_h\alpha_h\Lambda_H\mu_H(\mu_H+\gamma_H+\delta_H)[G_0\alpha_H(\mu_H+\delta_H)+N_h\alpha_h\Lambda_H]}{[G_0\alpha_H[\mu_H(\mu_H+\gamma_H+\delta_H)+V(\mu_H+\delta_H)]+N_h\alpha_h\Lambda_H V]^3},$$
$$< 0. \tag{6.3.0.14}$$

This demonstrates that $f_1(V)$ is an increasing concave down function which has no convexity. So there is a unique positive V^{**} such that $f_1(V^{**}) = H^{**} > 0$.

The function $f_2(H)$ produces the function

$$f_2(H) = \frac{\beta_V(T)N_v\alpha_v H[\Lambda_V(T)-(H^{**}+\mu_V(T))]}{P_0\phi_V\alpha_V(H+\mu_V(T))+N_v\alpha_v H[\Lambda_V(T)-(H+\mu_V(T))]}. \tag{6.3.0.15}$$

Since $f_2(0)=0$ and $\lim_{H\to\infty} f_2(H) = \beta_V(T) < \infty$. Thus, $0 \le f_2(H) < \infty$. This indicate that $f_2(H)$ is bounded.

$$\frac{\partial f_2(H)}{\partial H} = \frac{\psi_1\psi_2\psi_4\beta_V(T)}{(\psi_1(H+\mu_V(T))+\psi_2\psi_3 H)^2}, \tag{6.3.0.16}$$

$$\frac{\partial^2 f_2(H)}{\partial H^2} = -\frac{2\psi_1\psi_2\beta_V(T)\left[\psi_1(H+\mu_V(T))^2+\psi_1\psi_4+\psi_2\psi_3\psi_4+\psi_2\Lambda_V(T)H^2\right]}{(\psi_1(H+\mu_V(T))+\psi_2\psi_3 H)^3} \tag{6.3.0.17}$$

where

$$\begin{aligned}\psi_1 &= P_0\phi_V\alpha_V,\\ \psi_2 &= N_v\alpha_v,\\ \psi_3 &= [\Lambda_V(T)-(H+\mu_V(T))],\\ \psi_4 &= [\mu_V(T)\Lambda_V(T)-(H+\mu_V(T))^2].\end{aligned} \tag{6.3.0.18}$$

$$\begin{aligned}\frac{\partial f_2(H)}{\partial H} &> 0,\\ \frac{\partial^2 f_2(H)}{\partial H^2} &< 0,\end{aligned}$$

when $\Lambda_V(T) > (H+\mu_V(T))$ and $\mu_V(T)\Lambda_V(T) > (H+\mu_V(T))^2$.
This indicates that $f_2(H)$ is an increasing concave down function which has no change of convexity. Therefore, there exist a unique positive H^{**} such that $f_2(H^{**}) = V^{**} > 0$. However, (H^{**}, V^{**}) is a fixed point of which correspond to an endemic state E_2 of the multiscale model (6.2.1.12).

For testing the stability of (H^{**}, V^{**}), we expect that $|f'(H^{**}, V^{**})| < 1$ and for when there is instability of (H^{**}, V^{**}), we expect that $|f'(H^{**}, V^{**})| > 1$. The Jacobian matrix of f at (H^{**}, V^{**}) is given by

$$J^{**} = \begin{pmatrix} \dfrac{\partial f_1(V)}{\partial V}_{|(H^{**},V^{**})} & \dfrac{\partial f_1(V)}{\partial H}_{|(H^{**},V^{**})} \\ \dfrac{\partial f_2(H)}{\partial V}_{|(H^{**},V^{**})} & \dfrac{\partial f_2(H)}{\partial H}_{|(H^{**},V^{**})} \end{pmatrix}, \tag{6.3.0.19}$$

Therefore,

$$\begin{aligned}\frac{\partial f_1(V)}{\partial V} &= \frac{G_0\alpha_H\beta_H(T)N_h\alpha_h\Lambda_H\mu_H(\mu_H+\gamma_H+\delta_H)}{[G_0\alpha_H[\mu_H(\mu_H+\gamma_H+\delta_H)+V(\mu_H+\delta_H)]+N_h\alpha_h\Lambda_H V]^2} > 0,\\ \frac{\partial f_1(V)}{\partial H} &= 0,\\ \frac{\partial f_2(H)}{\partial V} &= 0,\\ \frac{\partial f_2(H)}{\partial H} &= \frac{\psi_1\psi_2\psi_4\beta_V(T)}{[\psi_1(H+\mu_V(T))+\psi_2\psi_3 H]^2} > 0.\end{aligned} \tag{6.3.0.20}$$

$$\begin{vmatrix} \dfrac{\partial f_1(V)}{\partial V}-\lambda & 0 \\ 0 & \dfrac{\partial f_2(H)}{\partial H}-\lambda \end{vmatrix} = 0. \tag{6.3.0.21}$$

Thus,

$$\left(\frac{\partial f_1(V)}{\partial V}-\lambda\right)\left(\frac{\partial f_2(H)}{\partial H}-\lambda\right)=0,$$
$$\lambda^2-\left(\frac{\partial f_1(V)}{\partial V}+\frac{\partial f_2(H)}{\partial H}\right)\lambda+\frac{\partial f_1(V)}{\partial V}\frac{\partial f_2(H)}{\partial H}=0. \tag{6.3.0.22}$$

The solution of equation (6.3.0.22) is given by

$$\begin{aligned} D_1 &= \frac{1}{2}\left[\left(\frac{\partial f_1(V)}{\partial V}+\frac{\partial f_2(H)}{\partial H}\right)+\sqrt{\left(\frac{\partial f_1(V)}{\partial V}+\frac{\partial f_2(H)}{\partial H}\right)^2-4\frac{\partial f_1(V)}{\partial V}\frac{\partial f_2(H)}{\partial H}}\right] \\ D_2 &= \frac{1}{2}\left[\left(\frac{\partial f_1(V)}{\partial V}+\frac{\partial f_2(H)}{\partial H}\right)-\sqrt{\left(\frac{\partial f_1(V)}{\partial V}+\frac{\partial f_2(H)}{\partial H}\right)^2-4\frac{\partial f_1(V)}{\partial V}\frac{\partial f_2(H)}{\partial H}}\right] \end{aligned} \tag{6.3.0.23}$$

Therefore

$$\begin{aligned} D_1 &= \frac{1}{2}\left[\left(\frac{\partial f_1(V)}{\partial V}+\frac{\partial f_2(H)}{\partial H}\right)+\sqrt{\left(\frac{\partial f_1(V)}{\partial V}-\frac{\partial f_2(H)}{\partial H}\right)^2}\right] \\ D_2 &= \frac{1}{2}\left[\left(\frac{\partial f_1(V)}{\partial V}+\frac{\partial f_2(H)}{\partial H}\right)-\sqrt{\left(\frac{\partial f_1(V)}{\partial V}-\frac{\partial f_2(H)}{\partial H}\right)^2}\right], \end{aligned} \tag{6.3.0.24}$$

where

$$\begin{aligned} D_1 &= \frac{\partial f_1(0)}{\partial V}=\frac{N_h\alpha_h\beta_H(T)\Lambda_H}{G_0\alpha_H\mu_H(\mu_H+\gamma_H+\delta_H)}=R_{0H}, \\ D_2 &= \frac{\partial f_2(0)}{\partial H}\frac{N_v\alpha_v\beta_V(T)[\Lambda_V(T)-\mu_V(T)]}{P_0\phi_V\alpha_V\mu_V(T)}=R_{0V}. \end{aligned} \tag{6.3.0.25}$$

The fact that $det(J^{**})>0$ implies that

$$\begin{aligned} \left|\frac{\partial f_1(V)}{\partial V}+\frac{\partial f_2(H)}{\partial H}\right| &> \sqrt{\left(\frac{\partial f_1(V)}{\partial V}-\frac{\partial f_2(H)}{\partial H}\right)^2}, \\ \left(\frac{\partial f_1(V)}{\partial V}+\frac{\partial f_2(H)}{\partial H}\right)^2 &> \left(\frac{\partial f_1(V)}{\partial V}-\frac{\partial f_2(H)}{\partial H}\right)^2, \\ \frac{\partial f_1(V)}{\partial V}\frac{\partial f_2(H)}{\partial H} &> 0. \end{aligned} \tag{6.3.0.26}$$

Thus, both $D_1>0$ and $D_2>0$. Since $D_i=\rho(J(H^{**},V^{**}))$ is the dominant eigenvalue of the Jacobian matrix where $i=1,2$, then the fixed point (H^{**},V^{**}) asymptotically stable when the dominant eigenvalue $D_i<1$ (i.e $D_1=R_{0H}<1$ and $D_2=R_{0V}<1$) and unstable when $D_i>1$.

6.4 Numerical results

We perform numerical simulations using the Runge-Kutta scheme in Python version 2.7 to verify some of the analytical results for stability of the system of equations (6.2.1.12). The parameter values that we utilise for numerical simulations are in Tables (6.2) - (6.4). For numerical simulations, the following initial values are used: $L_M(0) = 300000$, $S_V(0) = 100000$, $I_V = 200$, $G_v(0) = 100$, $G_m(0) = 100$, $Z_v(0) = 10$, $O_v = 10$, $P_v(0) = 10$, $P_V(0) = 40000$, $S_H(0) = 10000$, $I_H(0) = 70$, $R_h(0) = 500$, $R_m(0) = 5$, $M_h(0) = 50$, $G_h(0) = 15$ and $G_H(0) = 1000$.

Table 6.2: Parameter values and their description.

Parameter	Description	Value	Source
$a(T)$	Mosquito biting rate.	$0.000203T(T-11.7)\sqrt{(42.3-T)}$	[79]
$\Lambda_L(T)$	Recruitment by birth of juveniles	$2.325a(T)$	[79]
$\alpha_L(T)$	The rate at which juveniles develops into adult.	$\frac{2.325a(T)}{10}$	[79]
$\mu_L(T)$	Mortality rate of juveniles.	$0.0025T^2 - 0.094T + 1.0257$	[79]
$\mu_V(T)$	Mortality rate of mosquitoes.	$-\ln(\exp\{\frac{-1}{-0.03T^2+1.31T-4.4}\})$	[79]
b_V	Proportion of bites by susceptible mosquitoes on infected humans that produce infection.	0.04	[79]
b_H	Proportion of bites by infectious mosquitoes on susceptible humans that produce infection.	0.09	[79]
δ_L	The rate at which larvae reduced by other species.	0.08	Estimated
$\beta_V(T)$	Contact rate of susceptible humans with the infectious reservoir of mosquitoes.	$a(T)b_H$	
$\beta_H(T)$	Infection rate of susceptible mosquitoes which depends on temperature.	$a(T)b_V$	
ϕ_V	Proportion of new infected mosquitoes in the total infected mosquito population.	0.0001	[24]
δ_V	induced death rate of infected mosquitoes.	0.00000426	[24]
P_0	Half saturation constant associated with the infection of humans.	1×10^6	Estimated.
α_V	Rate of clearance of community sporozoite load.	0.3	[24]

Table 6.3: Parameter values and their description.

Parameter	Description	Initial Value	Range	Units	Source
Λ_H	Rate of recruitment of Susceptible humans.	600	10-800	Humans per day	[35]
μ_H	Natural death rate of humans.	0.00004	0.00001-0.00008	day^{-1}	[24]
δ_H	Disease induced death rate of humans.	0.0003454	$1 \times 10^{-15} - 4.1 \times 10^{-4}$	day^{-1}	[35]
γ_H	Natural recovery rate of humans.	0.0092	0.0014-0.017	day^{-1}	[35]
G_0	Half saturation constant associated with the infection of mosquitoes.	5×10^6	$1\times10^6 - 1\times10^9$	day^{-1}	[24]
α_H	Rate of clearance of community gametocyte load.	0.0000913	0.0000467-0.000274	day^{-1}	[24]
Λ_v	The rate of supply of gametocytes within infected mosquitoes.	3000	100-3000	Gametocytes per day	Assumed
α_g	Rate at which gametocyte infected erythrocytes burst within ifected mosquito.	96	90-100	day^{-1}	[24]
μ_g	Decay rate of gametocytes within infected mosquito.	0.0625	0.0326-0.0725	day^{-1}	[24]
N_g	Number of gametes produced per gametocyte infected erythrocyte within infected mosquito.	2	1-3	Gametes per day	[24]
α_z	Rate at which zygote develop into oocysts.	0.4240	0.01-0.5	day^{-1}	[24]
μ_z	Natural death rate of zygote.	1	1-4	day^{-1}	[24]
α_s	Fertilisation of gametes.	0.2	0.01-0.2	day^{-1}	[24]
μ_s	Natural death rate of gametes.	58	40-129	day^{-1}	[24]
α_k	Bursting rate of oocysts to produce sporozoites.	0.2	0-1	day^{-1}	[24]
N_k	Number of sporozoites produced per bursting oocysts.	3 000	1000-10000	Sporozoites per day	[24]
μ_k	Natural death rate of oocysts.	0.01	0.071-0.143	day^{-1}	[24]
α_v	Rate at which sporozoites become infectious to humans.	0.025	0.0167-1	day^{-1}	[24]
μ_v	Natural death rate of sporozoites.	0.0001	0.0001-0.01	day^{-1}	[24]
Λ_h	Rate of suppy of uninfected red blood cells.	200	100-300	Cells per day	[24]

Table 6.4: Between-human scale parameter values and their description.

Parameter	Description	Initial Value	Range	Units	Source
β_h	Rate of infection of red blood cells (erythrocytes).	0.3	2×10^{-9}-0.4	day^{-1}	Assumed
α_h	Rate at which gametocytes develop and become infectious within infected human.	0.4	0.01-0.9	day^{-1}	[24]
μ_h	Natural death rate of gametocyte infected erythrocytes within infected human.	0.0625	0.0600-0.0625	day^{-1}	[24]
μ_b	Natural decay rate of red blood cells.	0.0083	0.006-0.1	day^{-1}	[24]
μ_m	Natural decay rate of free merozoites	0.001	0.001-0.5	day^{-1}	[24]
π	Proportion of gametocytes infected erythrocytes.	0.4	0.1-0.5	day^{-1}	[24]
N_m	Number of merozoites produced per bursting erythrocytes.	16	10-30	Merozoites per day	[77]
α_m	Rate at which erythrocytes burst to produce merozoites.	0.5	0.1-1.0	day^{-1}	[24].

In figure (6.1), we notice the effects of varying temperature on the between-human host model (Juvenile mosquitoes L_M, susceptible mosquitoes S_V, infected mosquitoes I_V and community sporozites load P_V). We notice that as we increase the temperature values, the variables L_M, S_V, I_V and P_V also increases until it reach an optimal level as the temperature is between 28^0C and 32^0C. When the temperature is 32 and above, we notice the decline of population of L_M, S_V, I_V and P_V. Therefore, the increase in temperature have an influence of increasing the spread of malaria disease system in the community.

Figure (6.2) demonstrates the influence of varying temperature on between-human host scale variables(i.e. susceptible humans (S_H), infected humans (I_H) and community gametocytes load (G_H)). We discover that as temperature increases from 18^0C-34^0C, there is a decrease in susceptible humans. We notice that susceptible humans reach a minimum when the temperature is around 36^0C. The susceptible humans starts to increase when the temperature is above 36^0C. When temperature increase from 18^0C-36^0C, we observe a slightly increase in infected human (I_H) and community gametocytes load (G_H) and when the temperature continues to increase after 36^0C, we notice decline in I_H and G_H. Therefore, temperature has an influence in transmission of malaria disease system in the community.

Figure (6.3) indicates the time evolution of within-mosquito vector scale variables (i.e. erythrocytes gametocytes within infected mosquitoes (G_v), the population of gametes (G_m), population of zygotes (Z_v) and the population of sporozoites (P_v)), for changes in temperature. The numerical results also indicate that

the four variables (G_v, G_m, Z_v and P_v), are sensitive to temperature changes. As temperature increases we observe that the erythrocytes gametocytes within-infected mosquito (G_v), the population of gametes (G_m) and the population of zygotes (Z_v) quickly reach the peak of the graph or takes shorter time to reach the peak. We also notice that as temperature increases, the peak of the graph also rise. The results also implies that as the temperature increases, we also observe an increase in population of sporozoites. Therefore, temperature changes have an influence in the malaria parasite growth within the infected mosquito, which have an effect in malaria transmission at community level.

In Figure (6.4) demonstrates the changes in within-human host variables (i.e uninfected erythrocytes (R_h), infected erythrocytes (R_m), population of merozoites (M_h) and population of gametocytes (G_h)), for temperature variations. The numerical results show that the four within-human scale variables (R_h, R_m, M_h and G_h) are not sensitive to temperature changes.

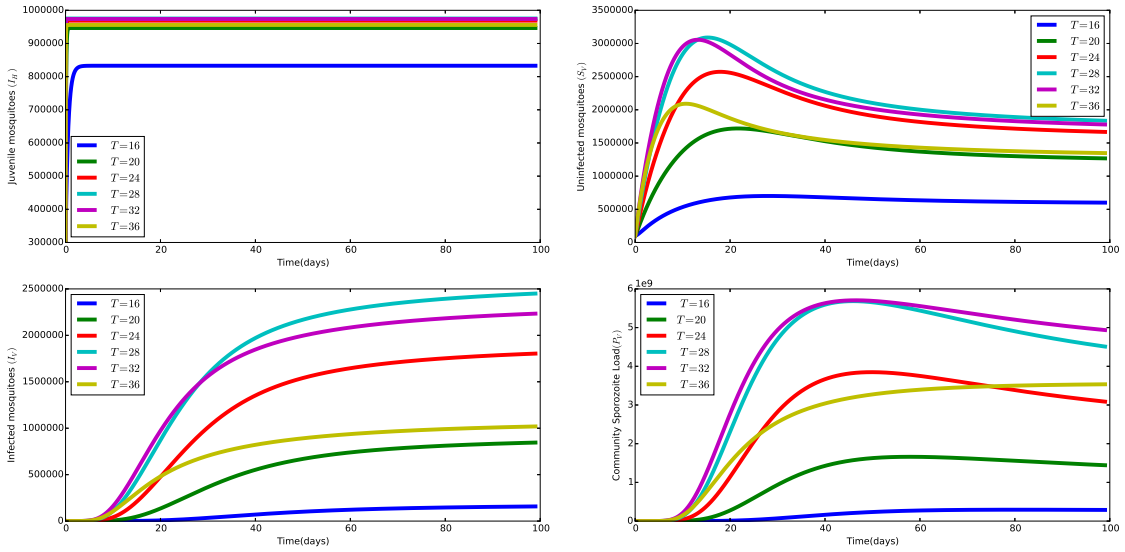

Figure 6.1: Graphs illustrating changes in Juvenile mosquitoes, susceptible mosquitoes, infected mosquitoes and community sporozoites load as temperature varies T: $T = 16$, $T = 20$, $T = 24$, $T = 28$, $T = 32$, $T = 36$

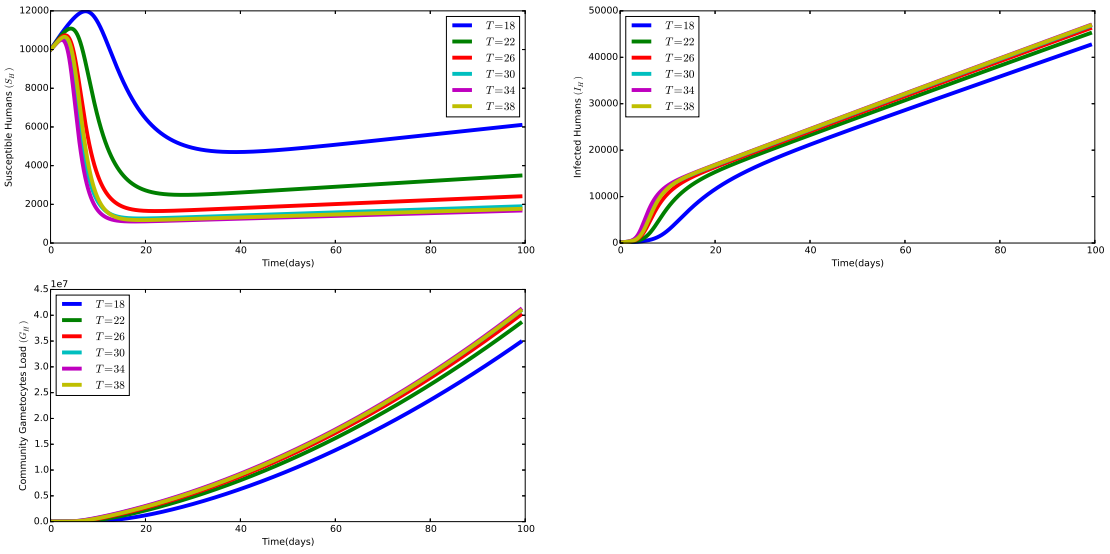

Figure 6.2: Graphs illustrating changes in susceptible Humans, infected humans and community gametocytes load as temperature varies T: $T = 18$, $T = 22$, $T = 26$, $T = 30$, $T = 34$, $T = 38$

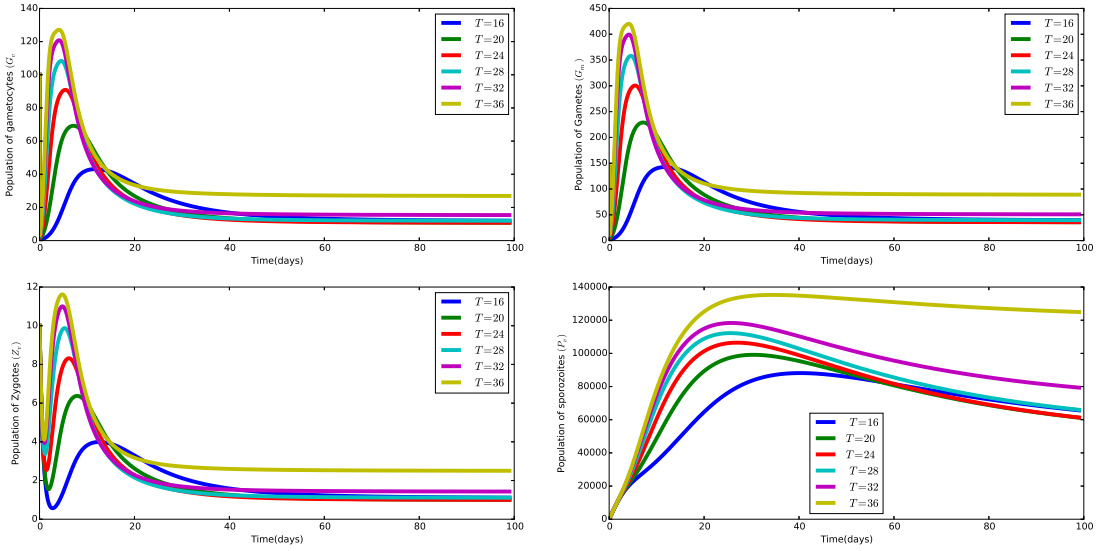

Figure 6.3: Graphs illustrating changes in population of gametocytes with infected mosquitoes, population of gametes, population of zygotes and population of sporozoites as temperature varies T: $T = 16$, $T = 20$, $T = 24$, $T = 28$, $T = 32$, $T = 36$

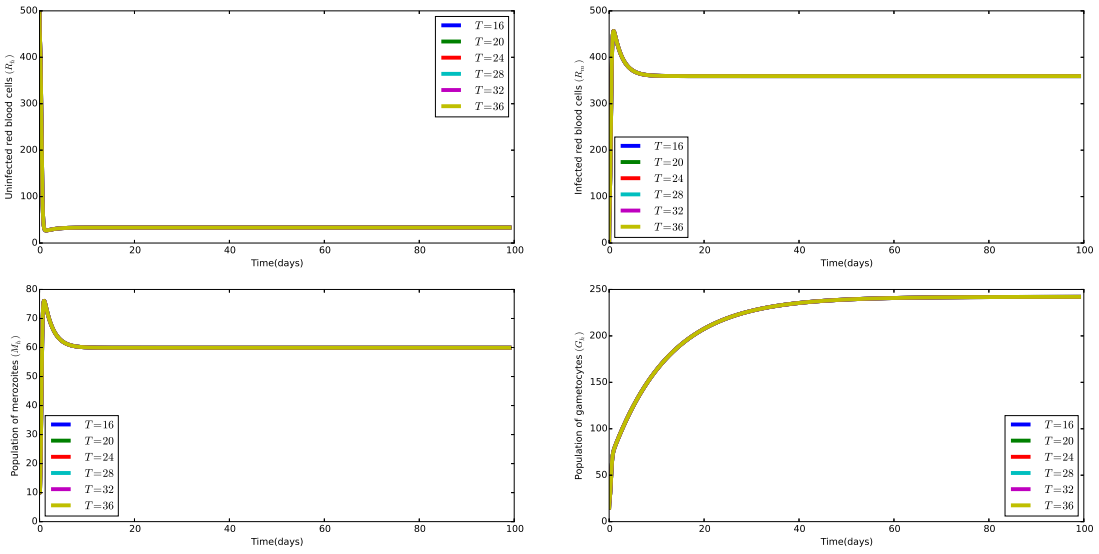

Figure 6.4: Graphs illustrating changes in uninfected erythrocytes, infected erythrocytes, population of merozoites and population of sporozoites as temperature varies T: $T = 16$, $T = 20$, $T = 24$, $T = 28$, $T = 32$, $T = 36$

6.5 Summary

In this study, we presented a multiscale model of malaria disease system to explore the impact of temperature changes on malaria pathogen replication-transmission using system of ordinary differential equations. The multi-scale model of malaria disease system we formulate in this study, explicitly traces the malaria pathogen life cycle between the two hosts (i.e human and mosquito) and on both scales (i.e. within-host scale and between-host scale). The disease-free equilibrium state was noted to be locally asymptotically stable. Using the fixed-point theorem, the stability of the endemic equilibrium was observed to be stable. The results from the graphs indicated that as the temperature increases the population of infected humans, population of infected mosquitoes, community gametocytes load and community sporozoites load increases and reach at maximum when temperature is around 32^0C and then decreases. These conclude that temperature have influence in increasing the malaria transmission. We also noticed that temperature have influence on increasing malaria progression for within-mosquito host scale. One of the key intervention controls recommended by World Health Organisation (WHO) in areas with high temperatures is the use of long-lasting insecticides treated nets (LLINs) for individuals and communities that are at high risk of malaria disease is one of the effective measures in malaria control. By considering the juvenile stage of mosquitoes in addition to the adult mosquito model enables to better understand the mosquito population dynamics and their impact on human population dynamics for malaria transmission dynamics. The incorporation of such juvenile stage may also provide some insights into designing larval control strategies in

reducing the spread of malaria disease. Therefore insecticides-treated bed nets use is one of the effective measures in malaria control. In conclusion, the results presented in this study are useful in advice the policy-makers and those who are responsible to implement the effective malaria health interventions in endemic regions with malaria disease and to adopt better strategies for improving controlling of malaria diseases.

Chapter 7

A Multiscale Model of Malaria Disease Dynamics with Mosquito life-cycle

7.1 Introduction

Infectious disease remains a significant public health challenge worldwide, despite the major development in the prevention and treatment [85]. Participating in battling against an infectious disease system involves combining the effort, among which incorporate a holistic understanding of the infectious mechanisms. Infectious disease system is the result of the interaction of three main sub-systems which are: (i) the host sub-system, (ii) the pathogen sub-system, and (iii) the environmental sub-system. These sub-systems result in infectious disease systems being structured into multi-level and multi-scale complex systems, where levels of organization range from the cell-level, tissue-level, organ-level, micro-ecosystem level, host-level, community-level, and macro-ecosystem level, which are demonstrated in the diagram (1.2). In this study, we describe the approach for the development of a multiscale model of type II vector-borne disease system, that is, we consider the malaria disease system as a case study. The malaria disease system is caused by a parasite called Plasmodium Falciparum. The parasite life cycle is strictly internal of the two inside-host environments (that is, within-human host scale and within-mosquito host scale) that are related to malaria transmission of multi-hosts infection [18]. There are two groups of type II vector-borne disease systems which are demonstrated in [18] which are:

(a) The type II vector-borne diseases with no pathogen replication cycle at the within-host scale (that is, there is no pathogen replication at the within-mosquito scale). The within-host scale pathogen load will increase through super-infection, which makes use of the embedded multiscale model.

(b) The other group of type II vector-borne disease systems with pathogen life stages has a pathogen-replication cycle at the within-host scale (that is, there is a replication cycle of merozoites at the within-human scale).

Our coupled multiscale model of malaria infectious disease system will use the combination of these two groups of type II vector-borne disease systems. The objective of this chapter is to investigate the influence of the mosquito life cycle on the multiscale model of the malaria disease system. Our multiscale model of malaria disease system with mosquito life cycle consists of three parts which are: (a) immature mosquito population, (b) mature mosquito population (within-mosquito scale and between-mosquito scale, and (c) human population (within-human scale and between-human scale).

The studies done on the mathematical models of mosquito life cycle are as follows: Abdelrazec [86] developed a mathematical model on transmission mechanism theory that incorporates the dynamics of immature and female adult Anopheles mosquitoes. They assess the impact of changes in temperature and rainfall on the density of mosquitoes in the community. White [87] develops a mathematical model using transmission mechanism theory to compare the influence of vector interventions applied against adult mosquitoes using long-lasting treated nets (LLNs), indoor residual spraying (IRS), and also used against immature mosquito stages, alone and in combination with mature mosquito density. These studies were only concentrated on transmission mechanism theory on the mosquito life cycle. Koutou ([88] presented a mathematical model of malaria disease system on transmission mechanism theory. Their model is an autonomous system constructed by considering two models, which are (i) model of vector population which includes immature and adult population, and (ii) model of pathogen transmission using the transmission mechanism theory on the between-host scale. The model on transmission mechanism theory in [89] present a mathematical model of malaria transmission dynamics with age-structured for the vector population (that is, immature and adult female Anopheles mosquitoes) and aperiodic biting rate of female Anopheles mosquitoes. In the human population, they use the between-host scale model where they divided the population into two major categories which are: the most vulnerable called non-immune, and the least vulnerable called semi-immune. We found out that majority of the models developed of malaria disease systems that include the mosquito life cycle focused on a single scale infection, that is, between-host (mosquito and human) scale.

From the previous works on pathogen replication transmission relativity theory of type II vector-borne diseases, there is none that consider the work on immature and adult mosquito stages (that is, within-mosquito scale and between-mosquito scale) in the control of malaria disease dynamics. Although most models on mosquitoes and vertebrate hosts dynamics are usually neglected the immature mosquito stage that could have an influence on malaria disease incidence in both spatial and temporal scales. There are models which are among the most significant novelties that address multiscale models (that is, pathogen replication transmission relativity theory) of the malaria parasite population dynamics within-infected human scale that includes human immunity and progression from infection of the individual host to between-host

scale [90]. The studies were done in [35] and [24] demonstrate on pathogen replication transmission relativity theory on malaria infectious disease dynamics, of which none address the influence of immature mosquito stage on the progression of malaria disease system.

Based on our coupled multiscale mode, we apply the intervention methods that will target stages in the mosquito life cycle that is the immature and the adult mosquitoes. and parasite life cycle. For intervention method for the immature mosquito stage will target the eggs, larva, and pupa. Intervention method targeted at the adult mosquito using community sporozoite load as a measure of intervention effectiveness. The intervention method targeted the human host population using the community gametocyte load as a measure of intervention effectiveness. The intervention method targeted the gametocytes and merozoites within the infected human scale, which helps to investigate the efficacy of the different drug interventions acting on multiple stages. These intervention methods have an impact on the reduction in transmission of malaria disease within the community. These will help to understand the impact of the mosquito life cycle on the multiscale model of the malaria disease system.

7.2 Model formulation

When the Anopheles mosquitoes get blood meal from biting human host population, they migrate to aquatic environment to lay their eggs, after about two-three days the eggs hatch into larval. The immature phase of the mosquito population is observed as the source of malaria disease system. The mosquito to pass through four separate and different phases of its life-cycle and these stages are as follows: eggs, larval, pupa and adult. Each of these phases can be easily recognised by its special appearance. All the female anopheles mosquitoes lay their eggs in a variety of water surfaces (aquatic environment). Anopheles mosquitoes can either lay their eggs one at a time or in groups called a raft every ten to fourteen days. Most eggs can survive the winter and hatch in spring. Most eggs hatch within a period of two days of being laid, the mosquito eggs hatch into larvae. The larvae live at the surface of the water and breathe through an air tube called a siphon. As they grow and develop, the larvae shed their skin several times. In the final underwater phase of development, the larvae develop into pupae, this process lasts between four to five days. They float to the surface of the water and breathe through the two small tubes called trumpets. At the end of this stage, the pupae encase themselves within a pupal case where they transform into adult mosquitoes. The complete developed mosquito then crawls to a protected place and rests while its external skeleton hardens. Once dry, the mature mosquito flies away to feed and seek a mate. While males feed on plants juices with their shorter mouth parts, females feed on human and animal blood with their longer mouth parts (proboscis). After feeding the females lay their eggs and the cycle will continues if the female Anopheles mosquito lives. Adult mosquito most especially anopheles' mosquito cannot survive in the absence of human and vertebrate host. When the human population and the female Anopheles mosquito population interact cause malaria which leads to serious sickness and death to the human host

population.

This model describes a mathematical dynamic model for mosquito-vector population, where their life-cycle is divided into two phases, the acquatic environment that is immature mosquito is divided into three subpopulation: eggs $(E_E(t))$, larval $(L_W(t))$ and pupal $(P_M(t))$, the aerial environment that is adult mosquito is divided into two sub-populations: Susceptible mosquito populations $S_V(t)$, infected mosquito populations $(I_V(t))$ and community sporozoites load $(P_V(t))$, within-infected mosquito variables: population of gametocytes within infected adult mosquito $(G_v(t))$, population of gametes $(G_m(t))$, population of zygotes $(Z_v(t))$, population of ookynetes $(O_v(t))$, and population of sporozoites within infected adult mosquito $(P_v(t))$, between-humans population includes: susceptible human populations $(S_H(t))$, infected human populations $(I_H(t))$ and community gametocytes load $G_H(t)$ and within-infected human variables includes: uninfected red-blood cells $(R_h(s))$, infected red blood cells $(R_m(s))$, merozoites populations $(M_h(s))$ and gametocytes populations within infected-humans $(G_h(s))$. This multiscale model of malaria disease system with mosquito life cycle has the following assumptions:

(a) There is no vertical transmission of the malaria disease system.

(b) The transmission of malaria disease is only caused through mosquito bites when the mosquito takes a blood meal, which is direct transmission.

(c) The infected mosquito population does not recover naturally from their infection, whilst the infected human population recovers naturally from their infection.

(d) All the newly supplied humans are assumed to be healthy and have not been previously contacted or exposed to malaria disease and also the newly supplied susceptible mosquitoes are assumed to be healthy and have been previously exposed to malaria disease.

(e) The supply of susceptible mosquito population are only mature female Anopheles mosquitoes.

(f) The supply of eggs is from both susceptible and infected mosquito populations, that is, the total production of eggs from the total population of mosquitoes (N_V).

Based on the assumptions above and the flow diagram displayed in (7.1), the coupled multiscale model of malaria disease system with mosquito cycle is given by the system of non-linear ordinary differential equations given in system of equation (7.2.0.1).

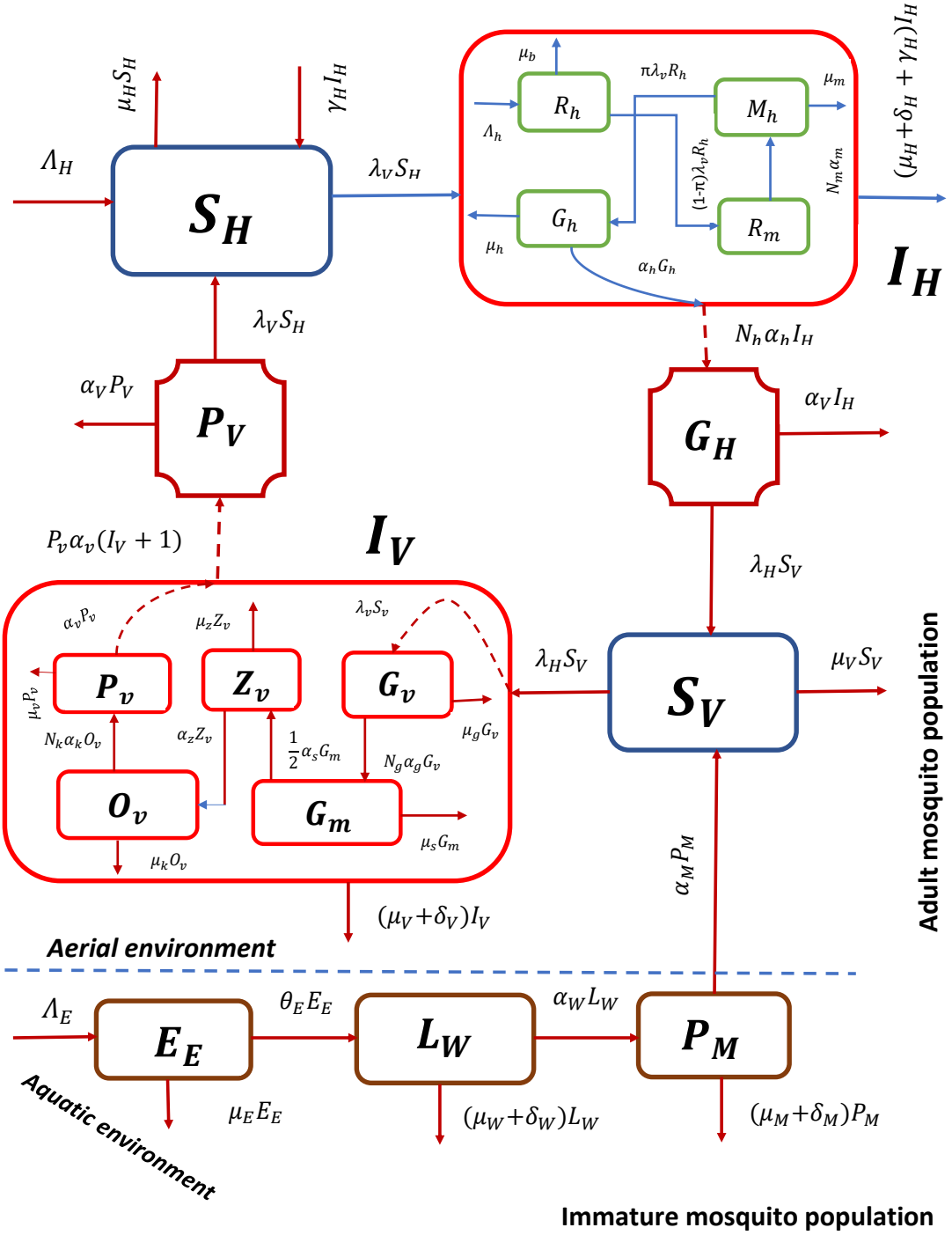

Figure 7.1: A conceptual diagram of the multiscale model of malaria disease dynamics with mosquito life cycle

$$
\begin{aligned}
1.\quad \frac{dE_E(t)}{dt} &= \Lambda_E - (\mu_E + \theta_E)E_E(t),\\
2.\quad \frac{dL_W(t)}{dt} &= \theta_E E_E(t) - (\mu_W + \alpha_W + \delta_W)L_W(t),\\
3.\quad \frac{dP_M(t)}{dt} &= \alpha_W L_W(t) - (\mu_M + \alpha_M + \delta_M)P_M(t),\\
4.\quad \frac{dS_V(t)}{dt} &= \frac{\alpha_M P_M(t)}{2} - \frac{\beta_H G_H(t) S_V(t)}{G_0 + G_H(t)} - \mu_V S_V(t),\\
5.\quad \frac{dI_V(t)}{dt} &= \frac{\beta_H G_H(t) S_V(t)}{G_0 + G_H(t)} - (\mu_V + \delta_V)I_V(t),\\
6.\quad \frac{dG_v(t)}{dt} &= \frac{\beta_H G_H(t)(S_V(t) - 1)}{(G_0 + G_H(t))\phi_V(I_V(t) + 1)} - [\alpha_g + \mu_g]\, G_v(t),\\
7.\quad \frac{dG_m(t)}{dt} &= N_g \alpha_g G_v(t) - [\alpha_s + \mu_s]\, G_m(t),\\
8.\quad \frac{dZ_v(t)}{dt} &= \frac{1}{2}\alpha_s G_m(t) - [\alpha_z + \mu_z]\, Z_v(t),\\
9.\quad \frac{dO_v(t)}{dt} &= \alpha_z Z_v(t) - [\alpha_k + \mu_k]\, O_v(t),\\
10.\quad \frac{dP_v(t)}{dt} &= N_k \alpha_k O_v(t) - [\alpha_v + \mu_v]\, P_v(t).\\
11.\quad \frac{dP_V(t)}{dt} &= P_v(t)\alpha_v(I_V(t) + 1) - \alpha_V P_V(t).\\
12.\quad \frac{dS_H(t)}{dt} &= \Lambda_H - \frac{\beta_V P_V(t) S_H(t)}{P_0 + P_V(t)} - \mu_H S_H(t) + \gamma_H I_H(t),\\
13.\quad \frac{dI_H(t)}{dt} &= \frac{\beta_V P_V(t) S_H(t)}{P_0 + P_V(t)} - (\mu_H + \gamma_H + \delta_H)I_H(t),\\
14.\quad \frac{dR_h(s)}{ds} &= \Lambda_h - \beta_h R_h(s) M_h(s) - \mu_b R_h(s),\\
15.\quad \frac{dR_m(s)}{ds} &= (1 - \pi)\beta_h R_h(s) M_h(s) - \alpha_m R_m(s),\\
16.\quad \frac{dM_h(s)}{ds} &= N_m \alpha_m R_m(s) - \mu_m M_h(s),\\
17.\quad \frac{dG_h(s)}{ds} &= \pi \beta_h R_h(s) M_h(s) - [\alpha_h + \mu_h] G_h(s),\\
18.\quad \frac{dG_H(t)}{dt} &= G_h(s)\alpha_h I_H(t) - \alpha_H G_H(t).
\end{aligned}
\tag{7.2.0.1}
$$

The first equation in system of equation (7.2.0.1) describe the dynanics of mosquito egg stage $(E_W(t))$. The first term on the right hand side of the mosquito egg stage is the supply of eggs from the total mosquito population $N_V(t)$ at a rate Λ_E. The mosquito egg stage is reduced by the natural decay at a rate μ_E and also by developing into larval at a rate θ_E. The second equation of the model (7.2.0.1) demonstrate the dynamics of mosquito larval stage $(L_W(t))$. The mosquito larval stage increase through the egg development at a rate θ_E and decrease by natural decay at a rate μ_W, by other species that feeds on larval mosquitoes at a rate δ_W, and through the development of larval into pupa at a rate α_W. The third equation of the model (7.2.1.1) describe the dynamics of mosquito pupa stage $(P_M(t))$. The first term on the right

hand side of the mosquito pupa stage increase through the larval development into pupa at a rate α_W and decrease through natural decay at a rate μ_M, through species that feeds on mosquito pupa at a rate δ_M, and through development of pupa into adult mosquito at a rate α_M. The fourth equation of model (7.2.0.1) demonstrate the dynamics of adult susceptible mosquito population $(S_V(t))$. The adult susceptible mosquito population is supplied by constant term $\frac{\alpha_M}{2}$, which is the rate of development of pupal mosquito into adult female Anopheles mosquito. The adult susceptible mosquito population is depleted through infection of adult susceptible mosquito at a variable rate $\frac{\beta_H G_H(t) S_V(t)}{G_0 + G_H(t)}$ and natural death at a constant rate μ_V, where β_H is the contact rate of susceptible mosquito with the human infectious reservoir. The fifth equation in system (7.2.0.1) demonstrates the dynamics of infected mosquitoes. This equation increase through the infection of susceptible mosquitoes and also decreased through natural death rate μ_V and also disease induced death rate δ_V.

The sixth equation in system (7.2.0.1) demonstrates the dynamics of gametocytes infected erythrocytes within an infected mosquito after a mosquito gets a blood meal from an infected human. The first term on the right-hand-side of this equation is the new infection at an individual mosquito at a variable rate $\frac{\beta_H G_H(t)(S_V(t)-1)}{(G_0+G_H(t))(I_V(t)+1)}$. This equation depleted through natural decay rate of gametocyte infected erythrocytes within an infected mosquito μ_g and also through α_g the rate at which gametocyte infected erythrocytes burst releasing sex cells called gametes. The seventh equation (7.2.0.1) describes the dynamics of the population of gametes within an infected mosquito. The first term of this equation is the rate of increase of gametes within an infected mosquito. The gametes decay at a rate μ_s and also depleted through male and female gametes fusing to form zygotes at a constant rate α_g. The eighth equation of system (7.2.0.1) demonstrates the dynamics of zygotes. The equation increase through gametes fuse to form zygotes at a rate $\frac{\alpha_s}{2}$ and depleted through natural decay μ_z and also through develop into oocysts at a rate α_s. The ninth equation of system (7.2.0.1) illustrates the dynamics of the population of oocysts in an infected mosquito. The first term in the right-hand-side of the ninth equation represent the rate of increase where the ookinetes transform into early oocysts. The second term is the rate of reduction of this population through either natural decay at a rate μ_k or burst and release sporozoites at a rate α_k. The tenth equation of system (7.2.0.1) describes the dynamics of sporozoites population in an infected mosquito. The first term of the RHS of the tenth equation is given by each oocysts bursts at a rate α_k releasing an average of N_k sporozoites upon bursting. Therefore, the rate of increase in sporozoites within an infected mosquito is given by $N_k \alpha_k O_v$. The tenth equation is reduced through either natural decay at a rate α_v or through the rate at which sporozoites mature and become infectious to humans and migrate to salivary glands of the infected mosquito. The eleventh equation of system (7.2.0.1) describes the community sporozoites load P_V. The equation increase by the up-scaling of within-host scale excretion/shedding of pathogen which is given by $P_v \alpha_v (I_V + 1)$ and reduced by α_V the rate of sporozoites eliminated from geographical area/ community area.

The twelveth equation in system (7.2.0.1) describes the dynamics of uninfected humans (susceptible)

$S_H(t)$.The population is assumed to increase at a constant rate Λ_H through birth and immigrants and also increase through natural recovered of infected individual at a rate γ_H. This population is reduced through infection of susceptible humans at a rate to $\frac{\beta V P_V(t)}{P_0 + P_V(t)}$, where β_V is the contact rate to a community sporozoite load $P_V(t)$ per unit time, P_0 is the community sporozoite load that yields 50% chance of getting a human host infected with malaria after a bite by a mosquito in a particular community. This equation also decreased by natural death at a constant rate μ_H. The thirteenth equation in system (7.2.0.1) demonstrates the dynamics of infected individuals. The equation increases through infection of susceptible humans and also depleted through natural death rate μ_H, recovery of the infected individual at rate γ_H and through disease induced death rate δ_H. The eighteenth equation in system (7.2.0.1), demonstrates the dynamics of the community gametocyte load (G_H). The first term in the right-hand-side of this equation describes the total number of gametocytes load contributed by all infected individuals from within-host process to the community gametocytes load pool, where $N_h = \widetilde{G_h}$ is defined as the measure of the total volume of gametocytes produced within an infected host throughout the entire period of host infectiousness and α_h is the proportion of individuals who are infected. α_H is the rate of degradation of this class.

The fourteenth equation in the system of equations (7.2.0.1), describes the dynamics of uninfected red blood cells within infected human $(R_h(s))$. The population of uninfected red blood cells is assumed to increase through the supply of red blood cells from the bone marrow at a rate Λ_h and the population of uninfected red blood cells decrease through the infection of red blood cells. $\beta_h R_h(s) M_h(s)$ models the rate at which the merozoites get contact with the uninfected red blood cells, where β_h is the infection rate or contact rate. The susceptible erythrocytes are also reduced through natural decay at a constant rate μ_b. The fifteenth equation of sub-model (7.2.0.1) illustrates the dynamics of merozoites infected red blood cells within infected human $(R_m(s))$. The dynamics of merozoites infected red blood cells increase through infection of susceptible red-blood cells with a propotion of $(1-\pi)$ and reduced through bursting of infected red blood cells to produce merozoites at a rate α_m. The sixteenth equation of sub-model (7.2.0.1) demonstrate the dynamics of population of merozoites. The dynamics of merozoites increase through the average number of merozoites releasedm in the human blood stream through bursting of infected red blood cells at a rate $N_m \alpha_m R_m(s)$. The population of merozoites reduced through natural decay at a rate μ_m. The last equation of sub-model (7.2.0.1) describe the dynamics of the population of gametocytes. The population of gametocytes increase through the population of gametocyte infected erythrocytes at a proportion π and the sub-model decrease through natural decay of gametocytes at a rate μ_h and through shedding/excretion of gametocytes at a rate α_h.

7.2.1 Simplification of the multiscale model

We adapt the simplifaction method in chapter 3 and the simplified multiscale model of model (7.2.0.1) is given by

$$
\begin{aligned}
1.\quad \frac{dE_E(t)}{dt} &= \Lambda_E - (\mu_E + \theta_E)E_E(t),\\
2.\quad \frac{dL_W(t)}{dt} &= \theta_E E_E(t) - (\mu_W + \alpha_W + \delta_W)L_W(t),\\
3.\quad \frac{dP_M(t)}{dt} &= \alpha_W L_W(t) - (\mu_M + \alpha_M + \delta_M)P_M(t),\\
4.\quad \frac{dS_V(t)}{dt} &= \frac{\alpha_M P_M(t)}{2} - \frac{\beta_H G_H(t) S_V(t)}{G_0 + G_H(t)} - \mu_V S_V(t),\\
5.\quad \frac{dI_V(t)}{dt} &= \frac{\beta_H G_H(t) S_V(t)}{G_0 + G_H(t)} - (\mu_V + \delta_V)I_V(t),\\
6.\quad \frac{dG_v(t)}{dt} &= \frac{\beta_H G_H(t)(S_V(t) - 1)}{(G_0 + G_H(t))\phi_V(I_V(t) + 1)} - [\alpha_g + \mu_g]\, G_v(t),\\
7.\quad \frac{dG_m(t)}{dt} &= N_g \alpha_g G_v(t) - [\alpha_s + \mu_s]\, G_m(t),\\
8.\quad \frac{dZ_v(t)}{dt} &= \frac{1}{2}\alpha_s G_m(t) - [\alpha_z + \mu_z]\, Z_v(t),\\
9.\quad \frac{dO_v(t)}{dt} &= \alpha_z Z_v(t) - [\alpha_k + \mu_k]\, O_v(t),\\
10.\quad \frac{dP_v(t)}{dt} &= N_k \alpha_k O_v(t) - [\alpha_v + \mu_v]\, P_v(t).\\
11.\quad \frac{dP_V(t)}{dt} &= P_v(t)\alpha_v(I_V(t) + 1) - \alpha_V P_V(t).\\
12.\quad \frac{dS_H(t)}{dt} &= \Lambda_H - \frac{\beta_V P_V(t) S_H(t)}{P_0 + P_V(t)} - \mu_H S_H(t) + \gamma_H I_H(t),\\
13.\quad \frac{dI_H(t)}{dt} &= \frac{\beta_V P_V(t) S_H(t)}{P_0 + P_V(t)} - (\mu_H + \gamma_H + \delta_H)I_H(t),\\
14.\quad \frac{dG_H(t)}{dt} &= N_h \alpha_h I_H(t) - \alpha_H G_H(t),
\end{aligned}
\tag{7.2.1.1}
$$

where N_h is a composite parameter that summarise the disease dynamics within an infected individual host. N_h models the average number of within-human host malaria parasite load available to be excreted into the between-host scale by each infected humanat a rate α_h. We make use of N_h obtained in chapter 3. Where

$$
N_h = \widetilde{G_h} = \frac{\pi}{(1-\pi)}\left[\frac{(1-\pi)N_m\beta_h\Lambda_h - \mu_b\mu_m}{N_m\beta_h(\alpha_h + \mu_h)}\right]. \tag{7.2.1.2}
$$

7.2.2 Positivity of Solutions

The system of equations (7.2.1.1) illustrates the dynamics of human, mosquito and parasite populations and it is essential to show that these populations are positive for all time $t \geq 0$. We have to prove the following theorem.

Theorem 7.1. *The solutions of the system of equations (7.2.1.1) satisfy the following initial conditions with strictly positive components i.e. ($E_E > 0$, $L_W > 0$, $P_M > 0$, $S_V > 0$,$I_V > 0$, $G_v > 0$, $G_m > 0$, $Z_v > 0$ $O_v > 0$, $P_v > 0$, $P_V > 0$, $S_H > 0$,$I_V > 0$ and $G_H > 0$) for all $t > 0$.*

Proof. We prove that the solution of system of equations (7.2.1.1) of which the solution starts from a strictly positive point, all components are positive for $0 \leq t \leq t_0$

$$\frac{dE_E(t)}{dt} \geq -(\mu_E + \theta_E)E_E(t).$$

The equation can be solved by the separation of variables as follows

$$\frac{dE_E(t)}{E_E(t)} =\geq -(\mu_E + \theta_E)dt, \tag{7.2.2.1}$$

By letting

$$\begin{aligned}\hat{t} \;=\; & \sup\{t > 0 : E_E > 0, L_W > 0, P_M > 0, S_V > 0, I_V, G_v > 0, G_m > 0, Z_v > 0,\\ & O_v > 0, P_v > 0, P_V, S_H > 0, I_H > 0, G_H > 0\} \in [0, t],\end{aligned}$$

and integrating equation (7.2.2.1), and we obtain

$$\begin{aligned}\ln(E_E(t)) &\geq -(\mu_E + \theta_E)t + \ln(E_E(0)),\\ E_E(t) &\geq E_E(0)\exp\{-(\mu_E + \theta_E)t\}\\ &> 0\end{aligned}$$

It implies that

$$\lim_{t\to\infty} \inf(E_E(t)) \geq 0.$$

Using the similar method , it can be shown that

$$\begin{aligned}\lim_{t\to\infty} \inf(L_W(t)) &\geq 0,\\ \lim_{t\to\infty} \inf(P_M(t)) &\geq 0.\end{aligned}$$

Using the similar method, we obtain

$$S_V(t) \geq S_V(0).\exp\left\{-\left(\mu_V t + \int_0^t \lambda_H(\hat{t})d\hat{t}\right)\right\}, \tag{7.2.2.2}$$

$$\lim_{t\to\infty} \inf(S_V(t)) \geq 0. \tag{7.2.2.3}$$

Using the similar method, we obtain

$$\begin{aligned} I_V(t) &\geq I_V(0).\exp\{-(\mu_V t + \delta_V(t))\}, && (7.2.2.4)\\ \lim_{t\to\infty}\inf(I_V(t)) &\geq 0. && (7.2.2.5)\end{aligned}$$

Using the same principle, it can be shown that

$$\begin{aligned} \lim_{t\to\infty}\inf(G_v(t)) &\geq 0,\\ \lim_{t\to\infty}\inf(G_m(t)) &\geq 0,\\ \lim_{t\to\infty}\inf(Z_v(t)) &\geq 0,\\ \lim_{t\to\infty}\inf(O_v(t)) &\geq 0,\\ \lim_{t\to\infty}\inf(P_v(t)) &\geq 0,\\ \lim_{t\to\infty}\inf(P_V(t)) &\geq 0,\\ \lim_{t\to\infty}\inf(S_H(t)) &\geq 0,\\ \lim_{t\to\infty}\inf(I_H(t)) &\geq 0,\\ \lim_{t\to\infty}\inf(G_H(t)) &\geq 0.\end{aligned}$$

Thus, when starting with non-negative initial value conditions in the systems of equations (7.2.1.1), the solutions of the model will remain non-negative for all $t \geq 0$, and this completes the proof. □

7.2.3 Feasible region of the equilibrium of the model

All the parameters and state variables for the model system (7.2.1.1) are assumed to be non-negative to be consistent with human and mosquito populations. Further, it can be verified that for system of equations (7.2.1.1), all solutions with non-negative initial conditions remain bounded and non-negative. We define N_V as the total mosquito population, N_H as the total human population and they are given by

$$\begin{aligned} N_V &= S_V + I_V\\ N_H &= S_H + I_H. && (7.2.3.1)\end{aligned}$$

$$\begin{aligned} \frac{dN_V(t)}{dt} &= \frac{dS_V(t)}{dt} + \frac{dI_V(t)}{dt},\\ &= \frac{1}{2}\frac{\alpha_M}{\mu_M+\alpha_M+\delta_M}\frac{\alpha_W}{\mu_W+\alpha_W+\delta_W}\frac{\theta_E\Lambda_E}{\mu_E+\theta_E} - \mu_V N_V(t) - \delta_V I_V(t), && (7.2.3.2)\\ &\leq \frac{1}{2}\frac{\alpha_M}{\mu_M+\alpha_M+\delta_M}\frac{\alpha_W}{\mu_W+\alpha_W+\delta_W}\frac{\theta_E\Lambda_E}{\mu_E+\theta_E} - \mu_V N_V(t).\end{aligned}$$

Therefore $\lim_{t\longrightarrow\infty} Sup(N_V(t)) = \frac{1}{2}\frac{1}{\mu_V}\frac{\alpha_M}{\mu_M+\alpha_M+\delta_M}\frac{\alpha_W}{\mu_W+\alpha_W+\delta_W}\frac{\theta_E\Lambda_E}{\mu_E+\theta_E}$.

$$\begin{aligned}\frac{dN_H(t)}{dt} &= \frac{dS_H(t)}{dt}+\frac{dI_H(t)}{dt},\\ \frac{dN_H(t)}{dt} &= \Lambda_H-\mu_H N_H(t)-\delta_H I_H(t),\\ &\leq \Lambda_H-\mu_H N_H(t).\end{aligned} \tag{7.2.3.3}$$

Therefore $\lim_{t\longrightarrow\infty} Sup(N_H(t)) = \frac{\Lambda_H}{\mu_H}$.
Therefore all feasible solutions of the model system (7.2.1.1) are positive and eventually enter the invariant attracting region

$$\Omega = (E_E, L_W, P_M, S_V, I_V, G_v, G_m, Z_v, O_v, P_v, P_V, S_H, I_H, G_H), \tag{7.2.3.4}$$

where

$$\begin{aligned}0 &\leq S_V+I_V \leq \frac{1}{2}\frac{1}{\mu_V}\frac{\alpha_M}{\mu_M+\alpha_M+\delta_M}\frac{\alpha_W}{\mu_W+\alpha_W+\delta_W}\frac{\theta_E\Lambda_E}{\mu_E+\theta_E},\\ 0 &\leq G_v \leq \frac{1}{\alpha_g+\mu_g}\frac{\beta_H(\alpha_M\alpha_W\theta_E\Lambda_E-A)}{A\phi_V(I_V+1)}\frac{G_H}{G_0+G_H},\\ 0 &\leq G_m \leq \frac{N_g\alpha_g}{\alpha_g+\mu_g}\frac{1}{\alpha_s+\mu_s}\frac{\beta_H(\alpha_M\alpha_W\theta_E\Lambda_E-A)}{A\phi_V(I_V+1)}\frac{G_H}{G_0+G_H},\\ 0 &\leq Z_v \leq \frac{1}{2}\frac{N_g\alpha_g}{\alpha_g+\mu_g}\frac{\alpha_s}{\alpha_s+\mu_s}\frac{1}{\alpha_z+\mu_z}\frac{\beta_H(\alpha_M\alpha_W\theta_E\Lambda_E-A)}{A\phi_V(I_V+1)}\frac{G_H}{G_0+G_H},\\ 0 &\leq O_v \leq \frac{1}{2}\frac{N_g\alpha_g}{\alpha_g+\mu_g}\frac{\alpha_s}{\alpha_s+\mu_s}\frac{\alpha_z}{\alpha_z+\mu_z}\frac{1}{\alpha_k+\mu_k}\frac{\beta_H(\alpha_M\alpha_W\theta_E\Lambda_E-A)}{A\phi_V(I_V+1)}\frac{G_H}{G_0+G_H},\\ 0 &\leq P_v \leq N_v\frac{\beta_H(\alpha_M\alpha_W\theta_E\Lambda_E-A)}{A\phi_V(I_V+1)}\frac{G_H}{G_0+G_H},\\ 0 &\leq P_V \leq \frac{N_v\alpha_v}{\alpha_V}\frac{\beta_H(\alpha_M\alpha_W\theta_E\Lambda_E-A)}{A\phi_V}\frac{G_H}{G_0+G_H},\\ 0 &\leq S_H+I_H \leq \frac{\Lambda_H}{\mu_H},\\ 0 &\leq G_H \leq \frac{N_h\alpha_h}{\alpha_H}\frac{\Lambda_H}{\mu_H},\end{aligned} \tag{7.2.3.5}$$

where

$$\begin{aligned}A &= 2\mu_V(\mu_M+\alpha_M+\delta_M)(\mu_W+\alpha_W+\delta_W)(\mu_E+\theta_E),\\ N_v &= \frac{1}{2}\frac{N_g\alpha_g}{\alpha_g+\mu_g}\frac{\alpha_s}{\alpha_s+\mu_s}\frac{\alpha_z}{\alpha_z+\mu_z}\frac{N_k\alpha_k}{\alpha_k+\mu_k}\frac{1}{\alpha_v+\mu_v}.\end{aligned} \tag{7.2.3.6}$$

7.2.4 Disease free Equilibrium

The disease free equilibrium point of the system of equations (7.2.1.1) is obtained by setting the right hand sides of differential equations (7.2.1.1) to zero and and assume that $I_V = G_H = I_H = P_V = G_v = G_m = Z_v = O_v = P_v = 0$. We obtain

$$\begin{aligned} E^0 &= (E_E^0, L_W^0, P_M^0, S_V^0, I_V^0, G_H^0, S_H^0, I_H^0, P_V^0, G_v^0, G_m^0, Z_v^0, O_v^0, P_v^0). \\ &= (E_E^0, L_W^0, , P_M^0, S_V^0, 0, 0, \frac{\Lambda_H}{\mu_H}, 0, 0, 0, 0, 0, 0, 0), \end{aligned} \tag{7.2.4.1}$$

Where

$$\begin{aligned} E_E^0 &= \frac{\Lambda_E}{(\mu_E + \theta_E)} \\ L_W^0 &= \frac{\Lambda_E}{(\mu_E + \theta_E)} \frac{\theta_E}{(\mu_W + \alpha_W + \delta_W)} \\ P_M^0 &= \frac{\Lambda_E}{(\mu_E + \theta_E)} \frac{\theta_E}{(\mu_W + \alpha_W + \delta_W)} \frac{\alpha_W}{(\mu_M + \alpha_M + \delta_M)} \\ S_V^0 &= \frac{\alpha_M}{2\mu_V} \frac{\alpha_W}{(\mu_M + \alpha_M + \delta_M)} \frac{\theta_E}{(\mu_W + \alpha_W + \delta_W)} \frac{\Lambda_E}{(\mu_E + \theta_E)}. \end{aligned} \tag{7.2.4.2}$$

7.2.5 Reproductive Number

We use the next-generation operator approach to compute the basic reproductive number and we use the [71]'s approach. The systems of equations (7.2.1.1) can be written in the form

$$\begin{aligned} \frac{dX}{dt} &= f(X, Y, Z), \\ \frac{dY}{dt} &= g(X, Y, Z), \\ \frac{dZ}{dt} &= h(X, Y, Z), \end{aligned} \tag{7.2.5.1}$$

where

i. $X = (E_E, L_W, P_M, S_V, S_H)$ represents the compartments of susceptible individuals.

ii. $Y = (I_V, I_H, G_v, G_m, Z_v, O_v, P_v)$ represents compartments of infected individuals that are not infectious.

iii. $Z = (G_H, P_V)$ represents compartments which are infectious who are capable of transmitting other diseases.

We define $\widetilde{g}(X^*, Z)$ by

$$\begin{aligned}
\widetilde{g}_1 &= \frac{\beta_H S_V}{(\mu_V+\delta_V)}\frac{G_H}{(G_0+G_H)},\\
\widetilde{g}_2 &= \frac{1}{\alpha_g+\mu_g}\frac{\beta_H(S_V-1)}{\phi_V(I_V+1)}\frac{G_H}{(G_0+G_H)},\\
\widetilde{g}_3 &= \frac{N_g\alpha_g}{\alpha_g+\mu_g}\frac{1}{\alpha_s+\mu_s}\frac{\beta_H(S_V-1)}{\phi_V(I_V+1)}\frac{G_H}{(G_0+G_H)},\\
\widetilde{g}_4 &= \frac{1}{2}\frac{N_g\alpha_g}{\alpha_g+\mu_g}\frac{\alpha_s}{\alpha_s+\mu_s}\frac{1}{\alpha_z+\mu_z}\frac{\beta_H(S_V-1)}{\phi_V(I_V+1)}\frac{G_H}{(G_0+G_H)},\\
\widetilde{g}_5 &= \frac{1}{2}\frac{N_g\alpha_g}{\alpha_g+\mu_g}\frac{\alpha_s}{\alpha_s+\mu_s}\frac{\alpha_z}{\alpha_z+\mu_z}\frac{1}{\alpha_k+\mu_k}\frac{\beta_H(S_V-1)}{\phi_V(I_V+1)}\frac{G_H}{(G_0+G_H)},
\end{aligned} \tag{7.2.5.2}$$

$$\begin{aligned}
\widetilde{g}_6 &= \frac{N_v\alpha_v}{\phi_V}\frac{\beta_H(S_V-1)}{(I_V+1)}\frac{G_H}{(G_0+G_H)},\\
\widetilde{g}_7 &= \frac{\beta_V S_H}{(\mu_H+\gamma_H+\delta_H)}\frac{P_V}{(P_0+P_V)}.
\end{aligned}$$

Let $h_1 = \dfrac{dG_H}{dt}$ and $h_2 = \dfrac{dP_V}{dt}$ and we obtain

$$\begin{aligned}
h_1 &= \frac{N_h\alpha_h}{\mu_H+\gamma_H+\delta_H}\frac{\beta_V\Lambda_H}{\mu_H}\frac{P_V}{(P_0+P_V)} - \alpha_H G_H,\\
h_2 &= N_v\alpha_v\frac{\beta_H(S_V-1)}{\phi_V}\frac{G_H}{(G_0+G_H)} - \alpha_V P_V.
\end{aligned} \tag{7.2.5.3}$$

We assume that A can be written in the form $A = M - D$, where $M \geq 0$ and $D \geq 0$, a diagonal matrix.

$$A = \begin{pmatrix} \dfrac{\partial h_1}{\partial G_H} & \dfrac{\partial h_1}{\partial P_V} \\ \dfrac{\partial h_2}{\partial G_H} & \dfrac{\partial h_2}{\partial P_V} \end{pmatrix},$$

then

$$A = \begin{pmatrix} -\alpha_H & \dfrac{N_h\alpha_h}{\mu_H+\gamma_H+\delta_H}\dfrac{1}{P_0}\dfrac{\beta_V\Lambda_H}{\mu_H} \\ \dfrac{N_v\alpha_v}{\phi_V}\dfrac{\beta_H q_1}{2\mu_V G_0 q_2} & -\alpha_V \end{pmatrix}.$$

We deduce matrices

$$M = \begin{pmatrix} 0 & \dfrac{N_h\alpha_h}{\mu_H+\gamma_H+\delta_H}\dfrac{1}{P_0}\dfrac{\beta_V\Lambda_H}{\mu_H} \\ \dfrac{N_v\alpha_v}{\phi_V}\dfrac{\beta_H q_1}{2\mu_V G_0 q_2} & 0 \end{pmatrix}$$

and

$$D = \begin{pmatrix} \alpha_H & 0 \\ 0 & \alpha_V \end{pmatrix} \Longrightarrow D^1 = \begin{pmatrix} \frac{1}{\alpha_H} & 0 \\ 0 & \frac{1}{\alpha_V} \end{pmatrix}. \tag{7.2.5.4}$$

The basic reproductive number is the special radius (dominant eigenvalue) of the matrix MD^{-1} that is

$$\begin{aligned} R_0 &= \rho(MD^{-1}) \qquad (7.2.5.5) \\ &= \sqrt{\left[\frac{1}{2}\frac{N_v\alpha_v}{(\mu_E+\theta_E)(\mu_W+\alpha_W+\delta_W)(\mu_M+\alpha_M+\delta_M)}\frac{1}{P_0}\frac{1}{\alpha_V}\frac{\beta_V\Lambda_H}{\mu_H}\right]\left[\frac{N_h\alpha_h}{\mu_H+\gamma_H+\delta_H}\frac{1}{G_0}\frac{1}{\alpha_H}\frac{\beta_H q_1}{\mu_V\phi_V}\right]}, \\ R_0 &= \sqrt{R_{0VH}R_{0HV}}. \qquad (7.2.5.6) \end{aligned}$$

where

$$\begin{aligned} N_v &= \frac{1}{2}\frac{N_g\alpha_g}{\alpha_g+\mu_g}\frac{N_k\alpha_k}{\alpha_k+\mu_k}\frac{\alpha_z}{\alpha_z+\mu_z}\frac{\alpha_s}{\alpha_s+\mu_s}\frac{1}{\alpha_v+\mu_v}, \\ q_1 &= (\alpha_M\alpha_W\theta_E\Lambda_E - 2\mu_V(\mu_E+\theta_E)(\mu_W+\alpha_W+\delta_W)(\mu_M+\alpha_M+\delta_M)), \\ \alpha_M\alpha_W\theta_E\Lambda_E &\geq 2\mu_V(\mu_E+\theta_E)(\mu_W+\alpha_W+\delta_W)(\mu_M+\alpha_M+\delta_M),, \qquad (7.2.5.7) \\ R_{0VH} &= \frac{1}{2}\frac{N_v\alpha_v}{(\mu_E+\theta_E)(\mu_W+\alpha_W+\delta_W)(\mu_M+\alpha_M+\delta_M)}\frac{1}{P_0}\frac{1}{\alpha_V}\frac{\beta_V\Lambda_H}{\mu_H}, \\ R_{0HV} &= \frac{N_h\alpha_h}{\mu_H+\gamma_H+\delta_H}\frac{1}{G_0}\frac{1}{\alpha_H}\frac{\beta_H q_1}{\mu_V\phi_V}. \end{aligned}$$

We deduce that the basic reproductive number has components of immature mosquito parameters, adult mosquito parameters and human parameters and also have the components of both within-host (mosquito and human) scale parameters and between host (mosquito and human) scale parameters.

7.2.6 Endemic equilibrium Points

The equilibrium points are obtained by setting the right-hand-side of systems of equations (7.2.1.1) to zero and we obtain

$$E^* = (E_E^*, L_W^*, P_M^*, S_V^*, I_V^*, G_v^*, G_m^*, Z_v^*, O_V^*, P_v^*, P_V^*, S_H^*, I_H^*, G_H^*),$$

where

$$
\begin{aligned}
E_E^* &= \frac{\Lambda_E}{\mu_E+\theta_E},\\
L_W^* &= \frac{1}{\mu_W+\alpha_W+\delta_W}\frac{\theta_E\Lambda_E}{\mu_E+\theta_E},\\
P_M^* &= \frac{1}{\mu_M+\alpha_W+\delta_M}\frac{\alpha_W}{\mu_W+\alpha_W+\delta_W}\frac{\theta_E\Lambda_E}{\mu_E+\theta_E},\\
S_V^* &= \frac{\alpha_M\alpha_W\theta_E\Lambda_E\left[N_h\alpha_h\beta_V\Lambda_H P_V^*+\alpha_H G_0[a_1(P_0+P_V^*)+a_2P_V^*]\right]}{a_3\left[N_h\alpha_h\beta_V\Lambda_H P_V^*(\beta_H+\mu_V)+\mu_V\alpha_H G_0[a_1(P_0+P_V^*)+a_2P_V^*]\right]},\\
I_V^* &= \frac{N_h\alpha_h\beta_H\alpha_M\alpha_W\theta_E\Lambda_E\beta_V\Lambda_H P_V^*}{a_3(\mu_V+\delta_V)\left[N_h\alpha_h\beta_V\Lambda_H P_V^*(\beta_H+\mu_V)+\mu_V\alpha_H G_0[a_1(P_0+P_V^*)+a_2P_V^*]\right]},\\
G_v &= \frac{1}{\alpha_g+\mu_g}\frac{N_h\alpha_h\beta_H\beta_V\Lambda_H P_V^*[b_1P_V^*+b_2]}{a_3\phi_V(I_V^*+1)\left[b_3P_V^*+\mu_V\alpha_H a_1G_0P_0\right]\left[b_4P_V^*+\alpha_H a_1G_0P_0\right]},\\
G_m^* &= \frac{N_g\alpha_g}{\alpha_g+\mu_g}\frac{1}{\alpha_s+\mu_s}\frac{N_h\alpha_h\beta_H\beta_V\Lambda_H P_V^*[b_1P_V^*+b_2]}{a_3\phi_V(I_V^*+1)\left[b_3P_V^*+\mu_V\alpha_H a_1G_0P_0\right]\left[b_4P_V^*+\alpha_H a_1G_0P_0\right]},\\
Z_v^* &= \frac{1}{2}\frac{N_g\alpha_g}{\alpha_g+\mu_g}\frac{\alpha_s}{\alpha_s+\mu_s}\frac{1}{\alpha_z+\mu_z}\frac{N_h\alpha_h\beta_H\beta_V\Lambda_H P_V^*[b_1P_V^*+b_2]}{a_3\phi_V(I_V^*+1)\left[b_3P_V^*+\mu_V\alpha_H a_1G_0P_0\right]\left[b_4P_V^*+\alpha_H a_1G_0P_0\right]},
\end{aligned}
\tag{7.2.6.1}
$$

$$
\begin{aligned}
O_v^* &= \frac{1}{2}\frac{N_g\alpha_g}{\alpha_g+\mu_g}\frac{\alpha_s}{\alpha_s+\mu_s}\frac{\alpha_z}{\alpha_z+\mu_z}\frac{1}{\alpha_k+\mu_k}\frac{N_h\alpha_h\beta_H\beta_V\Lambda_H P_V^*[b_1P_V^*+b_2]}{a_3\phi_V(I_V^*+1)\left[b_3P_V^*+\mu_V\alpha_H a_1G_0P_0\right]\left[b_4P_V^*+\alpha_H a_1G_0P_0\right]},\\
P_v^* &= N_v\frac{N_h\alpha_h\beta_H\beta_V\Lambda_H P_V^*[b_1P_V^*+b_2]}{a_3\phi_V(I_V^*+1)\left[b_3P_V^*+\mu_V\alpha_H a_1G_0P_0\right]\left[b_4P_V^*+\alpha_H a_1G_0P_0\right]},\\
S_H^* &= \frac{\Lambda_H(\mu_H+\gamma_H+\delta_H)(P_0+P_V^*)}{a_1(P_0+P_V^*)+a_2P_V^*},\\
I_H^* &= \frac{\beta_V\Lambda_H P_V^*}{a_1(P_0+P_V^*)+a_2P_V^*},\\
G_H^* &= \frac{N_h\alpha_h\beta_V\Lambda_H P_V^*}{\alpha_H[a_1(P_0+P_V^*)+a_2P_V^*]},\\
P_V^* &= \frac{-c_2+\sqrt{c_2^2-4c_1c_3}}{2c_1},
\end{aligned}
$$

where

$$\begin{aligned}
a_1 &= \mu_H(\mu_H+\gamma_H+\delta_H),\\
a_2 &= \beta_V(\mu_H+\delta_H),\\
a_3 &= 2(\mu_M+\alpha_M+\delta_M)(\mu_W+\alpha_W+\delta_W)(\mu_E+\theta_E),\\
b_1 &= N_h\alpha_h\beta_V\Lambda_H[\alpha_M\alpha_W\theta_E\Lambda_E-a_3(\beta_H+\mu_V)]+\alpha_H G_0(a_1+a_2)[\alpha_M\alpha_W\theta_E\Lambda_E-a_3\mu_V]>0,\\
b_2 &= \alpha_H a_1 G_0 P_0[\alpha_M\alpha_W\theta_E\Lambda_E-a_3\mu_V]>0,\\
b_3 &= N_h\alpha_h\beta_V\Lambda_H(\beta_H+\mu_V)+\mu_V\alpha_H G_0(a_1+a_2)>0,\\
b_4 &= N_h\alpha_h\beta_V\Lambda_H+\alpha_H G_0(a_1+a_2)>0,\\
c_1 &= \alpha_V\phi_V a_3 b_3 b_4>0,\\
c_2 &= N_h\alpha_h\beta_V\Lambda_H a_1 a_3\mu_V\alpha_V\alpha_H\phi_V G_0 P_0[2-R_0^2]+\alpha_H^2 G_0^2(a_1+a_2)a_1a_3\mu_V\alpha_V\phi_V P_0[2-R_0^2],\\
&\quad +N_h\alpha_h a_3\beta_V\Lambda_H\beta_H\left[\alpha_V\phi_V a_1 a_3\alpha_H G_0 P_0+N_v\alpha_v N_h\alpha_h\beta_H\beta_V\Lambda_H\right],\\
c_3 &= -\mu_V\alpha_V\phi_V a_3 a_1^2\alpha_H^2 G_0^2 P_0^2[R_0^2-1]<0.
\end{aligned} \tag{7.2.6.2}$$

Therefore P_V^* is positive when $R_0>1$, $c_1>0$, $c_3<0$ and c_2 could be either positive or negative. Therefore, we conclude that there exist a positive endemic equilibrium points when $R_0>1$.

7.3 Stability analysis

7.3.1 Local stability of disease free equilibrium (DFE)

In this sub-section, we determine the local stability of the DFE of the coupled multiscale model (7.2.1.1), where we linearize the multiscale model in order to obtain a Jacobian matrix. We examine the Jacobian matrix at the DFE.

$$\begin{aligned}
E_0 &= (E_{E0}, L_{W0}, P_{M0}, S_{V0}, I_{V0}, G_{H0}, S_{H0}, I_{H0}, P_{V0}, G_{v0}, G_{m0}, Z_{v0}, O_{v0}, P_{v0}). \quad (7.3.1.1)\\
&= (E_{E0}, L_{W0},, P_{M0}, S_{V0}, 0, 0, \frac{\Lambda_H}{\mu_H}, 0, 0, 0, 0, 0, 0, 0),
\end{aligned}$$

Where

$$\begin{aligned}
E_{E0} &= \frac{\Lambda_E}{(\mu_E+\theta_E)}\\
L_{W0} &= \frac{\Lambda_E}{(\mu_E+\theta_E)}\frac{\theta_E}{(\mu_W+\alpha_W+\delta_W)}\\
P_M &= \frac{\Lambda_E}{(\mu_E+\theta_E)}\frac{\theta_E}{(\mu_W+\alpha_W+\delta_W)}\frac{\alpha_W}{(\mu_M+\alpha_M+\delta_M)}\\
S_{V0} &= \frac{\alpha_M}{2\mu_V}\frac{\alpha_W}{(\mu_M+\alpha_M+\delta_M)}\frac{\theta_E}{(\mu_W+\alpha_W+\delta_W)}\frac{\Lambda_E}{(\mu_E+\theta_E)}.
\end{aligned} \tag{7.3.1.2}$$

We denote the DFE of the multiscale model (7.2.1.1). For examining the stability analysis, we use the basic reproductive number R_0, where R_0 is a threshold value that is used in public health to assess the transmission of a disease in a given community.

The Jacobian matrix of the model (7.2.1.1) computed at the DFE is given by $J(E_0) =$

$$\begin{pmatrix}
-F_1 & 0 & 0 & 0 & 0 & 0 & 0 & 0 & 0 & 0 & 0 & 0 & 0 & 0 \\
\theta_e & -F_2 & 0 & 0 & 0 & 0 & 0 & 0 & 0 & 0 & 0 & 0 & 0 & 0 \\
0 & \alpha_W & -F_3 & 0 & 0 & 0 & 0 & 0 & 0 & 0 & 0 & 0 & 0 & 0 \\
0 & 0 & \frac{\alpha_M}{2} & -\mu_V & 0 & 0 & 0 & 0 & 0 & 0 & 0 & 0 & 0 & -G_1 \\
0 & 0 & 0 & 0 & -F_4 & 0 & 0 & 0 & 0 & 0 & 0 & 0 & 0 & G_1 \\
0 & 0 & 0 & 0 & 0 & -F_5 & 0 & 0 & 0 & 0 & 0 & 0 & 0 & G_2 \\
0 & 0 & 0 & 0 & 0 & N_g\alpha_g & -F_6 & 0 & 0 & 0 & 0 & 0 & 0 & 0 \\
0 & 0 & 0 & 0 & 0 & 0 & 0.5\alpha_s & -F_7 & 0 & 0 & 0 & 0 & 0 & 0 \\
0 & 0 & 0 & 0 & 0 & 0 & 0 & \alpha_z & -F_8 & 0 & 0 & 0 & 0 & 0 \\
0 & 0 & 0 & 0 & 0 & 0 & 0 & 0 & N_k\alpha_k & -F_9 & 0 & 0 & 0 & 0 \\
0 & 0 & 0 & 0 & P_v\alpha_v & 0 & 0 & 0 & 0 & \alpha_v & -\alpha_V & 0 & 0 & 0 \\
0 & 0 & 0 & 0 & 0 & 0 & 0 & 0 & 0 & 0 & \frac{-\beta_V S_{H0}}{P_0} & -\mu_H & \gamma_H & 0 \\
0 & 0 & 0 & 0 & 0 & 0 & 0 & 0 & 0 & 0 & \frac{\beta_V S_{H0}}{P_0} & 0 & -F_{10} & 0 \\
0 & 0 & 0 & 0 & 0 & 0 & 0 & 0 & 0 & 0 & 0 & 0 & N_h\alpha_h & -\alpha_H
\end{pmatrix}, \tag{7.3.1.3}$$

where

$$\begin{aligned}
F_1 &= \theta_E + \mu_E, & F_2 &= \alpha_W + \delta_W + \mu_W, & F_3 &= \alpha_M + \delta_M + \mu_M, & F_4 &= \delta_V + \mu_V, \\
F_5 &= \alpha_g + \mu_g, & F_6 &= \alpha_s + \mu_s, & F_7 &= \alpha_z + \mu_z, & F_8 &= \alpha_k + \mu_k, \\
F_9 &= \alpha_v + \mu_v & F_{10} &= \delta_H + \gamma_H + \mu_H, & G_1 &= \frac{\beta_H S_{V0}}{G_0}, & G_2 &= \frac{\beta_H (S_{V0} - 1)}{G_0 \phi_V}.
\end{aligned}$$

The characteristic equation at the equilibrium E_0 is given by

$$\begin{aligned}
|J(E_0) - \lambda I| &= 0, \\
(F_1 + \lambda)(F_2 + \lambda)(F_3 + \lambda)(F_4 + \lambda)(\mu_V + \lambda)(\mu_H + \lambda) \left[\lambda^8 + \right. & \\
\left. b_1\lambda^7 + b_2\lambda^6 + b_3\lambda^5 + b_4\lambda^4 + b_5\lambda^3 + b_6\lambda^2 + b_7\lambda + b_8\right] &= 0,
\end{aligned} \tag{7.3.1.4}$$

where

$$b_1 = \alpha_H + \alpha_V + F_5 + F_6 + F_7 + F_8 + F_9 + F_{10}, \tag{7.3.1.5}$$

$$\begin{aligned} b_2 &= \alpha_H\alpha_V + \alpha_H F_5\alpha_H F_6 + \alpha_H F_7 + \alpha_H F_8 + \alpha_H F_9 + \alpha_H F_{10} + \alpha_V F_{10} + \alpha_V F_5 + \alpha_V F_6 \\ &= +\alpha_V F_7 + \alpha_V F_8 + \alpha_V F_9 + \alpha_V F_{10} + F_5F_6 + F_5F_7 + F_5F_8 + F_5F_9 + F_5F_{10} + F_6F_7 \\ &\quad +F_6F_8 + F_6F_9 + F_6F_{10} + F_7F_8 + F_7F_9 + F_7F_{10} + F_8F_9 + F_8F_{10} + F_9F_{10}, \end{aligned} \tag{7.3.1.6}$$

$$\begin{aligned} b_3 &= \alpha_H\alpha_V F_5 + \alpha_H\alpha_V F_6 + \alpha_H\alpha_V F_7 + \alpha_H\alpha_V F_8 + \alpha_H\alpha_V F_9 + \alpha_H\alpha_V F_{10} + \alpha_H F_5F_6 \\ &\quad +\alpha_H F_5F_7 + \alpha_H F_5F_8 + \alpha_H F_5F_9 + \alpha_H F_5F_{10} + \alpha_H F_6F_7 + \alpha_H F_6F_8 + \alpha_H F_6F_9 + \\ &\quad \alpha_H F_6F_{10} + \alpha_H F_7F_8 + \alpha_H F_7F_9 + \alpha_H F_7F_{10} + \alpha_H F_8F_9 + \alpha_H F_8F_{10} + \alpha_H F_9F_{10} + \\ &\quad \alpha_V F_5F_6 + \alpha_V F_5F_7 + \alpha_V F_5F_8 + \alpha_V F_5F_9 + \alpha_V F_5F_{10} + \alpha_V F_6F_7 + \alpha_V F_6F_8 + \alpha_V F_6F_9 \\ &\quad +\alpha_V F_6F_{10} + \alpha_V F_7F_8 + \alpha_V F_7F_9 + \alpha_V F_7F_{10} + \alpha_V F_8F_9 + \alpha_V F_8F_{10} + \alpha_V F_9F_{10} + \\ &\quad \alpha_V F_6F_7 + \alpha_V F_6F_8 + \alpha_V F_6F_9 + F_5F_6F_7 + F_5F_6F_8 + F_5F_6F_9 + F_5F_6F_{10} + F_5F_7F_8 + \\ &\quad F_5F_7F_9 + F_5F_7F_{10} + F_5F_8F_9 + F_5F_9F_{10} + F_6F_7F_8 + F_6F_7F_9 + F_6F_7F_{10} + F_7F_8F_9 + \\ &\quad F_7F_8F_{10} + F_7F_9F_{10} + F_8F_9F_{10}, \end{aligned}$$

$$\begin{aligned} b_4 &= \alpha_H\alpha_V F_5F_6 + \alpha_H\alpha_V F_5F_7 + \alpha_H\alpha_V F_5F_8 + \alpha_H\alpha_V F_5F_9 + \alpha_H\alpha_V F_5F_{10} + \alpha_H\alpha_V F_6F_7 + \\ &\quad \alpha_H\alpha_V F_6F_8 + \alpha_H\alpha_V F_6F_9 + \alpha_H\alpha_V F_6F_{10} + \alpha_H\alpha_V F_7F_8 + \alpha_H\alpha_V F_7F_9 + \alpha_H\alpha_V F_7F_{10} \\ &\quad +\alpha_H\alpha_V F_8F_9 + \alpha_H\alpha_V F_8F_{10} + \alpha_H\alpha_V F_9F_{10} + \alpha_H F_5F_6F_7 + \alpha_H F_5F_6F_8 + \alpha_H F_5F_6F_9 + \\ &\quad \alpha_H F_5F_6F_{10} + \alpha_H F_5F_7F_8 + \alpha_H F_5F_7F_9 + \alpha_H F_5F_7F_{10} + \alpha_H F_5F_8F_9 + \alpha_H F_5F_8F_{10} + \\ &\quad \alpha_H F_5F_9F_{10} + \alpha_H F_6F_7F_8 + \alpha_H F_6F_7F_9 + \alpha_H F_6F_7F_{10} + \alpha_H F_6F_8F_9 + \alpha_H F_6F_8F_{10} + \\ &\quad \alpha_H F_6F_9F_{10} + \alpha_H F_7F_8F_9 + \alpha_H F_7F_8F_{10} + \alpha_H F_7F_9F_{10} + \alpha_H F_8F_9F_{10}\alpha_H F_5F_6F_7 + \\ &\quad \alpha_H F_5F_6F_8 + \alpha_H F_5F_6F_9 + \alpha_V F_5F_6F_{10} + \alpha_V F_5F_7F_8 + \alpha_V F_5F_7F_9 + \alpha_V F_5F_7F_{10} + \\ &\quad \alpha_V F_5F_8F_9 + \alpha_V F_5F_8F_{10} + \alpha_V F_5F_9F_{10} + \alpha_V F_6F_7F_8 + \alpha_V F_6F_7F_9 + \alpha_V F_6F_7F_{10} + \\ &\quad \alpha_V F_6F_8F_9 + \alpha_V F_6F_8F_{10} + \alpha_V F_6F_9F_{10} + \alpha_V F_7F_8F_9 + \alpha_V F_7F_8F_{10} + \alpha_V F_7F_9F_{10} + \\ &\quad \alpha_V F_8F_9F_{10} + F_5F_6F_7F_8 + F_5F_6F_7F_9 + F_5F_6F_7F_{10} + F_5F_6F_8F_9 + F_5F_6F_8F_{10} + F_5F_6F_9F_{10} \\ &\quad +F_5F_7F_8F_9 + F_5F_7F_8F_{10} + F_5F_7F_9F_{10} + F_5F_8F_9F_{10} + F_6F_7F_8F_9 + F_6F_7F_8F_{10} + F_6F_7F_9F_{10} \\ &\quad +F_6F_8F_9F_{10} + F_7F_8F_9F_{10}, \end{aligned} \tag{7.3.1.7}$$

$$\begin{aligned} b_5 &= \alpha_H\alpha_V F_5F_6F_7 + \alpha_H\alpha_V F_5F_6F_8 + \alpha_H\alpha_V F_5F_6F_9 + \alpha_H\alpha_V F_5F_6F_{10} + \alpha_H\alpha_V F_5F_7F_8 + \\ &\quad \alpha_H\alpha_V F_5F_7F_9 + \alpha_H\alpha_V F_5F_7F_{10} + \alpha_H\alpha_V F_5F_8F_9 + \alpha_H\alpha_V F_5F_8F_{10} + \alpha_H\alpha_V F_5F_9F_{10} + \\ &\quad \alpha_H\alpha_V F_6F_7F_8 + \alpha_H\alpha_V F_6F_7F_9 + \alpha_H\alpha_V F_6F_7F_{10} + \alpha_H\alpha_V F_6F_8F_9 + \alpha_H\alpha_V F_6F_8F_{10} + \\ &\quad \alpha_H\alpha_V F_6F_9F_{10} + \alpha_H\alpha_V F_7F_8F_9 + \alpha_H\alpha_V F_7F_8F_{10} + \alpha_H\alpha_V F_7F_9F_{10} + \alpha_H\alpha_V F_8F_9F_{10} + \\ &\quad \alpha_H F_5F_6F_7F_8 + \alpha_H F_5F_6F_7F_9 + \alpha_H F_5F_6F_7F_{10} + \alpha_H F_5F_6F_8F_9 + \alpha_H F_5F_6F_8F_{10} + \\ &\quad \alpha_H F_5F_6F_9F_{10} + \alpha_H F_5F_7F_8F_9 + \alpha_H F_5F_7F_8F_{10} + \alpha_H F_5F_8F_9F_{10} + \alpha_H F_6F_7F_8F_9 + \\ &\quad \alpha_H F_6F_7F_8F_{10} + \alpha_H F_6F_7F_9F_{10} + \alpha_H F_6F_8F_9F_{10} + \alpha_H F_7F_8F_9F_{10} + \alpha_V F_5F_6F_7F_8 + \\ &\quad \alpha_V F_5F_6F_7F_9 + \alpha_V F_5F_6F_7F_{10} + \alpha_V F_5F_6F_8F_9 + \alpha_V F_5F_6F_8F_{10} + \alpha_V F_5F_6F_9F_{10} + \\ &\quad \alpha_V F_5F_7F_8F_9 + \alpha_V F_5F_7F_8F_{10} + \alpha_V F_5F_8F_9F_{10} + \alpha_V F_6F_7F_8F_9 + \alpha_V F_6F_7F_8F_{10} + \\ &\quad \alpha_V F_6F_7F_9F_{10} + \alpha_V F_6F_8F_9F_{10} + \alpha_V F_7F_8F_9F_{10} + F_5F_6F_7F_8F_9 + F_5F_6F_7F_8F_{10} + \\ &\quad F_5F_6F_7F_9F_{10} + F_5F_6F_8F_9F_{10} + F_5F_7F_8F_9F_{10} + F_6F_7F_8F_9F_{10}, \end{aligned} \tag{7.3.1.8}$$

$$
\begin{aligned}
b_6 &= \alpha_H\alpha_V F_5F_6F_7F_8 + \alpha_H\alpha_V F_5F_6F_7F_9 + \alpha_H\alpha_V F_5F_6F_7F_{10} + \alpha_H\alpha_V F_5F_6F_8F_9 + \\
&\quad \alpha_H\alpha_V F_5F_6F_9F_{10} + \alpha_H\alpha_V F_5F_7F_8F_9 + \alpha_H\alpha_V F_5F_7F_8F_{10} + \alpha_H\alpha_V F_5F_7F_9F_{10} + \\
&\quad \alpha_H\alpha_V F_5F_8F_9F_{10} + \alpha_H\alpha_V F_6F_7F_8F_9 + \alpha_H\alpha_V F_6F_7F_8F_{10} + \alpha_H\alpha_V F_6F_7F_9F_{10} + \\
&\quad \alpha_H\alpha_V F_6F_8F_9F_{10} + \alpha_H\alpha_V F_7F_8F_9F_{10} + \alpha_H F_5F_6F_7F_8F_9 + \alpha_H F_5F_6F_7F_8F_{10} + \\
&\quad \alpha_H F_5F_6F_7F_9F_{10} + \alpha_H F_5F_6F_8F_9F_{10} + \alpha_H F_5F_7F_8F_9F_{10} + \alpha_H F_6F_7F_8F_9F_{10} + \\
&\quad \alpha_V F_5F_6F_7F_8F_9 + \alpha_V F_5F_6F_7F_8F_{10} + \alpha_V F_5F_6F_7F_9F_{10} + \alpha_V F_5F_6F_8F_9F_{10} + \\
&\quad \alpha_V F_5F_7F_8F_9F_{10} + \alpha_V F_6F_7F_8F_9F_{10} + F_5F_6F_7F_8F_9F_{10}, \qquad (7.3.1.9)\\
b_7 &= \alpha_H\alpha_V F_5F_6F_7F_8F_9 + \alpha_H\alpha_V F_5F_6F_7F_8F_{10} + \alpha_H\alpha_V F_5F_6F_7F_9F_{10} + \\
&\quad \alpha_H\alpha_V F_5F_6F_8F_9F_{10} + \alpha_H\alpha_V F_5F_7F_8F_9F_{10} + \alpha_H\alpha_V F_6F_7F_8F_9F_{10} + \\
&\quad \alpha_H F_5F_6F_7F_8F_9F_{10} + \alpha_V F_5F_6F_7F_8F_9F_{10}, \qquad (7.3.1.10)\\
b_8 &= \alpha_H\alpha_V(\alpha_g+\mu_g)(\alpha_s+\mu_s)(\alpha_z+\mu_z)(\alpha_k+\mu_k)(\alpha_v+\mu_v)(\delta_H+\gamma_H+\mu_H)(1-R_0^2). \qquad (7.3.1.11)
\end{aligned}
$$

The eigenvalues are given by

$$
\begin{aligned}
&\lambda_1 = -F_1, && \lambda_2 = -F_2,\\
&\lambda_3 = -F_3, && \lambda_4 = -F_4,\\
&\lambda_5 = -\mu_V, && \lambda^8 + b_1\lambda^7 + b_2\lambda^6 + b_3\lambda^5 + b_4\lambda^4 + b_5\lambda^3 + b_6\lambda^2 + b_7\lambda + b_8 = 0
\end{aligned}
$$

The disease free equilibrium is stable when all the eigenvalues obtain from $J(E_0)$ are negatives or have negative real parts. λ_1, λ_2, λ_3, λ_4 and λ_5 are strictly negatives and the disease free equilibrium points are stable if and only if

$$\lambda^8 + b_1\lambda^7 + b_2\lambda^6 + b_3\lambda^5 + b_4\lambda^4 + b_5\lambda^3 + b_6\lambda^2 + b_7\lambda + b_8 = 0 \qquad (7.3.1.12)$$

has negative eigenvalues. The polynomial have negative eigenvalues if $b_1 > 0$, $b_2 > 0$, $b_3 > 0$, $b_4 > 0$, $b_5 > 0$, $b_6 > 0$, $b_7 > 0$ and $b_8 > 0$. Therefore the coefficients b_1, b_2, b_3, b_4, b_5, b_6 and b_7 are clearly positive and coefficient $b_8 > 0$ when $R_0 < 1$.

Table 7.1: Possible number of positive roots of equation (6.2.5.2)

	b_8	b_7	b_6	b_5	b_4	b_3	b_2	b_1	b_0	
$R_0 < 1$	+	+	+	+	+	+	+	+	+	0 positive roots
$R_0 > 1$	+	+	+	+	+	+	+	+	-	1 positive roots
$f(\lambda)$	+	+	+	+	+	+	+	+	+	0 positive roots
$f(-\lambda)$	+	-	+	-	+	-	+	-	+	8 or 6 or 4 or 2 or 0 negative eigenvalues

Using descartes sign rule of change show that when $R_0 < 1$, there is no change of sign of the characteristic equation and conclude that there are no positive roots. When $R_0 > 1$, we observe that there is only one

change of sign and conclude that the characteristics has one positive root. When we find $f(\lambda)$, we notice that there is no change of sign which mean that there is no positive roots. $f(-\lambda)$ has 8 change of sign which means that the characteristic equation has 8 negative eigenvalues. Therefore, the DFE is locally asymptotically stable when $R_0 < 1$ and unstable when $R_0 > 1$.

7.3.2 Global Stability of the disease free equilibrium

We obtain the global stability of disease free equilibrium of system of equations 7.2.1.1 using the next generation operator [71]. We can rewrite the system of equations 7.2.1.1 in the form

$$\begin{aligned} \frac{dX}{dt} &= F(X,Z), \\ \frac{dY}{dt} &= G(X,Z), \\ G(X,0) &= 0. \end{aligned} \tag{7.3.2.1}$$

where

$$X = (E_E, L_W, P_M, S_V, S_H),$$

comprises of the uninfected components and

$$Z = (I_V, G_v, G_m, Z_v, O_v, P_v, P_V, I_H, G_H)$$

comprises of the infected and infectious components.
We let

$$\begin{aligned} E_0 &= (X^*, 0), \\ &= \left(\frac{\Lambda_E}{\mu_E + theta_E}, \frac{1}{\mu_W + \alpha_W + \delta_W} \frac{\theta_E \Lambda_E}{\mu_E + \theta_E}, \frac{1}{\mu_M + \alpha_M + \delta_M} \frac{\alpha_W}{\mu_W + \alpha_W + \delta_W} \frac{\theta_E \Lambda_E}{\mu_E + \theta_E}, \right. \\ &\quad \left. \frac{1}{2\mu_V} \frac{\alpha_M}{\mu_M + \alpha_M + \delta_M} \frac{\alpha_W}{\mu_W + \alpha_W + \delta_W} \frac{\theta_E \Lambda_E}{\mu_E + \theta_E}, 0, 0, 0, 0, 0, 0, 0, \frac{\Lambda_H}{\mu_H}, 0, 0 \right), \end{aligned}$$

represent the disease-free equilibrium (DFE) of the system of equations 7.2.1.1. Where for X^* to be globally asymptotically stable, the following conditions $H1$ and $H2$ must be satisfied.
$H1$. For $\frac{dX}{dt} = F(X,0)$, X^* is globally asymptotically.
$H2$. $G(X,Y) = AZ - \hat{G}(X,Z)$, $\hat{G}(X,Z) \geq 0$ for $(X,Z) \in \mathbb{R}^{14}_+$, where $A = D_Z G(X^*, 0)$, which is an

M-matrix and $\mathbb{R}_+^{14}$ is the region where the model makes biological sense.

$$F(X,0) = \begin{bmatrix} \Lambda_E - (\mu_E + \theta_E)E_E \\ \\ \dfrac{\theta_E \Lambda_E}{\mu_E + \theta_E} - (\mu_W + \alpha_W + \delta_W)L_W \\ \\ \dfrac{\alpha_W}{\mu_W + \alpha_W + \delta_W} \dfrac{\theta_E \Lambda_E}{\mu_E + \theta_E} - (\mu_M + \alpha_M + \delta_M)P_M \\ \\ \dfrac{1}{2} \dfrac{\alpha_M}{\mu_M + \alpha_M + \delta_M} \dfrac{\alpha_W}{\mu_W + \alpha_W + \delta_W} \dfrac{\theta_E \Lambda_E}{\mu_E + \theta_E} - \mu_V S_V \\ \\ \Lambda_H - \mu_H S_H \end{bmatrix}, \tag{7.3.2.2}$$

and the matrix A is given by

$$A = \begin{bmatrix} -F_4 & 0 & 0 & 0 & 0 & 0 & 0 & 0 & G_1 \\ 0 & -F_5 & 0 & 0 & 0 & 0 & 0 & 0 & G_2 \\ 0 & N_g\alpha_g & -F_6 & 0 & 0 & 0 & 0 & 0 & 0 \\ 0 & 0 & \dfrac{\alpha_s}{2} & -F_7 & 0 & 0 & 0 & 0 & 0 \\ 0 & 0 & 0 & \alpha_z & -F_8 & 0 & 0 & 0 & 0 \\ 0 & 0 & 0 & 0 & N_k\alpha_k & -F_9 & 0 & 0 & 0 \\ 0 & 0 & 0 & 0 & 0 & \alpha_v & \alpha_V & 0 & 0 \\ 0 & 0 & 0 & 0 & 0 & 0 & \dfrac{\beta_V S_H}{P_0} & -F_{10} & 0 \\ 0 & 0 & 0 & 0 & 0 & 0 & 0 & N_h\alpha_h & -\alpha_H \end{bmatrix}, \tag{7.3.2.3}$$

and

$$\hat{G}(X,Z) = AZ - G(X,Z) \tag{7.3.2.4}$$

$$= \begin{bmatrix} \beta_H G_H \left[\dfrac{1}{2\mu_V G_0} \dfrac{\alpha_M}{\mu_M + \alpha_M + \delta_M} \dfrac{\alpha_W}{\mu_W + \alpha_W + \delta_W} \dfrac{\theta_E \Lambda_E}{\mu_E + \theta_E} - \dfrac{S_V}{G_0 + G_H} \right] \\ \dfrac{\beta_H G_H}{\phi_V} \left[\dfrac{(S_V^0 - 1)}{G_0} - \dfrac{(S_V - 1)}{(G_0 + G_H)(I_H + 1)} \right] \\ 0 \\ 0 \\ 0 \\ 0 \\ 0 \\ \beta_V P_V \left[\dfrac{\Lambda_H}{\mu_H P_0} - \dfrac{S_H}{P_0 + P_V} \right] \\ 0 \end{bmatrix}.$$

Since $\left[\frac{1}{2\mu_V G_0}\frac{\alpha_M}{\mu_M+\alpha_M+\delta_M}\frac{\alpha_W}{\mu_W+\alpha_W+\delta_W}\frac{\theta_E\Lambda_E}{\mu_E+\theta_E} \geq \frac{S_V}{G_0+G_H}\right]$, $\left[\frac{(S_V^0-1)}{G_0} \geq \frac{(S_V-1)}{(G_0+G_H)(I_H+1)}\right]$ and $\left[\frac{\Lambda_H}{\mu_H P_0} \geq \frac{S_H}{P_0+P_V}\right]$, it clear that $\hat{G}(X,Z) \geq 0$ for all $(X,Z) \in \mathbb{R}_+^{14}$. It is also clear that A is an M-matrix, since the off diagonal elements of A are non-negative. So, we state a theorem which summarises the above results.

Theorem 7.2. *The fixed point*

$$E_0 = (X^*, 0),$$

is global asymptotically stable equilibrium of the system of equations (7.2.1.1) when $R_0 < 1$ and then the assumptions $(H1)$ and $(H2)$ are satisfied.

7.3.3 Local stability of endemic equilibrium

We establish a local stability of the endemic equilibrium state by applying the center manifold theory [50, 91], as illustrated in [74]. We use the center manifold theory to obtain the local asymptotic stability of the endemic equilibrium points.

By applying the center manifold theory, We then introducing the change of variables. We let $E_E = x_1$, $L_W = x_2$, $P_M = x_3$, $S_V = x_4$, $I_V = x_5$, $G_v = x_6$, $G_m = x_7$, $Z_v = x_8$, $O_v = x_9$, $P_v = x_{10}$, $P_V = x_{11}$, $S_H = x_{12}$, $I_V = x_{13}$, $G_H = x_{14}$, $\beta^* = \beta_V$ and $\beta_H = k\beta_V$ and let β be the bifurcation parameter. We denote $x = (x_1, x_2, x_3, x_4, x_5, x_6, x_7, x_8, x_9, x_{10}, x_{11}, x_{12}, x_{13}, x_{14})^T$, then the model (7.2.1.1) can be written in the form

$$\frac{dX}{dt} = (f_1, f_2, f_3, f_4, f_5, f_6, f_7, f_8, f_9, f_{10}, f_{11}, f_{12}, f_{13}, f_{14})^T,$$

as follows

$$\begin{aligned}
f_1 &= \frac{dx_1}{dt} = \Lambda_E - (\mu_E + \theta_E)x_1, \\
f_2 &= \frac{dx_2}{dt} = \theta_E x_1 - (\mu_W + \alpha_W + \delta_W)x_2, \\
f_3 &= \frac{dx_3}{dt} = \alpha_W x_2 - (\mu_M + \alpha_M + \delta_M)x_3, \\
f_4 &= \frac{dx_4}{dt} = \frac{\alpha_M x_1}{2} - \frac{k\beta^* x_{14}x_4}{P_0 + x_{14}} - \mu_V x_4, \\
f_5 &= \frac{dx_5}{dt} = \frac{k\beta^* x_{14}x_4}{P_0 + x_{14}} - (\mu_V + \delta_V)x_5, \\
f_6 &= \frac{dx_6}{dt} = \frac{k\beta^* x_{14}(x_4 - 1)}{(P_0 + x_{14})\phi_V(x_5 + 1)} - (\alpha_g + \mu_g)x_6, \\
f_7 &= \frac{dx_7}{dt} = N_g\alpha_g x_6 - (\alpha_s + \mu_s)x_7 \qquad (7.3.3.1) \\
f_8 &= \frac{dx_8}{dt} = \frac{\alpha_s x_7}{2} - (\alpha_z + \mu_z)x_8, \\
f_9 &= \frac{dx_9}{dt} = \alpha_z x_8 - (\alpha_k + \mu_k)x_9, \\
f_{10} &= \frac{dx_{10}}{dt} = N_k\alpha_k x_9 - (\alpha_v + \mu_v)x_{10}, \\
f_{11} &= \frac{dx_{11}}{dt} = x_{10}\alpha_v(x_5 + 1) - \alpha_V x_{11}, \\
f_{12} &= \frac{dx_{12}}{dt} = \Lambda_H - \frac{\beta^* x_{11}x_{12}}{P_0 + x_{11}} - \mu_H x_{12} + \gamma_H x_{13}, \\
f_{13} &= \frac{\beta^* x_{11}x_{12}}{P_0 + x_{11}} - (\mu_H + \gamma_H + \delta_H)x_{13}, \\
f_{14} &= \frac{dx_{14}}{dt} = N_h\alpha_h x_{13} - \alpha_H x_{14}.
\end{aligned}$$

By considering $R_0 = 1$, and solving for β^*, we obtain

$$\beta^* = \sqrt{\left[\frac{2(\mu_E + \theta_E)(\mu_W + \alpha_W + \delta_W)(\mu_M + \alpha_M + \delta_M)}{N_v\alpha_v}\frac{P_0}{1}\frac{\alpha_V}{1}\frac{\mu_H}{\Lambda_H}\right]\left[\frac{\mu_H + \gamma_H + \delta_H}{N_h\alpha_h}\frac{G_0}{1}\frac{\alpha_H}{1}\frac{\phi_V\mu_V}{kq_1}\right]}, \qquad (7.3.3.2)$$

where

$$\begin{aligned}
q_1 &= \alpha_H\alpha_W\theta_E\Lambda_E - 2\mu_V(\mu_E + \theta_E)(\mu_W + \alpha_W + \delta_W)(\mu_M + \alpha_M + \delta_H), \qquad (7.3.3.3) \\
N_v &= \frac{1}{2}\frac{N_g\alpha_g}{\alpha_g + \mu_g}\frac{N_k\alpha_k}{\alpha_k + \mu_k}\frac{\alpha_z}{\alpha_z + \mu_z}\frac{\alpha_s}{\alpha_s + \mu_s}\frac{1}{\alpha_v + \mu_v}, \qquad (7.3.3.4) \\
N_h &= \frac{\pi}{(1 - \pi)}\left[\frac{(1 - \pi)N_m\beta_h\Lambda_h - \mu_b\mu_m}{N_m\beta_h(\alpha_h + \mu_h)}\right]. \qquad (7.3.3.5)
\end{aligned}$$

We linearize matrix of system of equations (7.3.3.1) around the DFE when $\beta_V = \beta$ and $\beta_H = k\beta_V$ which is similar to $J(E_0)$ in system (7.3.1.3). The right eigenvector are associated with zero eigenvalue and is given by $W = (w_1, w_2, w_3, w_4, w_5, w_6, w_7, w^8, w_9, w_{11}, w_{12}, w_{13}, w_{14})^T$. We determine the right

eigenvector by saying $(J(E_0))W = 0$. We obtain

$$\begin{aligned}
w_1 &= w_2 = w_3 = 0,\\
w_4 &= -\frac{k\beta^* x_4^0}{G_0\mu_V},\\
w_5 &= \frac{k\beta^* x_4^0}{G_0(\mu_V+\delta_V)},\\
w_6 &= \frac{1}{\alpha_g+\mu_g}\frac{k\beta^*(x_4^0-1)}{G_0\phi_V},\\
w_7 &= \frac{N_g\alpha_g}{\alpha_g+\mu_g}\frac{1}{\alpha_s+\mu_s}\frac{k\beta^*(x_4^0-1)}{G_0\phi_V},\\
w_8 &= \frac{1}{2}\frac{N_g\alpha_g}{\alpha_g+\mu_g}\frac{\alpha_s}{\alpha_s+\mu_s}\frac{1}{\alpha_z+\mu_z}\frac{k\beta^*(x_4^0-1)}{G_0\phi_V},\\
w_9 &= \frac{1}{2}\frac{N_g\alpha_g}{\alpha_g+\mu_g}\frac{\alpha_s}{\alpha_s+\mu_s}\frac{\alpha_z}{\alpha_z+\mu_z}\frac{1}{\alpha_k+\mu_k}\frac{k\beta^*(x_4^0-1)}{G_0\phi_V},\\
w_{10} &= \frac{1}{2}\frac{N_g\alpha_g}{\alpha_g+\mu_g}\frac{\alpha_s}{\alpha_s+\mu_s}\frac{\alpha_z}{\alpha_z+\mu_z}\frac{N_k\alpha_k}{\alpha_k+\mu_k}\frac{1}{\alpha_v+\mu_v}\frac{k\beta^*(x_4^0-1)}{G_0\phi_V},\\
w_{11} &= \frac{1}{2}\frac{N_g\alpha_g}{\alpha_g+\mu_g}\frac{\alpha_s}{\alpha_s+\mu_s}\frac{\alpha_z}{\alpha_z+\mu_z}\frac{N_k\alpha_k}{\alpha_k+\mu_k}\frac{\alpha_v}{\alpha_v+\mu_v}\frac{1}{\alpha_V}\frac{k\beta^*(x_4^0-1)}{G_0\phi_V},\\
w_{12} &= -\frac{1}{2}\frac{N_g\alpha_g}{\alpha_g+\mu_g}\frac{\alpha_s}{\alpha_s+\mu_s}\frac{\alpha_z}{\alpha_z+\mu_z}\frac{N_k\alpha_k}{\alpha_k+\mu_k}\frac{\alpha_v}{\alpha_v+\mu_v}\frac{\mu_H+\delta_H}{\mu_H+\gamma_H+\delta_H}\frac{1}{\alpha_V}\frac{k\beta^*(x_4^0-1)}{G_0\phi_V}\frac{\beta^* X_{12}^0}{P_0},\\
w_{13} &= \frac{1}{2}\frac{N_g\alpha_g}{\alpha_g+\mu_g}\frac{\alpha_s}{\alpha_s+\mu_s}\frac{\alpha_z}{\alpha_z+\mu_z}\frac{N_k\alpha_k}{\alpha_k+\mu_k}\frac{\alpha_v}{\alpha_v+\mu_v}\frac{1}{\mu_H+\gamma_H+\delta_H}\frac{1}{\alpha_V}\frac{k\beta^*(x_4^0-1)}{G_0\phi_V}\frac{\beta^* x_{12}^0}{P_0},\\
w_{14} &= 1.
\end{aligned} \tag{7.3.3.6}$$

We denote

$$V = (v_1, v_2, v_3, v_4, v_5, v_6, v_7, v_8, v_9' v_{10}, v_{11}, v_{12}, v_{13}, v_{14})^T$$

as the left eigenvector associated with zero eigenvalue. To find V, we employ

$$V^T(J(E_0, \beta^*)) = 0,$$

where $J(E0; \beta^*)$ is the Jacobian matrix at the disease free equilibrium point when $R_0 = 1$, where 0 is the zero vector.

$$\begin{aligned}
v_1 &= v_2 = v_3 = v_4 = V_5 = v_{12},\\
v_6 &= \frac{N_g\alpha_g}{\alpha_g+\mu_g},\\
v_7 &= 1,\\
v_8 &= \frac{N_g\alpha_g}{\alpha_g+\mu_g}\frac{N_h\alpha_h}{\mu_H+\gamma_H+\delta_H}\frac{N_k\alpha_k}{\alpha_k+\mu_k}\frac{\alpha_z}{\alpha_z+\mu_z}\frac{\alpha_v}{\alpha_v+\mu_v}\frac{k\beta^*(x_4^0-1)}{G_0\phi_V\alpha_H}\frac{\beta^* x_{12}^0}{\alpha_V P_0},\\
v_9 &= \frac{N_g\alpha_g}{\alpha_g+\mu_g}\frac{N_h\alpha_h}{\mu_H+\gamma_H+\delta_H}\frac{N_k\alpha_k}{\alpha_k+\mu_k}\frac{\alpha_v}{\alpha_v+\mu_v}\frac{k\beta^*(x_4^0-1)}{G_0\phi_V\alpha_H}\frac{\beta^* x_{12}^0}{\alpha_V P_0},
\end{aligned} \tag{7.3.3.7}$$

$$
\begin{aligned}
v_{10} &= \frac{N_g\alpha_g}{\alpha_g+\mu_g}\frac{N_h\alpha_h}{\mu_H+\gamma_H+\delta_H}\frac{\alpha_v}{\alpha_v+\mu_v}\frac{k\beta^*(x_4^0-1)}{G_0\phi_V\alpha_H}\frac{\beta^*x_{12}^0}{\alpha_V P_0},\\
v_{11} &= \frac{N_g\alpha_g}{\alpha_g+\mu_g}\frac{N_h\alpha_h}{\mu_H+\gamma_H+\delta_H}\frac{k\beta^*(x_4^0-1)}{G_0\phi_V\alpha_H}\frac{\beta^*x_{12}^0}{\alpha_V P_0},\\
v_{13} &= \frac{N_g\alpha_g}{\alpha_g+\mu_g}\frac{N_h\alpha_h}{\mu_H+\gamma_H+\delta_H}\frac{k\beta^*(x_4^0-1)}{G_0\phi_V\alpha_H},\\
v_{14} &= \frac{N_g\alpha_g}{\alpha_g+\mu_g}\frac{k\beta^*(x_4^0-1)}{G_0\phi_V\alpha_H},
\end{aligned}
\tag{7.3.3.8}
$$

where

$$
\begin{aligned}
x_4^0 &= \frac{1}{2\mu_V}\frac{\alpha_M}{\mu_M+\alpha_M+\delta_M}\frac{\alpha_W}{\mu_W+\alpha_W+\delta_W}\frac{\theta_E\Lambda_E}{\mu_E+\theta_E},\\
x_{12} &= \frac{\Lambda_H}{\mu_H}.
\end{aligned}
\tag{7.3.3.9}
$$

The bifurcation coefficients, a and b are defined as follows

$$
a = \sum_{k,i,j=1}^{14} v_k w_i w_j \frac{\partial^2 f_k}{\partial w_i \partial w_j}(E_0), \tag{7.3.3.10}
$$

$$
b = \sum_{k,i,j=1}^{14} v_k w_i \frac{\partial^2 f_k}{\partial x_i \partial \beta}(E_0). \tag{7.3.3.11}
$$

Since $v_1 = v_2 = v_3 = v_4 = v_5 = v_{12} = 0$, we have to compute the non-zero partial derivatives of F at disease free equilibrium are given by

$$
\frac{\partial^2 f_6}{\partial x_4 \partial x_{14}}(E_0) = \frac{\partial^2 f_6}{\partial x_{14} \partial x_4}(E_0) = \frac{k\beta^*}{\phi_V G_0}, \qquad \frac{\partial^2 f_6}{\partial x_{14}^2}(E_0) = -\frac{2k\beta^*(x_4^0-1)}{G_0^2\phi_V},
$$

$$
\frac{\partial^2 f_6}{\partial x_5 \partial x_{14}}(E_0) = \frac{\partial^2 f_6}{\partial x_{14} \partial x_5}(E_0) = -\frac{k\beta^*(x_4^0-1)}{G_0\phi_V}, \qquad \frac{\partial^2 f_{11}}{\partial x_5 \partial x_{10}}(E_0) = \frac{\partial^2 f_{11}}{\partial x_{10} \partial x_5}(E_0) = \alpha_v,
$$

$$
\frac{\partial^2 f_{13}}{\partial x_{11}^2}(E_0) = -\frac{2\beta^* x_{12}^0}{P_0^2}, \qquad \frac{\partial^2 f_{13}}{\partial x_{11} \partial x_{12}}(E_0) = \frac{\partial^2 f_{13}}{\partial x_{12} \partial x_{11}}(E_0) = \frac{\beta^*}{P_0},
$$

$$
\frac{\partial^2 f_6}{\partial x_{14} \partial \beta}(E_0) = \frac{k(x_4^*-1)}{G_0\phi_V}, \qquad \frac{\partial^2 f_{13}}{\partial x_{11} \partial \beta}(E_0) = \frac{X_{12}^0}{P_0}.
$$

It follows that

$$
\begin{aligned}
a = {} & v_6 w_4 w_{14} \frac{\partial^2 f_6}{\partial x_4 \partial x_{14}}(E_0) + v_6 w_{14}^2 \frac{\partial^2 f_6}{\partial x_{14}^2}(E_0) + v_6 w_5 w_{14} \frac{\partial^2 f_6}{\partial x_5 \partial x_{14}}(E_0) + v_{13} w_{11}^2 \frac{\partial^2 f_{13}}{\partial x_{11}^2}(E_0)\\
& + v_{11} w_5 w_{10} \frac{\partial^2 f_{11}}{\partial x_5 \partial x_{10}}(E_0) + v_{13} w_{11} w_{12} \frac{\partial^2 f_{13}}{\partial x_5 \partial x_{12}}(E_0),
\end{aligned}
$$

$$
\begin{aligned}
a &= -\frac{N_g\alpha_g}{\alpha_g+\mu_g}\frac{k\beta^*}{\phi_V G_0^2}\left[\frac{k\beta^* x_4^0}{\mu_V}+2(x_4^0-1)+\frac{k\beta^* x_4^0(x_4^0-1)}{\mu_V+\delta_V}\right] \\
&\quad -\frac{1}{2}\left(\frac{N_g\alpha_g}{\alpha_g+\mu_g}\frac{k\beta^*(x_4^0-1)}{G_0\phi_V}\right)^3\frac{N_h\alpha_h\beta^* x_{12}^0}{\mu_H+\gamma_H+\delta_H}\left(\frac{N_k\alpha_k}{\alpha_k+\mu_k}\frac{\alpha_z}{\alpha_z+\mu_z}\frac{\alpha_s}{\alpha_s+\mu_s}\frac{\alpha_v}{\alpha_v+\mu_v}\frac{1}{\alpha_V P_0}\right)^2 \\
&\quad -\frac{1}{2}\left(\frac{N_g\alpha_g}{\alpha_g+\mu_g}\frac{k\beta^*(x_4^0-1)}{G_0\phi_V}\right)^2\frac{N_h\alpha_h}{\mu_H+\gamma_H+\delta_H}\frac{N_k\alpha_k}{\alpha_k+\mu_k}\frac{\alpha_z}{\alpha_z+\mu_z}\frac{\alpha_s}{\alpha_s+\mu_s}\frac{\alpha_v}{\alpha_v+\mu_v}\frac{1}{\alpha_V}\frac{k\beta^{*2}x_{12}^0}{G_0P_0}[\cdot \\
&\quad \frac{N_v\alpha_v}{\alpha_V}\frac{\beta^*(x_4^0-1)}{P_0\phi_V\alpha_H}\frac{\mu_H+\delta_H}{\mu_H+\gamma_H+\delta_H}-\frac{x_4^0}{\mu_V+\delta_V}\Big] \qquad (7.3.3.12) \\
a &< 0
\end{aligned}
$$

when

$$\frac{N_v\alpha_v}{\alpha_V}\frac{\beta^*(x_4^0-1)}{P_0\phi_V\alpha_H}\frac{\mu_H+\delta_H}{\mu_H+\gamma_H+\delta_H}\geq\frac{x_4^0}{\mu_V+\delta_V}.$$

It also follows that

$$
\begin{aligned}
b &= v_6w_{14}\frac{\partial^2 f_6}{\partial x_{14}\partial\beta}(E_0)+v_{13}w_{11}\frac{\partial^2 f_{13}}{\partial x_{11}\partial\beta}(E_0) \\
&= \frac{N_g\alpha_g}{\alpha_g+\mu_g}\frac{k(x_4^0-1)}{G_0\phi_V}[1+ \qquad (7.3.3.13) \\
&\quad \frac{1}{2}\frac{N_g\alpha_g}{\alpha_g+\mu_g}\frac{k\beta^*(x_4^0-1)}{G_0\phi_V}\frac{N_h\alpha_h}{\mu_H+\gamma_H+\delta_H}\frac{N_k\alpha_k}{\alpha_k+\mu_k}\frac{\alpha_z}{\alpha_z+\mu_z}\frac{\alpha_s}{\alpha_s+\mu_s}\frac{\alpha_v}{\alpha_v+\mu_v}\frac{\beta^* x_{12}^*}{P_0\alpha_V}\Big], \\
b &> 0.
\end{aligned}
$$

Thus, $a<0$ and $b>0$, it follows that the model will undergo a trans-critical bifurcation at $R_0=1$. By using item (iv) of Theorem (4.1). in [74], we can conclude that the endemic equilibrium points of system of equations (7.2.1.1) is locally asymptotically stable when $R_0>1$ but close to 1. We summarize the results using the following theorem.

Theorem 7.3. *The presents of malaria infection equilibrium is locally asymptotically stable when $R_0>1$ but close to 1.*

7.4 Numerical results

In this section, we display out numerical simulations of the mosquito life cycle model for malaria infectious disease systems, with the aim of validating some of the critical results of the coupled multiscale model (7.2.1.1). We perform numerical simulations using Python program version 2.7 and Matlab version 2019, using the windows operating system (Windows 10). We utilise a package called odeint function in the python-scipy that solve any system of differentiated equations. The parameter values utilised in the model simulations are in Tables (7.2, 7.3, 7.4 , 7.5, 7.6). The parameter values employed in this study were taken from published literatures on mathematical and computational models and some parameter values were estimated from empirical studies.

Table 7.2: Between-mosquito scale parameter values and their description.

Parameter	Description	Initial Value	Range	Units	Source
β_V	Contact rate of susceptible humans with the infectious reservoir of mosquitoes.	0.52135	2.7×10^{-3}-0.64	day^{-1}	[35]
μ_V	Natural death rate of mosquitoes.	0.12	0.033-0.3	day^{-1}	[24]
δ_V	induced death rate of infected mosquitoes.	0.00000426	$4.26 \times 10^{-6} - 5.33 \times 10^{-6}$	day^{-1}	[24]
P_0	Half saturation constant associated with the infection of humans.	1×10^8	$1^7 - 5 \times 10^8$	day^{-1}	[24]
ϕ_V	Proportion of new infected mosquitoes in the total infected mosquito population.	0.0001	0.0001-0.01	day^{-1}	assumed
α_V	Rate of clearance of community sporozoite load.	0.3	0.09-0.99	day^{-1}	[24]

Table 7.3: Immature mosquito parameter values and their description.

Parameter	Description	Initial Value	Range	Units	Source
Λ_E	Rate at which mosquitoes lay eggs.	200	100-4000	Eggs per day	Assumed
θ_E	Hatching rate of eggs into larvae.	0.6	0.01-0.6	day^{-1}	[88]
μ_E	Mortality rate of eggs.	0.3	0.01-0.56	day^{-1}	[88]
α_W	The rate at which larvae develops into pupae.	0.4	0.14-0.4	day^{-1}	[88]
μ_W	Natural death rare of larvae.	0.3	0.05-0.3	day^{-1}	[88]
δ_W	The rate at which larvae reduced by other species.	0.08	0.01-0.1	day^{-1}	Assumed
α_M	The rate at which pupae develops into adult.	0.25	0.25-0.5	day^{-1}	[88]
μ_M	Mortality rate of pupae.	0.15	0.15-0.37	day^{-1}	[88]
δ_M	The rate at which pupae reduced by other species.	0.08	0.01-0.1	day^{-1}	Assumed

Table 7.4: Between-human scale parameter values and their description.

Parameter	Description	Initial Value	Range	Units	Source
Λ_H	Rate of recruitment of Susceptible humans.	400	10-800	Humans per day	[35]
β_H	Infection rate of susceptible mosquitoes.	0.356	0.072-0.64	day^{-1}	[35]
μ_H	Natural death rate of humans.	0.00004	0.00001-0.00008	day^{-1}	[24]
δ_H	Disease induced death rate of humans.	0.003454	$1 \times 10^{-15} - 4.1 \times 10^{-4}$	day^{-1}	[35]
γ_H	Natural recovery rate of humans.	0.0092	0.0014-0.017	day^{-1}	[35]
G_0	Half saturation constant associated with the infection of mosquitoes.	5×10^8	$1\times10^8 - 1\times10^9$	day^{-1}	[24]
ϕ_H	Proportion of new infected humans in the total infected human population.	0.0001	0.0001-0.01	day^{-1}	Assumed
α_H	Rate of clearance of community gametocyte load.	0.0000913	0.0000467-0.000274	day^{-1}	[24]

Table 7.5: Within-mosquito scale parameter values and their description.

Parameter	Description	Initial Value	Range	Units	Source
Λ_v	The rate of supply of gametocytes within infected mosquitoes.	300	100-300	Gametocytes per day	[24]
α_g	Rate at which gametocyte infected erythrocytes burst within ifected mosquito.	96	90-100	day^{-1}	[24]
μ_g	Decay rate of gametocytes within infected mosquito.	0.0625	0.0326-0.0725	day^{-1}	[24]
N_g	Number of gametes produced per gametocyte infected erythrocyte within infected mosquito.	2	1-3	Gametes per day	[24]
α_z	Rate at which zygote develop into oocysts.	0.4240	0.01-0.5	day^{-1}	[24]
μ_z	Natural death rate of zygote.	1	1-4	day^{-1}	[24]
α_s	Fertilisation of gametes.	0.08	0.01-0.2	day^{-1}	[24]
μ_s	Natural death rate of gametes.	58	40-129	day^{-1}	[24]
α_k	Bursting rate of oocysts to produce sporozoites.	0.2	0-1	day^{-1}	[24]
N_k	Number of sporozoites produced per bursting oocysts.	3 000	1000-10000	Sporozoites per day	[24]
μ_k	Natural death rate of oocysts.	0.01	0.071-0.143	day^{-1}	[24]
α_v	Rate at which sporozoites become infectious to humans.	0.025	0.0167-1	day^{-1}	[24]
μ_v	Natural death rate of sporozoites.	0.0001	0.0001-0.01	day^{-1}	[24]

Table 7.6: Within-human scale parameter values and their description.

Parameter	Description	Initial Value	Range	Units	Source
Λ_h	Rate of supply of uninfected red blood cells.	200	100-300	Cells per day	[24]
β_h	Rate of infection of red blood cells (erythrocytes).	0.1	2×10^{-9}-0.2	day^{-1}	[24]
α_h	Rate at which gametocytes develop and become infectious within infected human.	0.02	0.01-0.9	day^{-1}	[24]
μ_h	Natural death rate of gametocyte infected erythrocytes within infected human.	0.0625	0.0600-0.0625	day^{-1}	[24]
μ_b	Natural decay rate of red blood cells.	0.0083	0.006-0.1	day^{-1}	[24]
μ_m	Natural decay rate of free merozoites	0.001	0.001-0.5	day^{-1}	
π	Proportion of gametocytes infected erythrocytes.	0.1	0.1-0.5	day^{-1}	[24]
N_m	Number of merozoites produced per bursting erythrocytes.	16	10-30	Merozoites per day	[24]
α_m	Rate at which erythrocytes burst to produce merozoites.	0.5	0.1-1.0	day^{-1}	[24]

7.4.1 Sensitivity Analysis

This subsection provides some results concerning the sensitive of the model reproductive number (R_0) along with the community sporozoites load (P_V^*) and community gametocytes load (G_H^*) when the multi-scale model parameters changes. By using the partial rank correlation coefficients (PRCCs), we investigate the sensitivity of model parameter variations on R_0, P_V^* and G_H^*. PRCCs rank each parameter by the impact it has on the results when all other parameters are kept at median values. We explore the influence of each model parameters on the model R_0, P_V^* and G_H^*. The solutions of the simulations of global sensitivity analysis of parameters on R_0, P_V^* and G_H^* are shown I the tornado plots diagrams in Figures (7.2), (7.3) and (7.4), respectively.

From Figure(7.2)-figure (7.4), we present the degree of sensitivity of every parameter on R_0, P_V^* and G_H^*, respectively. We observed that some of the parameters have positive PRCCs and some have negative PRCCs. The parameters with having positive PRCCs will increase the value of R_0, P_V^* and G_H^* when the parameter values are increased, whilst the parameters with negative PRCCs will reduce the value of R_0, P_V^* and G_H^* when the parameter values are increased.

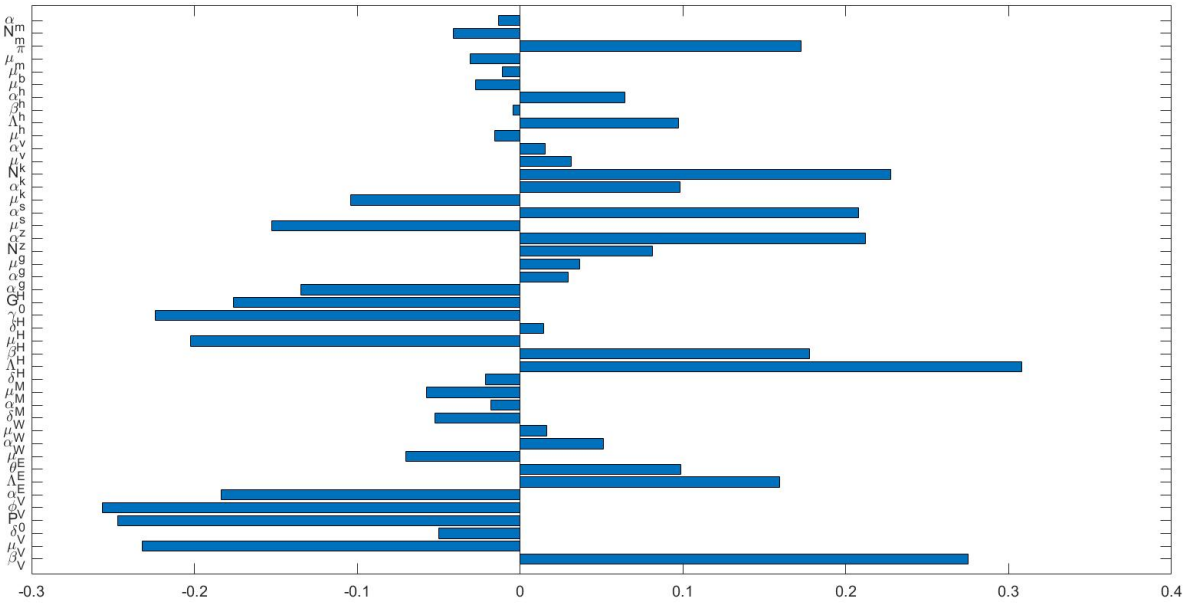

Figure 7.2: Global Sensitivity for Reproductive number (R_0)

In Figures (7.2), we present the global sensitivity analysis of R_0 using the tornado plot. The parameters β_V, Λ_H, Λ_E, β_H, π, α_s, N_k and α_z have the high impact in in raising the value of R_0 when these parameters values are increased. The parameters μ_V, P_0, ϕ_V, α_V, μ_V, γ_V, G_0, α_H, μ_z and μ_s have the high effect in reducing the value of R_0 when these parameter values are increased. The parameter values may have either positive or negative PRCCs, it is important to notice whether there is an increasing or decreasing trend when parameter values are varied.

In Figure (7.3), we present the tornado plot which showing the PRCCs of the community sporozoites load (P_V). The parameters P_0, Λ_E, θ_E, N_g, α_z, α_s, α_k and N_k have more influence in increasing the value of P_V when these parameter values are increased. Whilst these parameters β_V, μ_V, ϕ_V, α_V, μ_E, μ_W, δ_W, β_h, μ_s and μ_z have more impact on reducing the value of P_V, when the parameter values are increased.

Figure (7.4) illustrates on tornado plot which showing the PRCCs of the G_H. The parameters β_V, Λ_H, π and Λ_h have the influence in raising the value of G_H when the parameter values are increased. Whereas the parameters α_H, μ_V, P_0, ϕ_V and α_V have more influence in reducing the value of G_H when these parameter values are increased.

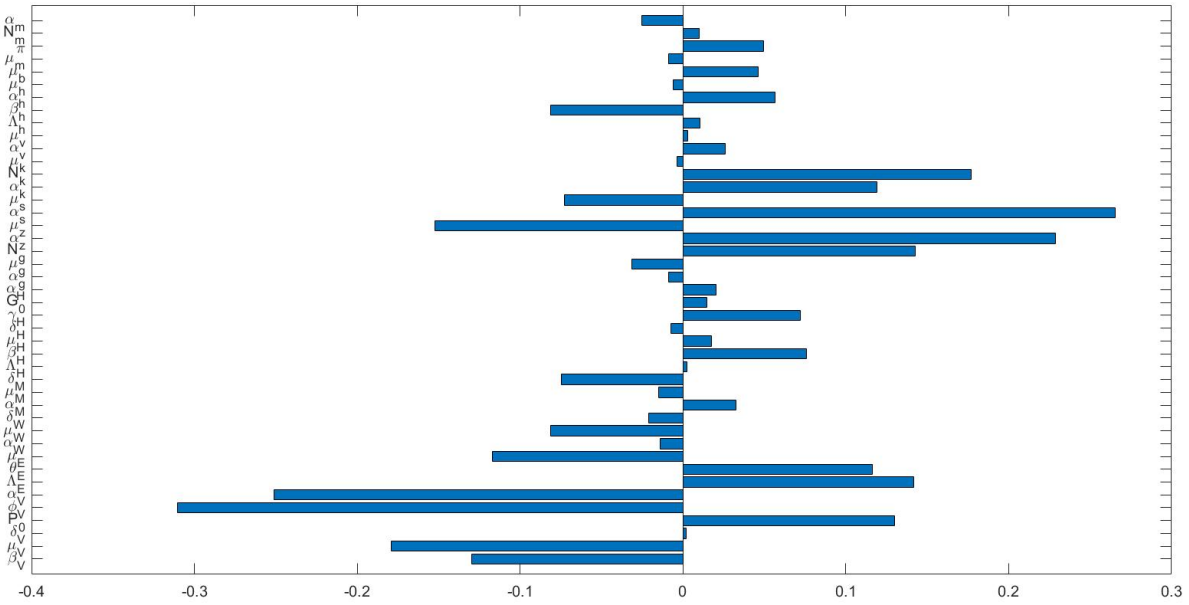

Figure 7.3: Global Sensitivity analysis for Community Sporozoites Load (P_V)

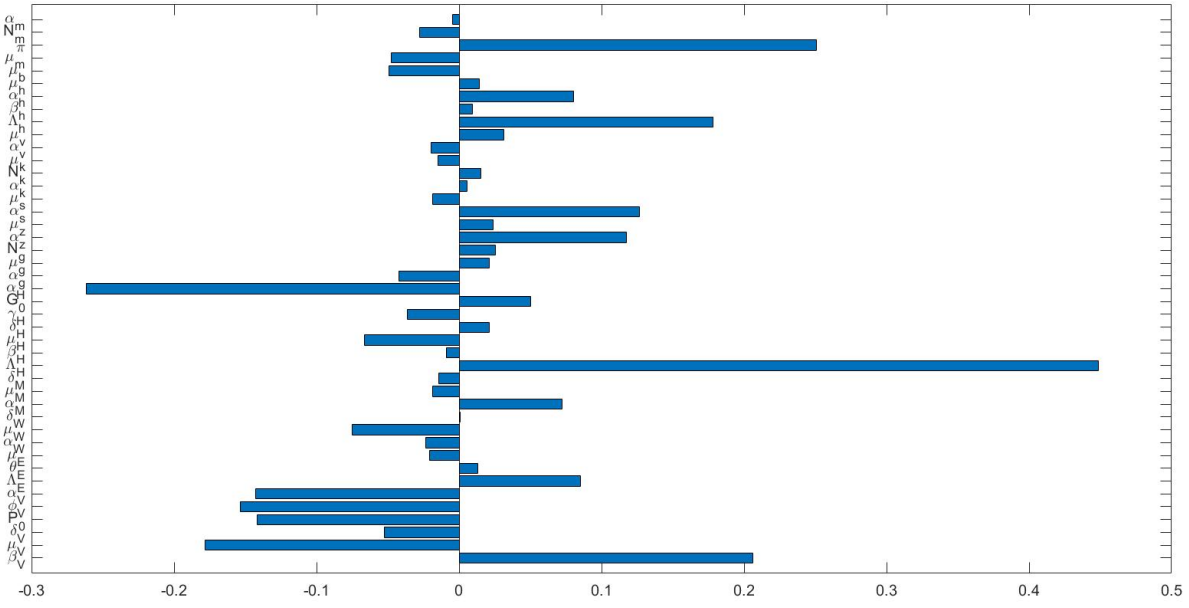

Figure 7.4: Global Sensitivity analysis for Community Gametocytes Load (G_H)

7.4.2 The Influence of Immature Mosquito Parameter on Within-Mosquito Scale Variables

In this sub-section, we examine through numerical simulation of the coupled multiscale model (7.2.1.1) the influence of immature mosquito parameters on the withi-mosquito scale sub-model dynamics of malaria. Figure (7.5)-figure (7.13) present the evidence of influence in the variation of immature mosquito scale parameters on the dynamics of within-mosquito variables ((a) population of gametocytes G_v, (b) population of gametes G_m, (c) population of zygotes Z_v, and (d) population of sporozoites P_v).

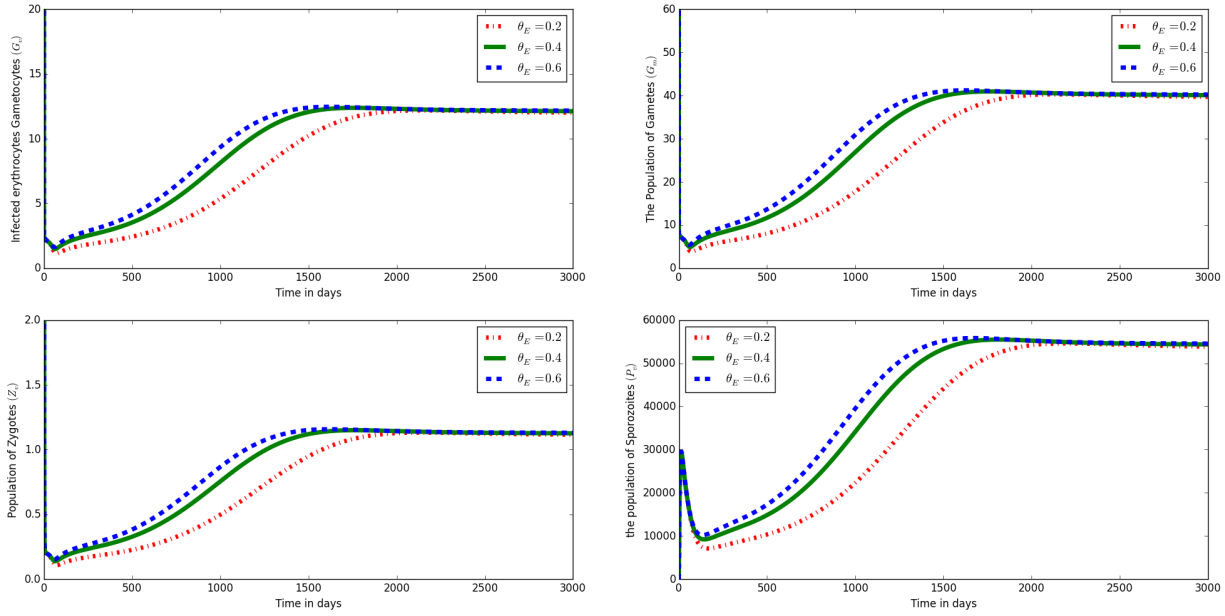

Figure 7.5: Graphs of numerical results of multiscale model (7.2.1.1) presenting the influence of variation of hatching of mosquito eggs into larvae at constant rate (θ_E) at the within-mosquito scale dynamics of (a) population of gametocytes G_v, (b) population of gametes G_m, (c) population of zygotes Z_v, and (d) population of sporozoites P_v for different values of θ_E: $\theta_E = 0.2$, $\theta_E = 0.4$ and $\theta_E = 0.6$

Figure (7.5) demonstrates the results of numerical simulation presenting the dynamics of (a) populations of gametocytes G_v, (b) population of gametes G_m, (c) population of zygotes Z_v, and (d) population of sporozoites P_v for different values of hatching of eggs into larvae at a rate θ_E: $\theta_E = 0.2$, $\theta_E = 0.4$, and $\theta_E = 0.6$. The results present that as the hatching of eggs into mosquito larvae increase, there is also visible increase in the malaria infection at the within-mosquito scale (that is, (a) population of gametocytes G_v, (b) population of gametes G_m, (c) population of zygotes Z_v, and (d) population of sporozoites P_v). The results indicate that control measures that reduce the hatching of eggs or increase the mortality of laid eggs has an impact in reducing the malaria infection at both within-mosquito scale and at community-level.

Figure (7.6) illustrates the solutions of numerical simulation showing the dynamics of (a) population of gametocytes G_v, (b) population of gametes G_m, (c) population of zygotes Z_v, and (d) population of

sporozoites P_v for different values of development of pupae into adult mosquito at a constant rate α_M: $\alpha_M = 0.25$, $\alpha_M = 0.35$, and $\alpha_M = 0.45$. The results present that as the rate of development of pupae into adult mosquito increase, there is a significant increase in the dynamics of (a) population of gametocytes G_v, (b) population of gametes G_m, (c) population of zygotes Z_v, and (d) population of sporozoites P_v. The results suggest that interventions that kills the pupae have an impact of reducing the mosquito density which has an influence in reducing malaria infection at both within-hosquito scale and between host scale.

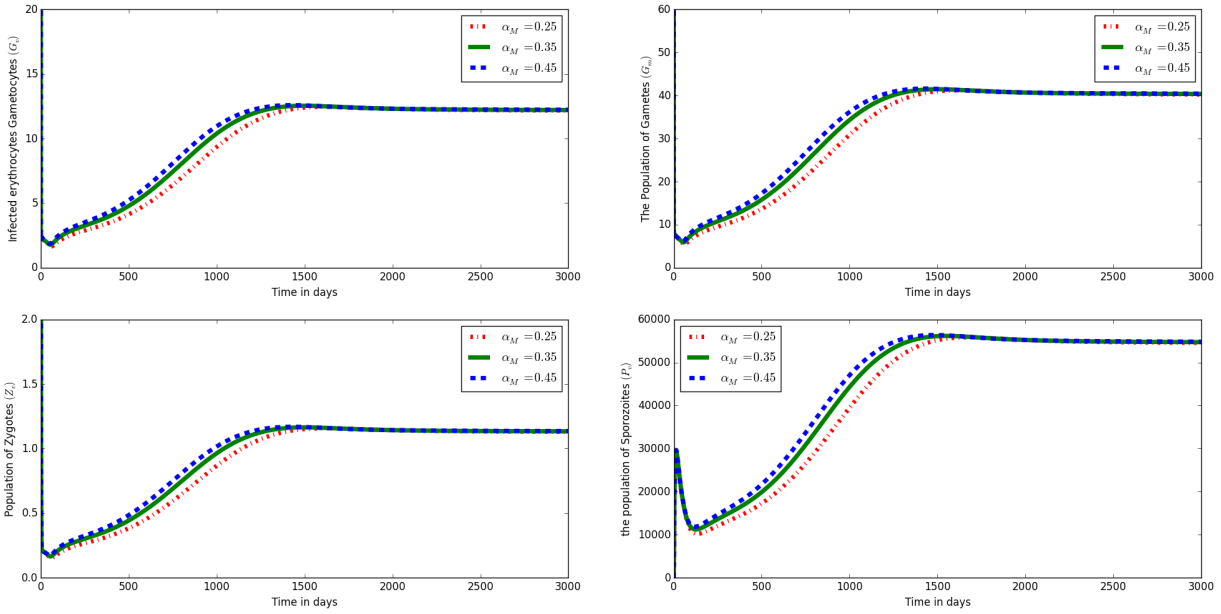

Figure 7.6: Graphs of numerical results of multiscale model (7.2.1.1) presenting the influence of variation of pupae develops into adult mosquito at a constant rate (α_M) at the within-mosquito scale dynamics of (a) population of gametocytes G_v, (b) population of gametes G_m, (c) population of zygotes Z_v, and (d) population of sporozoites P_v for different values of (α_M): $\alpha_M = 0.25$, $\alpha_M = 0.35$ and $\alpha_M = 0.45$

Figure (7.7) presents variations in (a) population of gametocytes G_v, (b) population of gametes G_m, (c) population of zygotes Z_v, and (d) population of sporozoites P_v for different values of development of larvae into mosquito pupae at a rate α_W: $\alpha_W = 0.2$, $\alpha_W = 0.4$, and $\alpha_W = 0.6$. From the results in figure (7.7), we observe that as the rate of development of larvae into mosquito pupae increase, we also observe an increase in the malaria infection on the dynamics of (a) population of gametocytes G_v, (b) population of gametes G_m, (c) population of zygotes Z_v, and (d) population of sporozoites P_v. The results suggest that control measures that targets the killing of larvae have an impact of reducing malaria infection at within-mosquito scale and also at population-level.

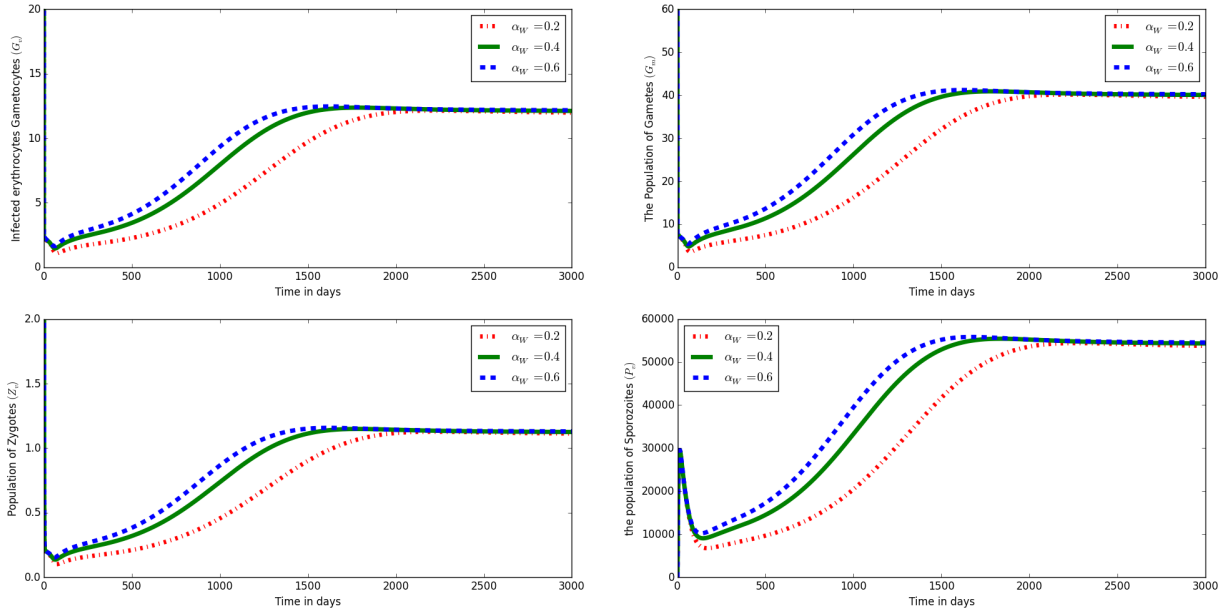

Figure 7.7: Graphs of numerical results of multiscale model (7.2.1.1) presenting the influence of variation of larvae develops into pupae (α_W) at the within-mosquito scale dynamics of (a) population of gametocytes G_v, (b) population of gametes G_m, (c) population of zygotes Z_v, and (d) population of sporozoites P_v for different values of (α_W): $\alpha_W = 0.2$, $\alpha_W = 0.4$ and $\alpha_W = 0.6$

Figure (7.8) illustrates the variations in (a) population of gametocytes G_v, (b) population of gametes G_m, (c) population of zygotes Z_v, and (d) population of sporozoites P_v for different values of pupae reduced by other species feed on them at a constant rate δ_M: $\delta_M = 0.008$, $\delta_M = 0.08$, and $\delta_M = 0.8$. From the results in figure (7.8), we observe that as the rate of pupae reduced by other species feed on them increase, there is a visible reduction in the malaria infection on the dynamics of within mosquito variables (that is, (a) population of gametocytes G_v, (b) population of gametes G_m, (c) population of zygotes Z_v, and (d) population of sporozoites P_v). The results suggests that interventions that aimed at increase the mortality of pupae have an impact in reducing the density of mosquitoes which results in reduction of malaria infection at both within-mosquito scale and at community-level.

Figure (7.9) demonstrates the dynamics of (a) population of gametocytes G_v, (b) population of gametes G_m, (c) population of zygotes Z_v, and (d) population of sporozoites P_v for differet values of reduction of larvae by other species that feeds on them at a rate δ_W: $\delta_W = 0.008$, $\delta_W = 0.08$, and $\delta_W = 0.8$. The results present that as the rate of larvae being reduced by other species that feeds on them increase, there is a significant reduction on the dynamics of (a) population of gametocytes G_v, (b) population of gametes G_m, (c) population of zygotes Z_v, and (d) population of sporozoites P_v. The results suggest that the intervention that increase the mortality of the larvae have an impact of reducing the mosquito density which have an effect in reducing the malaria infection at both within-mosquito scale and at population level.

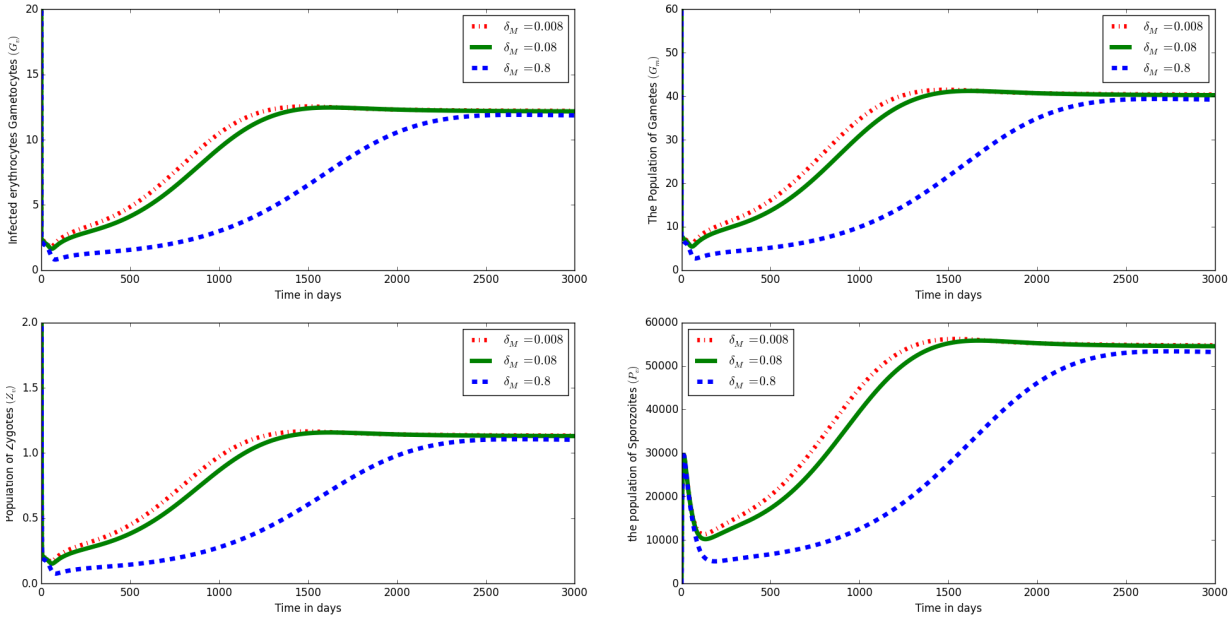

Figure 7.8: Graphs of numerical results of multiscale model (7.2.1.1) presenting the influence of variation of pupae reduced species that feeds on them at a rate (δ_M) at the within-mosquito scale dynamics of (a) population of gametocytes G_v, (b) population of gametes G_m, (c) population of zygotes Z_v, and (d) population of sporozoites P_v for different values of (δ_M): $\delta_M = 0.008$, $\delta_M = 0.08$ and $\delta_M = 0.8$

Figure (7.10) demonstrates the dynamics of (a) population of gametocytes G_v, (b) population of gametes G_m, (c) population of zygotes Z_v, and (d) population of sporozoites P_v for different values of which mosquitoes lay eggs at a constant rate Λ_E: $\Lambda_E = 100$, $\Lambda_E = 200$, and $\Lambda_E = 300$. The results in figure (7.10) pictures that as the rate at which mosquitoes lay eggs increase, there is visible increase in the dynamics of within-mosquito scale (that is, (a) population of gametocytes G_v, (b) population of gametes G_m, (c) population of zygotes Z_v, and (d) population of sporozoites P_v). The results suggest that interventions that destroys the laid eggs has an impact of reducing the mosquito density which also have influence in reduction of malaria infection on within-mosquito scale and at community level.

Figure (7.11) displays the dynamics of (a) population of gametocytes G_v, (b) population of gametes G_m, (c) population of zygotes Z_v, and (d) population of sporozoites P_v for different values of natural mortality rate Figure (7.10) demonstrates the dynamics of (a) population of gametocytes G_v, (b) population of gametes G_m, (c) population of zygotes Z_v, and (d) population of sporozoites P_v for different values of which mosquitoes lay eggs at a constant rate Λ_E: $\Lambda_E = 100$, $\Lambda_E = 200$, and $\Lambda_E = 300$. The results in figure (7.10) pictures that as the rate at which mosquitoes lay eggs increase, there is visible increase in the dynamics of within-mosquito scale (that is, (a) population of gametocytes G_v, (b) population of gametes G_m, (c) population of zygotes Z_v, and (d) population of sporozoites P_v). The results suggest that interventions that destroys the laid eggs has an impact of reducing the mosquito density which also have

influence in reduction of malaria infection on within-mosquito scale and at community level.

Figure (7.11) displays the dynamics of (a) population of gametocytes G_v, (b) population of gametes G_m, (c) population of zygotes Z_v, and (d) po of mosquito eggs μ_E: $\mu_E = 0.3$, $\mu_E = 0.6$, and $\mu_E = 0.9$. The results present that as the natural mortality of mosquito eggs increase, there is a significant reduction in the malaria dynamics of within-mosquito scale (that is, (a) population of gametocytes G_v, (b) population of gametes G_m, (c) population of zygotes Z_v, and (d) population of sporozoites P_v). The results imply that the interventions that aimed at the killing of the mosquito eggs have an influence in reducing the density of mosquitoes which have an effect of reducing the malaria infection in within-mosquito scale and at community-level.

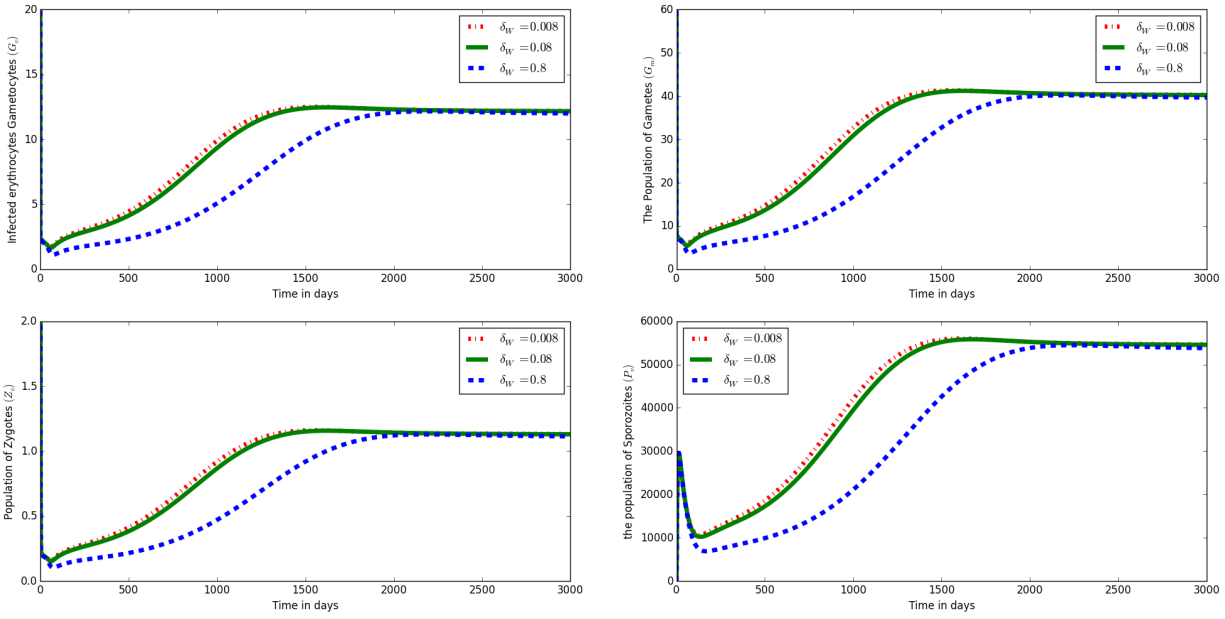

Figure 7.9: Graphs of numerical results of multiscale model (7.2.1.1) presenting the influence of variation of larvae reduced by species that feeds on them at a rate (δ_W) at the within-mosquito scale dynamics of (a) population of gametocytes G_v, (b) population of gametes G_m, (c) population of zygotes Z_v, and (d) population of sporozoites P_v for different values of (δ_W): $\delta_W = 0.008$, $\delta_W = 0.08$ and $\delta_W = 0.8$

Figure (7.12) Presents the dynamics of (a) population of gametocytes G_v, (b) population of gametes G_m, (c) population of zygotes Z_v, and (d) population of sporozoites P_v for different values of natural mortality rate of pupae μ_M: $\mu_M = 0.15$, $\mu_M = 0.35$, and $\mu_M = 0.55$. From the results in figure (7.12) show as the natural mortality of pupae increase, we also notice that there is reduction in the dynamics of (a) population of gametocytes G_v, (b) population of gametes G_m, (c) population of zygotes Z_v, and (d) population of sporozoites P_v. The results indicate that interventions that targets the killing of mosquito pupae has an impact in reducing the mosquito density which have influence in the reduction of malaria infection in both within-mosquito scale and between-host scale.

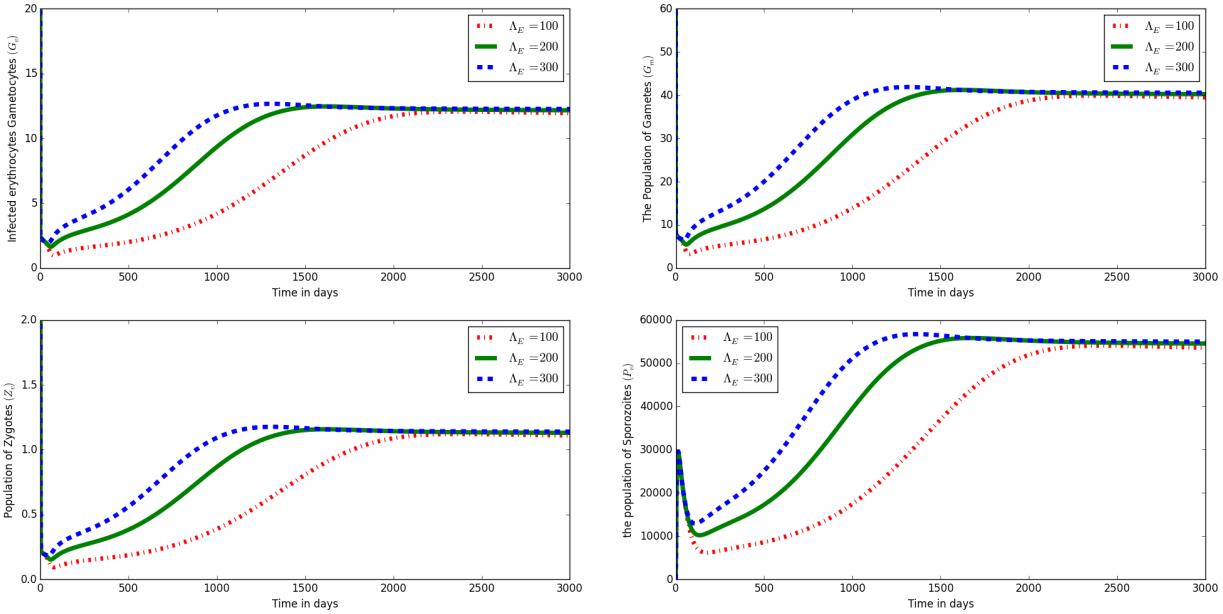

Figure 7.10: Graphs of numerical results of multiscale model (7.2.1.1) presenting the influence of variation of mosquitoes lay eggs at a rate (Λ_E) at the within-mosquito scale dynamics of (a) population of gametocytes G_v, (b) population of gametes G_m, (c) population of zygotes Z_v, and (d) population of sporozoites P_v for different values of (Λ_E): $\Lambda_E = 100$, $\Lambda_E = 200$ and $\Lambda_E = 300$

Figure (7.13) presents the dynamics of (a) population of gametocytes G_v, (b) population of gametes G_m, (c) population of zygotes Z_v, and (d) population of sporozoites P_v for different values of natural death rate of mosquito larvae μ_W: $\mu_W = 0.1$, $\mu_W = 0.3$, and $\mu_W = 0.5$. The results desplay that as the natural decay of mosquito larvae increase, there is a visible reduction on the dynamics of (a) population of gametocytes G_v, (b) population of gametes G_m, (c) population of zygotes Z_v, and (d) population of sporozoites P_v. The results indicate that the health interventions that target the killing of larvae that is use of larvicides which have an impact in reducing the density of mosquitoes.

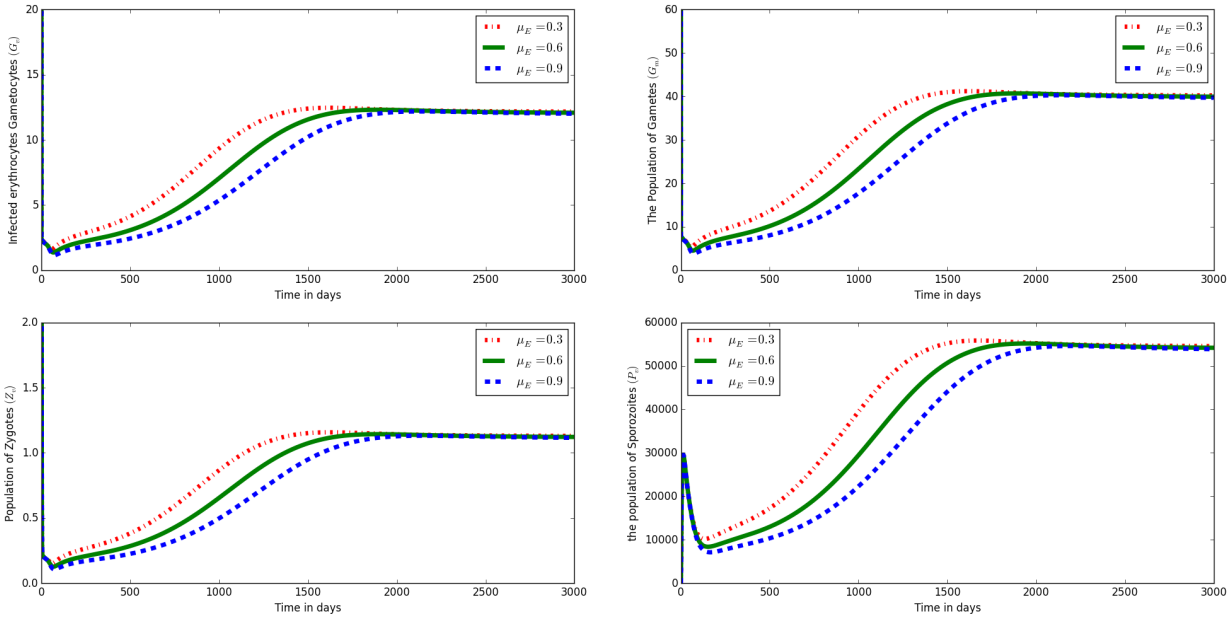

Figure 7.11: Graphs of numerical results of multiscale model (7.2.1.1) presenting the influence of variation of mortality rate of eggs (μ_E) at the within-mosquito scale dynamics of (a) population of gametocytes G_v, (b) population of gametes G_m, (c) population of zygotes Z_v, and (d) population of sporozoites P_v for different values of (μ_E): $\mu_E = 0.3$, $\mu_E = 0.6$ and $\mu_E = 0.9$

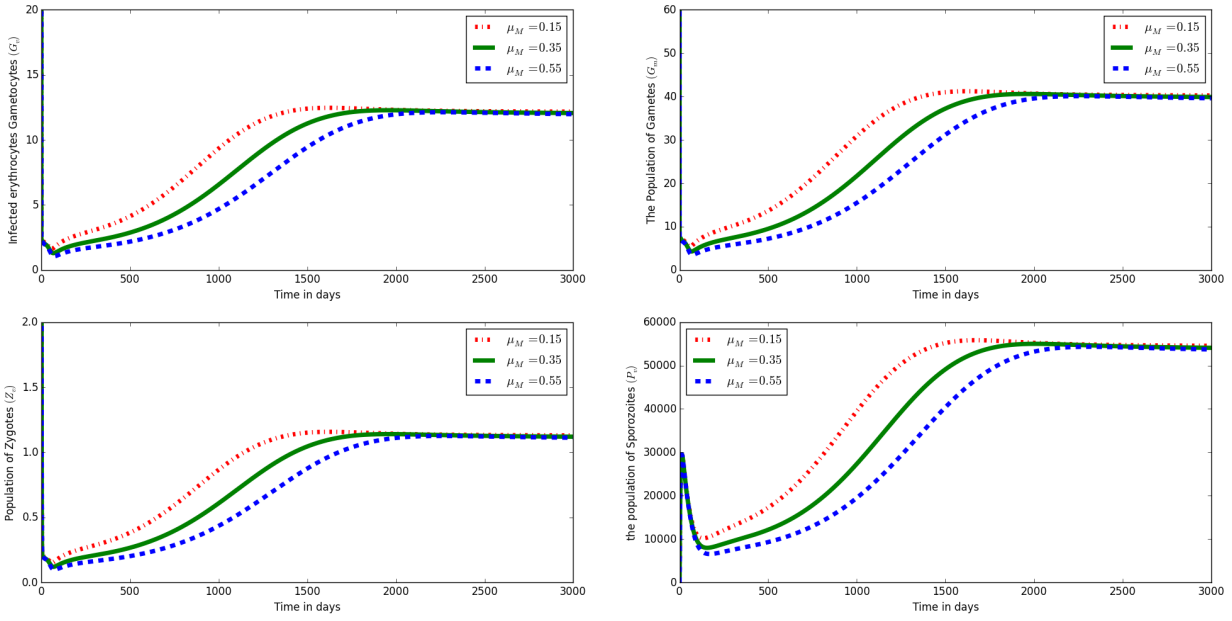

Figure 7.12: Graphs of numerical results of multiscale model (7.2.1.1) presenting the influence of variation of mortality rate of pupae (μ_M) at the within-mosquito scale dynamics of (a) population of gametocytes G_v, (b) population of gametes G_m, (c) population of zygotes Z_v, and (d) population of sporozoites P_v for different values of (μ_M): $\mu_M = 0.15$, $\mu_M = 0.35$ and $\mu_M = 0.55$

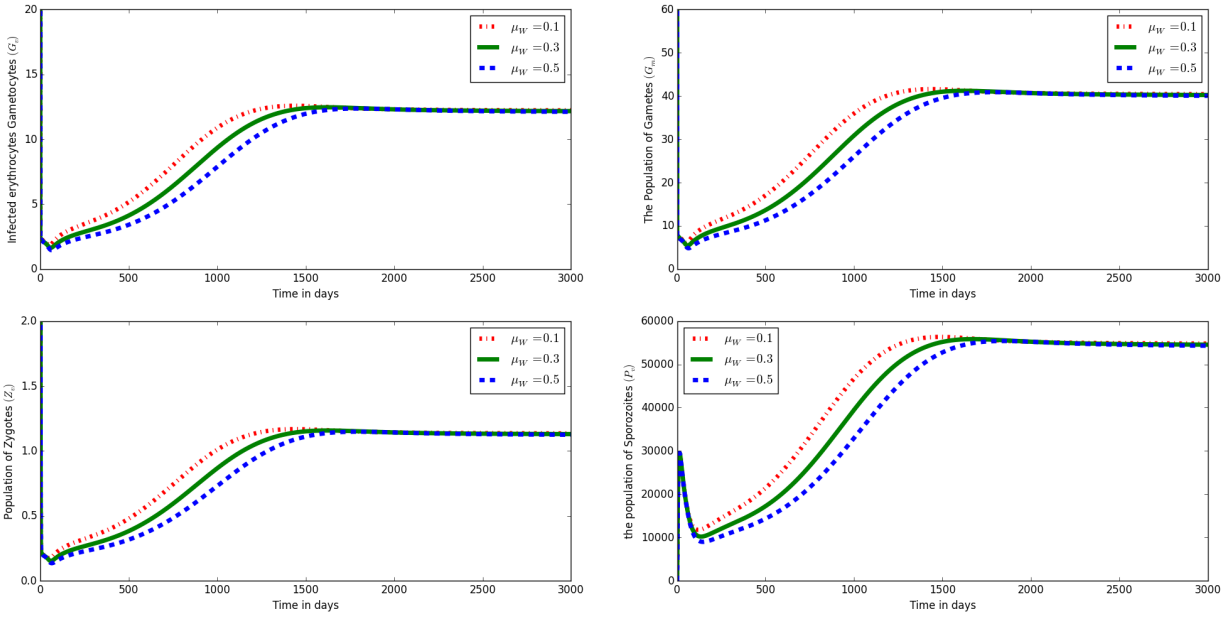

Figure 7.13: Graphs of numerical results of multiscale model (7.2.1.1) presenting the influence of variation of natural death rate of larvae (μ_W) at the within-mosquito scale dynamics of (a) population of gametocytes G_v, (b) population of gametes G_m, (c) population of zygotes Z_v, and (d) population of sporozoites P_v for different values of (μ_W): $\mu_W = 0.1$, $\mu_W = 0.3$ and $\mu_W = 0.5$

7.4.3 The Influence of Immature Mosquito Parameters on Between-Host Scale Variables.

In this sub-section, we use numerical results to demonstrate the influence of immature mosquito parameters on the between-host scale variables ((a) population of infected humans I_H, (b) community gametocytes load G_H, (c) population of infected mosquitoes I_V, and (d) community sporozoites load P_V). The immature mosquito parameters were used to demonstrate the effect of immature mosquito on between-host scale malaria infection dynamics. Figures (7.14)—(7.19), showing the evidence of the impact for immature-mosquito scale parameters (θ_E, α_M, α_W, δ_M, δ_W, Λ_E, μ_E, μ_M, μ_W) on between- human scale variables ((a)infected-human populations (I_H) and (b) community gametocytes load (G_H)) and also on between-mosquito scale variables ((c)infected-mosquito populations (I_V) and (d) community sporozoites load (P_V)) using the coupled multiscale model (7.2.1.1) for malaria disease systems.

Figure (7.14) demonstrates the changes in (a) population of infected humans I_H, (b) community gametocytes load G_H, (c) population of infected mosquitoes I_V, and (d) community sporozoites load P_V for different values of hatching of mosquito eggs θ_E: $\theta_E = 0.02$, $\theta_E = 0.04$, and $\theta_E = 0.06$. The results in figure (7.14) present that the increase in the hatching of mosquito eggs has an impact in the increasing the dynamics of (a) population of infected humans I_H, (b) community gametocytes load G_H, (c) population

of infected mosquitoes I_V, and (d) community sporozoites load P_V. The results suggest that any intervention that increase the mortality of mosquito eggs have an impact in reducing malaria transmission at between-host scale.

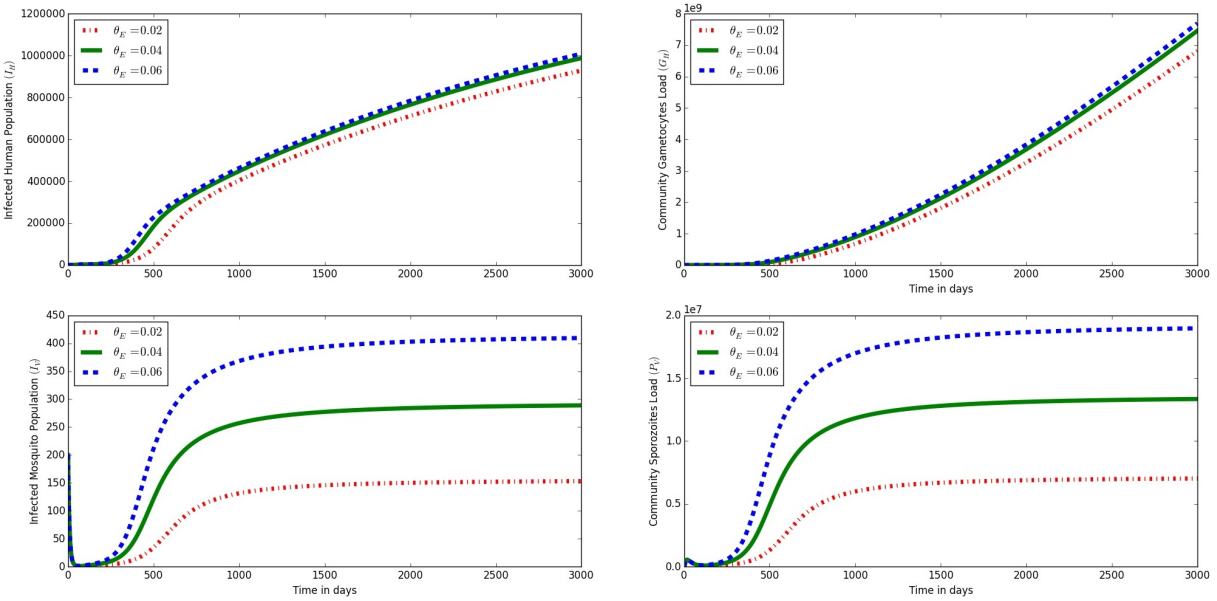

Figure 7.14: Simulation of multiscale model (7.2.1.1) presenting changes in population of infected humans (I_H), community gametocytes load (G_H), population of infected mosquitoes (I_V) and community sporozoites load (P_V) for distinct values of hatching rate of eggs into larvae (θ_E): $\theta_E = 0.02,\ 0.04$ and 0.06.

Figure (7.15) demonstrates the numerical simulation of multiscale model (7.2.1.1) presenting the dynamics of (a) population of infected humans I_H, (b) community gametocytes load G_H, (c) population of sporozoites load I_V, and (d) community sporozoites load P_V for different values of development of pupae into adult mosquitoes α_M: $\alpha_M = 0.25$, $\alpha_M = 0.35$, and $\alpha_M = 0.45$. From the results in Figure (7.15) present that as the rate of progression of pupae into adult mosquitoes increase, there is visible increase on the dynamics of (a) population of infected humans I_H, (b) community gametocytes load G_H, (c) population of infected mosquitoes I_V, and (d) community sporozoites load P_V.

Figure (7.16) demonstrates the numerical simulation of multiscale model (7.2.1.1) presenting the dynamics of (a) population of infected humans I_H, (b) community gametocytes load G_H, (c) population of sporozoites load I_V, and (d) community sporozoites load P_V for different values of the progression rate of larvae into mosquito pupae α_W: $\alpha_W = 0.2$, $\alpha_W = 0.4$ and $\alpha_W = 0.6$. These results in figure (7.16) present that as the progression rate of larval mosquito into pupae increases, we notice that malaria transmission at between-human scale and between-mosquito scale also increases. Therefore, any intervention that targets the larval and reduce the progression of larval into pupae have impact in reducing malaria transmission at population-level.

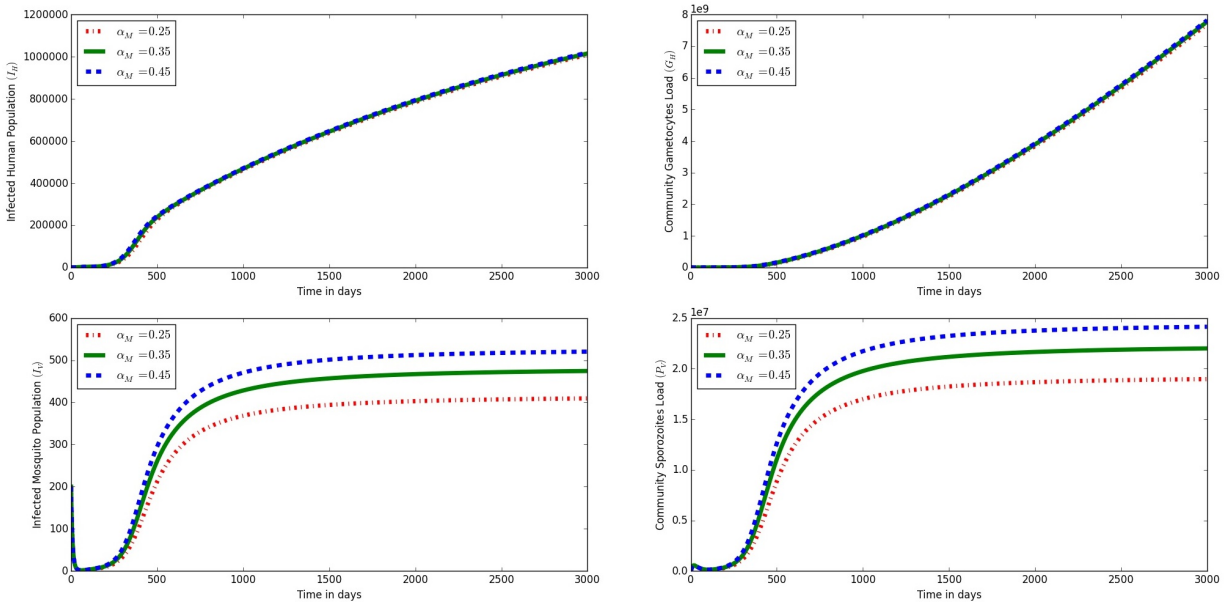

Figure 7.15: Simulation of multiscale model (7.2.1.1) presenting changes in population of infected humans (I_H), community gametocytes load (G_H), population of infected mosquitoes (I_V) and community sporozoites load (P_V) for distinct values of rate at which pupae develop into adult (α_M): $\alpha_M = 0.25,\ 0.35$ and 0.45.

Figure (7.17) illustrates the numerical simulation of multiscale model (7.2.1.1) presenting the dynamics of (a) population of infected humans I_H, (b) community gametocytes load G_H, (c) population of sporozoites load I_V, and (d) community sporozoites load P_V for different values of mortality of pupae due to species that feeds on them δ_M: $\delta_M = 0.008$, $\delta_M = 0.08$, and $\delta_M = 0.8$. From the results in figure (7.8), we observe that as the mortality of pupae due to species that feeds on them increase, there is also visible reduction in the dynamics of (a) population of infected humans I_H, (b) community gametocytes load G_H, (c) population of infected mosquitoes I_V, and (d) community sporozoites load P_V. These results suggest that use of pupacides has an impact of increasing the mortality of pupae have an impact on reducing the malaria transmission at the between-human-scale dynamics (that is, (a) population of infected humans and (b) community gametocyte load) and between-mosquito scale (i.e., (c) population of infected mosquitoes and (d) community sporozoites load).

Figure (7.18) describes the numerical simulation of multiscale model (7.2.1.1) presenting the changes (a) population of infected humans I_H, (b) community gametocytes load G_H, (c) population of sporozoites load I_V, and (d) community sporozoites load P_V for different values of mortality rate of larval due to species feeds on them δ_W: $\delta_W = 0.008$, $\delta_W = 0.08$ and $\delta_W = 0.8$. The results in figure (7.18) present that an increase in the mortality of larvae due to species feeds on them has an impact on the reduction of malaria transmission on the dynamics of (a) population of infected humans I_H, (b) community gametocytes load G_H, (c) population of infected mosquitoes I_V, and (d) community sporozoity load P_V. The results suggest

that the use of larvicides or interventions that increase the mortality of larval have an influence of reducing malaria transmission at the population-level.

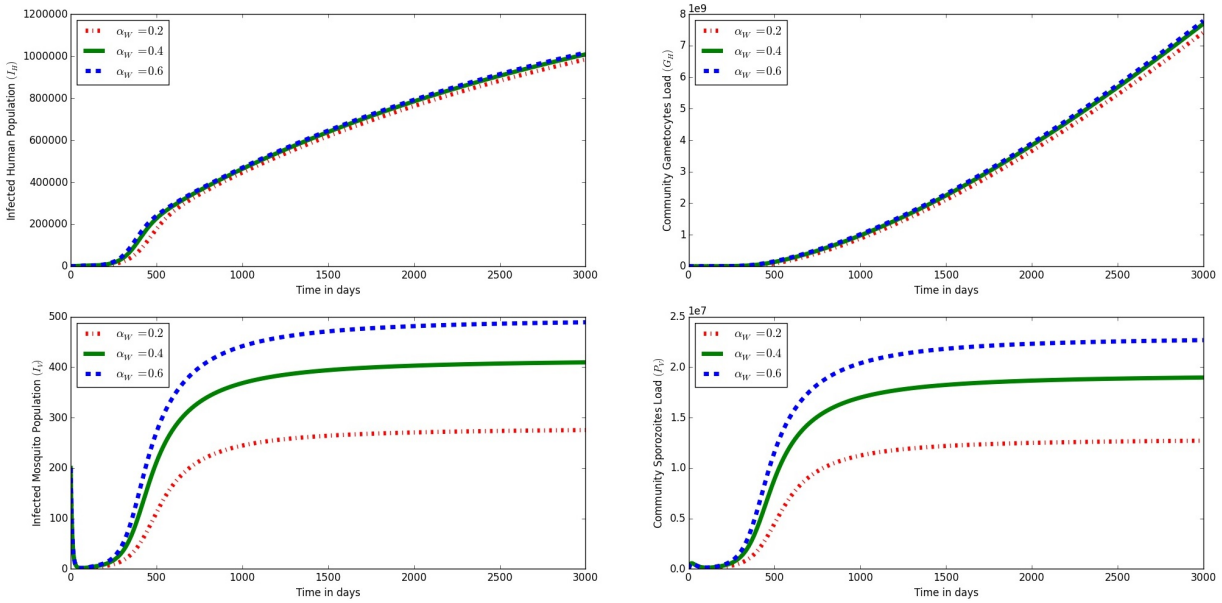

Figure 7.16: Simulation of multiscale model (7.2.1.1) presenting changes in population of infected humans (I_H), community gametocytes load (G_H), population of infected mosquitoes (I_V) and community sporozoites load (P_V) for distinct values of rate at which larvae develop into pupae (α_W): $\alpha_W = 0.2,\ 0.4$ and 0.6.

Figure (7.19) demonstrate the numerical simulation of multiscale model (7.2.1.1) presenting changes in (a) population of infected humans I_H, (b) community gametocytes load G_H, (c) population of sporozoites load I_V, and (d) community sporozoites load P_V for different values of mosquitoes laying eggs Λ_E: $\Lambda_E = 1000$, $\Lambda_E = 2000$ and $\Lambda_E = 3000$. The results in figure (7.19) present that increasing the rate of mosquito laying eggs has an effect of increasing the malaria transmission dynamics of (a) population of infected humans I_H, (b) community gametocytes load G_H, (c) population of sporozoites load I_V, and (d) community sporozoites load P_V. Therefore, the intervention that increasing the mortality of the mosquito eggs has an effect of reducing the malaria transmission at population-level.

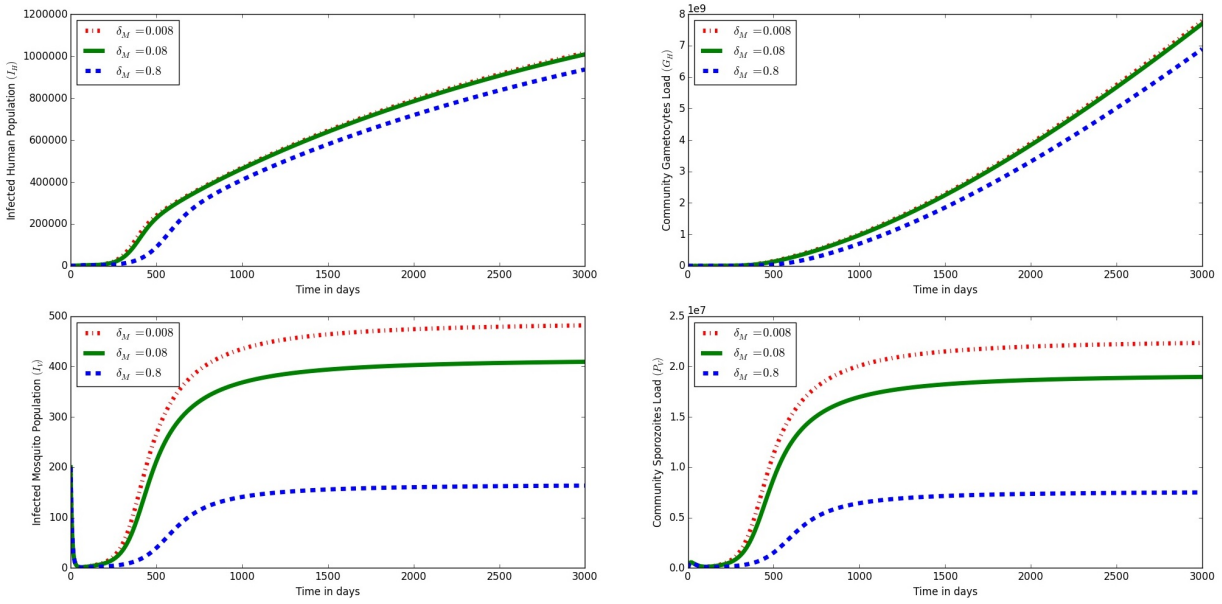

Figure 7.17: Simulation of multiscale model (7.2.1.1) presenting changes in population of infected humans (I_H), community gametocytes load (G_H), population of infected mosquitoes (I_V) and community sporozoites load (P_V) for distinct values of rate at which pupae reduced by other species (δ_M): $\delta_M = 0.008,\ 0.08$ and 0.8.

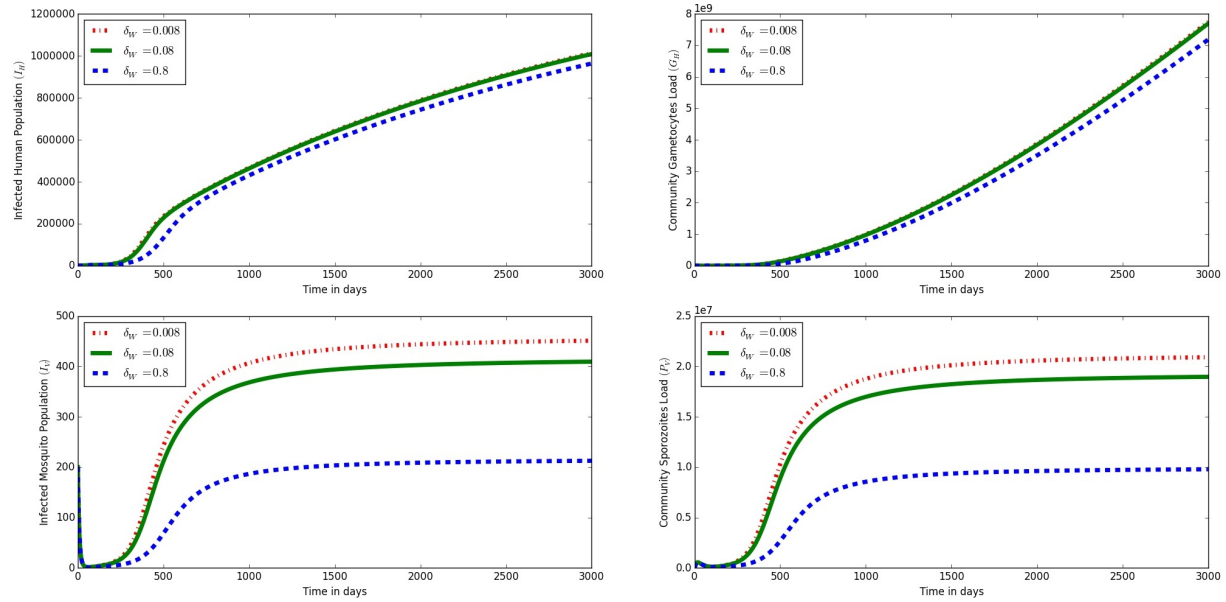

Figure 7.18: Simulation of multiscale model (7.2.1.1) presenting changes in population of infected humans (I_H), community gametocytes load (G_H), population of infected mosquitoes (I_V) and community sporozoites load (P_V) for distinct values of rate at which larvae reduced by other species (δ_W): $\delta_W = 0.008,\ 0.08$ and 0.8.

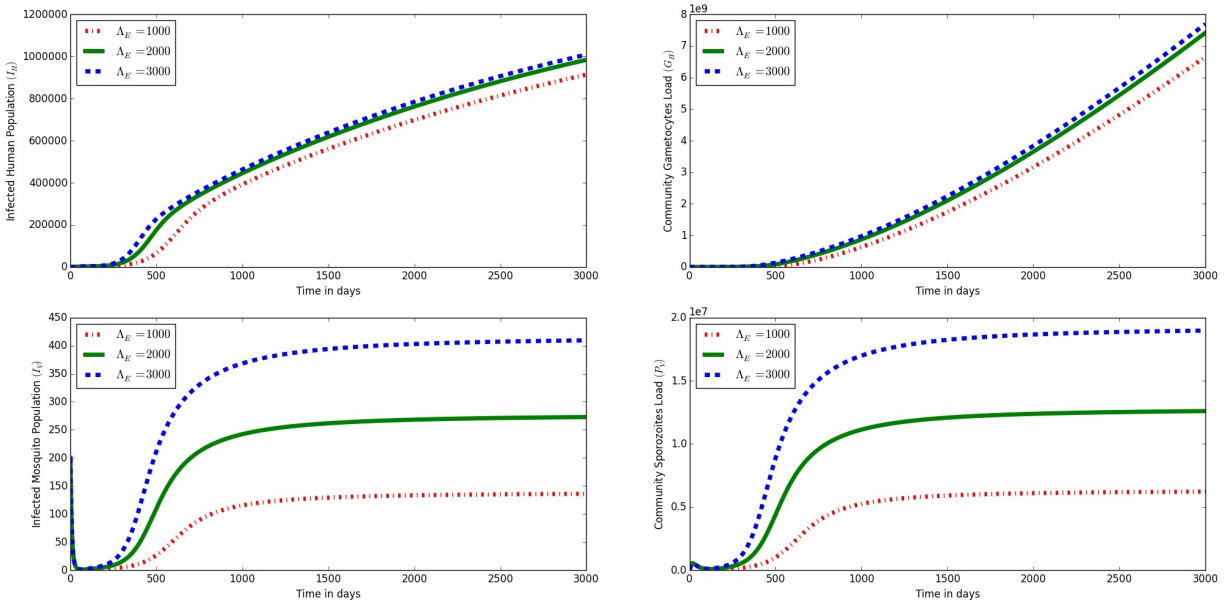

Figure 7.19: Simulation of multiscale model (7.2.1.1) presenting changes in population of infected humans (I_H), community gametocytes load (G_H), population of infected mosquitoes (I_V) and community sporozoites load (P_V) for distinct values of rate at which mosquitoes lay eggs (Λ_E): $\Lambda_E = 1000,\ 2000$ and 3000.

7.5 Extended Model

We extend the multiscale model (7.2.1.1) and to incorporates the effects of three malaria health interventions: (i) larvicides and pupacides, (ii) long-lasting insecticidal bed nets (LLINs) and (iii) artemisinin-based combination therapy (ACT). These malaria health interventions are employed at different scale domains of malaria infectious disease systems with larval source management functioning at immature mosquitoes population, LLINs functioning at between-host scale for adult mosquitoes and humans, and ACT functioning at within-infected human. In this section, we need the best strategies for controlling malaria disease systems by targeting immature and adult mosquitoes and treatment of infected humans. We extend model (7.2.1.1) for the dynamics of mosquito-human population and malaria transmission to includes: control strategies in targeting immatures mosquito population, control strategies in targeting adult mosquito population and also protection of humans from contacts with human populations and lastly treatment of infected-humans (i.e. within human-host scale). The number of malaria infected population increases due to the growth of mosquito population. We illustrate what will happen if we destroy the immature mosquitoes by drawing stagnant water where mosquitoes lay their eggs, control adult mosquitoes and protecting and treating the human population. The controlling of immature and adult mosquitoes is for aiming to reduce the mosquito vector population.

The control strategy of larval source management involves the methods such as the destroying of breeding sites of mosquitoes to reduce the densities of mosquitoes. These will result in experience an increase in eggs, larvae and pupae mortality rates. Destroying immature stages at eggs, larval and pupal stages has an impact in reducing the density of mosquitoes. By preventing their successful development into adult mosquito will also results in reduction of malaria transmission in the area or community.

The second control strategy is long-lasting insecticides-treated bed nets (LLINs) which reduce the transmission of malaria between human-populations and adults mosquito populations. We assume that LLINs have the influences on the adult mosquito populations. (i) It has impact on directly killing of adult mosquitoes that come to contact with nets, (ii) repelling of adult mosquitoes from house and diverting them to an animal blood meal host due to insecticides irritation or physical blockades of nets and (iii) increasing the duration of the gonotrophic cycle that directing to a reduction of oviposition rate.

The third and last control strategy that we are going to employ to our work is artemisinin-based combination therapy (ACT) which is the treatment process of within-infected humans. ACT has an impact on killing gametocytes and also killing merozoites populations. These will have an influence in reducing the malaria transmission in the community.The parameters of coupled multiscale model system (7.2.1.1)are modified as follows:

(i) Larvicides and pupacides: Killing effects on eggs by r_e, then μ_E is modified such that $\mu_E \longrightarrow \mu_E(1+r_e)$. Killing effect on larva by r_w, then μ_W is modified such that $\mu_W \longrightarrow \mu_W(1+r_w)$. Killing effect on pupa r_m, then $\mu_M \longrightarrow \mu_M(1+r_m)$.

(ii) Long-lasting insecticide-treated nets.

- **(a)** Directly killing of mosquitoes with killing efficacy of κ, then μ_V is modified to $\mu_V \longrightarrow \mu_V(1+\kappa)$,
- **(b)** The effect of mosquito repellent of υ, β_V is modified to $\beta_V \longrightarrow \beta_V(1-\upsilon)$, and β_H is modified to $\beta_H \longrightarrow \beta_H(1-\upsilon)$,
- **(c)** Protective efficacy of humans from mosquito bites φ, β_V is modified to $\beta_V \longrightarrow \beta_V(1-\varphi)$, and β_H is modified to $\beta_H \longrightarrow \beta_H(1-\varphi)$.

(iii) First line treatment by ACT

- **(a)** Killing efficacy on gametocytes is given by g, μ_h is modified to $\mu_h \longrightarrow \mu_h(1+g)$.
- **(b)** killing efficacy on merozoites is given by m, $\mu_m]$ is modified to $\mu_m \longrightarrow \mu_m(1+m)$
- **(c)** Emergent effect on reducing the disease induce death rate, $\delta_H \longrightarrow \delta_H(1-\rho)$.
- **(d)** Emergent effect on increase the patient's recovery rate, $\gamma_H \longrightarrow \gamma_H(1+\theta)$.

The model below is an extension of model (7.2.1.1) which incorporates the impacts of malaria health interventions, which is given by

$$
\begin{aligned}
1.\quad \frac{dE_E(t)}{dt} &= \Lambda_E - (\mu_E(1+r_e)+\theta_E)E_E(t),\\
2.\quad \frac{dL_W(t)}{dt} &= \theta_E E_E(t) - (\mu_W(1+r_w)+\alpha_W+\delta_W)L_W(t),\\
3.\quad \frac{dP_M(t)}{dt} &= \alpha_W L_W(t) - (\mu_M(1+r_m)+\alpha_M+\delta_M)P_M(t),\\
4.\quad \frac{dS_V(t)}{dt} &= \frac{\alpha_M P_M(t)}{2} - \frac{\beta_H(1-\upsilon)(1-\varphi)G_H(t)S_V(t)}{G_0+G_H(t)} - \mu_V(1+\kappa)S_V(t),\\
5.\quad \frac{dI_V(t)}{dt} &= \frac{\beta_H(1-\upsilon)(1-\varphi)G_H(t)S_V(t)}{G_0+G_H(t)} - (\mu_V(1+\kappa)+\delta_V)I_V(t),\\
6.\quad \frac{dG_v(t)}{dt} &= \frac{\beta_H(1-\upsilon)(1-\varphi)G_H(t)(S_V-1)}{(G_0+G_H)\phi_V(I_V+1)} - [\alpha_g+\mu_g]\,G_v(t),\\
7.\quad \frac{dG_m(t)}{dt} &= N_g\alpha_g G_v(t) - [\alpha_s+\mu_s]\,G_m(t),\\
8.\quad \frac{dZ_v(t)}{dt} &= \frac{1}{2}\alpha_s G_m(t) - [\alpha_z+\mu_z]\,Z_v(t),\\
9.\quad \frac{dO_v(t)}{dt} &= \alpha_z Z_v(t) - [\alpha_k+\mu_k]\,O_v(t),\\
10.\quad \frac{dP_v(t)}{dt} &= N_k\alpha_k O_v(t) - [\alpha_v+\mu_v]\,P_v(t).\\
11.\quad \frac{dP_V(t)}{dt} &= P_v\alpha_v(I_V(t)+1) - \alpha_V P_V(t).\\
12.\quad \frac{dS_H(t)}{dt} &= \Lambda_H - \frac{\beta_V(1-\upsilon)(1-\varphi)P_V(t)S_H(t)}{P_0+P_V(t)} - \mu_H S_H(t) + \gamma_H(1+\theta)I_H(t),\\
13.\quad \frac{dI_H(t)}{dt} &= \frac{\beta_V(1-\upsilon)(1-\varphi)P_V(t)S_H(t)}{P_0+P_V(t)} - [\mu_H+\gamma_H(1+\theta)+\delta_H(1-\rho)]\,I_H(t),\\
14.\quad \frac{dG_H(t)}{dt} &= N_{he}\alpha_h I_H(t) - \alpha_H G_H(t),
\end{aligned}
\tag{7.5.0.1}
$$

where N_{he} is the effective amount of malaria pathogens produced, during the entire period of host infectiousness after implementing the various health interventions and is given by

$$
N_{he} = \frac{\pi}{(1-\pi)}\left[\frac{(1-\pi)N_m\beta_h\Lambda_h - \mu_b\mu_m(1+m)}{N_m\beta_h(\alpha_h+\mu_h(1+g))}\right]. \tag{7.5.0.2}
$$

The reproductive number of extended model (7.5.0.1) is given by

$$
R_E = \sqrt{R_{VH}R_{HV}}. \tag{7.5.0.3}
$$

where

$$\begin{aligned}
R_{VH} &= \frac{1}{2}\frac{N_v\alpha_v}{Q_D}\frac{1}{P_0}\frac{1}{\alpha_V}\frac{\beta_V(1-\upsilon)(1-\varphi)\Lambda_H}{\mu_H},\\
R_{HV} &= \frac{N_{he}\alpha_h}{\mu_H+\gamma_H(1+\theta)+\delta_H(1-\rho)}\frac{1}{G_0}\frac{1}{\alpha_H}\frac{\beta_H(1-\upsilon)(1-\varphi)q_{1e}}{\mu_V(1+\kappa)\phi_V}.\\
N_v &= \frac{1}{2}\frac{N_g\alpha_g}{\alpha_g+\mu_g}\frac{N_k\alpha_k}{\alpha_k+\mu_k}\frac{\alpha_z}{\alpha_z+\mu_z}\frac{\alpha_s}{\alpha_s+\mu_s}\frac{1}{\alpha_v+\mu_v},\\
q_{1e} &= (\alpha_M\alpha_W\theta_E\Lambda_E-2\mu_V(1+\kappa)Q_D),\\
\alpha_M\alpha_W\theta_E\Lambda_E &\geq 2\mu_V(1+\kappa)Q_D,\\
Q_D &= [\mu_E(1+r_e)+\theta_E][\mu_W(1+r_w)+\alpha_W+\delta_W][\mu_M(1+r_m)+\alpha_M+\delta_M],
\end{aligned} \tag{7.5.0.4}$$

where R_{0E} is the effective reproductive number with various malaria health interventions which is derived from model (7.5.0.1), R_{VH} is vector to human effective reproductive number with various malaria heath interventions and R_{HV} is human to vector effective reproductive number with various malaria health interventions.

The disease free equibrium state of extended model (7.5.0.1) is given by

$$\begin{aligned}
E^0 &= (E_E^0, L_W^0, P_M^0, S_V^0, I_V^0, G_v^0, G_m^0, Z_v^0, O_v^0, P_v^0, P_V^0, S_H^0, I_H^0, G_H^0).\\
&= (E_E^0, L_W^0, P_M^0, S_V^0, 0, 0, 0, 0, 0, 0, 0, S_H^0, 0, 0),
\end{aligned} \tag{7.5.0.5}$$

Where

$$\begin{aligned}
E_E^1 &= \frac{\Lambda_E}{(\mu_E+\theta_E)},\\
L_W^1 &= \frac{\Lambda_E}{(\mu_E+\theta_E)}\frac{\theta_E}{(\mu_W+\alpha_W+\delta_W)},\\
P_M^1 &= \frac{\Lambda_E}{(\mu_E+\theta_E)}\frac{\theta_E}{(\mu_W+\alpha_W+\delta_W)}\frac{\alpha_W}{(\mu_M+\alpha_M+\delta_M)},\\
S_V^1 &= \frac{\alpha_M}{2\mu_V}\frac{\alpha_W}{(\mu_M+\alpha_M+\delta_M)}\frac{\theta_E}{(\mu_W+\alpha_W+\delta_W)}\frac{\Lambda_E}{(\mu_E+\theta_E)},\\
S_H^1 &= \frac{\Lambda_H}{\mu_H}.
\end{aligned} \tag{7.5.0.6}$$

The malaria health intervention induced endemic equilibrium states is given by

$$\overline{E} = (\overline{E}_E, \overline{L}_W, \overline{P}_M, \overline{S}_V, \overline{I}_V, \overline{G}_v, \overline{G}_m, \overline{Z}_v, \overline{P}_v, \overline{P}_V, \overline{S}_H, \overline{I}_H, \overline{G}_H),$$

where

$$
\begin{aligned}
\overline{E}_E &= \frac{\Lambda_E}{\mu_E(1+r_e)+\theta_E}, \\
\overline{L}_W &= \frac{1}{\mu_W(1+r_w)+\alpha_W+\delta_W}\frac{\theta_E\Lambda_E}{\mu_E(1+r_e)+\theta_E}, \\
\overline{P}_M &= \frac{\alpha_W\theta_E\Lambda_E}{Q_D}, \\
\overline{S}_V &= \frac{\alpha_M\alpha_W\theta_E\Lambda_E\left[N_{he}\alpha_h\beta_V(1-\upsilon)(1-\varphi)\Lambda_H\overline{P}_V+\alpha_H G_0[a_{1e}(P_0+\overline{P}_V)+a_{2e}\overline{P}_V]\right]}{a_{3e}Q_M}, \\
\overline{I}_V &= \frac{N_{he}\alpha_h\beta_H(1-\upsilon)(1-\varphi)\alpha_M\alpha_W\theta_E\Lambda_E\beta_V(1-\upsilon)(1-\varphi)\Lambda_H\overline{P}_V}{a_{3e}(\mu_V(1+\kappa)+\delta_V)Q_M}, \\
\overline{G}_v &= \frac{1}{\alpha_g+\mu_g}\frac{N_{he}\alpha_h\beta_H(1-\upsilon)^2(1-\varphi)^2\beta_V\Lambda_H\overline{P}_V[b_{1e}\overline{P}_V+b_{2e}]}{a_{3e}\phi_V(\overline{I}_V+1)Q_N}, \\
\overline{G}_m &= \frac{N_g\alpha_g}{\alpha_g+\mu_g}\frac{1}{\alpha_s+\mu_s}\frac{N_{he}\alpha_h\beta_H(1-\upsilon)^2(1-\varphi)^2\beta_V\Lambda_H\overline{P}_V[b_{1e}\overline{P}_V+b_{2e}]}{a_{3e}\phi_V(\overline{I}_V+1)Q_N}, \\
\overline{Z}_v &= \frac{1}{2}\frac{N_g\alpha_g}{\alpha_g+\mu_g}\frac{\alpha_s}{\alpha_s+\mu_s}\frac{1}{\alpha_z+\mu_z}\frac{N_{he}\alpha_h\beta_H(1-\upsilon)^2(1-\varphi)^2\beta_V\Lambda_H\overline{P}_V[b_{1e}\overline{P}_V+b_{2e}]}{a_{3e}\phi_V(\overline{I}_V+1)Q_N}, \\
\overline{O}_v &= \frac{1}{2}\frac{N_g\alpha_g}{\alpha_g+\mu_g}\frac{\alpha_s}{\alpha_s+\mu_s}\frac{\alpha_z}{\alpha_z+\mu_z}\frac{1}{\alpha_k+\mu_k}\frac{N_{he}\alpha_h\beta_H(1-\upsilon)^2(1-\varphi)^2\beta_V\Lambda_H\overline{P}_V[b_{1e}\overline{P}_V+b_{2e}]}{a_{3e}\phi_V(\overline{I}_V+1)Q_N}, \\
\overline{P}_v &= N_v\frac{N_{he}\alpha_h\beta_H(1-\upsilon)^2(1-\varphi)^2\beta_V\Lambda_H\overline{P}_V[b_{1e}\overline{P}_V+b_{2e}]}{a_{3e}\phi_V(\overline{I}_V+1)Q_N}, \\
\overline{P}_V &= \frac{-c_{2e}+\sqrt{c_{2e}^2-4c_{1e}c_{3e}}}{2c_{1e}}, \\
\overline{S}_H &= \frac{\Lambda_H(\mu_H+\gamma_H(1+\theta)+\delta_H(1-\rho))(P_0+\overline{P}_V)}{a_{1e}(P_0+\overline{P}_V)+a_{2e}\overline{P}_V}, \\
\overline{I}_H &= \frac{\beta_V(1-\upsilon)(1-\varphi)\Lambda_H\overline{P}_V}{a_{1e}(P_0+\overline{P}_V)+a_{2e}\overline{P}_V}, \\
\overline{G}_H &= \frac{N_{he}\alpha_h\beta_V(1-\upsilon)(1-\varphi)\Lambda_H\overline{P}_V}{\alpha_H[a_{1e}(P_0+\overline{P}_V)+a_{2e}\overline{P}_V]},
\end{aligned}
\tag{7.5.0.7}
$$

where

$$
\begin{aligned}
Q_M &= N_{he}\alpha_h\beta_V(1-\upsilon)(1-\varphi)\Lambda_H\overline{P}_V(\beta_H(1-\upsilon)(1-\varphi)+\mu_V(1+\kappa)) \\
&\quad +\mu_V(1+\kappa)\alpha_H G_0[a_{1e}(P_0+\overline{P}_V)+a_{2e}\overline{P}_V] \\
Q_N &= \left[b_{3e}\overline{P}_V+\mu_V(1+\kappa)\alpha_H a_{1e}G_0P_0\right]\left[b_{4e}\overline{P}_V+\alpha_H a_{1e}G_0P_0\right] \\
a_{1e} &= \mu_H[\mu_H+\gamma_H(1+\theta)+\delta_H(1-\rho)], \\
a_{2e} &= \beta_V(1-\upsilon)(1-\varphi)[\mu_H+\delta_H(1-\rho)], \\
a_{3e} &= 2Q_D, \\
b_{1e} &= N_{he}\alpha_h\beta_V(1-\upsilon)(1-\varphi)\Lambda_H[\alpha_M\alpha_W\theta_E\Lambda_E-a_3(\beta_H(1-\upsilon)(1-\varphi)+\mu_V(1+\kappa))] \\
&\quad +\alpha_H G_0(a_{1e}+a_{2e})[\alpha_M\alpha_W\theta_E\Lambda_E-a_{3e}\mu_V(1+\kappa)]>0, \\
b_{2e} &= \alpha_H a_{1e}G_0P_0[\alpha_M\alpha_W\theta_E\Lambda_E-a_{3e}\mu_V(1+\kappa)]>0, \qquad (7.5.0.8) \\
b_{3e} &= N_{he}\alpha_h\beta_V(1-\upsilon)(1-\varphi)\Lambda_H(\beta_H(1-\upsilon)(1-\varphi)+\mu_V(1+\kappa)) \\
&\quad +\mu_V(1+\kappa)\alpha_H G_0(a_{1e}+a_{2e})>0, \\
b_{4e} &= N_{he}\alpha_h\beta_V(1-\upsilon)(1-\varphi)\Lambda_H+\alpha_H G_0(a_{1e}+a_{2e})>0, \\
c_{1e} &= \alpha_V\phi_V a_{3e}b_{3e}b_{4e}>0, \\
c_{2e} &= N_{he}\alpha_h\beta_V(1-\upsilon)(1-\varphi)\Lambda_H a_{1e}a_{3e}\mu_V(1+\kappa)\alpha_V\alpha_H\phi_V G_0P_0[2-R_E^2]+\alpha_H^2G_0^2(a_{1e}+a_{2e})\times \\
&\quad a_{1e}a_{3e}\mu_V(1+\kappa)\alpha_V\phi_V P_0[2-R_E^2]+N_{he}\alpha_h a_{3e}\beta_V(1-\upsilon)^2(1-\varphi)^2\Lambda_H\beta_H\left[\alpha_V\phi_V a_{1e}a_{3e}\alpha_H G_0P_0\right. \\
&\quad \left.+N_v\alpha_v N_{he}\alpha_h\beta_H(1-\upsilon)^2(1-\varphi)^2\beta_V\Lambda_H\right], \\
c_{3e} &= -\mu_V(1+\kappa)\alpha_V\phi_V a_{3e}a_{1e}^2\alpha_H^2G_0^2P_0^2[R_E^2-1]<0.
\end{aligned}
$$

From model (7.5.0.1) we also deduce that there exist a unique positive endemic equilibrium state whenever $R_E>1$.

The comparative effectiveness of the different malaria health interventions in this model is assessed using R_E, $\overline{P}_V$ and $\overline{G}_H$ of equations (7.5.0.3) and (7.5.0.7), as an indication of the effectiveness of the intervention. We specially use these quantities (R_E, $\overline{P}_V$ and $\overline{G}_H$) to relate the efficiency at the individual level to population/ community level relative effectiveness of the health interventions against malaria disease system and certain results from combined interventions. We calculate the percentage reduction (%age) of R_0, P_V^* and G_H^* due to interventions that reduce them to R_E, $\overline{P}_V$ and $\overline{G}_H$ at three different efficiency levels, which (a) is the comparative effectiveness at low efficacy (CEL) of 0.3, (b) comparative effectiveness at medium efficacy (CEM) of 0.6 and comparative effectiveness at high efficacy (CEH) of 0.9 using the different health interventions utilising the expressions

$$\begin{aligned} \%\text{age reduction of } R_0 &= \left[\frac{R_0 - R_E}{R_0}\right] \times 100, \\ \%\text{age reduction of } P_V^* &= \left[\frac{P_V^* - \overline{P}_V}{P_V^*}\right] \times 100, \\ \%\text{age reduction of } G_H^* &= \left[\frac{G_H^* - \overline{G}_H}{G_H^*}\right] \times 100, \end{aligned} \tag{7.5.0.9}$$

where R_E, $\overline{P}_V$ and $\overline{G}_H$ are the effective reproductive number, the intervention induced endemic value of community sporozoites load and the intervention induced endemic value of the community gametocytes load, respectively. We assess the influence of health intervention components for malaria disease system by comparing their effectiveness when they are individual and even when they are combined using R_E, $\overline{P}_V$ and $\overline{G}_H$ as indicators. For each efficiency level, we rank the reduction percentages of R_0, P_V^* and G_H^* in ascending order from 1 to 37 corresponding to the different combinations of 8 health interventions considered in this work.

7.5.1 The impact of health intervention strategies against malaria disease using R_E as indicator of intervention effectiveness

Table (7.7) indicates the results of assessment of the comparative effectiveness of single and combined health intervention strategies of the percentage reduction of R_0 when the efficacy of each single and combined health intervention components are set to (a) comparative effectiveness at low efficacy level, (b) comparative effectiveness at medium efficacy level, and (c) comparative effectiveness at high efficacy level.

(i) From the results in the table (7.7), we can easily observe that when each of the health intervention components efficacy are set to CEL efficacy level, CEM efficacy level, and CEH efficacy level, respectively. The effect of mosquito repellent and protective efficacy of humans by the use of LLINs have the highest efficacy and equal comparative effectiveness whereas killing of merozoites by treating within within-infected human using ACT has the least comparative effectiveness that can lead a reduction of R_0. The killing of merozoites by using ACT does not show the influences of using this health intervention component.

(ii) The results from the table (7.7) also shows the assessment of the effectiveness of the combination of two health intervention strategies on the percentage reduction of R_0 when each of the health intervention components efficacy are set at (a) CEL efficacy level, (b) CEM efficacy level, and (c) CEH efficacy level. Comparing the results of the effectiveness of the possible combination of two health intervention components, we observe that the combination of direct killing of adult mosquitoes and protective efficacy of humans intervention strategies have highest comparative effectiveness in each efficacy level, followed by the combination of the killing effects on eggs for immature mosquitoes

and the efficacy of mosquito repellents by LLINs, followed by combination of killing effects on pupa for immature mosquitoes and the protective efficacy of humans by LLINs. The least combination of two health intervention components are killing efficacy on gametocytes and killing efficacy on merozoites by the ACT.

(iii) The results shows that the assessment of the comparison of combined three health intervention strategies for malaria disease system and when all interventions are combined on the reduction of R_0, when each of the combination interventions efficacy are set at (a) CEL efficacy level, (b) CEM efficacy level, and (c) CEH efficacy level. By comparing the outcome of the effectiveness of the possible combination of three health intervention components and we can easily identify that when the combination of killing efficacy of eggs of immature mosquitoes, the effects of mosquito repellent by LLINs and killing efficacy of merozoites by ACT has the highest comparative effectiveness that can lead to the reduction of R_0, whilst the least comparative effectiveness have a combination of health intervention components which are the killing efficacy of eggs for immature mosquitoes, killing efficacy of larval of immature mosquitoes and the killing efficacy of pupa of immature mosquitoes.

(iv) When we consider all eight health intervention components are implemented together at a time, we observe from the table (7.7) that this combination has the highest comparative effectiveness that lead to the reduction of R_0 than any other combination interventions which were presented in this work for assumed efficacy level.

Table 7.7: Results of the assessment of comparative effectiveness of Malaria interventions using percentage reduction of basic reproductive number (R_0) as the indicator of intervention effectiveness when each of the interventions is assumed to have: (a) low efficacy of 0.30, (b) medium efficacy of 0.60, and (c) high efficacy 0f 0.90. rate.

No.	**Indicator of Intervention effectiveness**	**Calculated R_0-L-eff**	**CEL**	**Calculated R_0-M-eff**	**CEM**	**Calculated R_0-H-eff**	**CEH**
1	R_0	0.0	1	0.0	1	0.0	1
2	R_{r_e}	4.69	6	8.77	6	12.38	6
3	R_{r_w}	5.35	7	9.93	7	13.91	7
4	R_{r_m}	4.41	5	8.29	5	11.74	5
5	R_{κ}	12.38	13	21.1	13	27.67	12
6	R_{υ}	30.0	25	60.0	25	90.0	25
7	R_{φ}	30.0	25	60.0	25	90.0	25
8	R_m	0.0	1	0.0	1	0.0	1
9	R_g	1.97	3	3.82	3	5.58	3
10	$R_{r_e r_w}$	9.79	11	17.85	11	24.6	11
11	$R_{r_e r_m}$	8.89	9	16.35	9	22.69	9
12	$R_{r_w r_m}$	9.53	10	17.41	10	24.04	10
13	$R_{r_e \kappa}$	16.5	16	28.06	16	36.69	15
14	$R_{r_e \upsilon}$	33.28	28	63.51	28	91.24	28
15	$R_{r_w \kappa}$	17.08	17	28.97	17	37.8	17
16	$R_{r_w m}$	5.35	7	9.93	7	13.91	7
17	$R_{r_m \varphi}$	33.09	27	63.32	27	91.17	27
18	$R_{\kappa \varphi}$	38.67	30	68.44	30	92.77	30
19	R_{mg}	1.97	3	3.82	3	5.58	3
20	$R_{r_e r_w r_m}$	13.78	14	24.68	14	33.5	14
21	$R_{r_e r_w \kappa}$	20.98	19	35.25	19	45.59	19
22	$R_{r_e r_m \kappa}$	20.19	18	34.06	18	44.2	18
23	$R_{r_e \upsilon m}$	33.28	28	63.51	28	91.24	28
24	$R_{r_e r_w r_m \kappa}$	24.48	21	40.67	21	52.09	21
25	$R_{r_e r_w \kappa \varphi}$	44.69	32	74.1	32	94.56	32
26	$R_{r_e r_w \kappa g}$	22.53	20	37.72	20	48.63	20
27	$R_{r_e r_w m g}$	11.56	12	20.99	12	28.8	13
28	$R_{r_e r_w r_m \kappa \upsilon}$	47.14	33	76.27	33	95.21	33
29	$R_{r_e r_w r_m \kappa g}$	25.97	23	42.94	23	54.76	23
30	$R_{r_e r_w r_m \varphi g}$	40.83	31	71.03	31	93.72	31
31	$R_{r_e r_w r_m m g}$	15.47	15	27.56	15	37.21	16
32	$R_{r_e r_w r_m \kappa \upsilon \varphi}$	63.0	35	90.51	35	99.52	35
33	$R_{r_e r_w r_m \kappa \upsilon m}$	24.48	21	40.67	21	52.09	21
34	$R_{r_e r_w r_m \kappa m g}$	25.97	23	42.94	23	54.76	23
35	$R_{r_e r_w r_m \kappa \upsilon \varphi m}$	63.0	35	90.51	35	99.52	35
36	$R_{r_e r_w r_m \kappa \upsilon m g}$	48.18	34	77.18	34	95.48	34
37	$R_{r_e r_w r_m \kappa \upsilon \varphi m g}$	63.72	37	90.87	37	99.55	37

7.5.2 The impact of health intervention strategies against malaria disease using community sporozoite load as indicator of intervention effectiveness

In this subsection, we investigate the impact of the health intervention components for malaria disease system by comparative effectiveness using the %age reduction in endemic value of community sporozoite load (P_V^*) as an indicator. We compar the effectiveness of the health intervention components when they are single and even when they are combined using P_V^* as an indicator. Table (7.8) shows the results of assessment of the comparative effectiveness of the 37 different combinations of malaria interventions which are considered. We assess the effectiveness of single and combined health intervention strategies on the %age reduction of P_V^* when the efficacy of each of the health intervention components are set to (a) CEL efficacy level, (b) CEM efficacy level, and (c) CEH efficacy level.

(i) From the single interventions, we observe that when each of the health intervention components are set to low, medium, and high efficacy level, respectively: the killing efficacy on larva has the highest comparative effectiveness on CEL efficacy level whilst the effect of mosquito repellent and protective efficacy of humans by the LLINs have the highest and equal comparative effectiveness on CEM and CEH efficacy levels, that can lead to the reduction of P_V^*. We also notice that killing efficacy on merozoites and killing efficacy on gametocytes by ACT interventions has the least comparative effectiveness in all efficacy levels that can lead to reduction of P_V^*.

(ii) When considering the combination of two health interventions at the same time, where each combination is coming from the eight individual health intervention strategies, we observe that the combination of killing efficacy of eggs of immature mosquitoes and killing efficacy of larva of immature mosquitoes has the highest comparative effectiveness on CEL efficacy level whilst the combination of direct killing efficacy of adult mosquitoes and the protective efficacy of humans by LLINs has the highest comparative effectiveness on CEM and CEH efficacy levels that can lead to the reduction of P_V^*. It then followed by the ranking of two health interventions, the combination of killing efficacy of larva and killing efficacy of pupa for immature mosquitoes in the CEL efficacy level whilst the combination of killing efficacy of eggs for immature mosquitoes and the effect of adult mosquito repellent by LLINs has the second highest comparative effectiveness on CEM and CEH efficacy levels that can lead to the reduction of P_V^*. Whereas the combination of killing efficacy of merozoites and killing efficacy of gametocytes has the least comparative effectiveness in the reduction of P_V^*.

(iii) When we take into account three health intervention strategies at the same time with each combination of three interventions coming from the eight individual malaria health intervention components, we observe that the combination of the killing efficacy of eggs, the killing efficacy of larva and the killing efficacy of pupa for immature mosquitoes has the highest compative effectiveness on CEL and CEM efficacy levels while the combination of killing efficacy of eggs for immature mosquitoes, the efficacy of adult mosquito repellent by LLINs and killing efficacy of merozoites by ACT has the

highest comparative effectiveness on CEH efficacy level in the reduction of P_V^*. The combination of the killing efficacy of eggs for immature mosquitoes, the efficacy of adult mosquito repellent by LLINs and the killing efficacy of merozoites by ACT has the least comparative effectiveness on CEL and CEM efficacy level whilst the combination of killing efficacy of eggs, killing efficacy of pupa for immature mosquitoes and the direct killing of adult mosquitoes by LLINs has the least comparative effectiveness on CEH efficacy level in the reduction of P_V^*.

(iv) Lastly, when we take into account the comparative effectiveness of malaria interventions when all the eight malaria intervention components are implemented at a time, we observe from the results that this combination has the highest comparative effectiveness in all efficacy levels in the reduction of P_V^*.

Table 7.8: Results of the assessment of comparative effectiveness of Malaria interventions using percentage reduction of endemic value of community sporozoites load (P_V^*) as the indicator of intervention effectiveness when each of the interventions is assumed to have: (a) low efficacy of 0.30, (b) medium efficacy of 0.60, and (c) high efficacy 0f 0.90. rate.

No.	**Indicator of Intervention effectiveness**	**Calculated P_V^*-L-eff**	**CEL**	**Calculated P_V^*-M-eff**	**CEM**	**Calculated P_V^*-H-eff**	**CEH**
1	P_V	0.0	1	0.0	1	0.0	1
2	P_{Vr_e}	9.34	9	17.12	7	23.71	7
3	P_{Vr_w}	10.63	10	19.26	8	26.42	8
4	P_{Vr_m}	8.81	6	16.22	6	22.55	6
5	$P_{V\kappa}$	7.22	5	13.5	5	19.0	5
6	$P_{V\upsilon}$	9.19	7	26.54	10	68.84	25
7	$P_{V\varphi}$	9.19	7	26.54	10	68.84	25
8	P_{Vm}	0.0	1	0.0	1	0.0	1
9	P_{Vg}	0.0	1	0.0	1	0.0	1
10	$P_{Vr_er_w}$	19.0	20	33.18	16	44.03	14
11	$P_{Vr_er_m}$	17.35	15	30.64	14	41.06	12
12	$P_{Vr_wr_m}$	18.52	19	32.45	15	43.18	12
13	$P_{Vr_e\kappa}$	15.91	12	28.37	12	38.33	10
14	$P_{Vr_e\upsilon}$	17.62	17	38.97	19	76.1	28
15	$P_{Vr_w\kappa}$	17.11	13	30.23	13	40.54	11
16	P_{Vr_wm}	10.63	10	19.26	8	26.42	8
17	$P_{Vr_m\varphi}$	17.14	14	38.32	18	75.74	27
18	$P_{V\kappa\varphi}$	17.43	10	42.6	24	81.72	30
19	P_{Vmg}	0.0	1	0.0	1	0.0	1
20	$P_{Vr_er_wr_m}$	26.18	25	44.16	25	56.92	19
21	$P_{Vr_er_w\kappa}$	24.89	23	42.32	22	54.89	17
22	$P_{Vr_er_m\kappa}$	23.35	22	40.12	21	52.47	16
23	$P_{Vr_e\upsilon m}$	17.62	17	38.97	19	76.1	28
24	$P_{Vr_er_wr_m\kappa}$	31.56	27	51.86	27	65.4	21
25	$P_{Vr_er_w\kappa\varphi}$	33.06	32	61.49	32	89.67	32
26	$P_{Vr_er_w\kappa g}$	24.89	23	42.32	22	54.89	17
27	$P_{Vr_er_wmg}$	19.0	20	33.18	16	44.03	14
28	$P_{Vr_er_wr_m\kappa\upsilon}$	38.96	33	67.74	33	92.0	33
29	$P_{Vr_er_wr_m\kappa g}$	31.56	27	51.86	27	65.4	21
30	$P_{Vr_er_wr_m\varphi g}$	32.82	31	58.59	31	86.26	31
31	$P_{Vr_er_wr_mmg}$	26.18	25	44.16	25	56.92	19
32	$P_{Vr_er_wr_m\kappa\upsilon\varphi}$	47.3	35	82.52	35	99.09	35
33	$P_{Vr_er_wr_m\kappa\upsilon m}$	31.56	27	51.86	27	65.4	21
34	$P_{Vr_er_wr_m\kappa mg}$	31.56	27	51.86	27	65.4	21
35	$P_{Vr_er_wr_m\kappa\upsilon\varphi m}$	47.3	35	82.52	35	99.09	35
36	$P_{Vr_er_wr_m\kappa\upsilon mg}$	38.96	33	67.74	33	92.0	33
37	$P_{Vr_er_wr_m\kappa\upsilon\varphi mg}$	47.3	35	82.52	35	99.09	35

7.5.3 The impact of health intervention strategies against malaria disease using community gametocyte load as indicator of intervention effectiveness

In this subsection, we assess the impact of the eight health intervention components for malaria disease system by comparing their effectiveness when they are single and even when they are combined using the endemic value of community gametocyte load (G_H^*) as an indicator of intervention effectiveness. Table (7.9) shows the results of the assessment of the comparative effectiveness of the malaria health intervention components using the %age reduction in the community gametocyte load as an indicator of intervention effectiveness. Community gametocyte load is a measure of the total infectious reservoir in humans, which we also propose in this study as an appropriate measure for public health to assess the overall performance of malaria health interventions targeted at the human host [24]. Community gametocyte load is useful in targeting the control and elimination of malaria in a given geographical environment as an indication of infectivity and the likelihood that malaria can be transmitted to mosquitoes.

a. By take into account the use of Larvicides and pupacides which has (i) killing efficacy on eggs, (ii) the killing efficacy on larva and (iii) the killing efficacy on pupa for immature mosquitoes. The results indicate that the killing efficacy on larva has the highest comparative effectiveness, followed by the killing efficacy on eggs while the killing efficacy of pupa have the least comparative effectiveness on larvicides and pupacides as a malaria health intervention.

b. When we take into account the use of LLINs as the only malaria health intervention, this intervention has three components which are (i) directly killing of adult mosquitoes, (ii) the effect of mosquito repellent and (iii) the protective efficacy of humans from mosquito bites. The results indicates that the effect of mosquito repellent and the protective efficacy of humans from mosquito bites have the highest but equal comparative effectiveness while the directly killing of adult mosquitoes has the least comparative effectiveness in reducing the G_H^*.

c. When we consider the use of ACT as the only malaria health intervention, we observe that this intervention has two components which are (i) the killing efficacy on gametocytes, and (ii) the killing efficacy of killing merozoites. We notice that the killing efficacy on gametocytes have higher comparative effectiveness than the killing efficacy of merozoites.

d. When we consider the comparative effectiveness of two components at a time of the malaria health interventions we observe the following results:

   i. The combination of the killing efficacy of merozoites and the killing efficacy of gametocytes has highest comparative effectiveness on CEL and CEM efficacy levels and the combination of directly killing of adult mosquitoes and the protective efficacy of humans from mosquito bites has also the highest comparative effectiveness on CEH efficacy level.

   ii. We consider the combination of the killing efficacy of eggs of immature mosquitoes and the effect of mosquito repellent on CEL and CEH efficacy levels and the combination of the direct

direct killing of adult mosquitoes and the protective efficacy of humans from mosquito bites on CEM efficacy level has the second highest comparative effectiveness that can lead to reduction of G_H^*.

iii. We consider the combination of directly killing of adult mosquitoes and the protective efficacy of humans from mosquito bites on CEL efficacy level, and on the other side the combination of the killing effecacy on eggs for immature mosquitoes and the effect of mosquito repellent on CEM efficacy level, and the combination of killing efficacy on pupa and the protective efficacy of humans from mosquito bites on CEH efficacy level has the third highest comparative effectiveness that can lead to the reduction of G_H^*.

iv. Furthermore, we observe that the combination of the killing efficacy of larva and the killing efficacy of merozoites has the lowest comparative effectiveness that can lead to the reduction of G_H^*.

e. When we take into account the comparative effectiveness of three intervention components which will be implemented at the same time of malaria health interventions, we observe the following results. The combination of the killing efficacy on eggs, the effect of mosquito repellent, and the killing efficacy on merozoites has the highest comparative effectiveness that can lead to the reduction of G_H^*. Whilst the combination of the killing efficacy on eggs, killing efficacy on pupa for immature mosquitoes and the directly killing of adult mosquitoes has the lowest comparative effectiveness that can lead to the reduction of G_H^*.

f. Lastly, when we consider the comparative effectiveness of all the intervention components of malaria health interventions are implemented at a time, we observe from the results that this combination has the highest comparative effectiveness compared to other combinations.

Table 7.9: Results of the assessment of comparative effectiveness of Malaria interventions using percentage reduction of endemic value of community gametocytes load (G_H^*) as the indicator of intervention effectiveness when each of the interventions is assumed to have: (a) low efficacy of 0.30, (b) medium efficacy of 0.60, and (c) high efficacy 0f 0.90. rate.

No.	**Indicator of Intervention effectiveness**	**Calculated G_H^*-L-eff**	**CEL**	**Calculated G_H^*-M-eff**	**CEM**	**Calculated G_H^*-H-eff**	**CEH**
1	G_H	0.0	1	0.0	1	0.0	1
2	G_{Hr_e}	0.19	5	0.37	5	0.56	5
3	G_{Hr_w}	0.21	6	0.43	6	0.64	6
4	G_{Hr_m}	0.17	4	0.35	4	0.52	4
5	$G_{H\kappa}$	0.14	3	0.28	3	0.42	3
6	$G_{H\upsilon}$	1.15	18	4.58	18	37.08	25
7	$G_{H\varphi}$	1.15	18	4.58	18	37.08	25
8	G_{Hm}	0.0	1	0.0	1	0.0	1
9	G_{Hg}	3.9	26	7.5	24	10.84	18
10	$G_{Hr_er_w}$	0.42	12	0.89	12	1.4	12
11	$G_{Hr_er_m}$	0.38	10	0.79	10	1.24	10
12	$G_{Hr_wr_m}$	0.41	11	0.86	11	1.35	11
13	$G_{Hr_e\kappa}$	0.34	8	0.71	8	1.11	8
14	$G_{Hr_e\upsilon}$	1.44	22	5.71	21	43.36	28
15	$G_{Hr_w\kappa}$	0.37	9	0.78	9	1.22	9
16	G_{Hr_wm}	0.21	6	0.43	6	0.64	6
17	$G_{Hr_m\varphi}$	1.42	20	5.64	20	43.0	27
18	$G_{H\kappa\varphi}$	1.43	21	6.12	23	49.95	30
19	G_{Hmg}	3.9	26	7.5	24	10.84	18
20	$G_{Hr_er_wr_m}$	0.64	15	1.41	15	2.33	15
21	$G_{Hr_er_w\kappa}$	0.6	14	1.31	14	2.15	14
22	$G_{Hr_er_m\kappa}$	0.55	13	1.2	13	1.96	13
23	$G_{Hr_e\upsilon m}$	1.44	22	5.71	21	43.36	28
24	$G_{Hr_er_wr_m\kappa}$	0.83	16	1.91	16	3.3	16
25	$G_{Hr_er_w\kappa\varphi}$	2.13	24	9.4	31	63.76	32
26	$G_{Hr_er_w\kappa g}$	4.47	29	8.71	27	12.76	21
27	$G_{Hr_er_wmg}$	4.3	28	8.32	26	12.09	20
28	$G_{Hr_er_wr_m\kappa\upsilon}$	2.49	25	11.23	32	69.41	33
29	$G_{Hr_er_wr_m\kappa g}$	4.69	31	9.27	29	13.79	23
30	$G_{Hr_er_wr_m\varphi g}$	5.93	35	15.57	33	61.64	31
31	$G_{Hr_er_wr_mmg}$	4.51	30	8.8	28	12.92	22
32	$G_{Hr_er_wr_m\kappa\upsilon\varphi}$	5.22	33	39.17	35	99.5	35
33	$G_{Hr_er_wr_m\kappa\upsilon m}$	0.83	16	1.91	16	3.3	16
34	$G_{Hr_er_wr_m\kappa mg}$	4.69	31	9.27	29	13.79	23
35	$G_{Hr_er_wr_m\kappa\upsilon\varphi m}$	5.22	33	39.17	35	99.5	35
36	$G_{Hr_er_wr_m\kappa\upsilon mg}$	6.29	36	17.89	34	72.72	34
37	$G_{Hr_er_wr_m\kappa\upsilon\varphi mg}$	8.91	37	43.74	37	99.55	37

7.6 Summary

In this chapter, we developed a multiscale model that described the replication-transmission multiscale cycle of type II- vector-borne disease system at the host level, and that incorporates the mosquito life cycle that is, immature mosquitoes and adult mosquitoes, using malaria as a reference. We applied the embedded multiscale on mosquito dynamics to investigate the effect of super-infection, whereas at human dynamics we used the nested multiscale model as a way to investigate the influence of initial infection on the multiscale model malaria disease system. The multiscale model was developed based on the combination of type I reciprocal influence between macro-scale and micro-scale on the human host, where there is a pathogen replication cycle at the within-host scale, and also based on type II reciprocal influence of between macro-scale and micro-scale, where there is no pathogen replication at the within-host scale. We performed the global sensitivity analysis of the basic reproductive number the community gametocytes load, and the community sporozoites load. We conducted the global sensitivity analysis as a way of identifying the parameters which have an influence on increasing or decreasing the disease dynamics. The results from mathematical analysis and numerical analysis present that immature mosquitoes have an influence on the dynamics of the malaria disease system. We extended the multiscale model of malaria disease dynamics with the mosquito life cycle by incorporating malaria health interventions. This multiscale model present allowed us to use the comparative effectiveness of malaria health interventions with associated of three different perspectives: (i) ACTs were applied at a within-human scale for killing merozoites and gametocytes which is a way of reducing or preventing the pathogen replication cycle process, (ii) LLINs were used at between-host scale for preventing the transmission cycle process, and (iii) the use of larvicides and pupacides targeted at the immature mosquitoes. In addition, we examined the effects of different possible combinations of malaria health interventions on the replication-transmission multiscale cycle of malaria among individuals in the community, and we learn that the combination of all three malaria health interventions can lead to significant elimination of malaria infections. The results of comparative effectiveness of malaria health interventions imply that the use of LLINs has the highest comparative efficacy, followed by the use of larvicides and pupacides and finally the use of ACT. The results of this study are useful for policymakers and members of the community in malaria-endemic areas to use better strategies in improving disease management.

Chapter 8

Conclusion and Future Research Direction

8.1 Conclusion

In this chapter, we summarized all the findings of this study and offer some recommendations that can be considered for preventing and controlling the pathogen replication-transmission and spread of malaria transmission at the individual level and at the population level. This study aimed at developing coupled multiscale models of type II vector-borne disease system that consider the replication-transmission relativity theory. We developed coupled multiscale models of type II vector-borne disease systems that demonstrate the pathogen replication-transmission multiscale cycle using the malaria disease system as an example. The coupled multiscale model developed has a combination of two other categories of multiscale models, which are as follows: (i) nested multiscale model and (ii) embedded multiscale model. We selected coupled multiscale model for the type II vector-borne disease system because of the complex life cycle which needs multiple hosts infection e.g., for malaria disease needs two hosts (human host and mosquito host) for the parasite to complete the life cycle of the infectious disease system. These coupled multiscale models considered the combination of sub-models with the following reciprocal influences: (i) type I reciprocal influence between the macroscale and microscale and this type of reciprocal influence has a replication cycle at the micro-scale, and (ii) type II reciprocal influence between-macroscale and microscale and this type of reciprocal influence has no pathogen replication at the microscale. This coupled multiscale model of the malaria disease system was derived from a general multiscale model of vector-borne diseases [18] and a coupled multiscale model of malaria disease [24].

In Chapter 2, we presented a single-scale model that was formulated based on the transmission mechanism theory of type II vector-borne disease systems. The single-scale models demonstrate the traditional methods which were used previously, and which can be tracked to Sir Ronald Ross. We introduced the disease dynamics transmission mechanism theory. We discuss the transmission mechanism's limitations and suggest a new modeling science for directly transmitted infectious diseases that is similar to an existing science for environmentally transmitted infectious diseases that considers pathogen load in both the host and the environment. We introduced a new epidemiological variable called community pathogen load (CPL), which is then utilized to define the force of infection and transmission probability. The single-scale model used N_h and N_v as the phenomenological parameters which were the production of community pathogen load coming from the within-infected host scale. The traditional method concentrates only on the transmission process which takes place at the microscale and neglects the replication process which happens at the microscale. The numerical results of the single-scale model were carried out based on the parameters which were more sensitive to the reproductive number R_0 and the endemic of the community pathogen loads (G_H and P_V).

In Chapter 3, we presented a basic coupled multiscale model of the malaria disease system, with the main objective of the study is to examine the influence of super-infection in mosquitoes has on the dynamics of type II vector-borne disease transmission without pathogen replication-cycle at the microscale and also to investigate the influence of initial infection in humans has on the dynamics of a multiscale model of malaria disease system with pathogen replication cycle at the microscale. This model presented described the application of pathogen replication-transmission relativity theory which incorporates events (that is, pathogen replication) that give rise to the transmission and thus accommodate variation in time and space. We analyzed the multiscale model on a fast-slow time scale by reducing the dimensions of the full nested multiscale model into a simplified multiscale model. We proved the feasible region where the model is mathematical well-posed. The equilibrium states were determined and the local stability of the model was established using the basic reproductive number. From the numerical simulation, we discovered that the nested multiscale model has a unidirectional flow of information, that is, the within-human scale influences the between-host scale throughout the infection whereas the between-host scale influences the within-human scale through initial infection and the within-human pathogen load is then maintained by the pathogen replication cycle. On the embedded multiscale model, we observed that there is a bi-directional flow of information, that is, the within-mosquito scale influences the between host scale throughout the infection, whilst the between-host scale influences the within-host scale through super-infection.

In Chapter 4, we presented a coupled multiscale model of the malaria disease system, with the objective of the study being to examine the influence of the human liver stage on the multiscale model for the malaria disease system. We proved the invariant region and feasible region where the model is mathematical well-posed. The multiscale model has a weakness in expressing the endemic equilibrium state in terms

of explicit parameters and the known reproductive number. We extended the multiscale model by incorporating the vaccine health intervention and used the comparative effectiveness on three subunits which are: (i) erythrocytic vaccine, (ii) blood-stage vaccine, and (iii) transmission-blocking stage vaccine. The results indicated that the combination of these vaccine interventions has the highest impact of reducing the reproductive number R_0. The combination of all three vaccine interventions has the transmission on both individual-level and at population-level.

In Chapter 5, we presented a coupled multiscale model of the malaria disease system with the human immune system. We used a coupled multiscale model of malaria with a combination of two nested multiscale models in human-host where there is pathogen replication cycle at the within-human scale and mosquito-host where there is no pathogen replication at the within-mosquito scale. We used the fast-slow time scale analysis to reduce the dimensions of the full-nested multiscale model into a simplified nested multiscale model. The role played by immune cells is to fight against the malaria parasite. From the numerical results, we discovered that the immune cells parameters have an influence on the reduction of malaria transmission at the community level. The results will help to identify the vaccines that boost the immune cells in the fight against malaria parasite at three sub-units stages which has an impact in reducing malaria at the individual level and at the population level. The results also suggested that malaria transmission can be controlled by reducing the rate of sporozoites that invades the human liver cells, which will lead to the reduction of merozoites that invade the red blood cells.

In Chapter 6, we presented a coupled multiscale model of the malaria disease system to explore the effect of temperature changes on the malaria pathogen replication transmission using a system of ordinary differential equations. The multiscale model formulated in this study explicitly traces the malaria parasite life cycle between two hosts (human host and mosquito host) and on two interacting scales (that is, within-host scale and between host scale). It was established with the aid of Castillo-Chavez's approach that the infection-free state is globally asymptotically stable when the basic reproductive number (R_0) is less than unity and also proved that the infection-free state is locally asymptotically stable when the basic number is less than unity. It was also proved with the aid of fixed point theory that the endemic equilibrium state is asymptotically stable when the R_0 is greater than unity. The existence and uniqueness of the endemic equilibrium state were proved. The numerical simulation of the multiscale model was conducted to explore the influence of temperature on the malaria transmission dynamics at the individual level and at the population level. From the numerical simulation, we observed that as the temperature increases, malaria transmission also increases at the population level and reaches a maximum when the temperature is between 32^0C and 34^0C. When the temperature continues to increase above 34^0C then the malaria transmission begins to decline at the population level. Therefore, the temperature changes influence increasing or reducing the malaria parasite replication and transmission cycle. The recommended control measures in areas of high temperatures are the use of LLINS to prevent the transmission of malaria and also the use of ACTs drugs and vaccines which are more effective on the within-human scale to prohibit

the replication cycle.

In Chapter 7, we presented a coupled multiscale model of the malaria disease system that incorporates the mosquito life cycle (that is, immature mosquitoes and adult mosquitoes). We examined the influence of the mosquito life cycle on the multiscale model of malaria transmission at the individual level and the population level. The mathematical properties of the multiscale model were investigated. The local stability and global stability of the disease-free equilibrium state were analyzed whenever R_0 is less than unity. The conditions for the existence and uniqueness of the endemic equilibrium state were well-posed. The result from the center Manifold theory shows that the model has endemic equilibrium which is asymptotically stable whenever the R_0 is greater than unity. The numerical results show that as the rate of immature mosquitoes developed to adult mosquitoes increased has an impact of increasing the density of mosquitoes, which will result in an increase in malaria transmission at the population level. The numerical results suggested that as more mosquitoes being mature there are more cases of malaria infection at the community level. Therefore, to rescue the life of the community, in the fight against malaria by reducing the number of mosquitoes from breeding sites by destroying eggs, larvae, and pupae, the use of recommended chemicals for protection, use of LLINs, and ACTs. The model suggests that the use of health interventions for malaria has an impact on reducing the transmission of malaria and the associated disease burden. We extended the multiscale model of the malaria disease system with mosquito life cycle by incorporating the three malaria health interventions: (i) larvicides and pupacides, (ii) LLINs, and (iii) ACTs. We used the comparative effectiveness of the combination of malaria health interventions targeting immature and adult mosquitoes, and humans, where these interventions work on both the within-host scale and between-host scale. From the results, the comparative effectiveness of the combination of all malaria health interventions (ACTs, LLINs, and larvicides/pupacides) has the greatest impact on the control of malaria transmission at the individual and population level.

8.2 Future Research Directions

Since the aim of this study was on development of coupled multiple models of malaria disease system. There are various aspects of the malaria disease system that are not considered in this study. Future research directions in which the following aspects can be taken into account:

1. Taking into account the immune response in humans and vectors against parasites. Since vectors have DNA like humans, they develop antibodies against malaria diseases.

2. It is important to study the coupled multiscale model of malaria disease system with multiple malaria patches that is when considering multiple geographical environments that have influence on controlling imported pathogens from other communities or countries.

3. The multiple scale model of chapter 4 did not take into account the other environmental effects that determine the dynamics of malaria disease such as precipitation and humidity, which play an important role in the population density of the vector. Since the rainfall plays an important role in the reproduction of vectors.

4. Inclusion of resistance to malaria drugs or consideration of multiple pathogen infections in disease dynamics. This includes the development of a multi-scale model of malaria parasites that studies the role of an antimalarial drug concentration gradient on the evolutionary dynamics of malaria parasites.

Bibliography

[1] A H Lee, L S Symington, and D A Fidock. Dna repair mechanisms and their biological roles in the malaria parasite plasmodium falciparum. *Microbiology and Molecular Biology Reviews*, 78(3): 469–486, 2014.

[2] M Vitoria, R Granich, C F Gilks, C Gunneberg, M Hosseini, W Were, M Raviglione, and K M De Cock. The global fight against hiv/aids, tuberculosis, and malariacurrent status and future perspectives. *American journal of clinical pathology*, 131(6):844–848, 2009.

[3] W Garira. A primer on multiscale modelling of infectious disease systems. *Infectious Disease Modelling*, 3:176–191, 2018.

[4] M L Barreto, M G Teixeira, and E H Carmo. Infectious diseases epidemiology. *Journal of Epidemiology & Community Health*, 60(3):192–195, 2006.

[5] F Messina, C Montaldo, I Abbate, M Antonioli, V Bordoni, G Matusali, A Sacchi, E Giombini, G M Fimia, M Piacentini, et al. Rationale and criteria for a covid-19 model framework. *Viruses*, 13(7): 1309, 2021.

[6] R B Garabed, A Jolles, W Garira, C Lanzas, J Gutierrez, and G Rempala. Multi-scale dynamics of infectious diseases. *Interface Focus*, 10(1):20190118, 2020.

[7] W Garira. A complete categorization of multiscale models of infectious disease systems. *Journal of biological dynamics*, 11(1):378–435, 2017.

[8] J B Gutierrez, M R Galinski, S Cantrell, and E O Voit. From within host dynamics to the epidemiology of infectious disease: scientific overview and challenges. *Mathematical biosciences*, 270: 143–155, 2015.

[9] D. L Smith, K. E Battle, S. I Hay, C M Barker, T W Scott, and F E McKenzie. Ross, macdonald, and a theory for the dynamics and control of mosquito-transmitted pathogens. *PLoS pathogens*, 8 (4):e1002588, 2012.

[10] H W Hethcote. The mathematics of infectious diseases. *SIAM review*, 42(4):599–653, 2000.

[11] W Garira. The replication-transmission relativity theory for multiscale modelling of infectious disease systems. *Scientific reports*, 9(1):1–17, 2019.

[12] B Maregere. Analysis of co-infection of human immunodeficiency virus with human papillomavirus. https://ukzn-dspace.ukzn.ac.za/handle/10413/10717, 2014. Accessed: 2022-07-02.

[13] E T Ngarakana-Gwasira. Modelling the impact of climate variability and change on human health and diseases. http://41.175.146.201/handle/10646/2893, 2016. Accessed: 2022-07-02.

[14] W Garira and M C Mafunda. From individual health to community health: towards multiscale modeling of directly transmitted infectious disease systems. *Journal of Biological Systems*, 27(01): 131–166, 2019.

[15] M H Cortez and J S Weitz. Distinguishing between indirect and direct modes of transmission using epidemiological time series. *The American Naturalist*, 181(2):E43–E52, 2013.

[16] L Cai, Z Li, Chayu Yang, and J Wang. Global analysis of an environmental disease transmission model linking within-host and between-host dynamics. *Applied Mathematical Modelling*, 86:404–423, 2020.

[17] C Lanzas, K Davies, S Erwin, and D Dawson. On modelling environmentally transmitted pathogens. *Interface focus*, 10(1):20190056, 2020.

[18] W Garira and F Chirove. A general method for multiscale modelling of vector-borne disease systems. *Interface focus*, 10(1):20190047, 2020.

[19] M O Souza. Multiscale analysis for a vector-borne epidemic model. *Journal of mathematical biology*, 68(5):1269–1293, 2014.

[20] W Garira, D Mathebula, and R Netshikweta. A mathematical modelling framework for linked within-host and between-host dynamics for infections with free-living pathogens in the environment. *Mathematical biosciences*, 256:58–78, 2014.

[21] R Netshikweta and W Garira. A multiscale model for the world's first parasitic disease targeted for eradication: guinea worm disease. *Computational and mathematical methods in medicine*, 2017, 2017.

[22] W Garira and D Mathebula. Development and application of multiscale models of acute viral infections in intervention research. *Mathematical Methods in the Applied Sciences*, 43(6):3280–3306, 2020.

[23] S. L Ott, S. J Wells, and B. A Wagner. Herd-level economic losses associated with johne's disease on us dairy operations. *Preventive veterinary medicine*, 40(3-4):179–192, 1999.

[24] W Garira and D Mathebula. A coupled multiscale model to guide malaria control and elimination. *Journal of theoretical biology*, 475:34–59, 2019.

[25] M J Keeling and K TD Eames. Networks and epidemic models. *Journal of the royal society interface*, 2(4):295–307, 2005.

[26] H C Tuckwell, L Toubiana, and J Vibert. Spatial epidemic network models with viral dynamics. *Physical Review E*, 57(2):2163, 1998.

[27] A V Diez Roux and A E Aiello. Multilevel analysis of infectious diseases. *The Journal of infectious diseases*, 191(Supplement_1):S25–S33, 2005.

[28] M A Gilchrist and D Coombs. Evolution of virulence: interdependence, constraints, and selection using nested models. *Theoretical population biology*, 69(2):145–153, 2006.

[29] J Labadin, CML Kon, and SFS Juan. Deterministic malaria transmission model with acquired immunity. In *Proceedings of the world congress on engineering and computer science*, volume 2, pages 20–22, 2009.

[30] H M Yang. Malaria transmission model for different levels of acquired immunity and temperature-dependent parameters (vector). *Revista de saude publica*, 34:223–231, 2000.

[31] Z Feng, J Velasco-Hernandez, B Tapia-Santos, and M C A Leite. A model for coupling within-host and between-host dynamics in an infectious disease. *Nonlinear Dynamics*, 68(3):401–411, 2012.

[32] M A Gilchrist and A Sasaki. Modeling host–parasite coevolution: a nested approach based on mechanistic models. *Journal of Theoretical Biology*, 218(3):289–308, 2002.

[33] M Martcheva and S S Pilyugin. An epidemic model structured by host immunity. *Journal of Biological Systems*, 14(02):185–203, 2006.

[34] L Cai, N Tuncer, and M Martcheva. How does within-host dynamics affect population-level dynamics? insights from an immuno-epidemiological model of malaria. *Mathematical Methods in the Applied Sciences*, 40(18):6424–6450, 2017.

[35] B Agusto, MCA Leite, and M E Orive. The transmission dynamics of a within-and between-hosts malaria model. *Ecological complexity*, 38:31–55, 2019.

[36] L Saker, K Lee, B Cannito, A Gilmore, D H Campbell-Lendrum, et al. Globalization and infectious diseases: a review of the linkages. https://apps.who.int/iris/bitstream/handle/10665/68726/TDR_STR_SEB_ST_04.2.pdf, 2004. Accessed: 2022-07-02.

[37] A Suryanto and I Darti. On the nonstandard numerical discretization of sir epidemic model with a saturated incidence rate and vaccination. *AIMS Math*, 6:141–155, 2021.

[38] W Garira. The research and development process for multiscale models of infectious disease systems. *PLoS computational biology*, 16(4):e1007734, 2020.

[39] ET Ngarakana-Gwasira, CP Bhunu, M Masocha, and E Mashonjowa. Assessing the role of climate change in malaria transmission in africa. *Malaria research and treatment*, 2016, 2016.

[40] G. A. Ngwa and W. S. Shu. A mathematical model for endemic malaria with variable human and mosquito populations. *Mathematical and Computer Modelling*, 32(7-8):747–763, 2000.

[41] A M Niger and A B Gumel. Mathematical analysis of the role of repeated exposure on malaria transmission dynamics. *Differential Equations and Dynamical Systems*, 16(3):251–287, 2008.

[42] J Tumwiine, JYT Mugisha, and L S Luboobi. A mathematical model for the dynamics of malaria in a human host and mosquito vector with temporary immunity. *Applied mathematics and computation*, 189(2):1953–1965, 2007.

[43] M I Teboh-Ewungkem and T Yuster. A within-vector mathematical model of plasmodium falciparum and implications of incomplete fertilization on optimal gametocyte sex ratio. *Journal of theoretical biology*, 264(2):273–286, 2010.

[44] B. Hellriegel. Modelling the immune response to malaria with ecological concepts: short-term behaviour against long-term equilibrium. *Proceedings of the Royal Society of London. Series B: Biological Sciences*, 250(1329):249–256, 1992.

[45] T. O. Orwa, R. W. Mbogo, and L. S. Luboobi. Mathematical model for hepatocytic-erythrocytic dynamics of malaria. *International Journal of Mathematics and Mathematical Sciences*, 2018, 2018.

[46] M. A. Selemani, L. S. Luboobi, and Y. Nkansah-Gyekye. Modelling of the in-human host and in mosquito dynamics of parasite. *Journal of Mathematical and Computational Science*, 7(3):430–455, 2017.

[47] M Legros and S Bonhoeffer. A combined within-host and between-hosts modelling framework for the evolution of resistance to antimalarial drugs. *Journal of the Royal Society Interface*, 13(117): 20160148, 2016.

[48] W C Miller, K A Powers, M K Smith, and M S Cohen. Community viral load as a measure for assessment of hiv treatment as prevention. *The Lancet infectious diseases*, 13(5):459–464, 2013.

[49] A D Castel, M Befus, S Willis, A Griffin, T West, S Hader, and A E Greenberg. Use of the community viral load as a population-based biomarker of hiv burden. *Aids*, 26(3):345–353, 2012.

[50] P. Van den Driessche and J. Watmough. Reproduction numbers and sub-threshold endemic equilibria for compartmental models of disease transmission. *Mathematical biosciences*, 180(1):29–48, 2002.

[51] M Bani-Yaghoub, R Gautam, Z Shuai, P Van Den Driessche, and R Ivanek. Reproduction numbers for infections with free-living pathogens growing in the environment. *Journal of biological dynamics*, 6(2):923–940, 2012.

[52] W. Garira and B. Maregere. The transmission mechanism theory of disease dynamics: Its aims, assumptions and limitations. *Infectious Disease Modelling*, Mauscript Number: IDM-D-22-00071, 2022.

[53] K Dietz and JAP Heesterbeek. Daniel bernoulli's epidemiological model revisited. *Mathematical biosciences*, 180(1-2):1–21, 2002.

[54] W O Kermack and A G McKendrick. A contribution to the mathematical theory of epidemics. *Proceedings of the royal society of london. Series A, Containing papers of a mathematical and physical character*, 115(772):700–721, 1927.

[55] W O Kermack and A G McKendrick. Contributions to the mathematical theory of epidemics. ii.—the problem of endemicity. *Proceedings of the Royal Society of London. Series A, containing papers of a mathematical and physical character*, 138(834):55–83, 1932.

[56] W O Kermack and A G McKendrick. Contributions to the mathematical theory of epidemics. iii.—further studies of the problem of endemicity. *Proceedings of the Royal Society of London. Series A, Containing Papers of a Mathematical and Physical Character*, 141(843):94–122, 1933.

[57] A. K Dasanna, U. S Schwarz, G. Gompper, and D. A Fedosov. Multiscale modeling of malaria-infected red blood cells. *Handbook of Materials Modeling: Applications: Current and Emerging Materials*, pages 2625–2648, 2020.

[58] S. K Sreenivasamurthy, G. Dey, M. Ramu, M. Kumar, M. K Gupta, A. K Mohanty, HC Harsha, P. Sharma, N. Kumar, A. Pandey, et al. A compendium of molecules involved in vector-pathogen interactions pertaining to malaria. *Malaria journal*, 12(1):1–7, 2013.

[59] C Chiyaka, W Garira, and S Dube. Modelling immune response and drug therapy in human malaria infection. *Computational and Mathematical Methods in Medicine*, 9(2):143–163, 2008.

[60] M. A. Selemani, L. S. Luboobi, and Y. Nkansah-Gyekye. The in-human host and in-mosquito dynamics of malaria parasites with immune responses. *New Trends in Mathematical Sciences*, 5(3): 182–207, 2017.

[61] C. Castillo-Chavez, Z. Feng, and W. Huang. On the computation of ro and its role on. *Mathematical approaches for emerging and reemerging infectious diseases: an introduction*, 1:229, 2002.

[62] N Chitnis, J M Cushing, and JM Hyman. Bifurcation analysis of a mathematical model for malaria transmission. *SIAM Journal on Applied Mathematics*, 67(1):24–45, 2006.

[63] M M Elloso, HC Van Der Heyde, JA Vande Waa, D D Manning, and W P Weidanz. Inhibition of plasmodium falciparum in vitro by human gamma delta t cells. *The Journal of Immunology*, 153(3): 1187–1194, 1994.

[64] D Gurarie, PA Zimmerman, and CH King. Dynamic regulation of single-and mixed-species malaria infection: insights to specific and non-specific mechanisms of control. *Journal of theoretical biology*, 240(2):185–199, 2006.

[65] R Netshikweta and W Garira. An embedded multiscale modelling to guide control and elimination of paratuberculosis in ruminants. *Computational and Mathematical Methods in Medicine*, 2021, 2021.

[66] MVI. Accelerating malaria vaccine development. https://www.malariavaccine.org/malaria-and-vaccines/need-vaccine. Accessed: 2021-12-22.

[67] C Chiyaka, W Garira, and S Dube. Mathematical modelling of the impact of vaccination on malaria epidemiology. *Qual. Theory Differ. Equ. Anal*, 1(1):28–58, 2007.

[68] S Mandal, R R Sarkar, and S Sinha. Mathematical models of malaria-a review. *Malaria journal*, 10 (1):1–19, 2011.

[69] World malaria report 2019. https://www.who.int/malaria/data/en/, 2019. Accessed: 2020-04-26.

[70] A M Niger and A B Gumel. Immune response and imperfect vaccine in malaria dynamics. *Mathematical Population Studies*, 18(2):55–86, 2011.

[71] C. Castillo-Chavez, Z. Feng, and W. Huang. On the computation of ro and its role on. *Mathematical approaches for emerging and reemerging infectious diseases: an introduction*, 1:229, 2002.

[72] C C McCluskey and P van den Driessche. Global analysis of two tuberculosis models. *Journal of Dynamics and Differential Equations*, 16(1):139–166, 2004.

[73] A. D Polyanin and A. V Manzhirov. Handbook of mathematics for engineers and scientists. *Taylor and Francis Group*, 2007.

[74] C Castillo-Chavez and B Song. Dynamical models of tuberculosis and their applications. *Mathematical Biosciences & Engineering*, 1(2):361, 2004.

[75] G Sun, J Xie, S Huang, Z Jin, M Li, and L Liu. Transmission dynamics of cholera: Mathematical modeling and control strategies. *Communications in Nonlinear Science and Numerical Simulation*, 45:235–244, 2017.

[76] JP LaSalle. The stability of dynamical systems, society for industrial and applied mathematics, philadelphia, pa., 1976. In *With an appendix:"Limiting equations and stability of nonautonomous ordinary differential equations" by Z. Artstein, Regional Conference Series in Applied Mathematics*, 1976. URL https://epubs.siam.org/doi/pdf/10.1137/1.9781611970432.appa.

[77] T O Orwa, R W Mbogo, and L S Luboobi. Uncertainty and sensitivity analysis applied to an in-host malaria model with multiple vaccine antigens. *International Journal of Applied and Computational Mathematics*, 5(3):1–32, 2019.

[78] K Okuneye, S E Eikenberry, and A B Gumel. Weather-driven malaria transmission model with gonotrophic and sporogonic cycles. *Journal of biological dynamics*, 13(sup1):288–324, 2019.

[79] ET Ngarakana-Gwasira, CP Bhunu, and E Mashonjowa. Assessing the impact of temperature on malaria transmission dynamics. *Afrika Matematika*, 25(4):1095–1112, 2014.

[80] S E Eikenberry and A B Gumel. Mathematical modeling of climate change and malaria transmission dynamics: a historical review. *Journal of mathematical biology*, 77(4):857–933, 2018.

[81] WJ Martens, L W Niessen, J Rotmans, T H Jetten, and A J McMichael. Potential impact of global climate change on malaria risk. *Environmental health perspectives*, 103(5):458–464, 1995.

[82] A B Gumel, S M Moghadas, and R E Mickens. Effect of a preventive vaccine on the dynamics of hiv transmission. *Communications in Nonlinear science and numerical simulation*, 9(6):649–659, 2004.

[83] O Sharomi and A B Gumel. Curtailing smoking dynamics: a mathematical modeling approach. *Applied Mathematics and Computation*, 195(2):475–499, 2008.

[84] S M Moghadas, A B Gumel, R G McLeod, and R Gordon. Could condoms stop the aids epidemic? *Journal of Theoretical Medicine*, 5(3-4):171–181, 2003.

[85] A. E. S. Almocera, V. Nguyen, and E. A. Hernandez-Vargas. Multiscale model within-host and between-host for viral infectious diseases. *Journal of mathematical biology*, 77(4):1035–1057, 2018.

[86] A. Abdelrazec and A B Gumel. Mathematical assessment of the role of temperature and rainfall on mosquito population dynamics. *Journal of mathematical biology*, 74(6):1351–1395, 2017.

[87] M. T. White, J. T Griffin, T. S. Churcher, N. M. Ferguson, M. Basáñez, and A. C Ghani. Modelling the impact of vector control interventions on anopheles gambiae population dynamics. *Parasites & vectors*, 4(1):153, 2011.

[88] O. Koutou, B. Traoré, and B. Sangaré. Mathematical modeling of malaria transmission global dynamics: Taking into account the immature stages of the vectors. *Advances in Difference Equations*, 2018(1):220, 2018.

[89] T. Bakary, S. Boureima, and T. Sado. A mathematical model of malaria transmission in a periodic environment. *Journal of biological dynamics*, 12(1):400–432, 2018.

[90] D. L. Smith, T. A. Perkins, R. C. Reiner Jr, C. M. Barker, T. Niu, L. F. Chaves, A. M. Ellis, D. B. George, A. Le Menach, J. RC. Pulliam, et al. Recasting the theory of mosquito-borne pathogen transmission dynamics and control. *Transactions of the Royal Society of Tropical Medicine and Hygiene*, 108(4):185–197, 2014.

[91] J. Carr. *Applications of centre manifold theory*, volume 35. Springer Science & Business Media, 2012.